



HAL
open science

Confinement of metal complexes in NHC-cyclodextrins : structure, electrochemistry and catalysis

Jorge Mejjide Suárez

► **To cite this version:**

Jorge Mejjide Suárez. Confinement of metal complexes in NHC-cyclodextrins : structure, electrochemistry and catalysis. Catalysis. Sorbonne Université, 2018. English. NNT : 2018SORUS539 . tel-03001250

HAL Id: tel-03001250

<https://theses.hal.science/tel-03001250v1>

Submitted on 12 Nov 2020

HAL is a multi-disciplinary open access archive for the deposit and dissemination of scientific research documents, whether they are published or not. The documents may come from teaching and research institutions in France or abroad, or from public or private research centers.

L'archive ouverte pluridisciplinaire **HAL**, est destinée au dépôt et à la diffusion de documents scientifiques de niveau recherche, publiés ou non, émanant des établissements d'enseignement et de recherche français ou étrangers, des laboratoires publics ou privés.

Sorbonne Université

ÉCOLE DOCTORALE : CHIMIE MOLÉCULAIRE - ED 406

Institut Parisien de Chimie Moléculaire -UMR 8232

Équipe Glycochimie Organique Biologique et Supramoléculaire

Confinement of metal complexes in NHC-cyclodextrins. Structure, electrochemistry and catalysis.

Par Jorge MEIJIDE SUÁREZ

Thèse de doctorat de chimie

Dirigée par Matthieu SOLLOGOUB, Sylvain ROLAND

Présentée et soutenue publiquement le 26 Octobre 2018

Devant un jury composé de :

M. Didier	BOURISSOU	Directeur de Recherche Université Paul Sabatier	Rapporteur
M. Clément	MAZET	Professeur Université de Genève	Rapporteur
Mme. Laurence	GRIMAUD	Directrice de Recherche École Normale Supérieure de Paris	Examinatrice
Mme. Florence	DJÉDAÏNI-PILARD	Professeure Université Jules Verne	Examinatrice
M. Matthieu	SOLLOGOUB	Professeur Sorbonne Université	Directeur de Thèse
M. Sylvain	ROLAND	Maître de Conférences Sorbonne Université	Directeur de Thèse

To my parents and Pilin

Acknowledgements	1
Abbreviations	3
CHAPTER I: Effects of discrete confinement of metal complexes. Structural and electrochemical properties and applications in catalysis	1
A. Introduction	1
B. Effect of the confinement on the structure and dynamics of the complex	2
1. Effect of the cavity in the trapping of organometallic complexes	2
2. Effect of the cavity in encapsulated dynamic species	5
C. Effect of the confinement in the electrochemical behavior	9
1. Effect of the cavity on redox-active host-guest complexes	9
2. Effect of the cavity on covalently linked complexes	14
D. Effect of the confinement of a metal on its catalytic properties	17
1. Cavity turning off the reactivity: On-off and product inhibition	17
2. Controlled environment to reduce deactivation pathways	19
3. Restricted cavities to form more reactive catalysts	22
4. Confined spaces for selective reactions	26
i. Regioselectivity	26
ii. Enantioselectivity	27
iii. Substrate selection	29
iv. Product distribution	33
E. Conclusions and outlook	37
CHAPTER II: Cyclodextrin based metal complexes. Structures and applications in catalysis	38
A. Nomenclature	38
B. Structure	39
C. Cyclodextrin-metal complexes	40
1. CD-metal complexes as second coordination sphere	41
2. CD-metal complexes as first and transient second coordination sphere	42
3. CD-metal complexes as first and second coordination spheres	49
D. The only introverted CD-metal complexes. NHC-capped cyclodextrins	52
1. Synthesis	52
2. Characterization	53
i. NMR	53
ii. DFT and X-Ray	57
iii. Weak interactions in (α -ICyD)AgCl complex	59
iv. First and second coordination sphere in (ICyD)MCl complexes	62
3. Catalytic applications: Cavity controlled selectivity	63
i. Regioselectivity: Hydroboration of alkynes	63
ii. Enantioselectivity: Enyne-cycloisomerisation	68
iii. Product distribution: Enyne-cycloisomerisation	69
E. Conclusion and perspectives	70
CHAPTER III: Synthesis and study of ICyD metal complexes	71
A. Increasing the size of the cyclodextrin	71
1. Linear coordination in gamma cyclodextrin : (γ -ICyD)AuCl	71
i. Synthesis	71
ii. Characterization	73
iii. Comparison of (γ -ICyD)AuCl shape with that of β and α -CD-derived complexes	79
B. Control of the metal position.	81
Confined versus non-confined gold (I) complexes	81
1. Synthesis of AuCl complexes via the silver route.	81
Comparison between α and β cyclodextrins	81
2. Synthesis of (ICyD)AuCl complexes via the free carbene route.	82
Comparison between α , β and γ cyclodextrin	82
C. Square planar gold (III) complexes:	90
Influence of the cyclodextrin in the geometry	90
1. Square planar coordination in gamma cyclodextrin: (γ -ICyD)AuCl ₃	90
i. Characterization	90

ii.	From NMR shifts to the structure of (γ -ICyD)AuCl ₃	92
iii.	From the structure to the shape of the (γ -AE-ICyD)AuCl ₃	94
2.	Oxidation of linear Au (I) complexes. Effect of narrower cyclodextrins	95
i.	Reported synthesis of NHC-Au(III) complexes	95
ii.	Screening of conditions with (γ -AE-ICyD)AuCl	95
iii.	NMR analysis of γ - based square planar gold (III) complexes	99
iv.	Effects on the NMR of (β -ICyD)-gold(III) complex	101
v.	Structure of (β -ICyD)-gold(III) complex	102
vi.	Comparison of structures and shapes of γ - and β -CD-based square planar gold(III) complexes	103
vii.	Electrochemistry of (ICyD)AuCl complexes	105
D.	To other geometries: CD-based Pd and Pt complexes	110
1.	Confinement of Pd. Square planar geometry in (ICyD)Pd complexes	110
i.	Described synthesis of NHC-Pd(II) complexes.	110
ii.	Synthesis of CD-based palladium (II) complexes via the silver route	111
iii.	Synthesis of CD-based palladium (II) complexes via the free NHC route	112
iv.	Analysis of structures.	114
-	Structure and behavior of α - β - and γ -CD based (ICyD)Pd(allyl)Cl complexes	114
-	Structures of γ - β - and α -CD-based (ICyD)PdCl ₂ (pyridine) complexes. Structure, shape and confirmation with DFT calculations	126
v.	QM-MM modeled structure of (β -ICyD)PdCl ₂ (pyridine).	131
vi.	Electrochemistry of (ICyD)PdCl ₂ (pyridine) compounds	132
2.	Confinement of Pt compounds.	139
	Square planar and trigonal geometry of (ICyD)Pt compounds.	139
i.	Synthesis of Pt-based-NHC.	139
ii.	Comparison between α and β - CD-based (ICyD)PtCl ₂ (pyridine) reactivity	139
iii.	Synthesis and structure of (β -rev-ICyD)Pt ₀ (dvtms)	142
iv.	Synthesis and structure of (β -ICyD)Pt ₀ (dvtms)	143
E.	General conclusion to chapter III.	146
CHAPTER IV: ICyD-metal complexes in catalysis. Effects of a discrete confinement		
A.	NHC-capped cyclodextrin in redox neutral catalytic cycles.	149
1.	Linear gold (I) catalyzed enyne cycloisomerization	149
i.	Effect of the cavity size on the enantioselectivity	149
ii.	Mechanism and selectivity.	151
iii.	Effect of the cavity size on the product distribution	154
2.	Copper (I) catalysis: Copper(I) Catalyzed Alkyne-Azide Cycloaddition	158
i.	Catalytic activity of (ICyD)CuCl complexes	159
ii.	Mechanistic studies	159
3.	Palladium (II) as Lewis Acid: Thiolation of triple bonds	161
i.	Reaction and mechanism	161
ii.	Scope of catalyst and kinetics	163
4.	Conclusion to part A:	165
B.	NHC capped cyclodextrin in redox active catalytic cycles.	166
1.	Increasing the oxidation state	166
iii.	Platinum(0)/platinum(II) catalysis : Hydrosilylation of triple bonds	166
iv.	Pt (0) /Pt (II) /Pt (IV) catalysis: C-H borylation of arenes.	167
2.	Gold(I) to gold(III)	169
i.	Bibliography: From linear to square planar.	169
ii.	Synthesis of (β -ICyD)Au(I) organogold species.	171
iii.	Stoichiometric studies.	172
iv.	Catalytic tests	174
3.	Reducing the oxidation state: Palladium(II) to palladium(0)	176
i.	Activation of the complex: Towards (β -ICyD)Pd(0) species.	176
ii.	Towards selectivity with (β -ICyD)Pd(II) complexes	180
iii.	Towards enantioselectivity with (β -ICyD)Pd(II) complexes: Allylation of aldehydes	188
C.	Conclusion to chapter IV	192
General conclusion and perspectives		193

Acknowledgements

First of all, I would like to thank all the jury members for taking the time to read my manuscript and for their advice and for their support, advice and ideas in a topic that can be far from their speciality.

I would also like to thank my advisors, Matthieu, who host me from the very beginning in the lab, for being human with his students and for the help to find something else for my postdoc.

Sylvain, I know that sometimes I can be quite stubborn, but I appreciated all the skills that you taught me during these years that I've spent working in the lab.

Special thanks also to all the GOBS members, who supported and helped me during these years. I have a special acknowledgment for Julien and Pinglu, who are the persons who showed me all that I have to know about the laboratory and how to deal with the cyclodextrins daily.

Last but not least, I couldn't possibly end this thesis without properly thanking Olivia, whose's teachings, encouragements and constant optimism about our work made the tough times at the lab bearable. She has always been helpful to every single one of us, no matter the project we were involved in. My PhD, would have not been the same without her in the team. I hope that everything will be better for your next steps, wherever you want ;).

I want also thank all the persons that made this history possible, starting with mis padres, que permitieron y apoyaron al máximo mis 5 años de vida en París. En los buenos y los no tan buenos momentos.

A mi hermano, que aunque hable poquito, siempre se preocupó por como avanzaba mi aventura en el extranjero. A mis primos, siempre dispuestos a olvidar los problemas con una (o más, muchas más) partidas en la grieta. Y a Marta y Javier que hicieron un gran esfuerzo para poder venir al día más largo y estresante de la tesis.

This trip could not be possible without Anne Lise et Ramón, qui ont suivi mon parcours des le début comme étudiant Erasmus.

J'ai un grand merci aux permanents de l'équipe, qui d'un côté un peu plus éloigné te font apprendre, qui encouragent a faire de ton mieux, et qui font ta vie au labo plus agréable. Mickaël pour sa curiosité et expertise en différents domaines, Berni pour toute la pédagogie qui partage avec tout le monde et Yongming, qui même en face de notre boîte de nuit, n'a rien dit de la musique qui tourne en continu dans le labo 509.

Merci a Guillaume (en paragraphe à part ;-)) pour surveiller le labo, pour les conseils et l'encouragement dans la vie professionnel qui m'ont donné la force pour postuler au postdoc que je commence dans quelques jours.

Un énorme merci à tous ceux qui ont été du début à la fin. Fares, la première personne que j'ai connu à Paris, qui a fait qu'un jeune espagnol qui tartina le français se sente accueilli. Mariecka, qui a toujours été une à côté, à Paris, en Belgique, à Vigo où aux manèges, toujours pas loin pour les bons moments, et les mauvais, merci pour les écoutes et tes conseils. Benji, collègue de master, de problèmes de labo, de bières, de restau et de voyages, toujours prêt à prendre un petit coup au bar pour noyer les problèmes de la vie, la manque de ce quotidien va me manquer énormément.

Gracias a Belén, aunque estemos separados por miles de km es como tenerla al lado, consciente de la vida en el extranjero, compartiendo las soluciones a todos los problemas que aparecen a mil km (dentro de poco millas).

J'ai pas de mots pour remercier à Sha, toujours à côté, à Paris où à Vancouver, au labo ou au bureau, au boulot ou au bar, autour d'un café ou d'une bière... Ton premier départ c'était compliqué, mais t'as réussi à me faire pleurer quand on s'est revu, merci encore.

Merci Lorien, Flo et Sawsen, votre arrivé dans ma vie m'a complètement touché. On passe tous par les mêmes problèmes pendant la thèse à un moment donné, mais on a réussi à les gérer petit à petit ensemble. Ravi de pouvoir refaire les prochains dimanches au soleil (où sous la pluie), peu importe où.

I keep a big space in the potato to those whom I shared my lab-life. Either in the lab or in the office. I never choose the colleagues of my office and lab, but I was the luckiest person sharing the lab with Zhihao (Chu-Oh) and Hugo. Always ready to smile and make the long days easier.

Kajetan (déso pour t'oublier le jour de ma soutenance), merci pour être capable de nous forcer à rigoler, même quand les choses vont mal, continue à sourire et à être de bonne humeur. Un gros merci aussi à Poporch, qui même s'il est un peu traître, tes 6 mois avec nous ont été excellents.

Merci à tous ceux avec lesquels j'ai eu la chance de partager mon passage par l'équipe, Renaud, Dmitri, Dan, Xiaolei, Bo, Léonid, Pierre, Changping, Zhonghang, Jiang, Wenting, Guangcan, Lisa, Manon, Marie, Pascaline, Fei et tous ceux que je risque d'oublier en écrivant la liste interminable.

Merci aussi à tous ceux de l'IPCM avec qui j'ai eu la chance de connaître et discuter. Sylvie, toujours prête à nous donner un coup de main, malgré son énorme quantité de travail. Virginie, avec qui j'ai eu la chance de collaborer. Omar (beau gosse), toujours souriant et flatteur Aurélie et Claire, pour l'énorme quantité de connaissances transmises, professionnelles ou personnels... Je trouverai jamais un bureau où aller râler aussi accueillant que le votre.

Merci finalement à celui qui trouvera cette thèse dans ses mains, qui lira la suite de ce texte.

Abbreviations

acac	Acetylacetonate
dba	dibenzylideneacetone
CD	Cyclodextrin
Cob ⁺	Cobaltocenium
COD	Cycloocta-1,5-diene
COSY	Correlation Spectroscopy
CuAAC	Copper-Catalyzed Alkyne-Azide Cycloaddition
CV	Cyclic Voltammetry
DCM	Dichloromethane
DEPT	Distorsionless Enhancement by Polarization Transfer
DFT	Density Functional Theory
DIBAL-H	Diisobutylaluminum Hydride
DMF	N,N-dimethylformamide
ESI	Electro-Spray Ionization
ee	Enantiomeric Excess
Fc	Ferrocene
HMBC	Heteronuclear Multiple Bond Correlation
HRMS	High Resolution Mass Spectrometry
HSQC	Heteronuclear Single-Quantum Coherence
IR	Infrared
Jmod	J-modulated spin-echo
IMes	1,3-Dimesitylimidazol-2-ylidene
IPr	1,3-Bis(2,6-diisopropylphenyl)imidazol-2-ylidene
Ms	Methanesulfonyl
NHC	N-Heterocyclic Carbene
NMR	Nuclear Magnetic Resonance
NOESY	Nuclear Overhauser Effect Spectroscopy
r.t.	Room Temperature
PEPPSI	Pyridine, Enhanced, Precatalyst, Preparation, Stabilization and Initiation
tren	tris(2-aminoethyl)amine
THF	Tetrahydrofuran
TLC	Thin-Layer Chromatography
TOCSY	Total Correlation Spectroscopy
TOF	TurnOver Frequency
TON	TurnOver Number

CHAPTER I

Effects of discrete confinement of metal complexes.
Structural and electrochemical properties.
Applications in catalysis

CHAPTER I: Effects of discrete confinement of metal complexes. Structural and electrochemical properties and applications in catalysis

A. Introduction

One of the most common dreams of a synthetic chemist is the synthesis of an artificial system as perfect as those made by Nature. Hence, metalloenzymes became a great source of inspiration. One common point in the structure of metalloenzymes is the presence of a catalytically active metal inside a well-defined pocket. The confining space of these pockets has been mimicked by chemists to add new properties to a metal complex.

Different approaches have been developed trying to mimic the active site. The most traditional one involves modifications on second coordination sphere of the metal complex.¹ Anchoring metal complexes to materials², direct inclusion of metal complexes to peptidic chains or proteins³ or ligand template approaches⁴ are just a few examples of how chemists of different fields have tried to reach the enzyme mimicry.

In the last few years, the relevance of the powerful effects of the encapsulation in the supramolecular catalysis field was stated by the publication of numerous reviews⁵. Some of them focused on the confining system, cavitands⁶, molecular flasks⁷ or nanoreactors.⁸ Others were focused on the nature of the second coordination sphere interacting with the metal, covalent or weak interactions⁹, hydrophobic effect,¹⁰ or biomimetic applications.¹¹

This review will focus on examples where discrete confining systems, independently of their nature, supramolecular assemblies, of covalently linked metals, but where the metal complex is fully encapsulated within. A special focus will be done on systems with direct interactions between the cavity and the metal atom. The effect of the cavity on the structural and electrochemical properties will be explained, as well as the effect on its reactivity for catalytic applications.

¹ Z. Liu, S. T. Schneebeli, J.F. Stoddart, *Chimia*, **2014**, *68*, 315 - 320

² S. Roland, J. Meijde Suárez, M. Sollogoub, *Chem. Eur. J.* **2018**, *24*, 12464 – 12473

³ P. Dydio, H. M. Key, A. Nazareno, J. Y.-E. Rha, V. Seyedkazemi, D.S. Clark, J. F. Hartwig, *Science*, **2016**, *354*, 102 - 106

⁴ V. F. Slagt, P. C. J. Kamer, P. W. N. M. van Leeuwen, J. N. H. Reek, *J. Am. Chem. Soc.* **2004**, *126*, 1526 - 1536

⁵ a) M. Raynal, P. Ballester, A. Vidal-Ferran, P. W. N. M. van Leeuwen, *Chem. Soc. Rev.*, **2014**, *43*, 1660-1733 b) M. Raynal, P. Ballester, A. Vidal-Ferran, P. W. N. M. van Leeuwen *Chem. Soc. Rev.*, **2014**, *43*, 1734–1787

⁶ R. Gramage-Doria, D. Armpach, D. Matt, *Coord. Chem. Rev.*, **2013**, *257*, 776–816

⁷ M. Yoshizawa, J. K. Klosterman, M. Fujita, *Angew. Chem. Int. Ed.* **2009**, *48*, 3418 – 3438

⁸ C. Deraedt, D. Astruc, *Coord. Chem. Rev.*, **2016**, *324*, 106 - 122

⁹ S. H. A. M. Leenders, R. Gramage-Doria, B. de Bruin, J. N. H. Reek, *Chem.Soc.Rev.*, **2015**, *44*, 433 - 448

¹⁰ L. Marchetti, M. Levine, *ACS Catal.* **2011**, *1*, 1090–1118

¹¹ J.-N. Rebilly, B. Colasson, O. Bistri, D. Over O. Reinaud, *Chem. Soc. Rev.*, **2015**, *44*, 467 - 489

B. Effect of the confinement on the structure and dynamics of the complex

Confinement of metal complexes has an important impact on the structure of the metal complex. The study of the behavior of the metal complex inside the cavity is the first step to understand the potential applications of the system.

1. Effect of the cavity in the trapping of organometallic complexes

One of the earliest examples in this field was proposed by Fujita *et al.*¹². In their report, the encapsulation of a $[(\eta^5\text{-indenyl})\text{Ru}(\text{CO})_2]_2$ dimer inside a Pd_6L_4 cage was studied. This complex, exists as a mixture of 4 different isomers in equilibrium in solution. In the presence of a Pd-based supramolecular assembled cage, the complex was quantitatively encapsulated. The driving force of the encapsulation is a π - π stacking between the indenyl groups and the aromatic wall that constituted the cage. Only one compound was observed in the $^1\text{H-NMR}$ spectrum of the encapsulated complex. Furthermore, only two peaks were observed for the CO ligands in $^{13}\text{C-NMR}$, one at 250 ppm and one at 190 ppm corresponding to the bridging CO ligand, and the terminal CO. Thus, the authors concluded that the encapsulated product was the *cis*-bridge isomer, displacing all the equilibria to form **1c2** (Figure I-1).

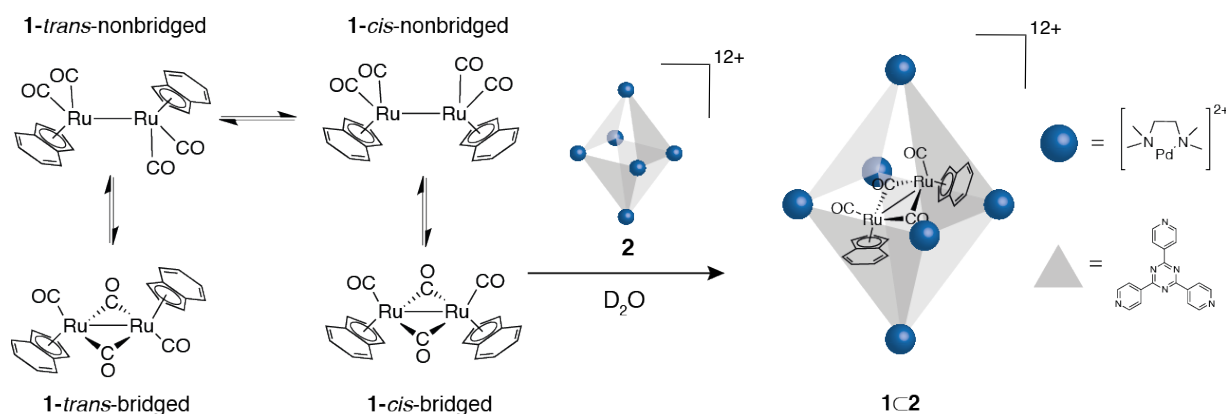


Figure I-1: Selective encapsulation of a *cis*- $[(\eta^5\text{-indenyl})\text{Ru}(\text{CO})_2]_2$ complex by a coordination cage.

They also report an increase of the lifetime of the complex, being stable during several months. Additionally, through NMR, IR and X-ray analysis, it was proved that the complex behaves similarly in solution and in the solid state.

¹² S Horiuchi, T. Murase, M. Fujita *J. Am. Chem. Soc.* **2011**, *133*, 12445–12447

At the same time,¹³ Love and coworkers showed that a cyclic polypyrrolic-Schiff base ligand can form metal complexes with different metal ions.¹⁴ In one of the reports, the authors showed that the monomeric Pacman-shaped ligand could coordinate MgBu_2 complexes. Addition of small amounts of water to the complex produces the hydrolysis of the MgBu salts. This hydrolyzed complex forms a $\text{Mg}_4(\text{OH})_4$ cubane inside two ligand molecules. This two ligands formed a dimeric capsule protecting the cubane within $([\text{Mg}_4(\text{OH})_4]c(\mathbf{3})_2)$. The driving force to stabilize it inside the assembly is the formation of a network of hydrogen bonding between the OH groups of the complex and the nitrogen atoms of the ligand, observed in the crystal structure. (Figure I-2).

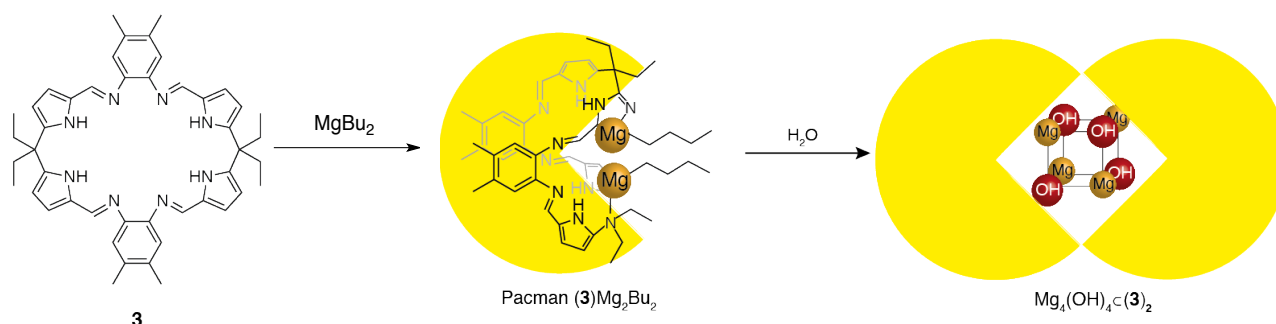
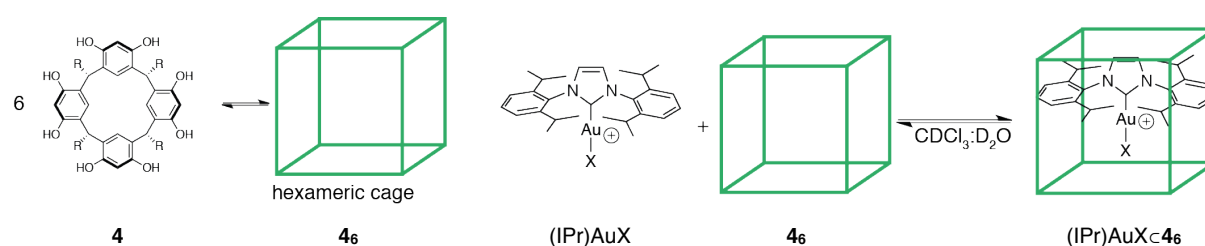


Figure I-2: Schematic structures of the Pacman shaped ligand and the encapsulated $\text{Mg}_4(\text{OH})_4$ cubane.

Few years later, Ballester and coworkers were interested in the confining mechanism of different gold catalysts inside a capsule.¹⁵ The nature of the capsule was based in a hydrogen bonded assembly of six resorcin[4]arenes ($\mathbf{4}$).¹⁶ Additionally, the formation of inclusion complexes with IPrAuX complexes was reported¹⁷ but the mechanism was not elucidated (Scheme I-1).



Scheme I-1: Schematic structures of the capsule and the studied complexes.

¹³ J. W. Leeland, F. J. White, J.B. Love, *J. Am. Chem. Soc.* **2011**, *133*, 7320-7323

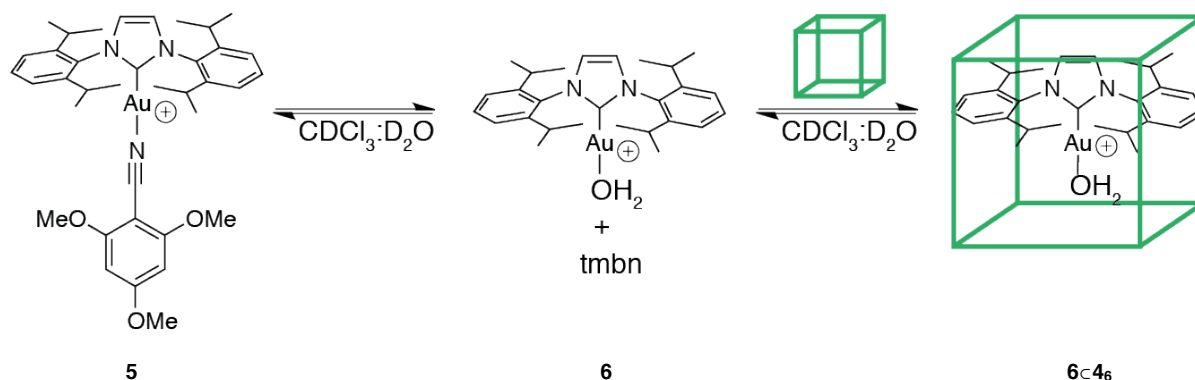
¹⁴ G. Givaja, A. J. Blake, C. Wilson, M. Schröder, J. B. Love, *Chem. Commun.*, **2003**, 2508-2509

¹⁵ L. Adriaenssens, A. Escribano-Cuesta, A. Homs, A. M. Echavarren, P. Ballester, *Eur. J. Org. Chem.* **2013**, 1494-1500.

¹⁶ L. R. MacGillivray, J. L. Atwood, *Nature*, **1997**, *389*, 469-472

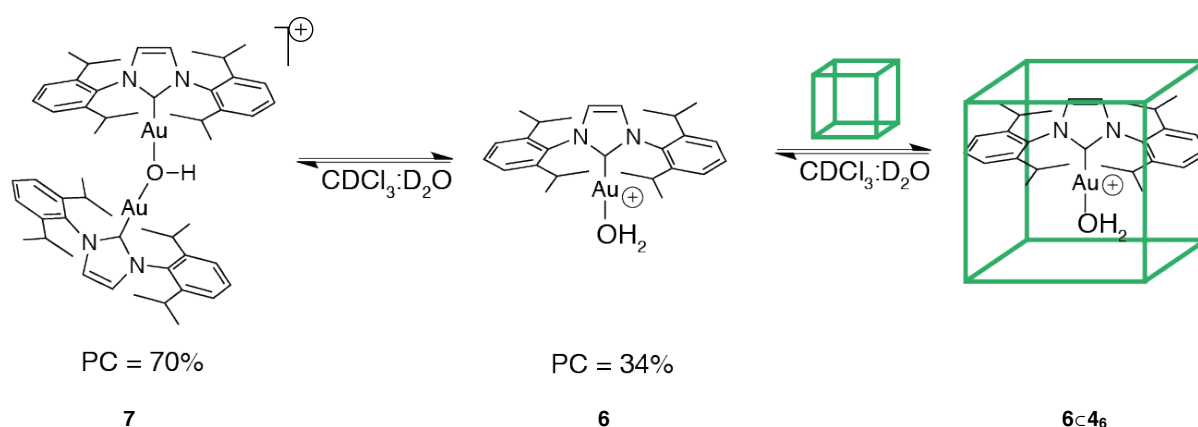
¹⁷ A. Carvazan, A. Scarso, P. Sgarbossa, G. Strukul, J. N. H. Reek, *J. Am. Chem. Soc.* **2011**, *133*, 2848 - 2851

During the encapsulation studies, the authors observed a kinetically slow encapsulation of the cationic IPrAu⁺ complex. Thus, the authors proposed that in a first instance IPrAu(tmbn)SbF₆ **5** must dissociate first its ligand. Then, the resulting aqua complex can be encapsulated driven by cation- π attractive interactions, forming a stable inclusion complex (Scheme I-2).



Scheme I-2: Schematic mechanism of the formation of the inclusion complex

To improve the rate of the encapsulation and avoid the rupture of the capsule due to an excess of water, the authors decided to form the aqua complex before the encapsulation. In this case, the complex was observed as a mixture of (IPr)Au(OH₂) and the dimeric (IPrAu)₂(μ -OH) complex (**7**).¹⁸ Nevertheless, in presence of **4₆** the authors observed only the encapsulation of the monomeric complex. To explain this observation, the packing coefficients (PC) were calculated.¹⁹ The PC of **7** is 70%, thus, higher than the ideal 55% postulated by Rebek. In conclusion, it cannot be encapsulated inside the cage. In contrast, the PC for the monomeric aqua complex **6** was calculated to be 34%, fitting inside the guest. Thus, the equilibrium is pushed to the thermodynamically stable **6@c₆** producing the complete dissociation of the dimer prior to the encapsulation (Scheme I-3).

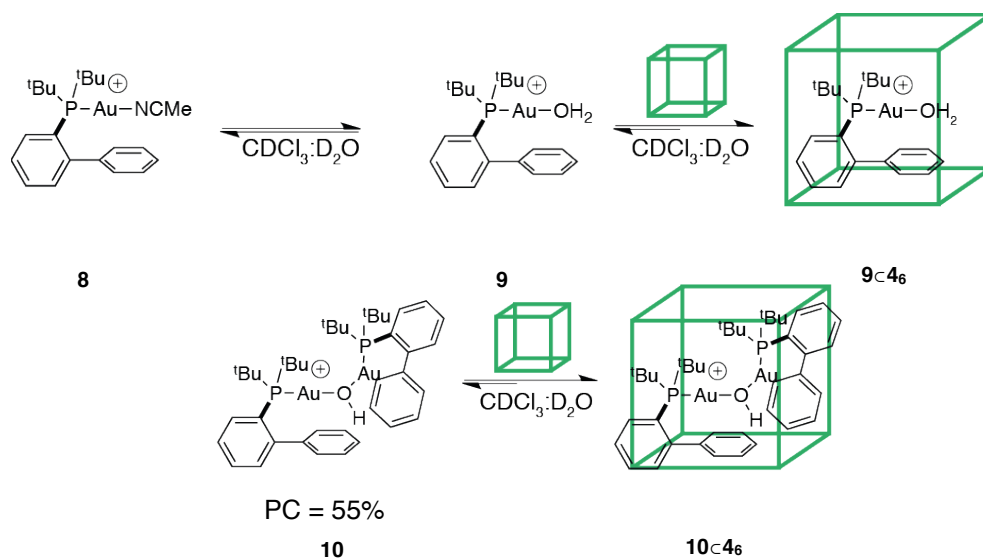


Scheme I-3: Schematic mechanism of the formation of the inclusion complex

¹⁸ R. S. Ramón, S. Gaillard, A. Poater, L. Cavallo, A. M. Z. Slawin, S. P. Nolan, *Chem. Eur. J.* **2011**, *17*, 1238–1246

¹⁹ S. Mecozzi, J. Rebek Jr, *Chem. Eur. J.*, **1998**, *4*, 1016 - 1022

To get more insights about the possibilities of this system, the authors were interested in the confinement of cationic phosphane complexes. Despite the appropriate PC for the monomeric **8**, the acetonitrile ligand was displaced to form the aqua complex **9**. Surprisingly, **9c4₆** was the only complex observed within. In contrast to **7**, when the the μ -OH dimer **10** is formed prior to the encapsulation, the host-guest complex is quantitatively observed inside the capsule without any dissociation. The authors explained this behavior with the ideal PC = 55% for the dimer, thus a ideal fitting inside the host (Scheme I-4).



Scheme I-4: Proposed equilibria in the encapsulation of different gold(I) phosphine complexes.

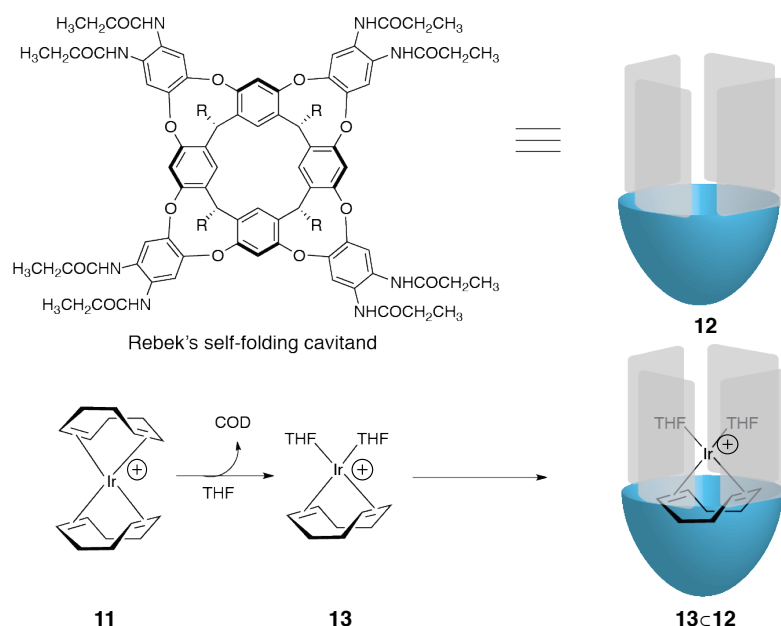
In these examples, the possibility of encapsulating discrete metal complexes was illustrated. Those systems showed how different natures of cavities can confine reactive metal complexes. The confinement of those complexes afforded stable structures with well-defined conformations. In addition, for the three cases, an additional stabilization was observed, which was reflected in increased lifetimes.

2. Effect of the cavity in encapsulated dynamic species

Studying the encapsulation of $[\text{Ir}(\text{COD})_2]^+$ (**11**)²⁰ inside a Rebek's self-folding cavitant (**12**)²¹, Ballester found that the included $[\text{Ir}]^+$ complex inside the vase-shaped cavitant had a particular motion and chiral properties. First, the encapsulation of the complex was detailed. It starts with a displacement of one of the COD ligands (cycloocta-1,5-diene) by two solvent molecules to form $\text{Ir}(\text{THF})_2(\text{COD})$ (**13**). This complex, driven by cation- π and CH- π interactions is included inside the host. (Scheme I-5)

²⁰ S. Korom, E. Martin, S. A. Serapian, C. Bo, P. Ballester, *J. Am. Chem. Soc.*, **2016**, *138*, 2273 - 2279

²¹ D. M. Rudkevich, G. Hilmersson, J. Rebek, *J. Am. Chem. Soc.* **1998**, *120*, 12216-12225

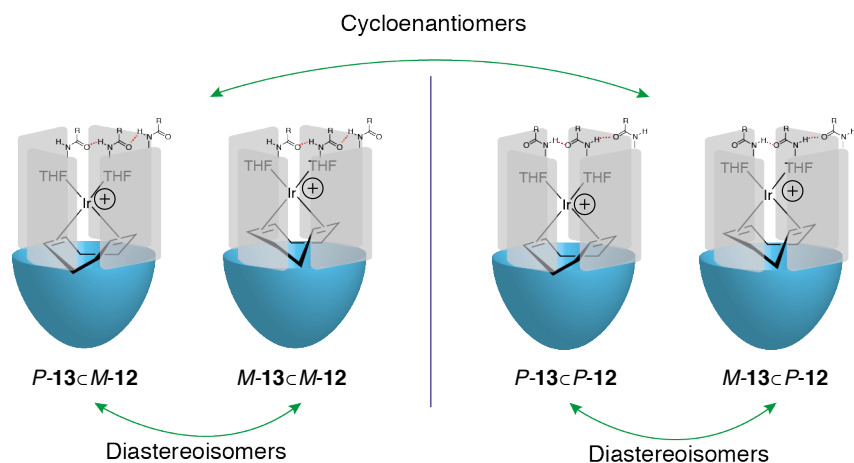


Scheme I-5: Structure of the Rebek's self folding cavitaand **12** and the proposed mechanism of the encapsulation of **13**.

Despite the chiral directionality of the hydrogen bonding of the amides, the NMR study of the host **12** showed a C_{4v} symmetry, pointing to a mixture of two cycloenantiomers in equilibrium in solution. DFT calculations of the system showed an interconversion barrier between the enantiomers of 18 kcal mol⁻¹, thus, both are conformationally stable. When the complex is encapsulated inside the vessel, the authors observed a reduction of the symmetry from a C_{4v} to a C_2 and the formation of two products in proton NMR. These two products were showed to be two different diastereoisomers, with a slow rotational motion on the NMR timescale.

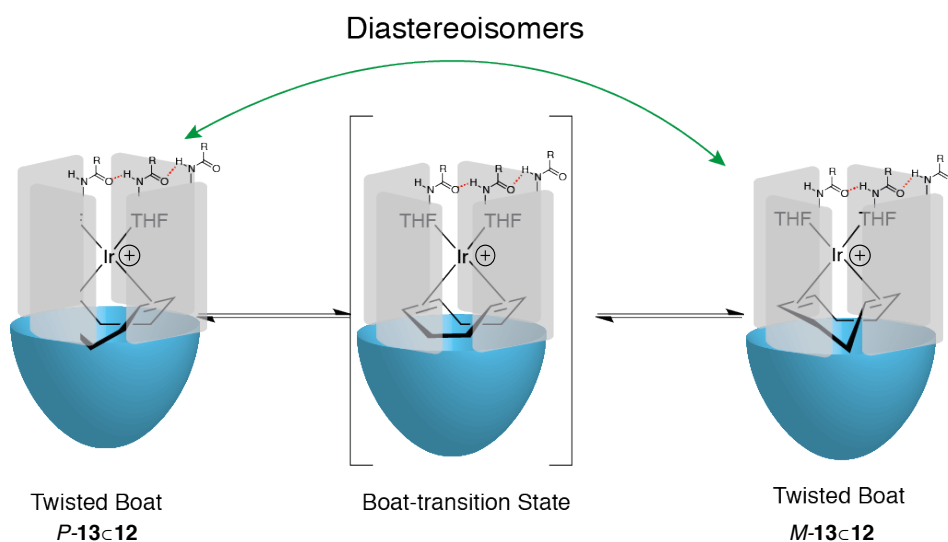
The diastereotopic chirality of the system was afforded by the chirality of the encapsulated Ir(COD)(THF)₂ (**13**). It was revealed by the resonances of the protons of the COD ligand. In their report, based on crystallographical data,²² the authors explained that despite the fact that the COD is usually drawn structure in a boat (B) conformation, the most stable structure is the twisted boat (**13-TB**). This TB conformation adds to the system the additional chirality to form two diastereoisomers. Thus, the formation of the host-guest system inside a chiral vessel **13c12**, forms 4 products, two pairs of diastereoisomers and two pairs of enantiomers (cycloenantiomers) (Scheme I-6).

²² Example structures with CCDC codes: JAMJOW and TUQWOS.



Scheme I-6: Structures of the four isomers of **13c12**.

Studying the mechanism of the isomerization of the system, the authors proved by DFT calculations that the isomerization must proceed without breaking the H-bonding network of the amides, thus, without guest exchange. Supported by variable temperature NMR experiments, the authors showed that the isomerization was achieved through a twisted boat to twisted boat isomerization, passing through a boat conformation (Scheme I-7). DFT calculations of this putative mechanism showed that this isomerization had a energy barrier of 8.6 kcal mol⁻¹, 2.5 times higher than the one calculated for the free complex in solution.



Scheme I-7: Mechanism of interconversion of both diastereoisomers.

In conclusion, the encapsulation of a metal complex added two new properties to the confined complex. The first one, a particular chirality, behaving inside the guest as pairs of diastereoisomers. The second one, an increase of the interconversion barrier between two diastereoisomers in comparison to the free complex.

In the following example, aiming to mimic the active site of a redox active enzyme,²³ Renaud and coworkers developed a tris(2-aminoethyl)amine (tren)-modified calix[6]arene cavitand able to form monomeric Cu²⁺ complexes **14** (Figure I-3). Thanks to the cavity, a monomeric Cu^I/Cu^{II} reactivity could be developed, avoiding dimerization of the Cu(tren) system. This system showed to produce guest exchanges driven by an electrochemical stimulus.²⁴

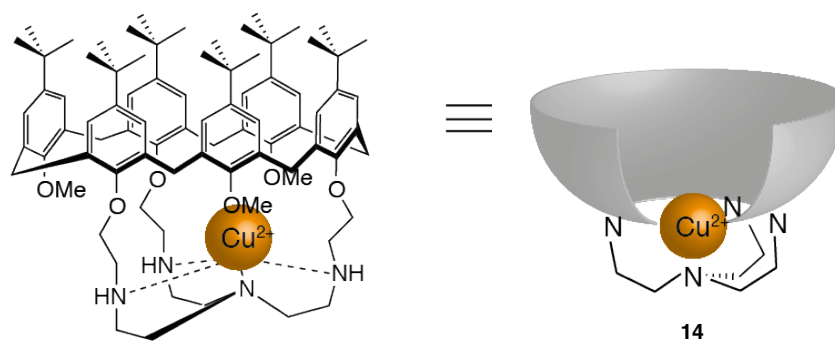


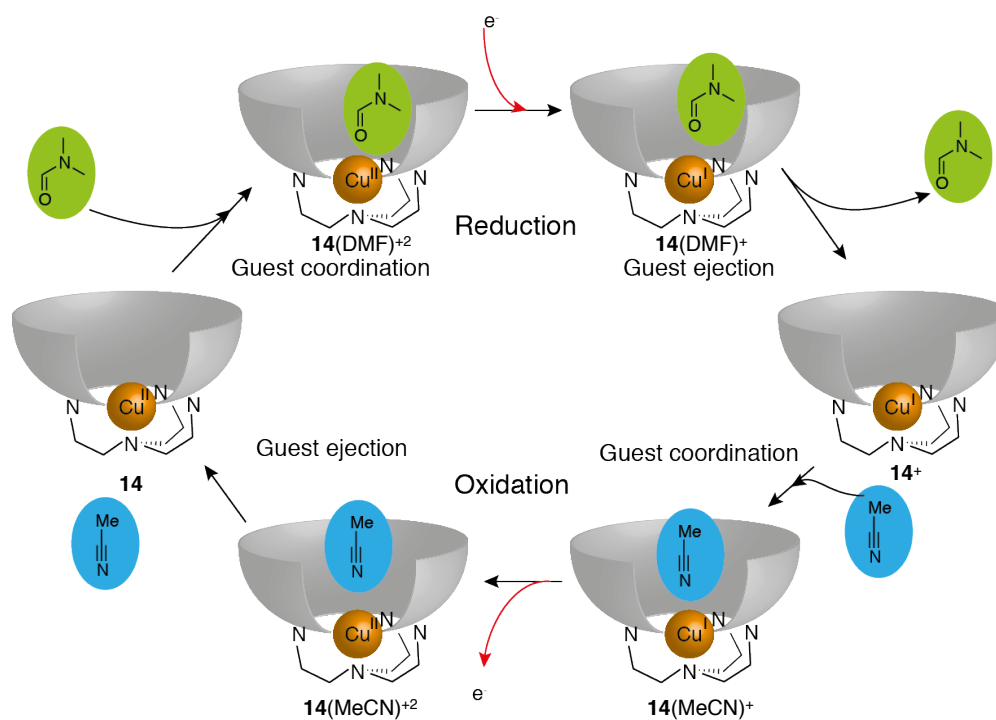
Figure I-3: Calix[6]trenCu **14** and its schematic representation.

For the [Cu(calix[6]tren)(H₂O)]²⁺ **14**(H₂O) where the water molecule is endo-coordinated to the copper(II) atom, an irreversible reduction peak at -0.94 V and a “sluggish” reoxidation wave at +0.03 V were observed. Since the use of different oxo-ligands (H₂O, EtOH, DMF) induced no change on the reoxidation peak, the authors proposed that the reduction of the oxophilic Cu(II) complex leads to a decoordination and ejection of the guest from the cavitand. Thus, the reoxidation peak is due to the guest-free Cu(I) complex.

When two competitive guest (MeCN and DMF) are present during the experiment, a redox-dependent interconversion of the endo-coordinated ligand is observed. Starting from [Cu(calix[6]tren)]²⁺ the coordination of the DMF is observed (**14**(DMF)²⁺). In the way of the reduction of the CV, an irreversible reduction of **14**(DMF)²⁺ is observed, producing an ejection of the DMF molecule and a coordination of a MeCN molecule **14**(MeCN)⁺. The pentacoordinated **14**(MeCN)⁺ complex was reoxidized at a different E_{pa} different that the one observed in absence of MeCN. This oxidation leads to a subsequent guest ejection and recoordination of the DMF molecule **14**(DMF)²⁺ in a completely reversible cycle (Scheme I-8)

²³ W. Kaim and J. Rall, *Angew. Chem., Int. Ed. Engl.*, **1996**, 35, 43 - 60

²⁴ G. Izzet, B. Douziech, T. Prangé, A. Tomas, I. Jabin, Y. Le Mest, O. Renaud. *Proc. Natl. Acad. Sci.*, **2005**, 102, 6831 - 6836



Scheme I-8: Redox cycle observed for **14**(DMF)

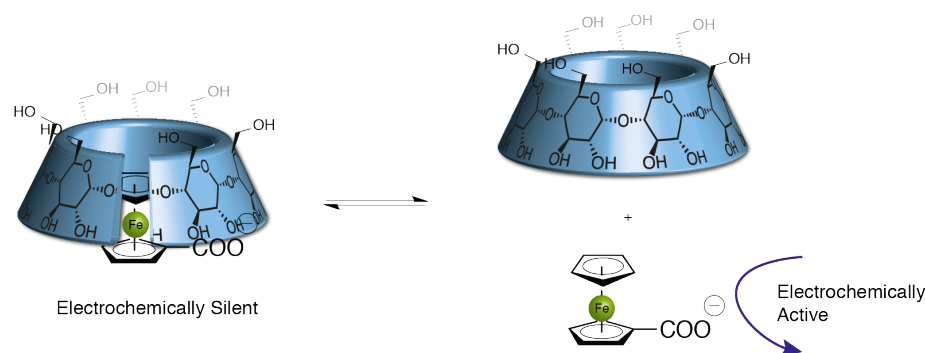
In this example, the confinement of a monometallic Cu^{2+} atom inside the cavitaund provides a protection of the system towards the formation of dimeric species. This protection allowed the authors to observe and study a dynamic behavior of a monometallic system.

C. Effect of the confinement in the electrochemical behavior

1. Effect of the cavity on redox-active host-guest complexes

The encapsulation of a metal complex inside a well-defined space can modify the redox properties of the free system. In this field, the most popular studies involved the encapsulation of a redox active center (used as guest) inside nanosized space (host) by weak interactions. The most popular redox active guests are the ferrocene (Fc) and cobaltocenium (Cob^+). In this part, some examples on how the nature of the cavity can influence the behavior in cyclic voltammetry of the encapsulated complex will be discussed.

One of the earliest reports of Evans. The authors studied the redox behavior of a water soluble Fc derivative and its host-guest complex with β -cyclodextrin (β -CD).²⁵ In their work, the authors found a decrease of the response of the Fc in cyclic voltammetry experiments. Additionally, a flattening of the oxidation wave at fast scan rates was also found. To explain this phenomenon, the authors proposed that the encapsulated Fc inside the cyclodextrin was electrochemically silent. Thus, to observe a signal in the CV voltammogram, the dissociation of the $Fc\subset\beta$ -CD must take place before the electron transfer (Figure). Therefore, the only signal observed is the one belonging to the free ferrocene in solution.



Scheme I-9: Observed process to explain the electrochemical behavior of $Fc\subset\beta$ -CD.

In the original paper, the origin of the redox inactivity was unknown. It was not established if the electron transfer did not take place because of a steric hindrance around the metal center (thus, kinetically hindered) or if the oxidized Fc^+ was unstable inside the β -CD (thus, thermodynamically hindered). To elucidate these different contributions, the behavior of different hosts was studied.²⁶

For example, the behavior of ferrocene complexes inside Cram's hemicarcerands²⁷ **15** was studied by Kaifer. In contrast to the experience with β -CD, the confined complex $Fc\subset$ **15** have responses in cyclic voltammetry, of a system that cannot release its guest²⁸. Besides, two different effects were observed in the experiments: A positive shift of the half-wave potential of ($E_{1/2}(F_c\subset$ **15**)) and a reduction of the intensity of response.

²⁵ T. Matsue, D.H. Evans, T. Osa, N. Kobayashi, *J. Am. Chem. Soc.* **1985**, *107*, 3411 - 3417

²⁶ For reviews about encapsulated redox centers: C. M. Cardona, S. Mendoza, A. E. Kaifer, *Chem. Soc. Rev.* **2000**, *29*, 37 - 42.

²⁷ M. L. Cuan, D. J. Cram, *J. Am. Chem. Soc.* **1991**, *113*, 2754 - 2755

²⁸ S. Mendoza, P. D. Davidov, A. E. Kaifer, *Chem. Eur. J.* **1998**, *4*, 864 - 870

The first effect was proposed to be a thermodynamic contribution due to the difficulty of formation of cationic species inside the guest. These cationic species inside the hemicarcerand are not able to complete their solvation sphere because of the steric hindrance afforded by the walls. Thus, this disruption leads to a less stable cationic Fc^+ , requiring a higher energy for the oxidation, translated in a higher oxidation potential.

The second effect was proposed to be related to the distance of the Fc from the electrode's surface. The authors proposed that the walls of the encapsulating hemicarcerand added an additional distance from the electrode. Using molecular dynamic methods, the authors estimate the size of the hemicarcerand complex to 1.8 nm x 3.0 nm, much bigger than the free ferrocene (0.7 nm diameter). This bigger size, increased significantly the distance of the ferrocene from 3.5 Å to 9 Å from the electrode's surface, thus, adding a kinetic constraint to the electron transfer (Figure I-4).

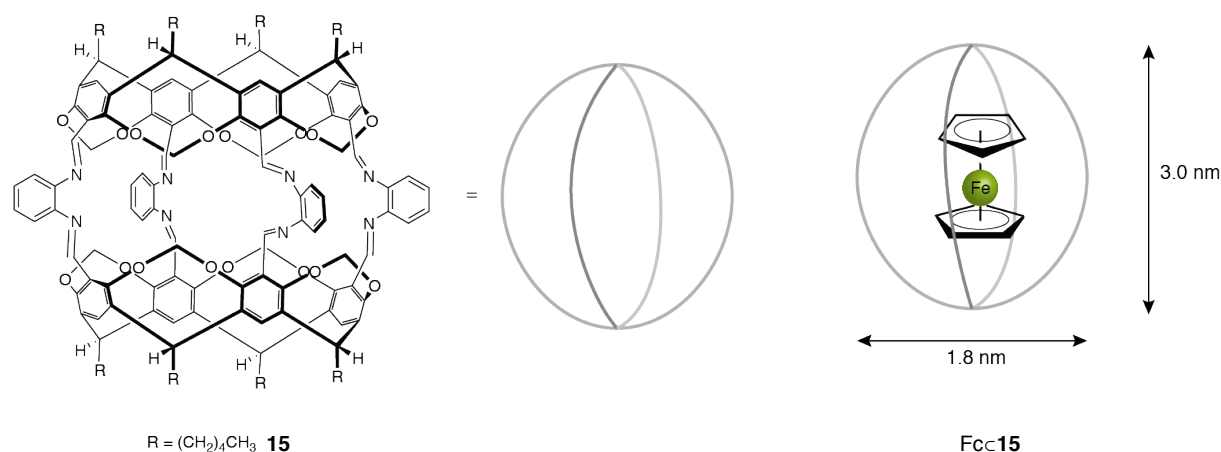
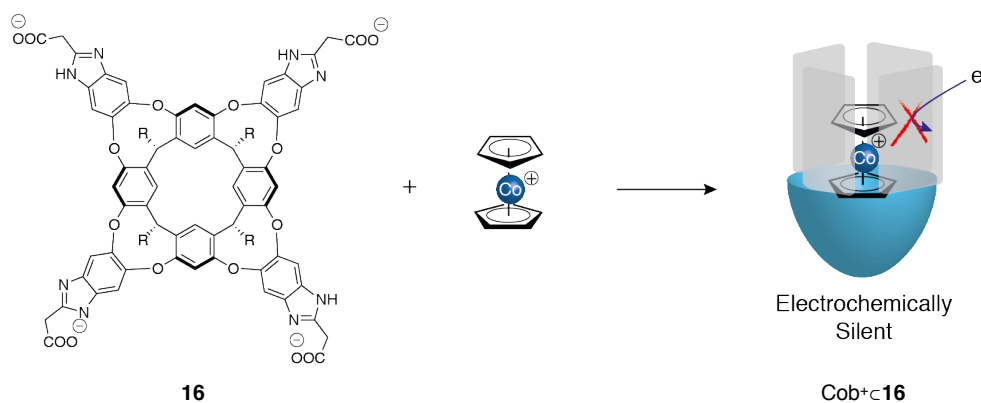


Figure I-4: Structure of the hemicarcerand and metrics of the encapsulated complex.

The use of Rebek's self-folding resorcin[4]arenes **16** was also studied to understand the behavior of Fc and Cob^+ based inclusion complexes. In this case, the encapsulation produced a loss of the electrochemical response of both inclusion complexes (Scheme I-10). $\text{Fc}\subset\mathbf{16}^{29}$ and $\text{Cob}^+\subset\mathbf{16}^{30}$ were electrochemically silent.

²⁹ D. Podkosielnny, I. Philip, C. L. D. Gibb, B. C. Gibb, A. E. Kaifer, *Chem. Eur. J.* **2008**, *14*, 4704 - 4710

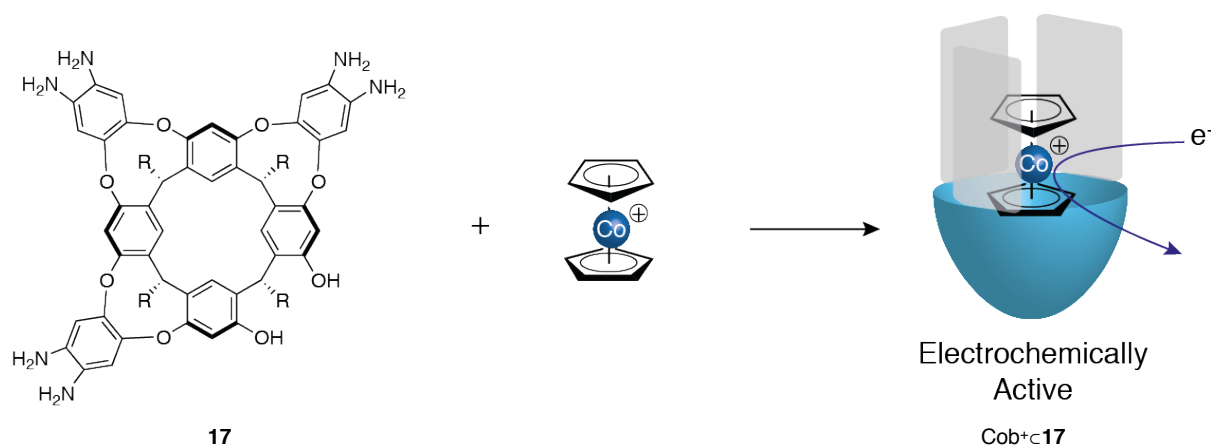
³⁰ D. Podkosielnny, R. J. Hooley, J. Rebek, A. E. Kaifer, *Org. Lett.* **2008**, *10*, 2865 - 2868



Scheme I-10: Formation of the electrochemically silent inclusion complex $\text{Cob}^+\text{c16}$.

A report of a structurally related resorcin[4]arene cavitand **17** was done by Ballester and Sarmentero.³¹ In their system, the cavitand structure was incomplete as one of the walls was missing, and the metal was only partially confined and exposed to the solvent. Despite the partial confinement of the complex, the association constant is $1.4 \times 10^5 \text{ M}^{-1}$, ten times higher than $\text{Fc}\beta\text{-CD}$ (Scheme I-11). The authors attribute this high association constants to CH- π and cation- π interactions, revealing a high affinity of these self folding cavitands for cationic guests.

Inside this new confining system, the CV of the host-guest complex showed a loss of 50% of the intensity of the signal, and a shift of the reduction of $\text{Co}^{\text{III}}/\text{Co}^{\text{II}}$ couple from -0.9 V (Cob^+) to -1.1 V ($\text{Fc}\text{c15}$). The reduction of the intensity was proposed to be related to the distance from the electrode.²⁵ The negative shift was proposed to be due to a stabilization of the cationic complex inside the host, that possesses a higher affinity for the charged Cob^+ .



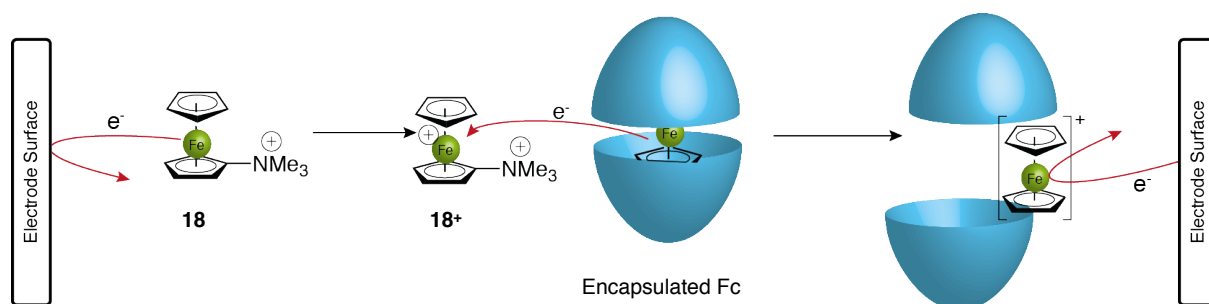
Scheme I-11: Structure of the cavitand and the host-guest complex.

³¹ M. A. Sarmentero, P. Ballester *Org. Biomol. Chem.*, **2007**, *5*, 3046–3054

In conclusion, two effects are observed at this point for the encapsulation. The kinetic constraint on the electron transfer due to the distance of the metal from the electrode produces a reduction of the intensity of the signal observed in CV.³² This reduction can be total, leading to electrochemically silent host-guest complexes.²⁶ The second one is related to the formation of complexes that are more stable than the free one. This stabilization produces changes on the redox potential of the system.

Different families of resorcin[4]arene capsules were studied in the literature.³⁴ In the next example, the authors studied the behavior of the host-guest complex based on dimeric resorcin[4]arene capsules with Fc hosts. CV experiments showed that the host-guest complex is electrochemically silent²⁹. In this work, the use of a mediator to prove that a redox activity inside the guest was studied.³³ When FcNMe₃ **18** is added to the solution and the CV is carried out, one oxidation and two reduction peaks are observed. The oxidation one was attributed to the FcNMe₃/FcNMe₃⁺ couple. The two peaks were found to correspond to FcNMe₃⁺/FcNMe₃ and to the free Fc⁺/Fc reductions.

The observation of the reduction of the free Fc⁺ let the authors state that a mediator can transfer the electrons from the electrode surface to the sterically hindered metal complex. Additionally in this case, the cationic Fc⁺ was not stable inside the dimeric capsule and the assembly was broken to release the guest to the solution. Superimposable CV on continuous scans proved that the assembly-disassembly was made in a reversible way.



Scheme I-12: Proposed mechanism in solution for the redox reactions of this system.

³² W. Ong, A. E. Kaifer, *Organometallics*, **2003**, *22*, 4181 - 4183.

³³ D. Podkoscilny, S. Gadde, A. E. Kaifer, *J. Am. Chem. Soc.*, **2009**, *131*, 12876 - 12877.

In conclusion, encapsulation of redox systems induces an increase of the distance from the electrode surface, translated in a reduction of the response. Nevertheless, this reduction of the signal is not a consequence of an inactive host guest complex.²⁷ The use of partially encapsulated complexes can recover the electrochemical activity.³¹ The effect of the encapsulation was showed to be dependent on the nature of the weak interactions between the metal center and the walls of the cavitand, as well as the size of the confining space. Besides, the addition of the correct mediator allows to transfer the electron from the surface of the electrode and the hindered metal center.

2. Effect of the cavity on covalently linked complexes

Later reports of encapsulated redox centers changed slightly the approach. Inspired by the usual N-coordinating histidines of the enzymes covalently linked metals were used as model systems.²⁴ N-cryptand-modified cavitands were thus used to develop models of the restricted space of the active site of enzymes, usually using copper as model redox center.²⁴

Martinez and coworkers showed that tren-modified hemicryptophanes can coordinate Cu²⁺ complexes with interesting redox properties.³⁴ In their report, the authors showed the same ligand exchange process observed by Reinaud with **14**,²⁴ driven by an electrochemical stimulus. In addition, the authors observed a dependence of the redox potential depending on the topology of the hemicryptophane. Additionally, since no deposit of Cu was observed during the electrochemical experiences, the authors suggest a stabilization afforded by the confinement.

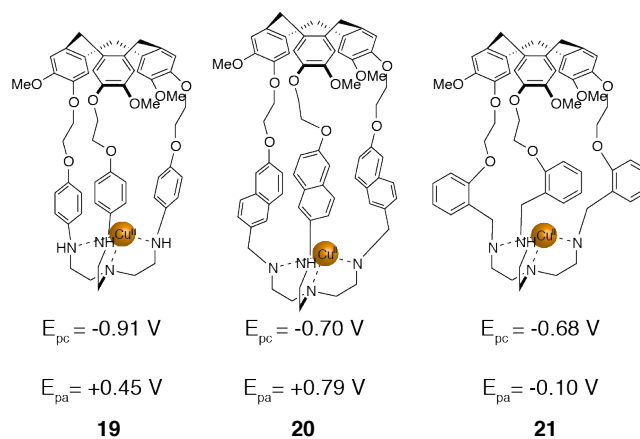
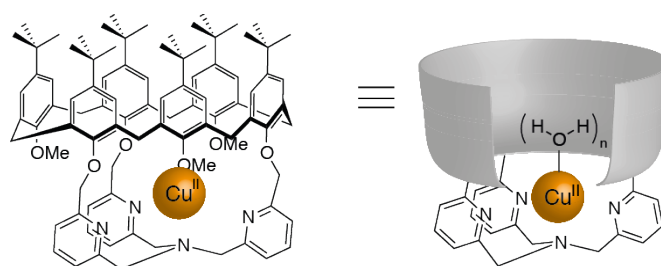


Figure I-5: Structures and redox potentials of the hemicryptophane-tren complexes

³⁴ O. Perraud, J.-B. Tommasino, V. Robert, B. Albeda, L. Khrouz, L. Bonneviot, J.-P. Dutasta, A. Martinez, *Dalton Trans.*, **2013**, 42, 1530-1535

The redox potentials of the Cu center were dependent on the topology of the cage varying from -0.68 V to -0.91 V for the reduction and from 0.1 V to 0.79 V for the reoxidation. This changes on the redox potentials, depending on the structures of the molecular cavitand, suggest a dependence on the topology of the confined space, and the size of the pocket. Nevertheless, the authors did not explained this effect (Figure I-5).

Recently, Le Mest and Reinaud described the electrochemical behavior of monocopper calix[6]arene(tmpa)³⁵ **22** (tmpa = tris(2-aminomethylpyridyl)amine). Mimicking the confined space of an active site of an enzyme, the authors were interested in the effect of the water molecules inside the cavity of the calixarene.



22

Figure I-6: Studied calix[6]arene(tmpa) and its schematic representation.

On the CV voltammogram of [calix[6]tmpaCu(H₂O)₁]⁺ under anhydrous conditions, the authors observed an irreversible reduction peak for the Cu^{II}/Cu^I couple at -0.20 V, and a irreversible oxidation peak at +0.75 V. Addition of controlled amounts of water (14 and 56 equivalents) lead to a shift of the oxidation peak at +0.25 V and 0.13 V. Due to the dependence of the redox potential on the amount of water, the authors proposed that small clusters of water molecules inside the cavity must be involved on the electrochemical properties.

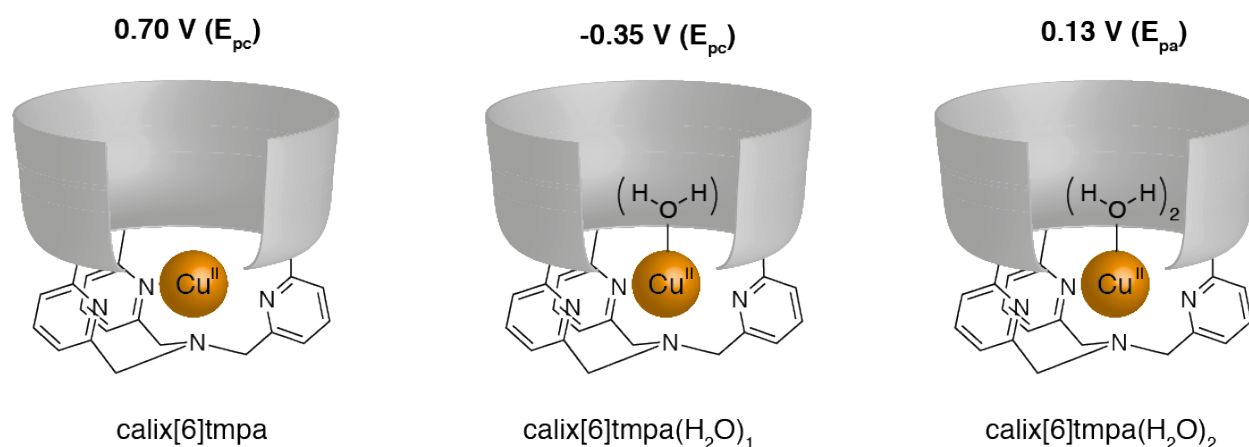
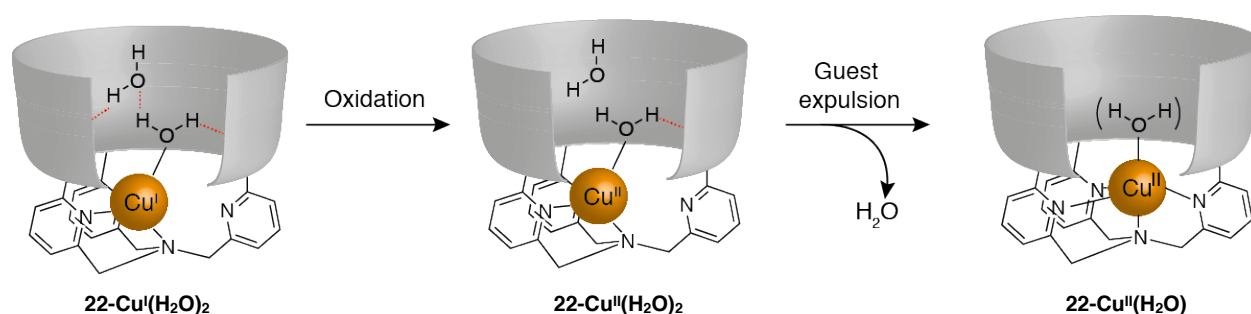


Figure I-7: Structures of **22** aqua complexes.

³⁵ N. Le Poul, B. Colasson, G. Thiabaud, D. J. Dit Fouque, C. Iacobucci, A. Memboeuf, B. Douziech, J. Rezac, T. Prange, A. de la Lande, O. Reinaud, Y. Le Mest *Chem. Sci.*, **2018**, Advance Article, DOI: 10.1039/c8sc03124j

In the report, the authors explain that the structural synergy between the conformation of the cavity and the coordination geometries of the Cu in different oxidation states are involved in the redox potentials. The Cu^I complex, coordinated to only three ligands of the tmpa³⁶ and one water molecule (**22**-Cu^I(H₂O)₂), favors a geometry where a network of H-bonding can stabilize a second water molecule inside the cavity. This geometry establish one H-bond between the two water molecules and the water molecules and the OMe groups of the calixarene. When the complex is oxidized, the Cu^{II} atom (**22**-Cu^{II}(H₂O)₂) is coordinated by the last pyridyl ligand and adopts a TBP geometry. This geometry cannot form the H-bonding with the second water molecule and forces the ejection of the guest (**22**-Cu^{II}(H₂O)).



Scheme I-13: Mechanism of the redox behavior of **22**

In conclusion, the impact of the cavity in the stabilization of a controlled amount of water was shown. In this example, the possibility of stabilization of different ligands by a confined metal, modifying its redox properties was illustrated.

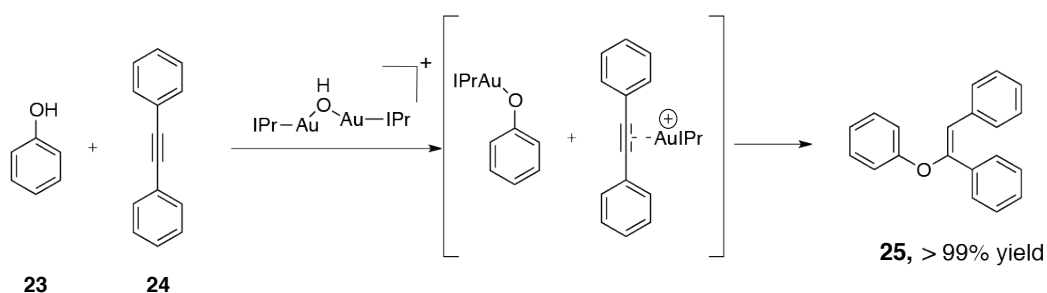
³⁶ L. Bonniard, A. de la Lande, S. Ulmer, J.-P. Piquemal, O. Parisel and H. Gérard, *Catal. Today*, **2011**, 177, 79–86

D. Effect of the confinement of a metal on its catalytic properties

In the following part, the effects of the encapsulation of a metal complex on its reactivity will be shown. The next examples will show how the presence of a restricted, well-defined cavity around a metal center can modify different aspects of the reactivity of a catalytic system.

1. Cavity turning off the reactivity: On-off and product inhibition

Reek and coworkers studied the effect of the encapsulation of a (IPrAu)₂OH catalyst on the reactivity in a hydroxyphenoxilation reaction.³⁷ The characteristic of this reaction is the requirement of two gold centers to activate simultaneously, the phenol and the alkyne (Scheme I-14).³⁸

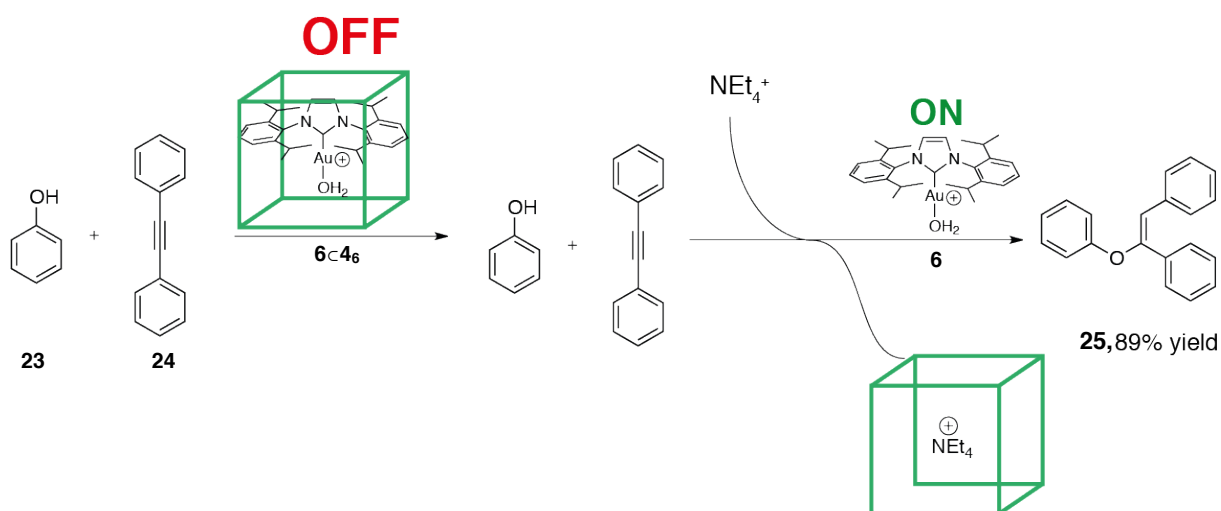


Scheme I-14: Dual activation of phenol and the alkyne.

Using the resorcinarene-assembled cage **4**₆, the authors were able to encapsulate the aqua complex within. Using the encapsulated IPrAu(OH₂)⁺ **6**⊂**4**₆ to catalyze the reaction no reactivity was observed in the formation of **25**. To recover the activity of **6** the authors added NEt₄⁺ salts, a better guest than the complex for the cage. Thus, the encapsulated complex was released from the cage leading to the recovery of the activity of the system. (Scheme I-15)

³⁷ A. C. H. Jans, A. Gómez-Suárez, S. P. Nolan, J. N. H. Reek, *Chem Eur, J.*, **2016**, *22*, 14836 - 14839

³⁸ P. H. Y. Cheong, P. Morganelli, M. R. Luzung, K. N. Houk, F. D. Toste, *J. Am. Chem. Soc.*, **2008**, *130*, 4517 - 4526

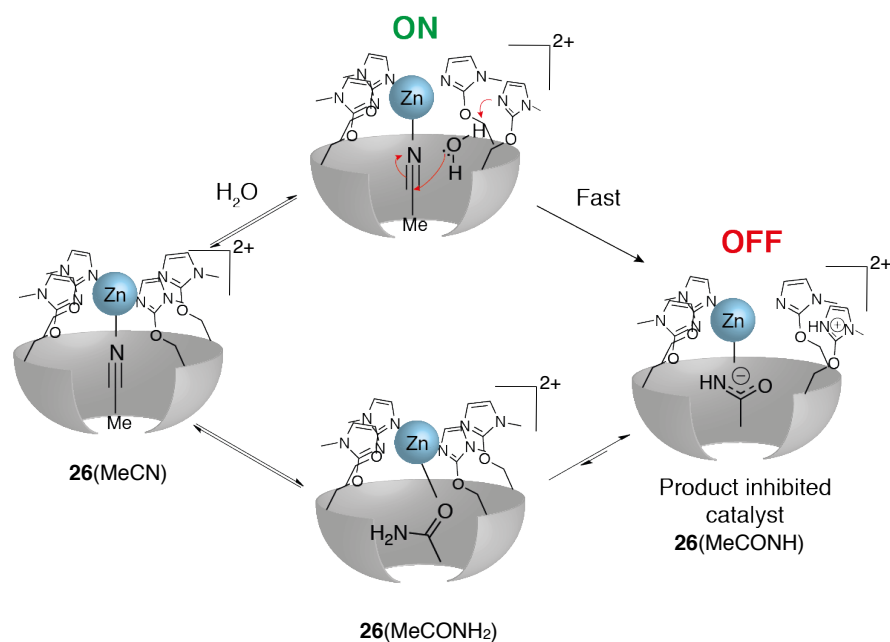


Scheme I-15: Switch of the reactivity of **6c46**

Studying the Zn catalyzed hydrolysis of MeCN inside a tetraimidazole substituted resorcinarene **26**(MeCN), Reinaud and coworkers observed a strong product inhibition of the catalytic site of the complex.³⁹ In their system, to allow the hydrolysis reaction, a simultaneous coordination of the MeCN and a water molecule is required. At the same time, the non-coordinated arm of the cavitand assisted the acid-base reaction and the nucleophilic attack to the *endo*-bounded MeCN. The resulting acetamide must be displaced by the MeCN to start again the catalytic cycle (Scheme).

During the study of the kinetics of the reaction, the authors observed a burst effect at the beginning of the reaction followed by a 5000 fold slowing down the reaction rate. To explain this behavior, the authors showed that the acetamido ligand (**26**(MeCONH)) produces a poisoning of the *endo*-coordination of the complex (OFF). To recover the catalytic activity of the complex, the addition of a high excess of water was required to displace the acetamide from the “catalytic site” (ON).

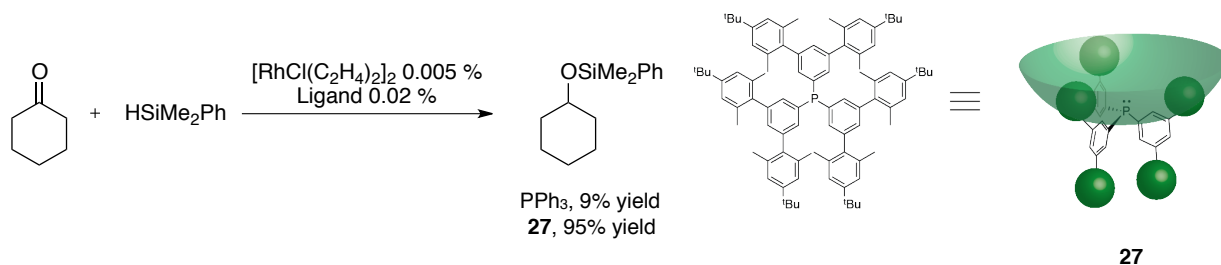
³⁹ A. Parrot, S. Collin, G. Bruylants, O.Reinaud, *Chem. Sci.*, **2018**, 9, 5479 - 5487



Scheme I-16: Proposed mechanism for the hydrolysis of the acetonitrile

2. Controlled environment to reduce deactivation pathways

Increasing the steric bulk around a metal complex can be used to improve the efficiency of some catalytic reactions.² In some cases, increasing the steric hindrance of a traditional ligand can lead to bowl shaped *pseudo-cavitands*.^{40,41} This phosphine bowl-shaped ligand **27** was used in a Rh-catalyzed hydrosilylation of ketones to give yields 10 fold higher than PPh₃.⁴² In their report, the authors rationalized this yield enhancement with by formation of mono-coordinated Rh complexes. These mono-phosphine Rh complexes are more reactive in hydrosilylation reaction. The three-dimensional bowl-shaped ligands avoids the deactivation by di- or tri-phosphine Rh complexes.⁴³



Scheme I-17: Structure of the Bowl-shape phosphine and catalytic application in a Rh-catalyzed hydrosilylation

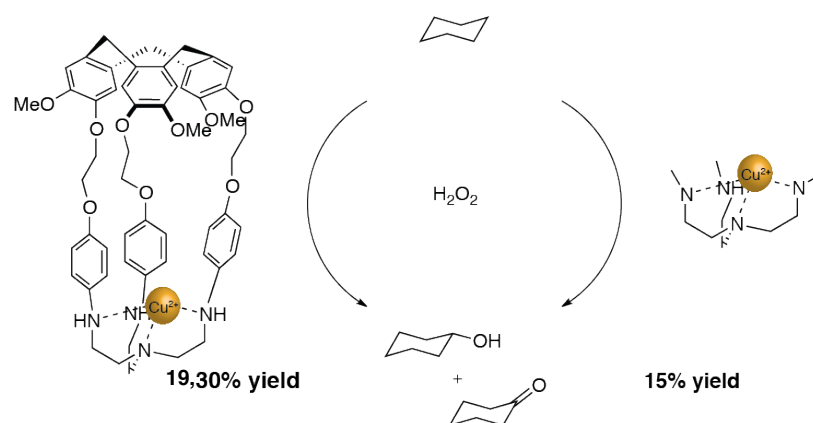
⁴⁰ H. Ohta, M. Tokunaga, Y. Obora, T. Iwai, T. Iwasawa, T. Fujihara, Y. Tsuji, *Org. Lett.*, **2007**, 9, 89 - 92

⁴¹ V. F. Slagt, J. N. H. Reek, P. C. J. Kamer, P. W. N. M. van Leeuwen, *Angew. Chem. Int. Ed.* **2001**, 40, 4271 - 4274

⁴² O. Niyomura, M. Tokunaga, Y. Obora, T. Iwasawa, Y. Tsuji, *Angew. Chem. Int. Ed.* **2003**, 42, 1287 - 1289

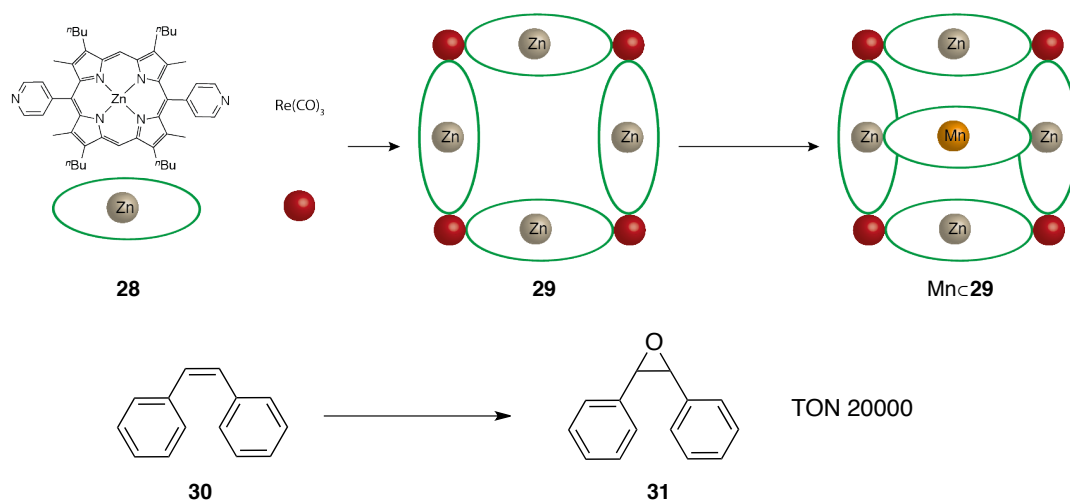
⁴³ H. M. Dickers, R. N. Haszeldine, L. S. Malkin, A. P. Mather, R. V. Parish, *J. Chem. Soc. Dalton Trans.* **1980**, 308 - 313

The synthesis of sterically demanding catalysts was also developed by confinement of transition metals inside molecular cavitands. Martinez groups developed tren-based hemycryptophane-copper complex **19** able to catalyze the oxidation of cycloalkanes with H₂O₂.⁴⁴ The complex **19** allowed the oxidation of cyclohexane in 30% yield. In contrast, when simple Cu(tren)(H₂O) complexes were used, the products were obtained in 15% yield. The authors suggest that the origin of this better performance was the stability of the confined metal, preventing intermolecular oxidative degradation.



Scheme I-18: Oxidation of cyclohexane by **19**

The use of porphyrin assemblies confining catalytically relevant porphyrins was developed by Hupp and coworkers.⁴⁵ In their first report, the authors observed an enhancement of the stability and turnover numbers (TON) in an epoxidation of alkenes catalyzed by Mn_c**29**. The better stability was explained by the blocking of degradative pathways involving the formation of Mn-O-Mn complexes.⁴⁶ This property, increased the stability and TON numbers up to 20000.



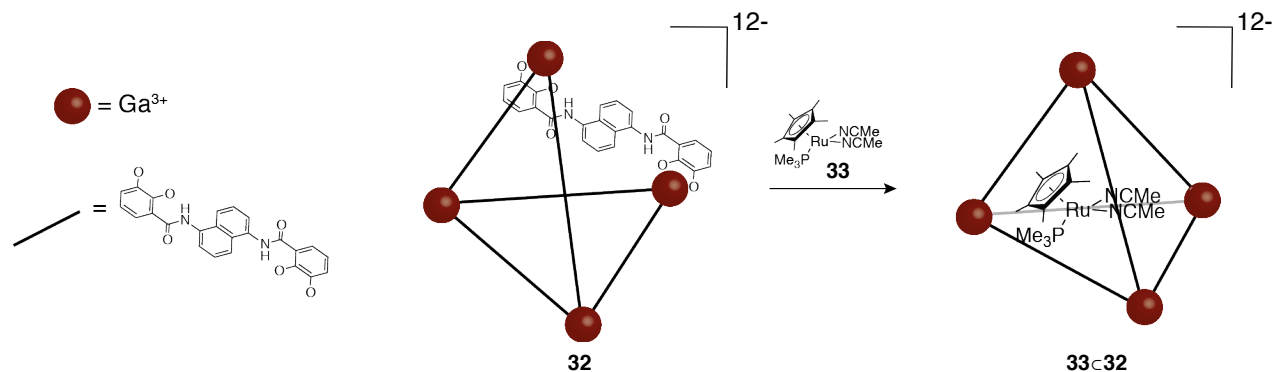
Scheme I-19: Schematic synthesis of the formation of the Mn_c**29** and catalytic application.

⁴⁴ O. Perraud, A. B. Sorokin, J.-P. Dutasta, A. Martinez, *Chem. Commun.*, **2013**, 49, 1288 - 1290

⁴⁵ M. L. Merlau, M. Del P. Mejía, S. T. Nguyen, J. T. Hupp, *Angew. Chem. Int. Ed.* **2001**, 40, 4239 - 4242

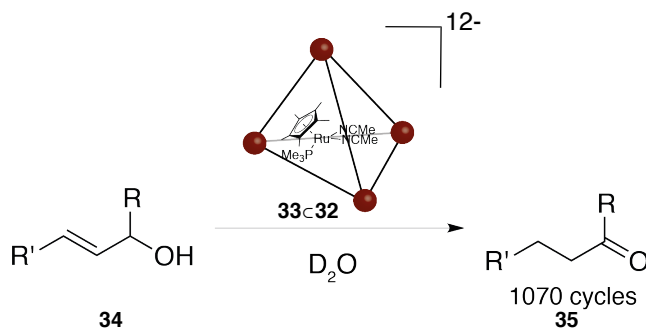
⁴⁶ M. L. Merlau, W. J. Grande, S. T. Nguyen, J. T. Hupp, *J. Mol. Catal. A* **2000**, 156, 79 - 84

In 2011, Raymond and Bergman reported the encapsulation of different transition metal complexes inside a $[\text{Ga}_4\text{L}_6]^{12-}$ supramolecular assembly **32**⁴⁷. In the case of $\text{RuCp}^*(\text{PMe}_3)(\text{MeCN})_2$ **33**,⁴⁸ the full encapsulation of the metal complex was produced with only one equivalent of the cage in D_2O . The complexation inside the assembly increased the lifetime and the solubility of the complex in water by at least an order of magnitude compared to **33**.



Scheme I-20: Structure and encapsulation of the **33c32**

The catalytic activity of the encapsulated complex was studied performing a Ru-catalyzed allyl-alcohol isomerization. Kinetic studies of the reaction showed that when **33c32** was used, a reduction of the turnover frequency from 44 to 16 $\text{M}^{-1} \text{h}^{-1}$ was obtained. In contrast, the turn over number (TON) of the catalyst increased by up to 1070 cycles, higher compared to the same complex in organic solvents. The authors attribute this high TON number to a protection from decomposition by the cage. This TON was the highest reported for a supramolecular catalyst at that time⁴⁹.



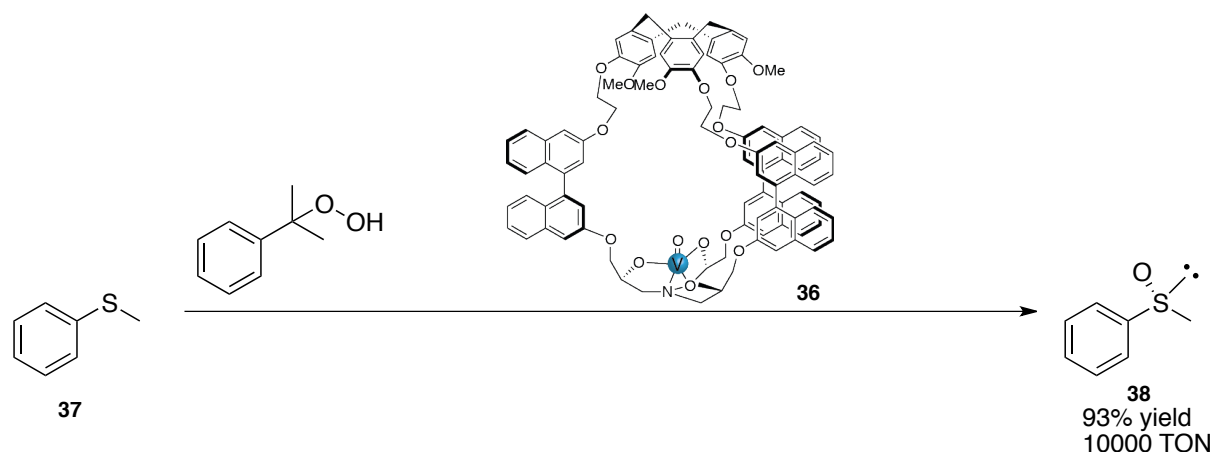
Scheme I-21: Allyl isomerization catalyzed by **33c32**

⁴⁷ D. H. Leung, R. G. Bergman, K. N. Raymond, *J. Am. Chem. Soc.* **2006**, *128*, 9781 - 9797

⁴⁸ C. J. Brown, G. M. Miller, M. W. Johnson, R. G. Bergman, K. N. Raymond, *J. Am. Chem. Soc.* **2011**, *133*, 11964–11966

⁴⁹ C. Slugovc, E. Ruba, R. Schmid, K. Kirchner, *Organometallics* **1999**, *18*, 4230-4233

The use of a confined space to increase the rates of a reaction was also explored by Martinez. Their system is based in an hemicryptophane that confines an oxido-vanadium complex inside a highly hydrophobic pocket.⁵⁰ Taking advantage to the hydrophobicity of the cage, the authors proved that the oxidation of thioanisole could reach turnover numbers of 10000, extremely high for a confining system. Additionally, the rates of the reaction are faster than non-confining oxido-vanadium complexes.⁵¹



Scheme I-22: Oxidation of thioanisole performed by a confined oxido-vanadium complex.

Besides, this catalytic reaction obeys a Michaelis-Menten mechanism, proved by saturation studies. In addition, inhibition by substrates that can fit inside the pocket was proved with NEt_4^+ salts. Thus, the system behaves as an enzyme mimic.

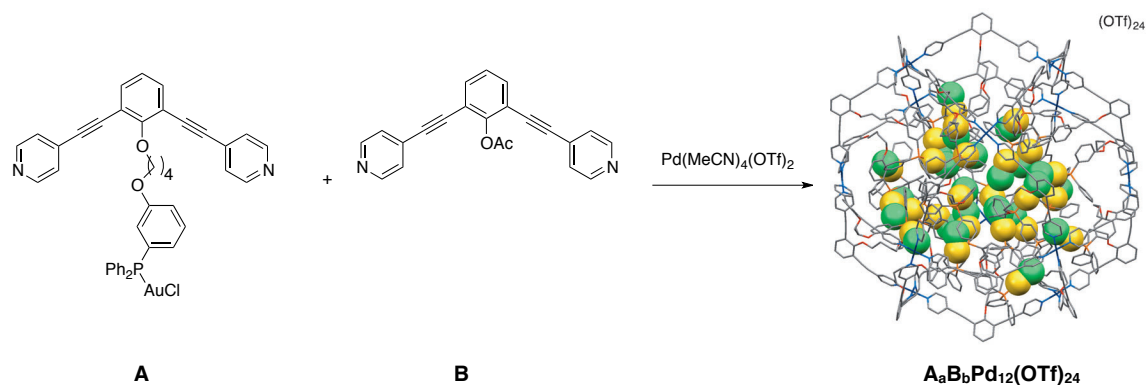
3. Restricted cavities to form more reactive catalysts

The use of a macromolecular assembly to increase the effective concentration of a catalyst inside a confined space was developed by Reek and coworkers.⁵² In their work, the concentration of the catalyst was increased inside a nanosphere, thus, in local spaces of the solution. The overall concentration depends on the A:B ratio of ligands. Thus, in a **A:B** = 18:6, at 5mM of nanosphere in solution, the concentration inside is increased to 0.27M. If the nanosphere is constituted only by A (**A:B** = 24:0) at 5mM the concentration inside is increased to 1.07M.

⁵⁰ D. Zhang, K. Jamieson, L. Guy, G. Gao, J. P. Dutasta, A. Martinez, *Chem. Sci.*, **2017**, 8, 789–794

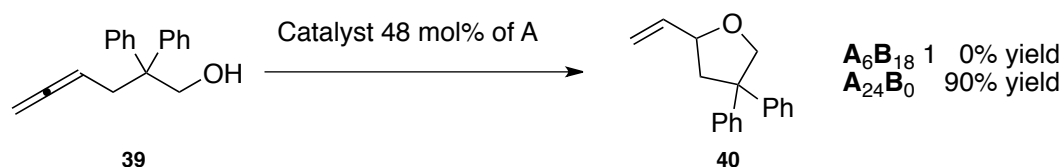
⁵¹ A. Martinez, J. P. Dutasta, *J. Catal.* **2009**, 267, 188 - 192

⁵² R. Gramage-Doria, J. Hessels, S. H. A. M. Leenders, O. Tröppner, M. Dürr, I. Ivanovic-Burmazovic, J. N. H. Reek, *Angew. Chem. Int. Ed.* **2014**, 53, 13380–13384



Scheme I-23: Synthesis of the nano spheres $A_a B_b Pd_{12}(OTf)_{24}$

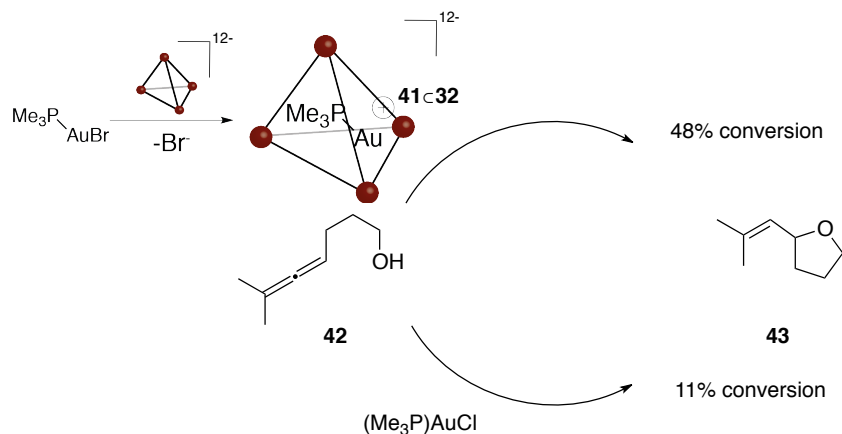
The use of the nanospheres was proved to increase the reactivity in a gold catalyzed hydroxyalkylation of allenes. Using the $A_6 B_{18}$ assembly, **40** was obtained only in 10% yield. In contrast, using the more gold-concentrated $A_{24} B_0$ nanosphere, the yield was significantly improved to 90%. This effect was proved to be related to the concentration of gold in the confined space.



Scheme I-24: Hydroxyalkylation of **39** catalyzed by the nanospheres.

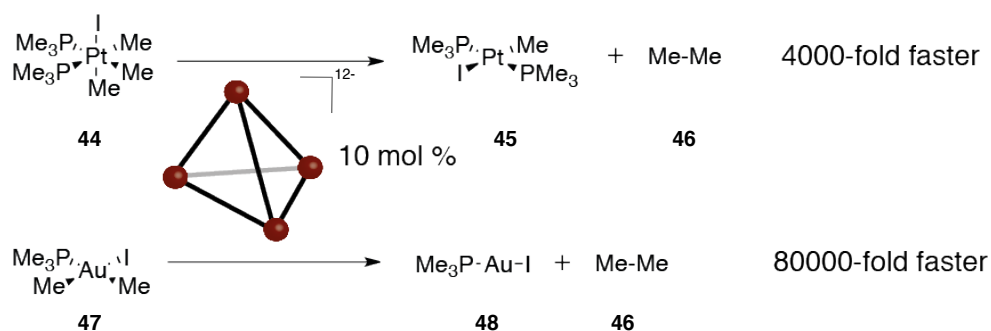
The $[Ga_4 L_6]^{12+}$ supramolecular assembly **32** was showed to be a good encapsulating system for $(Me_3P)AuBr$ complex **41**.⁵³ The use of the confined complex in a gold catalyzed hydroalkoxylation of allenes increases the reactivity, in comparison with the free catalyst. The use of the free complex to catalyze the cyclization of **42** produces a conversion of the starting material with 11% conversion. In contrast, using the confined complex **41**⊂**32**, the conversion was improved up to 48%. Studying the encapsulation of the complex inside the cage, the authors observed a full dissociation of the Br ligand. This dissociation encapsulates produces a more reactive cationic gold complex inside the guest without silver salts.

⁵³ Z. J. Wang, C. J. Brown, R. G. Bergman, K. N. Raymond, and F. D. Toste, *J. Am. Chem. Soc.* **2011**, *133*, 7358–7360



Scheme I-25: Gold-catalyzed hydroxyalkylation of **42**

Using the same supramolecular assembly **32**, Toste and Raymond showed that the encapsulation of high-valent Pt^{IV} **44** and Au^{III} **47** dialkyl complexes reduced the high kinetic barrier of the reductive elimination⁵⁴. The addition of catalytic amounts of the cage produced an increase of the rate of the reductive elimination. In the case of gold, the observed $t_{1/2}$ was reduced from 20 weeks to 53 minutes in the case of gold (4000 fold faster) and in the case of Pt^{IV} , from 45 days to 47 seconds (80000 fold faster). Kinetic studies showed a saturation behavior for both, Au and Pt complexes, consistent with a Michaelis-Menten like mechanism, thus, an enzyme-like kinetics (Scheme I-26).



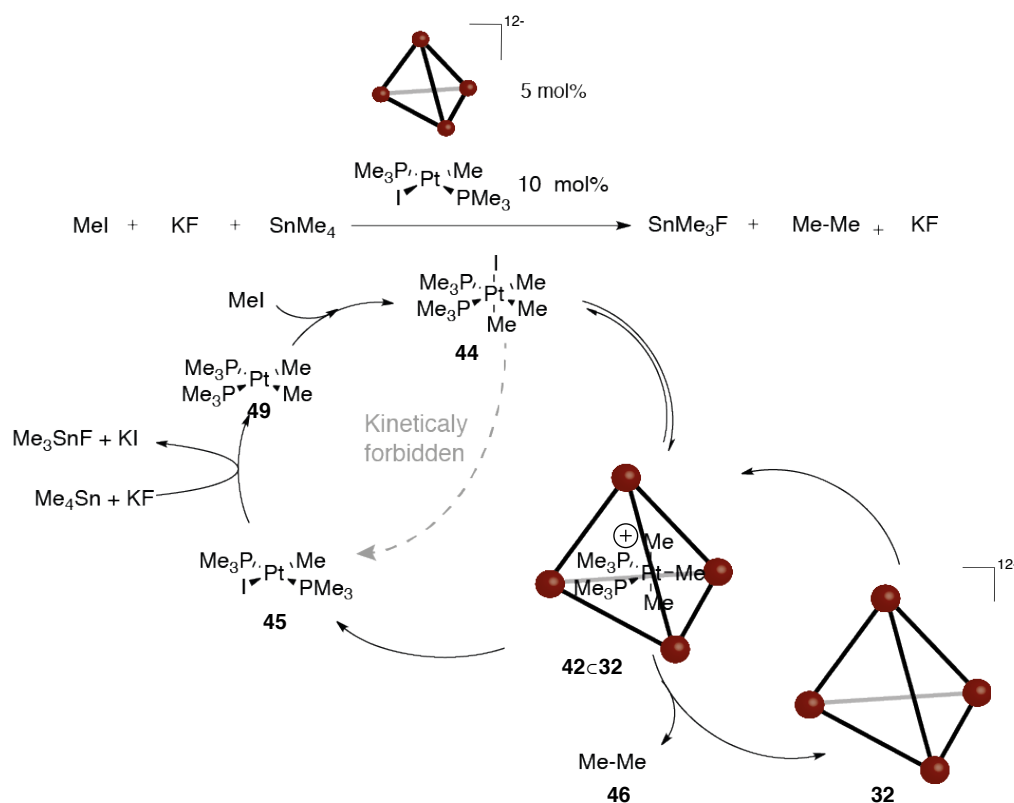
Scheme I-26: Reductive elimination of **44** and **45** catalyzed by **32**

The mechanism and the effect of the cavity is not well understood. The complexation is driven by the hydrophobic microenvironment created inside the cavitand. Further studies of the effects of the cavity on the mechanism suggests that the cage favors the ionization of the metal complex. This cationic metal complex undergoes faster the reductive elimination.⁵⁵

⁵⁴ D. M. Kaphan, M. D. Levin, R. G. Bergman, K. N. Raymond, F. D. Toste, *Science* **2015**, 350, 1235 - 1238

⁵⁵ M. D. Levin, D. M. Kaphan, C. M. Hong, R. G. Bergman, K. N. Raymond, F. D. Toste, *J. Am. Chem. Soc.*, **2016**, 138, 9682 - 9693

In addition, in a proof of concept, the authors took advantage of the assembly to develop a Pt-based dual catalytic cross-coupling reaction,⁵⁴ impossible to perform without the presence of the cage. To do so, starting from **45** the formation of the Pt complex **49** was done by transmetalation with Me_4Sn . This complex can undergo an oxidative addition of MeI to form **44**. **44** can then be encapsulated by the supramolecular assembly **42c32** to perform the reductive elimination and regenerate the catalyst **45**.



Scheme I-26: Reaction and mechanism of the dual catalysis.

4. Confined spaces for selective reactions

In addition to the differences in reactivity in terms of rates and TON explained previously, reactions developed inside a confined space can also vary in terms of selectivity.⁵⁹ The three-dimensional arrangement of the substrates and the catalyst can be structured differently by the effect of the cavity.⁵⁶ This selectivity can be classified in regioselectivity, enantioselectivity, as well as in terms of substrate selection and product distribution.

i. Regioselectivity

Alkyne-hydration of internal alkynes was proved to be a non-selective reaction when the substituents of the triple bond are different.⁵⁷ Nevertheless, the selectivity of this reaction could be improved using a resorcin[4]arene-based ligand. The chemical structure of the cavitand was designed with a ligand close to the cavity and a H-bonding acceptor in the other side of the macrocycle. In addition, the complexed gold center **50** is confined by two quinoxalines. This dual cavitand forced the complexation of the alkyne, favoring the approach of smallest substituents towards the pocket. The hydrogen bonded acceptor forced the intramolecular attack of the water molecule achieving selectivities higher than 91:9.⁵⁸

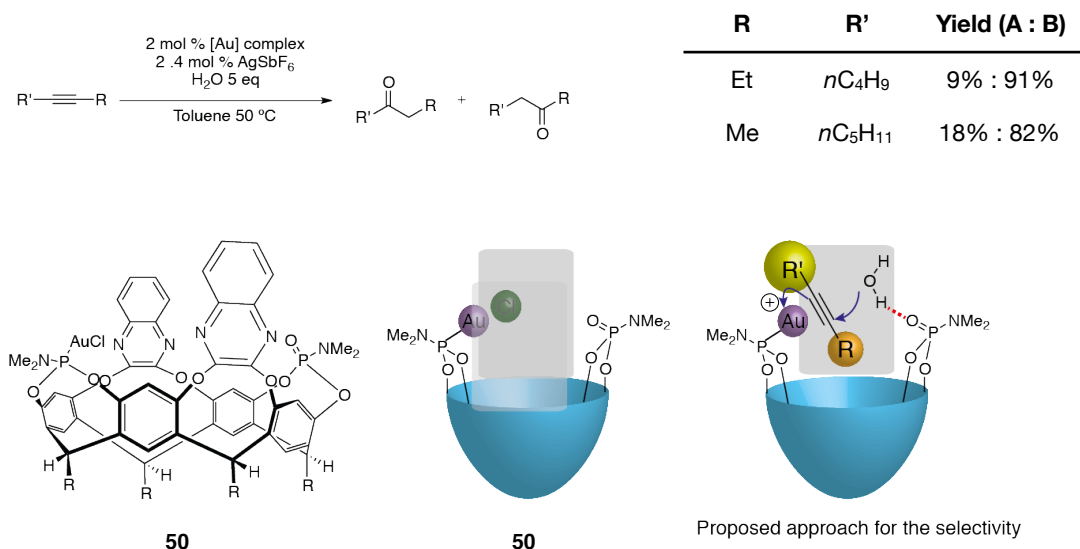


Figure I-7: Regioselective hydration of internal alkynes catalyzed by **50** complex.

In this field, NHC-capped cyclodextrins (ICyD) were efficient catalysts in a regioselective hydroboration of alkynes. The system will be detailed in chapter II.⁵⁹

⁵⁶ P. Zhang, C. Tugny, J. Mejjide Suárez, M. Guitet, E. Dérat, N. Vanthuyne, Y. Zhang, O. Bistri, V. Mourières-Mansuy, M. Ménand, S. Roland, L. Fensterbank, M. Sollogoub *Chem*, **2017**, 3, 174 - 191

⁵⁷ N. Marion, R. S. Ramón, S. P. Nolan, *J. Am. Chem. Soc.*, **2009**, 131, 448–449

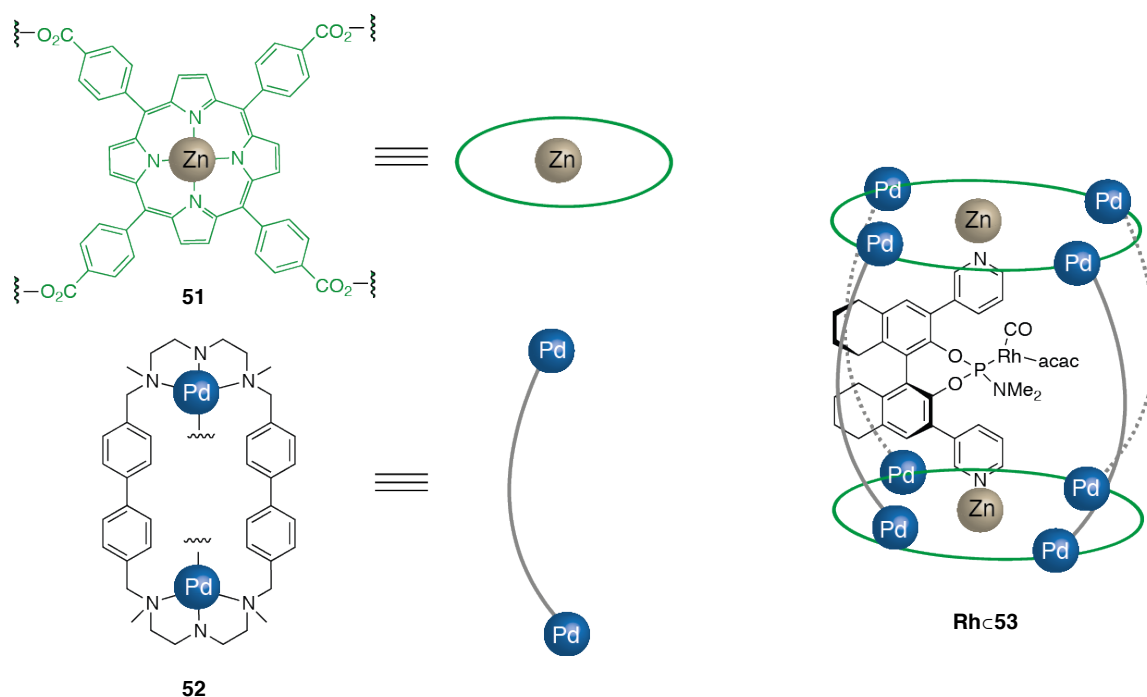
⁵⁸ N. Endo, M. Inoue, T. Iwasawa, *Eur. J. Org. Chem.*, **2018**, 1136 - 1140

⁵⁹ P. Zhang, J. Mejjide Suárez, T. Driant, E. Derat, Y. Zhang, M. Ménand, S. Roland, M. Sollogoub, *Angew. Chem. Int. Ed.* **2017**, 56, 10821–10825

ii. Enantioselectivity

Even if chiral supramolecular entities were largely studied, in most of the cases the metal is just placed close to the chiral moiety.^{60,61} Fully confined metals inside a discrete moiety, for asymmetric transformations remains limited. One of the first reports of fully confined metal inside a cavity to perform an enantioselective reaction was the use of Au-based ICyDs that will also be explained in detail later⁶².

The encapsulation of a chiral complex inside of a nonchiral supramolecular cage was the approach followed by Reek, Ribas and Costas.⁶³ The system was constituted of a Zn-porphyrin **51**, and a palladium ligand **52**. In a 2:1 ratio, the ligands are assembled forming a macromolecular assembly. The apical coordination site of the Zn can complex a BINOL-based Rh complex (**Rh****c****53**) inside the cage.



Scheme I-27: Structure of the macromolecular assembly **Rh****c****53**.

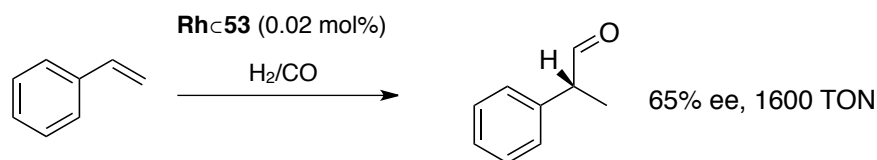
The confined **Rh****c****53** was used in an enantioselective hydroformylation of styrene. The reaction gave high TONs at very low concentration of catalyst (0.02 mol%). The products of the reaction were obtained with enantiomeric excesses up to 74% ee and TONs of 1600. A significant improvement can be observed by comparison with the free Rh-complex that performs the reaction with 7% ee and a TON of 41.

⁶⁰ T. Gadzikwa, R. Bellini, H. L. Dekker, J. N. H. Reek, *J. Am. Chem. Soc.* **2012**, *134*, 2860–2863

⁶¹ M. Jouffroy, R. Gramage-Doria, D. Armspach, D. Sémeril, W. Oberhauser, D. Matt, L. Toupet, *Angew. Chem. Int. Ed.* **2014**, *53*, 3937 - 3940.

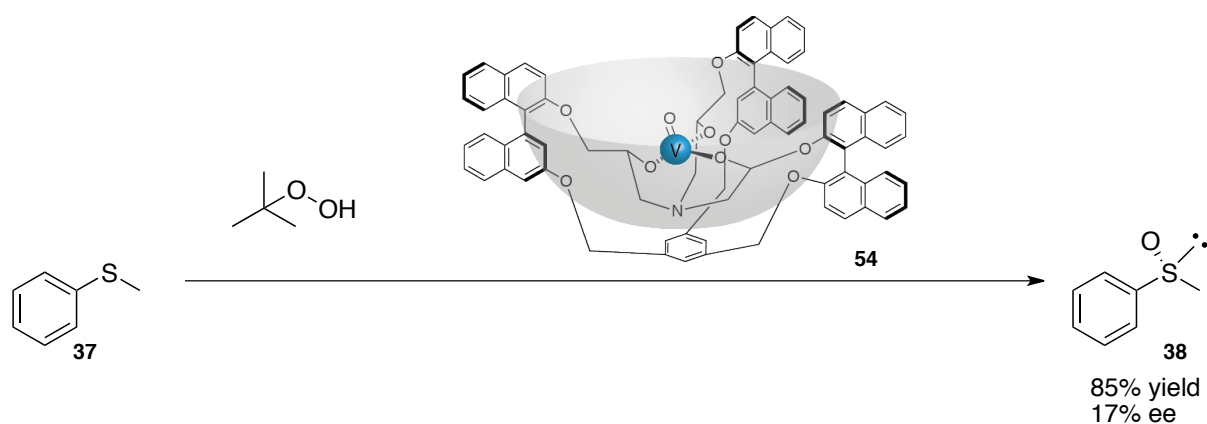
⁶² M. Guitet, P. Zhang, F. Marcelo, C. Tugny, J. Jiménez-Barbero, O. Buriez, C. Amatore, V. Mouriès-Mansuy, JP. Goddard, L. Fensterbank, Y. Zhang, S. Roland, M. Ménand, M. Sollogoub, *Angew. Chem. Int. Ed.* **2013**, *52*, 7213–7218

⁶³ C. García-Simon, R. Gramage-Doria, S. Raoufoghaddam, T. Parella, M. Costas, X. Ribas, J. N. H. Reek *J. Am. Chem. Soc.* **2015**, *137*, 2680–2687



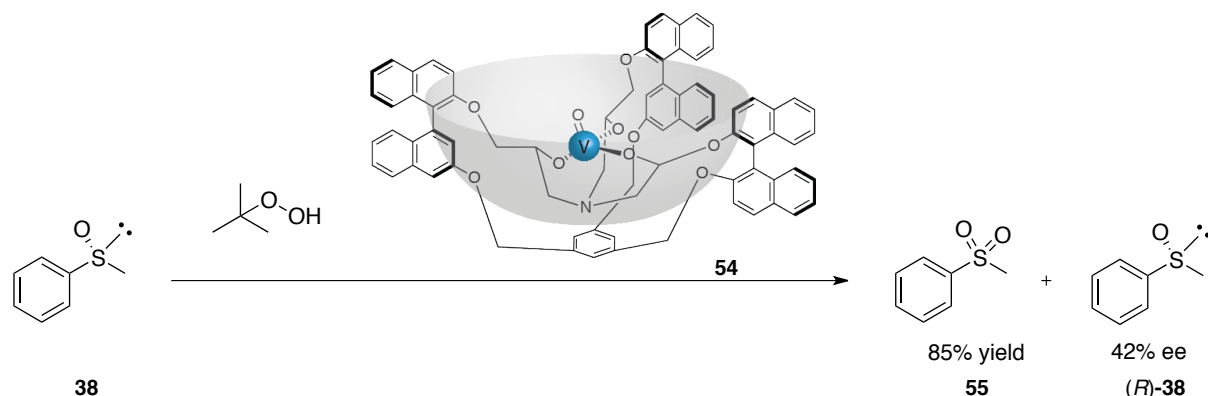
Scheme I-28. Hydroformylation reaction catalyzed by RhC53

Using a bowl-shaped confining chiral vanatrane, Martinez et al showed that confined vanadium inside the hydrophobic pocket **54** could perform the oxidation of thioethers in ee up to 42%.⁶⁴ In their report, the authors showed that the formation of the (*R*)-enantiomer **38** was 1.5 times faster than (*S*)-**38**, obtaining a 18% ee.



Scheme I-29: Enantioselective oxidation of **37** catalyzed by **54**.

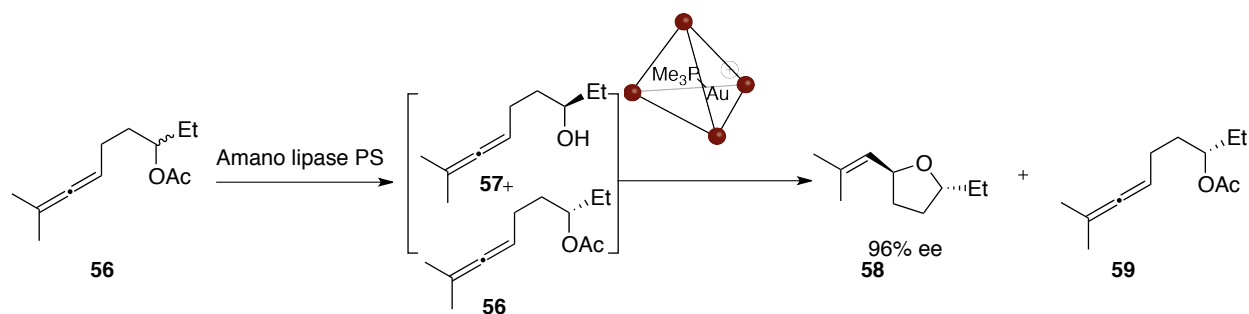
Furthermore, addition of one equivalent of oxidant to the mixture produced the oxidation of the sulfoxide. In contrast, the (*S*) enantiomer reacted faster. Using this kinetic resolution, ee's were improved up to 42% in favor of the (*R*) enantiomer.



Scheme I-30: Kinetic resolution catalyzed by **54**

⁶⁴ D. Zhang, J.-P. Dutasta, V. Dufaud, L. Guy, A. Martinez, *ACS Catal.* **2017**, 7,7340-7345.

An enantioselective reaction can also be obtained by coupling enzyme catalysis with transition metal catalysis. Nevertheless, direct interactions of the metal with the active enzyme must be avoided.⁶⁵ To perform an enzymatic gold catalyzed tandem reaction, the authors used the encapsulated **41** in the supramolecular cage **32**.⁶⁶ In this system, an esterase-mediated kinetic resolution could be coupled to a gold-catalyzed hydroxycyclization affording **58** with enantiomeric excesses up to 96%.

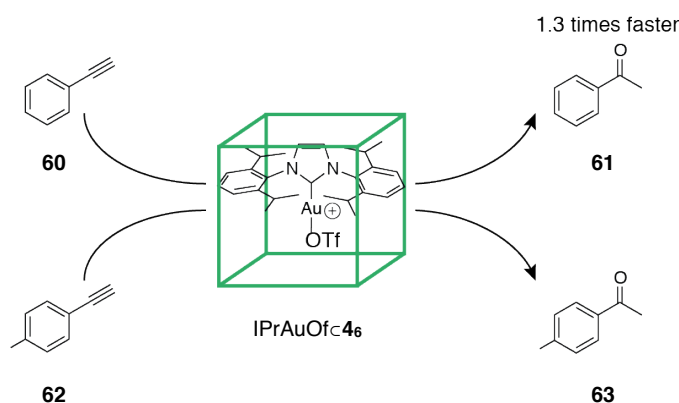


Scheme I-31: Confined gold catalysis coupled to a tandem enzyme catalysis

iii. Substrate selection

As showed previously, metal encapsulation can produce a deactivation of the catalytic system.³⁷ Nevertheless, a controlled and well-defined steric hindrance around the metal center can produce a selective deactivation of the catalyst towards substrates that differs only by their size.⁶⁷ Developing size-selective reactions, selective transformations of equivalent positions, depending on the differences on the steric hindrance around the reactive sites could be done.⁶⁸

Kinetic studies showed that IPrAuOTf complexes encapsulated inside **46** reacted 1.3 times faster with phenylacetylene **60** than with the slightly bigger *p*-tolylacetylene **62** in a Au-catalyzed hydration of triple bonds.⁶⁹



Scheme I-32: Kinetic substrate selection catalyzed by IPrAuOTf-**46**

⁶⁵ F. G. Mutti, A. Orthaber, J. H. Schrittwieser, J. G. de Vries, R. Pietschnig, W. Kroutil, *Chem. Commun.* **2010**, 46, 8046–8048

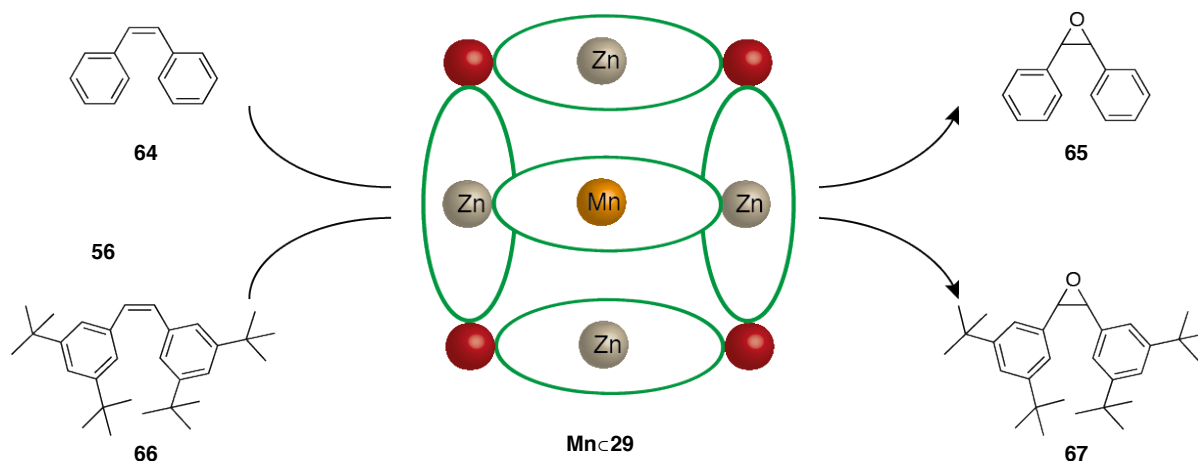
⁶⁶ Z. J. Wang, K. N. Clary, R. G. Bergman, K. N. Raymond, F. D. Toste, *Nat. Chem.* **2013**, 5, 100–103

⁶⁷ M. Otte, *ACS Catal.* **2016**, 6, 6491–6510

⁶⁸ T. Chavagnan, C. Bauder, D. Sémeril, D. Matt, L. Toupet, *Eur. J. Org. Chem.* **2017**, 70–76

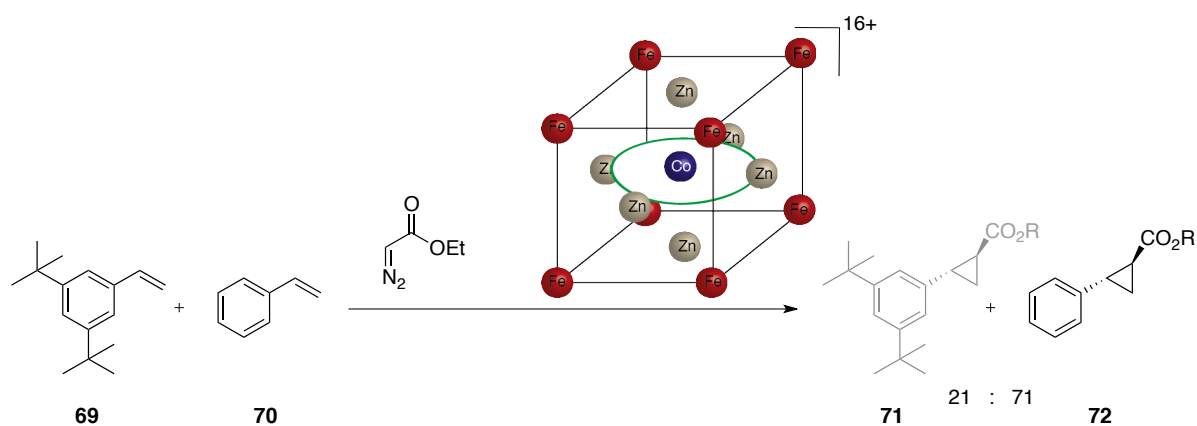
⁶⁹ A. Carvazan, J. N. H. Reek, F. Trentin, A. Scarso, G. Strukul, *Catal. Sci. Technol.*, **2013**, 3, 2898 – 2901

The supramolecular assemblies based on porphyrins were revealed to be substrate selective catalysts.⁷⁰ The coordination of the porphyrin inside the supramolecular assembly Mn@Zn₄ produces the formation of big cavities. The epoxidation reaction of an equimolar mixture of **64** and **66** produced the corresponding epoxides **65:67** in a 65:35 ratio.⁷¹ It is interesting to notice that the use of the big pores to develop substrate selective reactions requires extremely big differences on the sizes of both substrates.



Scheme I-33: Competitive substrate selective reaction catalyzed by the Mn@Zn₄

De Bruin and coworkers also used porphyrin-based supramolecular assemblies to confine a Co-porphyrin and develop a size selective cyclopropanation reaction.⁷² The cubic assembly was able to encapsulate one single Co porphyrin within **68**. This assembly, was an active catalyst in a size-selective and diastereoselective cyclopropanation reaction of alkenes (d.r. = 80 : 20). Additionally, the authors proved that the reaction of a 1:1 mixture of **69** and **70**, the products of the reaction were obtained in a 71:21 ratio in favor of the smallest one **72**.



Scheme I-34: Competitive substrate selective reaction catalyzed by the Fe@Zn₁₆

⁷⁰ P. F. Kuijpers, M. Otte, M. Dürr, I. Ivanovic-Burmazovic, J. N. H. Reek, B. De Bruin, *ACS Catal.* **2016**, *6*, 3106 - 3112

⁷¹ M. L. Merlau, M. Del P. Mejía, S. T. Nguyen, J. T. Hupp, *Angew. Chem. Int. Ed.* **2001**, *40*, 4239 - 4242

⁷² M. Otte, P. F. Kuijpers, O. Troepfner, I. Ivanovic-Burmazovic, J. N. H. Reek, B. de Bruin, *Chem. Eur. J.* **2014**, *20*, 4880 - 4884

The Mn=O-porphyrine **73** was shown to be prefolded in a molecular basket-shape. The control of the coordination modes of this cavitand led the authors to develop size selective reactions.⁷³ In their report, the authors showed that the different coordination modes of the Mn center could be controlled. Besides those coordination modes have different impacts on the reactivity of the complex.

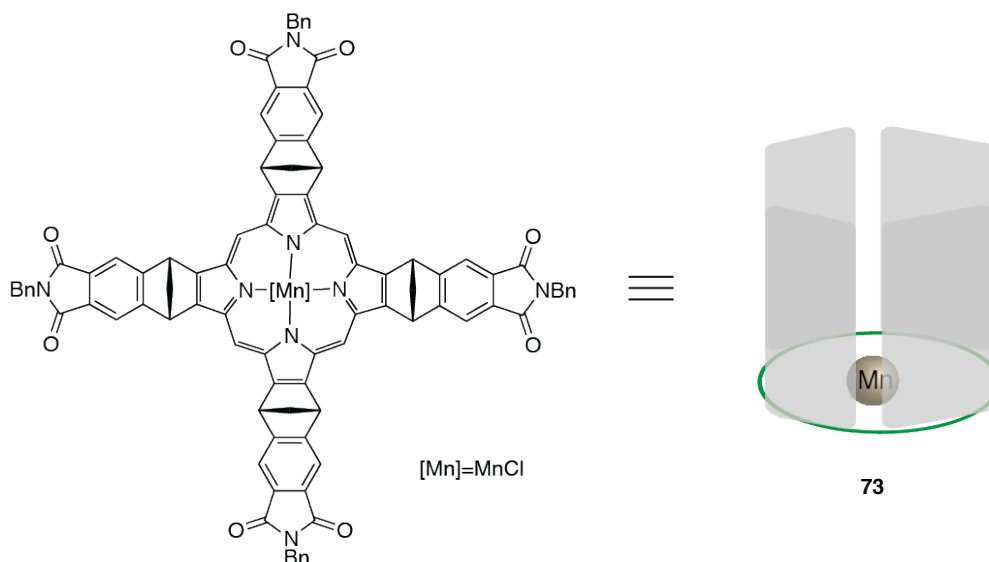
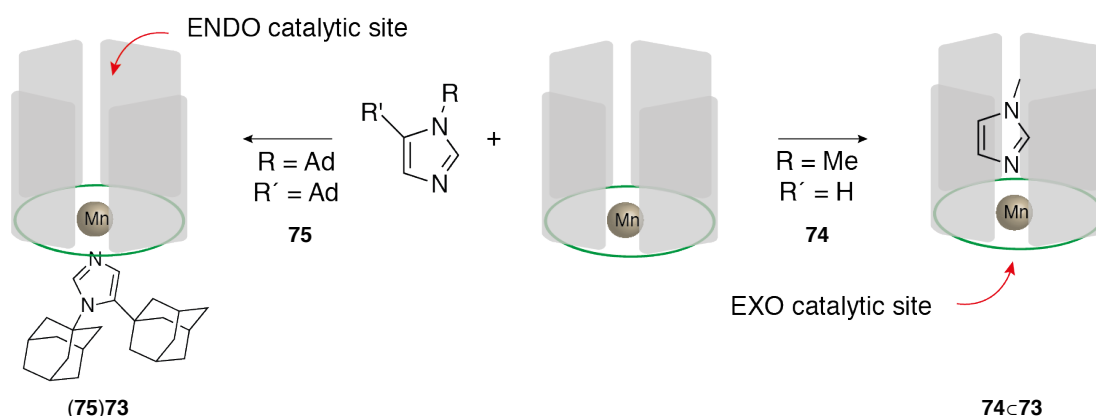


Figure I-8: Studied molecular basket

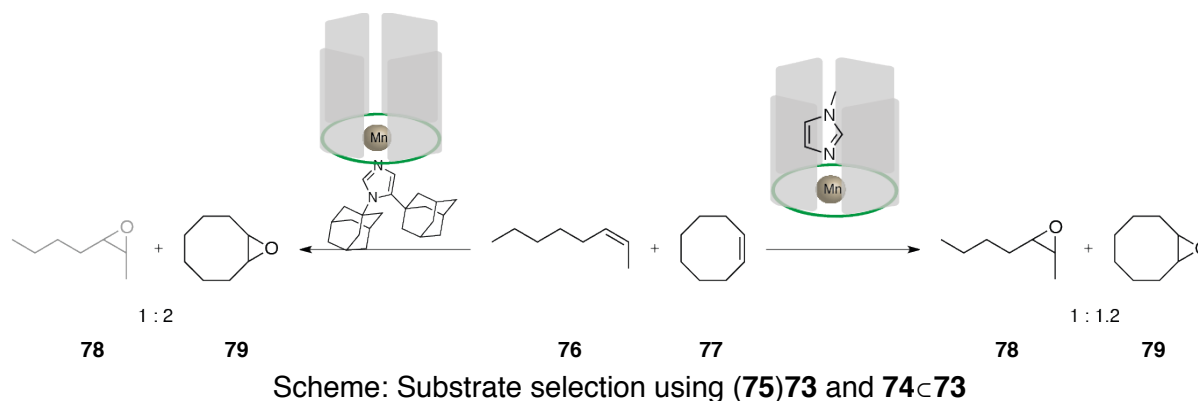
Based on NMR studies, the use of N-methyl imidazole **74** was proved to coordinate the Mn center inside the prefolded cavitand **74**⊂**73**. This inner complexation, let the only possible reactive site outside of the cavity. In contrast, using more hindered imidazole derivatives **75**, the authors proved the outer coordination (**75**)**73**. In this case, free reactive site is found inside the basket.



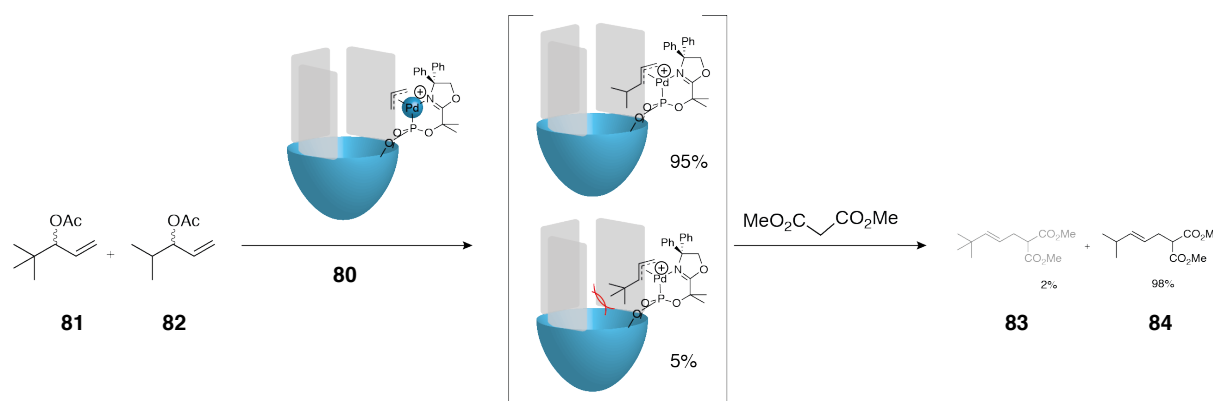
Scheme I-35: Coordination modes of **74**⊂**73** and (**75**)**73**.

⁷³ B.Y. Wang, T. Zudovic, D. A. Turner, C. M. Hadad, J. D. Badjic, *J. Org. Chem.*, **2012**, *77*, 2675 - 2688

The substrate selectivity was showed in an epoxidation of alkenes. The use of exo-free Mn basket **74**c**73** produced the epoxidation of the 1:1 mixture of **76**:**77** in a 1.2 ratio, in favor of the cyclic product **79**. In contrast, using the endo-free basket (**75**)**73**, the selectivity was improved to a 1:2 ratio of **78**:**79** in favor of the smallest one.

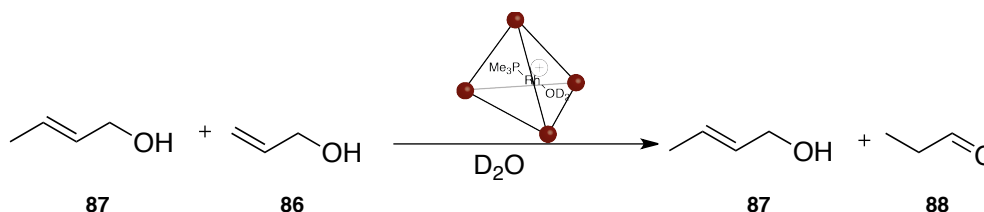


Rebek *et al*⁷⁴ synthesized a resorcinarene-based Pd **80** complex active in Tsuji-Trost reactions. Competition studies in 1 : 1 mixtures of allylic acetates differing on the size of the substituent (**81** and **82**) showed that the smallest ones react faster than bigger ones. In their report, the authors proved by mass spectrometry of the reaction mixtures that the smaller (η^3 -allyl) complexes were formed prior to the bigger ones. The ratios obtained in the mass spectra were preserved in the product distribution at the end of the reaction. The authors used this observation to suggest that the substituent of the allyl is hosted inside the cavity. Remarkably the use of this smaller cavitand, in contrast to the bigger porphyrin assemblies, reaches ratios up to 98:2 in substrates differing by one single carbon **81**:**82**.



⁷⁴ C. Gibson, J. Rebek Jr, *Org. Lett.* **2002**, 4,1887 - 1890.

Raymond and Bergman showed that small phosphine complexes could be encapsulated inside the **32** supramolecular assembly.⁷⁵ The complex $[(\text{PMe}_3)\text{Rh}(\text{D}_2\text{O})]^+$ **85** was an active catalyst in an isomerization of small allyl alcohols.⁷⁶ The reaction of a 1:1 mixture of allyl alcohol **86** and crotyl alcohol **87** catalyzed by **85**⊂**32** takes place only with the smaller one. The quantitative formation of propionic acid **88** and the total recovery of the crotyl alcohol **86** were observed.



Scheme I-38: Substrate selection catalyzed by **85**⊂**32**

iv. Product distribution

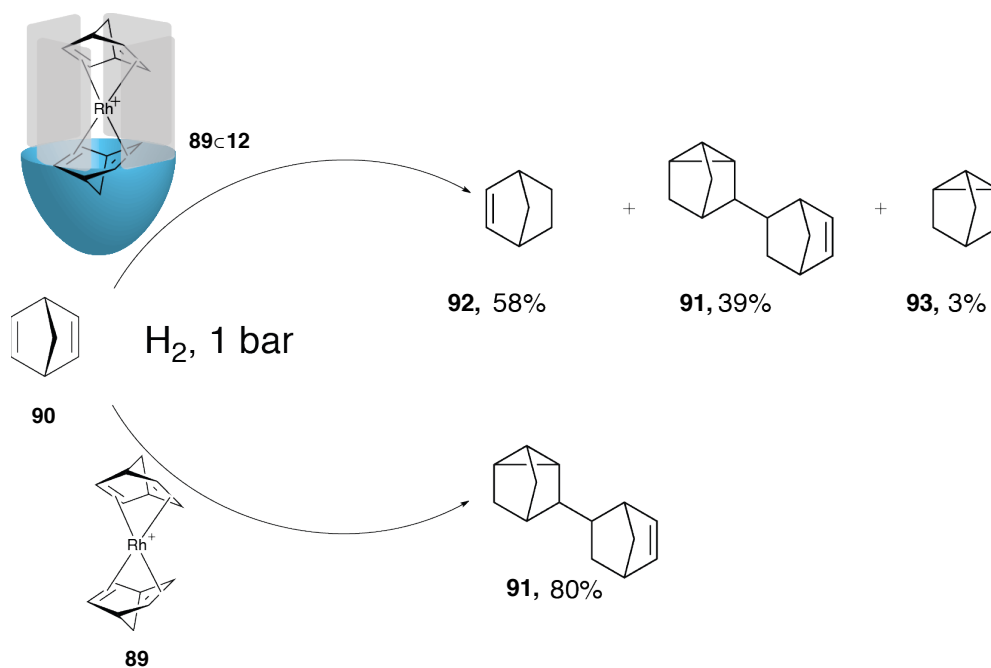
$\text{Rh}(\text{nbd})_2$ complexes encapsulated inside a self folding cavitand **12** showed a reactivity that differs from the one observed for the free $\text{Rh}(\text{nbd})_2$ complex **89**.⁷⁷ The hydrogenation of norbornadiene **90** catalyzed by the free $\text{Rh}(\text{nbd})_2$ complex produced the dimerization of the substrate in more than a 80% of the reaction mixture. In contrast, when the **89**⊂**12** is used as catalyst, norbornene **92** is obtained in 58% of the sample. To justify the product distribution, the authors explained that the confined space of the cavitand blocks the transition state required to dimerize. This example illustrates how the encapsulation can change the reactivity of a catalyst, producing products that are not achieved by the free complex.⁷⁸

⁷⁵ D. H. Leung, D. Fiedler, R. G. Bergman, K. N. Raymond, *Angew. Chem. Int. Ed.* **2004**, *43*, 963 - 966.

⁷⁶ D. H. Leung, R. G. Bergman, K. N. Raymond, *J. Am. Chem. Soc.* **2007**, *129*, 2746 - 2747.

⁷⁷ M. A. Sarmentero, H. Fernández-Pérez, E. Zuidema, C. Bo, A. Vidal-Ferran, P. Ballester *Angew. Chem. Int. Ed.* **2010**, *49*, 7489 - 7492

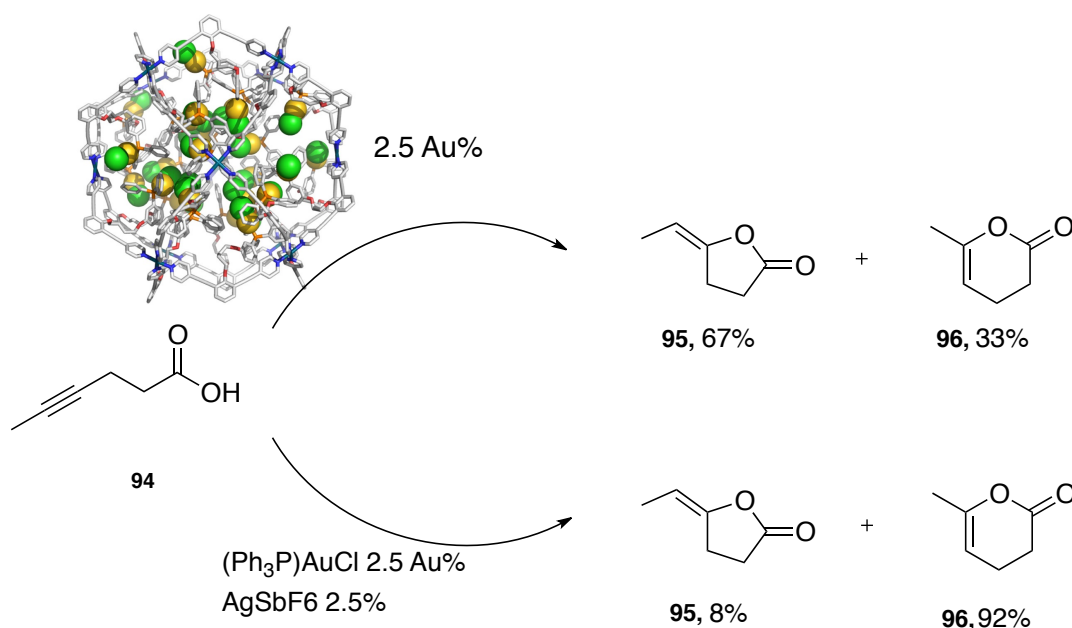
⁷⁸ S. Korom, P. Ballester, *Eur. J. Org. Chem.*, **2014**, 4276 - 4282.



Scheme I-39: Product distribution catalyzed by **89c12**

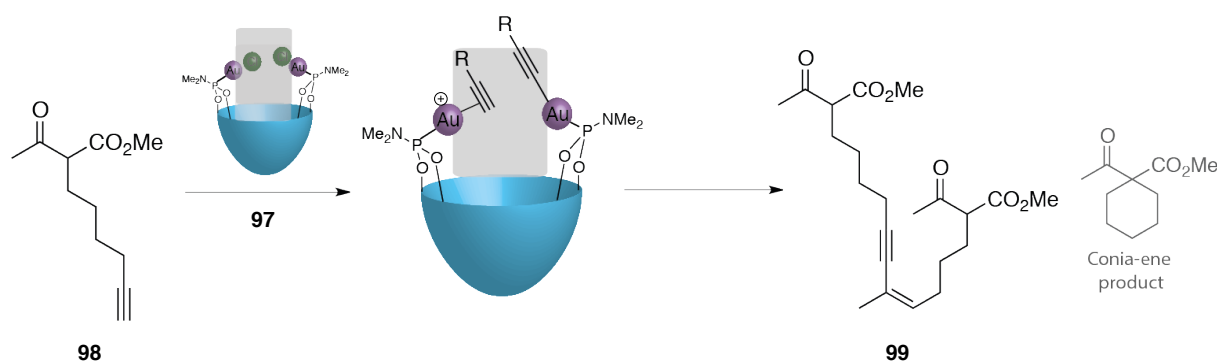
Pt-based supramolecular assembled nanospheres were also used in this field to increase the amount of Au atoms in a confined space.⁷⁹ The use of the (Ph₃P)AuCl to catalyze the lactonization of **94** produces the 6-endo product **96** and the 5-exo product **95** in a 92:8 ratio. In contrast, using the nano spheres to catalyze the cyclization, the ratio is reduced to a 67:33. The authors justified this selectivity by a lower rate of the isomerization of the product of the reaction, afforded by a increased amount of gold atoms inside the nanosphere.

⁷⁹ S. H. A. M. Leenders, M. Dürr, I. Ivanovic-Burmazovic, J. N. H. Reek, *Adv. Synth. Catal.* **2016**, 358, 1509 - 1518.



Scheme I-40: Substrate selection catalyzed by Au confining nanospheres.
Nanosphere obtained from the original paper⁷⁹

The use of gold in confining systems to develop substrate selective reaction was exploited using different shapes of cavities.⁸⁰ A bis-Au resorcinarene **97** was studied in a dual activation of alkynes. The use of the introverted complex **97** to catalyze the Conia-ene reaction⁸¹ afforded the dimeric compound **99** as single product of the reaction. The influence of the cavity is not well understood in the selectivity of the reaction. The authors suggest that the double coordination and the proximity of both substrates could be a key step in the mechanistic pathway. Additionally, this complex was used in a broad scope of substrates, illustrating the efficiency of this system in the dimerization of terminal alkynes.

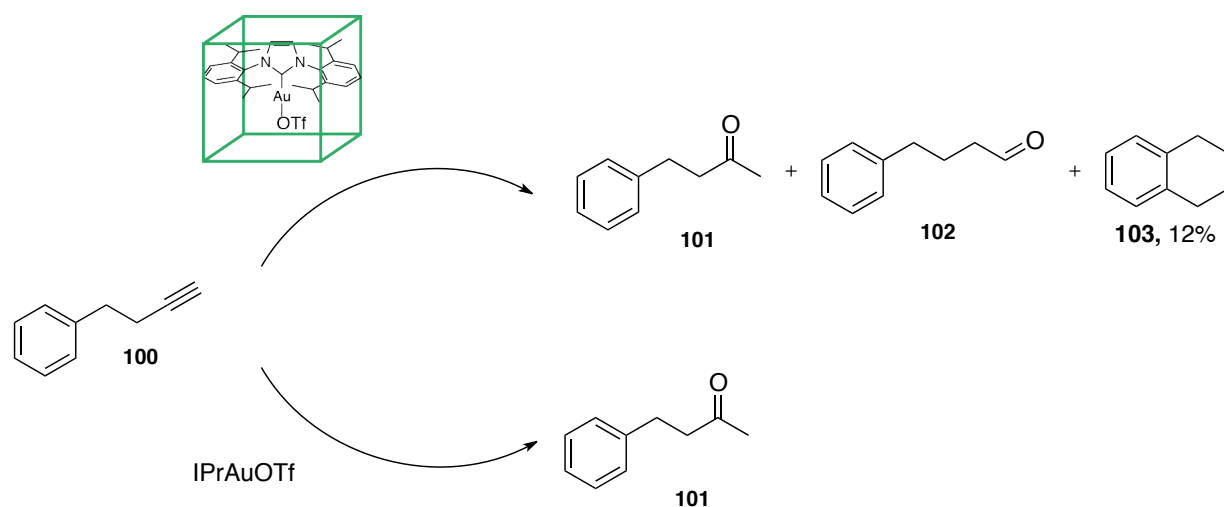


Scheme I-41: Product distribution catalyzed by **97**

⁸⁰ N. Endo, M. Kanaura, M. P. Schramm, T. Iwasawa, *Eur. J. Org. Chem.* **2016**, 2514 - 2521

⁸¹ J. J. Kennedy-Smith, S. T. Staben, F. D. Toste, *J. Am. Chem. Soc.* **2004**, 126, 4526-4527

The use of monomeric Au complexes inside cavitands has a complete different reactivity. Reek and coworkers showed that using IPrAuOTf inside the hexameric cage **4₆**, the distribution of the products is different that the one observed with IPrAuOTf.⁸² The use of the free gold complex produces the exclusive formation of the ketone **101**. In contrast, by using the confined complex, the dihydronaphtalene **103** and the ketone **101** was obtained in a 12% yield each. Additionally, the aldehyde **102** never observed with a gold catalyst was obtained in 4% yield. The origin of this selectivity was suggested to be an unusual folding of the substrate afforded by the nanoenvironment of the cage. Alternatively or additionally, the capsule can also impose a barrier, avoiding the entrance of water inside the cage to form **103**.



Scheme I-42: Observed product distribution with a confined IPrAuOTf complex

Au-ICyDs were also used in a enyne-cycloisomerization reaction showing different product distributions depending on the topology of the catalyst. This studies will be shown in the next chapter.⁵⁹

⁸² A. Carvazan, A. Scarso, P. Sgarbossa, G. Strukul, J. N. H. Reek, *J. Am. Chem. Soc.*, **2011**, *133*, 2848 – 2851.

E. Conclusions and outlook

Through this review, the effect of differently shaped cavities in the properties of an encapsulated metal complex was shown. From a structural point of view, an increased stability could be observed upon encapsulation of reactive species. It was shown that depending on the nature of the cavity and the metal complex, the corresponding confined complexes could have different dynamic behaviors inside the host.

Additionally, the close presence of a cavity around encapsulated redox centers can change their electrochemical properties. Cavity-induced changes of their redox potentials could be result of direct weak interactions with the metal or by different topologies of the cavity. Additionally, the arrangement of ligands inside the cavity can also produce ON/OFF reversible systems. The applications in catalysis were also studied herein.

The impact of different cavity shapes and sizes was studied, and their effects on the development of selective reactions was illustrated. It was showed that regio-, enantioselective, and size selective reactions could be developed using different confining systems. The improvement of a catalytic system by a confining space was highlighted by the increase of rates and yields of a reaction. Besides, the use of cavitands could be also used to add new mechanistic steps to a metal catalyzed transformation. Finally, the possibility of change the products of a reaction was illustrated.

Most of the examples presented here are beautiful proofs of concepts of the possibilities of a confined space. More research is now required to develop useful and applicable systems with a broader scope of applications.

CHAPTER II

Cyclodextrin based metal complexes.
Structures and applications in catalysis

CHAPTER II: Cyclodextrin based metal complexes. Structures and applications in catalysis

Cyclodextrins are a family of natural macrocycles produced by the enzymatic degradation of starch⁸³. The only building block of the structure is glucopyranose. These units are linked in the macrocycle through α -1,4 glycosidic bonds. This precise linking gives the cyclodextrin a well-defined conic structure, where all the primary alcohols of the glucose units are placed on the narrower rim, the primary rim of the cyclodextrin, and all of the secondary alcohols of the cyclodextrin are placed on the wider secondary rim of the macrocycle. (Figure II-1)

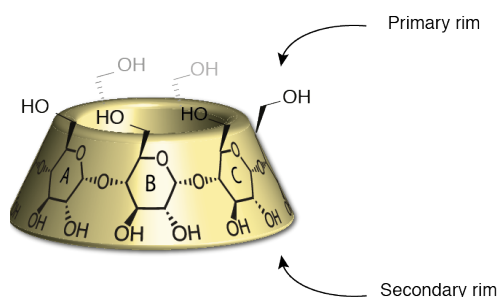


Figure II-1: Three dimensional structure of native α cyclodextrin

A. Nomenclature

Each sugar unit of the macrocycle is labeled with a capital letter starting from the most functionalized one and following the order of the 1,4 glycosidic bond.

On each sugar unit, each carbon is numbered starting from the most oxidized carbon, the anomeric one (Figure II-2).

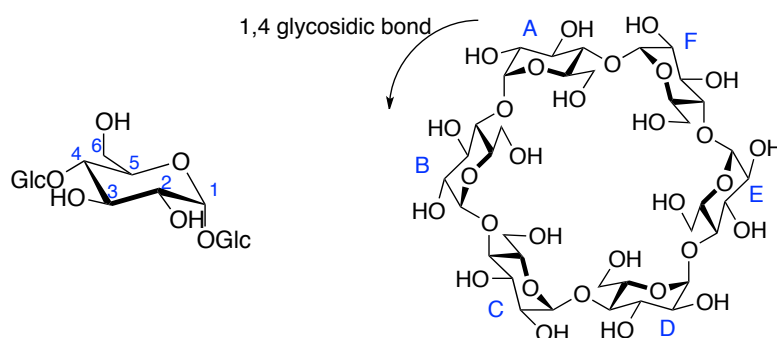


Figure II-2: Nomenclature of cyclodextrins

⁸³ J. Szejtli, *Pure Appl. Chem.* **2004**, *76*, 1825–1845

B. Structure

The three main classes of cyclodextrins are: α cyclodextrin with six glucose units (yellow), β cyclodextrin with seven (blue) and γ with eight (green). Structures and dimension of the three native cyclodextrins are well known⁸⁴. All the cyclodextrins have the same height of 7.9 Å but different width (Figure II-3). Cavity volumes are 174 Å³, 262 Å³ and 472 Å³ for α , β and γ cyclodextrins, respectively.

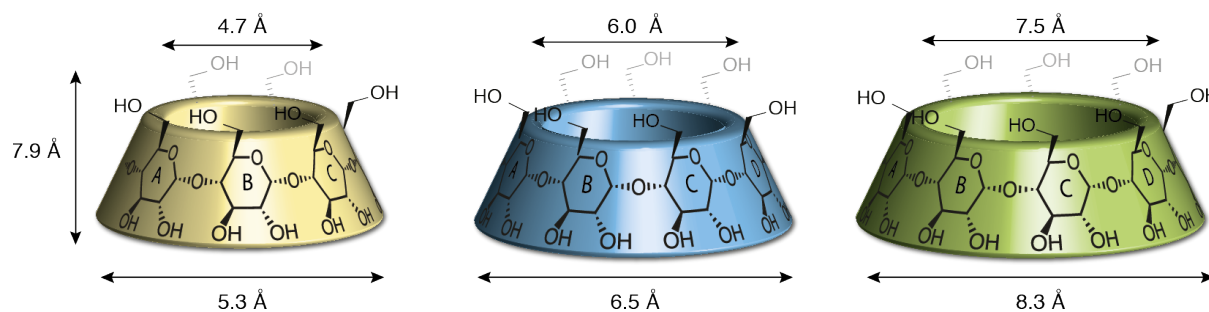


Figure II-3: Dimensions of α , β and γ cyclodextrins.

Due to the rigid ⁴C₁ conformation of each sugar unit, two faces are clearly differentiated. All of the H3 and H5 of the cavitand are pointing towards the inside of the cavity while the rest of the hydrogens of the glucose units are pointing towards the outside (Figure II-4).

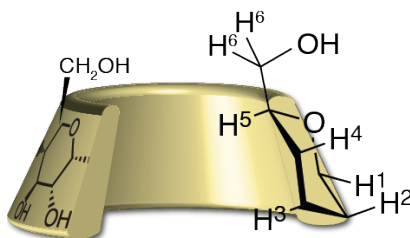


Figure II-4: Hydrogen orientation on conic cyclodextrins

⁸⁴ W. Saenger, J. Jacob, K. Gessler, T. Steiner, D. Hoffmann, H. Sanbe, K. Koizumi, S. M. Smith, T. Takaha *Chem. Rev.* **1998**, *98*, 1787–1802

C. Cyclodextrin-metal complexes

Because of their well-defined and chiral structure, natural origin, water solubility and encapsulation properties,⁸⁵ cyclodextrins were used as skeleton to develop enzyme mimetic systems for more than 40 years.⁸⁶

Since the NMR characterization of the first transition metal-cyclodextrin host-guest complex in solution by Stoddart⁸⁷, the search for metal complexes where the cyclodextrin acts as second coordination sphere started to rise.

In the use of cyclodextrins as second coordination sphere for supramolecular catalysis and metalloenzyme mimicry, two approaches were followed:

1) Formation of a host-guest complex between the cyclodextrin and one or more of the ligands of the organometallic complex (Figure II-5-a). In this case, the cyclodextrin only acts as a second coordination sphere, conferring new properties such as water solubility⁸⁸ or selectivity.

2) Covalent linkage between the cyclodextrin and the metal complex. In this precise situation, the cyclodextrin is part of the first and second coordination sphere. Traditional approaches in this field are still based on a host-guest interaction between the cyclodextrin and the substrate, without any weak interaction with the ligand. These systems will be thus considered as transient second coordination spheres⁸⁹ (Figure II-5-b). In contrast, more recent approaches developed covalent bonding to a metal complex,⁵⁶ where the ligand interacts through well-defined weak interactions with the CD-skeleton⁹⁰ in the precatalytic system, being at the same time, first and second coordination spheres (Figure II-5-c).

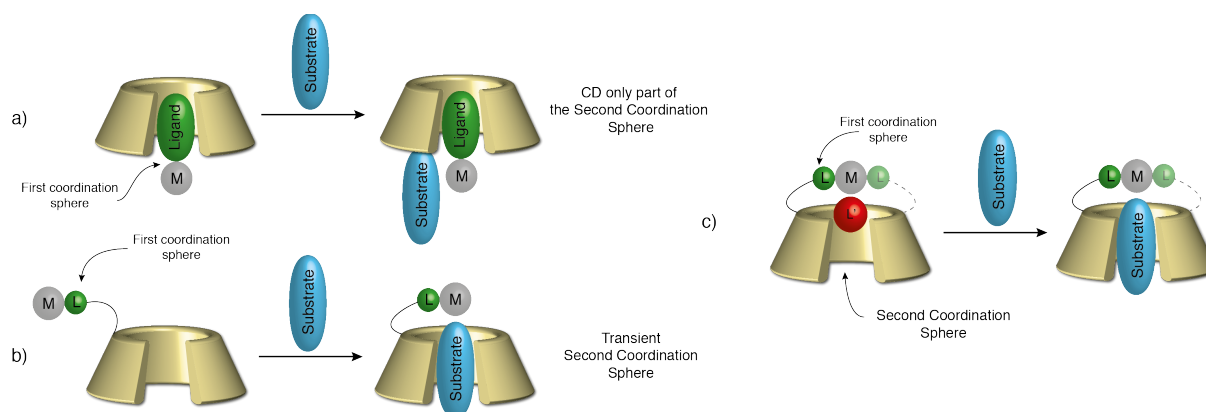


Figure II-5: Catalytic approaches based on the second coordination sphere.

⁸⁵ P. Evenou, J. Rossignol, G. Pembouong, A. Gothland, D. Colesnic, R. Barbeyron, S. Rudiuk, A.-G. Marcelin, M. Ménand, D. Baigl, V. Calvez, L. Bouteiller, M. Sollogoub, *Angew. Chem. Int. Ed. Engl.*, **2018**, *57*, 7753 - 7758

⁸⁶ Cramer, F., G. Mackensen: *Angew. Chem., Int. Ed. Engl.*, **1966**, *5*, 601 - 602

⁸⁷ D. R. Alston, A. M. Z. Slawin, J. F. Stoddart, D. J. Williams, R. Zarzycki, *Angew. Chem. Int. Ed. Engl.* **1988**, *27*, 1184 - 1185.

⁸⁸ F.X. Legrand, M. Ménand, M. Sollogoub, S. Tilloy, E. Monflier, *New J. Chem.*, **2011**, *35*, 2061 - 2065.

⁸⁹ For a review with the same classification: F. Hapiot, S. Tilloy, and E. Monflier *Chem. Rev.* **2006**, *106*, 767 - 781

⁹⁰ E. Engeldinger, D. Armspach, D. Matt, P. G. Jones, R. Welter *Angew. Chem. Int. Ed.* **2002**, *41*, 2593 - 2596

1. CD-metal complexes as second coordination sphere

Thanks to the study of the encapsulation and host-guest chemistry with cyclodextrins,⁸⁷ cyclodextrins were used as encapsulating agents to solubilize one or more partners of a catalytic system (ligand, metal complex or substrate)

Preliminary results showed that cyclodextrins could be used as phase transfer agents to carry an organic substrate to an aqueous phase in a Wacker oxidation of long chain alkenes.⁹¹

One of the early examples where the cyclodextrin acts only as a second coordination sphere was presented by Monflier *et al.* In their work, the authors showed that the phosphane ligand **104** was able to form 1 : 1 host-guest complexes with the permethylated β -cyclodextrin.⁹² These adducts behave as water soluble ligands that, in presence of Pd(OAc)₂, could catalyze the allylic amination of long chain allyl carbamates in a binary phase system.

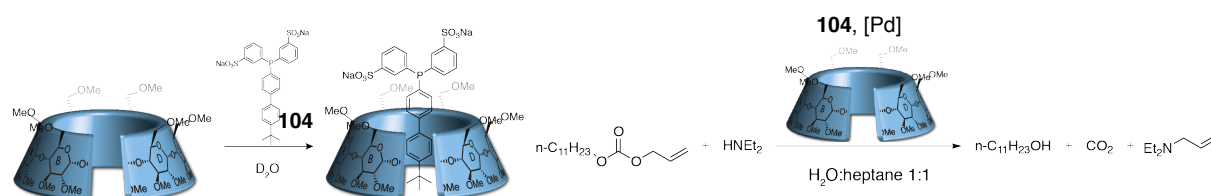


Figure II-6: Two phase system reaction performed with a β -CD-ligand inclusion complex.

Other results of the same group showed that surprisingly, even water soluble phosphines like P(*m*-C₆H₄SO₃Na)₃ (TPPTS) could form host-guest complexes in water with native β -cyclodextrin.⁹³ This result allowed the group to develop a broad scope of systems, based on permethylated cyclodextrin/ligand combinations to improve Rh catalyzed hydroformylation of alkenes.⁹⁴ One of the proposed examples consisted in the cyclodextrin dimer **105**, encapsulating the phosphane ligand **106**.

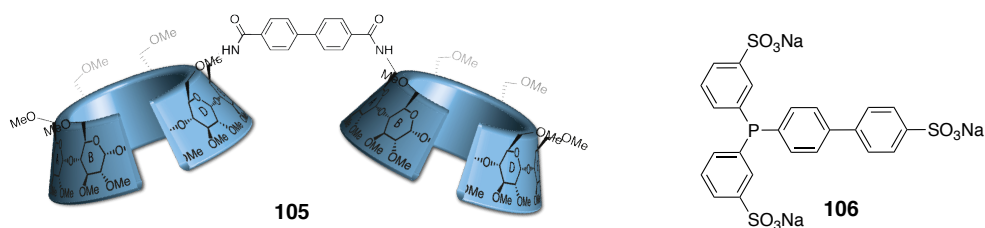


Figure II-7: Structure of the cyclodextrin dimer **105** and ligand **106**

⁹¹ E. Monflier, E. Blouet, Y. Barbaux, and A. Mortreux, *Angew. Chem. Int. Ed. Engl.*, **1994**, *33*, 2100-2102

⁹² L. Caron, H. Bricout, S. Tilloy, A. Ponchel, D. Landy, S. Fourmentin, E. Monflier, *Adv. Synth. Catal.* **2004**, *346*, 1449–1456

⁹³ E. Monflier, S. Tilloy, C. Méliet, A. Mortreux, S. Fourmentin, D. Landy, G. Surpateanu *New J. Chem.*, **1999**, *23*, 469 - 472

⁹⁴ C. Blaszkiewicz, H. Bricout, E. Leonard, C. Len, D. Landy, C. Cezard, F. Djedaïni-Pilard, E. Monflier, S. Tilloy, *Chem. Commun.*, **2013**, *49*, 6989 - 6991

In the tested conditions, this dimeric platform, performed the reaction with better conversions and TON than the water Rh-TPPTS complex or other traditional cyclodextrin based hydroformylation systems⁹⁵ (Table II-1). The simultaneous encapsulation of the catalyst and the substrate was used as an explanation for the better performance of this system.

Catalyst	Conversion	Aldehyde selectivity	Ratio L/B
Rh(TPPTS) ₂ (cod)	5 %	65 %	2.7
Rh(104)(105)	99 %	94 %	2.1

Table II-1: Hydroformylation reaction in presence and absence of the CD dimer **105**.

These two examples showed how through a simple host-guest encapsulation, a given catalytic system can be improved in terms of selectivity or water solubility. What can happen if the complexity of the system is increased to a well-defined covalent cyclodextrin-ligand complexed to a metal center?

2. CD-metal complexes as first and transient second coordination sphere

A well-defined structure of a cyclodextrin covalently linked to the ligand can have other properties than water solubility of a metal complex and phase transfer. The very first reported covalent system of a CD-ligand was developed by Cramer in 1966 where a imidazol-substituted α -cyclodextrin catalyzed the hydrolysis of aromatic esters in water 2000 fold faster through a acid-base catalyzed reaction.⁸⁶

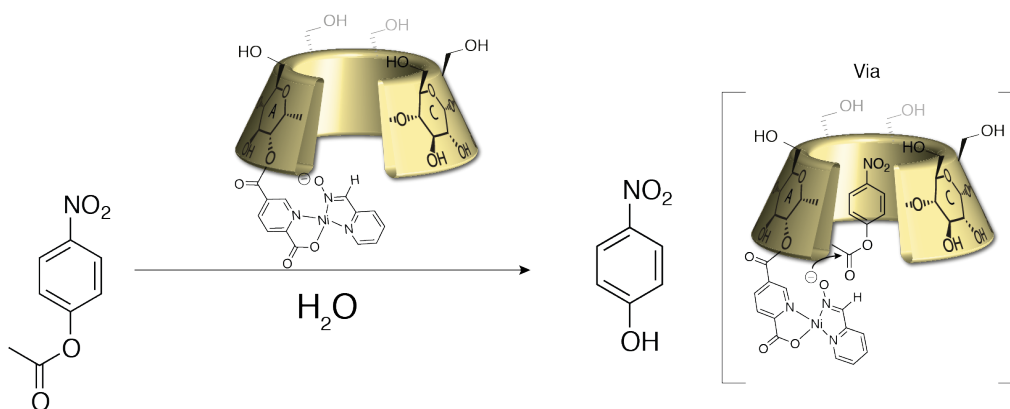
Four years after Cramer, Breslow and coworkers reported the first cyclodextrin-based metal complex able to enhance a catalytic activity.^{96,97} In this early example, the authors synthesized a chemically functionalized cyclodextrin by a pyridyl ligand on the secondary rim. This pyridine ligand could form catalytically active Ni²⁺ complexes able to catalyze efficiently the hydrolysis of aromatic acetates.

In their system, supported by binding constants between the *p*-nitrophenyl acetate and the metal complex as well as competition studies, the authors proved an enhancement of the hydrolysis rate of almost 3000 times over the non-catalyzed reaction. In their report, the authors proposed that this enhancement of rate is a result of the binding of the substrate with the catalyst thanks to the hydrophobic effect (Scheme II-1).

⁹⁵ F. Hapiot, L. Leclercq, N. Azaroual, S. Fourmentin, S. Tilloy, E. Monflier, *Curr. Org. Synth.*, **2008**, *5*, 162 - 172

⁹⁶ R. Breslow, L. E. Overmann, *J. Am. Chem. Soc.* **1970**, *92*, 1075 - 1077

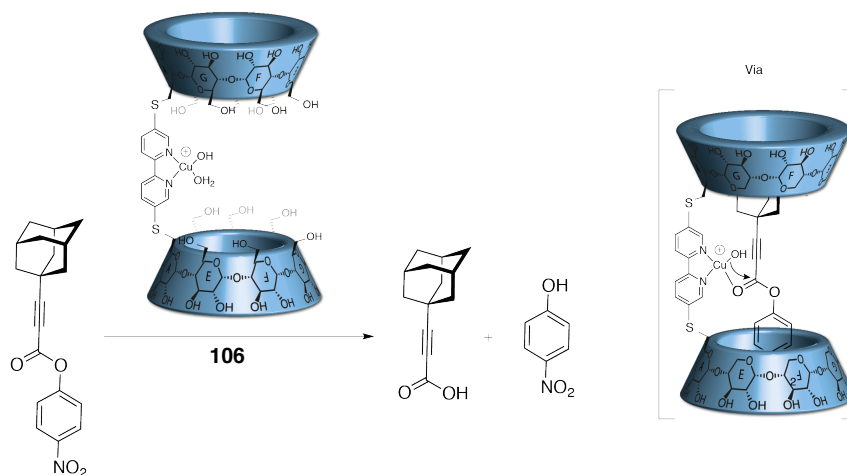
⁹⁷ B. Zhang, R. Breslow, *J. Am. Chem. Soc.* **1997**, *119*, 1676 - 1681



Scheme II-1: Early example of a CD-based complex with a catalytic activity.

Later studies by Breslow showed that a bipyridyl-linked β -cyclodextrin dimer could form Cu^{2+} metal complexes (**106**) able to hydrolyze ditopic hydrophobic esters in physiological conditions⁹⁸. This metal complex, enhanced the rate of the saponification of ditopic esters with two different hydrophobic groups up to 220000 fold faster over than non-catalyzed reaction.

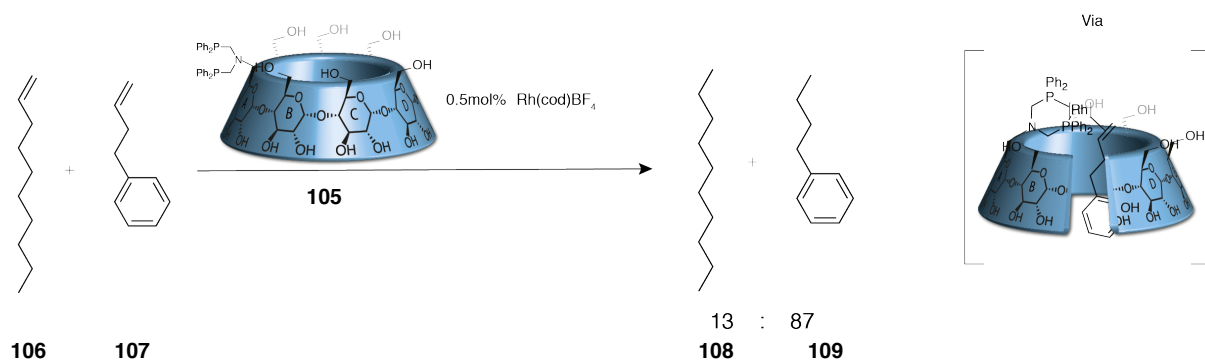
The authors suggested that the rates are increased because of the binding of both hydrophobic groups, that approaches the ester from the copper alkoxide **106** (Scheme II-2). In his report, the authors also suggest that the rates of this reaction are comparable to those of some acylating antibodies.



Scheme II-2: Hydrolysis of ditopic esters by a **106** complex.

⁹⁸ R. Breslow, B. Zhang, *J. Am. Chem. Soc.*, **1992**, *114*, 5883 - 5884

This hydrophobic binding was used by Reetz and coworkers to develop a system able to perform a substrate selection in a catalytic hydrogenation of alkenes.⁹⁹ To do so, the authors synthesized a β -cyclodextrin-modified diphosphane **107** which in the catalytic system forms **108** prior to **109** (scheme II-3). The rationalization of the origin of the substrate selection was suggested to be a better entrance and affinity constants between the phenyl ring and the β -cyclodextrin cavity.



Scheme II-3: Substrate selection promoted by a β -cyclodextrin-Rh complex.

One of the early examples of an asymmetric reduction promoted by the chirality of a cyclodextrin was developed by Woggon *et al.* The metal complexes developed in this example were amino alcohol derivatives from the native β -cyclodextrin **110**.¹⁰⁰

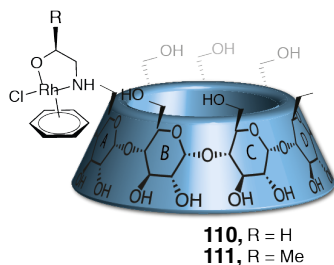
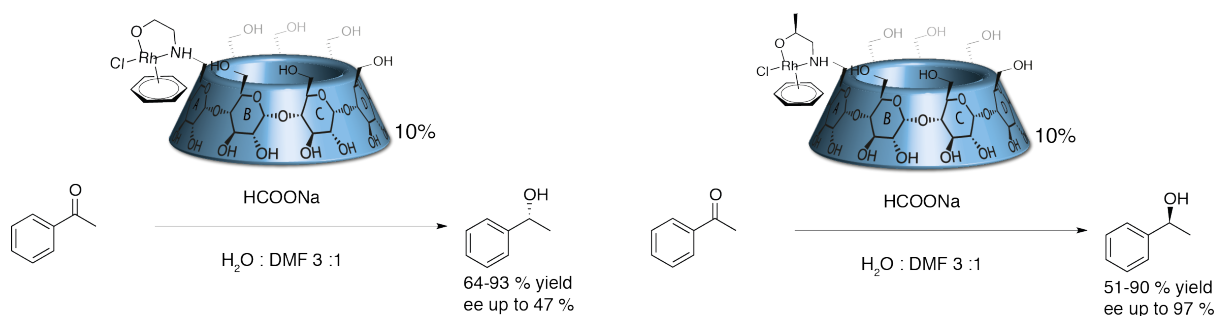


Figure II-8: Structure of (CD)Rh complexes **110** and **111**

In their seminal work, the use of these ligands in a Ru-catalyzed enantioselective reduction of ketones was studied. First, the use of the “achiral” ligand **110** produced the (*R*)-alcohols in good yields and enantiomeric excess up to 50% ee. Surprisingly, by addition of a chiral center at the α position of the alcohol, the complex **111**, formed the enantiomeric (*S*)-alcohols in 51% yield but in 97% ee (Figure II-9).

⁹⁹ M. T. Reetz, S. R. Waldvogel, *Angew. Chem. Int. Ed. Engl.*, **1997**, *36*, 865 - 867

¹⁰⁰ A. Schalter, M. K Kundu, W.D. Woggon, *Angew. Chem. Int. Ed.*, **2004**, *43*, 6731 - 6734



Scheme II-4: Reduction of aromatic ketones by **110** and **111**.

The origin of enantioselectivity was suggested to be the formation of a host-guest complex inside the cavity of the cyclodextrin with an additional hydrogen bonding between the N-H of the amine and the ketone. This example is one of the first and unusual systems where a cyclodextrin core, promoted an enantioselective reaction, that can be inverted. Additionally, the applicability to a broad scope of substrates showed the robustness of the catalytic system.

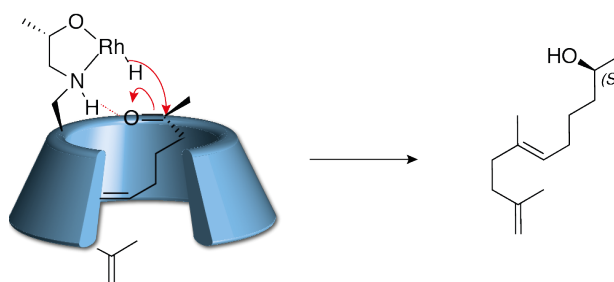
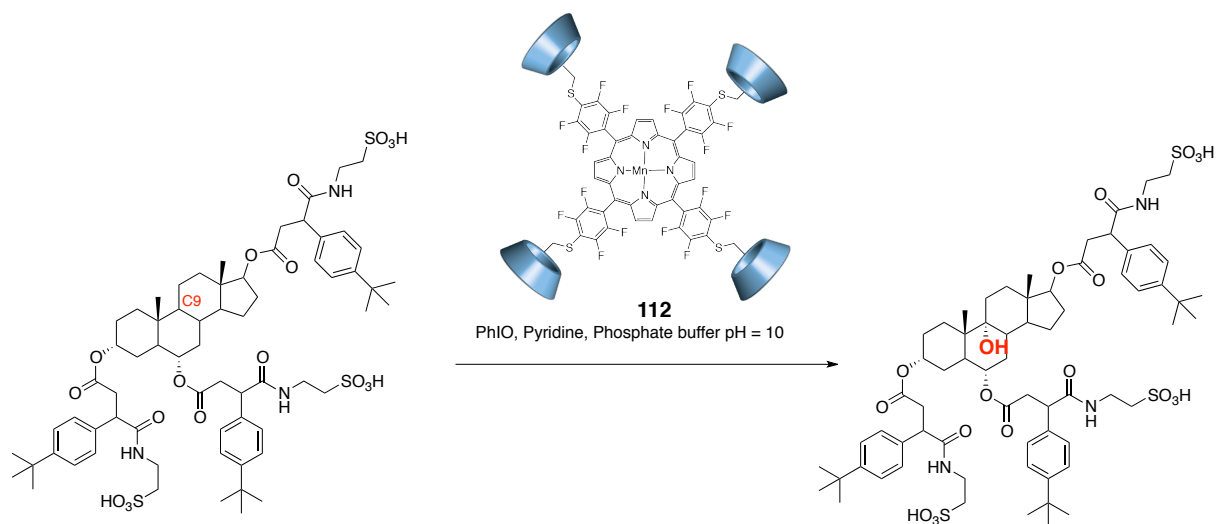


Figure II-9: Suggested hydrogen transfer (Re attack)

One of the latest works by Breslow in this field used a tetra-cyclodextrin molecule linked to a Mn porphyrin **112** (Scheme II-5). In this system, a late stage oxidation of the C6 position of a sterol skeleton was performed in a regio- and stereospecific manner. The selectivity of the system is justified by the recognition through hydrophobic effect of the diametrically opposed substituents of the sterol derivative.

This recognition places the steroid skeleton with the C9 carbon next to the catalytic Mn center, oxidizing selectively in a late step of synthesis, the C9 carbon of the sterol derivative (Figure II-10).¹⁰¹

¹⁰¹ J. Yang, B. Gabriele, S. Belvedere, Y. Huang, R. Breslow, *J. Org. Chem.*, **2002**, *67*, 5057 - 5067



Scheme II-5: Selective hydroxylation at C9 by a (CD)₄Mn- porphyrin complex

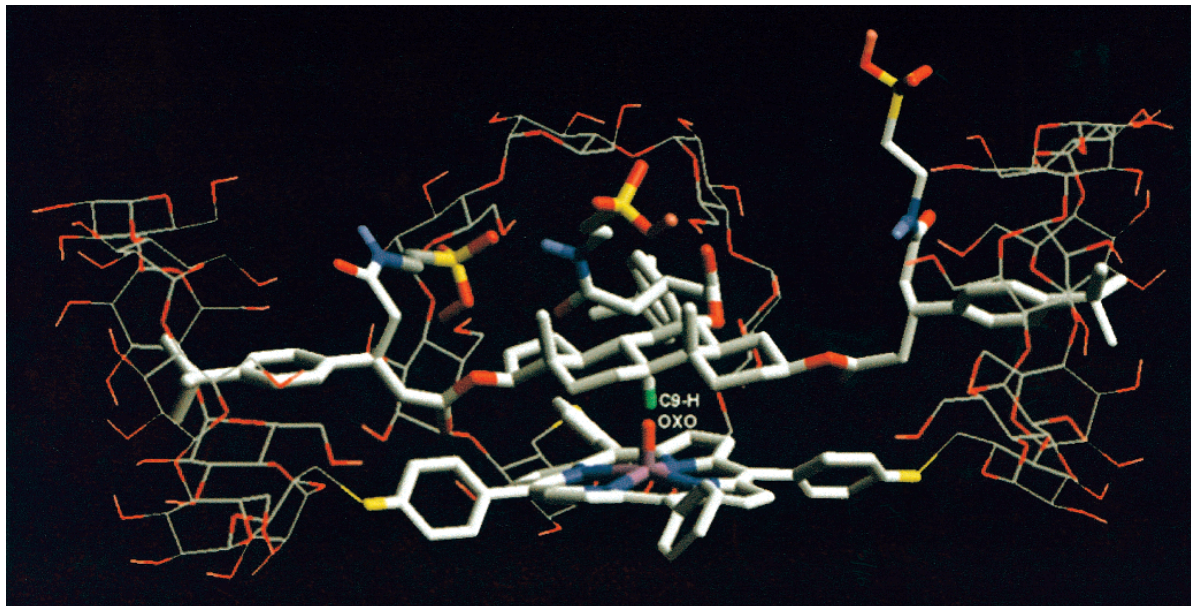


Figure II-10 : Computer model of the complex of the substrate with **112**. For clarity, the cyclodextrin ring not involved in binding is hidden. Image extracted from the reference 101.

The hydrophobic effect and the recognition of phenyl rings of the β -cyclodextrin was also exploited by Kostic and coworkers to develop a biomimetic peptidase.¹⁰² In this example a palladium(II) β -cyclodextrin conjugate was synthesized. In this complex, the cyclodextrin played the role of recognition site and the palladium, the active catalytic site of a synthetic peptidase. Thus, by complexation of a phenylalanine residue, in a 0.1 M aqueous phosphate buffer, the system cleaved selectively the proline peptidic bond 2 residues after a Phe, that was recognized by the cyclodextrin.

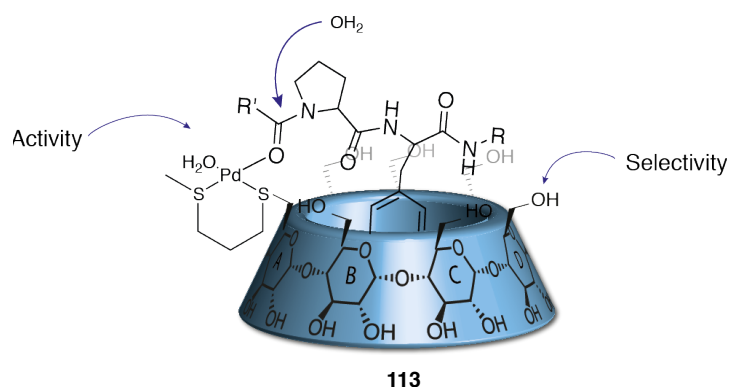


Figure II-11: Selective peptide bond cleavage of the Pro-Phe sequence.

To verify the role of the host guest complex, the complexation of the Phe of the sequence was proved to be inside the cavity by ROESY experiments. In this experiments, the aromatic ring showed cross peak correlations between the phenyl ring and the intra-cavity protons H3 and H5.

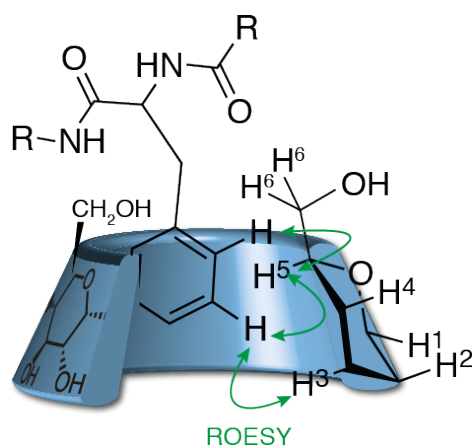
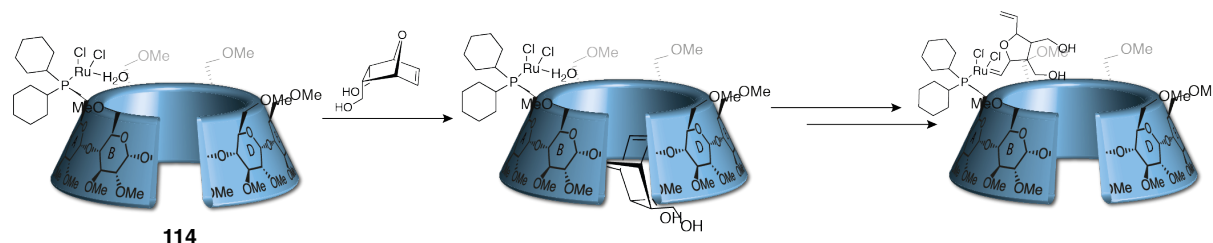


Figure II-12: Observed ROESY cross correlations observed between the Pro and the β -CD.

¹⁰² N. M. Milovic, J. D. Badjic, N. M. Kostic, *J. Am. Chem. Soc.*, **2004**, *126*, 696 - 697

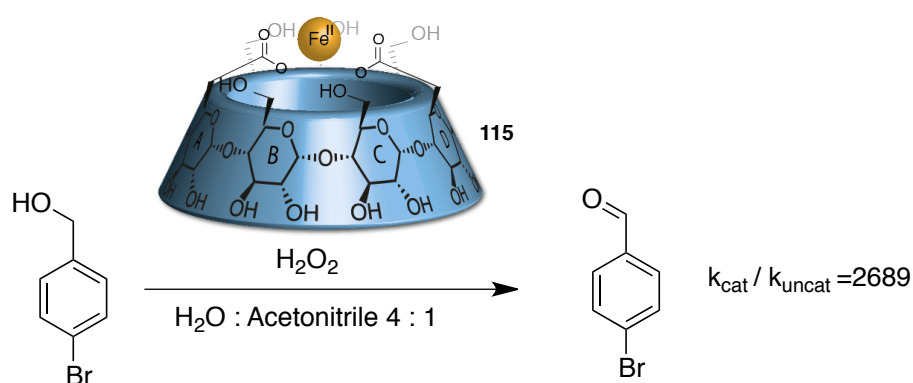
Harada and coworkers also contributed to this field by using a β -CD-phosphane derivative **114**, able to form Ru-based metal complexes¹⁰³. This water soluble Ru complexes could perform a Ring-Opening Metathesis Polymerization (ROMP) in aqueous media. Through association constants and competition studies, the key role of the recognition of the monomer developed by the cavity in the ROMP mechanism was proved.



Scheme II-6: (CD)Ru catalyzed Ring Opening Metathesis Polymerization

The last report describing a transient second coordination sphere cyclodextrin was shown last year by Bols and coworkers. In this study a β -cyclodextrin dicarboxylate **115** as ligand for transition metals of the first row was synthesized¹⁰⁴. The complexation of Zn^{2+} , Fe^{2+} or Cu^{2+} and the different acid-base constants of the aquo complexes was described.

Finally, the $CD(COO)_2Fe$ complex was used as catalyst in an oxidation of benzylic alcohols showing for all the substrates an enhanced rate up to 2689 fold for the *p*-bromo derivative. Additionally, Hanes plot for the oxidation revealed an enzyme-like rate enhancing effect, allowing the authors to propose their systems as an artificial metalloenzyme (Scheme II-7).



Scheme II-7: Oxidation of benzylic alcohols by a $CD(COO)_2Fe$ complex

¹⁰³ Y. Takashima, K. Uramatsu, D. Jomori, A. Harima, M. Otsubo, H. Yamaguchi, A. Harada, *ACS Macro Lett.* **2014**, *2*, 384 - 387

¹⁰⁴ B. Wang, R. Breslow, *Chem. Eur. J.* **2017**, *23*, 13766 - 13775

3. CD-metal complexes as first and second coordination spheres

First results on CD-based metal complexes where the cyclodextrin acts as second coordination sphere at the same time as the first coordination one, were started by Matt and Armspach with very structurally different phosphane-based ligands. Different applications this system such as the use of the cyclodextrin cavities as probes for ligand exchange processes were shown.⁹⁰

One of their main contributions in the synthesis of cyclodextrin-based metal complexes field was a primary rim modified permethylated α -CD-diphosphane used as ligand for transition metal complexes.⁹⁰ The formation of coordinated organometallic complexes such as (CD)PdMeCl produced a singular downfield shift of the H5 of sugar units A and D (H-5A,D). This downfield shift (around 0.8 ppm by comparison with the free ligand) was proved to be related with a weak interaction of the H5 and the chlorido ligands of the metal complex.

In this seminal work, the authors proved this weak-interaction thanks to proton NMR downfield shifts of the H5 involved, ROESY with the phenyl rings of the phosphine and the H6 of the cyclodextrin. These NMR data were correlated with the crystal structures of the metal complexes. Based on the crystal structure, the authors estimate the H5-Cl distance at 2.6 Å and rationalized the downfield shift of the H5 with a C-H \cdots Cl interaction (Figure II-13).

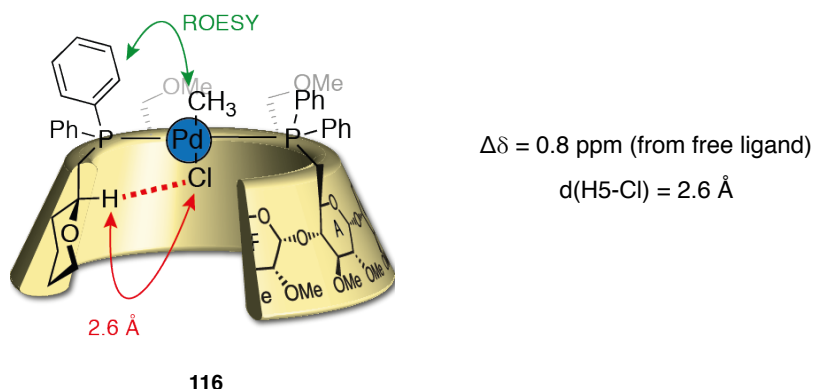
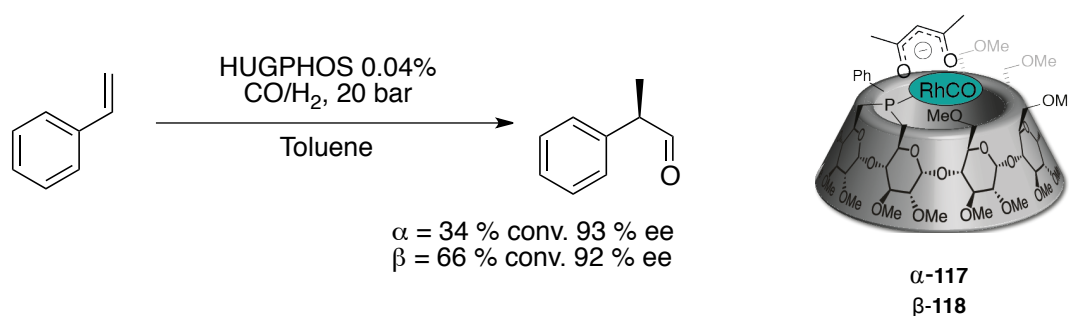


Figure II-13: Structure of the complex **116** with the first identified CH⁵-Cl interaction

These cyclodextrin-based ligands allowed the group to develop a second generation of confining phosphanes, based either on α - or β -cyclodextrin, with two anchoring point on the primary rim (α -HUGHPHOS **117** and β -HUGHPHOS **118**). These derivatives, with well-defined structures⁹⁰, were proved to be extremely efficient catalysts in regio- and enantioselective hydroformylation of styrene¹⁰⁵. In this reaction, both systems, α -HUGHPHOS **117** and β -HUGHPHOS **118**-Rhodium complexes perform the reaction under 40 bar of a H₂/CO atmosphere with selectivities Branched : Linear higher than 98:2 and 93% ee.



Scheme II-8 : HUGPHOS catalyzed hydroformylation of styrene.

Subsequently, Sollogoub described diametrically opposed Pd-based CD-bis-NHC and CD-bis-MIC ligands¹⁰⁶ where the same downfield shift on the H5 proved the presence of the metal complex in the entrance of the primary rim of the cyclodextrin. In this work, the authors demonstrated that the palladium complexes **108** and **109** were good candidates to perform Suzuki cross-coupling reactions. Additionally, as for all the examples presented before, the water solubility of the cyclodextrin made good water soluble palladium-based catalysts.

Through all these examples, a broad scope of possibilities for the use of cyclodextrins as platforms in catalysis were developed. Since the first example of Breslow, different approaches concerning the coordination spheres were taken conferring the metal complexes many different properties: water solubility, stability, or different selectivities in catalysis such as regioselectivity, enantioselectivity or substrate selection.

¹⁰⁵ a) M. Jouffroy, R. Gramage-Doria, D. Armspach, D. Sémeril, W. Oberhauser, D. Matt, L. Toupet, *Angew. Chem. Int. Ed.* **2014**, *53*, 3937 - 3940. b) *Beilstein J. Org. Chem.*, **2014**, *10*, 2388 - 2405

¹⁰⁶ M. Guitet, F. Marcelo, S. Adam de Beaumais, Y. Zhang, J. Jiménez-Barbero, S. Tilloy, E. Monflier, M. Ménand, M. Sollogoub *Eur. J. Org. Chem.* **2013**, 3691–3699.

D. The only introverted CD-metal complexes. NHC-capped cyclodextrins

Previous work in the laboratory showed the synthesis of introverted mono-imidazolium salts in cyclodextrins, called ICyDs⁵⁹ (Figure II-14). These mono-NHC-bridged cyclodextrins can coordinate group 11 metal complexes inside the cavity. These complexes have been proved to be the only introverted cyclodextrin-based complexes with interesting applications in catalysis.

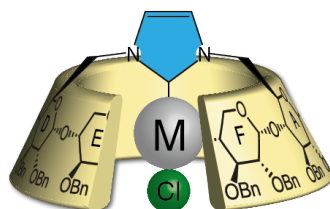
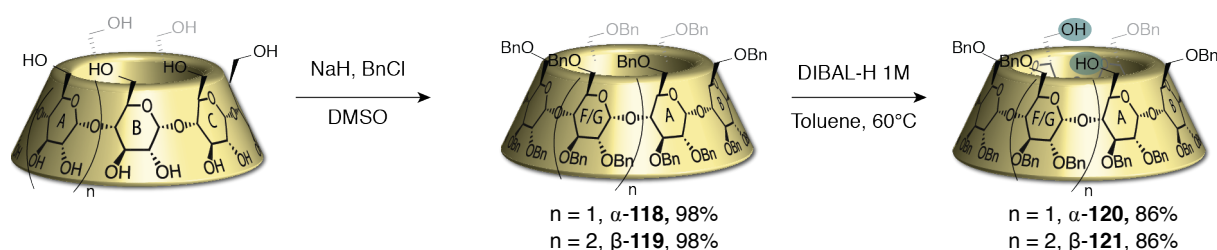


Figure II-14 : Structure of (α -ICyD)MCl complexes

1. Synthesis

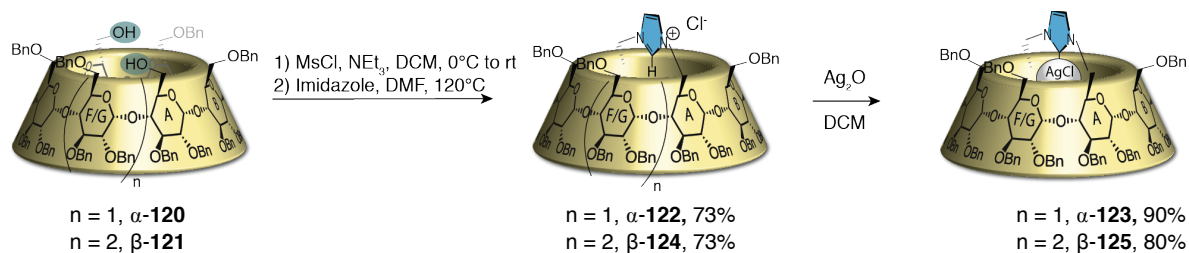
These complexes are obtained using the synthetic methodology developed in the laboratory.¹⁰⁷ Protection of α or β native cyclodextrin in the presence of benzyl chloride and sodium hydride in DMSO afforded the protected perbenzylated cyclodextrins in 98% yield. These protected cyclodextrins can be regioselectively deprotected using DIBAL-H in toluene, 1M in the medium at 60 °C to give α -CD-AD-diol **120** and β -CD-AD-diol **121** in 86% yield in both cases (Scheme II-10).



Scheme II-10: Synthesis of α and β -CD(OH)₂

Mesylation of these diols in the presence of mesyl chloride and triethylamine afforded the α -CD(OMs)₂ and β -CD(OMs)₂ in quantitative yields. Nucleophilic substitution using an excess of imidazole in DMF at 120 °C afforded the introverted imidazolium-capped cyclodextrins in 73% yield. Metalation of the imidazolium precursors in presence of Ag₂O afforded the introverted (α -ICyD)AgCl and (β -ICyD)AgCl in 90% and 80% yield respectively (Scheme II-11).

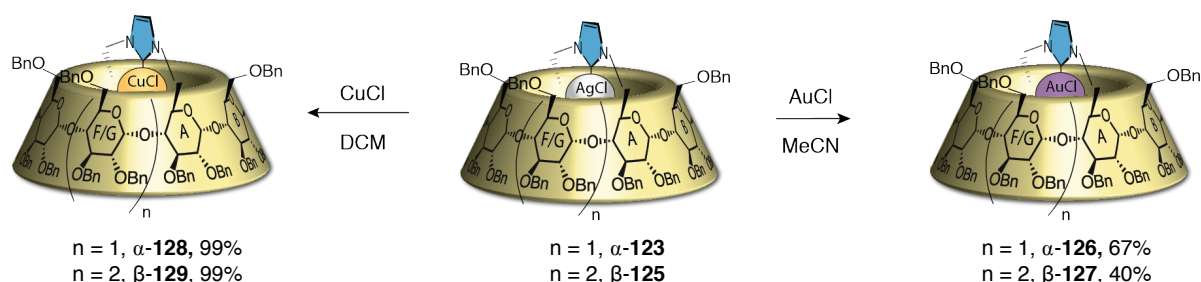
¹⁰⁷ T. Lecourt, A. Herault, A. J. Pearce, M. Sollogoub, P. Sinay, *Chem. Eur. J.* **2004**, *10*, 2960 - 2971



Scheme II-11: Synthesis of (α-ICyD)AgCl and (β-ICyD)AgCl.

(ICyD)AgCl can be engaged in transmetalation reactions with 10 equivalents of AuCl in acetonitrile affording (α-ICyD)AuCl and (β-ICyD)AuCl in 67% and 40% yield respectively (Scheme II-12). These complexes could be obtained thus in 6 steps, in 33% overall yield for the α-CD derivative and 20% yield for the β-CD analogue.

By treatment of the silver precursors with a large excess of freshly prepared CuCl in DCM, (α-ICyD)CuCl and (β-ICyD)CuCl were obtained after a silica gel purification in quantitative yields. The copper complexes are thus synthesized in 6 steps in 50% overall yield. The scale up of the complexes could be increased up to 10 g for copper complexes, affording silica gel, air and moisture stable compounds.



Scheme II-12: Synthesis of (α-ICyD)CuCl, (α-ICyD)AuCl, (β-ICyD)CuCl and (β-ICyD)AuCl

2. Characterization

i. NMR

Due to the difficulty to obtain monocrystals suitable to perform X-Ray analysis, all the characterization of these compounds were done by NMR. First indications of the introversion of the ligand were observed by NOESY experiments on the cyclodextrin-capped azolium salt **128** (α-ICyD).HCl. First, a single clear cross-correlation is observed between the acidic proton of the imidazolyl ring and the intra-cavity proton H5 of sugar units A and D (H-5A,D) (Figure II-15A). Besides, another cross correlation is observed between the H of the N-heterocyclic ring (H-NHC) and one of the H-6A,D of the primary rim of the cyclodextrin (Figure II-15B).

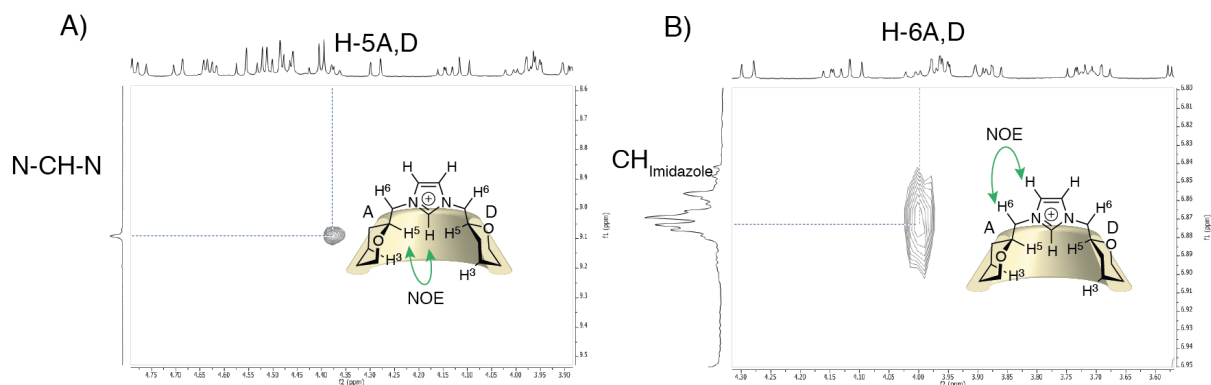


Figure II-15 : Key NOESY cross correlations of $(\alpha\text{-ICyD})\text{HCl}$. CD_3CN , 600 MHz, 300 K

The same type of NOESY cross correlations were found on the copper complex derivative (Figure II-16). The proton of the NHC showed intense cross peak correlations with the H6 of sugar units A,D as well as weaker correlations with the H6 of the adjacent sugar units B and E. Thus, the complexation takes place without changes on the orientation of the NHC.

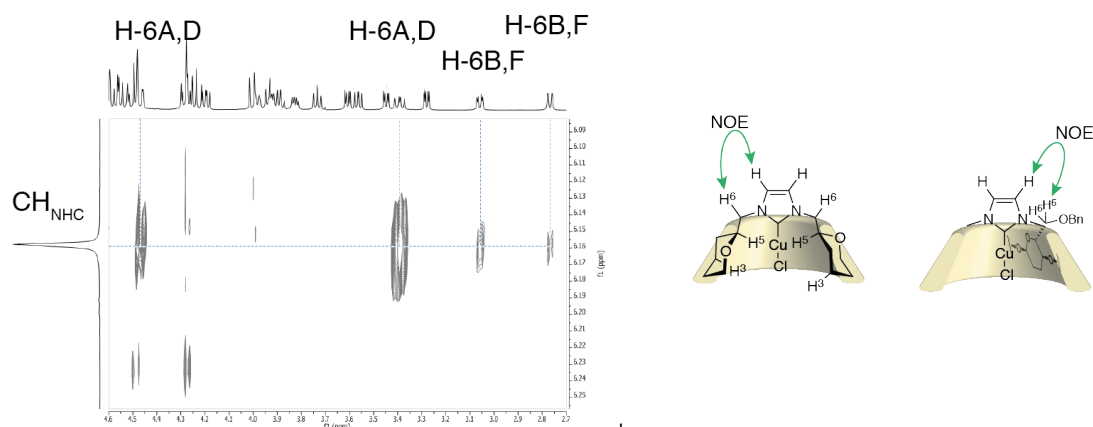


Figure II-16: Key NOESY cross correlations of $(\alpha\text{-ICyD})\text{CuCl}$. CDCl_3 , 600 MHz, 300 K

In addition to this NOESY experiment, an important deshielding of the intra-cavity protons H-5A,D and H-3C,F was observed in the NMR, proving the interaction of the cyclodextrin with the metal ion.⁹⁰ Through different NMR experiments, the authors proposed to reveal the real position of the metal and the ligand inside the cavity. First, by comparing the three metal complexes $(\alpha\text{-ICyD})\text{AuCl}$ **126**, $(\alpha\text{-ICyD})\text{AgCl}$ **123** and $(\alpha\text{-ICyD})\text{CuCl}$ **128**, a metal-dependent downfield shift was observed for the H-5A,D. Comparing its chemical shift to the other H5s, a downfield shift of 2.4 ppm was observed for the gold(I) complex **128**, 1.7 ppm for the silver(I) and 1.8 ppm for the copper(I) complex. It was therefore deduced that the metal atom is placed at the same level than the H5 of the macrocycle.

In addition to the observed downfield shift of the H-5A,D, the H-3C,F are also deshielded by 1 ppm (compared with the other H3s). Since no relevant changes were observed between the Cu, Ag, or Au complexes in the shift of the H3 (Figure II-17), the authors deduced that this chemical shift is independent of the metal but of the chlorine atom is situated at the same level as the H3.

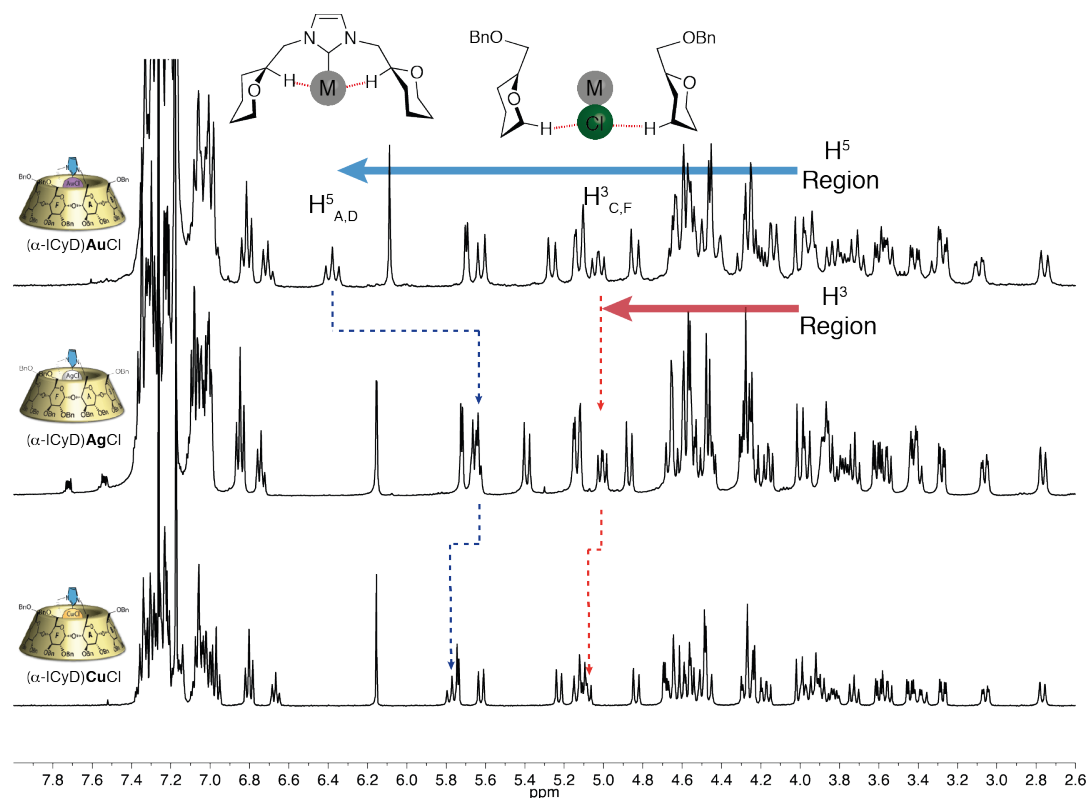


Figure II-17: Stacked NMR spectra of $(\alpha\text{-ICyD})\text{AuCl}$, $(\alpha\text{-ICyD})\text{AgCl}$ and $(\alpha\text{-ICyD})\text{CuCl}$. 600MHz, CDCl_3 , 300K

To verify this deduction and to study the influence of the chlorine atom on the NMR, different ligands and counterions such as bromine, iodine, acetate or triflate were compared on the $(\alpha\text{-ICyD})\text{AgX}$ complex. This experiment showed that halogens induced a stronger downfield shift (1 ppm), than carboxylates or triflates (around 0.5 ppm) proving the ligand-dependency of the chemical shift of the H-3C,F (Figure II-18). The ligand and the H3 are thus placed at the same level inside the cavity. Additional shifts were observed on the H5 chemical shifts, attributed to the modifications on the electronic density of the metal due to ligand exchange.

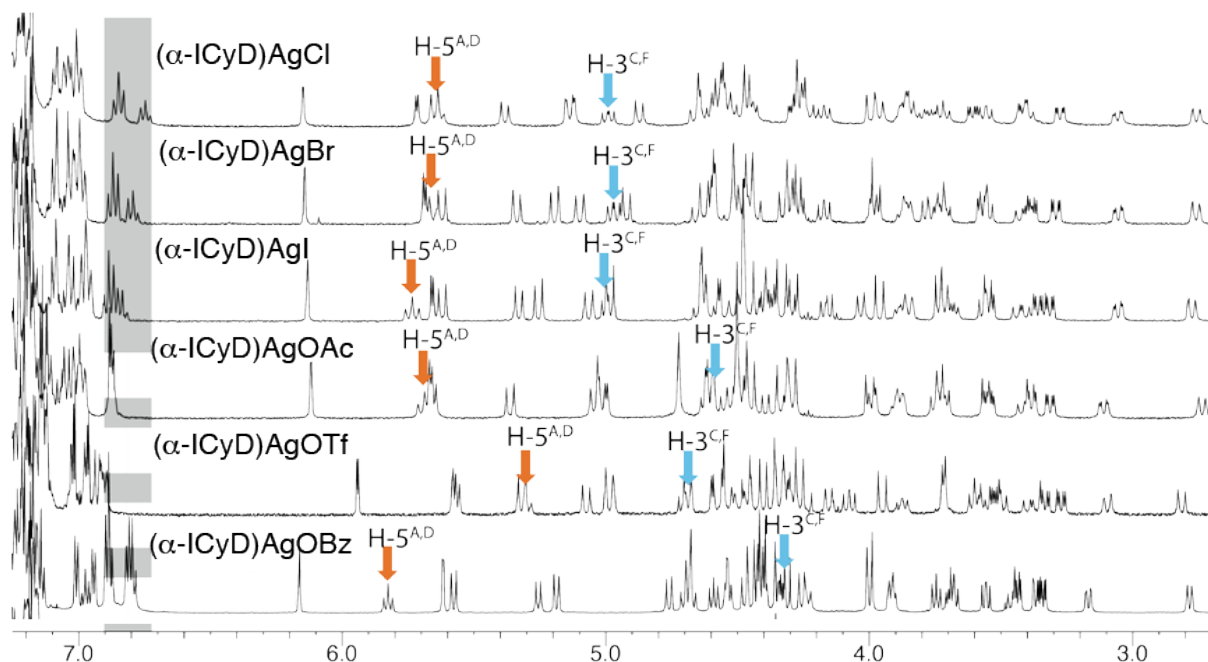


Figure II-18 : Stacked ^1H -NMR spectra of different $(\alpha\text{-ICyD})\text{AgX}$ complexes. CDCl_3 , 400 MHz, 300 K

To better understand the structure of this system, a three-dimensional model of the system was constructed. To do so, the chemical shifts of the intra-cavity protons were related to the distances between the H5 and the metal, as well as the H3 and the chlorine. Since, the $\delta(\text{H-5A,D}) > \delta(\text{H-5C,F}) > \delta(\text{H-5B,E})$, the relative distances of the H5 and the metal were supposed to follow the same order, $d(\text{H-5A,D-M}) > d(\text{H-5C,F-M}) > d(\text{H-5B,E-M})$. The same reasoning was followed to study the distances between the H3 and the chlorine, resulting thus in $d(\text{H-3C,F-Cl}) > d(\text{H-3B,F-Cl}) > d(\text{H-3A,D})$.

Finally, with this information, a model of the $(\alpha\text{-ICyD})\text{AgCl}$ was constructed using Avogadro. Starting from the crystal structure of the permethylated α -cyclodextrin, the imidazolyl bridge was constructed, and the structure was optimized a first time using the universal force field (UFF). The AgCl part was then added and the sugar units were tilted and arranged according to the NMR deduced distances and the structure was optimized a last time using the UFF giving the structure shown in Figure II-19

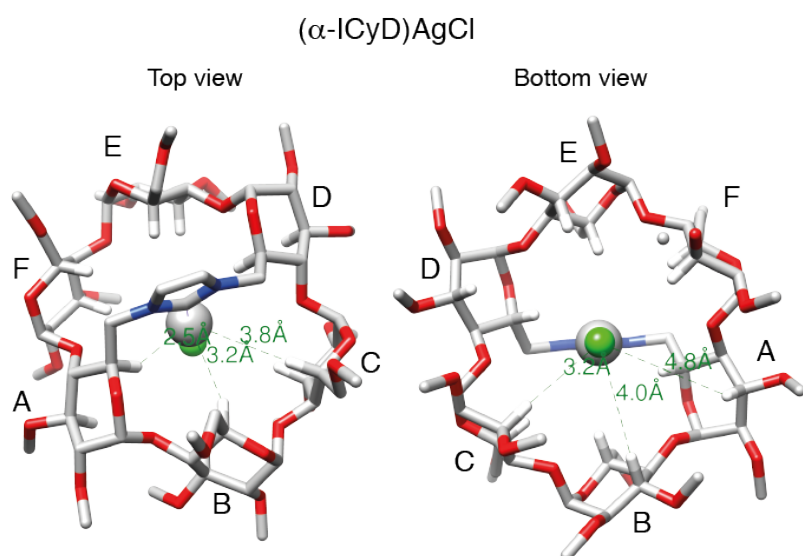


Figure II-19: Modeled structure of (α -ICyD)AgCl.

ii. DFT and X-Ray

Later studies of this system involved DFT calculations to confirm the structure obtained by molecular mechanics.⁵⁶ Indeed, superimposition of the modeled (α -ICyD)AgCl with the one obtained by DFT gives very similar structures, validating the followed approach.

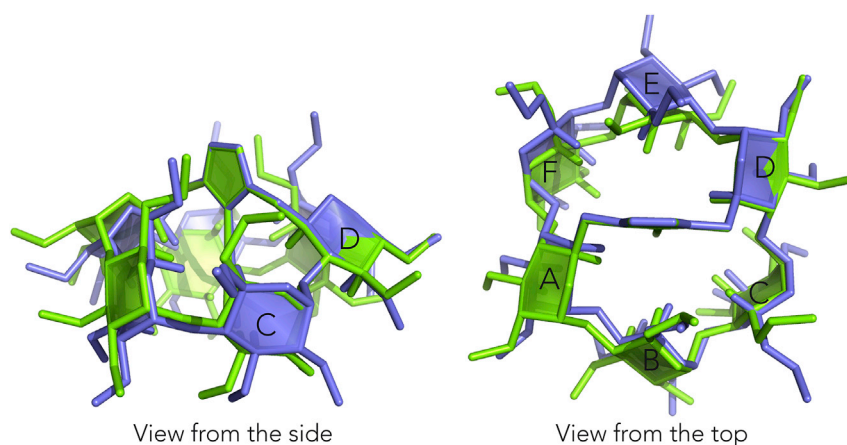


Figure II-16 : Superimposition of modeled (α -ICyD)AgCl (blue) with the DFT calculated structure (green).

Finally, as a second confirmation, the synthesis and the crystallization of the permethylated-(α -ICyD)AgCl was performed¹⁰⁸ (Figure II-21). The X-Ray structure of the complex confirmed both the DFT-calculated one and the NMR-modeled structure, validating with an experimental data the process of modelization with Avogadro and the DFT.

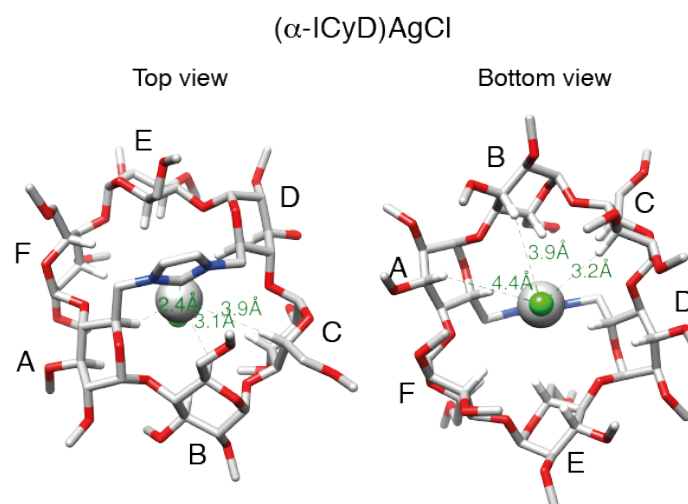


Figure II-17: Cristal structure of (α -ICyD)AgCl

Chemical shifts of H5 and H3 of (α -ICyD)AgCl, as well as the distances of the intracavity protons obtained on the structure deduced from the NMR data, and the crystallographic structure are reported in Table II-1. It is interesting to mention the accuracy of the H5-Ag distances found to be at 0.1 Å from the real one. In addition, the distances between the H3 and the chlorine are obtained with less than 15% error. In conclusion, the Avogadro modeling was confirmed to be a useful and valid tool to access the structures of the α -ICyD metal complexes.

Sugar unit	δ (H5) ppm	$\Delta\delta^a$ ppm	d(H5-Ag) Å (MM)	d(H5-Ag) Å (XRay)	δ (H3) ppm	$\Delta\delta^a$ ppm	d(H3-Cl) Å (MM)	d(H3-Cl) Å (XRay)
A/D	5.64	1.76	2.5	2.4	4.18	-	4.8	4.4
B/E	3.88	-	3.2	3.1	4.29	0.11	4.0	3.9
C/F	3.89	0.01	3.8	3.9	4.98	0.80	3.8	3.2

Table II-2: Chemical shifts of H5 and H3, H5-Ag and H3-Cl distances of (α -ICyD)AgCl. ^a $\Delta\delta$ were calculated from the most deshielded H and the most shielded one.

iii. Weak interactions in (α -ICyD)AgCl complex

As presented in Chapter I, the understanding of the weak interactions of both, first and second coordination spheres is a key step in the design of a catalyst,^{5a} the catalytic performances or the understanding of the properties of the system.^{5b} NMR of ICyD-metal complexes shows that indeed, this system can induce unusual downfield shifts on the intracavity protons, probably because of weak interactions.

Sugar unit	δ (H5) ppm	$\Delta\delta$ ppm	d(H5-Ag) Å (MM)	d(H5-Ag) Å (XRay)	Angle From XRay
A/D	5.64	1.76	2.5	2.4	136 °
B/E	3.88	-	3.2	3.1	159 °
C/F	3.89	0.01	3.8	3.9	153 °

Table II-3: Comparison of metrics of H5-M in the MM and X-ray and NMR data

It was shown previously that the H3s of the cyclodextrin were influenced by the presence of the second ligand of the complex. When this ligand is a halogen, the effect on the NMR was shown to deshield these protons. This downfield shift is in accordance with a C-H...halogen interaction, present in different previously presented cyclodextrin-based complexes.⁹⁰ This weak interaction is a hydrogen bond-like between a C-H bond and a halogen, widely studied for very different examples like anion recognition¹⁰⁹ or template assembly.¹¹⁰

This interaction is maximized when the C-H ... X angle is bigger than 150° and the distances are less than 4Å. The presence of this bonding produces a downfield shift in the ¹H-NMR of the protons concerned.¹¹¹ Comparing the NMR based modeled distances and the crystallographic data, both are in agreement to this weak interaction.

Sugar unit	δ (H3) ppm	$\Delta\delta$ ppm	d(H3-Cl) Å (XRay)	Angle From Xray
A/D	4.18	-	4.4	136 °
B/E	4.29	0.11	3.9	159 °
C/F	4.98	0.80	3.2	153 °

Table II-2: Chemical shifts of H3, H3-Cl distances of (α -ICyD)AgCl.

¹⁰⁹ a) C. Lee, H. Na, D. Yoon, D. Won, W.S. Cho, V. M. Lynch, Sergey V. Shevchuk, and J. L. Sessler *J. Am. Chem. Soc.*, **2003**, *125*, 7301 - 7306 b) K. J. Wallace, W. J. Belcher, D. R. Turner, K. F. Syed, J. W. Steed, *J. Am. Chem. Soc.*, **2003**, *125*, 9699 - 9715

¹¹⁰ M. R. Sambrook, P. D. Beer, J. A. Wisner, R. L. Paul, A. R. Cowley, F. Szemes, M. J. B. Drew *Am. Chem. Soc.* **2005**, *127*, 2292 - 2302

¹¹¹ G. Shi, Z. A. Tehrani, D. Kim, W. J. Cho, I. Youn, H. M. Lee, M. Yousuf, N. Ahmed, B. Shiringar, A. J. Teator, D. N. Lastovickova, L. Rasheed, M. S. Lah, C. W. Bielawski, K. S. Kim., *Sci. Rep.*, **2016**, *6*, 1 - 10

The intriguing effect was the deshielding of the H5. It was proved that the downfield shift was dependent on the nature of the metal. CH ... M interactions are widely studied because of the influence that a weak interaction can have in the reactivity of a transition metal complex¹¹² with an special focus on d⁸ transition metals. Studies on unpolarized CH ... M interactions with metals of the d⁸ configuration are classified in three different classes: Anagostic, agostic or preagostic (Figure II-20).¹¹³

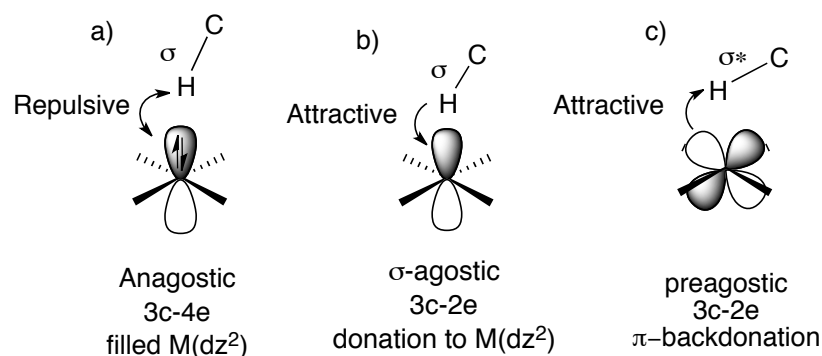


Figure II-20: Main weak interactions in d⁸ transition metal complexes

Anagostic interactions (Figure II-20, a), were first observed by Lippard and coworkers in a cis diamino-Pt(II) complex **130** (Figure II-21).¹¹⁴ In this first report, the authors proposed that this remote interaction (bond distance > 3) is produced because of a steric constraint of the complex. This proximity from the metal, produces an electronic repulsion between the d(z²) and the electrons of the σ (C-H) bond, producing a downfield shift of the H engaged on the interaction¹¹⁵. This 4 electron-3 center interaction is observed when a steric hindrance places the metal and the H at less than 3 Å. To reduce the electronic repulsion between the σ (C-H) bond and the filled d(z²), the C-H-M angle must be between 130 and 180°.

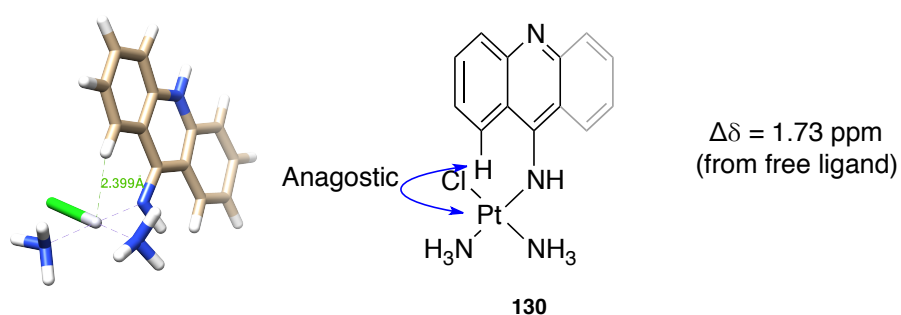


Figure II-21: First complex with a described anagostic interaction

¹¹² D L. Davies, S. M. A. Donald, S. A. Macgregor. *J. Am. Chem. Soc.* **2005**, *127*, 13754 - 13755.

¹¹³ W. Scherer, A. C. Dunbar, J. E. Barquera-Lozada, D. Schmitz, G. Eickerling, D. Kratzert, D. Stalke, A. Lanza, P. Macchi, Ni. P. M. Casati, J. Ebad-Allah, C. Kuntscher, *Angew. Chem. Int. Ed.* **2015**, *54*, 2505 - 2509.

¹¹⁴ W. I. Sundquist, D. P. Bancroft, S. J. Lippard, *J. Am. Chem. Soc.* **1990**, *112*, 1590-1596

¹¹⁵ Y. Zhang, J. C. Lewis, R. G. Bergman, J. A. Ellman, and E. Oldfield, *Organometallics* **2006**, *25*, 3515 - 3519

In contrast, if the $d(z_2)$ is empty and the electronic donation is given from the σ (C-H) bond to this empty orbital, coordination of the σ -bond to a metal is classified now as agostic (Figure 20, b). This interaction is usual in d^6 complexes like Ir^{III} or Re^{III} ¹¹⁶, also observed in d^8 transition metal complexes such as Pd^{II} complexes¹¹⁷ and only one recent example in the case of Au^{III} ¹¹⁸. This interaction, due to the full filled orbitals, cannot exist in d^{10} complexes such as Au^{I} ¹¹⁹. This 3 center-2 electron interaction is partially covalent, thus, to achieve the best overlapping of orbitals, distances ranging from 1.8 Å to 2.3 Å and angles between 90° and 140° were usually observed. (Figure II-22)¹²⁰. The effect on the NMR is metal dependent, but in the most cases a hydride shift is observed.¹²¹ Furthermore, a characteristic reduction of the $^1\text{J}(\text{C-H})$ is systematically observed¹²⁰.

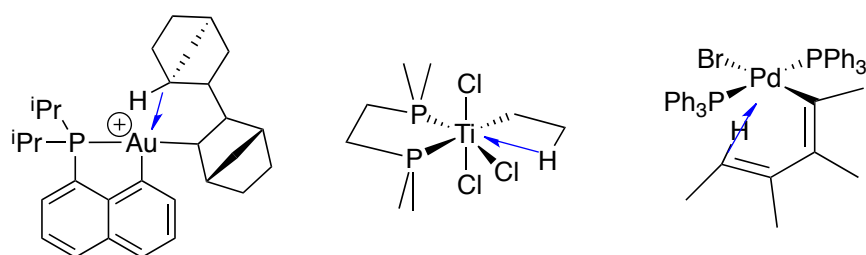


Figure II-22: Structures of some Ti, Au, Pd agostic complexes.

If for different reasons, the system could not achieve these geometric parameters, a preagostic interaction would be observed **131**. Similar in metrics to the anagostic, this partially covalent interaction does not involve the $d(z_2)$ orbital of the metal¹²² and only a retro-donation from the metal to the σ^* (C-H) is observed. This preagostic interaction also deshields the involved proton in the NMR but in contrast to the anagostic one, only 2 electrons are involved in the 3 centers. To differentiate this interaction from the anagostic, careful theoretical calculations must be done to know the origin of the deshielding, to determine if it is produced by an electrostatic repulsion (anagostic) or if it is a covalent bonding (preagostic).

¹¹⁶ V. Fernández-Moreira, F. L. Thorp-Greenwood, M. P. Coogan *Chem. Commun.*, **2010**, 46, 186–202

¹¹⁷ A.J. Nielson *J. Chem. Soc., Dalton Trans.*, **1981**, 0, 205 - 211.

¹¹⁸ F. Rekhroukh, L. Estévez, C. Bijani, K. Miqueu, A. Amgoune, D. Bourissou, *Angew. Chem. Int. Ed.* **2016**, 55, 3414–3418

¹¹⁹ G. Klatt, R. Xu, M. Pernpointner, L. Molinari, T. QuangHung, F. Rominger, A.S. Hashmi, H. Köppel, *Chem. Eur. J.* **2013**, 19, 3954–3961.

¹²⁰ a) Z. Dawoodi, M.L.H. Green, V.S.B. Mtetwa, K. Prout, A.J. Schultz, J.M. Williams, T.F. Koetzle, *J. Chem. Soc. Dalton. Trans.*, **1986** 1629–1637. B) *J. Chem. Soc. Chem. Commun.* **1972**, 1237.

¹²¹ W. Scherer, A. C. Dunbar, J. E. Barquera-Lozada, D. Schmitz, G. Eickerling, D. Kratzert, D. Stalke, A. Lanza, P. Macchi, N. P. M. Casati, J. Ebad-Allah, C. Kuntscher, *Angew. Chem. Int. Ed.* **2015**, 54, 2505 - 2509

¹²² J. C. Lewis, J. Wu, R. G. Bergman, J. A. Ellman, *Organometallics*, **2005**, 24, 5737 - 5746

Preagostic interactions are widely studied to improve the efficiency of a catalytic system. It is known in the literature that agostic interactions are widely involved in C-H activation steps such as σ -bond metathesis,¹²³ β -hydride elimination¹²⁴ or oxidative additions¹²⁵. Furthermore, the study of these interactions becomes more interesting on d^8 transition metal complexes because of the versatility of the possible interactions, translate thus, in different possible reactivities.

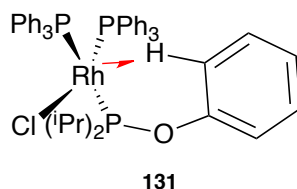


Figure II-23: example of a Rh complex with a preagostic interaction.

Looking now at the chemical shift of the H5-A,D and the distances obtained from the modeling and the X-Ray structure of the (α -ICyD)AgCl (table II-3), a short 2.4 Å distance between the Ag atom and the H-5A,D with a 136° angle is observed. According to the classification shown by Kuntscher *et al* this interaction could be either anagostic, either preagostic. Since the frontier between both requires powerful DFT calculations,¹²⁶ the interaction will be named as C-H \cdots M interaction.

iv. First and second coordination sphere in (ICyD)MCl complexes

Now that intra-cavity interactions have been shown and described, the coordination spheres can be defined in the (ICyD)MCl complexes. The different weak interactions of this system make this ligand a simultaneous multi-coordinating first- and second-coordination sphere.

As presented previously, the first coordination sphere of a metal complex is formed by the ligands and the interaction with it, in this case, the NHC and the C-H5 \cdots M interaction and the chlorido ligand build the first coordination sphere. The second one, formed by weak interactions with the ligand is formed by the C-H3 \cdots halogen interaction between the H3 and the Cl ligand (Figure II-24).

¹²³ J. Mathew, N. Koga, C. H. Suresh, *Organometallics*, **2008**, *27*, 4666–4670

¹²⁴ D. R. Jensen, M. J. Schultz, J. A. Mueller, M. S. Sigman *Angew. Chem. Int. Ed.* **2003**, *42*, 3810–3813

¹²⁵ a) W. I. Sundquist, D. P. Bancroft, S. J. Lippard, *J. Am. Chem. Soc.* **1990**, *112*, 1590–1596; b) M. Brookhart, M. L. H. Green, G. Parkin, *Proc. Natl. Acad. Sci.* **2007**, *104*, 6908–6914.

¹²⁶ A. Sajjad, P. Schwerdtfeger, J. Harrison, A. J. Nielson, *Eur. J. Inorg. Chem.* **2017**, *46*, 5485 - 5496

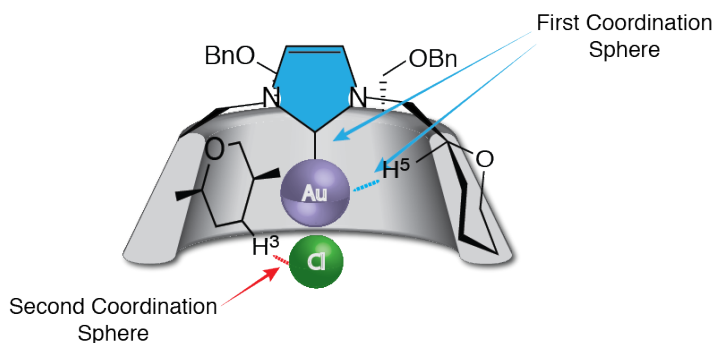


Figure II-24: First and second coordination spheres on (ICyD)MCl complexes.

3. Catalytic applications: Cavity controlled selectivity

As demonstrated in the introduction, encapsulation of a metal complex inside a cavity confers him with unusual catalytic properties, and in particular, allows to envisage specific selectivities. In the case of ICyD ligands, very different structures have been determined for α and β cyclodextrins. It was therefore of great interest to test if these different cavities could induce different selectivities in a catalytic reaction and if these selectivities could be rationalized in terms of the different shapes.

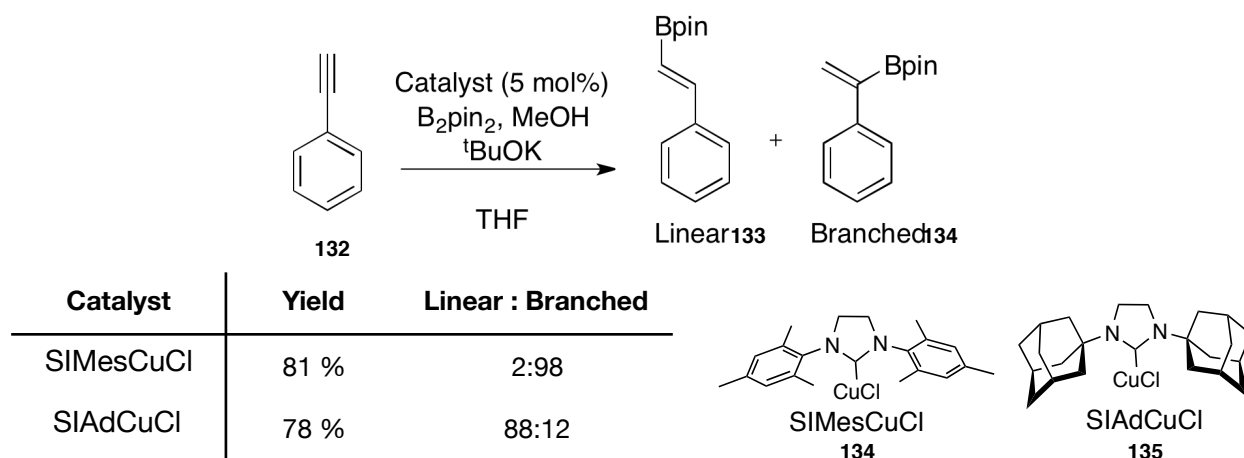
Three different selectivities were therefore studied: First, a regioselective reaction was studied with (ICyD)CuCl complexes and finally, the enantioselectivity and product distribution were studied using (ICyD)AuCl complexes.

i. Regioselectivity: Hydroboration of alkynes

The ability to induce regioselective reactions of this family of complexes was tested in a catalytic hydroboration of triple bonds.⁵⁶ In this work, the regioselectivity of a copper-catalyzed hydroboration reaction is only depending on the size and shape of the (α -ICyD)CuCl or (β -ICyD)CuCl cavity.

Hoveyda's original work on this copper-catalyzed reaction showed that the selectivity depends on the substitution of the nitrogens on the NHC. N-Alkyl-substituted NHC such as (SIAd)CuCl give the linear (*E*) **133** since N-aryl-substituted NHCs such as (SIMes)CuCl give the branched **134** (Scheme II-12).¹²⁷

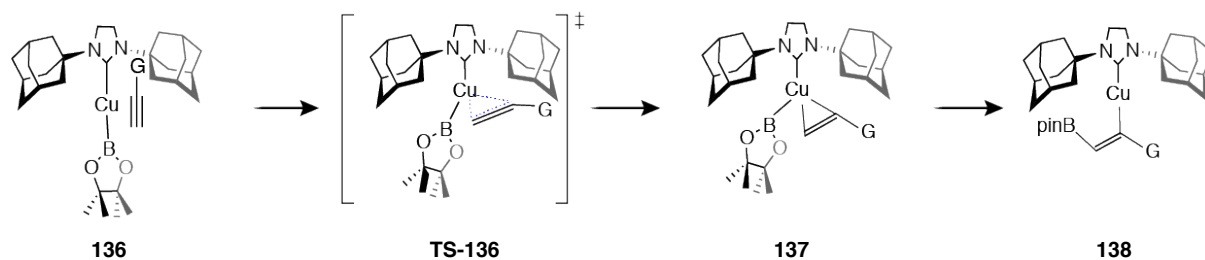
¹²⁷ H. Jang, A. R. Zhugralin, Y. Lee, A. H. Hoveyda, *J. Am. Chem. Soc.*, **2011**, *133*, 7859 – 7871



Scheme II-12: Original copper catalyzed hydroboration of alkynes.

DFT calculations showed that the regio-determining step is the insertion of the Cu-Bpin complex in the triple bond, more precisely, the approach of the triple bond to the complex **136**. It was proven that strongly donating alkyl-substituted NHC such as SIAdCuCl, due to electronic parameters favors the approach of the terminal carbon of the triple bond parallel with the substituent G *cis* to the NHC. Thus, the insertion of the copper is done in the terminal carbon of the alkyne, forming the vinyl-copper complex **138** that after protodemetalation gives the linear hydroborated compound **133** (Scheme II-13).

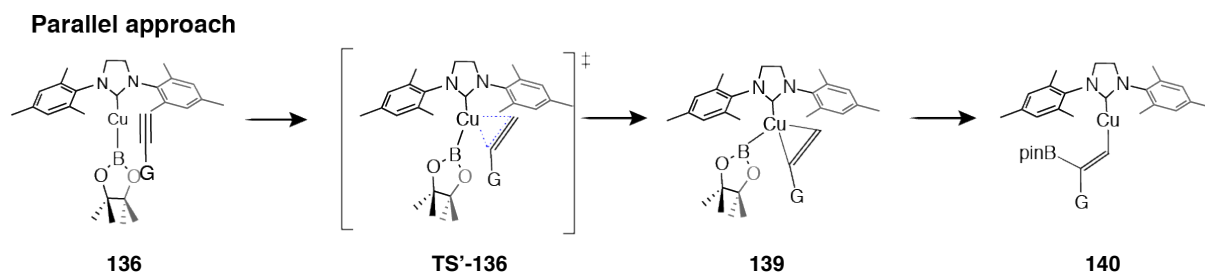
Parallel approach



Electronically driven: Less hindered and electron-rich NHC

Scheme II-13: Proposed mechanism of the regiodeterminant step of (SIAd)CuCl ligands.

In contrast, less electron-rich but more hindered aromatic-substituted NHC as SIMesCuCl, due to stereo-electronic parameters, forces the terminal carbon of the triple bond to be *trans* to the NHC, favoring now the approach of the internal carbon of the triple bond closer to the copper forming the vinyl-copper complex **140** that after protodemetalation forms the branched compound (Scheme II-14).

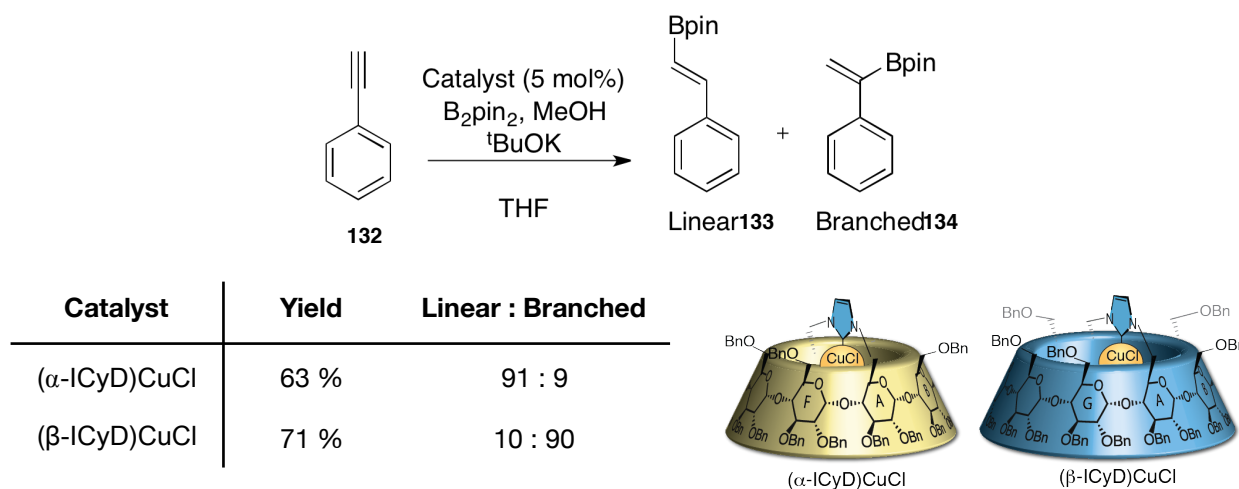


Stereo-electronically driven: More hindered and less electron-rich NHC

Scheme II-14: Proposed mechanism of the regiodeterminant step of (SIMes)CuCl ligands.

Hence, the contrast of the regioselectivity is mainly governed by electronic factors in this case. That is why it was interesting to study the differences of selectivity imposed by the α -cyclodextrin cavity, and the β -cyclodextrin NHC complexes, which would be purely steric.

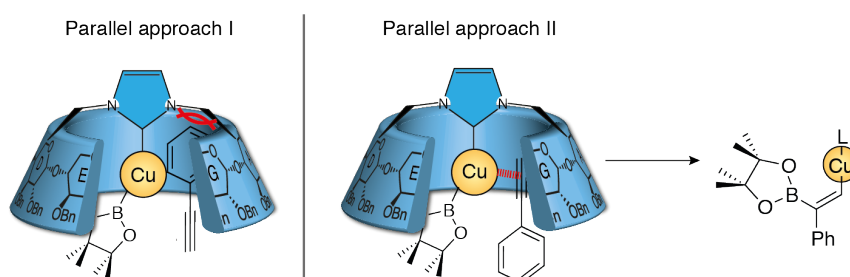
In the case of (α -ICyD)CuCl,^[ref] performing the reaction in the same conditions revealed that, as expected, an electron-rich, alkyl-substituted NHC affords the linear regioisomer as the major one. In contrast, (β -ICyD)CuCl, while being also alkyl-substituted NHC affords surprisingly the branched regioisomer with similar yields in both cases (Scheme II-15).



Scheme II-15: ICyD-catalyzed hydroboration of alkynes

As these two NHCs are both alkyl-substituted, the electronics of the ligand cannot account for this difference in selectivity. In addition, in contrast to Hoveyda's observation, the most hindered complex was the one that gave the linear compound and the less sterically demanding the one that formed the branched one.

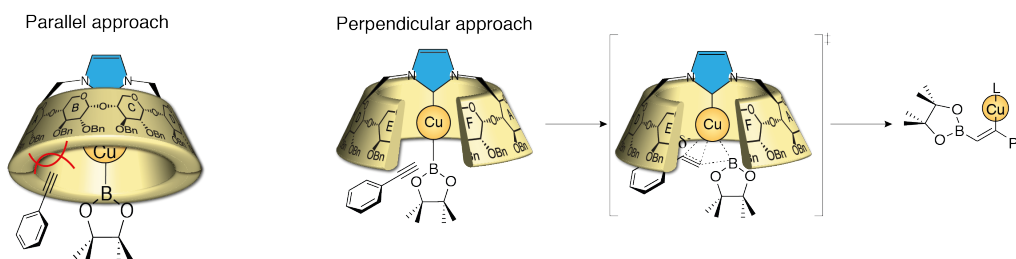
DFT calculations were performed to understand the effect of the cavity on this opposite selectivity. In fact, if the aryl of the phenylacetylene enters into the cavity first (Scheme II-16, parallel approach I) the steric hindrance imposed by the cavity prevents the access of the copper by the triple bond. The only way for the triple bond to reach the metal is to enter as in the parallel approach II. In this case, the steric hindrance imposed by the cavity overrules the electronics of the ligand, reversing the approach compared to the alkyl-functionalised (SIAd)CuCl described by Hoveyda.¹²⁹



Scheme II-16 : Two parallel approaches for phenylacetylene to the (β -ICyD)CuBpin complex

The case of the (α -ICyD)CuCl is completely different. The smaller cavity of the (α -ICyD) wraps the metal with the walls of the cyclodextrin. Therefore, a parallel approach to form the π -complex with the alkyne is not possible (Scheme II-17-parallel approach). However, DFT calculations showed another possible route for the mechanistic pathway which is not a parallel approach anymore but a perpendicular to the Cu-B bond.

Furthermore, the regioselectivity is likely to be governed by the development of a partial negative charge in the transition state stabilized by the phenyl ring at the benzylic position.¹²⁸



Scheme II-17: Parallel and perpendicular approaches of phenylacetylene to the (α -ICyD)CuBpin

¹²⁸ J. H. Moon, H.-Y. Jung, Y. J. Lee, S. W. Lee, J. Yun, J. Y. Lee, *Organometallics* **2015**, *34*, 2151 - 2159

In addition, in this work it was also proved, in contrast to many other confined space catalysts,[ref] that both systems could be used in a broad scope of substrates. In the case of (α -ICyD)CuCl in any case, the selectivity of the reaction (Linear : Branched < 85 :15) was not altered by the electronic or the steric modifications on the aromatic ring. In the case of the (β -ICyD)CuCl, the selectivity of the reaction was only disturbed by the steric hindrance on the *ortho* substitution, while the electronics of the aromatic ring produced negligible changes on the selectivity (Table II-5).

Catalyst (5 mol%)
B₂pin₂, MeOH
tBuOK
THF

Linear + Branched

Catalyst	Substitution	R = OMe	R = Me	R = Cl	R = F	R = CF ₃
(α-ICyD)CuCl	<i>ortho</i> -	55% (93 : 7)	49% (92 : 8)	68% (94 : 6)	68% (94 : 6)	55% (91 : 9)
	<i>meta</i> -	71% (94 : 6)	48% (93 : 7)	70% (97 : 3)	70% (97 : 3)	63% (86 : 14)
	<i>para</i> -	67% (91 : 9)	39% (93 : 7)	61% (95 : 5)	48% (86 : 14)	64% (98 : 2)
(β-ICyD)CuCl	<i>ortho</i> -	64% (46 : 54)	74% (19 : 81)	68% (9 : 91)	67% (7 : 93)	44% (10 : 90)
	<i>meta</i> -	82% (12 : 88)	78% (14 : 86)	40% (6 : 94)	48% (4 : 96)	48% (4 : 96)
	<i>para</i> -	87% (10 : 90)	66% (8 : 92)	25% (9 : 91)	65% (7 : 93)	44% (10 : 90)

Table II-5: Scope of the (ICyD)CuCl catalyzed reaction. Linear : Branched ratio is reported in brackets

Conclusion:

In this example, the value of (ICyD)CuCl complexes has been demonstrated by a catalytic regioselective reaction. This regioselectivity was proved to be directly linked to the shape of the cavity. It was confirmed that using the (α -ICyD)CuCl complex, the regioselectivity obtained is the same that the one already described in the literature. However, DFT calculations proved that the steric hindrance brought by the cavity produces a switch in the mechanism from a parallel to a perpendicular approach.

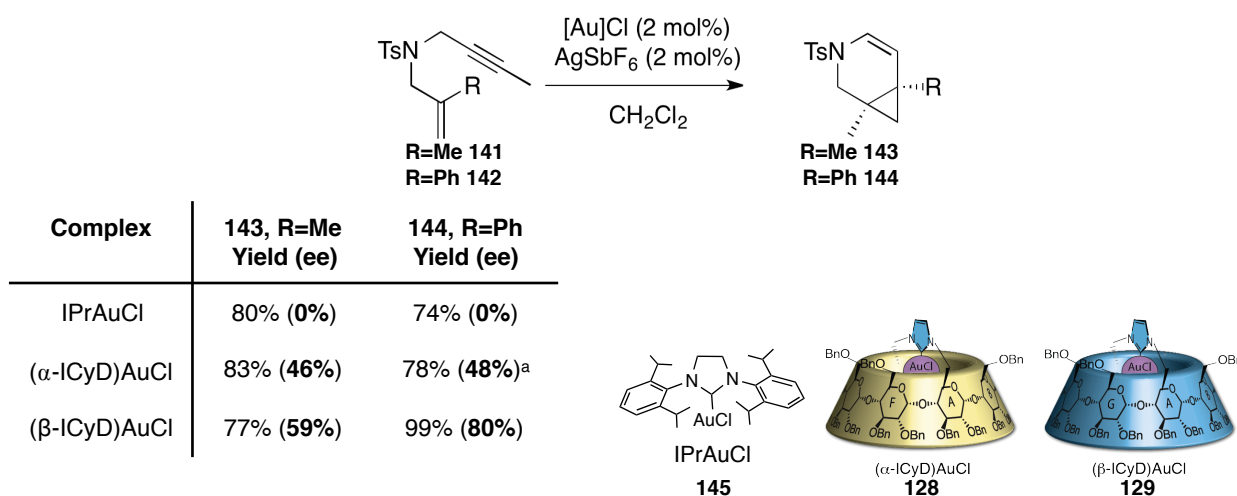
In contrast, using (β -ICyD)CuCl complex, the obtained regioselectivity was inverted, affording now the opposite regioisomer but with a usual parallel mechanism. Therefore, passing from α to β ICyD induces a mechanistic switch in this hydroboration reaction.

In addition, a broad scope of substrates has been studied, proving the efficiency of this system in a laboratory-scale methodology. This methodological application remains exceptional in the case of supramolecular complexes.

ii. Enantioselectivity: Enyne-cycloisomerisation

Due to the linear coordination of gold (I), in addition of a outer-sphere nucleophilic attack, chirality transfer from the ligand to the substrate is the main limitation on the development of gold catalyzed enantioselective reactions. (ICyD)AuCl compounds are perfect candidates in the field thanks to the chiral wrapping of the gold atom. Hence, in collaboration with Pr. Fensterbank's group, it was shown that (α -ICyD)AuCl and (β -ICyD)AuCl could be used as catalysts in classical enyne-cycloisomerisations.⁶² Using AgSbF₆ and (α -ICyD)AuCl with the enyne **141**, the cycloisomerization product **143** is obtained in a 83% yield with 46% enantiomeric excess (ee). The same substrate using (β -ICyD)AuCl and the same silver salt, affords the same product in 77% yield and 59% ee (Scheme II-18).

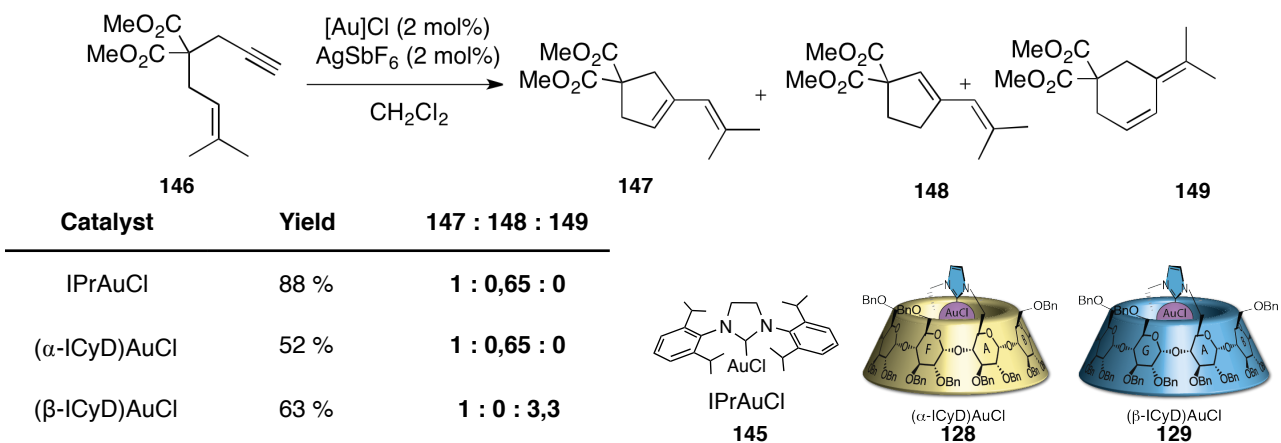
In the case of enyne **142**, (α -ICyD)AuCl forms the cycloisomerization product **144** in 78% yield and 48% ee, while (β -ICyD)AuCl also gives the same product in almost quantitative yields and 80% ee, which represents an excellent ee in gold (I) chemistry. By comparing to the IPrAuCl, used as model complex for this reaction, it is worth noting that both complexes perform the reaction without any loss of yield or, in some cases, even better, proving the value of these ligands in catalytic reactions.



Scheme II-18: (ICyD)AuCl enantioselective cycloisomerisation of N-tethered enynes. ^aReaction performed at 40 °C.

iii. Product distribution: Enyne-cycloisomerisation

In the supramolecular catalysis field, it is sometimes possible to obtain a new product not formed when using the model catalyst.⁷⁹ In this example, using IPrAuCl complex **145**, the enyne **146** gives the cyclopentenenes **147** and **148** in a 1 : 0,65 ratio. Same results are obtained by using (α -ICyD)AuCl. Nevertheless, when the (β -ICyD)AuCl complex is used as catalyst, no traces of **148** are observed, and the major compound is now a formal 6-endo cycloisomerisation cyclohexene **149**. (Scheme II-19)



Scheme II-19: Product distribution in (ICyD)AuCl catalyzed cycloisomerisation of enynes.

E. Conclusion and perspectives

With these examples, the value of the NHC-capped cyclodextrin metal complexes as ligands for laboratory scale regio- and enantioselective methods has been demonstrated.

Nevertheless, for the gold (I) complexes, a dependence on the cavity size is observed, bigger β -cyclodextrin derivatives gave in both reactions better enantiomeric excesses, and better substrate selection. These results are obtained just by adding one sugar unit in one of the loops of the macrocycle.

The remaining question is, can we synthesize even bigger analogues based on γ -cyclodextrin, and by using more distorted macrocycles improve even more the performances of this systems? (figure) This question is the starting point of this dissertation.

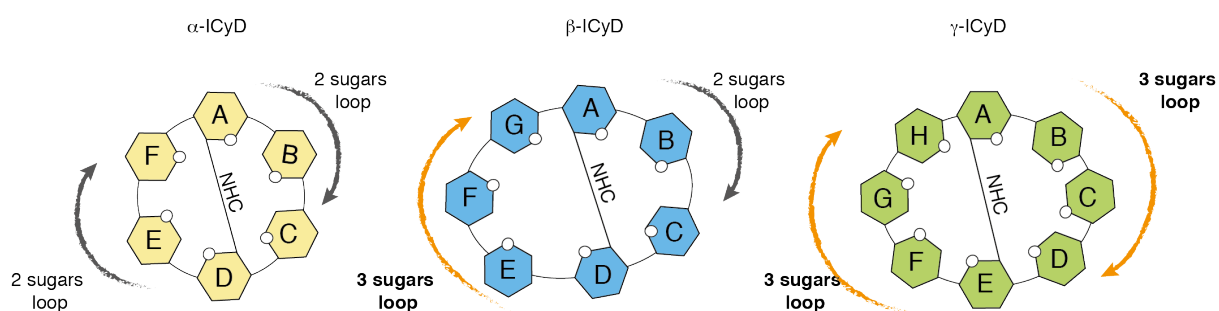


Figure II-23: Schematic representations of the α , β and γ NHC-capped cyclodextrins. View from the secondary rim.

Hence, my PhD work starts with the synthesis, characterization and three-dimensional elucidation of the (γ -ICyD)AuCl to further study how the distortion and the cavity size and shape can change the effects of the second coordination sphere in the previously described enyne cycloisomerisation.

CHAPTER III

Synthesis and study of ICyD metal complexes

CHAPTER III: Synthesis and study of ICyD metal complexes

A. Increasing the size of the cyclodextrin

As proposed in chapter II, the study of γ -cyclodextrin-based metal complexes, characterized by a larger CD core, would be of interest to better understand the effect of the second coordination sphere in catalytic applications. To obtain the desired (γ -ICyD)AuCl complexes, a synthetic route similar to the one developed for the smaller α and β CD analogues has been considered.

1. Linear coordination in gamma cyclodextrin : (γ -ICyD)AuCl

i. Synthesis

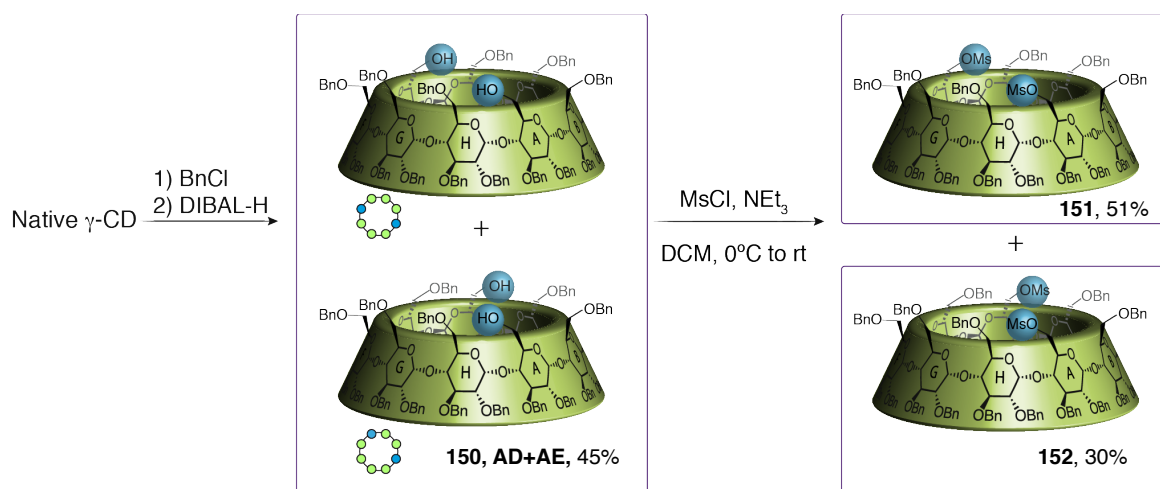
Starting from native γ -cyclodextrin, full protection in the presence of benzyl chloride and sodium hydride afforded the perbenzylated γ -cyclodextrin in quantitative yield. Next, the DIBAL-H mediated strategy for selective deprotection of perbenzylated cyclodextrins was applied.¹²⁹

However, the deprotection with DIBAL-H was found to be less selective than with α and β cyclodextrins, leading to a mixture of two non-separable AE (symmetrical) and AD (non-symmetrical) isomers. Previous studies in the laboratory already showed that the AE/AD selectivity is low and strongly dependent on the concentration of DIBAL-H and temperature¹³⁰. In this work, the reaction was performed at 60 °C with 20 equivalents of DIBAL-H (1M in the medium) to afford a 1 : 1 mixture of non-separable AD and AE diols in 45% yield.

Treatment of the mixture with mesyl chloride and NEt₃ gave the bis-mesylated derivatives. At this stage, the separation was performed by silica gel flash chromatography affording 51% of the pure AE isomer, 30% of the AD isomer and a 19% of mixture of both (Scheme III-1).

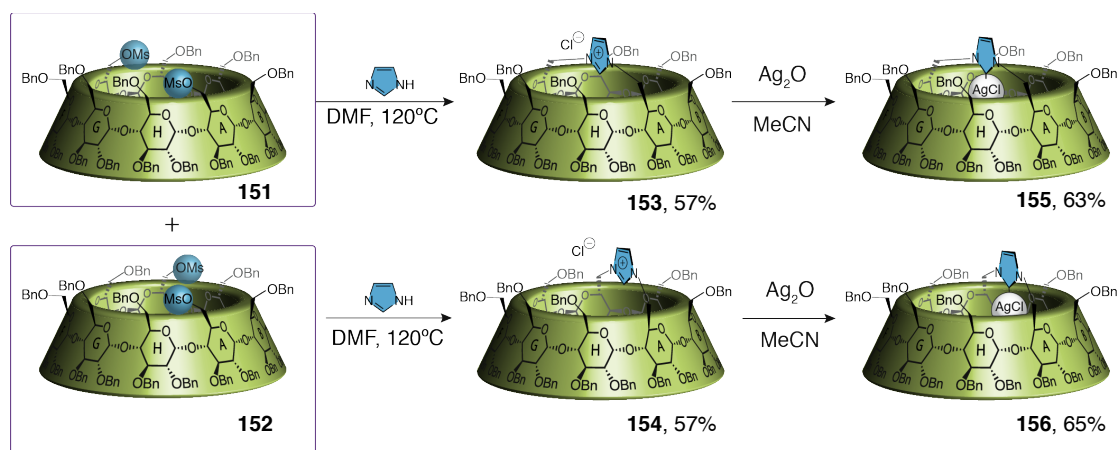
¹²⁹ T. Lecourt, A. Herault, A. J. Pearce, M. Sollogoub, P. Sinay, *Chem. Eur. J.* **2004**, *10*, 2960 - 2971

¹³⁰ P. Zhang, Cyclodextrin-(N-Heterocyclic Carbene)-Metal Complexes for Cavity-Dependent Catalysis, PhD dissertation, Université Pierre et Marie Curie, Paris, France, **2015**.



Scheme III-1: Synthesis of both regioisomers of γ -CD(OMs)₂

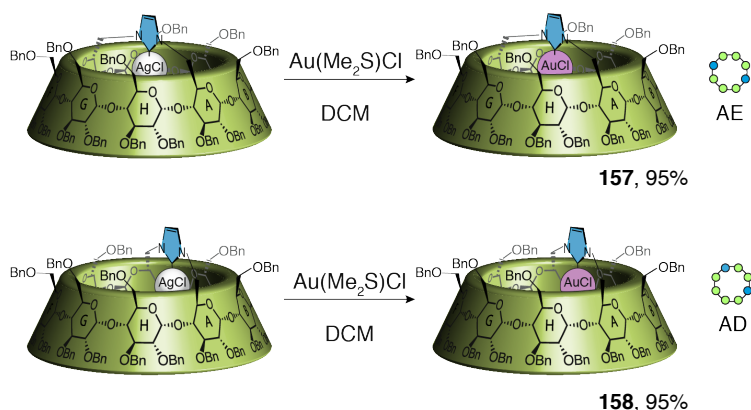
As for α - and β - cyclodextrins, the reaction of the γ -CD(OMs)₂ compounds with an excess of imidazole at 120 °C in DMF afforded the azolium-capped salt in 57% and 40% yield for the symmetrical (AE, **153**) or non-symmetrical (AD, **154**) isomer, respectively (scheme III-2). A final metalation with silver oxide gave the (γ -ICyD)AgCl complex with an overall yield of 8% for the AE (symmetrical) isomer **155** and 3% for the AD (non-symmetrical) isomer **156** over 6 steps.



Scheme III-2: Synthesis of (γ -ICyD)AgCl complexes **155** and **156**

To obtain the desired (γ -ICyD)AuCl complexes, transmetalation of the silver precursor was considered. After optimization, the reaction was carried out with one equivalent of Au(Me₂S)Cl in dichloromethane,¹³¹ affording the expected (γ -ICyD)AuCl in 95% yield for both isomers (Scheme III-3).

¹³¹ S. Gaillard, A. M. Z. Slawin, A. T. Bonura, E. D. Stevens, S. P. Nolan *Organometallics* **2010**, *29*, 394–402



Scheme III-3: Transmetalation conditions to obtain (γ -ICyD)AuCl

ii. Characterization

The reactivity of a catalytic system is intrinsically dependent on the electronics and the steric environment around the metal. Therefore, the three-dimensional structures of the (γ -ICyD)AuCl complexes must be elucidated. Because of the difficulty to get monocrystals suitable for X-ray analysis with CD-benzylated derivatives, the structures of the ICyD-metal complexes were analyzed by NMR.¹³⁴ For clarity, because of the C_2 symmetry of the AE isomer, the analysis and the methodology to elucidate the 3D structures will be shown first for the (γ -AE-ICyD)AuCl complex, and then for the most complex the non-symmetrical (γ -AD-ICyD)AuCl.

- (γ -AE-ICyD)AuCl

The general method to obtain the structure of (γ -ICyD)AuCl **157** required first the attribution of all the protons of each sugar unit. The attribution of each proton of each sugar unit was made following the COSY and TOCSY correlations. The carbons attached to each proton were found with the HSQC spectrum. Then, the order of attachment of each sugar unit in the CD was deduced from the NOESY and HMBC experiments (see the experimental part for a detailed attribution). The coordination of the metal, as well as the nature of the complex, was characterized by the chemical shift of the carbene. Then, a study of shielding and deshielding of the intra-cavity protons (H5 and H3) was done in order to relate the chemical shifts to relative distances between the different sugar units and the gold and chloride atoms. Finally, with these relative distances, the sugars were tilted and arranged on the macrocycle skeleton to build a three-dimensional model of the complex.

The complexation of gold was verified by HMBC (Figure III-1). An unambiguous cross correlation peak was observed between the C-H of the NHC ring and the quaternary carbene. For the (γ -AE-ICyD)AuCl complex studied here, the observed chemical shift of the ^{13}C at 172.2 ppm of the carbene is consistent with the literature and confirms the presence of a NHC-AuCl complex.¹³¹

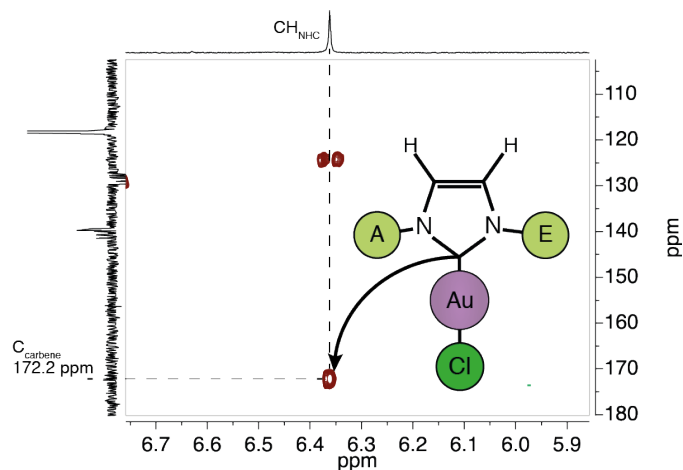


FIGURE III-1 : HMBC of (γ -ICyD)AuCl **157** showing the chemical shift of the C_{carbene} .
 CD_3CN , 400 MHz, 300 K

The position of the AuCl moiety inside the cavity was first demonstrated by NOE cross-correlations between the CH of the NHC ring and protons of the position 6 of the sugars of the cyclodextrin (Figure III-2). 2D-NOESY, stacked with HSQC of the complex, shows two clear cross correlations: An intense one with one of the diastereotopic H6 protons from the AE sugar units and a less intense one with one of the diastereotopic protons of the BF sugar units, confirming the introversion of the complex.

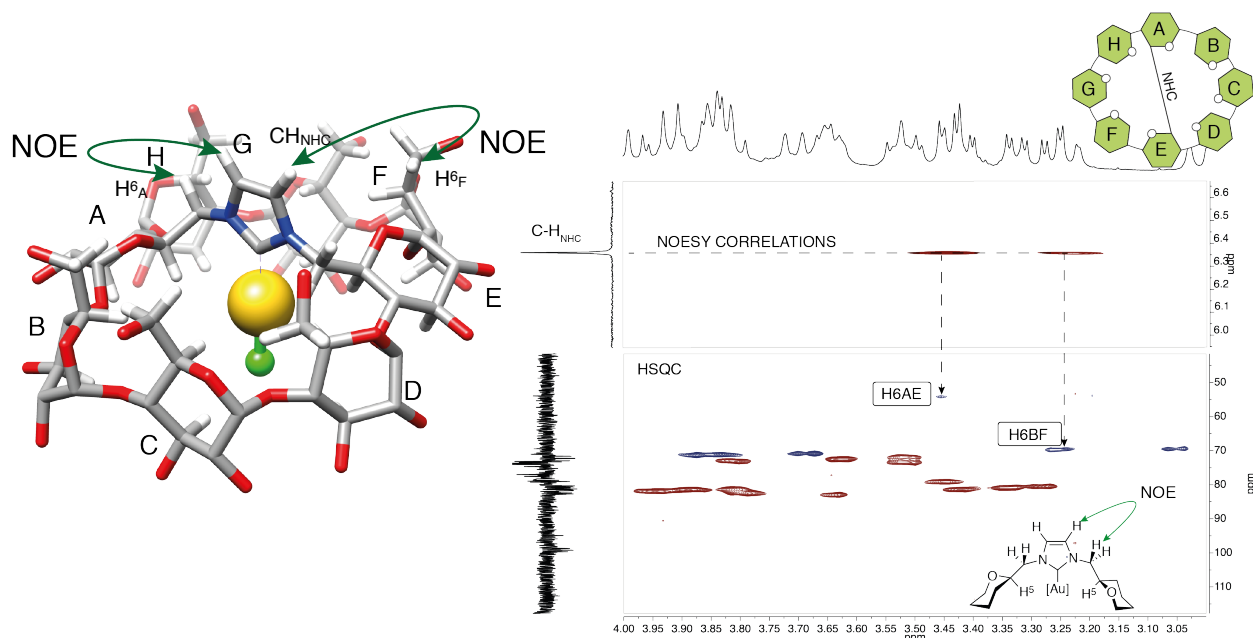


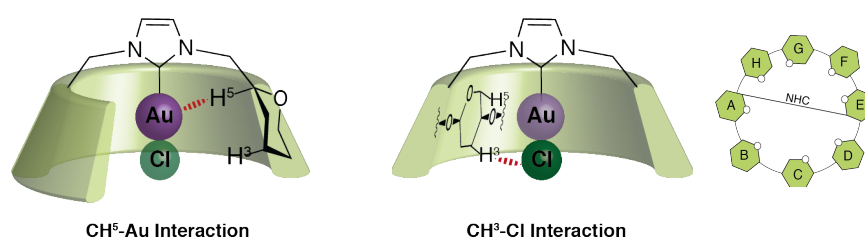
Figure III-2: NOESY (top) and HSQC (bottom) of (γ -AE-ICyD)AuCl **157** complex showing cross-correlations between the C-H of the imidazole and two H6.
 CD_3CN , 600 MHz, 300K

The chemical shifts of the intra-cavity protons (H5 and H3) are also used as proofs for the position of the complex. $\delta(\text{H3})$ and $\delta(\text{H5})$ of $(\gamma\text{-ICyD})\text{HCl}$, $(\gamma\text{-ICyD})\text{AgCl}$ and $(\gamma\text{-ICyD})\text{AuCl}$ are compiled in Table III-1. By comparison of the chemical shifts on the H5 of the metal complexes with its precursor, a downfield shift of 0.33 ppm for the H5-AE is observed between the silver complex and the azolium precursor. As for α - and β -ICyD complexes presented previously, this deshielding is symptomatic of a proximity between this proton and the silver atom.

In addition, the same H5 is deshielded by another +0.13 ppm in the case of the gold analogue. This trend, produced by an enrichment of the metal, confirms the position of the metal inside the cavity.

Looking now at the chemical shifts of the H3, two pairs of sugar units are affected by a deshielding of its protons. By comparison of the chemical shifts of the H3 of the metal complexes and the azolium salt, H3 of cycles C and G are deshielded by +0.28 ppm for the Ag^{I} complex and by +0.21 ppm for the Au^{I} complex. In addition, H3 of sugar units DH are also deshielded by +0.12 ppm and +0.15 ppm for the Ag^{I} and the Au^{I} complexes, respectively

When comparing the trends on the H5-AE chemical shifts for the Ag^{I} and Au^{I} with its azolium precursor, a dependance of the chemical shift on the metal can be observed, even if the effect is less important than the one observed for $(\alpha\text{-ICyD})\text{MCl}$, presented in last chapter. On the other hand, the downfield shift of the H3 remains close for both analogues. This confirms that as for α -CD and β -CD analogues, the H5 are at the same level than the metal, and the H3 at the same level than the chlorine.



Sugar unit	A/E		B/F		C/G		D/H	
	H5	H3	H5	H3	H5	H3	H5	H3
$(\gamma\text{-ICyD})\text{HCl}$	3.84	3.93	3.80	3.79	3.58	3.89	3.80	3.96
$(\gamma\text{-ICyD})\text{AgCl}$	4.17 (+0.33)	3.97	3.62	3.97	3.79	4.17 (+0.28)	3.62	4.08 (+0.12)
$(\gamma\text{-ICyD})\text{AuCl}$	4.30 (+0.46)	3.95	3.52	3.90	3.81	4.10 (+0.21)	3.52	4.11 (+0.15)

Table III-1: Chemical shift differences of the intra-cavity H3 and H5 protons of $(\gamma\text{-ICyD})\text{HCl}$ **153**, $(\gamma\text{-ICyD})\text{AgCl}$ **155** and $(\gamma\text{-ICyD})\text{AuCl}$ **157**
 CD_3CN , 600 MHz, 300 K

With all these chemical shifts and interactions deduced from the NMR data in mind, a relative proximity of each H5 and H3 proton with the metal and halogen centers can be established and modeled structures can be proposed. Models of the structures have been done with Avogadro starting from the crystal structure of the native γ -cyclodextrin. Then the NHC-bridge and metal complex are placed with the metal atom at the same height as the H5 and the chlorine atom at the same level as the H3. Then, the system is optimized by reducing the energy with the UFF force field. Finally, sugars are arranged following the distances deduced from the NMR. The construction of the models has been done by removing all the benzyl groups from the molecule to avoid a possible ambiguity due to flexible substituents.

For the (γ -AE-ICyD)AuCl complex, the relative H-5...metal distances are ordered depending on their proton NMR chemical shifts, being shorter for the most deshielded ones. The order deduced is then: first AE sugar units, followed by CG and DH cycles, and finally the farthest BF units.

Following then the same reasoning for the H3, we hypothesized that H3 of CG and DF units are the closest to the chlorine atom, followed by those of the AE and the BF units. Placing and tilting then the sugar units according to this criteria gave the modeled structures shown in figure III.3.

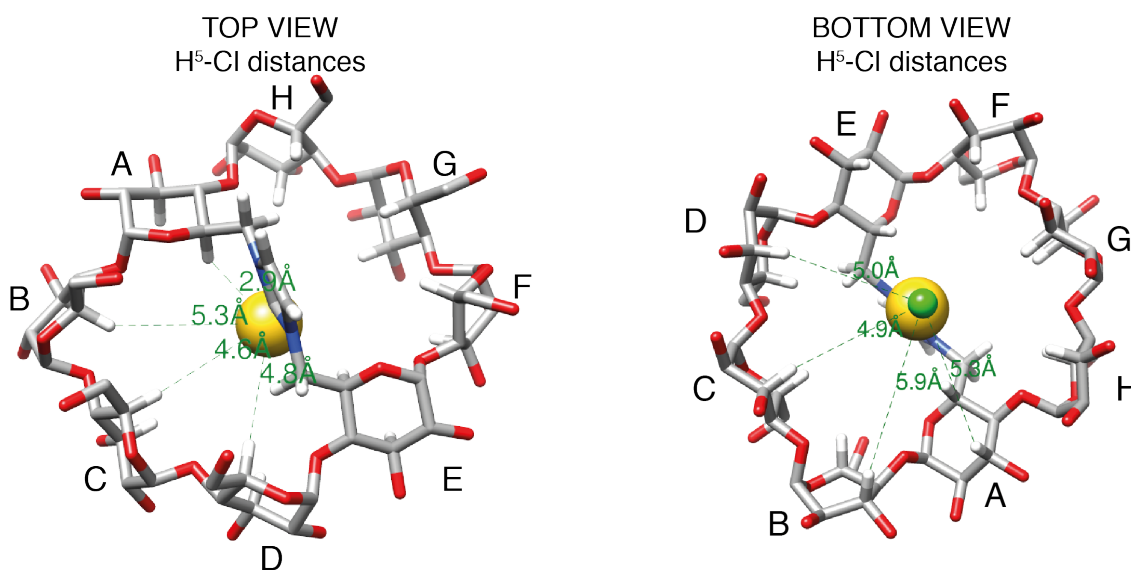


FIGURE III-3: Top and bottom views of modeled (γ -ICyD)AuCl. H⁵...Au (left) and H³...Cl (right) distances are shown in the structures.

A distortion of the macrocycle and important tilts of the C and D units are clearly observed in the modeled structures. Distances ranging from 2.9 to 5.3 Å are observed for the H5 and the Au atom, and distances between 4.9 and 5.9 Å for the H3 and the chlorido ligand. Due to the complexity of the NMR data, the elucidation of the (γ -AD-ICyD)AuCl complex was directly done on the gold (I) complex, following the same procedure as the one showed for its symmetrical analogue.

- (γ -AD-ICyD)AuCl

The non-symmetrical bridging of the (γ -AD-ICyD)AuCl **158** leads to a C_1 symmetry, verified by the presence of eight characteristic anomeric signals on the C1-H1 region of the HSQC, as well as for the presence of 2 cross correlation peaks of the CH of the NHC. (Figure III-4).

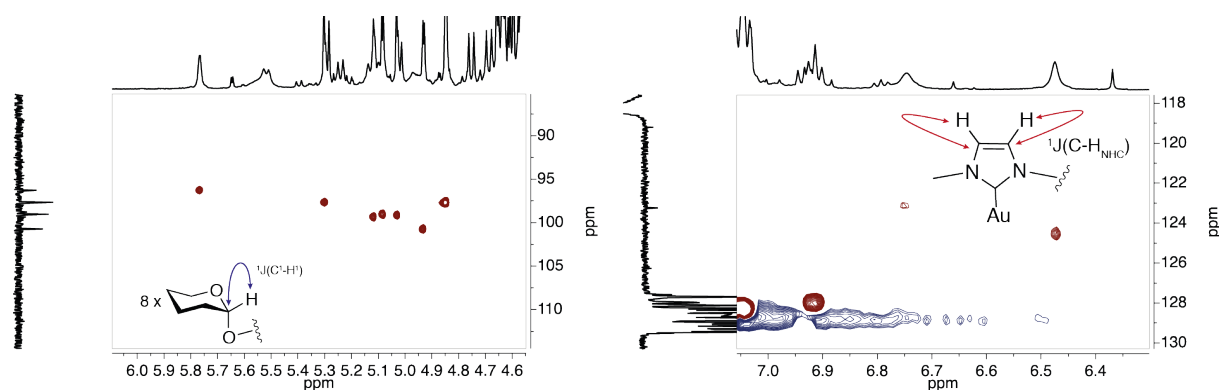


Figure III-4: HSQC of the anomeric (left) and NHC (right) of (γ -AD-ICyD)AuCl. CD₃CN, 600 MHz, 300 K

As for its symmetrical analogue, the introverted coordination of the gold center was determined by the presence of cross correlation peaks between the CH of the NHC and the both H6 of both A and D sugar units.(Figure III-4)

The analysis of all the NMR experiments and attribution of all the signals of the proton NMR was performed as previously. The chemical shifts of the intra-cavity protons of this complex are reported on the table III-2.

	A	B	C	D	E	F	G	H
H5	4.19	3.96	3.72	4.34	3.75	3.80	3.80	4.19
H3	3.86	4.18	4.36	4.01	3.90	3.90	3.90	3.94

Table III-2: chemical shifts of the H5 and H3 of (γ -AD-ICyD)AuCl. CD₃CN, 600 MHz, 300 K

As for its symmetrical analogue the downfield shifts of the different H5 and H3 could be related to the relative distances between the H5 and the gold atom, and the H3 and the chloride atom. The closest H5 were thus, H5A, H5D and H5H, and the closest H3, H3B and H3C. With these informations, an approximated model of the (γ -AD-ICyD)AuCl was constructed following the same steps as for the γ -AE analogue (Figure III-5).

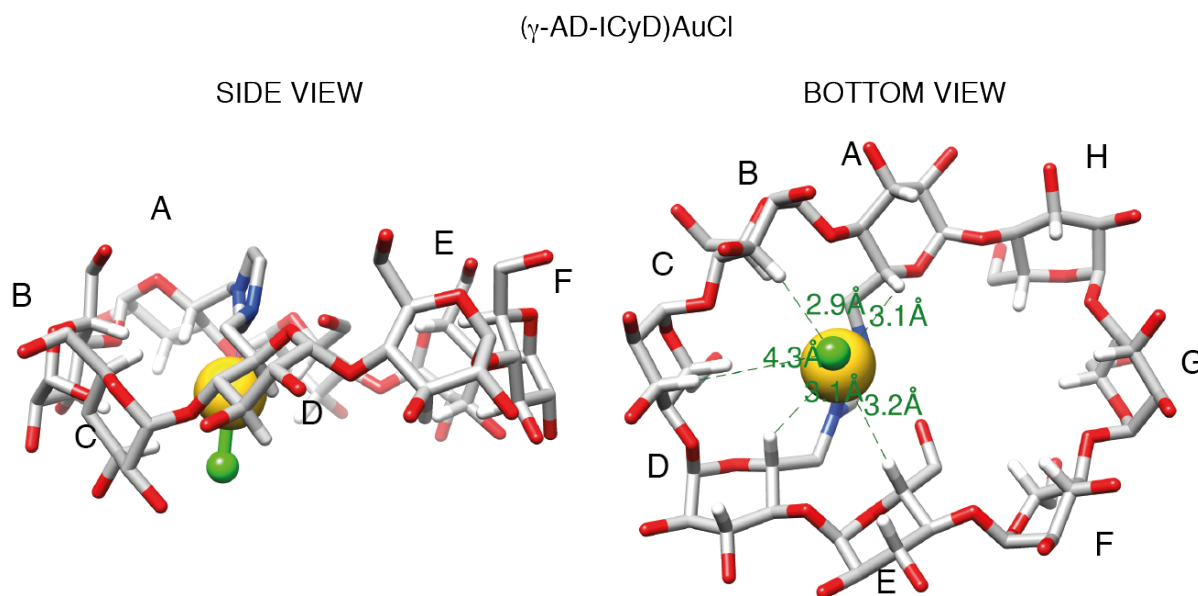


Figure II-5: Modeled structure of (γ -AD-ICyD)AuCl.

iii. Comparison of (γ -ICyD)AuCl shape with that of β and α -CD-derived complexes

For future rationalization of the properties of the metal center inside the cavity and to better understand the impact of the second coordination sphere, Connolly's surfaces have been built for the four α -, β -, and γ -AD and γ -AE gold derivatives (Figure III-6). Connolly's surfaces are three-dimensional contours around molecules that show the atoms accessible to the solvent molecules.¹³²

(α -ICyD)AuCl possesses a C₂ - symmetrical shape, where the gold atom is completely wrapped by the inner walls of the cyclodextrin. The symmetrical bridge between the sugar units A and D (sugar units bearing the bridge) produced a tilt of these sugar units and a groove through the entrance of the cavity. In addition, an important steric hindrance afforded by the proximity of the cycles C and F is observed around the gold atom (represented in red).

The addition of one sugar unit on one of the loops of the (β -ICyD)AuCl analogue produces a loss of the symmetry of the shape. As for the narrowest analogue the NHC bridge of the CD macrocycle through A,D units generates two different macrocyclic subunits which differ in their size by only one glucose unit. The narrow side, containing B and C sugar units on the loop, is much closer from the metal, affording an steric hindrance around only one face of the gold atom. The other face of the gold atom is now sterically released thanks to the presence of one more one sugar unit in the larger macrocyclic loop (sugar units E,F and G). Additionally, a tilted coordination of the NHC-Au-Cl was observed.

The same tilted coordination of the NHC-Au-Cl was found on the non-symmetrical (γ -AD-ICyD)AuCl, in addition of a complete distorted form of the cyclodextrin skeleton. As for the (β -ICyD) analogue, the steric hindrance afforded by the smaller loop of the macrocycle (B,C sugar units) is also present. On the opposite side of the cyclodextrin, a distancing of the inner walls of the macrocycle was also found.

Finally, the (γ -AE-ICyD)AuCl showed a completely symmetrical shape, with the AuCl complex in the middle of the cavity. The presence of three sugar units on each loop of the macrocycle produced a complete release of the steric hindrance around the metal center without any interaction with the inner walls of the cyclodextrin core.

During the following studies, the effect of these different structures and shapes can influence different structural, electrochemical, and reactivity properties.

¹³² M. L. Connolly, *Science* **1983**, 221, 709 - 713

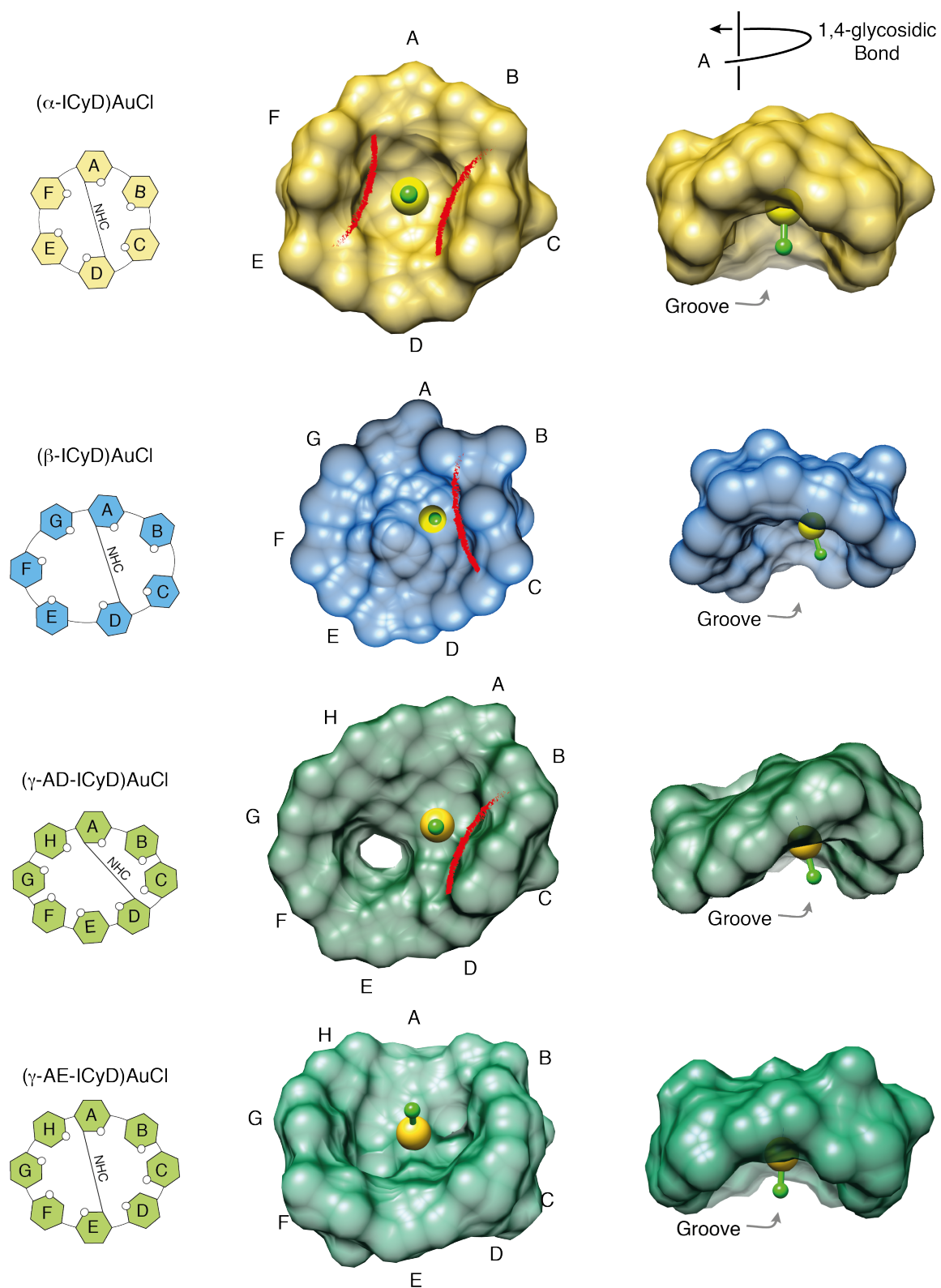


Figure III-6: Modeled Conolly's surfaces of $(\alpha\text{-ICyD})\text{AuCl}$, $(\beta\text{-ICyD})\text{AuCl}$, $(\gamma\text{-AD-ICyD})\text{AuCl}$ and $(\gamma\text{-AE-ICyD})\text{AuCl}$

B. Control of the metal position.

Confined versus non-confined gold (I) complexes

During the synthesis of (α -ICyD)AuCl and (β -ICyD)AuCl, a problem of reproducibility of the last transmetallation step of the synthesis was observed. The origin was the requirement of an excess of AuCl to push the equilibrium to completion. The excess of a strong Lewis acid, concentrated at the moment of the evaporation of the solvent produced a degradation of the cyclodextrin skeleton. Additional economical factors, such as the price of the salt and successive silica gel purifications to get rid of the excess of gold salts encouraged us to look for a better synthesis of the complexes. As discussed before, Au(Me₂S)Cl was used as transmetalating agent with (γ -ICyD)AgCl to get the desired Au(I) compound.¹³¹

The question is now, can we optimize the previous syntheses, affording better yields on higher scale? In this section, starting by a simple optimization of the previous reaction conditions, new synthetic procedures were developed affording new metal complexes and new coordination modes. In the following studies, the consequences of the confinement of the metal will be detailed.

1. Synthesis of AuCl complexes via the silver route.

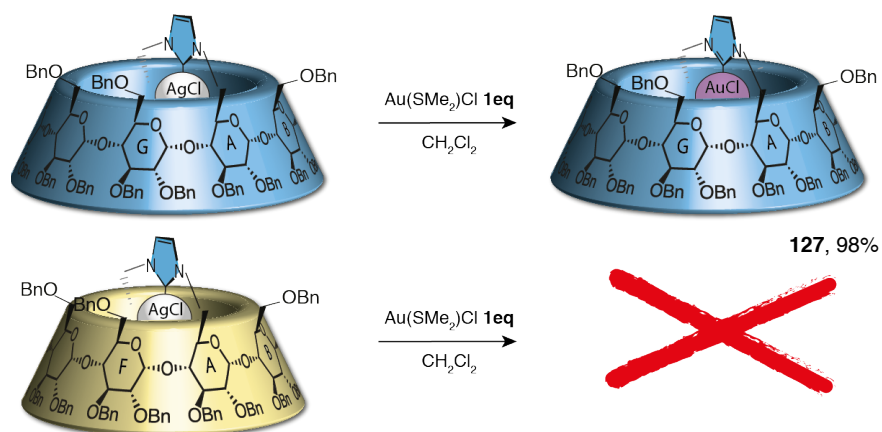
Comparison between α and β cyclodextrins

Based on the last step of (γ -ICyD)AuCl complex, the first tested conditions were the use of only one equivalent of Au(Me₂S)Cl.

Formation of (β -ICyD)AuCl was previously described by reaction of (β -ICyD)AgCl with 8 equivalents of AuCl affording at maximum 300 mg of the desired complex in 70% yield. Transmetalation with only one equivalent of Au(Me₂S)Cl in dichloromethane induce an instantaneous precipitation of AgCl salts and the formation of the desired (β -ICyD)AuCl complex in 98% yield carried out up to 1.7 g of product (Scheme III-4). However, the same reaction conditions in the case of the (α -ICyD)AuCl gave no conversion after 18h of reaction.

This result can be related to the shape of the cavity of the (α -ICyD)AuCl. The steric hindrance caused by the cavity, wrapping the whole silver atom may prevent a possible associative mechanism with Au(Me₂S)Cl to take place.

The following trials towards the optimization of the (α -ICyD)AuCl synthesis will be based on the use of the free carbene route in the synthesis of metal complexes.



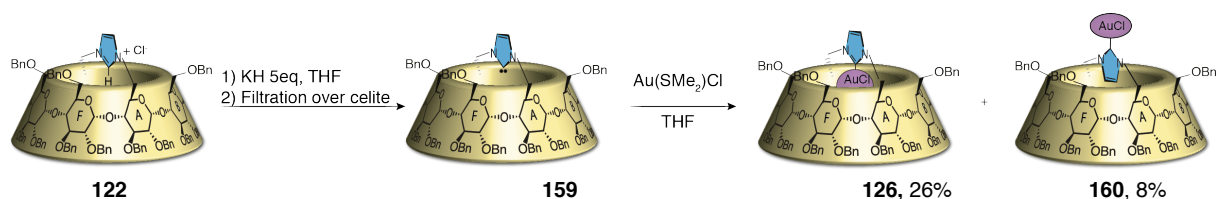
Scheme III-4: Formation of (ICyD)AuCl complexes via the silver route with Au(Me₂S)Cl

2. Synthesis of (ICyD)AuCl complexes via the free carbene route.

Comparison between α , β and γ cyclodextrin

Synthesis of free (α -ICyD) was previously optimized in the laboratory, showing that the best conditions to obtain the free carbene were by treatment of the azolium salt (α -ICyD)HCl with 5 equivalents of KH in THF. After a filtration over celite to remove the excess of KH and KCl, the free carbene (α -ICyD) **159** was obtained in quantitative yield (Scheme III-5)

Reaction of α -ICyD carbene with Au(Me₂S)Cl in THF affords a mixture of two complexes. Purification by silica gel, followed by preparative TLC led to the isolation of the expected (α -ICyD)AuCl **126** in a 26% yield. A second fraction containing a 23:77 ratio of (α -ICyD)AuCl and another compound having the same m/z value. This second complex was found to be an unprecedented isomer where the AuCl unit is coordinated via de normal NHC outside the cavity.



Scheme III-5: Reaction conditions of the formation of the free NHC and metallation with Au(SMe₂)Cl

¹H-NMR of the minor fraction containing a 23:77 mixture of both isomers is shown in Figure III-7. Characteristic signals of the (α -ICyD)AuCl complex were observed: The protons of the imidazole (highlighted in blue), the deshielded H-5A,D (in green) and the confirmed the presence of the (α -ICyD)AuCl as minor isomer. A deshielded proton for the (α -rev-ICyD)AuCl was observed at 7.7 ppm. By integration of the isolated imidazole protons of both complexes, the presence of the new compound in 77% of mixture is proved (Figure III-7).

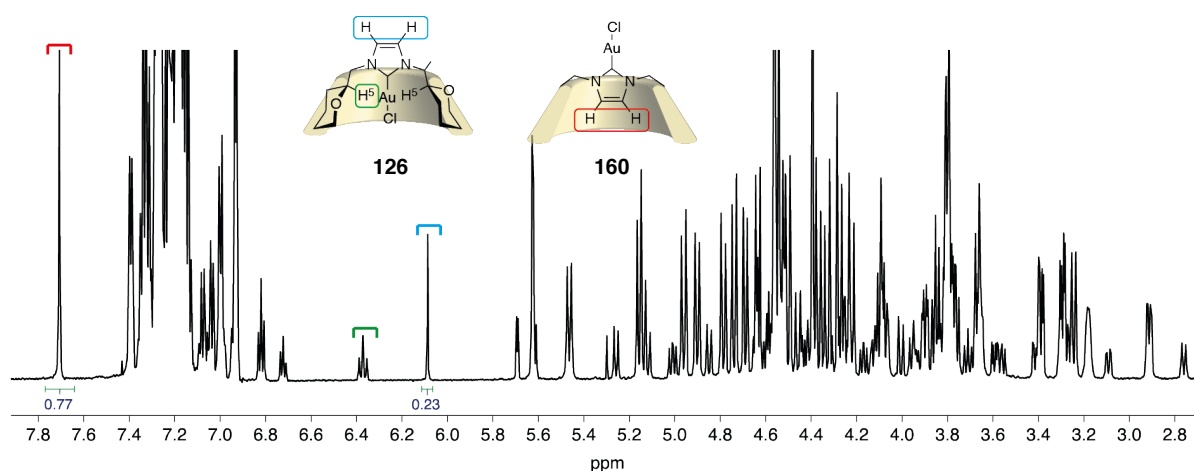


Figure III-7: $^1\text{H-NMR}$ of the mixture of compounds isolated after preparative TLC.
 CDCl_3 , 600 MHz, 300 K

As for all ICyDs due to the difficulty to obtain monocrystals, the structure of the major isomer of the mixture was elucidated through NMR analysis. The following presented NMR studies show that this compound is an unprecedented isomer where the gold atom is coordinated outside of the cavity, named as (α -rev-ICyD)AuCl.

Only two sets of three anomeric carbons are observed in the HSQC (Figure III-8). The three minor signals correspond to the previously described (α -ICyD)AuCl and the three major signals correspond to the new (α -rev-ICyD)AuCl. The presence of only three anomeric carbons indicates a C_2 symmetry for the entire molecule, excluding the possibility of an abnormal carbene.

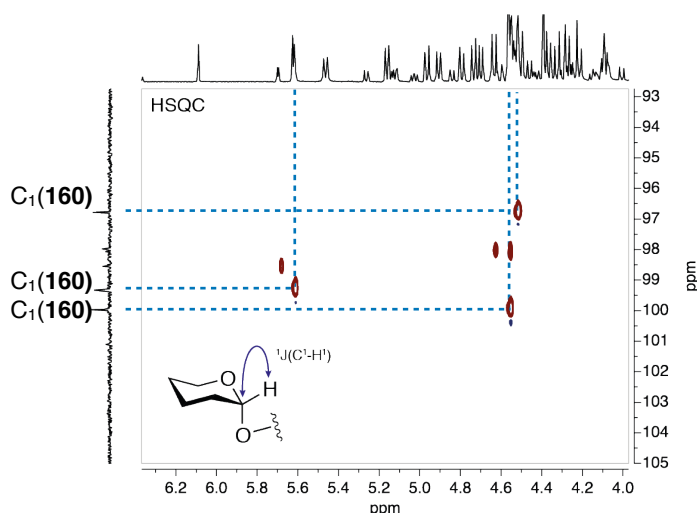


Figure III-8 : Extract of HSQC of the mixture showing two sets of three signals showing the C_2 symmetry.
 CDCl_3 , 600 MHz, 300K

For (α -rev-ICyD)AuCl, a cross-correlation peak is also observed between the proton at 7.7 ppm and a carbon at 120 ppm, confirming the presence of the imidazolyl moiety. This value is consistent with the chemical shift of the CH of normal NHC.¹³¹ Besides, the C₂ symmetry of the complex, observed also in the imidazolyl bridge, confirmed the normal-type coordination of the NHC (Figure III-9).

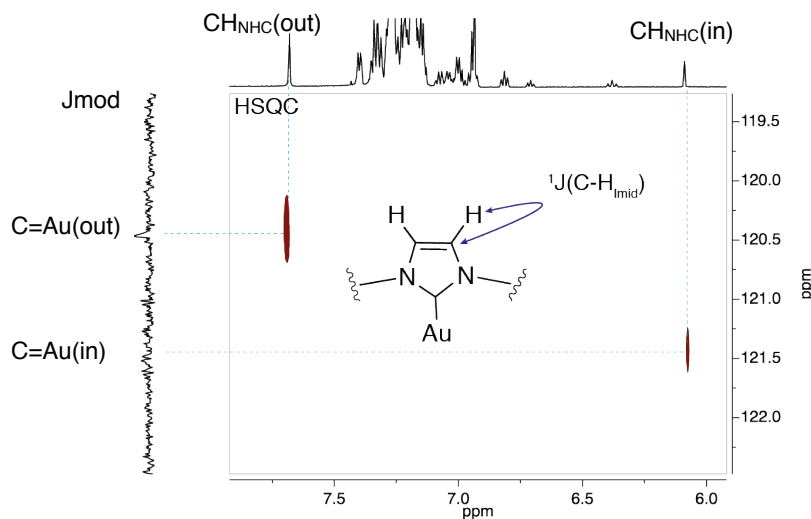


Figure III-9: Extract of HSQC showing one single correlation between the C and the H of the NHC. CDCl₃, 600 MHz, 300K

HMBC correlations of the CH at 7.7 ppm shows one single clear cross-correlation peak with the CH of the NHC ring (marked in blue) and a cross-correlation peak with a quaternary carbon at 172.1 ppm (marked in green) corresponding to the carbenic carbon of the NHC-AuCl unit (Figure III-10).

In addition, cross correlations peaks are observed between the same carbons with the H6 of the sugar units AD, the sugar units bearing the NHC bridge (marked in dark blue and orange). The C₂ symmetry, and this additional chemical shift of the carbene at 172.1 ppm confirms the coordination of a bridged normal NHC-AuCl complex.

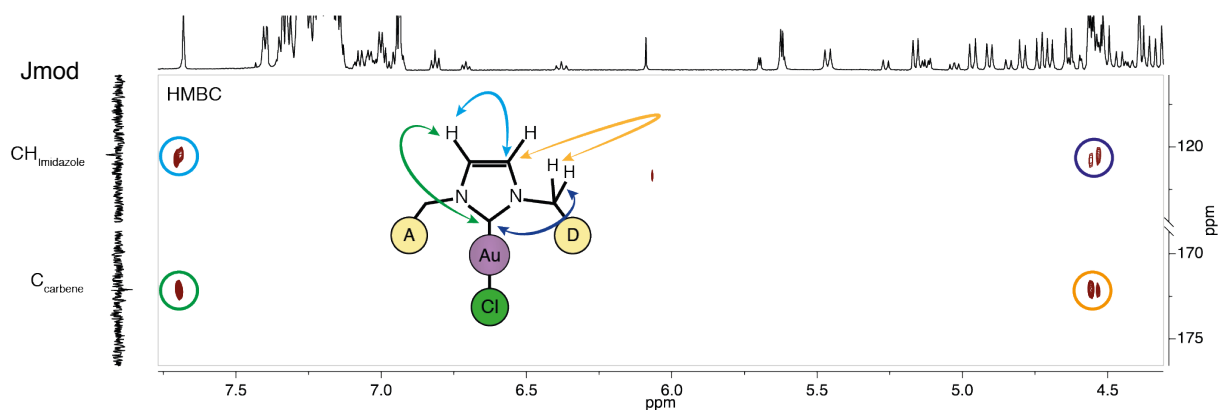


Figure III-10: Extract of HMBC showing all the cross correlations between the carbons of the NHC moiety and the surrounding protons
 CDCl_3 , 600 MHz, 300K

The reversal of the imidazolyl moiety was proved by 2D-NOESY experiments. In contrast to $(\gamma\text{-ICyD})\text{AuCl}$ complexes, $(\alpha\text{-rev-ICyD})\text{AuCl}$ exhibits very a clear NOESY cross correlations between the deshielded CH of the imidazole and the H-5 of the sugar units A,D (highlighted in orange) and the intra-cavity protons H3 and H5 on sugar units C and F (highlighted in green and blue, respectively) (Figure III-11). To clarify the attribution of the signals, the NOESY spectra was stacked with the HSQC, showing the corresponding correlations with the signals of the intracavity CH mentioned before. Additionally, 2D -NOESY experiments, recorded at long mixing times ($\tau_{\text{mix}} = 0.8$ secs) did not show any exchange signal, suggesting the presence of two discrete non-equilibrated complexes.

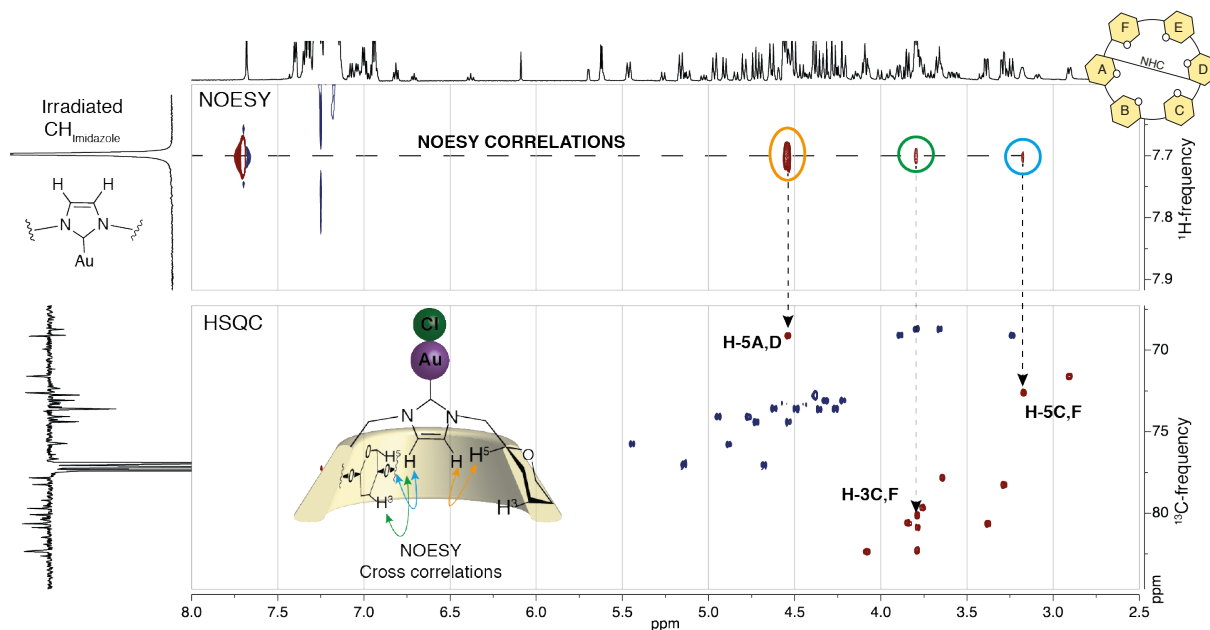
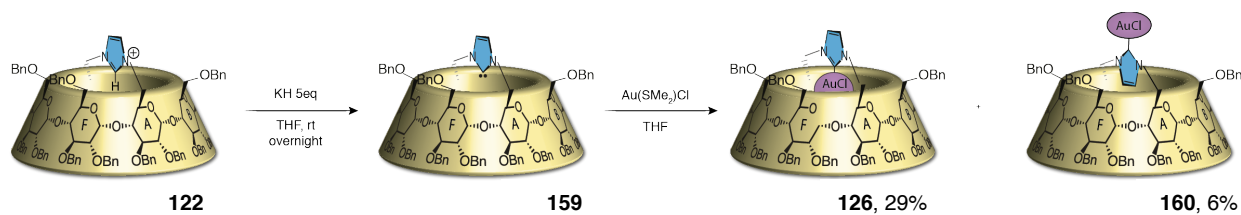


Figure III-11: Extract of NOESY experience of $(\alpha\text{-rev-ICyD})\text{AuCl}$ stacked with the HSQC showing NOE correlations between the CH of the NHC and the intra cavity protons H3 and H5.
 CDCl_3 , 600 MHz, 300K



Scheme III-6 : Formation of the free α -ICyD and metalation with $\text{Au}(\text{Me}_2\text{S})\text{Cl}$ affording a mixture of $(\alpha\text{-ICyD})\text{AuCl}$ and $(\alpha\text{-rev-ICyD})\text{AuCl}$

All these experiments proved that the gold complex is coordinated outside of the cavity, and that this unprecedented reversed coordination mode is possible with ICyD ligands. However, the reason and mechanism of the flipping out of the free α -ICyD remains unclear.

To understand it, and to verify the non-equilibrated mixture of both isomers, a mixture of $(\alpha\text{-ICyD})\text{AuCl}$ and $(\alpha\text{-rev-ICyD})\text{AuCl}$ was heated in toluene- d_8 at 360 K showing no change of the ratio of both isomers (Figure III-12), concluding that the inversion must occur in the metallation step.

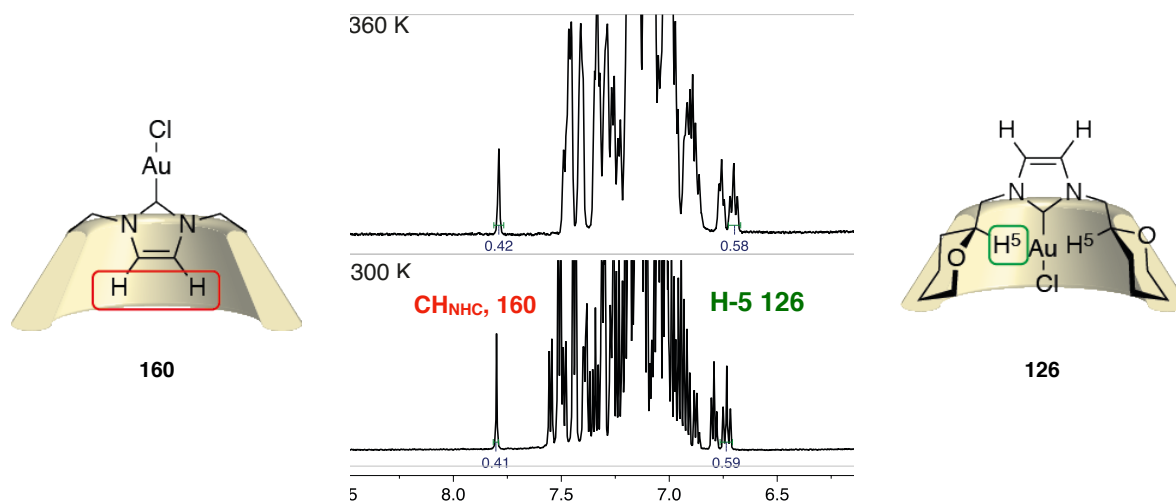


Figure III-12: ^1H -NMR spectrum of a mixture α -ICyD)AuCl and $(\alpha\text{-rev-ICyD})\text{AuCl}$ at 300 K and 360 K. 600 MHz, toluene- d_8

To understand the behavior of the free NHC, a NMR study of the free $(\alpha\text{-ICyD})$ was done. The NOESY of the compound shows a very clear cross correlation peak between the CH of the NHC and the H6 of the sugar units A,D; similar to the one observed for all the introverted complexes and the imidazolium salts.

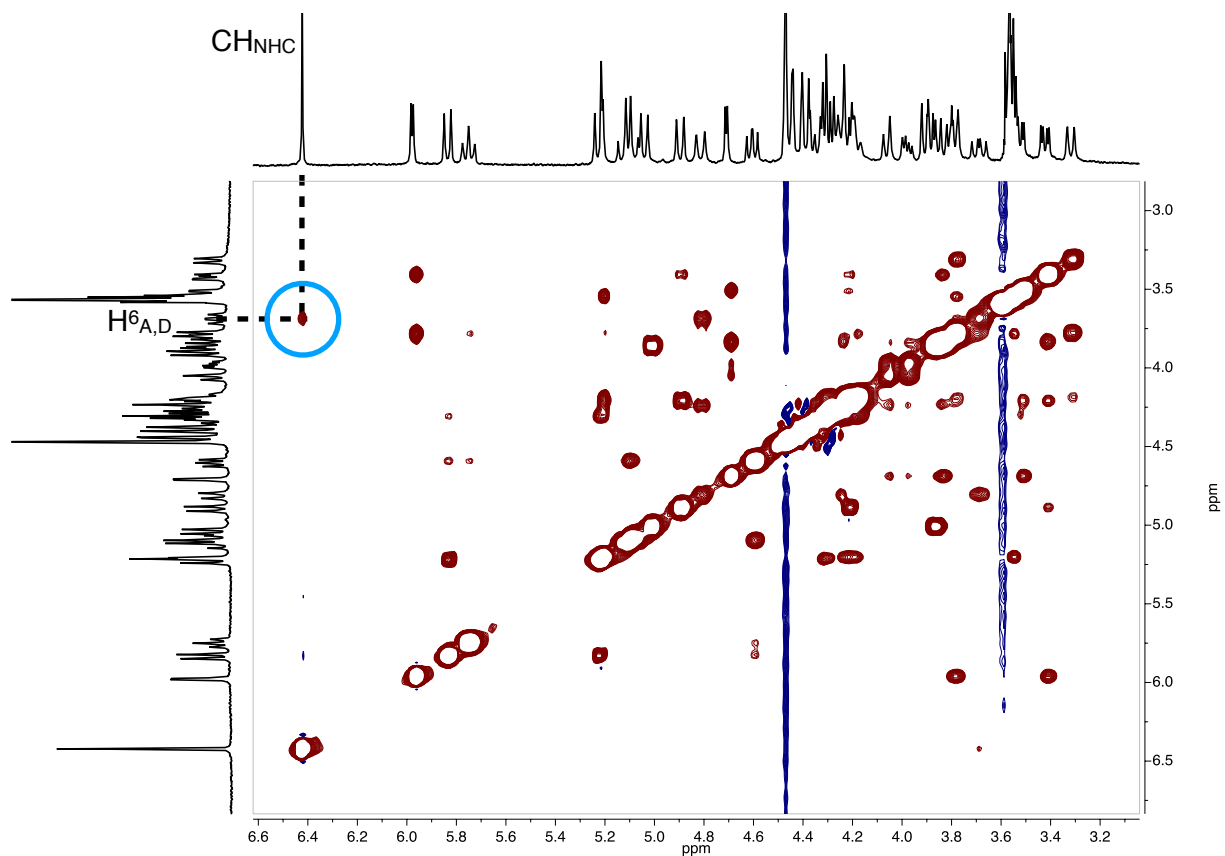


Figure III-13: 2D-NOESY of the free (α -ICyD). C_6D_6 , 400 MHz, 300 K

¹H-NMR of the free NHC is sharp and only one compound is observed, the coalescence temperature must be thus under 300 K, to look for a rotation around the NHC coexisting in solution, the free (α -ICyD) was cooled down until 202 K. Nevertheless, cooling down to -70 °C in toluene- d_8 did not show any apparition of another compound.

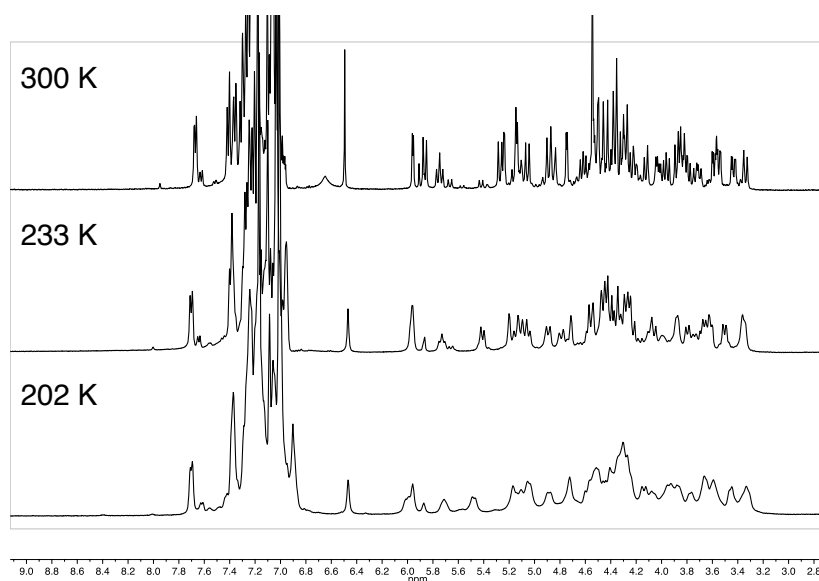
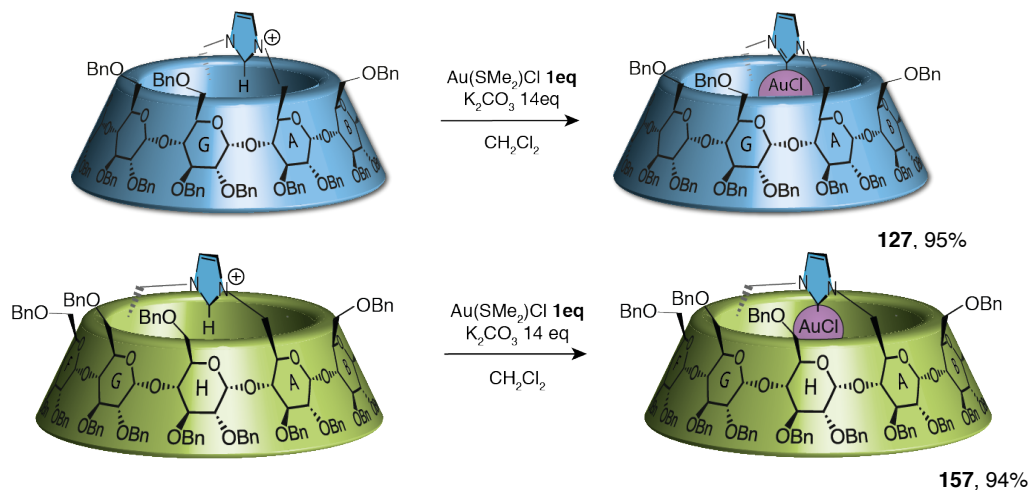


Figure III-14: Temperature variation of free (α -ICyD). 400 MHz, toluene- d_8 .

The remaining question is now, can the $K_2CO_3/Au(SMe_2)Cl$ methodology be extended to (β - and γ -ICyD) precursors to obtain, an inner complex or an outer one depending on the synthetic route? By using the conditions previously described for (α -ICyD)HCl, $K_2CO_3/Au(SMe_2)Cl$, both (β -ICyD)HCl and (γ -AE-ICyD)HCl complexes gave the previously described “inner” complexes (β -ICyD)AuCl and (γ -AE-ICyD)AuCl in 90% and 94% yield, respectively, with no detectable trace of the “outer” coordinated gold complexes (Scheme III-9).

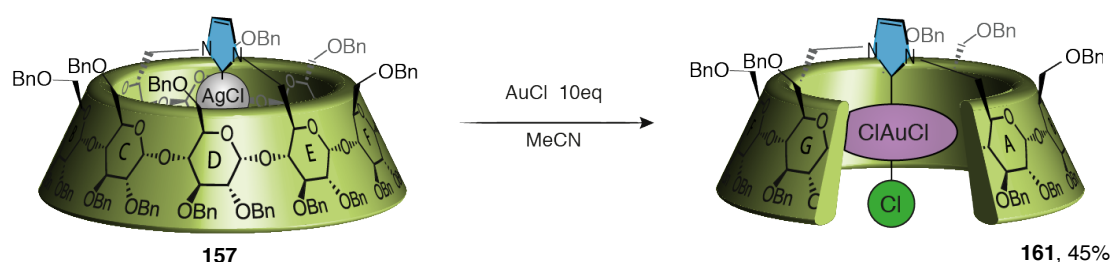


Scheme III-9: Optimized synthetic route to the obtention of (ICyD)AuCl complexes

C. Square planar gold (III) complexes:

Influence of the cyclodextrin in the geometry

While the only way to synthesize (α -ICyD)AuCl and (β -ICyD)AuCl consisted in the transmetalation of (α - and β -ICyD)AgCl with 10 equivalents of AuCl in acetonitrile, this reaction gave a different result in the case of the γ analogue. Instead, the only compound isolated during this reaction was the (γ -ICyD)AuCl₃ **161**. This unexpected gold(III) complex resulted from disproportionation of the intermediate gold (I) complex and was obtained in 45% yield (Scheme III-10). Other conditions have been tried to obtain the (γ -ICyD)AuCl, such as a lower amount of gold and exclusion of light, but the gold (I) complex was never observed. This unexpected result, formed an unprecedented square planar complex inside the CD cavity opening the possibility to synthesize new complexes, with different geometries inside ICyDs.



Scheme III-10: Transmetalation conditions to obtain (γ -ICyD)AuCl₃ complexes.

1. Square planar coordination in gamma cyclodextrin: (γ -ICyD)AuCl₃

i. Characterization

The oxidation state of the complex was proved by ¹³C NMR of the C-carbene chemical shift. Nolan and co-workers have already shown that oxidation of the gold(I) to gold(III) produces an upfield shift around 30 ppm from gold (I) to gold (III).¹³¹ In the case of the (γ -ICyD)AuCl₃, a resonance frequency for the C-carbene at 142.4 ppm was observed, in contrast to the 172 ppm for the Au^I analogue. In addition, the mass spectrum shows a clear isotopic pattern, also in agreement with the presence of three chlorine atoms (Figure III-15)

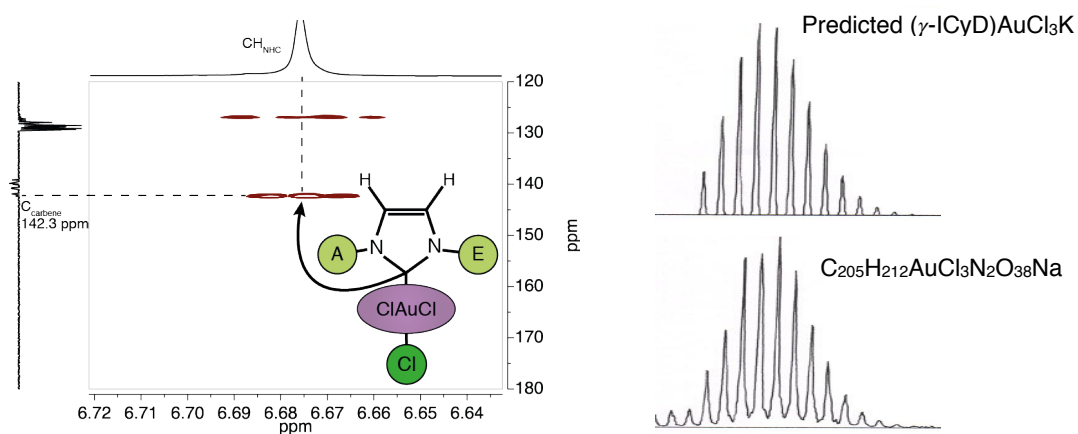


Figure III-15 : HMBC of (γ -AE-ICyD)AuCl₃ showing the chemical shift of the C_{carbene}.
 HMBC: CD₃CN, 400MHz, 300K ESI-TOF: Injection in MeCN

As in the Au^I complex, the encapsulation of the gold center was proved with the NOESY spectra, showing cross correlation picks between the CH of the NHC and H-6 of the sugar units A/E and B/F (Figure III-16).

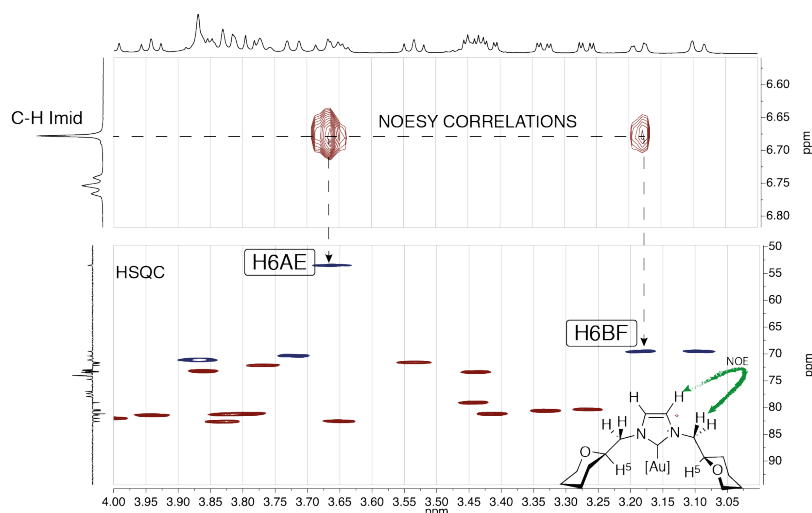


Figure III-16: NOESY (top) and HSQC (bottom) showing cross correlations between the C-H of the imidazole and the H6-AE and BF

By analogy with the Au^I analogue, chemical shifts of the intracavity protons H5 and H3 were used to prove the encapsulation of the AuCl₃ moiety. Due to the large size of the cyclodextrin the effects are weak, but some slight deshieldings could be appreciated at the H5 level (Figure III-17).

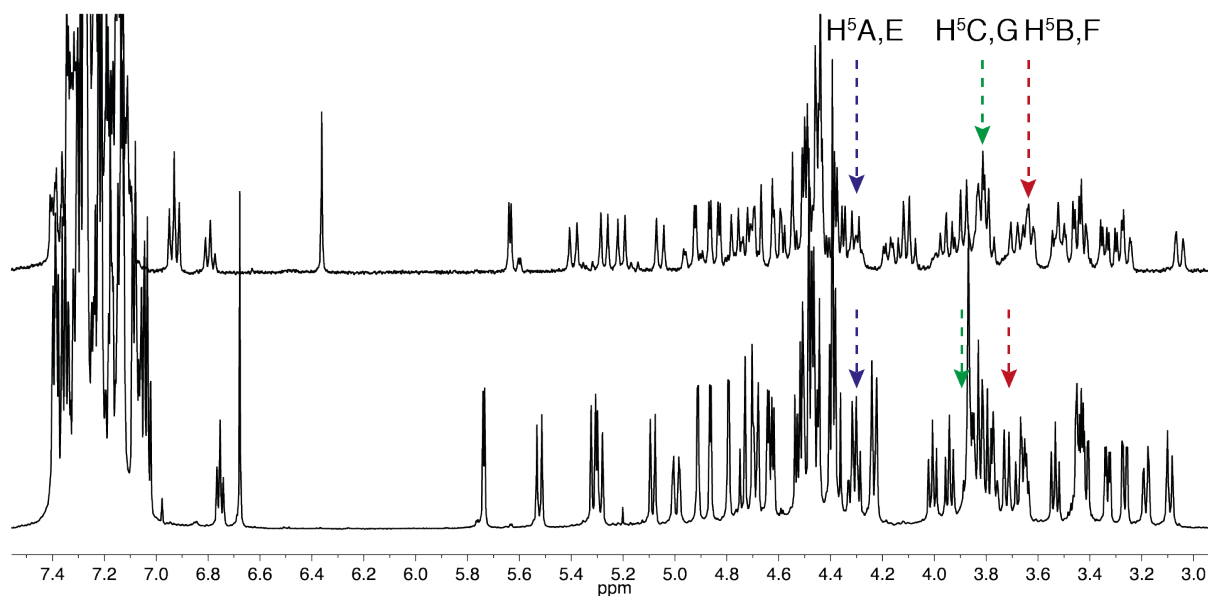


Figure III-17 : Stacked $^1\text{H-NMR}$ of $(\gamma\text{-ICyD})\text{AuCl}$ **161** (top) and $(\gamma\text{-ICyD})\text{AuCl}_3$ (bottom). CD_3CN , 600 MHz, 300 K.

ii. From NMR shifts to the structure of $(\gamma\text{-ICyD})\text{AuCl}_3$

To elucidate the structure some preliminary hypotheses were done. Due to the position in the macrocycle (Figure III-18), upfield shifts on the H5 of sugar units A and E were attributed only to the presence of the metal. Following the same reasoning, due to the height in the cavity, all the deshieldings of the rest of the H5 of the cavity were attributed to the presence of the equatorial chlorines, thus, a C-H...halogen interaction. Finally, for the H3, the effects were only attributed to the axial chlorido ligand.

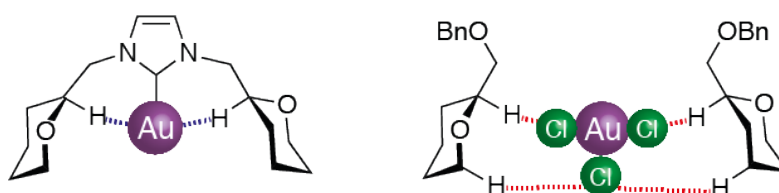


Figure III-18: Orientation of intra-cavity protons in the cyclodextrin and hypothesized interactions

Comparing the real values of the chemical shifts in both complexes (Table III-2), no changes were observed in the sugar units A,E and C,G; this lack of changes may be produced by small changes in the conformation of the macrocycle.

On the opposite hand, the only H5s that followed a “significant” downfield shift were those of sugar units B and F (+0.14 ppm). This shift can be justified by the presence of the equatorial chlorines, close to these sugar units. Finally, a deshielded H3 was found on the sugar units D and H, due to a proximity from the C-H3 ... Cl-axial ligand.

Sugar unit	A/E		B/F		C/G		D/H	
	H5	H3	H5	H3	H5	H3	H5	H3
(γ -ICyD)AuCl	4.30	3.95	3.62	3.90	3.81	4.10	3.52	4.11
(γ -ICyD)AuCl ₃	4.31	3.94	3.76 (+0.14)	3.82	3.86(+0.05)	4.00	3.44(-0.08)	4.30(+0.19)

Table III-3: Chemical shifts of the intra-cavity protons of (γ -AE-ICyD)AuCl and (γ -AE-ICyD)AuCl₃.
¹H-NMR, CD₃CN, 600MHz, 300K

With all these chemical shifts, starting from the previous model of (γ -ICyD)AuCl, the equatorial chlorine atoms were placed next to the most deshielded sugar units B and F assuming that the square planar geometry is not distorted inside the cavity. Those sugar cycles were tilted until the H5 was closer than the H5 of C,G units. The complex is optimized by reducing the energy with the UFF force field. Finally, bond distances around the metal atom were corrected with an average of those reported in the literature (2 Å for Au-C and 2.25 Å for Au-Cl bonds) affording the model showed on figure III-19.

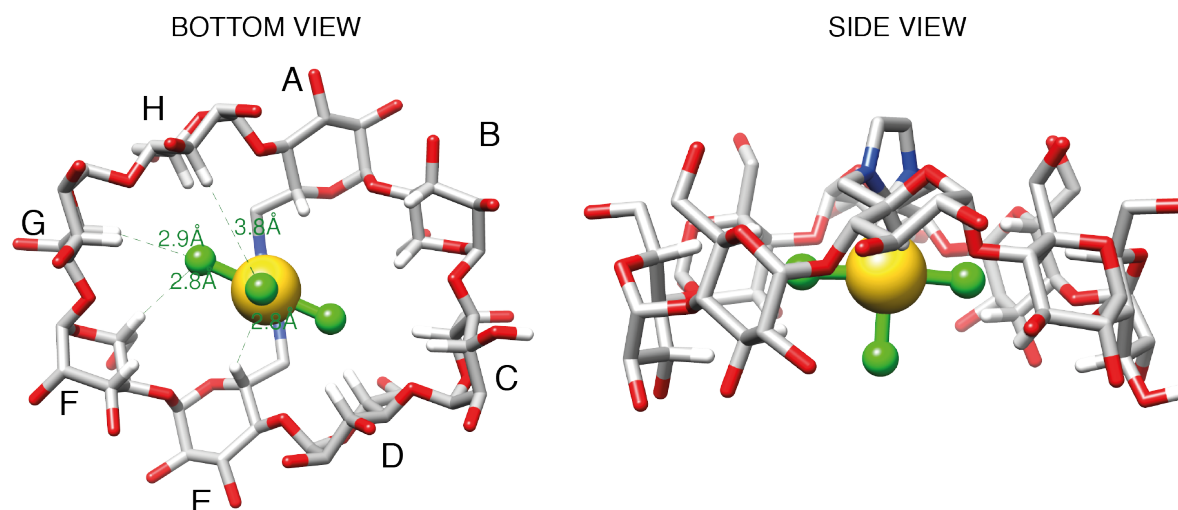


Figure III-19 : Modeled structure of (γ -ICyD)AuCl₃

As it can be observed in the modeled structures, the H5-A,D ... M distance, as well as other H5-Cl and H3-Cl are consistent to distances reported in the literature to C-H ... M¹³⁴ and C-H-Cl⁹⁰ interactions, suggesting a valid procedure and confirming the initial hypothesis.

iii. From the structure to the shape of the $(\gamma\text{-AE-ICyD})\text{AuCl}_3$

To deduce more insights about the second coordination sphere of this square planar complex, the Connolly's surface of the modeled structure of $(\gamma\text{-ICyD})\text{AuCl}$ and $(\gamma\text{-ICyD})\text{AuCl}_3$ were built to have a better vision of the three-dimensional structure of the complex.

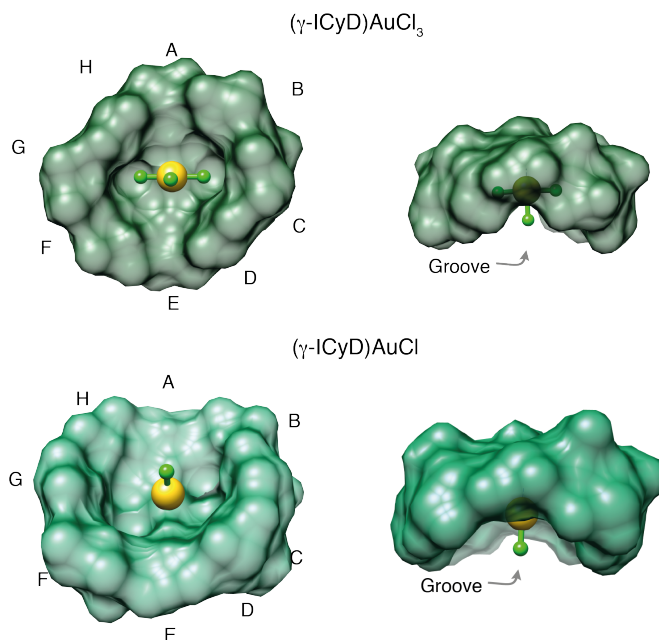


Figure III-20: Bottom and side views of the Connolly's surfaces of $(\gamma\text{-ICyD})\text{AuCl}_3$ and $(\gamma\text{-ICyD})\text{AuCl}$

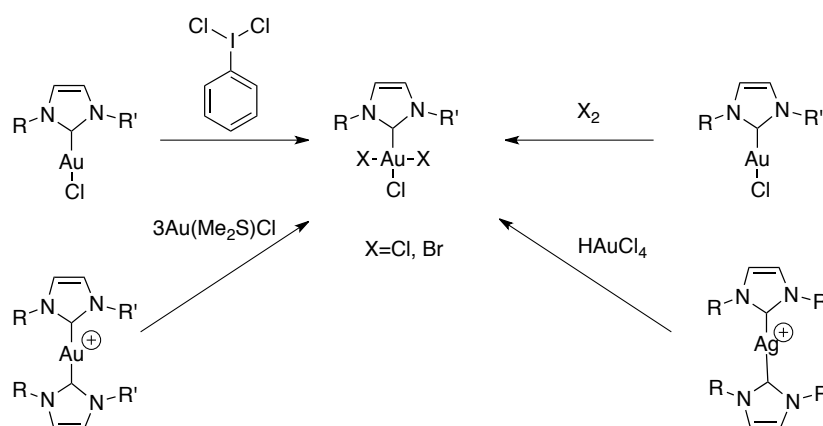
As it can be observed on the Figure III-20, a similar shape to the one of the $(\gamma\text{-ICyD})\text{AuCl}$ analogue was obtained. Both shapes are symmetrical, both possess a groove due to the bridging with a short imidazolyl moiety, more important in the case of the AuCl_3 complex. In both cases, the metal is far away from the inner walls of the cyclodextrin but in the case of the Au^{III} complex the sugar units D and H were brought closer, probably to optimize the interaction with the axial chlorido ligands.

To further understand the structure of the $\text{ICyD-Au}^{\text{III}}$ complexes, a library of CD-based Au^{III} complexes was synthesized starting with $(\gamma\text{-ICyD})\text{AuX}_3$ ($\text{X}=\text{Br}$ and I). Then, the possibility of synthesis of the same Au^{III} complexes was studied.

2. Oxidation of linear Au (I) complexes. Effect of narrower cyclodextrins

i. Reported synthesis of NHC-Au(III) complexes

As presented before, a spontaneous oxidation of (γ -ICyD)Au(I) to Au(III) complex was observed in the case of the largest γ -ICyD ligand. Gold (III) complexes are nowadays exhaustively studied because of their catalytic¹³⁵, biological¹³⁶, or luminescent¹³⁷ properties. In the case of NHC-AuClX₂ (X = halogen), the described syntheses are limited to an oxidation of Au^I complexes either with PhICl₂,¹³¹ or X₂¹³⁸ and only one recent example of transmetalation in presence of HAuCl₄ is reported¹³⁹ (Scheme III-11). Furthermore, the synthesis of this family of complexes seems to be substrate-dependent.



Scheme III-11 : synthesis of NHC-Au^{III} complexes

ii. Screening of conditions with (γ -AE-ICyD)AuCl

To control the reactivity and stability of (ICyD)AuCl complexes towards these oxidative conditions, the oxidation reactions were first tested on the γ -ICyD analogue, for which the corresponding gold (III) complex **161** was already isolated and characterized.

¹³⁵ C.Y. Wu, T. Horibe, C.B. Jacobsen, F.D. Toste, *Nature* **2015**, *517*, 449 - 454., M. Hofer, A. Genoux, R. Kumar, C. Nevado *Angew. Chem. Int. Ed.* **2017**, *56*, 1021 - 1025, A. Zeineddine, L. Estévez, S. Mallet-Ladeira, K. Miqueu, A. Amgoune, D. Bourissou *Nat. Commun.* **2017**, *8*, 565

¹³⁶ J. Dinda, T. Samanta, A. Nandy, K. Das Saha, S. K. Seth, S. K. Chattopadhyay, C. W. Bielawski, *New J. Chem.*, **2014**, *38*, 1218 - 1224

¹³⁷ R. Kumar, C. Nevado, *Angew. Chem. Int. Ed.* **2017**, *56*, 1994 - 2015

¹³⁸ C. Topf, C. Hirtenlehner, M. Zabel, M. List, M. Fleck, U. Monkowius, *Organometallics* **2011**, *30*, 2755-2764

¹³⁹ A. G. Nair, R. T. McBurney, M. R. D. Gatus, S. C. Binding, B. A. Messerle, *Inorg. Chem.* **2017**, *56*, 12067-12075

The oxidation of the complex with 8 equivalents of iodosobenzene dichloride¹⁴⁰ was followed by NMR (Figure III-21). Formation of the expected gold (III) complex was observed after 18 hours, without a total conversion of the starting material. Furthermore, before the completion of the reaction, a degradation product appeared as a major product of the reaction (highlighted in green).

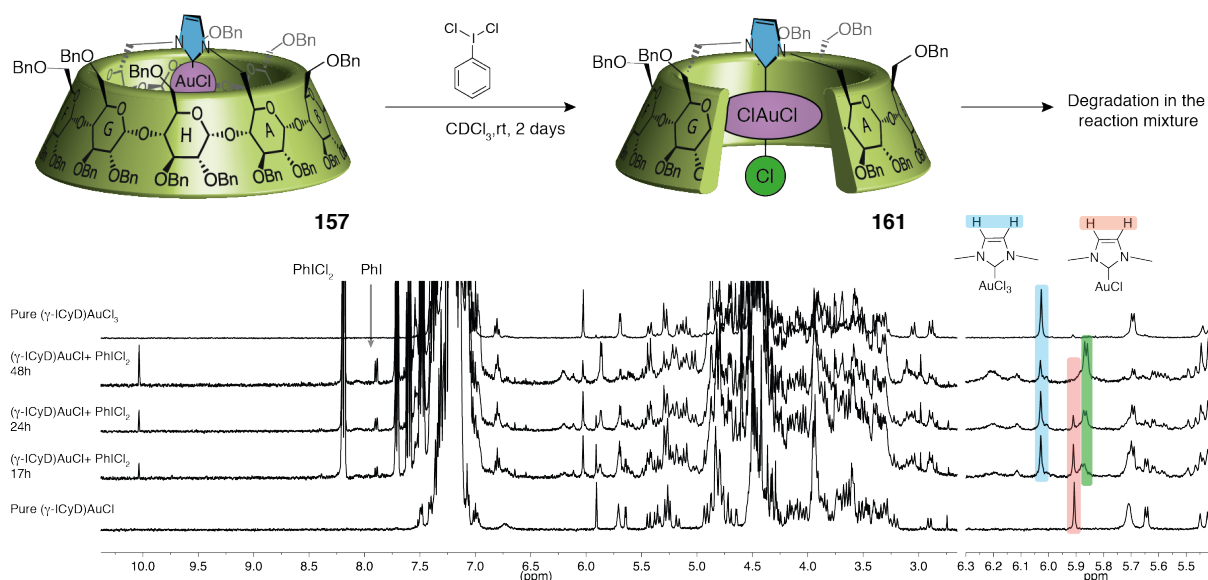
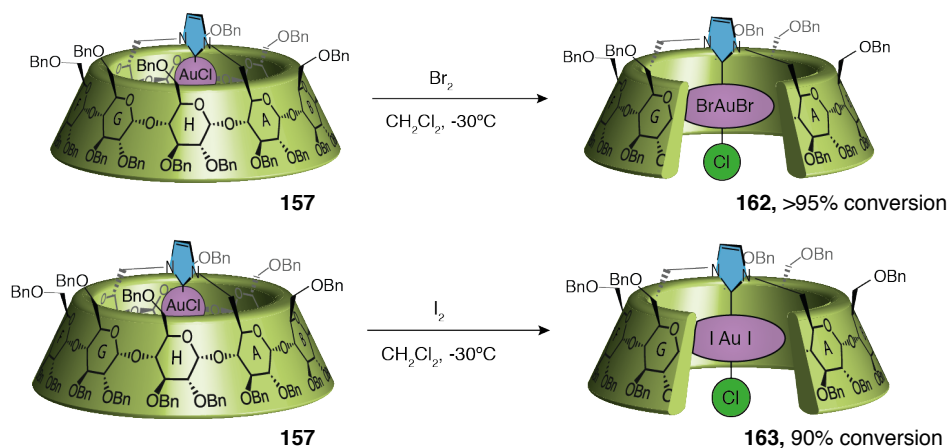


Figure III-21 : NMR monitoring of the reaction of $(\gamma\text{-ICyD})\text{AuCl}$ with PhICl_2 .
Zoom of the CH_{NHC} and anomeric region is shown on the right.

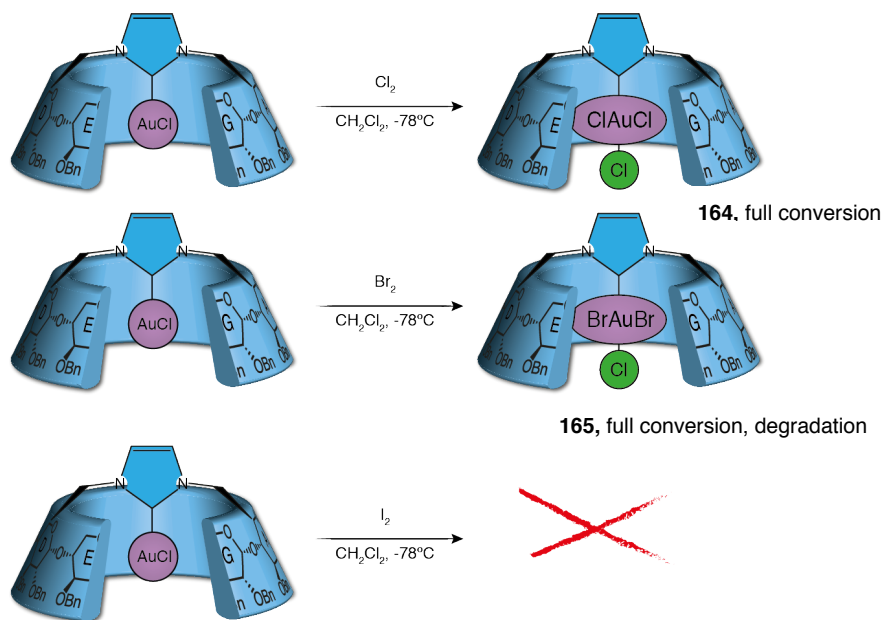
Oxidations with Br_2 and I_2 were performed at -30°C in dichloromethane.¹³¹ After evaporation of the solvent, crude NMR conversions superior to 90% were calculated by integration of the starting $(\gamma\text{-AE-ICyD})\text{AuCl}$ and the products. Both, $(\gamma\text{-AE-ICyD})\text{AuBr}_2$ **162** and $(\gamma\text{-AE-ICyD})\text{AuI}_2\text{Cl}$ **163** were characterized by NMR without any further purification (Scheme III-12).



Scheme III-12 : Oxidations with Br_2 and I_2 of $(\gamma\text{-ICyD})\text{AuCl}$

¹⁴⁰ X. Zhao, C. Zhang, *Synthesis* **2007**, 4, 551 - 557.

Moving to the nearest narrower (β -ICyD)AuCl, oxidation was carried out by bubbling Cl_2^{141} into a solution of (β -ICyD)AuCl at -78°C in dichloromethane. After evaporation of the solvent, crude NMR showed the formation the expected (β -ICyD)AuCl₃ **164** with full conversion by NMR.



Scheme III-13: Oxidation fo (β -ICyD)AuCl with Cl_2

The same procedure was followed to perform the reaction with Br_2 . Addition of bromine at -78°C produced the expected (β -ICyD)AuBr₂Cl complex. Oxidation of the gold (I) complex was confirmed by a shift of the carbenic carbon from 171.9 ppm to 141.3 ppm. Mass spectrometry also shows the formation of the expected compound.(Figure III-22) Nevertheless, a degradation of the complex was observed during the acquisition of the NMR analysis, making impossible any further analysis.

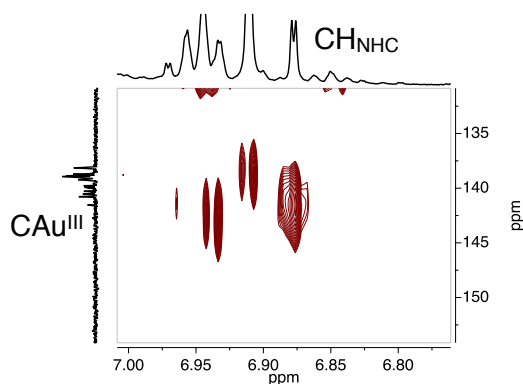
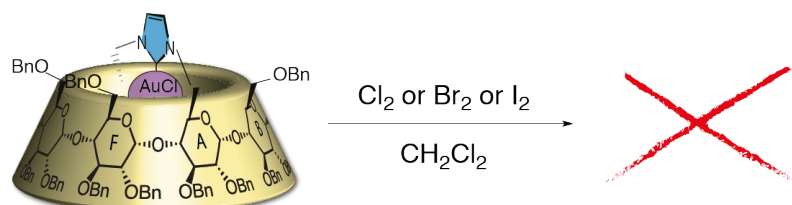


Figure III-22: HMBC of (β -ICyD)AuBr₂Cl showing the cross peak correlation between the CHNHC and the carbene. Acetone- d_6 , 600 MHz, 300 K.

¹⁴¹ Generated in situ by dropwise addition of concentrated HCl on solid KMnO_4 , washed by bubbling in water, dried by bubbling in concentrated H_2SO_4 and bubbled directly in the reaction mixture.

Surprisingly, the reaction of I₂ with the (β-ICyD)AuCl in dichloromethane at -78 °C did not take place. Pushing the conditions to room temperature and longer reaction times only led to a degradation of the cyclodextrin skeleton.

To conclude the synthesis of (ICyD)AuX₃ cyclodextrin complexes, reactions were performed on (α-ICyD)AuCl. No oxidation products were observed in any of the cases.



Scheme I-14: Attempts of oxidation of (α-ICyD)AuCl

All these experiments illustrated the variation of the reactivity of the previously described NHC-based cyclodextrin gold (I) complexes. The non-reactivity towards oxidants of the (α-ICyD)AuCl demonstrates in this case the protection of the metal center by the steric hindrance afforded by the cavity.

Then, (β-ICyD)AuCl can be oxidized by the smallest Cl₂, whereas oxidation with Br₂ occurs but the obtained complex was revealed unstable. This linear (β-ICyD) gold (I) complex shown to be unreactive against I₂. This size-dependent discrimination between oxidants can be an interesting starting point to develop site-selective reactions.

Finally, (γ-ICyD)AuClX₂ complexes were formed without difficulty with both Br₂ and I₂ leading to discrete well-defined introverted complexes. In addition, the AuCl₃ analogue was obtained through a different method (Table III-3).

Oxidant	Cl ₂	Br ₂	I ₂
Complex	NMR conversion		
(α-ICyD)AuCl	0 %	0 %	0 %
(β-ICyD)AuCl	100 %	Observed but unstable	0 %
(γ-ICyD)AuCl	45% ^a	95 %	92 %

Table III-3: Summary of conversion of oxidations with Cl₂, Br₂, and I₂ of the different NHC-based cyclodextrin gold (I) complexes. a) Obtained by a different method.

With all these different reactivities, the same NMR studies as the one done for the linear (γ-ICyD)AuCl complex were done to understand the possible changes on the three dimensional structures of the cyclodextrin core, aiming to synthesize new square planar complexes and develop new reactivities in the case of the easy accessible α and β complexes.

iii. NMR analysis of γ -based square planar gold (III) complexes

The same methodology as for the $(\gamma\text{-ICyD})\text{AuCl}_3$ was followed to study the structures of the $(\gamma\text{-ICyD})\text{AuClX}_2$. To elucidate the structures, the differences between all the intra-cavity protons of the three compounds were compared. By analogy with the $(\gamma\text{-AE-ICyD})\text{AuCl}$, the downfield shift of the H5A,E will be treated as a metal-hydrogen interaction, and the rest of effects on the intra-cavity protons as CH-halogen interactions.

All of the complexes appeared in the NMR as a set of 4 sugar units, being all thus, C_2 symmetric (Figure III-23). This symmetry, is a direct consequence of a *trans*- addition of the included halogens.

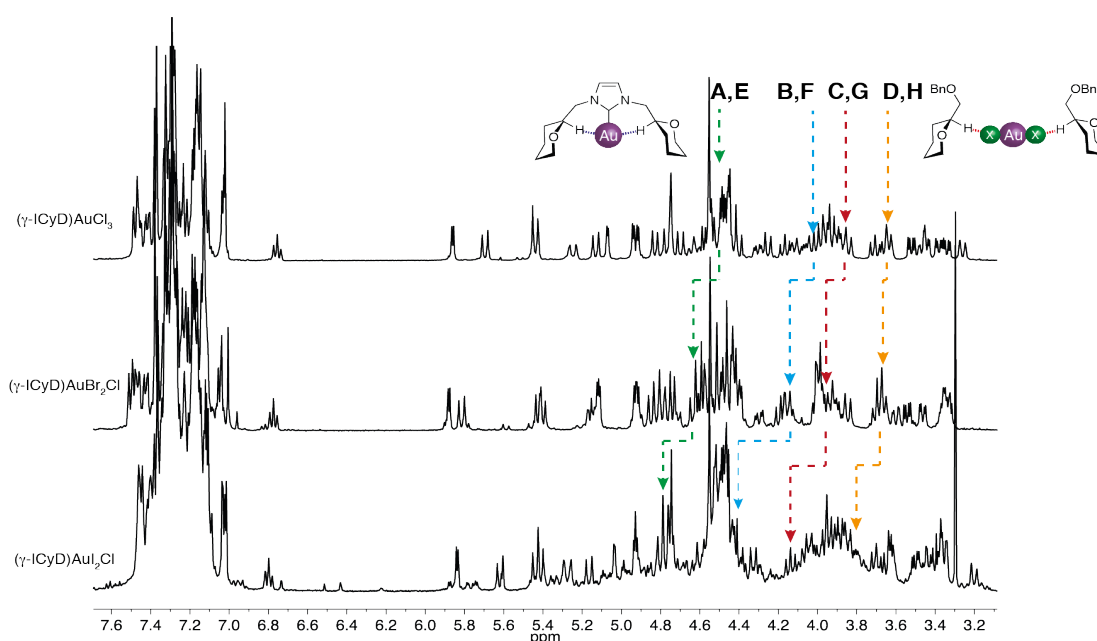


Figure III-23: $^1\text{H-NMR}$ of $(\gamma\text{-ICyD})\text{AuCl}_3$, $(\gamma\text{-ICyD})\text{AuBr}_2\text{Cl}$ and $(\gamma\text{-ICyD})\text{AuI}_2\text{Cl}$. Acetone- d_6 , 600 MHz, 300 K

Chemical shifts of the intra-cavity protons H5 and H3 of the cyclodextrin as well as the chemical shifts of the C-carbene are reported in Table III-4. Looking at the chemical shift of the carbene, a slight upfield shift of 1.5 ppm is observed between the $(\gamma\text{-ICyD})\text{AuCl}_3$ **161** and its brominated analogue **162**, showing a negligible change of the electronic density around the gold atom.¹⁴² In contrast, a more relevant upfield shift of 12.3 ppm is observed in the case of the $(\gamma\text{-ICyD})\text{AuI}_2\text{Cl}$ **163**, appearing at 131.5 ppm. This shift is consequence of a more important electron density around the gold center due to a lower electronegativity of the iodine atom ($\chi = 2.66$ against $\chi = 3.16$ in Pauling's scale).

¹⁴² C. Hirtenlehner, C. Krims, J. Hölbling, M. List, M. Zabel, M. Fleck, R. J. F. Berger, W. Schoefberger, U. Monkowius, *Dalton Trans.*, **2011**, 40, 9899 - 9910

Sugar unit	δ_{carbene}	A/E		B/F		C/G		D/H	
		H5	H3	H5	H3	H5	H3	H5	H3
(γ -ICyD)AuCl ₃	143.8	4.54	4.05	4.04	4.15	3.93	3.96	3.62	4.51
(γ -ICyD)AuBr ₂ Cl	142.3	4.63 (+0.09)	4.02	4.11(+0.07)	3.97	4.06 (+0.13)	4.17	3.63	4.52
(γ -ICyD)AuI ₂ Cl	131.5	4.81 (+0.27)	3.98	4.39 (+0.35)	4.00	4.13 (+0.20)	4.18 (0.22)	3.80 (+0.18)	4.56

Table III-4: Key resonances of (γ -ICyD)AuCl₃, (γ -ICyD)AuBr₂Cl and (γ -ICyD)AuI₂Cl
600MHz, acetone-d₆, 300K

This change on the electron density could be related to the chemical shift of the H-5A,E of the cyclodextrin. More electron rich metals produce a more important downfield shift of the influenced protons of a M ... H-C bonding,¹¹⁷ being also a proof of the inner coordination of the gold atom.

Since the same behavior of chemical shifts was observed, $\delta(\text{H5B,F}) > \delta(\text{H5C,G}) > \delta(\text{H5D,H})$ for the same complexes, thus, the same relative distances, both structures were built just by replacing the equatorial ligands without moving the skeleton of the cyclodextrin, obtaining thus the same three-dimensional system (Figure III-24).

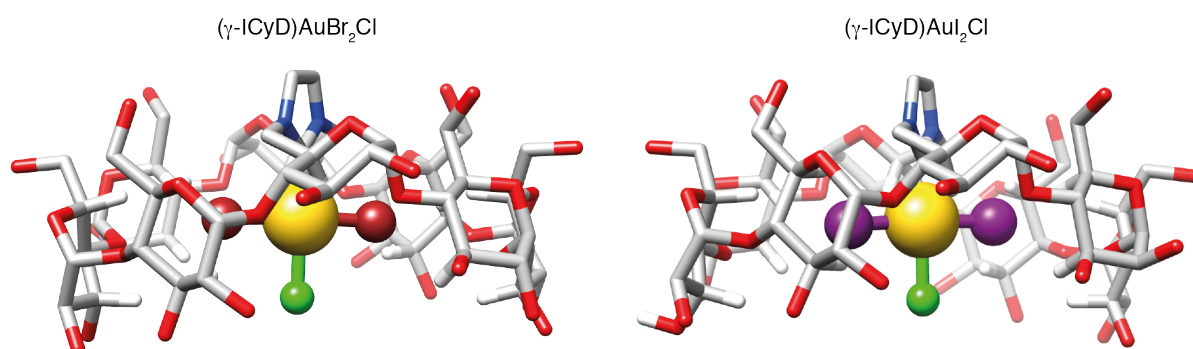


Figure III-24: Modeled structures of (γ -ICyD)AuBr₂Cl and (γ -ICyD)AuI₂Cl.

iv. Effects on the NMR of (β -ICyD)-gold(III) complex

Studying now the case of the narrowest cavity hosting a Au(III) square planar complex, (β -ICyD)AuCl₃ **164**, the same comparative study of the intra-cavity protons with the linear analogue was done (Figure III-25).

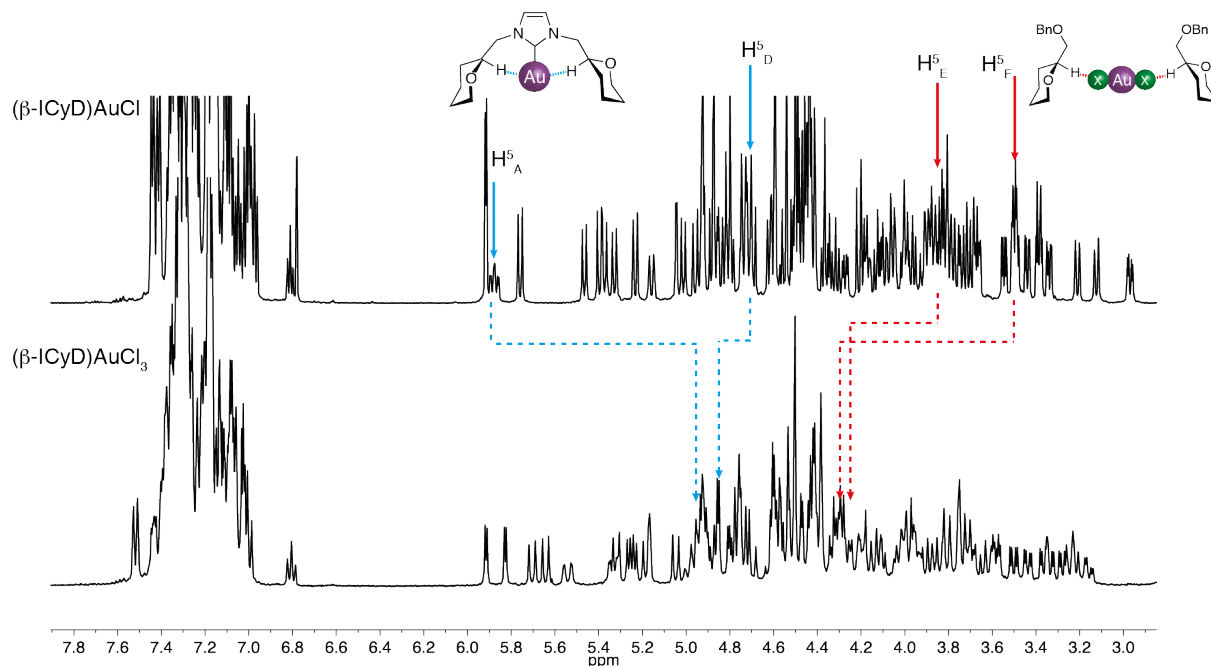


Figure III-25: Superposition of ¹H-NMR spectra of (β -ICyD)AuCl (up) and (β -ICyD)AuCl₃ (bottom)
Acetone-d₆, 600 MHz, 300 K.

The comparison of both complexes starts with the chemical shifts of the H-5A,D. Because of a less electron rich Au^{III} metal, an important upfield shift for the H5A was observed for the (β -ICyD)AuCl₃ complex in comparison for the Au^I analogue.

Interestingly, the H-5D is deshielded of 0.27 ppm, an opposite effect that the expected. This change on the chemical shift can be due to a new arrangement of the gold atom inside the cavity, reflected in a similar chemical shift for both H-5A and D. Additional downfield shifts of H5 of sugar units E and F (0.81 and 0.38 ppm, respectively) were observed. According to the same hypothesis than in the case of the (γ -ICyD)AuX₂Cl analogues, it is reasonable to assume that these shifts are due to the presence of an equatorial chlorine placed next to the sugar units E and F.^{59,90}

Sugar unit	A	B	C	D	E	F	G
(β -ICyD)AuCl	5.88	4.17	3.91	4.72	3.50	3.87	3.99
(β -ICyD)AuCl ₃	4.95(-0.93)	4.20	3.95	4.99(+0.27)	4.31(+0.81)	4.29 (+0.38)	3.95

Table III-5: Key resonances of H5 of (β -ICyD)AuCl and (β -ICyD)AuCl₃.600MHz, 300K, Acetone-d₆

Now analyzing the H3 of the macrocycle, an important upfield shift of 0.22 ppm is observed on the sugar unit G. This upfield shift of this precise proton confirmed the hypothesis of a structural change because its chemical shift was influenced by the presence of the axial chlorido ligand.

Additional downfield shifts of H3s were observed around all of the cyclodextrin. H-3C is deshielded of 0.54 ppm, H-3E 0.13 ppm and H-3F 0.22 ppm. In these three cases, the rationalization of the chemical shift was the presence of a chlorine atom.

Sugar unit	A	B	C	D	E	F	G
(β -ICyD)AuCl	4,10	4,32	4,37	4,12	4,00	4,06	4,80
(β -ICyD)AuCl ₃	4,00	4,28	4.91(+0.54)	4,17	4.13(+0.13)	4.32(+0.26)	4.58(-0.22)

Table III-6: Key resonances of H³ of (β -ICyD)AuCl and (β -ICyD)AuCl₃.600MHz, 300K, Acetone-d₆

v. Structure of (β -ICyD)-gold(III) complex

Once again, by placing all the atoms of the metal ion, the three-dimensional structure of the complex was deduced. To do so, as for all the structures elucidated previously, the relative distances between the H5 and the gold, as well as the H5-Cl and H3-Cl were deduced from the NMR.

Due to a similar chemical shift of the H-5A and the H-5D, thus similar interactions with the metal, the gold atom was placed exactly in between them both. Deshieldings on the H5-E and F suggests the presence of one of the equatorial chlorido ligands on this side of cavity. In contrast, no significant change is observed on the chemical shift of the diametrically opposed H5-B and C, showing that the previous hypothesis is not valid for this complex, indicating potential a tilt of the gold complex inside the cavity.

Finally, the H3 of the sugar unit C, the most deshielded of the compound, was rationalized with the presence of an equatorial chlorido ligand, justifying the tilting of the complex inside the cavity.

With all these informations, the structures were modeled following the same procedure as presented previously. The metal complex was placed in the middle-slightly closer to the H5A of the cyclodextrin, the chlorido ligands are placed according to the previous deductions and the sugar units are tilted according to relative distances. A final UFF optimization is done to obtain the structure showed in Figure III-26. As observed for the (γ -ICyD)AuCl complex, a consistent modeled structure was deduced from the NMR data, founding relative distances to build a three-dimensional model with C-H \cdots Cl and C-H \cdots M distances in agreement to the ones described in the literature for weak interactions.

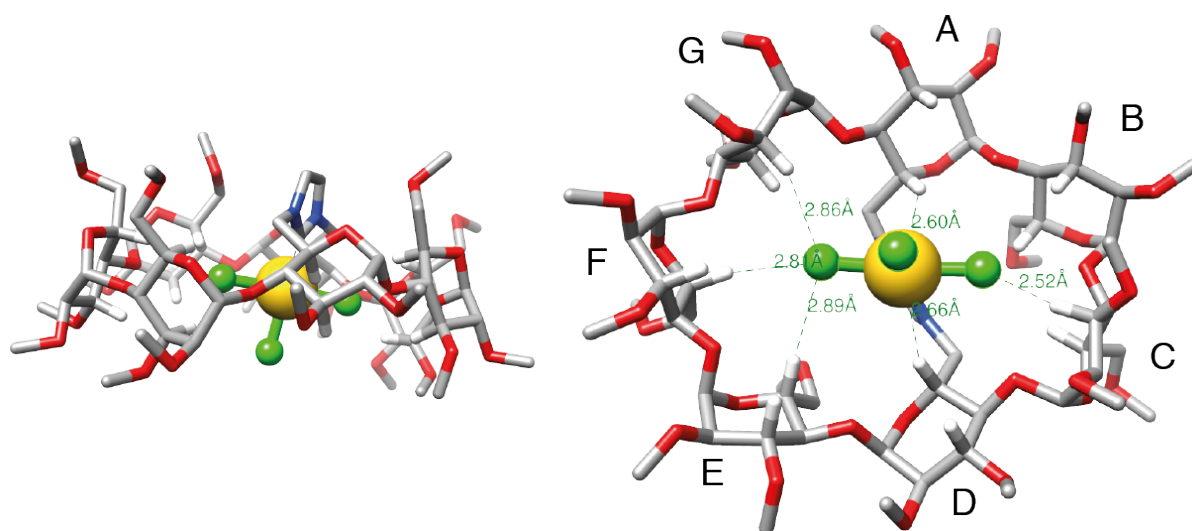


Figure III-26: Side view and bottom view of the modeled structures of (β -ICyD)AuCl₃

vi. Comparison of structures and shapes of γ - and β -CD-based square planar gold(III) complexes

As presented for the linear (ICyD)AuCl complexes, by modeling the three-dimensional structure of the cyclodextrin, Connolly's shape¹³⁵ of the macrocycle is created again to analyze the steric environment around the metal center.

In the case of (γ -ICyD)AuCl₃ a similar shape from the one of the linear complex was observed. In contrast, in the case of the (β -ICyD)AuCl₃ the presence of a network of weak interactions between the H5 of sugar units E,F and the H-3,G forces the metal to be moved away from the inner walls of the small loop of the cyclodextrin, constituted by the sugar units B and C in agreement with the observed shifts of the H-5A and D. This displacement of the metal center makes the gold atom to be more exposed inside the cavity.

As observed for the (γ -ICyD)AuCl analogue **157**, the sugar unit G (anti-clockwise from the sugar unit A), is tilted to establish a C-H \cdots Cl interaction with the equatorial chlorido ligand, slightly changing the shape of the cyclodextrin on this side.

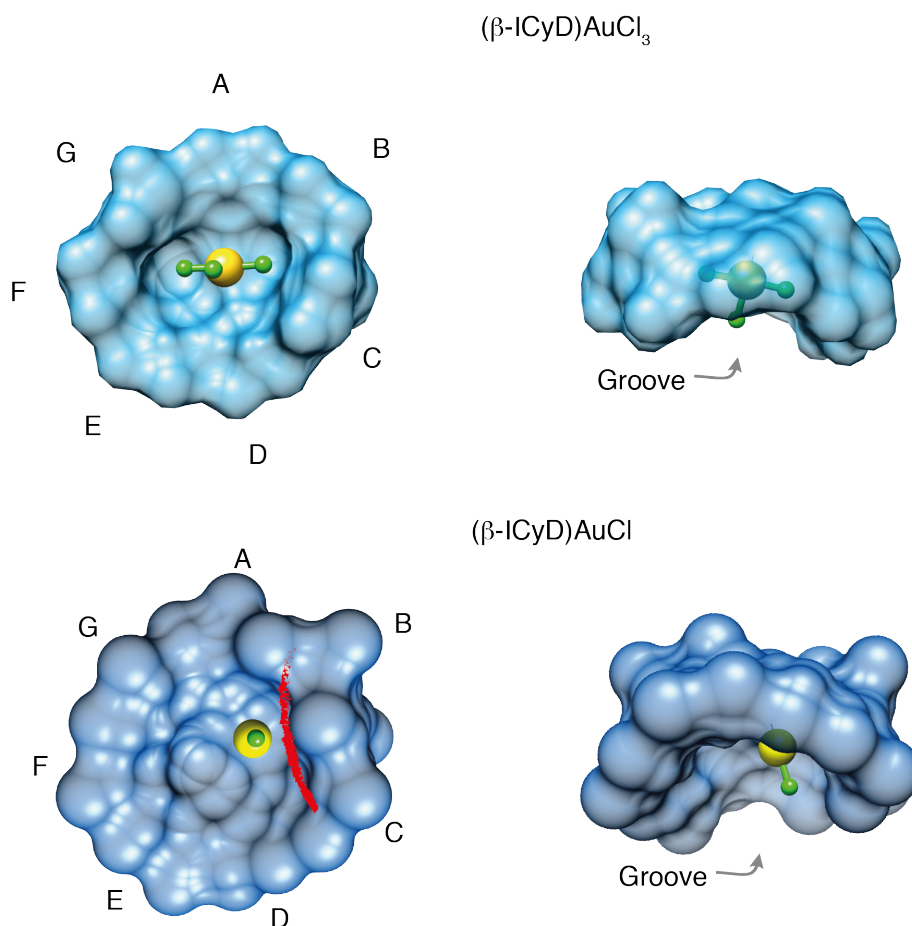


Figure III-27: Shape comparison of (β -ICyD)AuCl and (β -ICyD)AuCl₃ complexes

In conclusion, it was found that three different cyclodextrin-gold-complexes, (α -ICyD)AuCl, (β -ICyD)AuCl and (γ -ICyD)AuCl, differing only in their cavity size, differed also in their reactivity towards the oxidation and in the structure of the different Au^I and Au^{III} complexes. As showed in chapter I, redox properties of encapsulated redox centers has been a subject of study for more than 30 years.²⁵ In our case, we obtained four different complexes with different cavity sizes and coordination modes. In the literature, it was reported that the redox behavior of confined metals can be influenced by the nature of the confining system, the size and the topology.⁴⁴ What can afford a cyclodextrin as confining system in the redox behavior of a metal complex?

vii. Electrochemistry of (ICyD)AuCl complexes

As presented in chapter I, encapsulation of redox centers in confined spaces is an interesting research field in redox-metalloenzymes mimicry. Nevertheless, a risk of this encapsulation inside a big cavitand is a reduction in intensity or a loss of the signal in cyclic voltammetry.⁶² Previous studies of the electrochemical properties of (ICyD)-CuCl complexes showed that the encapsulation of the CuCl moiety inside the α -cyclodextrin cavity leads to a complete loss of the redox properties of the redox center³⁸. This property was used as a proof of the encapsulation of the Cu atom. Thus, the reversal of the NHC should be then proved by the redox properties.

Since in the previous reports of electrochemistry with ICyDs only the α -derivative was studied, at this stage, three different encapsulated complexes with different reactivities towards the oxidation, encouraged us to revisit the electrochemistry of ICyDs and look for cavity-size depending redox potentials. All the electrochemistry was done in a collaboration with Dr. Grimaud of ENS de Paris.

Electrochemistry of NHC-based gold complexes is an almost unexplored research field, only few examples of cyclic voltammetry studies with simple NHC are reported in the literature¹⁴³. The only complete report of the properties of NHC-AuX complexes has been done by Wu studying the redox properties of different benzimidazolin-2-ylidenes-based AuX complexes (X=halogen). Wu and coworkers proved in their study the nature of the waves in a cyclic voltammogram of (**166**)AuX complexes. Only one reduction wave (R1) corresponding to a monoelectronic reduction of the Au^I in Au⁰. This reoxidation is diffusion dependent being irreversible at low scan rates and quasi reversible at 0.2V/s, where a reoxidation wave (O1) emerges.

Comparing the voltammograms of chlorine, bromine and iodine derivatives, 3 different oxidation waves (O2, O3, and O4 respectively) are observed. The authors proposed there oxidation waves as Au^I/Au^{III} oxidation can be overlapped with the Cl⁻/Cl₂ oxidation process without rejecting any of the processes.

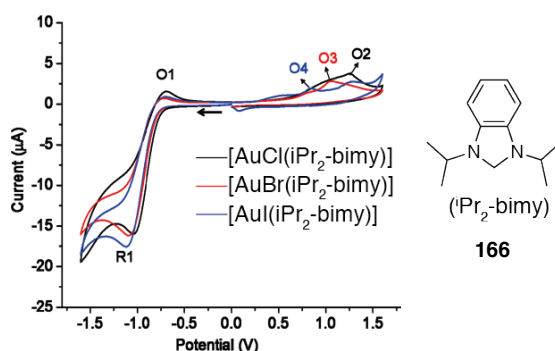


Figure III-28: Overlaid cyclic voltammograms of Au(I) complexes. CH₂Cl₂ 0.1V/s, 0.1M TBAPF₆ as supporting electrolyte.

¹⁴³ H.V- Huynh, S. Guo, W. Wu, *Organometallics* **2013**, 32, 4591–4600

In their study, the authors also showed, according to Hashmi¹⁴⁴ and Raubenheimer¹⁴⁵ that the R2 reduction of Au^{III} to Au^I wave emerged on continuous scans (Figure III-29). Two possibilities were proposed, either the oxidation of Cl⁻, Br⁻ or I⁻ and the generated X₂ can quickly oxidize the gold complex and the Au^{III} is generated chemically, either the Au^{III} is electrogenerated but overlapped with this wave.

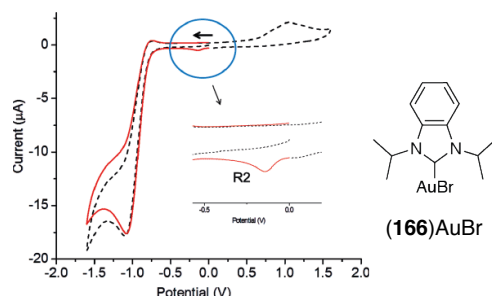


Figure III-29: Cyclic voltammogram of [AuBr(iPr₂-bimy)] complex. Dashed line first cyclic scan, red line second half scan. CH₂Cl₂ 0.1V/s, 0.1M TBAPF₆ as supporting electrolyte.

First trials on this system were done reproducing conditions of Wu's work presented before. Nevertheless, no oxidation or reduction has been observed on the voltammogram of IBnAuCl **167** in dichloromethane, used as model complex. On the opposite hand, better results were found using acetonitrile as solvent (Figure III-30). Similar results were found, a characteristic O₁ oxidation wave of Cl⁻, R₃ reduction from Au^{III} to Au^I, R₂ Au^I to Au⁰. An additional R₁ wave emerged at low reduction potentials, probably due to a reduction of the coordinated acetonitrile used as solvent to the complex.

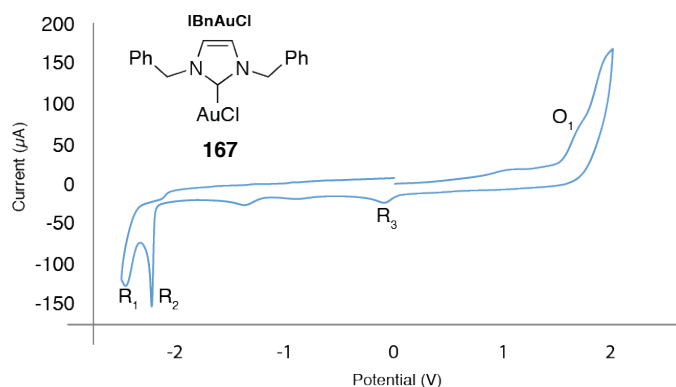


Figure III-30: Cyclic voltammogram of (IBn)AuCl complex. MeCN, [(IBn)AuCl] = 2 mM, 0.5 V/s, 0.1 M TBAPF₆ as supporting electrolyte.

As expected, due to a hindered metal complex¹⁴⁶, in agreement with the (α-ICyD)CuCl analogue, a complete loss of the signal in cyclic voltammetry was observed for the (α-ICyD)AuCl complex.

¹⁴⁴ M Pazický, A. Loos, M. J. Ferreira, D. Serra, N. Vinokurov, F. Rominger, C. Jakel, A. S. Hashmi, K.; M. Limbach, *Organometallics* **2010**, *29*, 4448

¹⁴⁵ P. Kühlkamp, H. G. Raubenheimer, J. S. Field, M. Desmet, *J. Organomet. Chem.* **1998**, *552*, 69

¹⁴⁶ S. Mendoza, P. D. Davidov, A. E. Kaifer, *Chem. Eur. J.*, **1998**, *4*, 864 - 870.

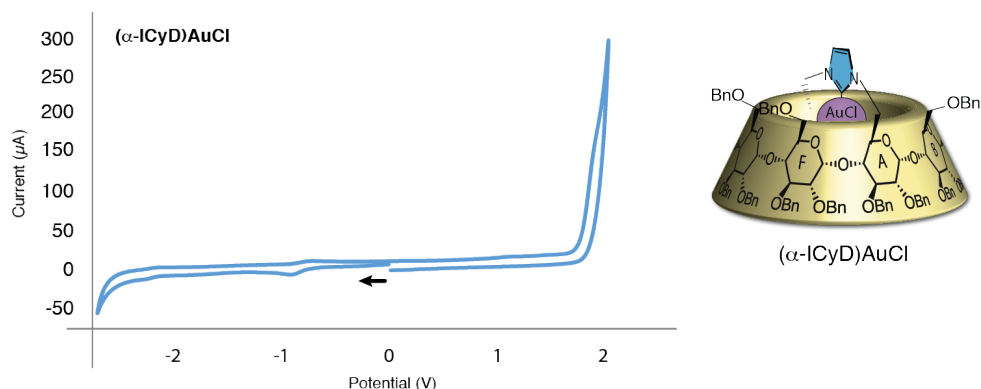


Figure III-31: Cyclic voltammogram of $(\alpha\text{-ICyD})\text{AuCl}$ complex. MeCN, 0.5 V/s, $[(\text{ICyD})\text{AuCl}] = 2\text{mM}$, 0.1M TBAPF_6 as supporting electrolyte.

In contrast, when the cyclic voltammetry is run in the same conditions with the $(\alpha\text{-rev-ICyD})\text{AuCl}$ ¹⁴⁷, a response similar to the one obtained with the IBnAuCl was obtained. In the oxidation way, the oxidation of chlorine ($\text{O}_1 = 1.40\text{ V}$), several reductions between 1 V and -0.5 V are observed, probably because a limited stability of the complex. A reduction of the gold complex was observed at $\text{R}_2 = -1.87\text{ V}$, proving the outer coordination of the gold center.

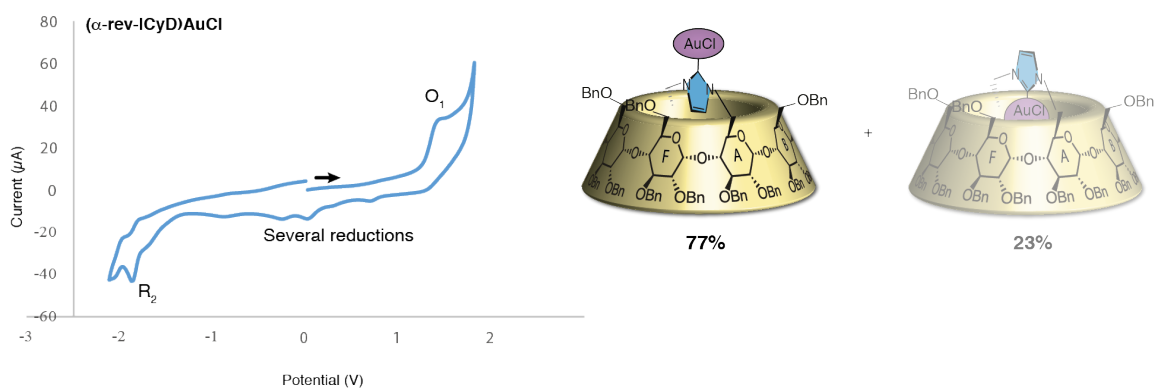


Figure III-32: Cyclic voltammogram of $(\alpha\text{-rev-ICyD})\text{AuCl}$ complex. MeCN 0.5 V/s, $[(\text{ICyD})\text{AuCl}] = 2\text{mM}$, 0.1M TBAPF_6 as supporting electrolyte.

¹⁴⁷ In a mixture with a 23% of the silent $(\text{ICyD})\text{AuCl}$

(β -ICyD)AuCl showed in the same conditions a similar behavior. Once again, oxidation of Cl⁻ ligands at 1.19 V (O₁) but this time no reduction of an electrogenerated Au^{III} was observed. Finally, the same two reduction waves were observed, R₂ due to a reduction of the Au^I in Au⁰, and the reduction of the coordinated acetonitrile molecule were observed at -1.86 V and -2.20 V respectively.

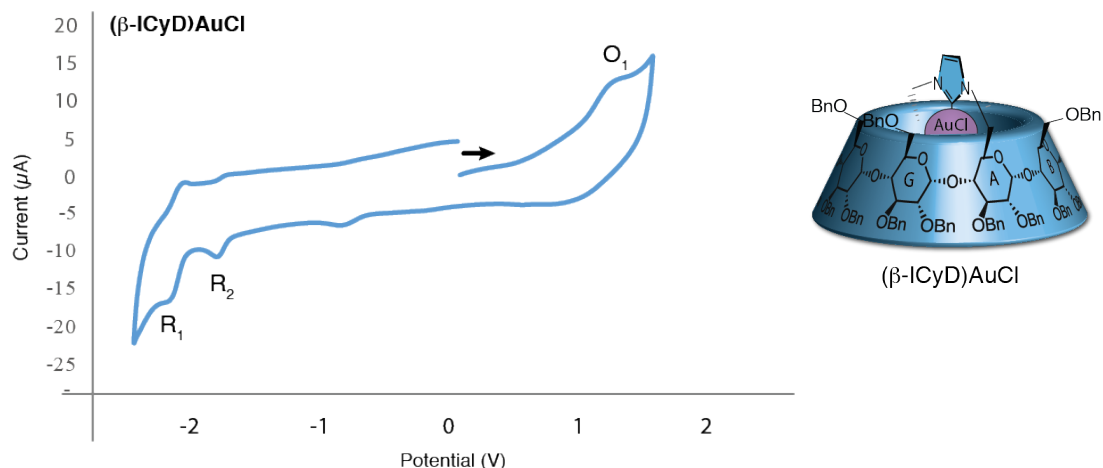


Figure: Cyclic voltammogram of (β -ICyD)AuCl complex. MeCN 0.5V/s, [(ICyD)AuCl] = 2 mM, 0.1M TBAPF₆ as supporting electrolyte.

Similar behavior was found with the largest (γ -AE-ICyD)AuCl, same oxidation wave, now with the apparition of a corresponding reduction of the generated Au^{III} (R₃) and the two corresponding reductions of the Au^I (R₂) and the proposed coordinated MeCN (R₁).

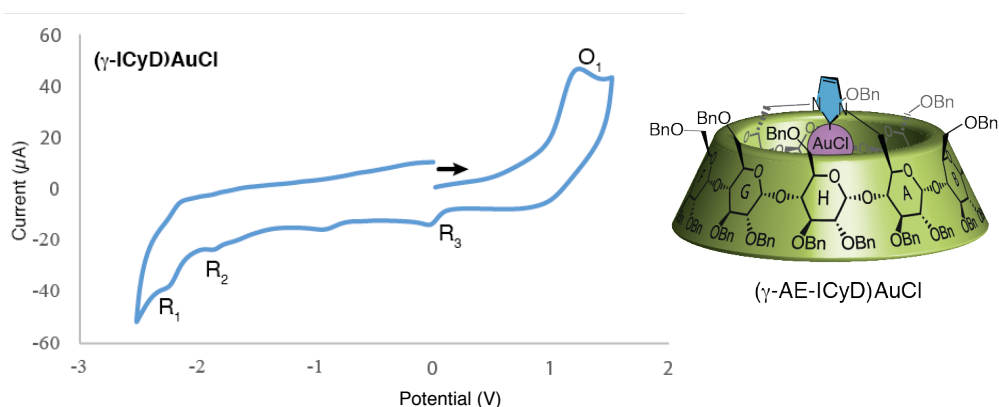


Figure: Cyclic voltammogram of (γ -ICyD)AuCl complex. MeCN 0.5 V/s, [(ICyD)AuCl] = 2 mM, 0.1 M TBAPF₆ as supporting electrolyte.

In conclusion, preliminary results on (ICyD)AuCl complexes proved their activity in electrochemistry being, to our knowledge, the first non-silent cyclodextrin-based encapsulated redox complexes. Additionally, four different behaviors were observed depending on the cavity size and the coordination mode (compiled in table III-5).

The first one, with (α -ICyD)AuCl, which is inert in cyclic voltammetry, constituted an expected result according to all the encapsulated redox centers inside cyclodextrins¹⁴⁸. Also expected, when the coordination mode is changed to the outer complex, and the complex is released of the steric hindrance afforded by the cavity, thus, the metal center can be closer to the electrode and the redox signals were recovered.¹⁴⁹

(β -ICyD)AuCl also showed a response on cyclic voltammetry, unprecedented for confining cyclodextrins and ICyDs. In this case, redox potentials of the involved oxido-reduction processes changed substantially from the ones observed for the IBnAuCl, which is easier to oxidize and reduce. In addition, the R3 wave, attributed to a Au^{III}/Au^I reduction was no observed. Two reasons can explain this fact: Either the confinement produced an increase of the redox potential and the gold is not oxidized during the experiment.¹⁴⁸ Or the chemical oxidation is kinetically slow, thus, it did not happen on the time of the experiment. Furthermore, (γ -AE-ICyD)AuCl, showed a cyclic voltammogram similar to the one of the β -analogue, with the additional signal of the reduction of the Au^{III} complex. This recovery could be observed thanks to a less hindered metal center, favoring the kinetic factors of the process.

Complex	R ₁	R ₂ (Au ^I /Au ⁰)	R ₃ Au ^{III} /Au ^I	O ₁
IBnAuCl	-2.46 V	-2.22 V	-0.1 V	Broad 1.5-1.7 V
(α -rev-ICyD)AuCl	—	-1.87 V	Several waves	1.40 V
(α -ICyD)AuCl	—	—	—	-
(β -ICyD)AuCl	-2.20 V	-1.86 V	—	1.19 V
(γ -AE-ICyD)AuCl	-2.25V	-1.87 V	0 V	1.25 V

Table III-5: Summary of R1, R2 and O1 potentials for the studied gold(I) complexes.

These results, unprecedented for encapsulated redox centers, showed the interest of a study of the redox behavior of these compounds. To gain more details about this phenomenon, more studies will be done using other encapsulated metal centers.

¹⁴⁸ T. Matsue, D.H. Evans, T. Osa, N. Kobayashi, *J. Am. Chem. Soc.*, **1985**, *107*, 3411 - 3417

¹⁴⁹ M. A. Sarmentero, P. Ballester *Org. Biomol. Chem.*, **2007**, *5*, 3046–3054

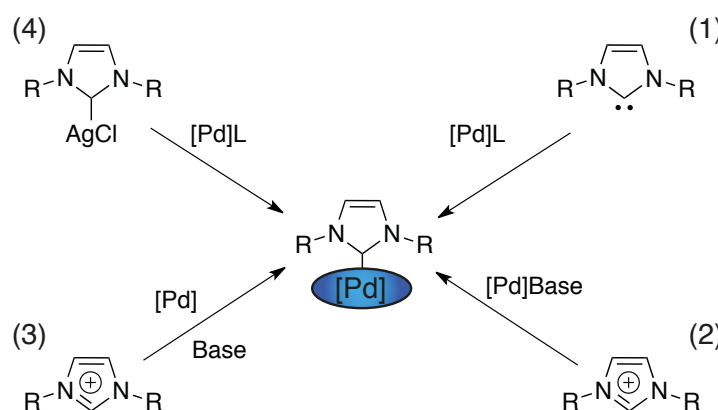
D. To other geometries: CD-based Pd and Pt complexes

1. Confinement of Pd. Square planar geometry in (ICyD)Pd complexes

i. Described synthesis of NHC-Pd^{II} complexes.

Now that the access to CD-encapsulated square planar geometries has been revealed possible, at least for β -ICyD and γ -ICyD, the access to other square planar complexes has been the first step to new metals inside ICyDs. Since the first report in 1995,¹⁵⁰ the interest of palladium-NHC complexes has grown, with interesting applications in the catalytic field. To synthesize Pd^{II}-NHC, the main reported synthetic routes are:

- 1) Direct displacement of a labile two electron ligand L with the free NHC, the most common labile complexes are $[\text{Pd}(\eta^3\text{-allyl})\text{Cl}_2]_2$ ¹⁵¹ and $\text{PdCl}_2(\text{NCR})_2$.¹⁵²
- 2) In situ deprotonation-metalation with a Pd bearing a basic conteranion such as $[\text{Pd}(\text{OAc})_2]$.¹⁵³
- 3) In situ deprotonation-metallation with an external base such as ^tBuOK or K_2CO_3 .¹⁵⁴
- 4) Transmetalation from a silver NHC.¹⁵⁵



Scheme III-14: Main synthetic routes for the formation of Pd-NHC

Since both, the silver route and the free NHC route have been proved as useful tools to obtain gold NHC-capped cyclodextrin complexes, both synthetic methodologies will be tested to get square planar palladium based-ICyDs.

¹⁵⁰ W. A. Herrmann, M. Elison, J. Fischer, C. Köcher, G. R. J. Artus, *Angew. Chem. Int. Ed. Engl.*, **1995**, *34*, 2371–2374

¹⁵¹ N. Marion, O. Navarro, J. Mei, E. D. Stevens, N. M. Scott, S. P. Nolan, *J. Am. Chem. Soc.* **2006**, *128*, 4101 - 4111

¹⁵² D. R. Jensen, M. S. Sigman, *Org Lett*, **2003**, *5*, 63 - 65

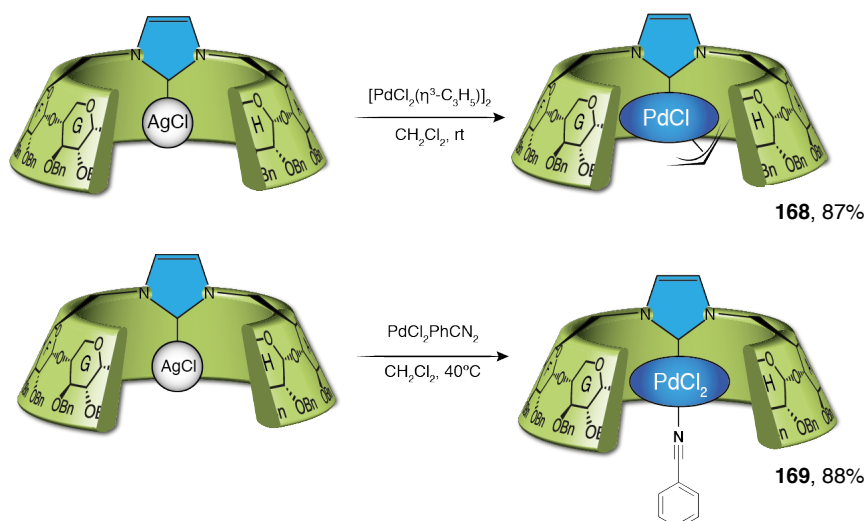
¹⁵³ L.-C. Campeau, P. Thansandote, K. Fagnou *Org. Lett.*, **2005**, *7*, 1857 - 1860

¹⁵⁴ C. J. O'Brien, E. A. B. Kantchev, C. Valente, N. Hadei, G. A. Chass, A. Lough, A. C. Hopkinson, M. G. Organ, *Chem. Eur. J.* **2006**, *12*, 4743 – 4748

¹⁵⁵ S. Roland, M. Audouin, P. Mangeney, *Organometallics*, **2004**, *23*, 3075 - 3078

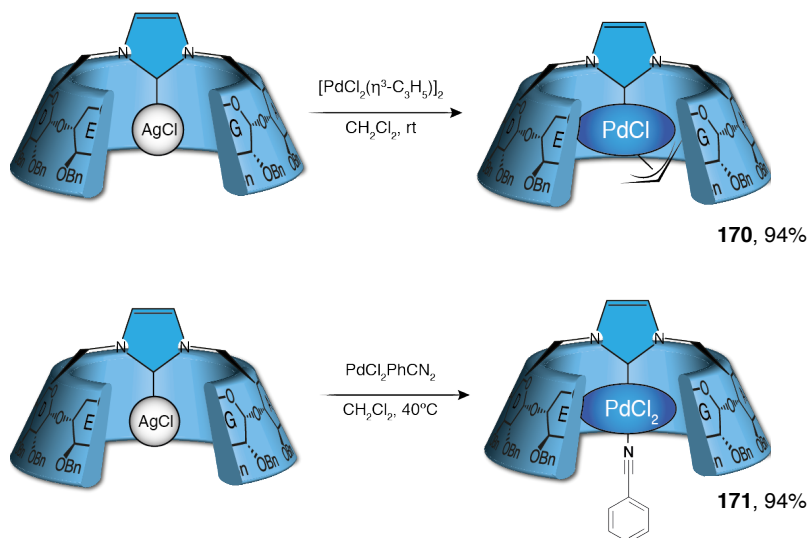
ii. Synthesis of CD-based palladium (II) complexes via the silver route

Even if this synthetic procedure is the less employed for the synthesis of these complexes, transmetalation of (γ -ICyD)AgCl was found to be an efficient method to obtain (γ -ICyD)PdCl₂(PhCN) and (γ -ICyD)PdCl(η^3 -allyl). These two complexes were obtained after silica gel purification in 88% yield by using one equivalent of PdCl₂(PhCN)₂, or 0.5 equivalents of [Pd(η^3 -allyl)Cl]₂ in dichloromethane, respectively (Scheme III-15).



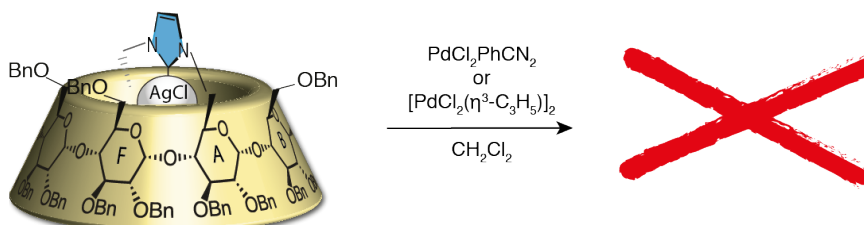
Scheme III-15: Synthesis by transmetalation of (γ -ICyD)PdCl₂(PhCN) and (γ -ICyD)PdCl(η^3 -allyl)

Same results were observed with (β -ICyD) analogues. The reaction of (β -ICyD)AgCl with one equivalent of PdCl₂(PhCN)₂ at 40 °C afforded (β -ICyD)PdCl₂(PhCN) in 94% yield, and the reaction of (β -ICyD)AgCl in presence of 0.5 equivalents of [Pd(η^3 -allyl)Cl]₂ afforded (β -ICyD)PdCl(η^3 -allyl) in excellent yields (Scheme II-16).



Scheme III-16: Synthesis of (β -ICyD)PdCl₂(PhCN) and (β -ICyD)PdCl(η^3 -allyl)

By analogy with the previously studied gold oxidations, it was not unexpected that transmetalations of (α -ICyD)AgCl gave no traces of square planar Pd^{II} compounds, either with [Pd(η^3 -allyl)Cl₂]₂ or PdCl₂(PhCN)₂ (Scheme III-17).

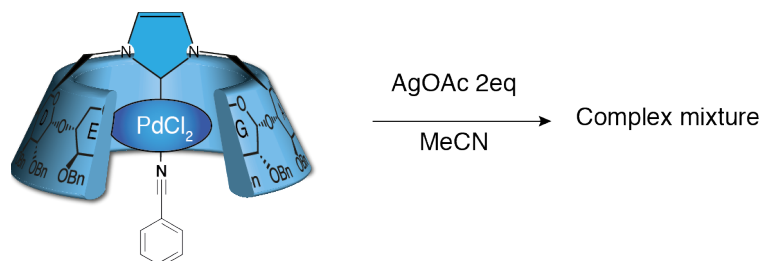


Scheme III-17: Reaction conditions for the transmetalation of (α -ICyD)AgCl

iii. Synthesis of CD-based palladium (II) complexes via the free NHC route

Transmetalations of silver-NHCs were proved as a powerful tool to obtain a diversity of NHC-metal complexes, nevertheless, this synthetic route is the less used for the synthesis of Pd-NHCs. We were interested in the synthesis of a broad library of Pd complexes due to the strong dependence on the reaction efficiency and the nature of the precatalyst.¹⁵⁶

For example, [Pd(OAc)₂] complexes are the best catalysts for CH activation reactions. However, standard reaction conditions to form this complexes did not show any evolution.¹⁵⁷



Scheme III-18: Attempt of ligand exchange of **171**

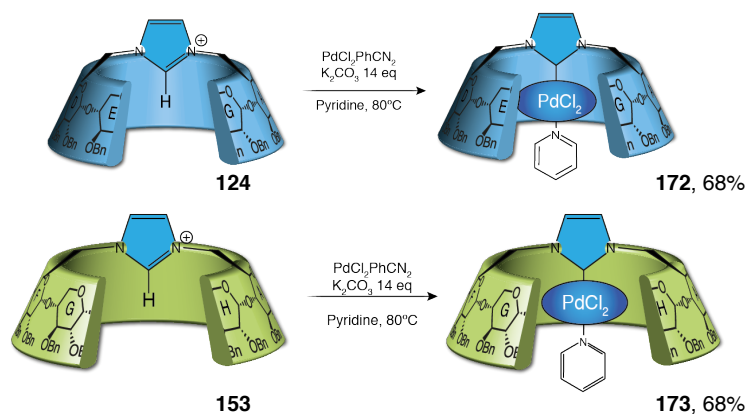
PEPPSI™-like palladium(II) (Pyridine, Enhanced, Precatalyst, Preparation, Stabilization and Initiation) complexes were recently developed by Organ as powerful and stable precatalysts, extremely active in cross-coupling reactions¹⁶⁰. Standard conditions to synthesize these complexes are treatment of an azolium precursor with K₂CO₃ in presence of a palladium salt using pyridine as solvent at 80 °C.¹⁵⁸

By using this synthetic procedure, (β -ICyD)PdCl₂(pyridine) and (γ -AE-ICyD)PdCl₂(pyridine) were obtained after a silica gel column purification in 68% and 88% yield, respectively.

¹⁵⁶ N. Hadei, E. A. B. Kantchev, C. J. O'Brien, and M. G. Organ, *Org. Lett.*, **2005**, 7, 3805 - 3807

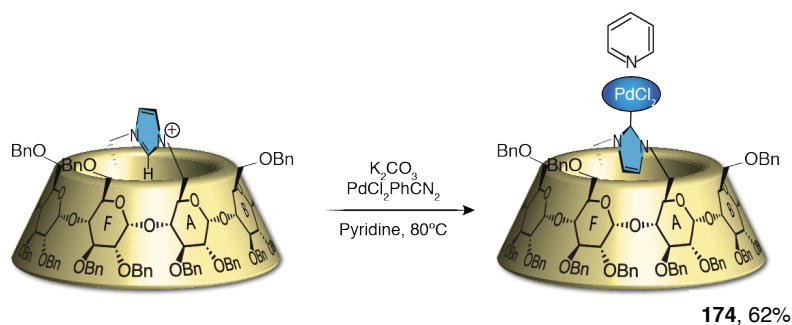
¹⁵⁷ Q. Cao, N. L. Hughes, M. J. Muldon, *Chem. Eur. J.*, **2016**, 22, 11982–11985

¹⁵⁸ M. G. Organ, S. Avola, I. Dubovyk, N. Hadei, E. A. B. Kantchev, C. J. O'Brien, C. Valente, *Chem. Eur. J.*, **2006**, 12, 4749 – 4755



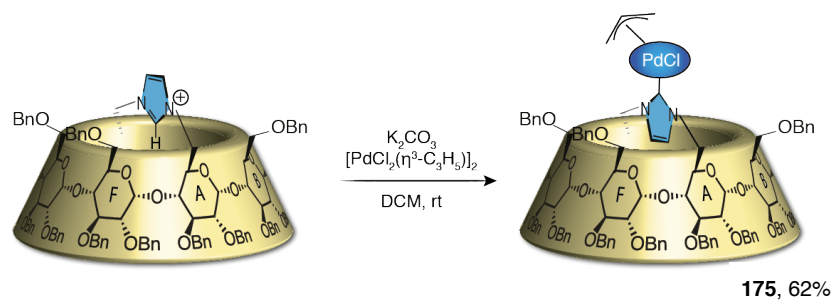
Scheme III-19: Synthesis of (γ-ICyD)PdCl₂(pyridine) and (β-ICyD)PdCl₂(pyridine).

The same reaction conditions were used with (α-ICyD)HCl. These reaction conditions afforded the reversed (α-rev-ICyD)PdCl₂(pyridine) compound in 62% yield without traces of the introverted square planar complex.



Scheme III-20: Synthesis of (α-rev-ICyD)PdCl₂(pyridine) complex.

Finally, (α-ICyD)HCl was treated with K_2CO_3 and 0.5 equivalents of $[\text{Pd}(\eta^3\text{-allyl})\text{Cl}_2]_2$ in dichloromethane to give the (α-rev-ICyD)PdCl(η³-allyl) in 62% yield after silica gel filtration (Scheme III-20).



Scheme III-21: Synthesis of (α-rev-ICyD)PdCl(η³-allyl)

iv. Analysis of structures.

- Structure and behavior of α - β - and γ -CD based (ICyD)Pd(allyl)Cl complexes

Nomenclature and structural characteristics

Due to the non-symmetrical coordination of a η^3 -allyl ligand, its complexation to a NHC-PdCl complex produces the formation of a stereogenic center on the palladium atom.¹⁵⁶ The formation of this stereogenic center leads to the formation of two different enantiomers if the NHC is achiral (Figure III-35). In the case of a chiral NHC, the product is observed as a mixture of diastereoisomers.¹⁵⁹ In addition, the five protons of the allyl moiety are not equivalent and all of them are observed in the NMR spectrum as five different signals.

Both CH_2 carbons are easily differentiated because of the reduced electron delocalization of the allyl moiety induced by the carbene implies a downfield shift in the ^{13}C -NMR of the *trans* carbon and a upfield shift of the *cis* one.¹⁶⁰

The η^3 -allyl will be named as shown in Figure III-, *cis*- and *trans*- will refer the position with respect to the NHC, and the *syn* and *anti* will be with respect to the central meso proton of the allyl.

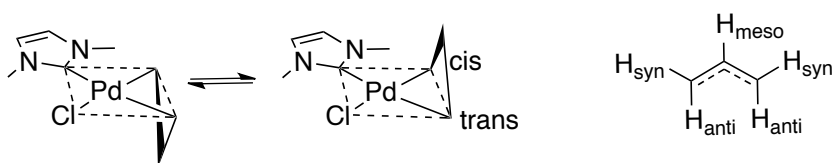


Figure III-35: Stereoisomers and nomenclature of a generic NHC-Pd(η^3 -allyl)Cl

(γ -AE-ICyD)PdCl(η^3 -allyl)

^1H -NMR of the (γ -AE-ICyD)PdCl(η^3 -allyl) **168** shows, as expected, the formation of two diastereoisomers. By integration of two isolated signals of the allyl ligand, a 6:4 ratio could be calculated, demonstrating that the asymmetric structure of the cyclodextrin cavity induced some stereoselectivity in the isomerization of the allyl ligand.

¹⁵⁹ P. G. A. Kumar, P. Dotta, R. Hermatschweiler, P. S. Pregosin, *Organometallics* **2005**, *24*, 1306 - 1314

¹⁶⁰ E. S. Chernyshova, R. Goddard, K-R. Porschke, *Organometallics* **2007**, *26*, 3236 - 3251

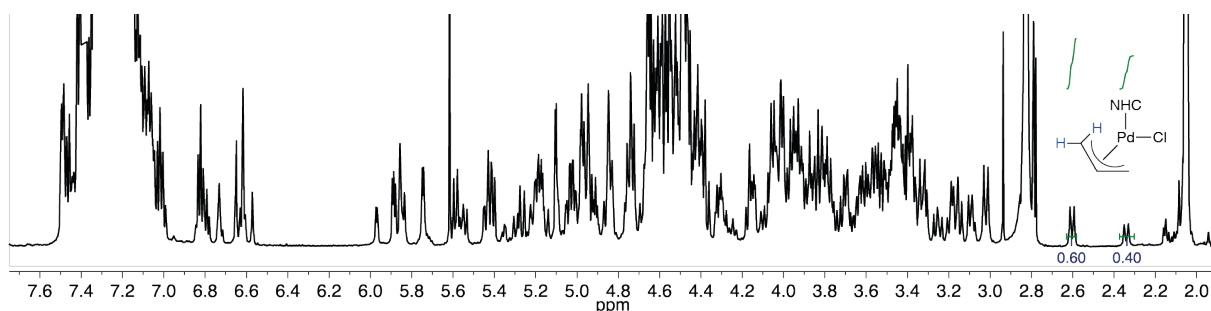


Figure III-36: $^1\text{H-NMR}$ of $(\gamma\text{-AE-ICyD})\text{PdCl}(\eta^3\text{-allyl})$. Acetone- d_6 , 600 MHz, 300 K.

From the anomeric region in the HSQC spectrum of $(\gamma\text{-AE-ICyD})\text{PdCl}(\eta^3\text{-allyl})$ complex sixteen H1-C1 cross correlations were observed (Figure III-37). These sixteen signals are the consequence of a reduction of the C2 symmetry of the cyclodextrin to a C1 symmetry, thus, all the sugars of the cyclodextrin are observed in the NMR. This loss of symmetry was produced by the complexation of a stereogenic $(\text{NHC})\text{PdCl}(\eta^3\text{-allyl})$ moiety.¹⁶¹ Thus, only two different isomers are observed.

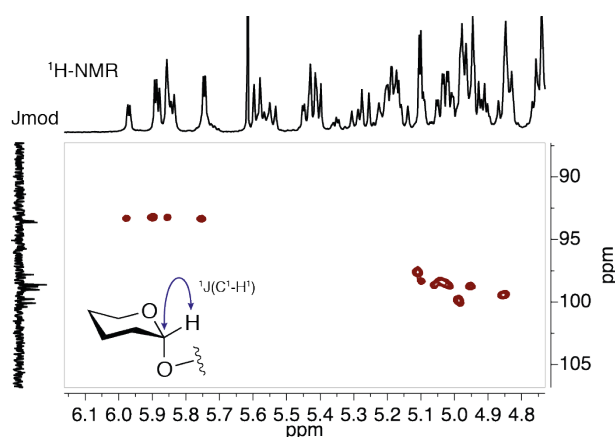


Figure III-37 : Extract of the anomeric region of the HSQC of $(\gamma\text{-ICyD})\text{PdCl}(\eta^3\text{-allyl})$ complex

The presence of two allyl complexes was verified by the presence of characteristic signals of palladium coordinated allyl complexes. Two *meso* carbon-proton correlations are observed in the frequency of carbon at 114.9 and 115.7 ppm according to a η^3 -coordination, and two sets of *cis* proton-carbon cross correlations at 44.5 and 45.7 ppm. These chemical shifts are in agreement with previously described NHC-based $\text{PdCl}(\eta^3\text{-allyl})$ complexes,^{162,163} confirming the formation of the expected complex as a mixture of diastereoisomers (Figure III-38).

¹⁶¹ S. Filipuzzi, P. S. Pregosin, A. Albinati, S. Rizzato, *Organometallics*, **2008**, *27*, 437–444

¹⁶² H. M. Peng, G. Song, Y. Li, X. Li, *Inorg. Chem.*, **2008**, *47*, 8031–8043

¹⁶³ M. S. Viciu, R. F. Germaneau, O. Navarro-Fernandez, E. D. Stevens, S. P. Nolan, *Organometallics*, **2002**, *21*, 5470–5472

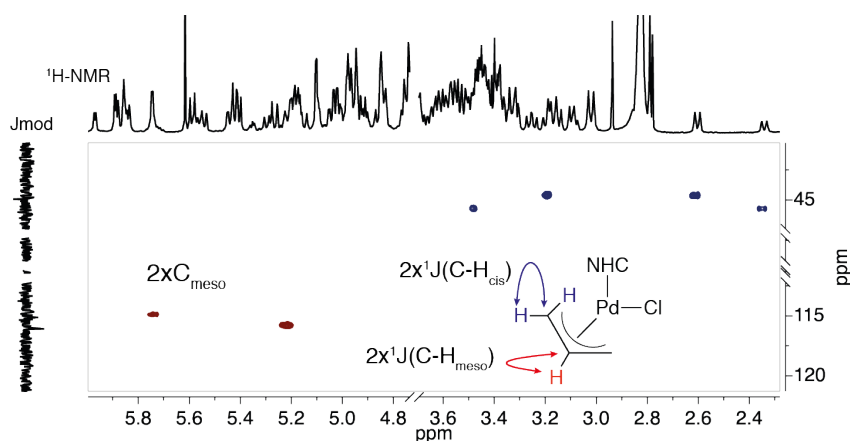


Figure III-38 : Extract of the allyl region of the HSQC of $(\gamma\text{-ICyD})\text{PdCl}(\eta^3\text{-allyl})$ complex

A particular 2D-NOESY spectrum was obtained. In addition to usual cross correlation peaks (Figure III-39 green), exchange signals between both isomers were observed (Figure III-39-blue). More precisely, in the region of H_{cis}-anti protons of the allyl ligand, key exchange cross correlations were observed at $\tau_{\text{mix}} = 800$ ms.

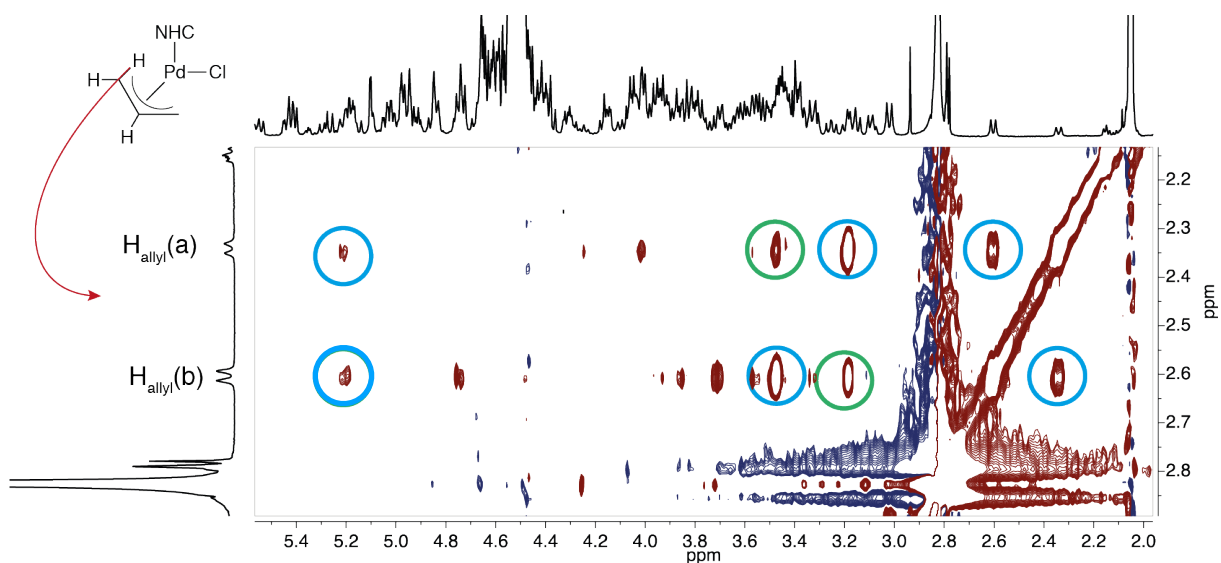


Figure III-40: NOESY of **170** at $\tau_{\text{mix}}=800\text{ms}$. Exchange signals are marked in blue and NOESY signals in green. Acetone- d_6 , 600 MHz, 300 K

Four correlations were identified in the 2D-NOESY spectra of **170** for each H-cis-anti proton. From all of them, only one was attributed to a pure NOE effect. To these signals, three different exchange signals were additionally observed for each isomer (Figure III-40).

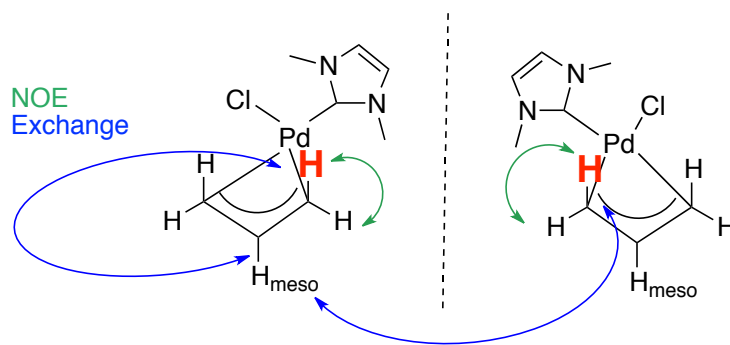
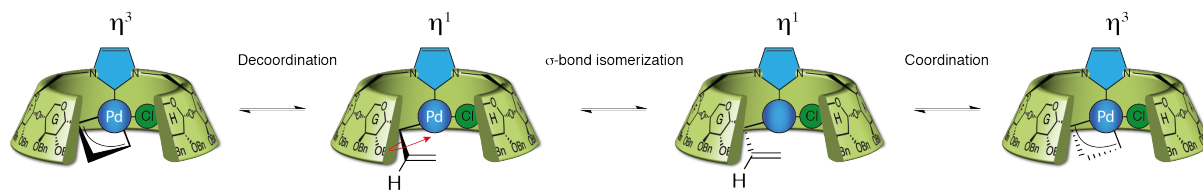


Figure III-40 :Observed signals in 2D-NOESY.

In other words, the diastereoisomerization takes place through an isomerization of the Cis-Cmeso bond¹⁶⁴. Thus, formation of a σ -bond between the palladium and the Cis carbon with the corresponding decooordination of the double bond. Formation of a σ -allyl complex able to follow a rotation around the σ -Csyn-Cmeso bond to finally form η^3 -allyl complex again. The relative position of the Hanti and Hsyn of the Cis are thus inverted (Scheme III-21). This result is in agreement with Pregosin's observations.¹⁶⁸



Scheme III-21: Proposed mechanism of the diastereomerization of (γ -AE-ICyD)PdCl(allyl)

(β -ICyD)PdCl(η^3 -allyl)

Complexation to the PdCl(allyl) inside the cavity of the β -ICyD **170** should lead also to the formation of a mixture of diastereoisomers. Surprisingly, unlike its γ -ICyD analogue, one major diastereoisomer is observed, in a ratio superior to 97:3 calculated by NMR (Figure III-41). This result shows that the cavity can control the position of the allyl moiety, and therefore, the diastereoselectivity of the complexation of the allyl.¹⁶⁸

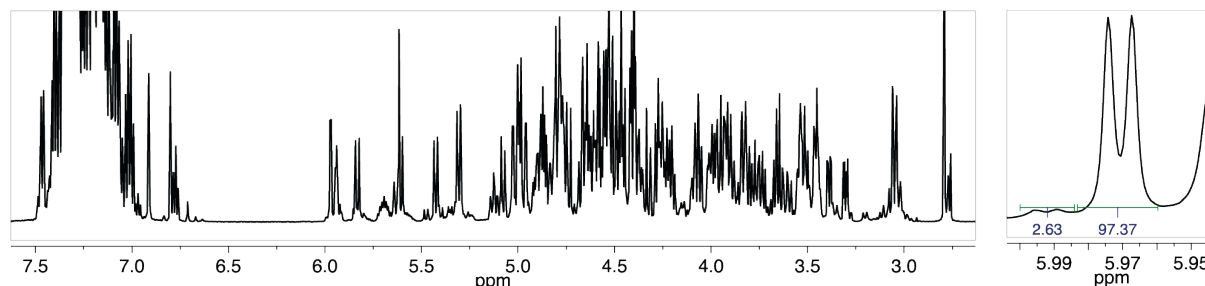


Figure III-41: Extract of $^1\text{H-NMR}$ of (β -ICyD)PdCl(η^3 -allyl) **170**. Integration of two anomeric protons of both species is shown on the right. Acetone- d_6 , 600 MHz, 300K

¹⁶⁴ H. Meyer A. Zschunke, *J. Organomet. Chem.* **1984**, 269, 209 - 216

From the anomeric region of the HSQC a single group of seven signals, confirms the presence of a major isomer (Figure III-42).

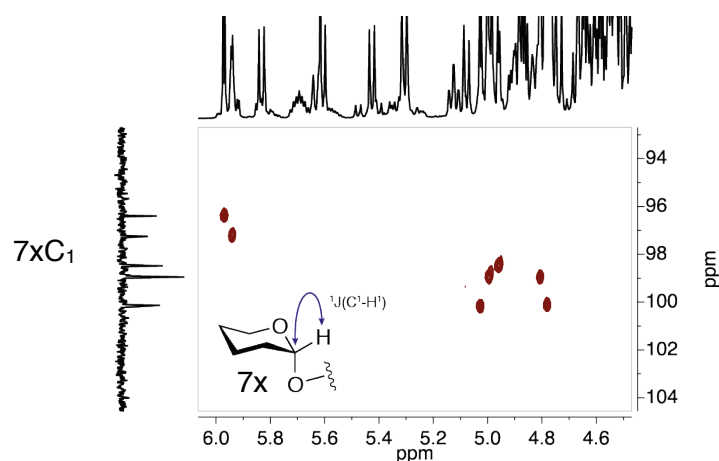


Figure III-42: Extract of HSQC of $(\beta\text{-ICyD})\text{PdCl}(\eta^3\text{-allyl})$ showing the presence of only one major isomer.
Acetone- d_6 , 600 MHz, 300K

The same information can be obtained from the allyl ligand. One single signal is observed for the meso proton-carbon correlation, and two cross correlations for the diastereotopic cis proton-carbon correlations. The split on the chemical shift of these two protons made the differentiation easy by simple comparison to the literature¹⁶⁹. The most shielded one corresponds to the *anti* one and the most deshielded one to the *syn* proton (Figure III-43).

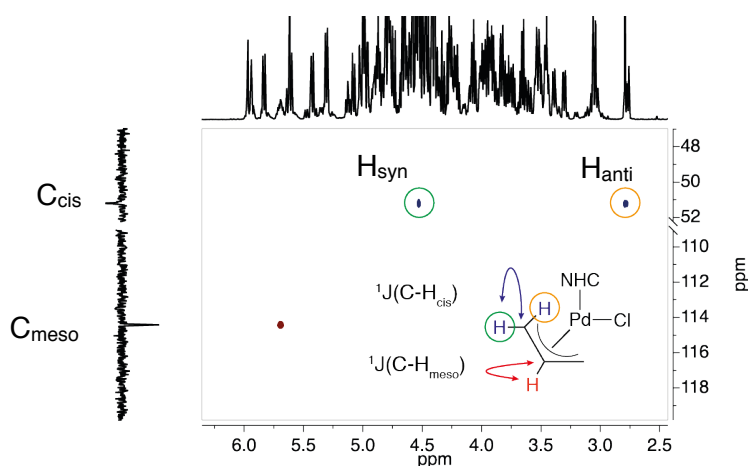


Figure III-43: Extract of HSQC of $(\beta\text{-ICyD})\text{PdCl}(\eta^3\text{-allyl})$ showing the cross correlations of the major allyl, (the minor one is not visible) acetone- d_6 , 600 MHz, 300 K

2D-NOESY shows a very clear cross-correlation peak between the H *cis* and *anti* from the allyl moiety and the H-5 of the sugar unit A that bears the NHC-bridge (Figure III-44).

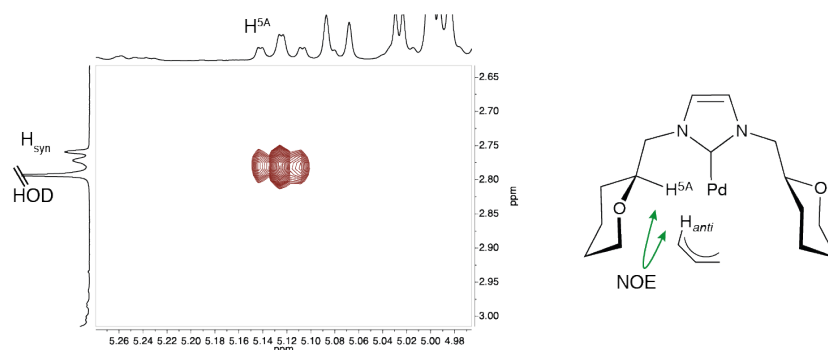


Figure III-44: NOESY extract of (β-ICyD)PdCl(η³-allyl) showing a cross correlation between the H-5A and the *anti/cis* proton of the allyl.
Acetone-d₆, 600MHz, 300K

Since this allyl proton has only one cross correlation peak with the cyclodextrin, the C-carbene—Pd bond rotation will be considered as slow, on the analysis timescale ($\tau_{\text{mix}} = 800\text{ms}$). This NOESY cross correlation was used as key data in the structural determination of the complex. Either the allyl ligand is included in the bigger loop of the macrocycle, (E,F,G sugar units, Figure III-45B), either it is encapsulated in the smaller one (B, C sugar units, Figure III-45A). In any case, as observed for all the complexes presented previously, the downfield shifts of the H5 and H3 will be the other key structural informations in the elucidation of the structure. Additionally, assuming the square planar geometry around the palladium atom, the chlorido ligand will be placed on the opposite side of the macrocycle.

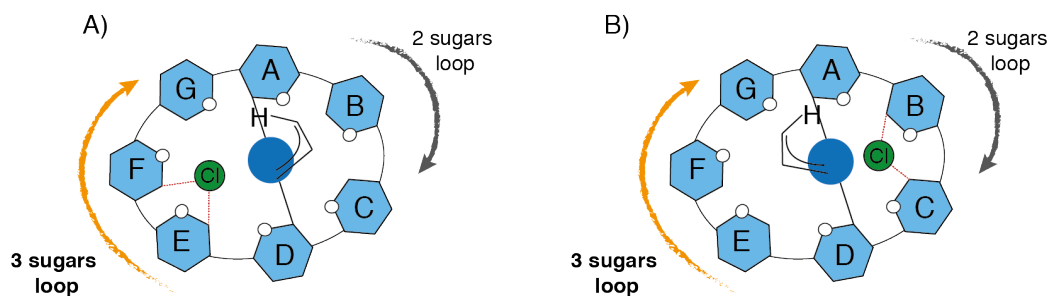


Figure III-45: Schematic representation of the two structures according to the NOESY cross correlations

To discriminate between these two possible structures, the chemical shifts of the intra-cavity protons were studied. As for all the introverted complexes, a downfield shift of the H5 A and D is observed (Table III-6) due to the C-H \cdots M interaction with the metal. Comparing the rest of the H5, a downfield shift is observed on the H5 of sugar units E and F (deshielded almost by 1 ppm in comparison with C and G) and on the H3 F and G (deshielded by 0.5 and 0.75 ppm in comparison of the rest of H3). In contrast, there are no deshieldings on the sugar units B and C, confirming the presence of the allyl in the smallest loop of the macrocycle, as proposed in the Figure III-45B.

Complex	H	Cycle A	Cycle B	Cycle C	Cycle D	Cycle E	Cycle F	Cycle G
$(\beta\text{-ICyD})\text{PdCl}_2(\eta^3\text{-allyl})$	H5	5.13	3.54	4.01	4.79	4.82	4.91	4.09
	H3	3.81	4.08	4.13	4.13	4.08	4.50	4.75

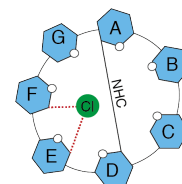


Table III-6: $^1\text{H-NMR}$ chemical shifts of the intra-cavity protons of $(\beta\text{-ICyD})\text{AuCl}_3$ and $(\beta\text{-ICyD})\text{PdCl}_2(\eta^3\text{-allyl})$. Acetone- d_6 , 600 MHz, 300 K

With all this information, as for the rest of the complexes, the Pd atom was placed between the H5 A and D according to the NMR deductions. To model the E,F,G sugars, the chlorido ligand was placed in the between the H3 and the H5 of the cyclodextrin, and the sugars were tilted to obtain relative distances in agreement with the other of the NMR chemical shifts. After a final UFF optimization the structures obtained are shown in the figure III-46.

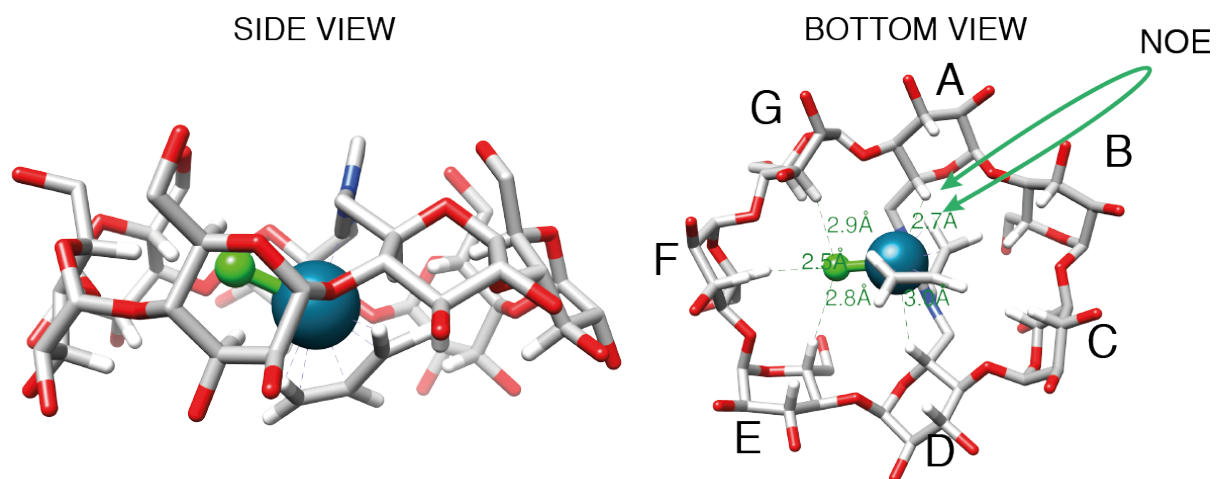


Figure III-46: Modeled structures of $(\beta\text{-ICyD})\text{PdCl}(\eta^3\text{-allyl})$ **170**

In contrast to the linear complexes, the Pd atom is moved away from the walls of the B,C sugar units, placed in the exact middle of the cavity. The chlorine atom is deeply included at the H5 level of the cyclodextrin and the allyl ligand partially included inside the cavity. The distances obtained for the different parts of the complex are consistent with the downfield shifts described in the literature for C-H \cdots M and C-H \cdots Cl interactions.^{90,117}

$(\alpha\text{-rev-ICyD})\text{PdCl}(\eta^3\text{-allyl})$

In the case of the $\alpha\text{-rev-ICyD}$ complex, two species are also observed in the $^1\text{H-NMR}$. As for the $(\gamma\text{-ICyD})\text{PdCl}(\eta^3\text{-allyl})$ analogue, by integration of the two shielded protons of the allyl ligand of both isomers a 1:1 ratio is deduced (Figure III-47). The anomeric protons H1-C,F isolated in the $^1\text{H-NMR}$ as well as the characteristic deshielded protons of the NHC, integrates for four protons, compared to one of the allyl, suggesting a C_2 symmetry for both complexes.

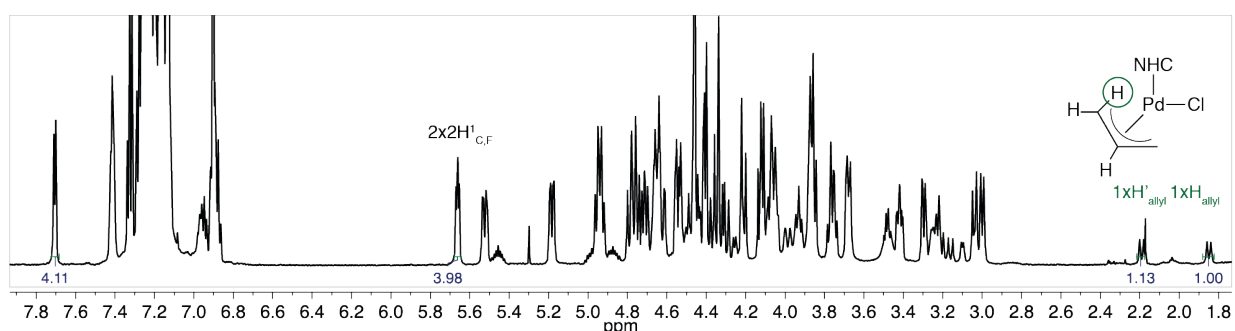


Figure III-47: $^1\text{H-NMR}$ of $(\alpha\text{-rev-ICyD})\text{PdCl}(\eta^3\text{-allyl})$
 CDCl_3 , 600MHz, 300K

By analyzing the anomeric region of the HSQC six signals corresponding to six different H1-C1 cross-correlations were found (Figure III-48). Also in accordance with a possible mixture of two C₂ symmetric complexes., which is, this time, in contrast with γ -ICyD and non-confined NHC complexes,¹⁷⁰ where C₁ symmetries are observed

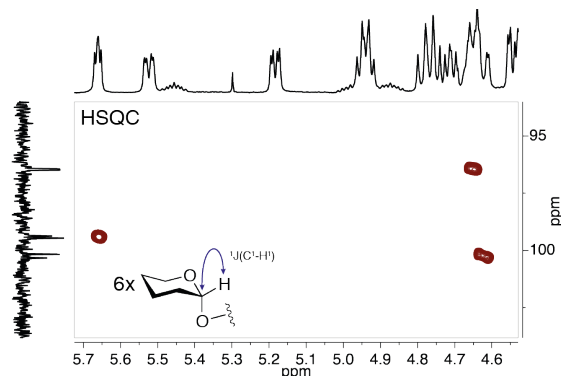


Figure III-48: HSQC of the anomeric region of (α -rev-ICyD)PdCl(η^3 -allyl) CDCl₃, 600MHz, 300K

The presence of two allyl moieties was also confirmed by HSQC since two different signals at 114.8 and 114.9 ppm are observed, corresponding to the proton-carbon *meso* cross-correlations. Multiplicities and chemical shifts also suggested to two η^3 -coordinated species.¹⁶⁹

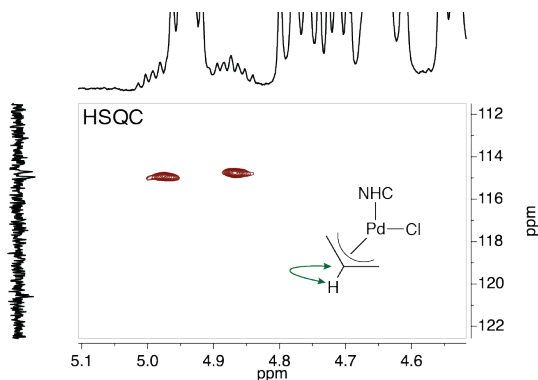


Figure III-49: HSQC of the *meso*-allyl region of (α -rev-ICyD)PdCl(η^3 -allyl) CDCl₃, 600MHz, 300K

Two cross correlation peaks were observed between the CH of the NHC and the carbenic carbon in the HMBC spectra (Figure III-50). Confirming the coexistence of two C₂-symmetrical complexes.

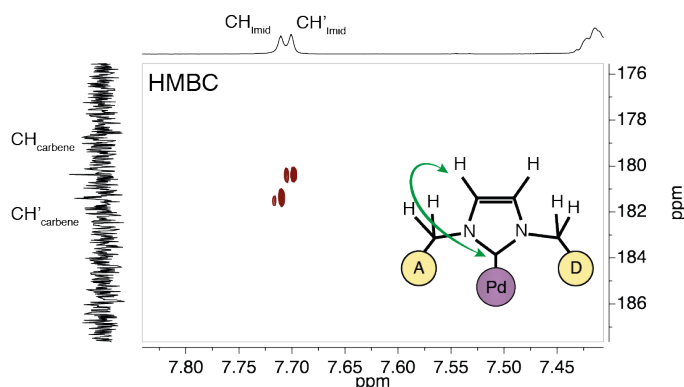


Figure III-51: HMBC of the carbene region of $(\alpha\text{-rev-ICyD})\text{PdCl}(\eta^3\text{-allyl})$ showing the presence of two carbenes.
 CDCl_3 , 600MHz, 300K

As for the $(\alpha\text{-rev-ICyD})\text{AuCl}$ analogue, three cross correlation peaks were observed on the 2D-NOESY between the CH of the NHC and the intra-cavity protons H-5A,D, H-3C,F and the H5C,F (Figure III-51).

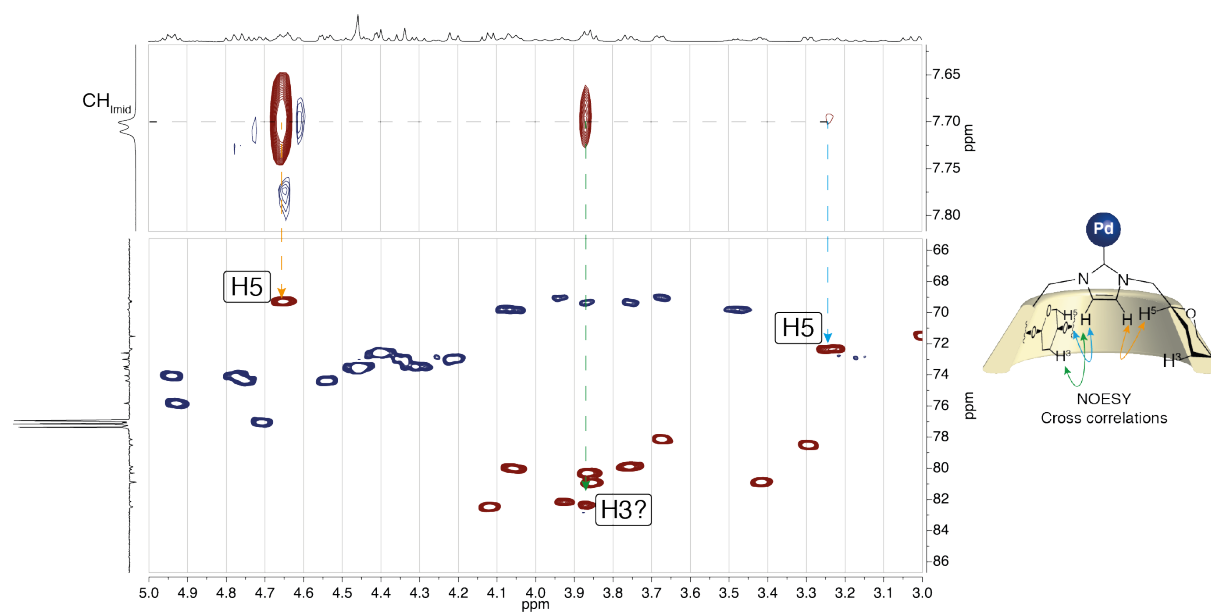


Figure III-51: NOESY and HSQC of $(\alpha\text{-rev-ICyD})\text{PdCl}(\eta^3\text{-allyl})$ showing cross correlations between the CH of the imidazole and some intra-cavity protons.
 CDCl_3 , 600 MHz, 300K

In contrast to its γ -analogue, a different pattern on the 2D-NOESY was observed on the allyl part. In this complex, 2D-NOESY and exchange cross correlations signals were observed between the four H_{cis} of the allyl moiety (Figure III-52, green NOESY, blue exchange). In contrast, no cross correlations were observed with the H_{meso} of the allyl (region showed on the image with a yellow rectangle).

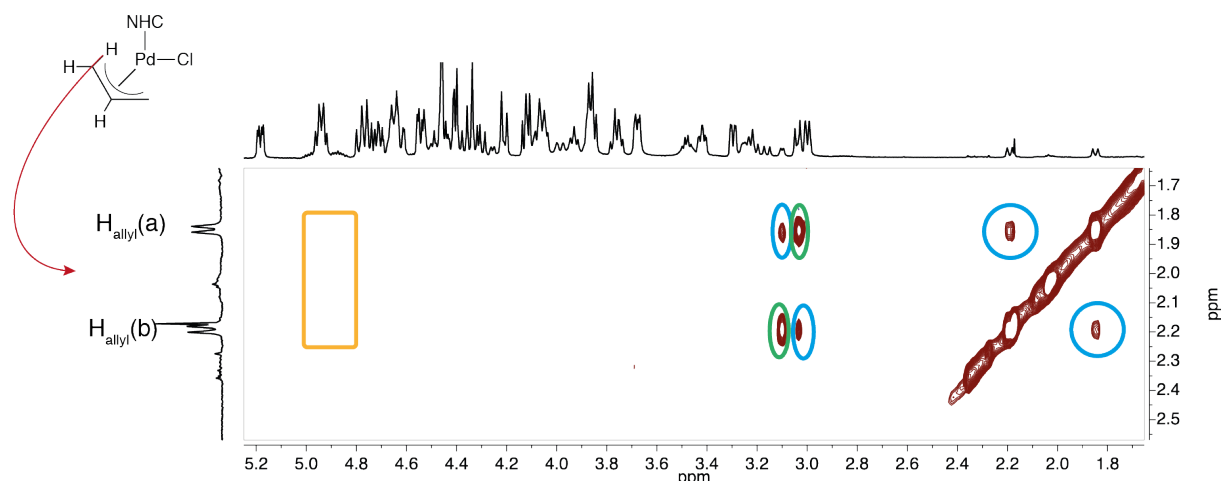
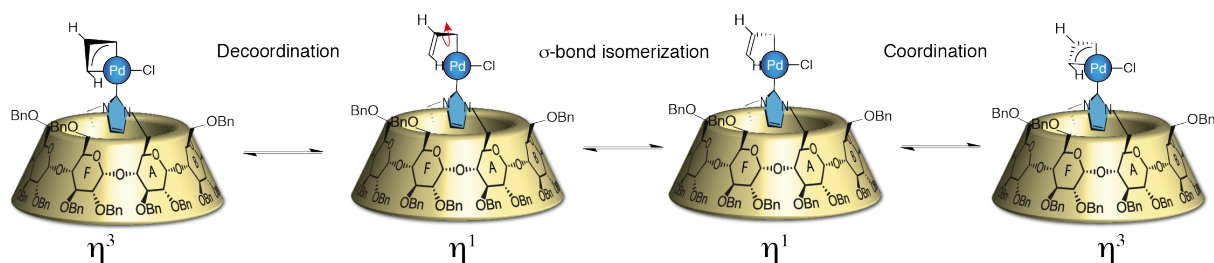


Figure III-52: Extract of 2D-NOESY spectra of (α -rev-ICyD)PdCl(allyl). Exchange signals are marked in blue, NOESY in green and the region of the H_{meso} is marked with a yellow rectangle.
CDCl₃, 600 MHz, 300 K $\tau_{\text{mix}} = 800$ ms

This different 2D-NOESY pattern suggests that the diastereoisomerization mechanism differs for this complex. What is clear is that the stereochemistry between the C_{cis} and the C_{meso} is conserved. The most probable mechanism in agreement for this observation involves, in analogy to the one presented for the γ -ICyD-complex,¹⁶⁸ a isomerization through the C_{meso}-C_{trans} bond. This mechanism starts with the formation of the η^1 -allyl complex by decooordination of the double bond to form a σ -bond between the Pd and the C_{trans} carbon. Then, rotation around the σ -C_{trans}-C_{meso} bond, this one, after a final complexation of the double bond gives the diastereoisomer of the palladium center without changing the relative position of the H_{cis} and the H_{meso} (Scheme III-22).



Scheme III-22: Proposed mechanism of diastereoisomerization of (α -rev-ICyD)PdCl(allyl)

Due to the overlapping of signals in the NMR experiments, cross correlations between the *Htrans* and the *Hmeso* could not be found in 2D-NOESY experiments. To elucidate this mechanism, cleanEXSY sequences are under development.

In conclusion, with this three (ICyD)PdCl(allyl) complexes, three different effects of the encapsulation and the coordination mode on the dynamic behavior of a complex were observed. It was found that the complexation in the chiral pocket of the (γ -AE-ICyD)PdCl(allyl) complex formed a mixture of diastereoisomers in a 6 : 4 ratio. When the complexation is done inside a narrower cavity (β -ICyD), the ratio of diastereoisomers was significantly increased at more than 97 : 3. Finally, the outer coordination of the (α -rev-ICyD) afford a 1 : 1 mixture of complexes. This complex was revealed as C_2 symmetric, unexpected for monodentated NHC.

168

Additionally, the observed mechanisms of diastereoisomerization for the (α -rev-ICyD) and the (γ -ICyD)-based complexes were different in both cases. (α -rev-ICyD) was found to isomerize with the η^1 -allyl complex coordinated by the *Ctrans* carbon. In contrast, with the (γ -ICyD)PdCl(allyl) complex the carbon found to be bonded to the Pd atom was the *Ccis* one. These differences in the isomerization mechanism will be tried to be applied in the development of selective allylation reactions.

- Structures of γ - β - and α -CD-based (ICyD)PdCl₂(pyridine) complexes. Structure, shape and confirmation with DFT calculations

Bulky NHC-based Pd pyridine compounds are more and more exploited as catalysts in palladium chemistry¹⁶⁵. To understand the reactivity of ICyD-based Pd complexes the three-dimensional structure is required first.

The same methodology was followed to elucidate the shape of all the (ICyD)PdCl₂(pyridine) complexes. Analysis of the chemical shifts of the H5 and H3 pointing inside the cavity allowed us to deduce relative distances depending on the δ . Finally, the metal and the sugar units were placed according to this relative distances. As for the square planar (γ -ICyD)AuCl₃, it will be considered that the only interaction of the H5-A and E was the one with the metal. The rest of the downfield shifts will be considered to be an interaction with the equatorial chlorido ligands.

As observed on the NMR, the order of H5 proton chemical shifts in the (γ -ICyD)PdCl₂(pyridine) **173** complex is H5-A,E (the most deshielded), then B,F; C,G and finally D,H (Figure III-53). According to the previous hypothesis and experiences, H5-A,E is deshielded because of the presence of a M-H interaction, and the rest of H5 due to the presence of the two diametrically opposed equatorial chlorido ligands of the square planar palladium complex.

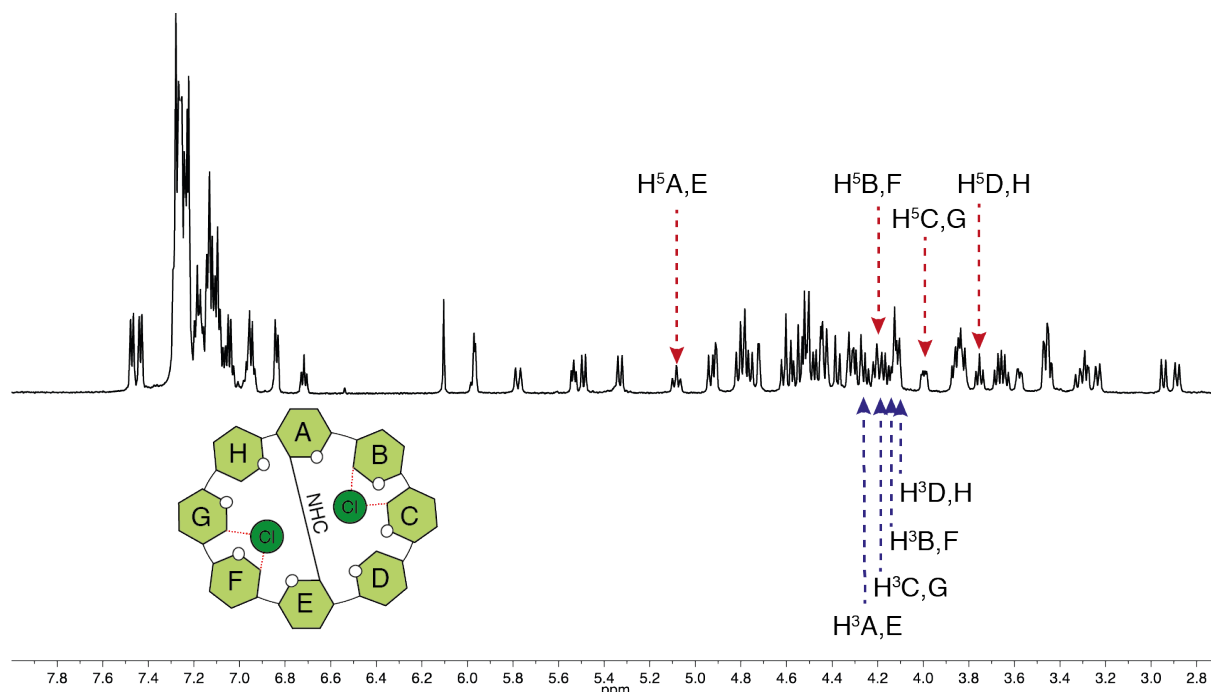


Figure III-53: ¹H-NMR of (γ -ICyD)PdCl₂(py). CDCl₃, 600 MHz, 300 K.

¹⁶⁵ R. D. J. Froese, C. Lombardi, M. Pompeo, R. P. Rucker, M. G. Organ, *Acc. Chem. Res.* **2017**, *50*, 2244 - 2253

As presented for the rest of complexes, the model was constructed placing the palladium atom in the middle of the cavity between the sugar units A and E, then, the equatorial chloride ligands were placed next to the most deshielded sugar units H5-B,F and the rest were tilted according to the relative distances deduced from the NMR. The resulting modeled structure is presented in the figure III-54 and the measured distances and the chemical shifts are reported in table III-7.

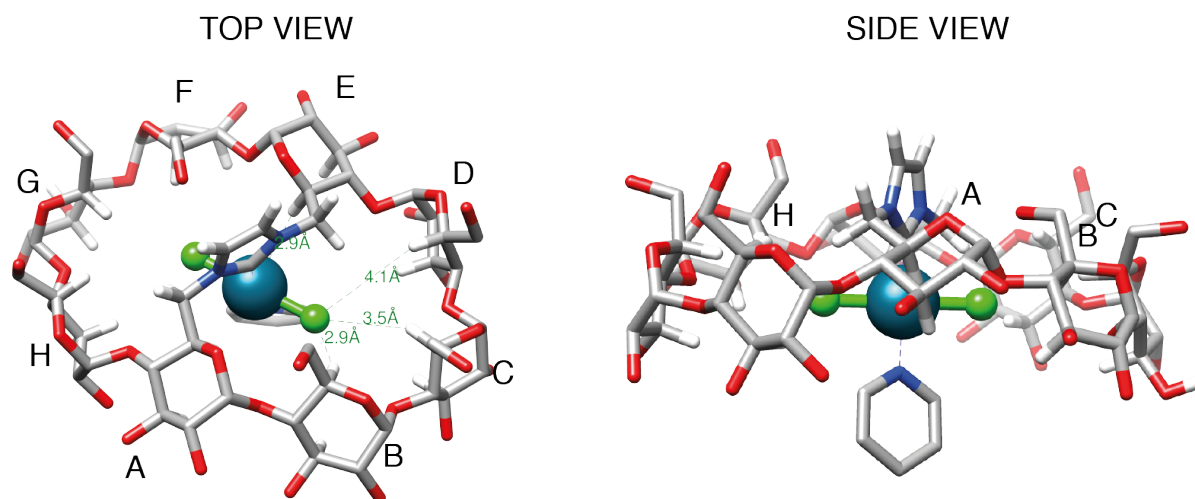


Figure III-54: Modeled structure of $(\gamma\text{-ICyD})\text{PdCl}_2(\text{pyridine})$

$(\gamma\text{-ICyD})\text{PdCl}_2(\text{py})$		A/E	B,F	C,G	D,H
δ / ppm	H5	5.08	4.21	3.99	3.58
	H3	4.25	4.11	4.16	4.12
DISTANCES-H5-Cl _{axial} /Å		-	2.9	3.5	4.3

Table III-7: Chemical shifts of intra-cavity protons $(\gamma\text{-AE-ICyD})\text{PdCl}_2(\text{pyridine})$ **173** complex and distances obtained from the modeled structure.

It can be observed on the modeled structure a complete inclusion of the PdCl_2 moiety at the level of the H5. In contrast, the pyridine is placed at the entrance of the cavity, coordinated in axial position of the complex. This *trans* complexation of the pyridine can be verified with the observed upfield shift of the H-3D,H (-0.18 ppm by comparison with the AuCl_3 analogue) downfield shift attributed in the $(\gamma\text{-ICyD})\text{AuCl}_3$ complexes to a $\text{CH}_3\text{-Cl}$ interaction. Unfortunately, any NOESY signal was observed between the pyridine and the protons of the cyclodextrin, probably, because a fast rotation of the Pd-N bond.

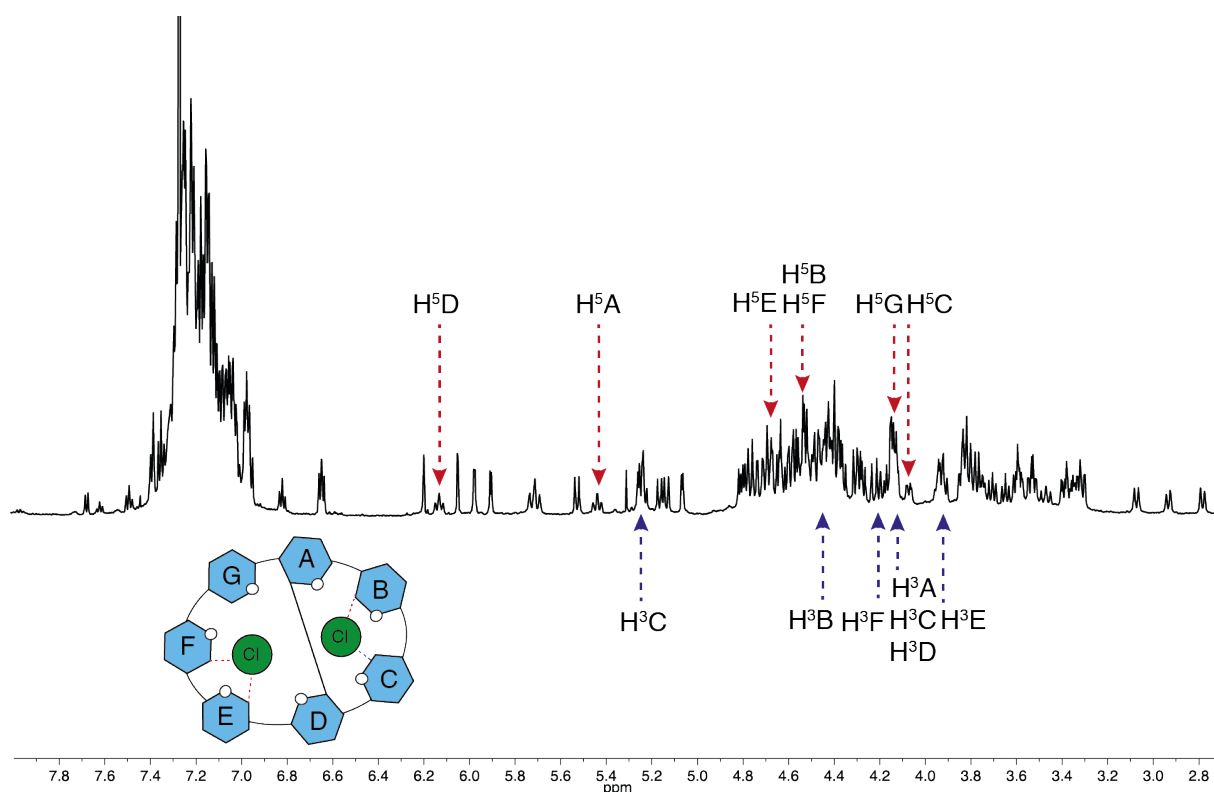


Figure III-55: $^1\text{H-NMR}$ of $(\beta\text{-ICyD})\text{PdCl}_2(\text{pyridine})$ **172**. CDCl_3 , 600 MHz, 300 K.

The same reasoning was followed to deduce the structure of the $(\beta\text{-ICyD})\text{PdCl}_2(\text{pyridine})$. After analysis all the NMR, the chemical shifts of the intra-cavity protons were analyzed to find where the chlorido ligands of the palladium complex were placed inside the cavity (Figure III-55).

Then as presented several times during this chapter, the sugar units of the macrocycle were tilted according to the relative distances obtained from the NMR. Thus, once again, the palladium atom is placed in the inside of the cavity, slightly closer from the most deshielded H-5D. Then, chlorido ligands are placed inside the cavity, the first one, in the big loop next to the H5 E and F, and the second one, between the H5-B and the H3-C the only one deshielded. After a final UFF optimization of the system the result is shown on the figure III-56 and the measured distance on the table III-8.

$(\beta\text{-ICyD})\text{PdCl}_2(\text{py})$	A	B	C	D	E	F	G
δ / ppm	H5 5.42	4.49	3.93	6.12	4.68	4.52	4.12
	H3 4.14	4.40	5.22	4.12	3.91	4.19	4.14
Distances H5-Cl	-	4.1Å	5.6Å	-	4.0Å	4.8Å	4.3Å

Table III-8: Chemical shifts of intra-cavity protons $(\beta\text{-ICyD})\text{PdCl}_2(\text{pyridine})$ complex and distances obtained from the modeled structure. CDCl_3 , 600 MHz, 300 K.

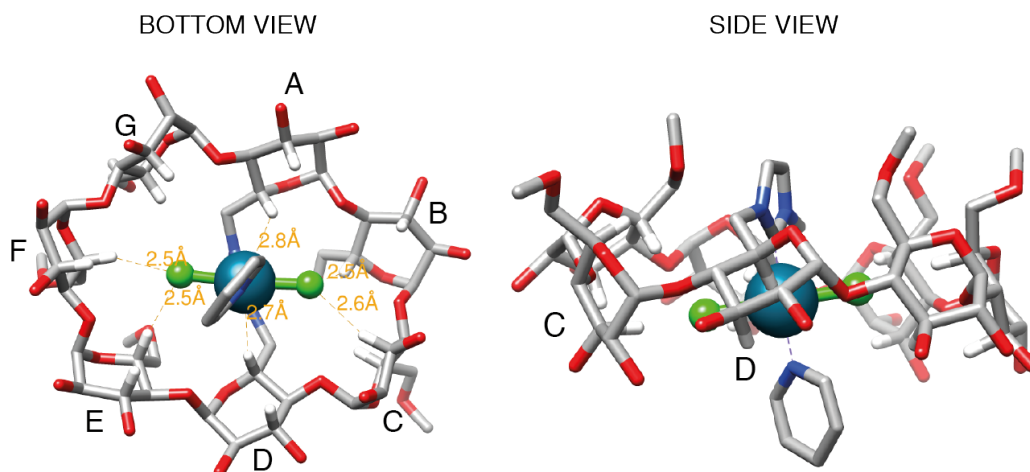


Figure III-56: Top view and side view of the modeled structures of $(\beta\text{-ICyD})\text{PdCl}_2(\text{pyridine})$.

It can be observed on the modeled structure a slightly distorted coordination, with extremely tilted C and B sugars. As observed for the AuCl_3 analogue, one of the Cl atoms is closer to the entrance of the cavity, closer to the H3; and the other one, completely included at the H5 level. The pyridine ligand, also coordinated at the axial position, is as observed previously, placed at the entrance of the cyclodextrin.

To finish the analysis of the $(\text{ICyD})\text{PdCl}_2(\text{pyridine})$ compounds, the $(\alpha\text{-ICyD})$ analogue was studied. To avoid the overlapping of signals in the 2D-NOESY experiment and confirm the cross correlations with the intra-cavity protons, selective 1D NOESY was performed by irradiation of the CH of the imidazole to suppress all the signals of the 1D- ^1H -NMR spectrum without NOE effect (Figure III-57).

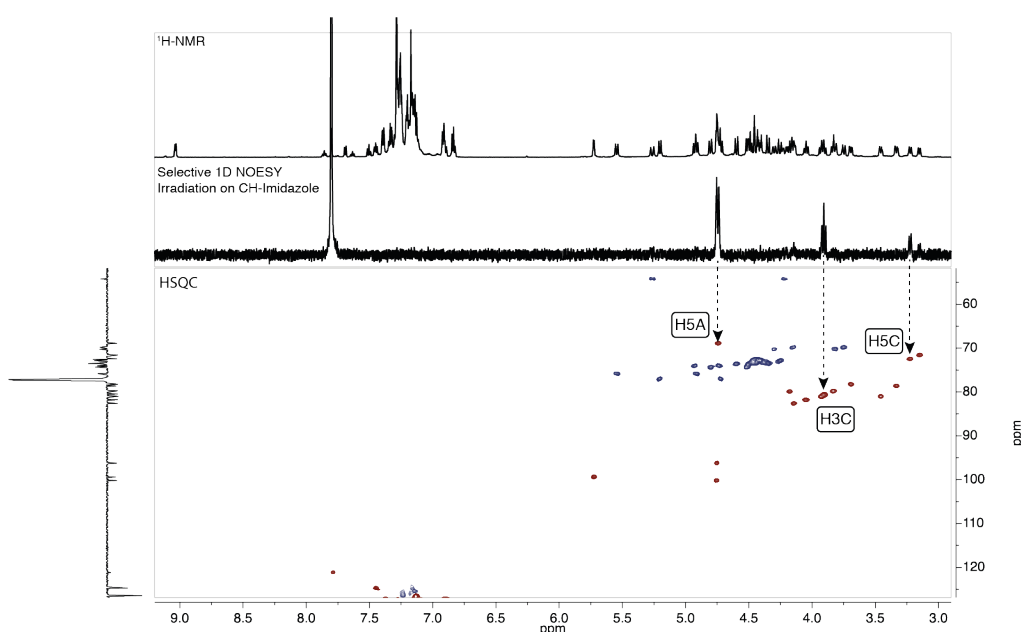


Figure III-57: Stacked of ^1H -NMR, NOESY and HSQC showing the spatial proximity of the CH of the NHC and the intra-cavity protons H5A, H5C and H3C. CDCl_3 , 600MHz, 300K

The structure of this compound was estimated starting with the (α -rev-ICyD)AuCl complex. By returning the NHC and adding the PdCl₂(pyridine) complex, after a UFF optimization the structure obtained is showed in Figure III-58 with the NOE distances marked in green.

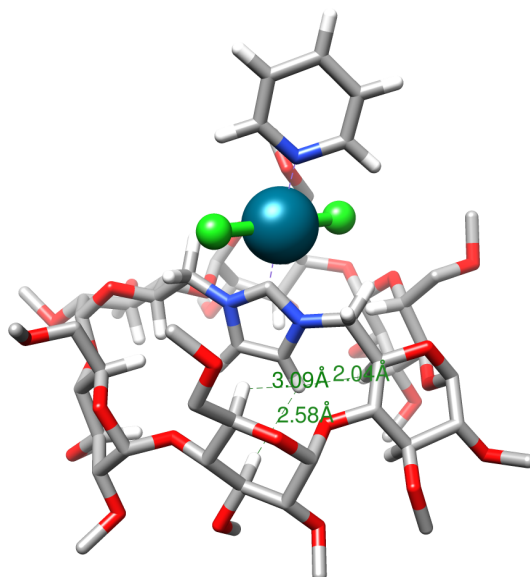


Figure III-58: Modeled three-dimensional structure of (α -rev-ICyD)PdCl₂(pyridine). Distances according to the NOE are shown in green.

The position of the NHC was verified, in addition to the NOESY correlations, with the coupling constants between the H5 and both H6. As it can be observed in the 1D-NOESY spectrum, the H5 are observed as broad doublets and not as the usual triplet observed for the introverted ICyDs. The calculated dihedral angle using Haasnot's method¹⁶⁶ are 59°, 108°, 247° and 294° using the coupling constant of $^3J_{H5-H6a} = ^3J_{H5-H6b} = 2.8$ Hz obtained from the 2D-Jres spectrum. Only two conformations fit with this dihedral angles, the staggered one with the two H6 at 60°, or the eclipsed one with the H5 and both H6 at 120° (Figure III-59).

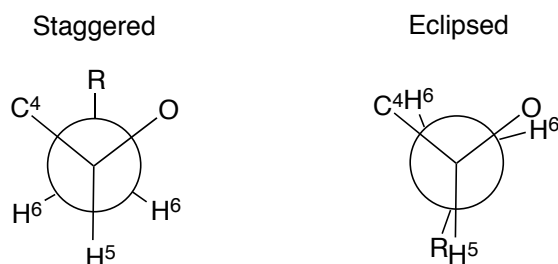


Figure III-59: Staggered and eclipsed conformations around the C5-C6 bond.

¹⁶⁶ C. A. G. Haasnoot, F. A. A. M. Leeuw, C. Altona, *Tetrahedron* **1980** 36 2783 - 2792

As it can be observed on the modeled structures, the structure directly obtained is the eclipsed one, with a internalization of the NHC and a complete exposition of the Pd center to the outside of the cyclodextrin.

The internalization of the NHC and the eclipsed conformer with the H-5A,D, places this last protons exactly in the anisotropic cone of the aromatic ring. This fact, explains the downfield shifted H-5A,D at 4.75 ppm of a complex where the metal atom is placed outside of the cavity.

v. QM-MM modeled structure of (β -ICyD)PdCl₂(pyridine).

To validate all the procedure of the modeling based on NMR, QM-MM calculations were performed to get the structure of the (β -ICyD)PdCl₂(pyridine) complex¹⁶⁷. The obtained structure, compared to the NMR deduced, is shown on the Figure III-60 (Benzyl groups and non-intra-cavity hydrogens were removed for clarity). A slight distortion of the square planar geometry with an 160° C-Pd-N(pyridine) angle of the complex was obtained by DFT structure. To appreciate the similarity between both structures distances between the H5 and the metal (used as reference point) were measured and reported on the table III-9.

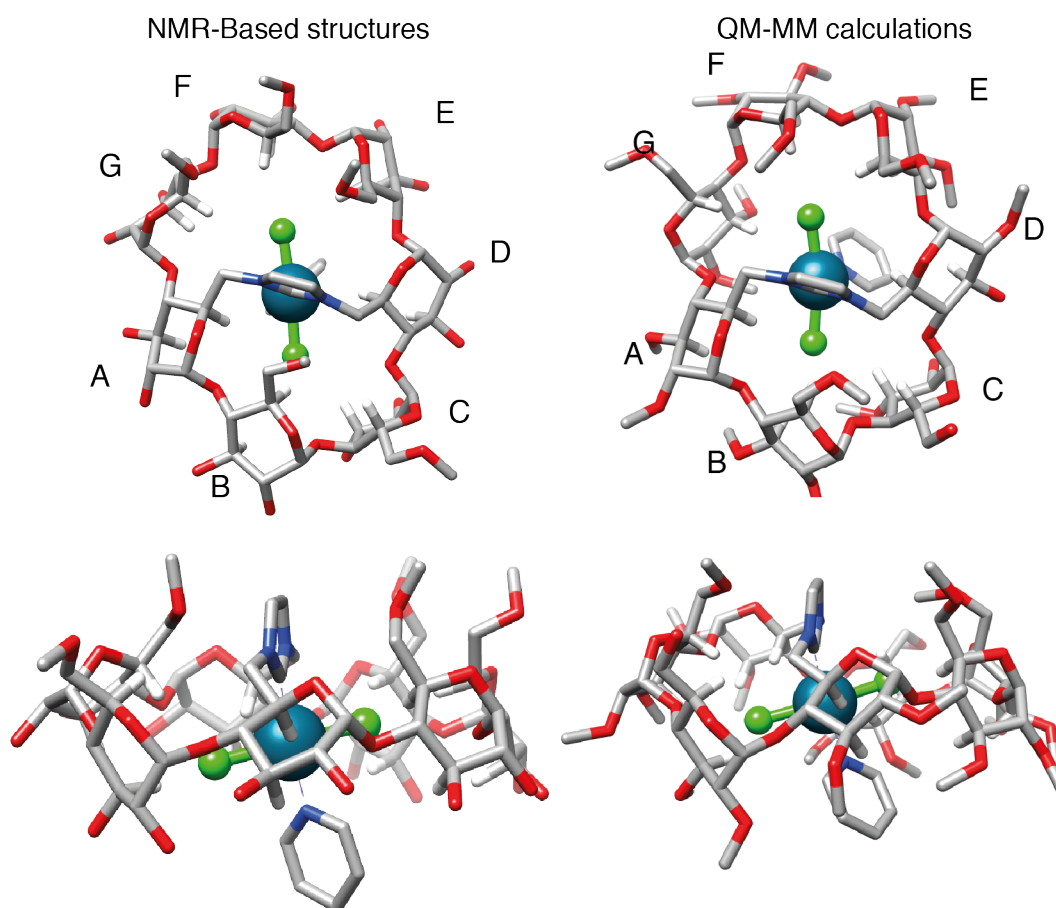


Figure III-60: NMR-based structures (left) and QM-MM calculated structures of β -ICyD)PdCl₂(py)

¹⁶⁷ Structures calculated by Dr Etienne Derat. Benzyl groups have been removed for clarity.

Proton	A	B	C	D	E	F	G	C-Pd
NMR models	2.8Å	4.1Å	5.6Å	2.7Å	4.0Å	4.8Å	4.3Å	1.9Å
QM-MM	3Å	4.2Å	5.0Å	2.8Å	4.2Å	4.8Å	4.5Å	2Å

Table III-9: Distances between the H5 of each sugar and the Pd center of the NMR-based proposed structures and the calculated one

It can be appreciated in the reported distances a precision of less than 0.2 Å (~10%) for all the H5 of the cyclodextrin except the sugar unit C, because is the only sugar unit without weak interactions, thus, without any probe of the position. These two similar structures validate the whole methodology and all the hypotheses done during the elucidation of the structure of the cyclodextrin-based square planar complexes.

vi. Electrochemistry of (ICyD)PdCl₂(pyridine) compounds

As presented previously, (ICyD)AuCl complexes showed, for the first time, an activity on cyclic voltammetry that differs from a model complex (IBn)AuCl. This fact, aroused our interest to study the behavior of the Pd analogues.

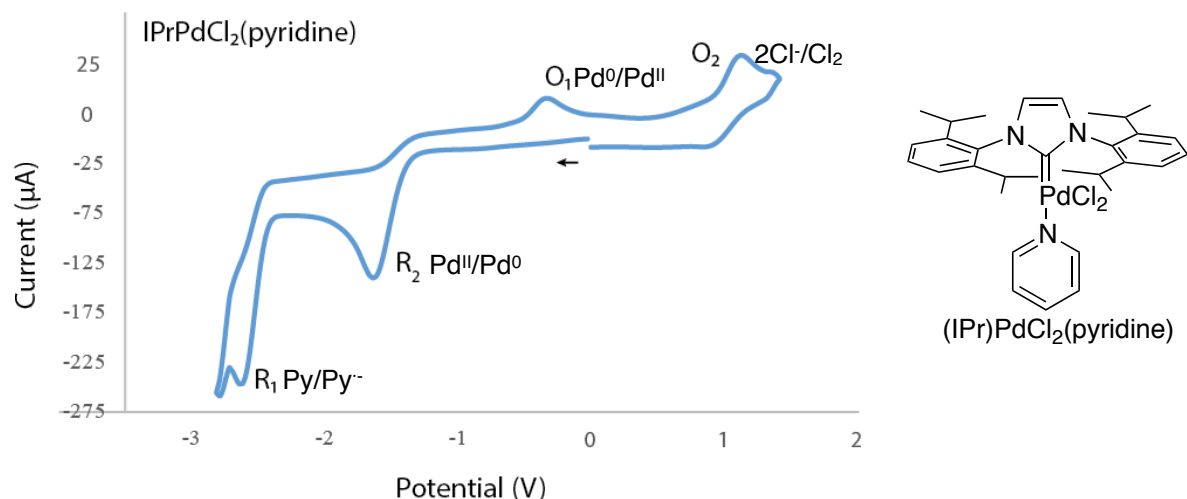
To continue the study of the effect of the cavity size and coordination modes of in the redox properties of these compounds, cyclic voltammetry of the cyclodextrin-based PdCl₂(pyridine) complexes were performed. As for NHC-gold complexes, only a couple of studies of the electrochemical properties of simple NHC ligands are reported in the literature^{168,169}

To get a model complex with the redox potentials of an imidazolylidene compound, control experiences were carried out with (IPr)PdCl₂(pyridine) in acetonitrile. In the reduction direction, this complex shows two reduction waves, one irreversible at -1.67 V (R2) produced by a two electron reduction of the Pd^{II} to Pd⁰, and the reversible R1, probably due to a reduction of the complexed acetonitrile (solvent), pyridine, or both, at -2.61 V.

Two oxidation waves are then observed on the reoxidation way, the O1 reoxidation of the electrogenerated Pd⁰ to Pd^{II} at -0,29 V and the oxidation of Cl⁻ in Cl₂ at 1.15V (Figure III-61).

¹⁶⁸ J. Pytkowicz, S. Roland, P. Mangeney, G. Meyer, A. Jutand, *J. Organomet. Chem.*, **2003**, 678, 166 - 179

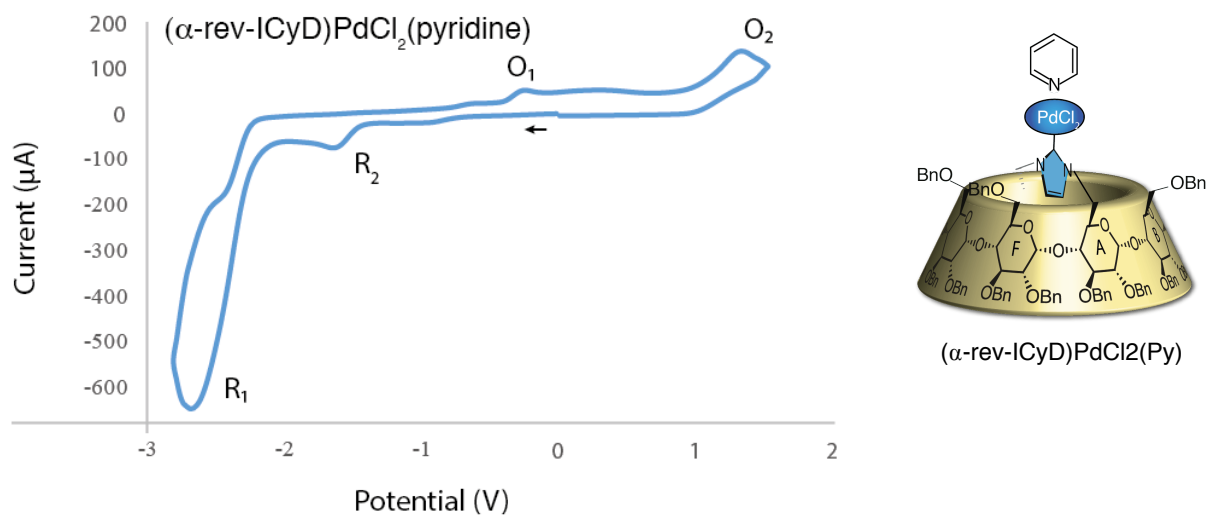
¹⁶⁹ J. A. Therrien, M. O. Wolf, B. O. Patrick, *Inorg. Chem.*, **2014**, 53, 12962 - 12972



Complex	R ₁	R ₂ (Pd ^{II} /Pd ⁰)	O ₁ Pd ⁰ /Pd ^{II}	ΔE (R ₂ /O ₁)
(IPr)PdCl ₂ (pyridine)	-2.61 V	-1.64 V	-0.29 V	1.35 V

Figure III-61: Cyclic voltammogram of (IPr)PdCl₂(pyridine). MeCN, [(IPr)PdCl₂] = 2 mM TBABF₄, 0.1M, GC 3 mm, CE Pt wire, SCE, 20°C, 0.5 V/s 2mM.

Same results have been observed for the (α-rev-ICyD)PdCl₂(pyridine) complex. Two reduction waves and two oxidations involving the same couples at the same redox potentials were observed (Figure III-62).



Complex	R ₁	R ₂ (Pd ^{II} /Pd ⁰)	O ₁ Pd ⁰ /Pd ^{II}	ΔE (R ₂ /O ₁)
(α-rev-ICyD)PdCl ₂ (pyridine)	-2.64 V	-1.68 V	-0.22 V	1.46 V

Figure III-62: Cyclic voltammogram of (α-rev-ICyD)PdCl₂(pyridine). [(IPr)PdCl₂] = 2 mM TBABF₄, 0.1M, GC 3 mm, CE Pt wire, SCE, 20°C, 0.5 V/s.

Analyzing now the nearest larger (β -ICyD)PdCl₂(pyridine) analogue, a surprisingly different behavior was observed. The irreversible R2 reduction from Pd^{II} to Pd⁰ is now shifted at -2.02 V while the R1 reversible reduction of is also observed at -2.6 V. The same O1 reoxidation of the electrogenerated palladium at -0.22 V and O2 oxidation of Cl⁻ to Cl₂ at 1.16V (Figure III-63).

Surprisingly, an additional reversible reduction R3 is observed at -2.44 V, this additional reduction wave is still not determined.

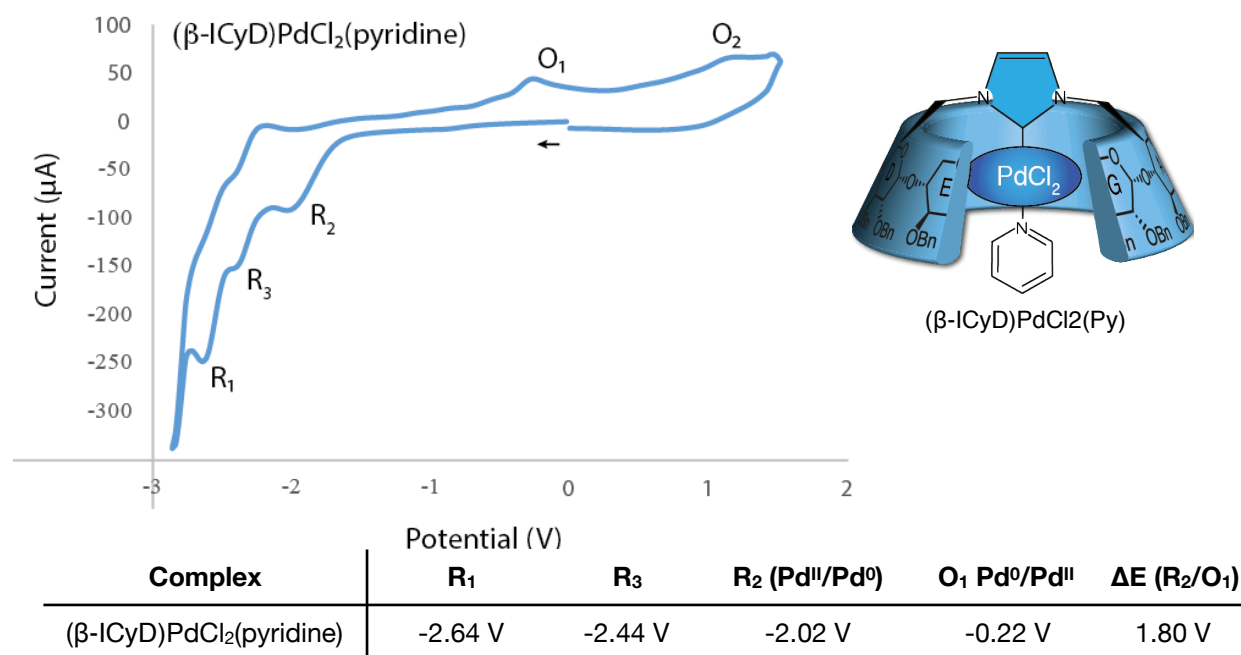


Figure III-63: Cyclic voltammogram of (β -ICyD)PdCl₂(pyridine). [(ICyD)PdCl₂] = 2 mM TBABF₄ 0.1M, GC 3 mm, CE Pt wire, SCE, 20°C, 0.5 V/s.

Finally, cyclic voltammetry of the largest analogue (γ -ICyD)PdCl₂(pyridine) shows a new shift of the R2 Pd^{II} to Pd⁰ to a even lower potential (-2.32 V) while the reversible reduction R1 is still observed at -2.6 V. On the oxidation way, O1 oxidation of the electrogenerated palladium (0) is now observed at +0.07 V and finally the O2 oxidation of Cl⁻ to Cl₂ is observed at the same potential (1.20V)

In conclusion, a cathodic shift of the reduction of Pd^{II}/Pd⁰ was observed, as well as an anodic shift for the oxidation of the electrogenerated Pd⁰ to Pd^{II}, for the γ -ICyD analogue (Figure III-64).

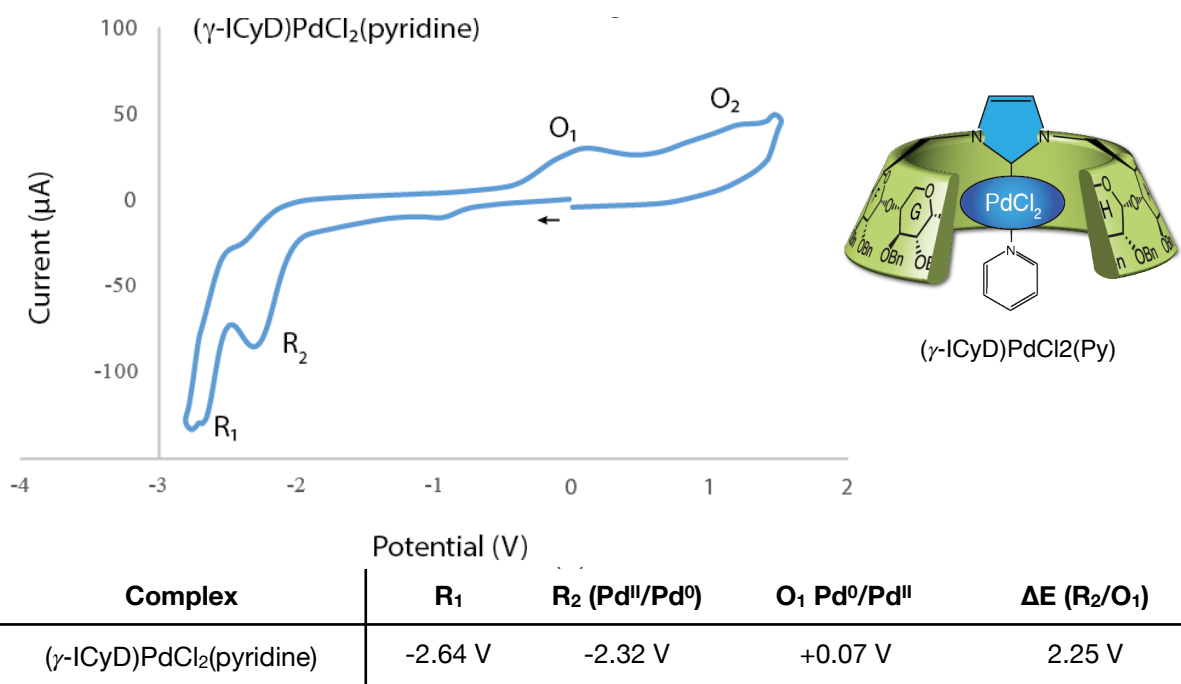


Figure III-64: Cyclic voltammogram of $(\gamma\text{-ICyD})\text{PdCl}_2(\text{pyridine})$ $[(\text{ICyD})\text{PdCl}_2] = 1.5 \text{ mM}$.
 TBABF₄ 0.1M, GC 3 mm, CE Pt wire, SCE, 20°C, 0.5 V/s.

The redox potentials obtained from the cyclic voltammetry experiences are summarized in table III-10. Since the reduction potential of the R₁ wave remains negligibly unchanged in the four different complexes, it can be deduced that the reduction potential of the coordinated pyridine is not affected either by the steric around the metal center either by the diffusion coefficient.

Looking now at the palladium center redox peaks, it can be observed that the redox behavior of the extroverted $\alpha\text{-ICyD}$ based complex is similar to the one observed for the control complex $\text{IPrPdCl}_2(\text{pyridine})$. This result means that the diffusion coefficient of the bigger ($\alpha\text{-rev-ICyD})\text{PdCl}_2(\text{pyridine})$ complex is not relevant on the redox potential of the system.¹⁷⁰ To exclude this factor, showed to have an effect in other encapsulated redox centers,¹⁷¹ diffusion coefficients were calculated by DOSY-NMR for all the $(\text{ICyD})\text{PdCl}_2(\text{pyridine})$ complexes, being $6 \times 10^{-10} \text{ m}^2 \text{ s}^{-1}$ for the three complexes.

By comparison of the $\alpha\text{-}$ and $\beta\text{-ICyD PdCl}_2(\text{pyridine})$ complexes, the reduction of the palladium is now shifted to a lower potential ($\Delta E(\text{R}_1) = -0.34 \text{ V}$), in addition, the reoxidation of the electrogenerated palladium (0) stays at -0.22 V .

¹⁷⁰ F. Vögtle, M. Plevoets, M. Nieger, G. C. Azzellini, A. Cred, L. De Cola, V. De Marchis, M. Venturi, V. Balzani, *J. Am. Chem. Soc.*, **1999**, *121*, 6290-6298.

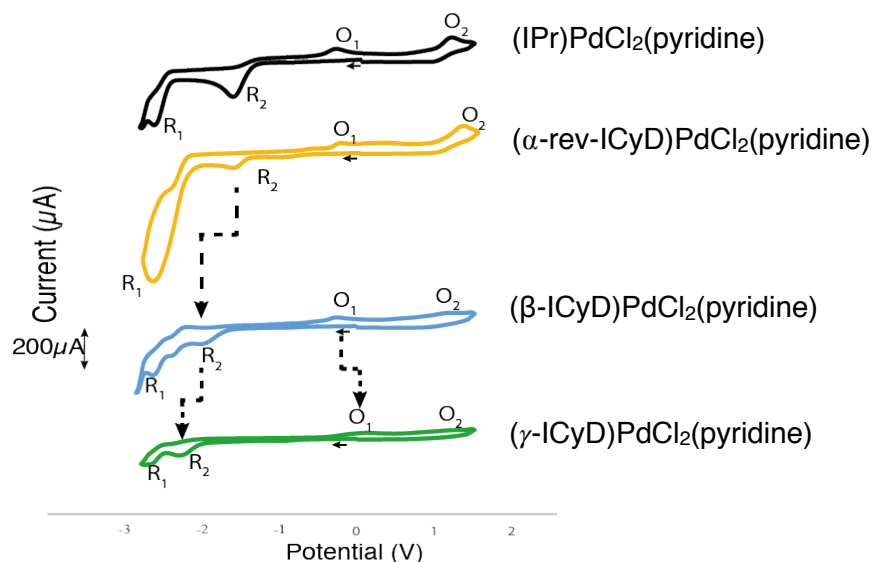


Figure III-65: Stacked cyclic voltammogram of the studied complexes. $[(\text{NHC})\text{Pd}] = 2 \text{ mM}$, $[(\gamma\text{-ICyD})\text{PdCl}_2] = 1.5 \text{ mM}$, $\text{TBABF}_4 0.1 \text{ M}$, GC 3 mm, CE Pt wire, SCE, 20°C , 0.5 V/s .

Moving now to the biggest analogue $(\gamma\text{-ICyD})\text{PdCl}_2(\text{pyridine})$ the reduction potential R_2 of the palladium center is shifted again to lower potentials at -2.32 V , again shifted to lower potentials. Furthermore, the reoxidation wave of the electrogenerated palladium (0) appears now at 0.07 V , at upper potentials.

Complex	R_1	$\text{R}_2 (\text{Pd}^{\text{II}}/\text{Pd}^0)$	$\text{O}_1 \text{ Pd}^0/\text{Pd}^{\text{II}}$	$\Delta E (\text{R}_2/\text{O}_1)$
$\text{IPrPdCl}_2(\text{pyridine})$	-2.61 V	-1.64 V	-0.29 V	1.35 V
$(\alpha\text{-rev-ICyD})\text{PdCl}_2(\text{pyridine})$	-2.64 V	-1.68 V	-0.22 V	1.46 V
$(\beta\text{-ICyD})\text{PdCl}_2(\text{pyridine})$	-2.64 V	-2.02 V	-0.22 V	1.80 V
$(\gamma\text{-ICyD})\text{PdCl}_2(\text{pyridine})$	-2.64 V	-2.32 V	$+0.07 \text{ V}$	2.25 V

Table III-10: Summary of R_1 , R_2 and O_1 potentials for the studied complexes.

The proposed rationalization of this behavior is based in previous reports of encapsulated redox active metal complexes, such as the already presented calixarenes³⁵ or hemicryptophanes.³⁴

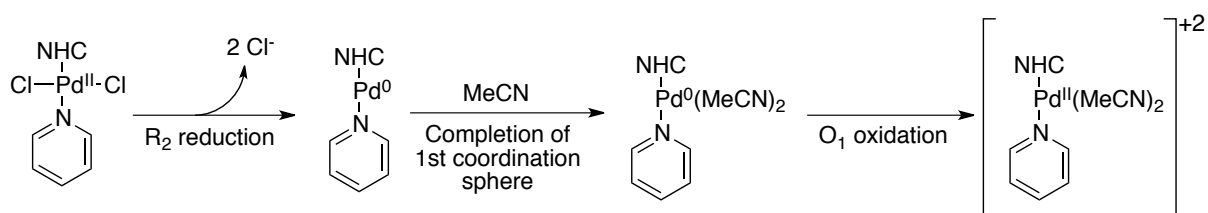
One key aspect on the CV, is the necessity of completion of the first coordination sphere, and the effect of these ligands in the redox potential.¹⁷¹ The ligands and the stability of a metal complex are determinant on the redox potential of a metal complex,³¹ and the evolution during the CV can be considered as a chemical reaction.¹⁷² Additionally, in different Fc-based host-guest complexes, another important factor is the solvation sphere.²⁶ The close presence of a

¹⁷¹ N. Elgrishi, D. A. Kurtz, J. L. Dempsey, *J. Am. Chem. Soc.* **2017**, *139*, 239–244

¹⁷² N. Elgrishi, K. J. Rountree, B. D. McCarthy, E. S. Rountree, T. T. Eisenhart, J. L. Dempsey, *J. Chem. Educ.* **2018**, *95*, 197–206

cavitand, can disturb these factors in the different species generated by an electrochemical reaction,¹⁷³ the exchange of “guests” are thus involved in the process.²⁴

The model system started thus with a (NHC)PdCl₂(pyridine) complex reduced in a (NHC)Pd⁰(pyridine) complex. At this stage, both chlorido ligands must get out of the first coordination sphere and the palladium with 14 valency electrons needed to complete its coordination sphere, thus a rearrangement of the first coordination sphere should be involved to complete the coordination sphere and the electrogenerated complex (NHC)Pd(pyridine) accepts 2 electron ligands to complete its valency electrons (ideally 2 to complete the 18 valency electrons). Then, this different complex is reoxidized to generate a cationic (NHC)Pd²⁺(pyridine). (Scheme III-23)



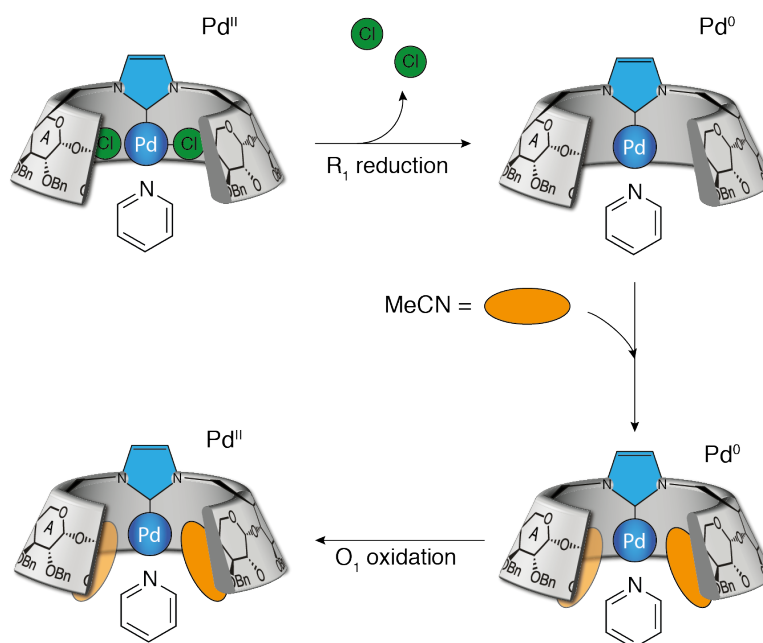
Scheme III-23: Proposed generic pathways of the electrochemical process.

In the case of the (IPr) and the (α -ICyD) ligands, no steric hindrance disturbs the process of coordination and expulsion of ligands around the metal center. Nevertheless in the case of the confined complexes of (β -ICyD) and (γ -ICyD), the steric hindrance afforded by the cavity implies an additional cost in energy for the coordination-expulsion of ligands to happen.

The proposal of this process is thus, that the expulsion of the chlorido ligands requires an additional energy. This additional energy is lower for the (β -ICyD)PdCl₂(pyridine), where tilt of the metal complex places one of the equatorial chlorido ligands at the entrance of the cavity. Nevertheless, in the case of (γ -ICyD)PdCl₂(pyridine), a deeper coordination of the chlorides requires an additional energy to expel the guest from the cavity (Scheme III-24), reflected in a lower redox potential.

¹⁷³ W. S. Jeon, K. Moon, S. Hyun Park, H. Chun, Y. Ho Ko, J. Yong Lee, E. Sung Lee, S. Samal, N. Selvapalam, M. V. Rekharsky, V. Sindelar, D. Sobransingh, Y. Inoue, A. E. Kaifer, K. Kim, *J. Am. Chem. Soc.* **2005**, *127*, 12984 - 12989

In addition, the completion of the first coordination sphere of the Pd⁰ complex is also influenced by the same steric hindrance, requiring the entrance into the cavity of a new guest. In this case, this new ligand is a solvent MeCN molecule. The entrance inside the cavity requires also an additional energy cost, reflected in a higher redox potential.



Scheme III-24 : Proposed pathways for the electrochemical process of (β - and γ -ICyD)PdCl₂(pyridine)

In conclusion, through all the electrochemical experiments, the study of ICyD-confined Pd complexes was done. Relating all the CV performed (gold and palladium), a strong dependence on the position of the ligands of the metal inside the cavity was found. Due to the linear coordination of gold, (ICyD)AuCl complexes placed all the reactivity at the entrance of the cavity, reflected in any change on the redox potentials between (α -, β - and γ -ICyD)AuCl complexes.

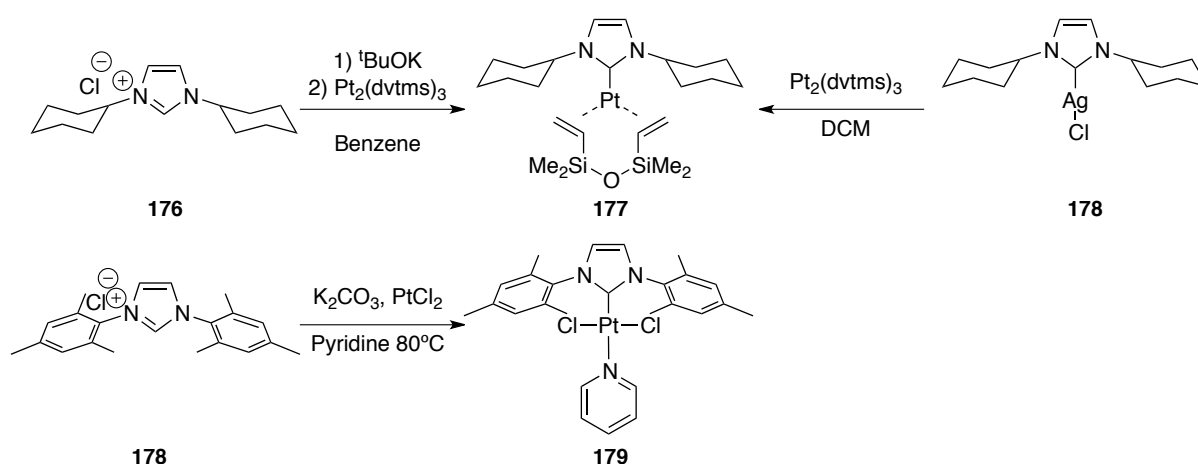
In contrast, in the case of (β - and γ -ICyD) Pd complexes, the reactivity of the ligands happened at the *cis* position of the Pd atom, thus, inside the cavity. This inner reactivity was reflected in strong changes on the redox potentials of the complex. The reduction peaks were observed at lower potentials when the coordination-expulsion of ligands take place in a higher position on the cavity (Scheme). This result is, to the best of our knowledge, the first study of the dependance of the position of the metal in a cavitand on the redox potentials of the complex.

2. Confinement of Pt compounds.

Square planar and trigonal geometry of (ICyD)Pt compounds.

i. Synthesis of Pt-based-NHC.

While Pd-based NHC's exists mainly in Pd(II) oxidation state, Pt are reported under many different geometries and oxidation states. (Scheme III-25). In this work the only considered complexes will be the NHC-Pt^{II}Cl₂(pyridine) as a PEPPSI structural analogue, as well as the NHC-Pt⁰(dvtms) for recent interest as catalysts in the hydrosilylation¹⁷⁴ and borylation¹⁷⁵ reactions. Synthetic methods for this compounds are, as for most of NHC-transition metal complexes, complexation with a free NHC¹⁷⁶ or transmetalation of the silver carbene.¹⁷⁷



Scheme III-25: Synthetic methods for the selected Pt complexes

ii. Comparison between α and β - CD-based (ICyD)PtCl₂(pyridine) reactivity

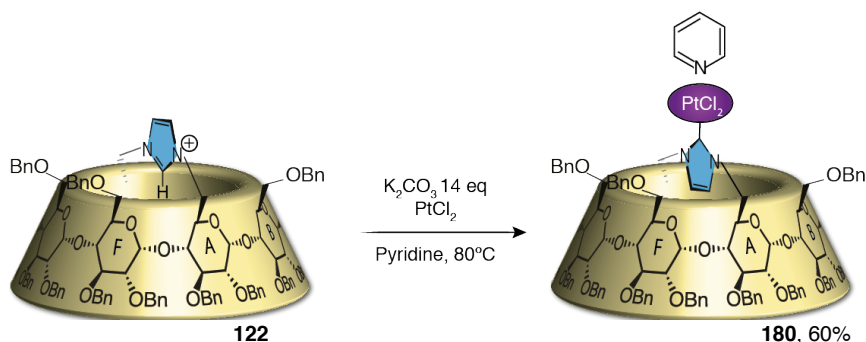
The synthesis of the (α -rev-ICyD)Pt(pyridine) complex has been performed in the same conditions reported in the literature.¹⁸⁷ Deprotonation of the azolium salt (α -ICyD)HCl **122** with an excess of K₂CO₃ in presence of PtCl₂ in pyridine at 80°C affords the expected reversed (α -rev-ICyD)PtCl₂(pyridine) **180** complex in 60% yield (Scheme III-26)

¹⁷⁴ T. K. Meister, K. Riener, P. Gigler, J. Stohrer, W. A. Herrmann, F. E. Kühn, *ACS Catal.* **2016**, 6, 1274–1284

¹⁷⁵ T. Furukawa, M. Tobisu, N. Chatani, *J. Am. Chem. Soc.* **2015**, 137, 12211–12214

¹⁷⁶ E. Bolbat, K. Suarez-Alcantara, S. E. Canton, O. F. Wendt, *Inor. Chim. Acta*, **2016**, 445 129 - 133

¹⁷⁷ V. Lillo, Jose Mata, J. Ramirez, E. Peris, and E. Fernandez, *Organometallics* **2006**, 25, 5829 - 5831



Scheme III-26: Synthesis of (α -rev-ICyD)Pt(pyridine)

As for its Pd analogue (α -ICyD)PdCl₂(pyridine), the external coordination of the metal center was verified by 1D-NOESY experiments. Irradiation of the deshielded C-H proton of the NHC shows an unambiguous spatial proximity with the intra-cavity protons H-5A,D H-3C,F and H-5C,F. As showed previously, the same conformational change observed on the (α -rev-ICyD)PdCl₂(pyridine) can be deduced from the multiplicity of the H-5A,D (Figure III-66).

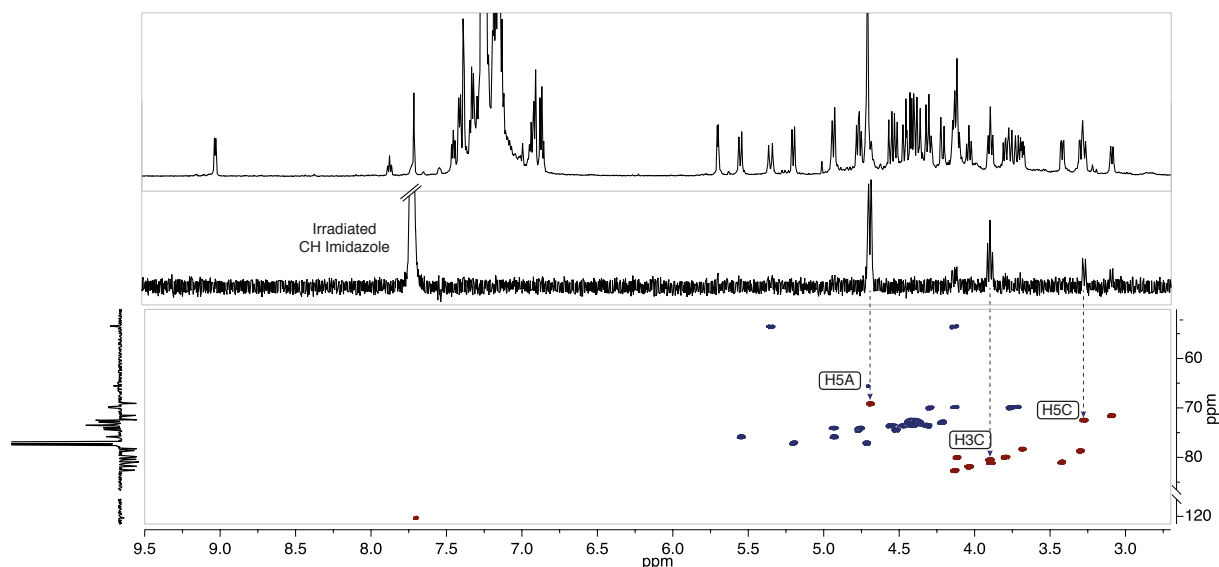
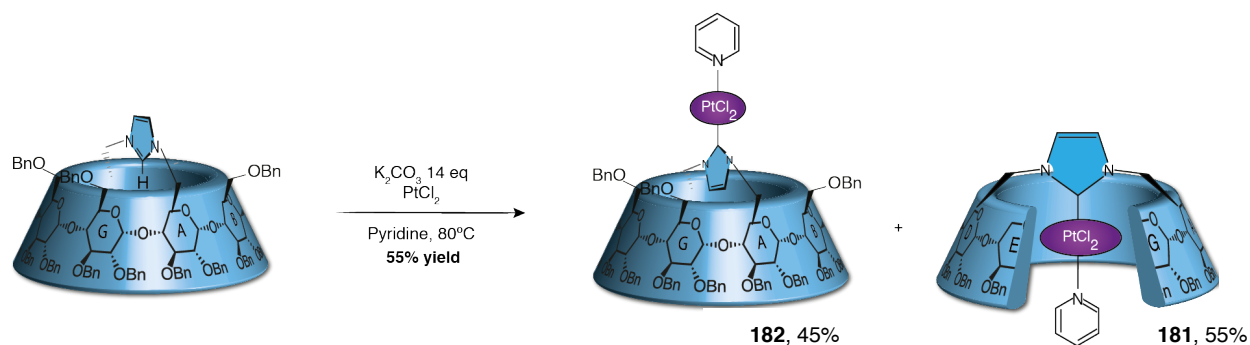


Figure III-66: ¹H-NMR, selective 1D-NOE and HSQC of (α -rev-ICyD)PtCl₂(pyridine) **181**. CDCl₃, 600 MHz, 300 K (irradiation at 7.4 ppm)

In contrast, the same reaction conditions with (β -ICyD)HCl afforded a non-separable mixture of the expected (β -ICyD)PtCl₂(pyridine) **181**, and the reversed (β -rev-ICyD)PtCl₂(pyridine) **182**. This reversed complex is the first observed with β -cyclodextrin. A 45:55 mixture of both compounds in favor of **181** was obtained in 55% yield after two silica gel purifications.



Scheme III-27: Synthesis of (β -rev-ICyD)Pt(pyridine)

From the HSQC (Figure III-67), the presence of 14 anomeric carbons, two pairs of C6 attached to the NHC, two pairs of *ortho* carbons of the coordinated pyridine and two pairs of CH of the NHC (two shielded at 6.13 and 6.03 ppm corresponding to the inner one, and two deshielded at 7.95 and 7.92 ppm) and 2 characteristic *ortho* protons of the complexed pyridine.

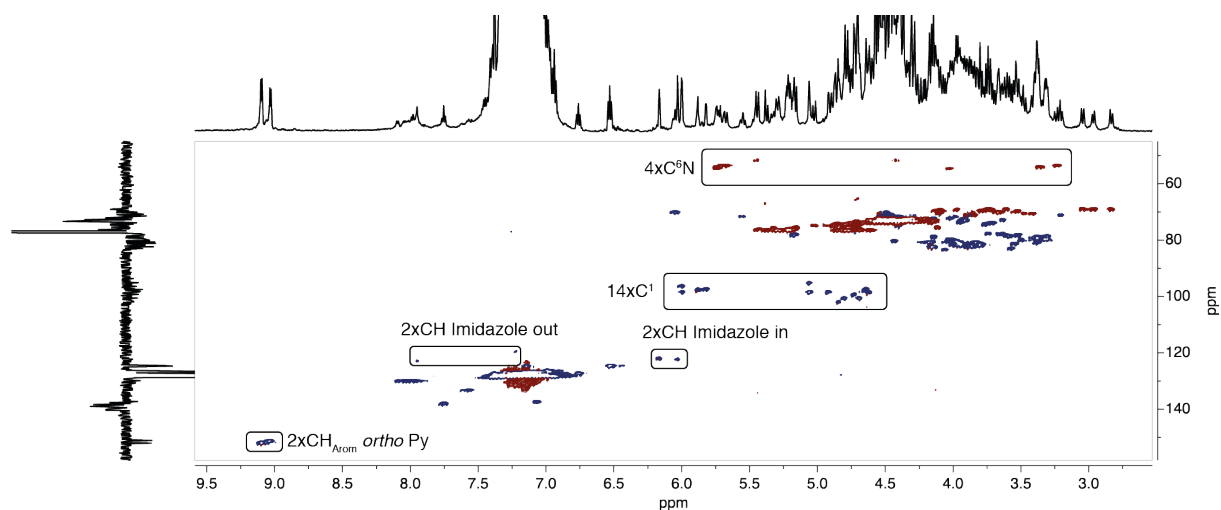


Figure III-67: HSQC of a mixture of (β -ICyD)PtCl₂(pyridine) and (β -rev-ICyD)PtCl₂(pyridine)
CDCl₃, 600 MHz, 300 K

The possibility to obtain Pt complexes with α -ICyD and β -ICyD ligands made us consider the possibility to obtain other Pt-based complexes found more frequently in synthetic applications.

The outer coordination of the carbene was verified by 2D-NOESY experiments. Cross correlation peaks were observed between both CH of the NHC and H5 and H3 intra cavity protons, as it was observed for all the (α -rev-ICyD) complexes.

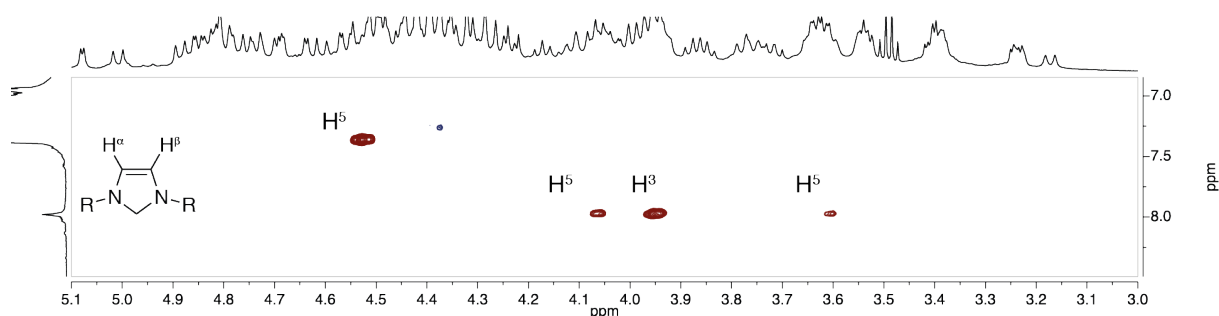
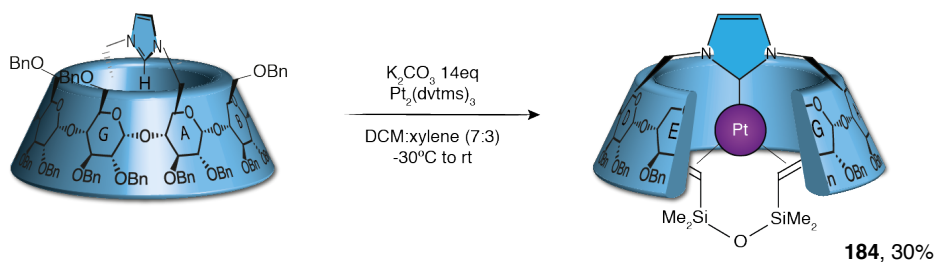


Figure III-69: 2D-NOESY spectrum of (β -rev-ICyD)Pt(dvtms). CDCl_3 600 MHz, 300 K $\tau_{\text{mix}} = 800$ ms.

iv. Synthesis and structure of (β -ICyD)Pt⁰(dvtms)

In contrast, using K_2CO_3 as base and the same $\text{Pt}_2(\text{dvtms})_3$ compound in a dichloromethane : xylene 7 : 3 mixture. The reaction was started at -30°C and slowly warmed up to room temperature to obtain the inner (β -ICyD)Pt(dvtms), also isolated from the mixture by silica gel chromatography in 30% yield (Scheme III-29).



Scheme III-29: Synthesis of (β -ICyD)Pt(dvtms)

Once again, a different conformational behavior could be observed in the NMR. At room temperature in CDCl_3 , three different complexes in slow exchange on the NMR timescale were observed. This equilibrium was suggested by the presence of 6 signals of the CH of the NHC. Several groups of vinyl signals between 2 and 2.6 ppm and the same observation could be done for the Si- CH_3 signals between 0 and 0.5 ppm. All the signals were in agreement with the literature, confirming the presence of a coordinated divinyltetramethylsiloxane (Figure III-70).

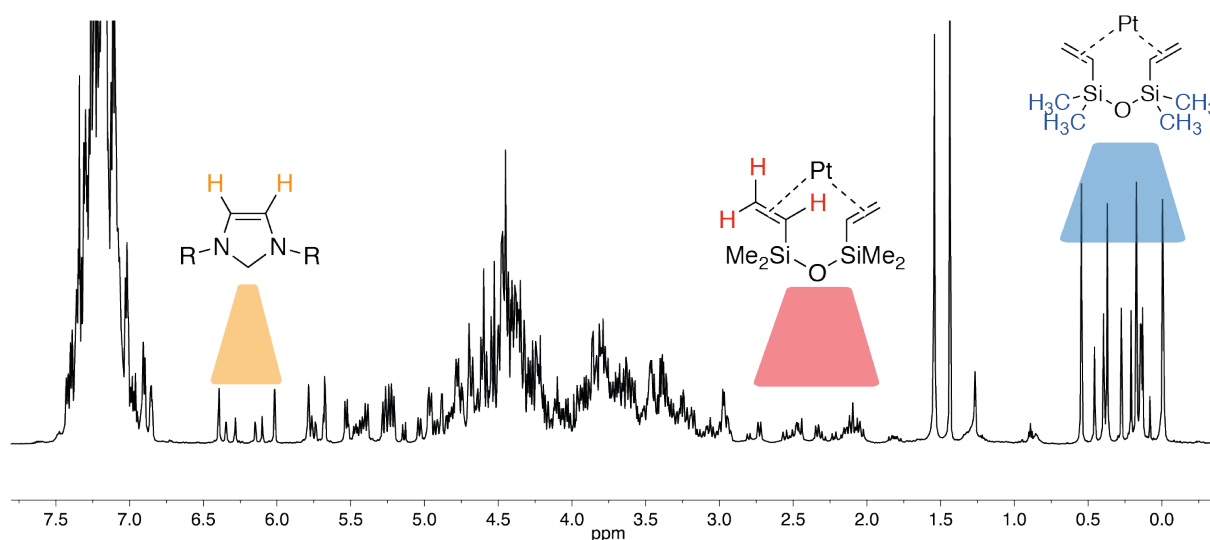


Figure III-70: $^1\text{H-NMR}$ of $(\beta\text{-ICyD})\text{Pt}(\text{dvtms})$ **184**. CDCl_3 , 600 MHz, 300 K

As already presented several times during this chapter, chemical shift of the carbene, used as key information of the nature of the NHC was obtained through the HMBC cross correlation with the CH of the NHC at 185.8, according with already reported complexes¹⁷⁸ confirming the presence of a Pt^0 complex (Figure III-72).

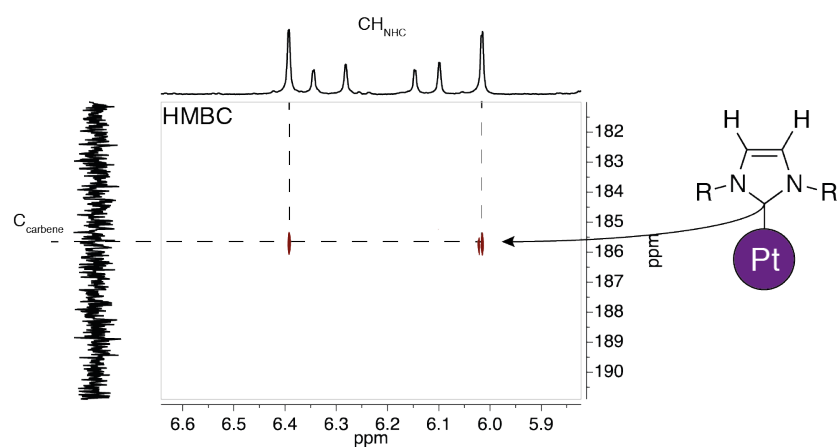


Figure III-71: HMBC of $(\beta\text{-ICyD})\text{Pt}(\text{dvtms})$ **184**. CDCl_3 , 600 MHz, 300 K

To study the dynamic behavior of the compound, the complex was heated in toluene- d_8 . A clear approach of the NHC signals of the NHC and the dtms could be observed between 300 K to 360 K due to a possible coalescence at more than 360 K (Figure III-72).

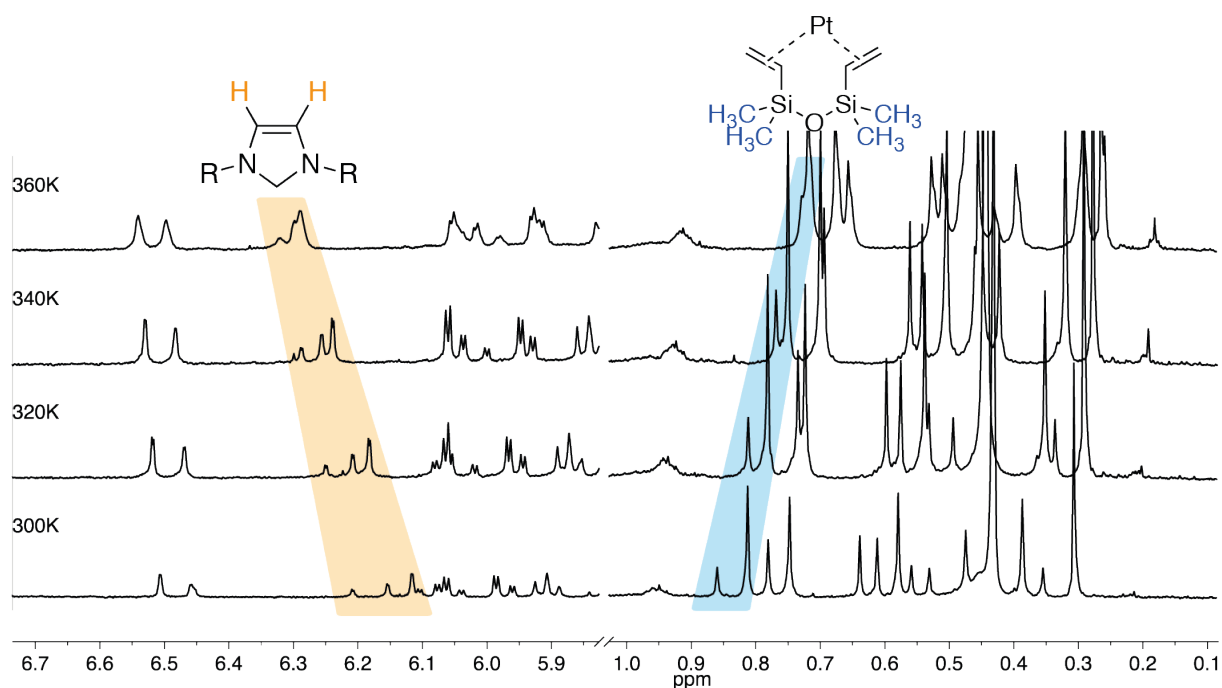


Figure III-72: Temperature variation of (β-ICyD)Pt(dvtms). Tol-d₈, 300 K.

In conclusion, different Pt-based complexes, with different geometries were synthesized inside and outside the α- and β-ICyD ligands. In the case of α-rev-ICyD)PtCl₂(pyridine), a single outer coordinated complex was obtained without traces of the inner one. In the case of the (β-ICyD) ligand, a non-separable mixture of (β-ICyD)PtCl₂(pyridine) and (β-rev-ICyD)PtCl₂(pyridine) complexes was obtained. In addition, when the reaction is performed with the Pt₂(dvtms)₃ precursor, a dependance on the base was observed in the major product of the reaction. If KHMDS is used as base to form the free NHC, the outer (β-rev-ICyD)Pt(dvtms) complex is isolated as major product of the reaction. If in contrast, K₂CO₃ is used as base to form the free (β-ICyD), the inner (β-ICyD)Pt(dvtms) is obtained as major compound of the reaction.

E. General conclusion to chapter III.

Through all this chapter, a synthesis of new NHC-capped cyclodextrins were presented. This synthetic work started with the synthesis of a targeted (γ -ICyD)AuCl complex, for a enyne-cycloisomerization that will be studied in the next chapter.

Studying the optimization of the synthesis, passing through the free-NHC, either in a two steps or a one pot reaction, an unprecedented reversed coordination mode of the AuCl was found for α -cyclodextrin. This (α -rev-ICyD)AuCl was first observed as side product of the reaction, to finally develop a method to synthesize it in a preparative scale.

Also during the synthesis of (γ -ICyD)AuCl complex, an unexpected oxidation of the gold complex at the last step of the synthesis, producing a unprecedented square planar (γ -AE-ICyD)AuCl₃ complex inside the cavity of a cyclodextrin. This preliminary result, opened a synthetic route to square planar complexes, with an important interest on Pd-based complexes. First, inside of the largest γ -cyclodextrin cavity, to then develop the synthesis in narrower easily accessible analogues in β -cyclodextrin, with the expected inner coordination; and α -cyclodextrin, where the coordination mode was observed to be exclusively outside of the cavity. Finally, the methodology was extended to Pd and Pt complexes, showing that the different metals, square planar or trigonal could be also accessible inside the cavity of ICyDs.

All these complexes contributed to a better understanding of the behavior of ICyDs. From a structural point of view of the dynamics of the complexes it was found that the cavity size and the coordination mode had an important impact on the mechanism of the isomerization of the simplest η^3 -allyl ligand of a Pd complex. In the case of the (γ -ICyD)PdCl(η^3 -allyl) complex, the mechanism found was in agreement with a η^3 - η^1 - η^3 isomerization around the *Ccis* of the ligand. In the case of (α -rev-ICyD), the mechanism found showed no rotation around this bond. Finally, in the case of the (β -ICyD)PdCl(η^3 -allyl), the cavity restricted the position of the allyl, found to be in a ratio higher than 97 : 3.

This first study showed how the size of a cavitand, in cooperation with the size of the metal complex can influence the dynamic behavior of a metal complex. This behavior is the first clue towards selective allylations, either regio- or enantioselective, that will be studied during the next chapter.

Another interesting result of this chapter were the electrochemistry results, being to the best of our knowledge, the first metal complexes, confined in cyclodextrins that exhibit a response in CV. This study related the structure of the complexes to the electrochemical properties. In this work, a relationship of the position of the ligands inside the cavitand and the redox potentials was showed, suggesting that the redox potentials are not only dependent on the confining system but also in the position within. This results showed that more confining systems lead to lower reduction and higher oxidation potentials.

CHAPTER IV

ICyD-metal complexes in catalysis.
Effects of a discrete confinement

CHAPTER IV: ICyD-metal complexes in catalysis.

Effects of a discrete confinement

In chapter III different cyclodextrin-based metal complexes were presented. In all of the synthesized complexes, different structural parameters were studied such as the cavity size and its deformation, the coordination modes depending on the cavity size, as well as the influence of the cavity size on the redox potentials.

In the following chapter, the structure-reactivity of all the ICyD complexes presented in the last chapter will be studied. Different aspects will be presented, as for example the effect of the coordination mode and the encapsulation in the efficiency of the system or the different geometries of a complex. This study will start with the previously presented enyne cycloisomerization, followed by other reactions where the oxidation state of the complex remains unchanged (Cu(I) and Pd(II)). In a second part, the study of redox active catalytic cycles will be studied, starting with higher oxidation states of Pt and Au, and finishing with lower oxidation states of Pd.

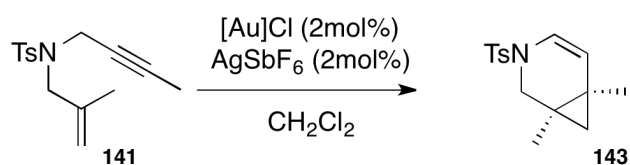
A. NHC-capped cyclodextrin in redox neutral catalytic cycles.

1. Linear gold (I) catalyzed enyne cycloisomerization

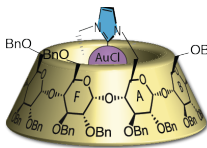
As presented in chapter II, increasing the cavity size of (ICyD)AuCl catalysts from α -cyclodextrin to β -cyclodextrin produced an improvement of the enantiomeric excess⁵⁶ up to 80%. The main goal of the synthesis of the (γ -ICyD)AuCl analogues was to see if even a larger cavity size could also increase the efficiency in terms of selectivity. With these largest analogues, the understanding of the behavior of the ICyD ligands in enyne-cycloisomerization will be completed.

i. Effect of the cavity size on the enantioselectivity

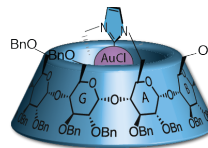
As observed in table IV-1, the use of the largest (γ -AE-ICyD)AuCl analogues lead to an important drop of the enantioselectivity and yield in the cycloisomerization reaction for **141**. With this symmetrical isomer, a slightly drop of yield from 77% (for β -ICyD) to 50%, as well as and a complete loss of enantioselectivity (0%) were observed.⁵⁶ In the case of the non-symmetrical isomer (γ -AD-ICyD)AuCl, the system kept the efficiency with 77% yield, but an almost total loss of enantioselectivity was unfortunately observed (7%).⁵⁶



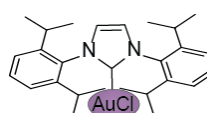
Complex	Yield (ee)
IPrAuCl	80% (0%)
(α -ICyD)AuCl	83% (46%)
(β -ICyD)AuCl	77% (59%)
(γ -AE-ICyD)AuCl	50% (0%)
(γ -AD-ICyD)AuCl	77% (7%)



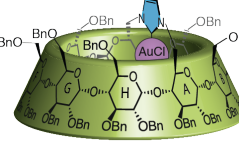
(α -ICyD)AuCl



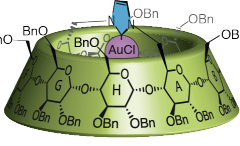
(β -ICyD)AuCl



(IPr)AuCl



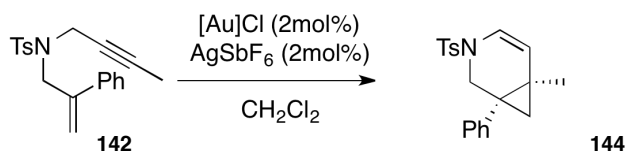
(γ -AD-ICyD)AuCl



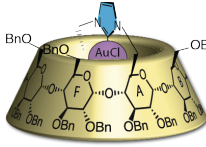
(γ -AE-ICyD)AuCl

Table IV-1: Yields and values of ee of the cycloisomerization of enyne **141**

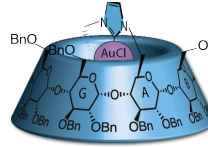
The same trend was observed when using enyne **142** with a more hindered phenyl ring (Table IV-2). This time, both catalysts are as active as (β -ICyD)AuCl giving quantitative yields. In terms of ee, both γ -ICyD complexes gave lower ee: 22%, in the case of the (γ -AE-ICyD)AuCl, and 42% ee of the opposite enantiomer (!) was obtained in the case of the non-symmetrical isomer (γ -AD-ICyD)AuCl. To understand the origin of the enantioselectivity, a study of the mechanism of the reaction was operated using the cyclodextrin shapes as steric constraints.



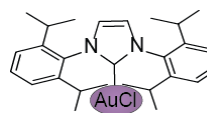
Complex	Yield (ee)
IPrAuCl	74% (0%)
(α -ICyD)AuCl	78% (48%)
(β -ICyD)AuCl	99% (80%)
(γ -AE-ICyD)AuCl	99% (22%)
(γ -AD-ICyD)AuCl	99% (-42%)



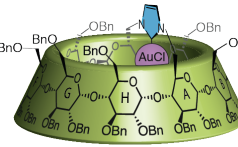
(α -ICyD)AuCl



(β -ICyD)AuCl



(IPr)AuCl



(γ -AD-ICyD)AuCl

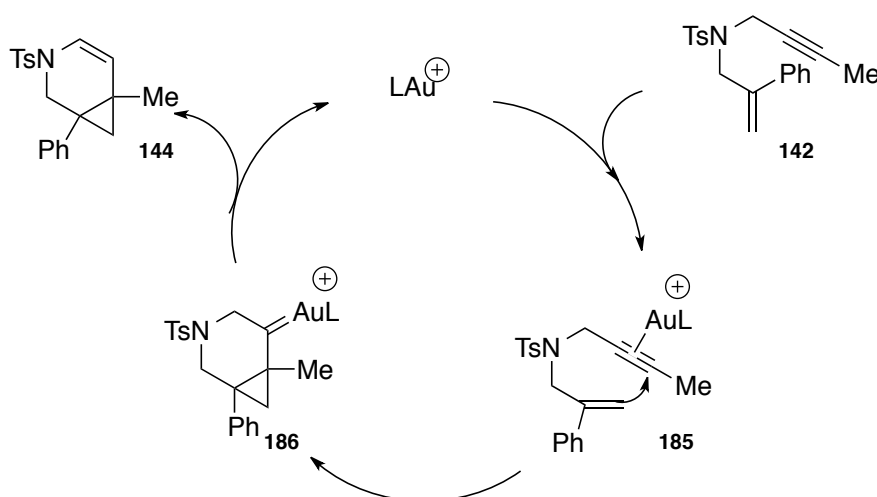


(γ -AE-ICyD)AuCl

Table IV-2: Yields and values of ee of the cycloisomerization of enyne **142**

ii. Mechanism and selectivity.

Cycloisomerization of 1,5 enynes were first reported by Toste¹⁷⁹ and the proposed mechanism was confirmed by later studies of Echavarren's group¹⁸⁰. The catalytic cycle starts with a coordination of the alkyne to the cationic gold(I) complex. This activated triple bond undergoes a nucleophilic attack of the olefin to form the key intermediate **186**. This gold carbene, after a 1,2 hydrogen shift and elimination of the complex forms the product of the reaction **144** regenerating the cationic gold(I) catalyst (Scheme IV-1).



Scheme IV-1: Mechanism of the cycloisomerisation compound **42**

The enantiodeterminant step was shown to be the attack of the double bond on the activated alkyne.^{191c} Thus, the enantioselectivity must be determined by the approach of the double bond to the coordinated alkyne, directed by the different topologies of each cyclodextrin. To visually appreciate the influence of the irregular steric hindrance of the cavity, the different approaches will be presented using the Connolly's surfaces in analogy with the model of quadrants.¹⁸¹

To coordinate the triple bond of the substrate, it seemed evident to place it through the groove produced by the short bridging of the NHC. Then, to discriminate between both approaches, the steric hindrance induced by the secondary rim was analyzed. In the case of β -ICyD the closest sugar units are the B and C, thus, the less sterically demanding vinylic-CH₂ of the double bond must approach through this side. Substituents of the double bond had to approach therefore closer to the E,F,G sugar units, the biggest loop of the cyclodextrin. Then, only two possibilities were left, either the phenyl ring approached closer to the E and F sugar units, or it approached closer to the F and G sugars. From the results obtained by NMR, sugar units F and G are closer to the metal center, as it can be observed in the Figure IV-1. Thus, the

¹⁷⁹ M. R. Luzung, J. P. Markham, F. D. Toste, *J. Am. Chem. Soc.*, **2004**, *126*, 10858 - 10859

¹⁸⁰ a) C. Nieto-Oberhuber, M. P. Muñoz, E. Buñuel, C. Nevado, D. J. Cárdenas, A. M. Echavarren, *Angew. Chem. Int. Ed.* **2004**, *43*, 2402 - 2406 b) C. Nieto-Oberhuber, M. Paz Muñoz, S. López, E. Jiménez-Núñez, C. Nevado, E. Herrero-Gómez, M. Raducan, A. M. Echavarren, *Chem. Eur. J.* **2006**, *12*, 1677 - 1693. c) For a general review on mechanisms of gold catalyzed reactions. D. J. Gorin, F. D. Toste, *Nature*, **2007**, *446*, 395 - 403.

¹⁸¹ I. D. Gridnev, T. Imamoto *Acc. Chem. Res.*, **2004**, *37*, 633-644

less sterically hindered approach is the one where the phenyl ring approaches next to the sugar unit E, for both (α -ICyD) and (β -ICyD). In addition, these two approaches, with less steric clash, produce the same enantiomer as the one obtained in the experiments.

To verify this approach, DFT, calculations were performed on each approach, founding that for (α -ICyD) and (β -ICyD) the deduced favored approaches are energetically favored by 3.7 kcal/mol and 4.1 kcal/mol, respectively.⁵⁶

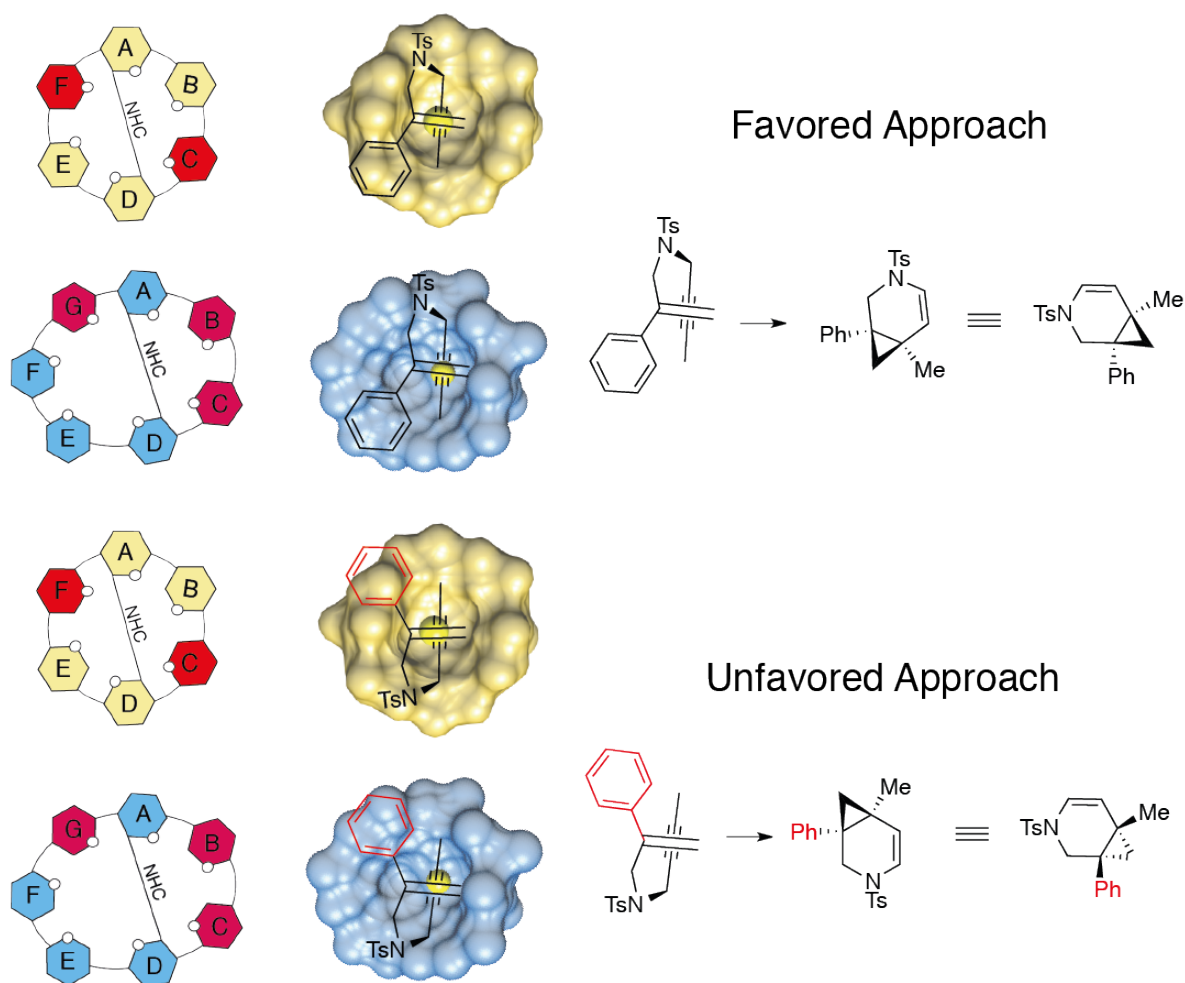


Figure IV-1: Favored and unfavored approach for (α -ICyD) and (β -ICyD).

Using a larger and symmetrical analogue, (γ -AE-ICyD)AuCl, the obtained enantioselectivity drop to 22%. Due to this lower selectivity, we assume that the approach is similar to the one of the narrower α and β analogues.

In the case of the non-symmetrical (γ -AD-ICyD) complex, a notably inversion of the enantioselectivity was observed for the same substrate. To explain this unexpected result, the same study of the possible approaches with the shape was done. As for its α - and β -analogues, it seemed reasonable to place the triple bond parallel to the closest B and C sugar units, and the smaller CH₂ of the alkene approaching closer to this part of the macrocycle. In contrast to the narrower analogues, three H5 were deshielded on the proton NMR as consequence of their proximity to the metal center. A steric clash between the H5H and the NTs, not present in the other analogues, was considered to explain this reversed enantioselectivity. Thus, placing the NTs on the opposite side of the macrocycle (D,E), and the phenyl substituent close to the sugar unit G the approach founded gives the correct isomer.

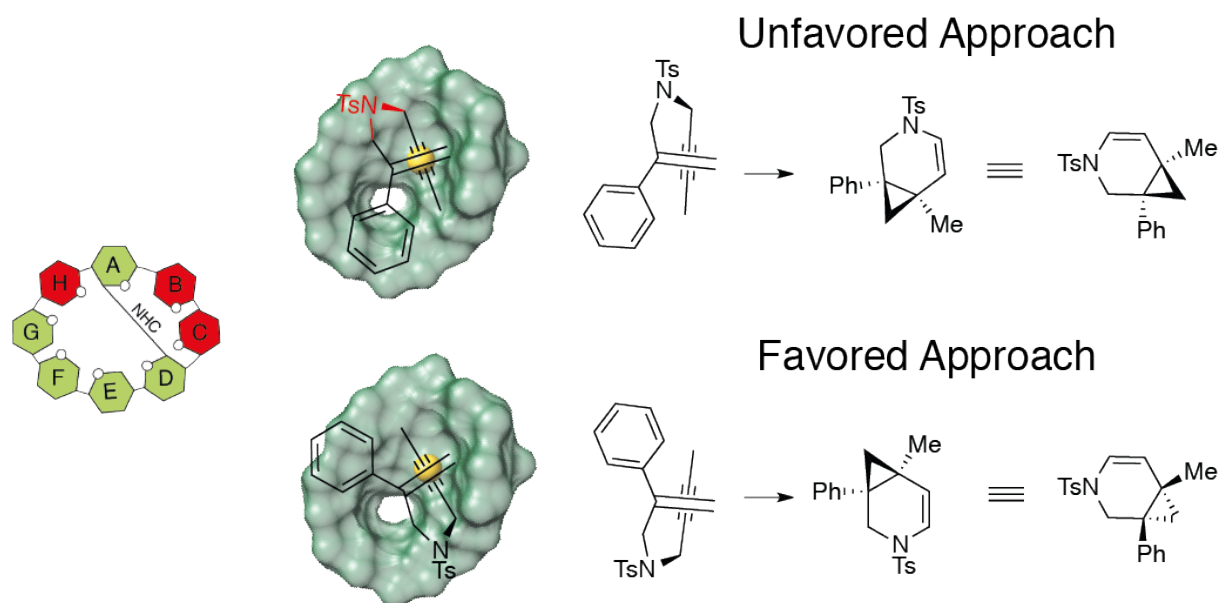


Figure IV-2: Favoured and unfavored approaches to rationalize the enantioselectivity of the (γ -AD-ICyD)AuCl

iii. Effect of the cavity size on the product distribution

First results of our laboratory,⁵⁹ a substrate distribution in the cycloisomerization reaction of **146** was observed. While (α -ICyD)AuCl gave the same formal 5-exo cycloisomerization products as the model catalyst IPrAuCl, (β -ICyD)AuCl gave as major compound the formal 6-endo (**3**) product without traces of the *s*-trans isomer.

Using (γ -ICyD)AuCl catalysts, the selectivity started to drop. Using the (γ -AE-ICyD)AuCl isomer, a quantitative yield was obtained, leading to the products **147**:**148**:**149** in a 1 : 0.14 : 1 ratio. In the case of the (γ -AD-ICyD)AuCl isomer, compounds **147**:**148**:**149** were obtained in a 1 : 0.56 : 0.6 ratio, with a total yield of 80%.

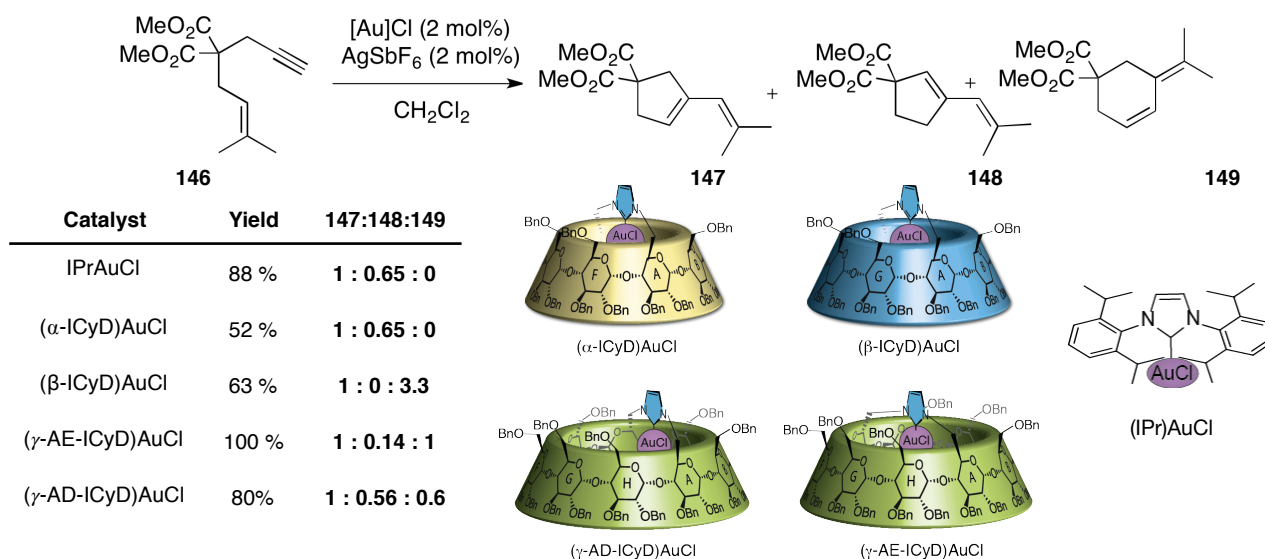


Table IV-3: Yields and values of ee of the cycloisomerization of enyne **146**

To rationalize this product distribution, the mechanism was studied by DFT calculations. Gold-catalyzed cycloisomerization mechanisms affording 5- or 6- member rings products were studied in detail by Echavarren with several revisitations of the calculations¹⁸². As for the main reactions of gold (I), the mechanism starts with a complexation of the triple bond to the cationic Au^I complex, this complexation activates the triple bond and this one is attacked by the olefin. This nucleophilic attack forms a [3.1.0]bicycle with an external gold carbene **187** (Scheme IV-2).

This gold carbene, depending on the catalyst and the substitution pattern of the enyne¹⁸³ has three different pathways to evolve:

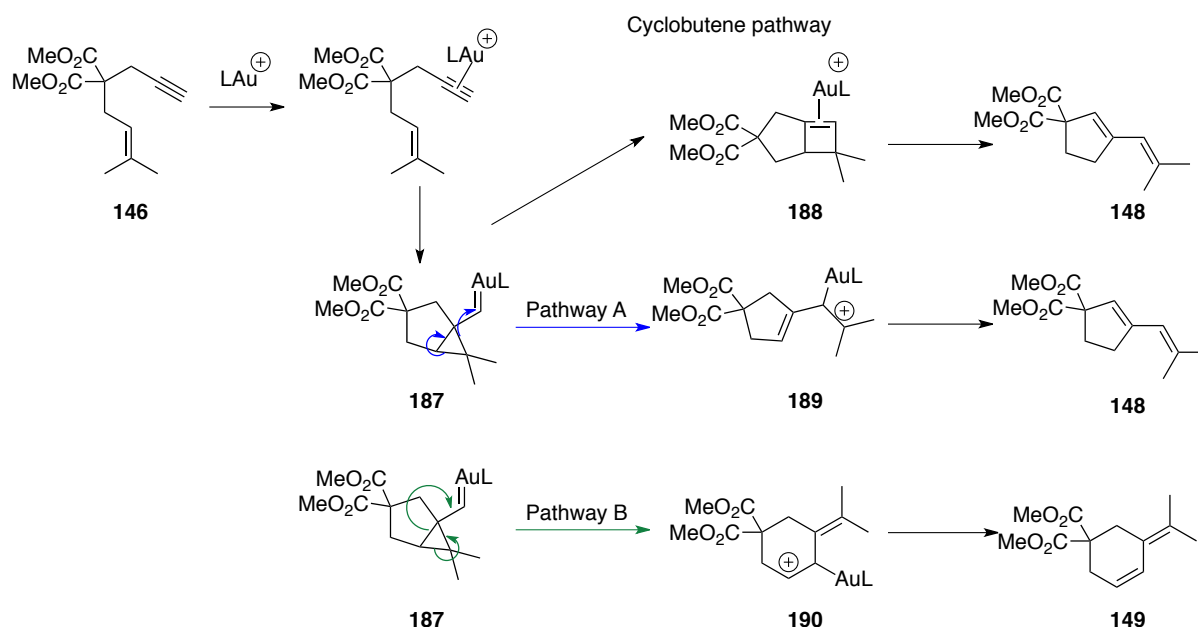
1) Expansion of the cyclopropane forms the cyclobutene **188**, intermediate that can follow an electrocyclic reaction to form the formal 5-exo cyclopentene **148**.

¹⁸² a) C. Obradors, A. M. Echavarren, *Chem. Commun.*, **2014**, 50, 16 - 28 b) N. Cabello, E. Jiménez-Núñez, E. Buñuel, D. J. Cárdenas, A. M. Echavarren, *Eur. J. Org. Chem.* **2007**, 4217–4223

¹⁸³ A. Escribano-Cuesta, P. Pérez-Galan, E. Herrero-Gómez, M. Sekine, A.A.C. Braga, F. Maserasa, A. M. Echavarren, *Org. Biomol. Chem.*, **2012**, 10, 6105 - 61111

2) Opening of the cyclopropane **187** through the pathway A forms the cyclopentane **189** that by elimination of the gold complex gives **148**, the same product as the electrocyclic reaction.

3) Ring expansion of the cyclopropane **187** forms the cyclohexane **190**, this pathway B forms the product of the reaction that after elimination of the LAu⁺ catalyst, produces directly the product **149**.

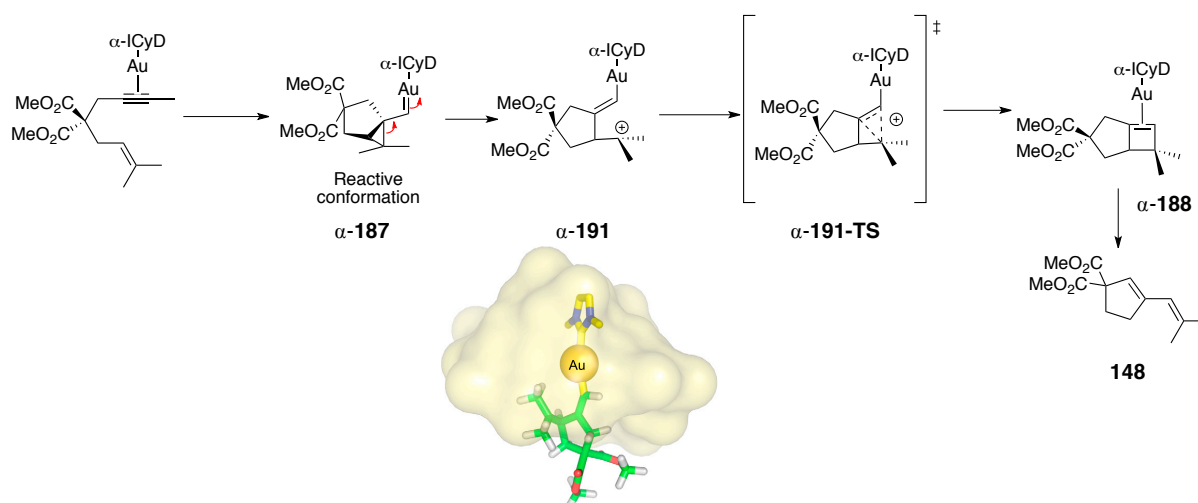


Scheme IV-2 : Mechanistic pathways to form in the formation of **148** and **149**

Mechanistic pathways are strongly dependent on the substitution pattern of the enyne, and the metal complex.^{180a} But in our case, due to similar electronics of the four ICyD ligands, it seemed logical to suppose that the factor dictating the mechanistic pathways is the different topologies of the different ligands. To understand the origin of the product distribution, and the mechanism of the reaction, DFT calculations¹⁸⁴ were performed with (α -ICyD) and (β -ICyD).

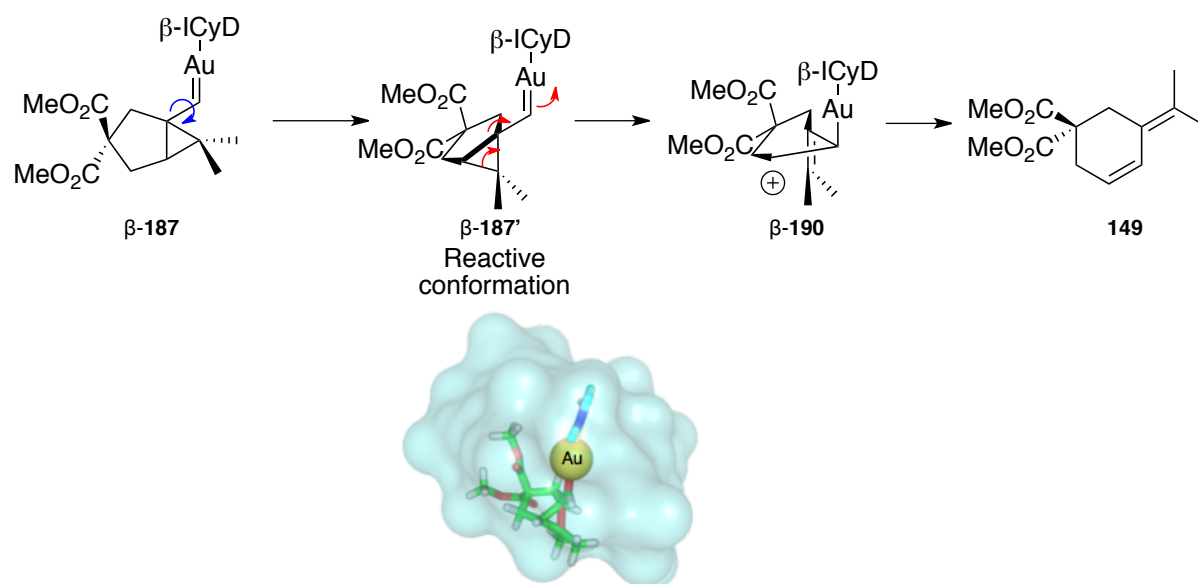
For (α -ICyD), calculations showed that the conformation imposed by the cyclodextrin of the cyclopropane intermediate α -**187** forced the spontaneous formation of a new carbocationic intermediate α -**191**. This carbocation evolved through a transition state (TS α -**191**) low in energy (0.95 kcal/mol) to form the cyclobutene α -**188**. This intermediate, evolved through a electrocyclic reaction forming product **148** (Scheme II-3). This mechanistic pathway is consistent with both experimental and theoretical results.^{180a}

¹⁸⁴ B3LYP-D3/def2-SV(P). Calculations performed by Dr. E. Derat.



Scheme IV-3: Mechanistic pathway and TS for the $(\alpha\text{-ICyD})\text{AuCl}$ catalyzed formation of **149**

In the case of $(\beta\text{-ICyD})$, the cyclopropane carbene $\beta\text{-187}$ intermediate was found to correspond to a local minimum, and any spontaneous evolution could be found. Furthermore, calculations showed that a new conformation of the cyclopropane carbene must be adopted. In this new conformation, both methyl groups are placed away from the metal center ($\beta\text{-187}'$), evolving to the cyclohexene $\beta\text{-190}$. Finally, $\beta\text{-190}$ evolves directly to the product of the reaction by elimination of the gold complex, in agreement with the experimental results and the mechanism proposed by Echavarren^{180a} (Scheme IV-4).



Scheme IV-4: Calculated mechanistic pathway and conformation for the $(\beta\text{-ICyD})\text{AuCl}$ catalyzed formation of **149**.

In conclusion for (α -ICyD) and (β -ICyD), two different conformations imposed by the different topologies of the cyclodextrin forced the system to evolve through different mechanistic pathways. In these two conformations, for (α -ICyD) both CO₂Me substituents are placed totally outside of the cyclodextrin cavity. In contrast, the conformation found to be the most reactive in the case of (β -ICyD) is one where one of the CO₂Me is included into the cavity. Due to the largest cavity size of (γ -ICyD), and the possible conformations of the macrocycle, mechanistic DFT calculations could not be performed.

For the symmetrical isomer (γ -AE-ICyD)AuCl, the results were more selective than in the case of the non-symmetrical AD isomer. 1 : 0.9, against 1:0.4, respectively (**147+148:149**). This points to a more important effect of the cavity in the case of the AE isomer. Nevertheless, both are much less selective than (β -ICyD)AuCl that formed the product in a 1:3.3 ratio. This suggests that the larger size of the cavity is less discriminating between the possible conformers of the intermediate **187**. Therefore, all the products are made in similar amounts.

To conclude, the use of confined cationic gold complexes, in this case, based on a cyclodextrin skeleton, was proved to be a useful approach to develop enantioselective enyne cycloisomerization reactions. The enantioselectivity was found to be dependent on the topology of the catalyst obtaining ee's up to 80%, extremely elevated in gold-catalyzed reactions.^{191c} More surprisingly, different enantiomers could be obtained depending on the arrangement of the walls of the macrocycle, and not on the chirality of the sugars.

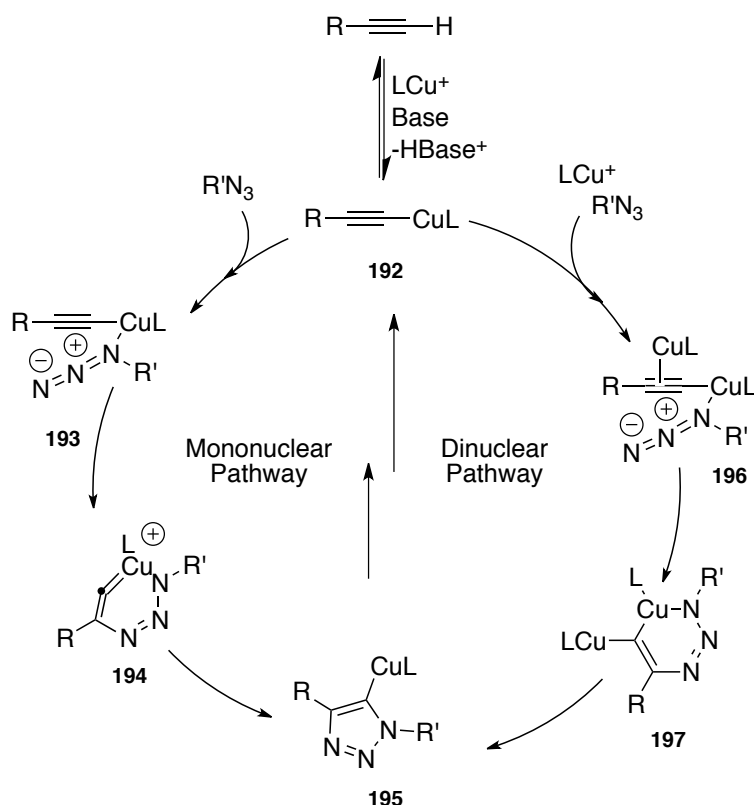
These complexes were also studied in another enyne cycloisomerization, showing to be an important effect on the distribution of the obtained products. In this case, based on DFT calculations, it was shown that the product distribution was dictated by the conformation adopted by one common intermediate. Additionally, these conformations were dictated, as for the enantioselectivity, by the topology of the macrocycle.

These results showed that ICyD metal complexes are powerful catalysts in laboratory scale reactions and the understanding of reaction mechanisms. The following parts of this PhD dissertation will be based on the use of ICyD complexes to develop synthetic useful reactions.

2. Copper (I) catalysis: Copper(I) Catalyzed Alkyne-Azide Cycloaddition

Since the discovery by Sharpless and Fokin in 2002,¹⁸⁵ the CuAAC made a place as an almost universal reaction in different fields of chemistry. From bioconjugation¹⁸⁶ to surface grafting¹⁸⁷ the Cu(I) catalyzed click reaction gained an important interest in organic chemistry. As for all of chemical reactions, understanding its mechanism helps to improve the system.

In the first report, the proposed mechanism involved only one Cu(I) atom to activate the alkyne (Scheme IV-Mononuclear Pathway). Later experimental studies on the mechanism showed that two copper atoms are involved: one that forms a copper acetylide **192** and another one to activate the triple bond.¹⁸⁸



Scheme IV-5: Mononuclear and dinuclear pathways in the CuAAC reaction.

Nevertheless, even if the presence of both copper atoms were proved experimentally, all of the studies consider the mononuclear pathway as feasible but less favorable.¹⁸⁹ Since (ICyD)CuCl are complexes with a second coordination sphere wrapping the Cu atom inside the cavity, the dinuclear pathway must be deleted. This makes our complexes as perfect candidates to study the mononuclear pathway.

¹⁸⁵ V. V. Rostovtsev, L. G. Green, V. V. Fokin, K. B. Sharpless, *Angew. Chem. Int. Ed.*, **2002**, *41*, 2596 - 2599.

¹⁸⁶ H. Díaz Velázquez, Y. Ruiz García, M. Vandichel, A. Madder, F. Verpoort, *Org. Biomol. Chem.*, **2014**, *12*, 9350 - 9356

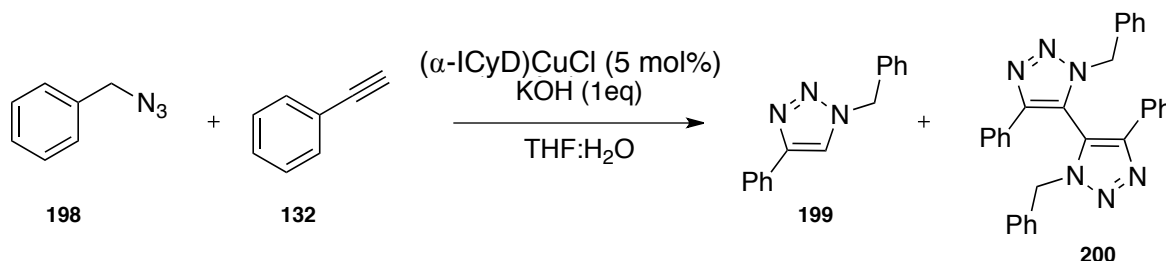
¹⁸⁷ R. G. Kultyshev, Y. Kawanishi, M. Nishioka, A. Miyazawa, *Organic Chemistry*, **2014**, *44*, 556 - 563

¹⁸⁸ B. T. Worrell, J. A. Malik, V. V. Fokin, *Science*, **2013**, *34*, 457 - 460, b) L. Jin, D. R. Tolentino, M. Melaimi, G. Bertrand, *Sci. Adv.* **2015**, *1*, 1 - 5

¹⁸⁹ A. Makarem, R. Berg, F. Rominger, B. F. Straub, *Angew. Chem. Int. Ed.* **2015**, *54*, 7431 - 7435

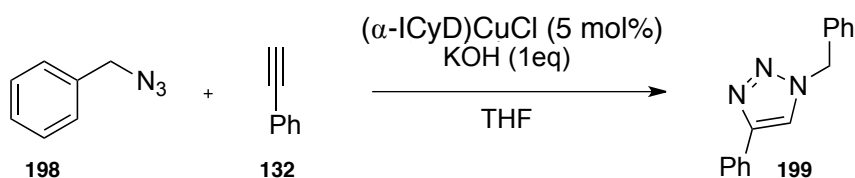
i. Catalytic activity of (α -ICyD)CuCl complexes

The first test was tried in a catalytic reaction conditions. The reaction of benzyl azide **198** with phenylacetylene **132** in presence of (α -ICyD)CuCl and KOH in a 1:1 mixture of THF : water, led to the formation of the 1,4-triazole **199** in 31% yield and an unexpected bistriazole **200** as a major compound in 63% yield.



Scheme I-6: (α -ICyD)CuCl catalyzed CuAAC

Bistriazoles were reported on the original report as oxidative coupling side-products of the CuAAC reaction. Ten years ago, Burgess and Angell were able to improve the formation of this bistriazoles up to the preparative scale. These bistriazoles were obtained in quantitative yields proposed to be assisted by inorganic bases in aqueous media.¹⁹⁰ To avoid the formation of bistriazoles, the reaction was carried out in the absence of water using pure THF as solvent, obtaining exclusively the 1,4 triazole **199** in 74% yield.



Scheme I-7: (α -ICyD)CuCl catalyzed synthesis of triazole **199**

ii. Mechanistic studies

To get more insights into the reaction mechanism, the putative intermediates of the mononuclear pathway were synthesized stepwise. Reaction of (α -ICyD)CuCl **128** with an excess of KOH formed instantaneously (α -ICyD)CuOH **201**. After filtration of the excess of KOH and KCl, the copper hydroxide intermediate reacted slowly with 2 equivalents of phenylacetylene to afford the monomeric copper acetylide (α -ICyD)CuCCPh **202** (Figure IV-3). The formation of these species was monitored by NMR. The complete shift of the characteristic deshielded H-5A,D indicated the completion of the reaction.

¹⁹⁰ Y. Angell, K. Burgess, *Angew. Chem. Int. Ed.* **2007**, 46, 3649–3651

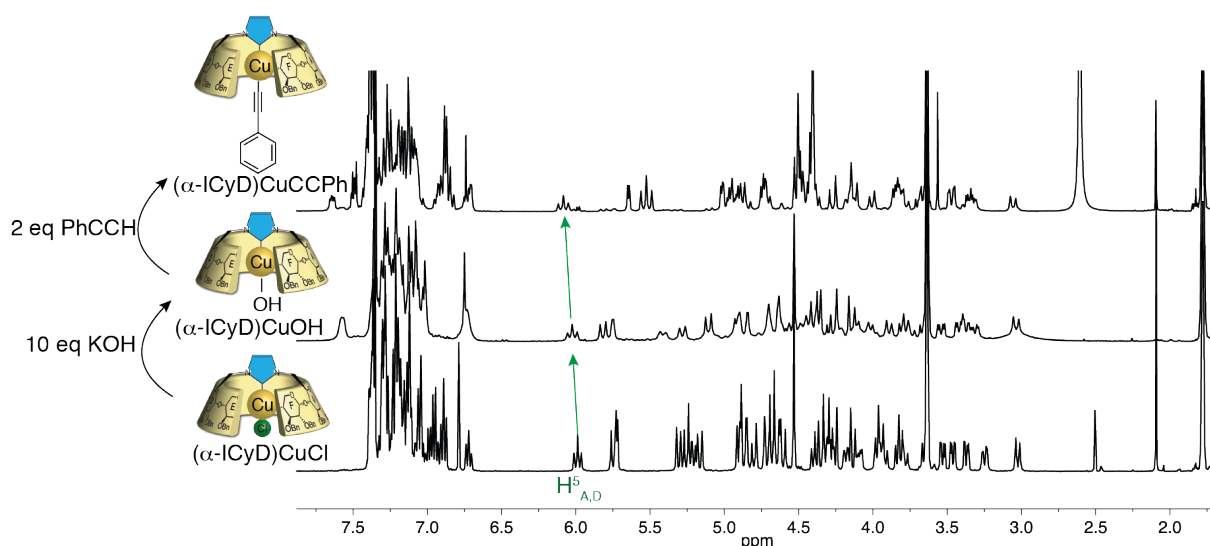


Figure IV-3: Monitoring of the stepwise formation of key reactive species.

After addition of an excess of benzyl azide, an extremely slow reaction was observed. After 70 hours of reaction, a consumption of the excess of phenylacetylene of the previous step and formation of 1-benzyl-4-phenyl-1,2,3-triazole of the reaction were observed. Nevertheless, no transformation of the $(\alpha\text{-ICyD})\text{CuCCPh}$ **202** was observed, confirming the monomeric copper-acetylide as resting state. This means that the cycloaddition is the rate limiting step thus, slow on the mononuclear complex (Figure IV-4).

In conclusion for this reaction, even if the stoichiometric reactivity was slower than expected, the structural differences of $(\alpha\text{-ICyD})\text{CuCl}$ allowed us to briefly study a mechanistic pathway not accessible to traditional catalysts. Unfortunately, results were in agreement with the literature: The mononuclear pathway is slower and less favorable than the reported dinuclear one.

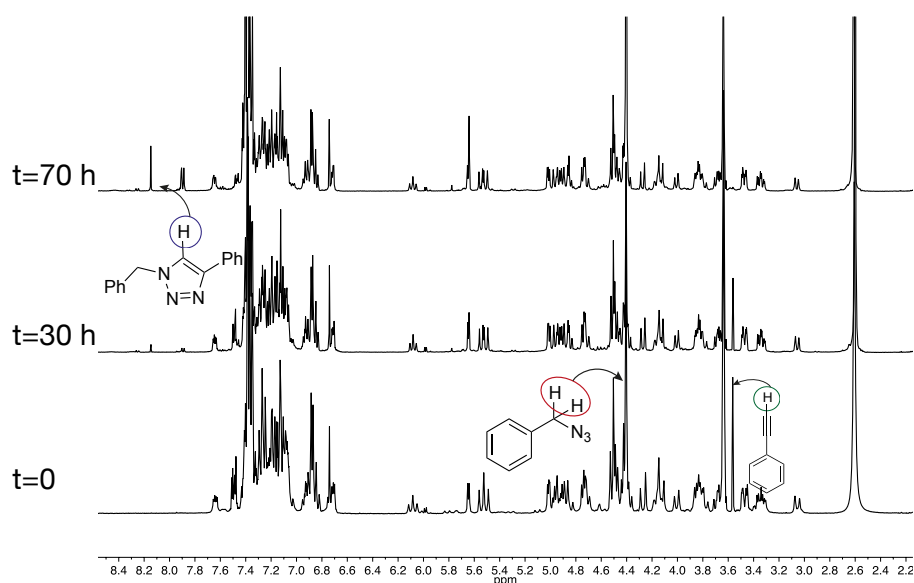


Figure IV-4: Monitoring of the reaction of $(\alpha\text{-ICyD})\text{CuCCPh}$ with BnN_3 .

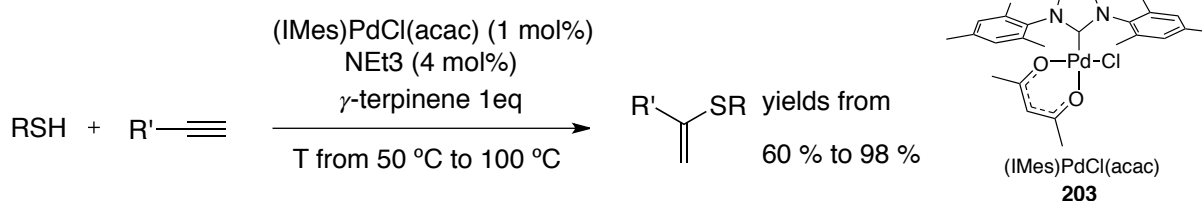
3. Palladium (II) as Lewis Acid: Thiolation of triple bonds

To start the study of (ICyD)Pd^{II} in catalytic applications, the simplest case to study was the use of the complex in a reaction where the oxidation state remains unchanged during the whole catalytic cycle, thus, a Lewis acid reactivity. The chosen reaction was a hydrothiolation of triple bonds.

i. Reaction and mechanism

C-sp² heteroatom substituted vinyl monomers are building blocks of interest in the development of functional polymers,¹⁹¹ from an economically point of view, development of mild and selective conditions to synthesize the monomers are required to develop a scalable method.

Transition metal-catalyzed synthesis of Markovnikov-type vinyl sulfides was shown as a tolerant method but sensitive to the structure of the catalyst as well as to the substitution of the thiol¹⁹². Different methods were developed in a hydrothiolation of triple bonds with different advantages and drawbacks¹⁹³. In this context, we were interested in a Pd^{II} catalyzed hydrothiolation of alkynes proposed by Hirao¹⁹⁴, recently revisited by Ananikov¹⁹⁵. In the latest report, Ananikov *et al* proposed the following conditions to obtain the industrially valuable branched vinyl sulfides (Scheme IV-8).



Scheme IV-8: Pd-NHC catalyzed synthesis of branched vinyl sulfides.

¹⁹¹ Y. Iwakura, F. Toda, K. Hattori, *J. Polym. Sci. A*, **1968**, 6, 1633 - 1642

¹⁹² L. Palacios, M.J. Artigas, V. Polo, F. J. Lahoz, R. Castarlenas, J. J. Pérez-Torrente, L. Oro, *ACS Catal.* **2013**, 3, 2910–2919

¹⁹³ Rh catalyzed : a) C. Cao, L. R. Fraser, J. A. Love, *J. Am. Chem. Soc.* **2005**, 127, 17614–17615

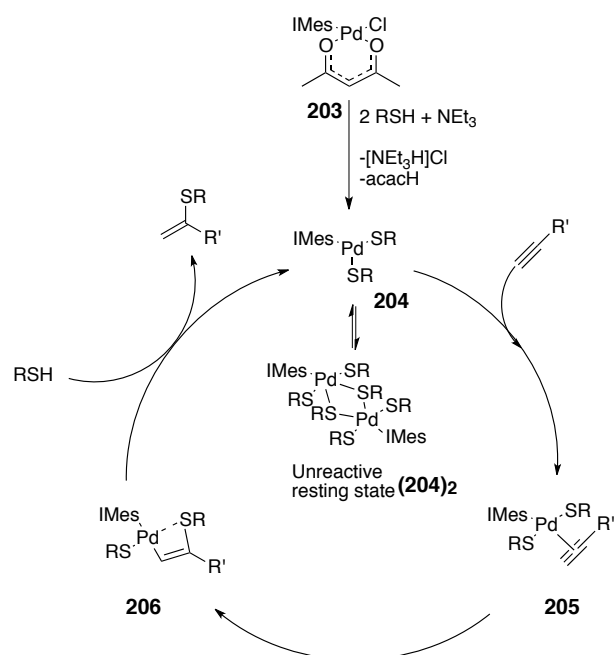
Zr catalyzed C. J. Weiss, T. J. Marks, *J. Am. Chem. Soc.* **2010**, 132, 10533–10546

¹⁹⁴ A. Ogawa, T. Ikeda, K. Kimura, T. Hirao, *J. Am. Chem. Soc.* **1999**, 121, 5108–5114

¹⁹⁵ E. S. Degtyareva, J. V. Burykina, A. N. Fakhrutdinov, E. G. Gordeev, V. N. Khrustalev, V. P. Ananikov *ACS Catal.* **2015**, 5, 7208 – 7213

The mechanism of the reaction starts with a NEt_3 mediated double substitution of the chloride ligand and the acac ligand to afford the intermediate I. Coordination of the alkyne(II), followed by an insertion of the thiol on the triple bond affords the vinyl palladium complex III that after acid-base reaction release the product and regenerates the intermediate I.

Stepwise mechanistic studies¹⁹⁵ showed that the Pd-dimer **(204)**₂ was an unreactive resting state. This low reactivity was confirmed by theoretical studies showing that the alkyne insertion on the dimer **(204)**₂ was 4 times higher in energy than on the monomer **204**. From an experimental point of view, higher temperatures were required when the dimer **(204)**₂ was used as precatalyst.



Scheme IV-9: Mechanism of the Pd-catalyzed alkyne thiolation.

The idea of the study of this reaction was to perform the reaction with (ICyD)-palladium(II) complexes, more precisely of (β -ICyD) which due to the steric hindrance induced by the cyclodextrin *a priori* cannot form dimeric species. This monomeric reactivity, would avoid the unreactive resting state, and carry out the reaction in milder conditions and faster rates.

ii. Scope of catalyst and kinetics

To start the study of the reaction, a test of the catalyst from the library of β -Pd(II) complexes synthesized previously was done, as well as the (α -rev-ICyD)Pd^{II} complexes, to better understand the reversed coordination. As simplest system to study, to reduce the steric hindrance around the Pd(II) center, *p*-thiocresol **207** and 4-phenyl-1-butyne **100** were used as substrates. Reaction with (β -ICyD)PdCl₂(PhCN) at room temperature afforded the expected vinyl-sulfide **208** in 89% yield (table IV-entry 1). Changing the PhCN ligand by a more coordinating pyridine produced a drop on the yield of the reaction to 8% (Entry 2), reflecting a poisoning effect of the coordinating pyridine.

The same effect was found with the less sterically demanding (α -rev-ICyD). The axial coordinated pyridine ligand produced a significant drop in the yield affording the desired product only in 33% yield. In contrast, (α -rev-ICyD)PdCl allyl afforded the product in 79% yield in the same conditions. Finally IPrPdCl₂PEPPSI **209** and (IPrPdCl₂)₂ **210** were used as model catalyst for this reaction, affording the vinyl sulfide **208** in 51% and 70% yield, respectively.

The use of bigger alkynes with the inner (β -ICyD)PdCl₂(PhCN) produced a drop of the yield to 34%, showing the limits to reach the metal center for hindered substrates (Table-entry 7)

208
R=CH₂CH₂Ph, 100
209

Entry	R'	Catalyst (2%)	NMR yield ^a
1	PhCH ₂ CH ₂	(β -ICyD)PdCl ₂ (PhCN)	89 %
2	PhCH ₂ CH ₂	(β -ICyD)PdCl ₂ (Pyridine)	8 %
3	PhCH ₂ CH ₂	(α -rev-ICyD)PdCl ₂ (pyridine)	33 %
4	PhCH ₂ CH ₂	(α -rev-ICyD)PdCl(allyl)	79 %
5	PhCH ₂ CH ₂	(IPrPdCl ₂) ₂	70 %
6	PhCH ₂ CH ₂	IPrPdCl ₂ PEPPSI TM	51 %
7	C(CH ₃) ₂ OH	(β -ICyD)PdCl ₂ (PhCN)	34 %

Table IV-4: Scope of catalysts for the α -hydrothiolation of alkynes

^aUsing 1,4-dinitrobenzene as internal reference.

In conclusion, among the introverted complexes, $(\beta\text{-ICyD})\text{PdCl}_2(\text{PhCN})$ is the one that showed the best efficiency to catalyze this reaction, probably, because of the presence of a labile PhCN ligand, easily substituted by weakly coordinating triple bonds. The same deduction was followed to chose $(\text{IPrPdCl}_2)_2$ as model catalys to study the kinetics of the reaction.

Kinetics of the reaction were followed by NMR¹⁹⁶ recording a $^1\text{H-NMR}$ spectrum each 5 minutes, using 0.3 equivalents of 1,4-dinitrobenzene as internal reference (Figure IV-5). In the case of $(\text{IPrPdCl}_2)_2$, a kinetic profile reaching a maximum of 81% yield at 7 hours of reaction was obtained.

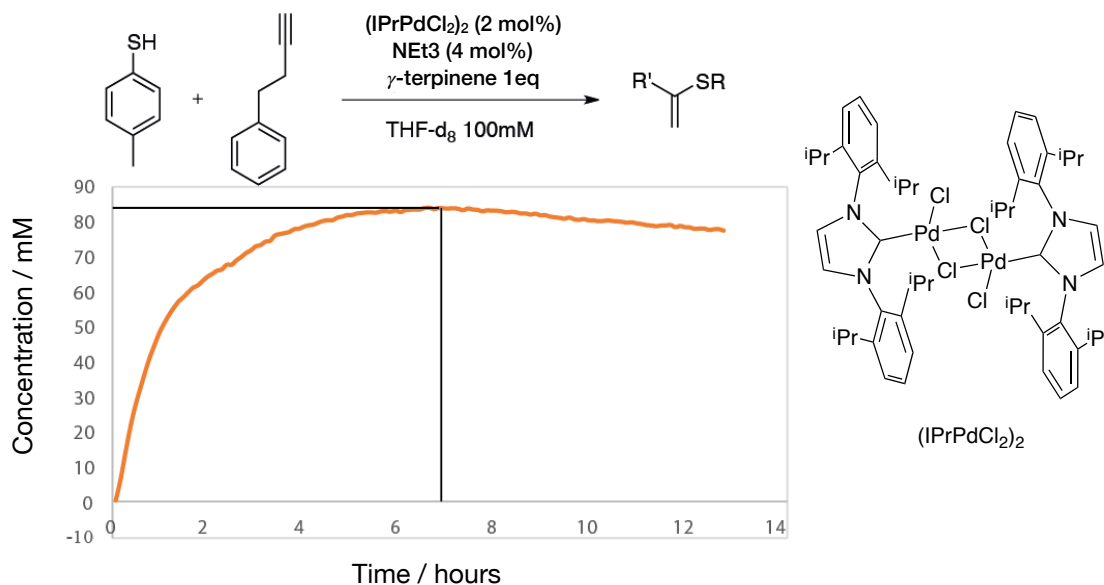


Figure IV-5 : Kinetic profile of the $(\text{IPrPdCl}_2)_2$ catalyzed hydrothiolation.

In contrast, $(\beta\text{-ICyD})\text{PdCl}_2(\text{PhCN})$ showed a much different kinetic profile. An accelerating rate profile is observed during the first seven hours of reaction where an inflection point was obtained. After this point the reaction is faster and reach a maximum yield of 83% at 11 hours.

Evaluating the initial rates of both reactions by linearization of the first eight points of the reaction, the $v_0(\text{IPr}) = 4.7 \mu\text{M sec}^{-1}$ and $v_0(\beta\text{-ICyD}) = 0.44 \mu\text{M sec}^{-1}$, 11 times faster for the non-confined complex.

This different behavior could be due to two different reasons: The first possibility, a slow activation of the catalyst, either because of the steric hindrance or poisoning of the Pd induced by the PhCN ligand. This slow activation could produce an increase of the effective concentration of catalyst over time (Figure IV-6). The second one, the product reacted with the catalyst and formed more active catalytic species, thus, the concentration of these active species increased over time, generating more active catalytic species.¹⁹⁷

¹⁹⁶ THF-d_8 , 300 K, 300 MHz

¹⁹⁷ For a similar kinetic profile see the Figure 4: D. G. Blackmond, *J. Am. Chem. Soc.*, **2015**, *137*, 10852 – 10866

In conclusion, a different mechanistic behavior was observed. (IPrPdCl₂)₂ showed at 27 °C a fast reaction since the beginning of the experiment. In contrast, (β-ICyD)PdCl₂(PhCN) required an activation time to form the most active catalytic species.

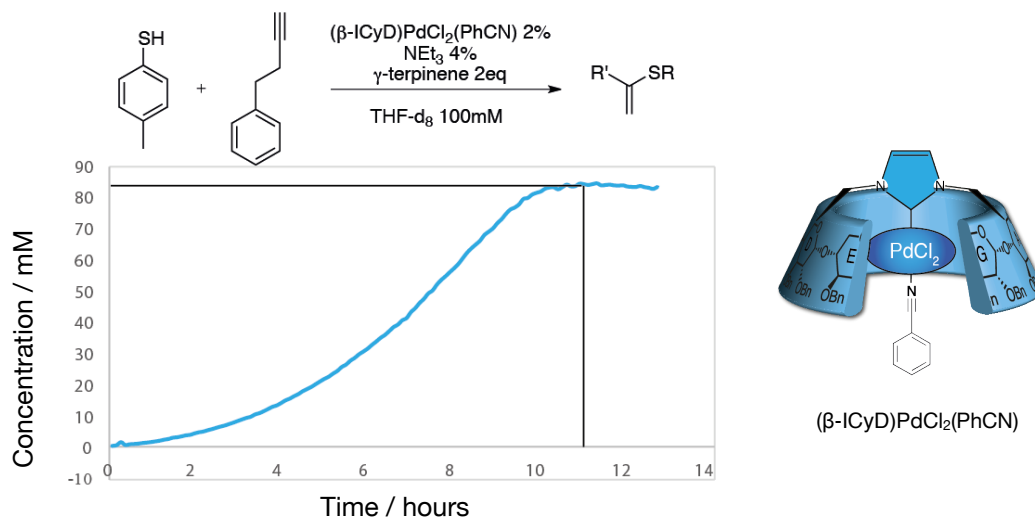


Figure IV-6 : Kinetic profile of the (β-ICyD)PdCl₂(PhCN) catalyzed hydrothiolation.

Once again, a different behavior during a reaction was observed with an ICyD ligand. Nevertheless, this reaction showed that even if the cavity of the (β-ICyD)PdCl₂(PhCN) complex seemed to be extremely crowded, reactions are still possible with the square planar complexes.

4. Conclusion to part A:

Through these three different reactions, using the previously described linear complexes (α-, β-, and γ-ICyD)AuCl, (α- and β- ICyD)CuCl and the additional square planar (ICyD)Pd^{II}-complexes and (α-rev-ICyD)Pd^{II} different behaviors, either positive or negative were observed.

(ICyD)AuCl complexes are efficient catalysts in enyne cycloisomerization, and more importantly, the steric hindrance around a gold center can influence the mechanism of gold(I)-catalyzed enyne cycloisomerization.

Copper(I) complexes showed again a small application in the understanding of Cu-catalyzed reactions. Using this complexes in a well-studied CuAAC reaction, according to previous reported studies on the CuAAC reaction,¹⁹⁶ a slow but not forbidden reaction catalyzed by a monomeric Cu atom.

Finally, the first studies in a hydrothiolation with Pd^{II} complexes showed that even with an important steric hindrance around the square planar palladium atom complexes, the activity is not lost.³⁷

The following studies will show, in addition to the electrochemistry showed before, how the second coordination sphere depending on the cavity size of the cyclodextrin can influence reactions where the oxidation state changes during the catalytic cycle.

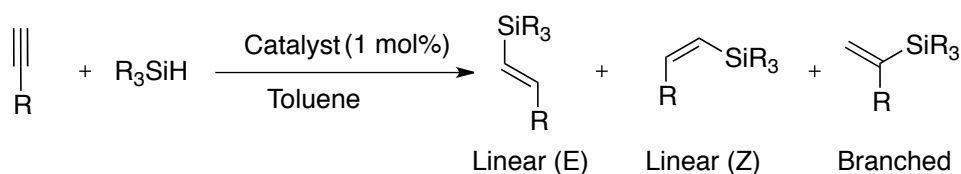
B. NHC capped cyclodextrin in redox active catalytic cycles.

During this part of the dissertation, the study of the reactivity of ICyDs in catalytic cycles where the geometry of the metal evolves was studied. In the first place, tests will be studied with Pt-catalyzed reactions where the geometry can dramatically change between two or three different oxidation states. Then, trials of oxidations from organometallic Au^I to Au^{III} were studied, to finally move to cross-coupling-type reactions where Pd^{II} complexes are reduced to Pd⁰.

1. Increasing the oxidation state

iii. Platinum(0)/platinum(II) catalysis : Hydrosilylation of triple bonds

Since the synthesis of the Marko's catalyst¹⁹⁸, NHC-Pt⁰-complexes were developed as one of the most powerful catalysts in alkene or alkyne hydrosilylation, due to the ability to insert into silicon-hydrogen bonds at extremely low loadings of catalyst¹⁹⁹. In the reaction of triple bonds with silanes, three different products could be obtained: the linear (E) isomer, the linear (Z) and the branched compound (Scheme IV). Due to the industrial interest of this reaction²⁰⁰, selective reactions in mild conditions are the objectives for the study of cyclodextrin-based Pt complexes.



Scheme IV-10: Generic Pt(0) catalyzed hydrosilylation of alkynes

For all these reactions, (β -rev-ICyD)Pt(dvtms) will be used as the model complex as it possesses the same electronic features as the inner (β -ICyD)Pt(dvtms), but with a less sterically crowded metal center.

A generic hydrosilylation reaction was carried out using phenylacetylene **132** and triethylsilane in toluene²⁰¹. When the reaction was catalyzed by the outer (β -rev-ICyD)Pt(dvtms) at room temperature, a mixture of the linear isomer and the branched one in a 9 : 1 ratio was obtained (without traces of the linear (Z) compound). When the inner (β -ICyD)Pt(dvtms) is used as catalyst, a mixture of both compounds was obtained in a 8 : 2 ratio, also in favor of the linear (E) isomer.

¹⁹⁸ I. E. Marko, S. Stérin, O. Buisine, G. Mignani, Paul B, B. Tinant, J.-P. Declercq, *Science*, **2002**, 298, 204 - 206.

¹⁹⁹ S Dierick, I.E Marko, NHC Platinum(0) Complexes: Unique Catalysts for the Hydrosilylation of Alkenes and Alkenes (Ed S.P. Nolan) Wiley-VCH, **2014**, 111 - 149

²⁰⁰ L. N. Lewis, J. Stein, Y. Gao, R. E. Colborn, G. Hutchins, *Platinum Met. Rev.*, **1997**, 41, 66 - 75

²⁰¹ P. Žak, M. Bořt, M. Kubicki, C. Pietraszuk, *Dalton Trans.* **2018**, 47, 1903 - 1910

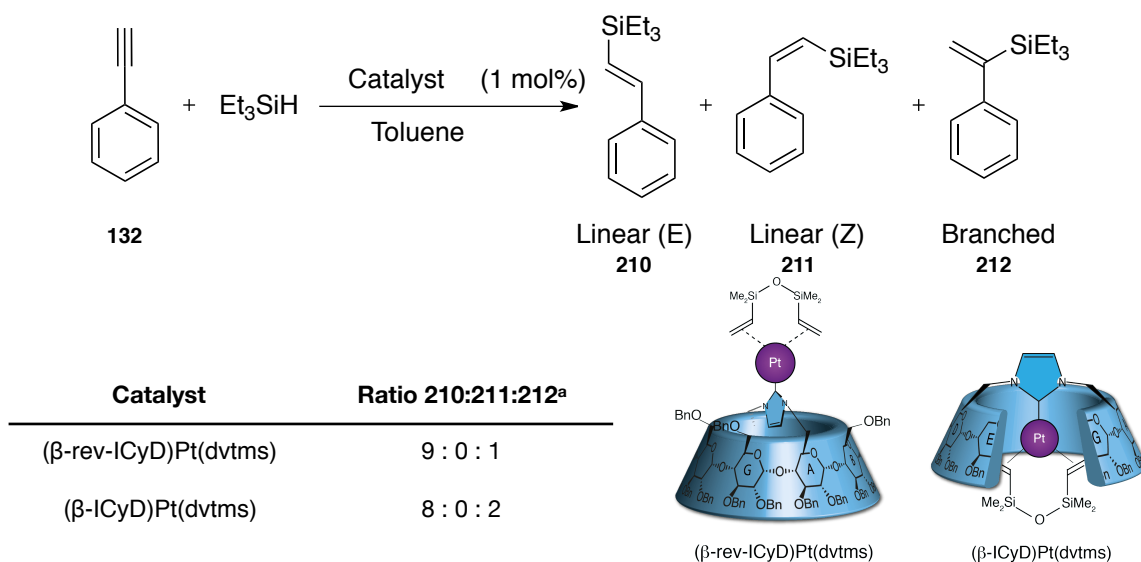


Table IV-5: Synthesis of triethylsilylstyrenes catalyzed by β -ICyD-based Pt(0) complexes.

^a Ratio calculated in the crude NMR.

These first catalytic tests showed the activity of NHC-based-Pt(0) catalysts proving that in a catalytic cycle sterically demanding substituents such as Et_3SiH could be in the first coordination sphere of the metal complex, thus, inside the cavity. Due to a modest selectivity of the catalyst, this reaction was abandoned to move towards a more challenging reactivity with more coordinated octahedral Pt complexes.

iv. Pt (0) /Pt (II) /Pt (IV) catalysis: C-H borylation of arenes.

Since the discovery of C-H activation, a broad variety of systems were developed to functionalize unactivated C-H bonds²⁰². Despite of the development of systems and methods, directing groups are required to perform selective activation of C-H bonds, frequently at *ortho* - or *para*- positions of aromatic rings. In this field, activation of *para* C-H bonds were developed with hindered ligands in synergy with hindered substitutions on the aryl substrate²⁰³.

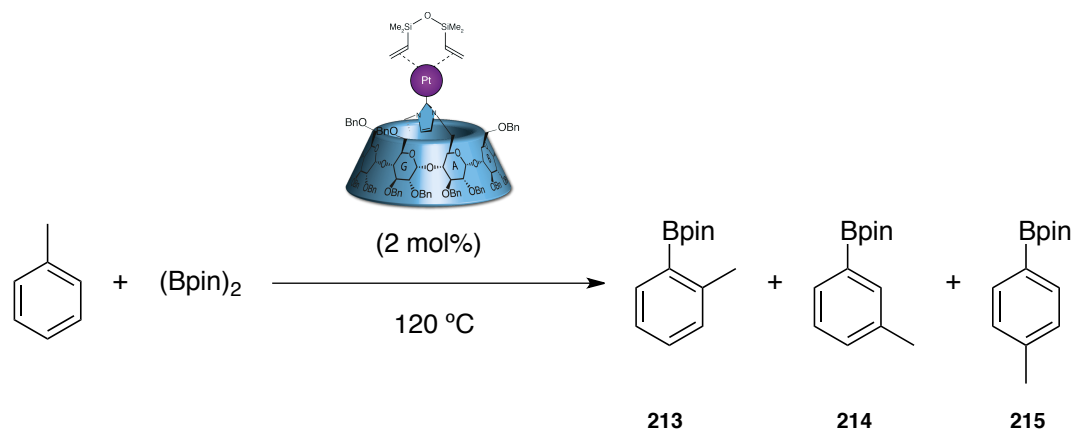
²⁰² X. Chen, K. M. Engle, D.-H. Wang, J.-Q. Yu *Angew. Chem. Int. Ed.* **2009**, *48*, 5094 – 5115

²⁰³ Y. Saito, Y. Segawa, K. Itami, *J. Am. Chem. Soc.*, **2015**, *137* 5193–5198

The first remote C-H bond functionalization was developed by Hartwig using a Rh-complex²⁰⁴. Due to the steric hindrance afforded by the substituents on the aromatic ring and the hindered ligands, the C-H silylation did not take place at the *ortho* position and the selectivity was directed by the rate of the reductive elimination.²⁰⁵

Later results showed that the use of bulky phosphines in an iridium(I) complexes can direct the C-H borylation to the *para* position of bulky mono substituted arenes.²⁰⁶ The same year, a C-H borylation of arenes was developed using (ICy)Pt(dvtms) complexes²⁰⁷. This reaction was not affected by the steric hindrance of the substituents of the arene, reacting in extremely crowded positions. Based on this result, we expect that the use of sterically crowded (β -ICyD)Pt(dvtms) could favor the reaction at the *para*- position of non-directing substrates.

Reaction of (Bpin)₂ with toluene catalyzed by the external (β -rev-ICyD)Pt(dvtms) complex at 120 °C afforded the Bpin substituted arenes in a ratio **213:214:215** of 13:55:32, similar to the one reported with the non-confined ICyPt(dvtms) (ICy = 1,3-bis-dicyclohexyl-Imidazol-2-ylidene) **177** (Scheme IV-11).



Scheme IV-11: (β -rev-ICyD)Pt(dvtms) catalyzed C-H borylation of toluene.

Unfortunately, the inner (β -ICyD)Pt(dvtms) appeared to be inert in this reaction. In this example, a negative effect of the hindrance of the cavity was observed, producing a complete deactivation of the complex.

²⁰⁴ C. Cheng, J. F. Hartwig, *Science*, **2014**, 343, 853 - 857.

²⁰⁵ C. CHeng, J. F. Hartwig, *J. Am. Chem. Soc.*, **2014**, 136, 12064–12072

²⁰⁶ Y. Saito, Y. Segawa, K. Itami, *J. Am. Chem. Soc.*, **2015**, 137, 5193–5198

²⁰⁷ T. Furukawa, M. Tobisu, N. Chatani, *J. Am. Chem. Soc.*, **2015**, 137, 12211–12214

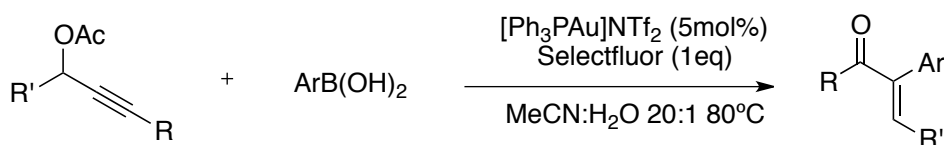
2. Gold(I) to gold(III)

i. Bibliography: From linear to square planar.

Despite the existence of a wide variety of organometallic Au^I and Au^{III} complexes, catalytic cycles where gold changes its oxidation state are rare²⁰⁸. Main challenges of gold chemistry are the stability of the organogold complexes²⁰⁹ and extremely high activation barriers between both oxidation states^{210,211}. Nevertheless, in the last decade, exciting reports were published with cross-coupling cycles, oxidative arylations or migratory insertions, thought to be forbidden for gold complexes.

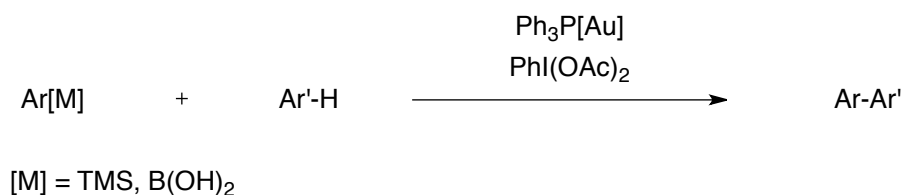
To set up catalytic cycles between Au^I and Au^{III} different approaches were reported in the literature:

Early reports in this field started with a classical activation of an unsaturated C-C bond and nucleophilic attack to form a organogold complex. Then, oxidation with selectfluor® and transmetalation with a boronic acid²¹² forms a gold(III) complex that finishes the catalytic cycle with a reductive elimination (Scheme IV-12).^{191c}



Scheme IV-12: Early report of a reaction with a Au(I)/Au(III) catalytic cycle.

Lloyd-Jones and then Nevado, showed that oxidative direct arylation can be performed with aryl silanes or boronic acids using hypervalent iodine as stoichiometric external oxidant²¹³ (Scheme IV-13).



Scheme IV-13: Au(I)/Au(III) catalyzed oxidative direct arylation.

²⁰⁸ C.-Y. Wu, T. Horibe, C. B. Jacobsen, F. D. Toste *Nature* **2015**, *517*, 449 - 454

²⁰⁹ M. D. Levin, T. Q. Chen, M. E. Neubig, C. M. Hong, C. A. Theulier, I. J. Kobylanski, M. Janabi, J. P. O'Neil F. D. Toste, *Science* **2017** *356*, 1272 - 1276.

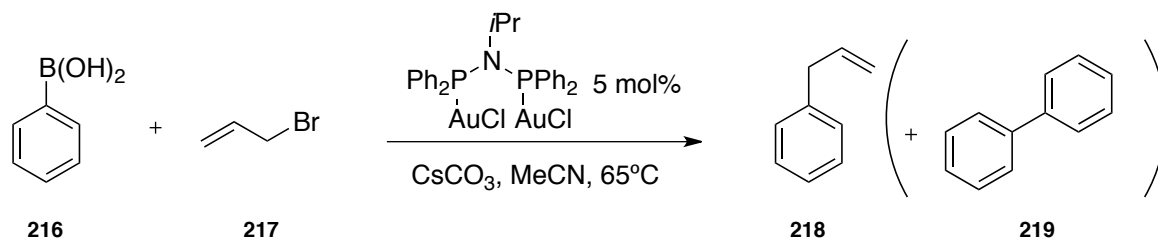
²¹⁰ M. Livendahl, C. Goehry, F. Maseras, A. M. Echavarren *Chem. Commun.*, **2014**, *50*, 1533 - 1536

²¹¹ G. Klatt, R. Xu, M. Pernpointner, L. Molinari, T. Q. Hung, F. Rominger, A. S. K. Hashmi, H. Koppel, *Chem. Eur. J.* **2013**, *19*, 3954 - 3961

²¹² R. Kumar, A. Linden, C. Nevado *J. Am. Chem. Soc.* **2016**, *138*, 13790-13793

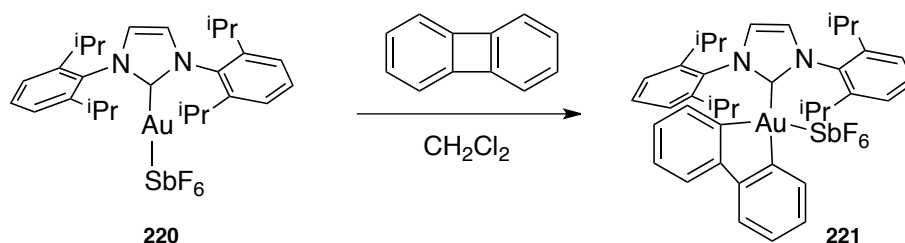
²¹³ a) L. T. Ball, G. Lloyd-Jones, C. R. Russell, *Science*, **2012**, *337*, 1644 - 1648. b) M. Hofer, A. Genoux, R. Kumar, C. Nevado, *Angew. Chem. Int. Ed.* **2017**, *56*, 1021 -1025.

The use of gold in a cross coupling reaction with a Au(I)/Au(III) catalytic cycle without external oxidant was first reported by Toste in a allylation of aromatic boronic acids.²¹⁴ The mechanism was shown to be polar but intermolecular Au(I) - Au(III) transmetalations produced homocoupled biaryl byproducts (**219**).



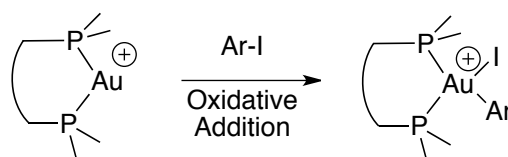
Scheme IV-14: Gold catalyzed allylation of aryl-boronic acids.

Later studies by Toste's group showed that C-C bonds could perform oxidative additions into a cationic IPrAuSbF₆ complex. In their report, the authors showed that an antiaromatic biphenylene could form a stable gold (III) complex by oxidative addition into a cationic NHC-Au^I complex **220**.²¹¹ Despite the fast reductive elimination reported on Au(III) complexes²¹⁵, the stability of this complex remains on the high energy barrier to produce again the 4 member ring antiaromatic biphenylene (Scheme IV-17).



Scheme IV-15: Oxidative addition of phenylene into a IPrAuSbF₆ complex.

Another approach to avoid the high energy activation barriers for the oxidative addition²¹¹ was proposed by Bourissou, and coworkers (Scheme IV-16). The first one, a distorted non-linear geometry of the initial dicoordinated gold(I) complex²¹⁶ allowed the authors to perform oxidative additions on aryl-iodides in a stoichiometric manner. (Scheme IV-16).



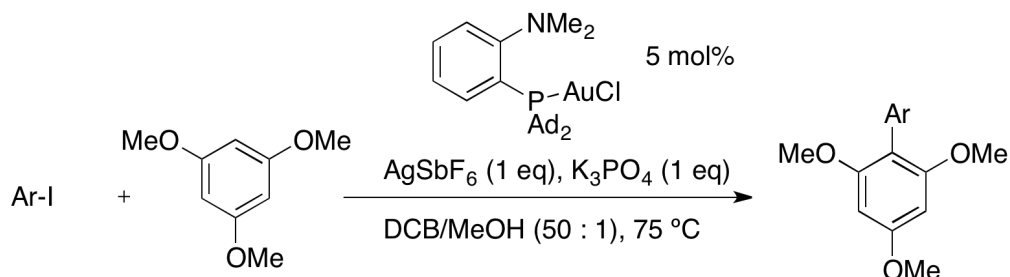
Scheme IV-16: Oxidative addition in bent coordinated gold(I) complex.

²¹⁴ M. D. Levin, F. D. Toste, *Angew. Chem. Int. Ed.* **2014**, 53, 6211 – 6215

²¹⁵ W. J. Wolf, M. S. Winston, F. D. Toste, *Nat Chem.* **2014**, 6, 159–164

²¹⁶ M. Joost, A. Zeineddine, L. Estévez, S. Mallet-Ladeira, K. Miqueu, A. Amgoune, D. Bourissou, *J. Am. Chem. Soc.*, **2014**, 136, 14654 – 14657

Another approach followed by the same group was the use of a ligand possessing an additional hemilabile ligand.²¹⁷ In this case, the generated gold(III) complex is stabilized by the ancillary ligand allowing the system to react in a controlled manner. Using this approach, the authors set up a cross-coupling reaction, without external oxidants between aryl-iodides and trimethoxybenzene (Scheme IV-17).



Scheme IV-17: Cross-coupling reaction catalyzed by a Au(I)/Au(III) catalytic cycle

In conclusion, common points on the approaches to force oxidative additions are the use of a distorted partner of the reaction. Either an antiaromatic substrate with a contracted cycle, either a distorted complex to reduce the activation barrier of the step. Our hypothesis, is that the presence of the cyclodextrin, with a well-defined environment, could produce conformations that could force the oxidative addition step. The approach followed to do so, was the synthesis of (β -ICyD)Au^I organogold complexes and try different elementary steps. To do so, different alkyl and aryl ICyD organogold complexes were synthesized and different elementary reactions were tested.

ii. Synthesis of (β -ICyD)Au(I) organogold species.

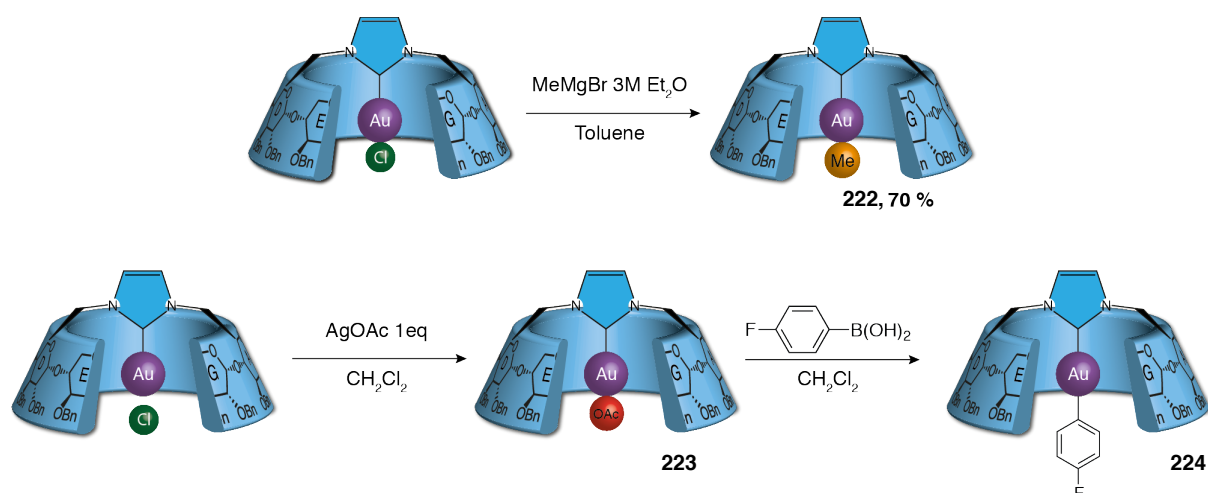
To obtain the β -ICyD organometallic precursors described methods with NHC-Au were used. (β -ICyD)AuMe **222** was obtained by reaction of (β -ICyD)AuCl with MeMgBr²¹⁸ in toluene in 70% yield after silica gel purification.

Aromatic (β -ICyD)Au(*p*-C₆H₄F) **224** was synthesized in two steps: first, ligand exchange with AgOAc afforded the (β -ICyD)AuOAc **223** precursor, after transmetalation with one equivalent of *p*-C₆H₄F-boronic acid the desired (β -ICyD)Au(*p*-C₆H₄F) **224** in 83% yield.^{213a}

²¹⁷ A. Zeineddine, L. Estévez, S. Mallet-Ladeira, K. Miqueu, A. Amgoune D. Bourissou, *Nat. Commun.*, **2017**, *8*, 1 - 8

²¹⁸ M. T. Johnson, J. M. J. van Rensburg, M. Axelsson, M. S. G. Ahlquist, O. F. Wendt *Chem. Sci.*, **2011**, *2*, 2373–2377

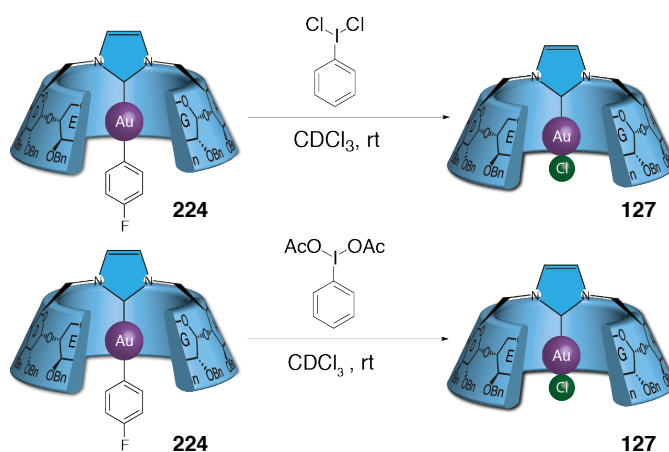
iii. Stoichiometric studies.



Scheme IV-18: Synthesis of $(\beta\text{-ICyD})\text{AuMe}$ **222** and $(\beta\text{-ICyD})\text{AuAr}$ **224**.

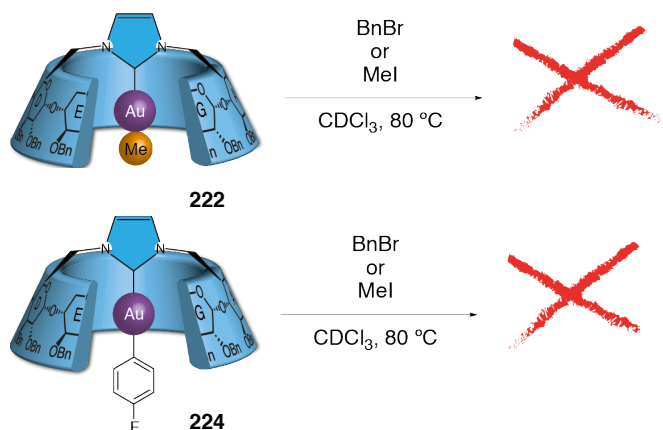
226 To first understand the stability of these organogold complexes, $(\beta\text{-ICyD})\text{AuAr}$ **224** was engaged in oxidation reactions using hypervalent iodine. Reaction of $(\beta\text{-ICyD})\text{AuAr}$ with PhICl_2 in CDCl_3 at room temperature formed $(\beta\text{-ICyD})\text{AuCl}$ **127** after 18 hours of reaction. If $\text{PhI}(\text{OAc})_2$ was used instead of the chlorinated analogue, after three days at room temperature $(\beta\text{-ICyD})\text{AuCl}$ is formed as major compound (Scheme IV-19). To avoid chloride donors in the reaction medium the reaction was carried out in C_6D_6 . In this solvent, a degradation of the cyclodextrin was observed.

In conclusion, a reactivity of the organometallic complexes was observed, but unfortunately, in any case the presence of 1-chloro-4-fluorobenzene was observed. Thus, any evidence of the oxidation of the complexes.



Scheme IV-19: oxidations with hypervalent iodine of **224**

Looking for a reactivity of these complexes, first tests were done with the electron rich (β -ICyD)AuMe complex. Mixture of (β -ICyD)AuMe with benzyl bromide or allyl bromide showed no evolution at 80 °C in CDCl₃. Reaction of (β -ICyD)AuAr **224** with MeI in CDCl₃ gave, the same result in the same reaction conditions.



Scheme IV-20: Investigation of the oxidative addition of (β -ICyD)AuR complexes.

Reactivity towards triple bonds was also tested. The reaction of (β -ICyD)AuAr with phenylacetylene in CDCl₃ afforded the corresponding (β -ICyD)AuCCPh **225** through an acid-base reaction.²¹⁹

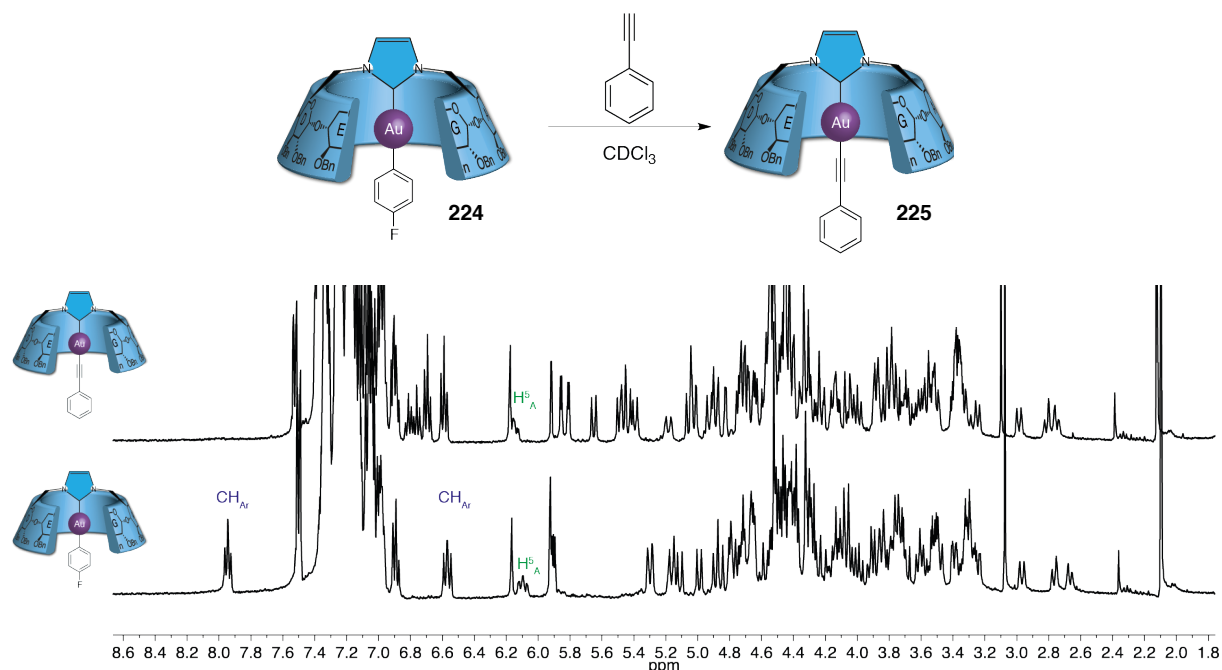


Figure IV-7: Synthesis of (β -ICyD)AuCCPh **225**

²¹⁹ K. E. Roth, S. A. Blum, *Organometallics* **2010**, *29*, 1712–1716

To avoid the acid-base reactivity, the substituted version of the phenylacetylene, PhCCMe was used as triple bond. While no evolution was observed at room temperature, when heating the reaction mixture at 60 °C, the system evolved towards the formation of a mixture of non-characterized compounds observed by ¹H-NMR. This mixture of complexes, after cooling down again the mixture at room temperature evolved to the precursor (β-ICyD)AuCl **127** (?) (Figure IV-8).

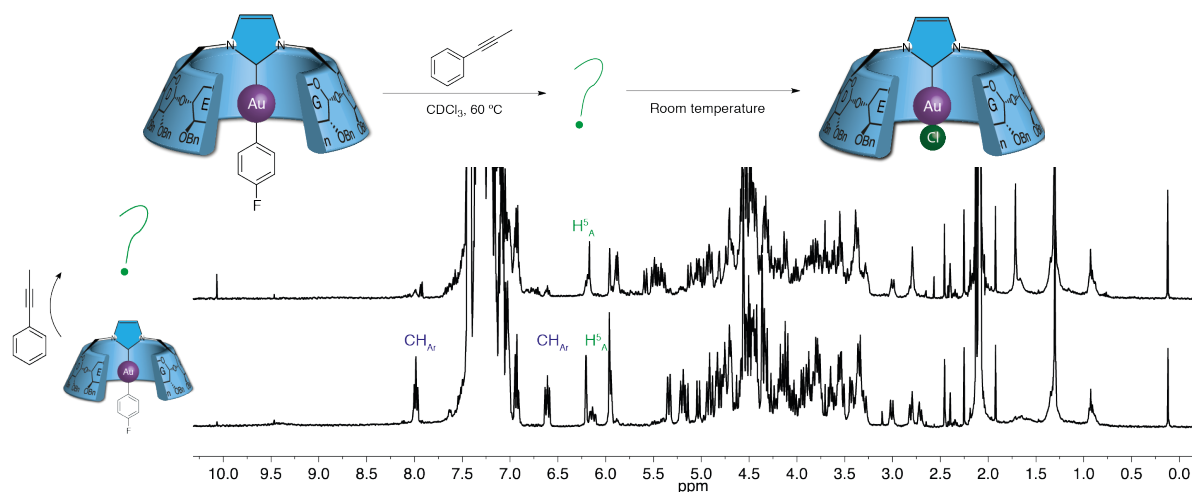
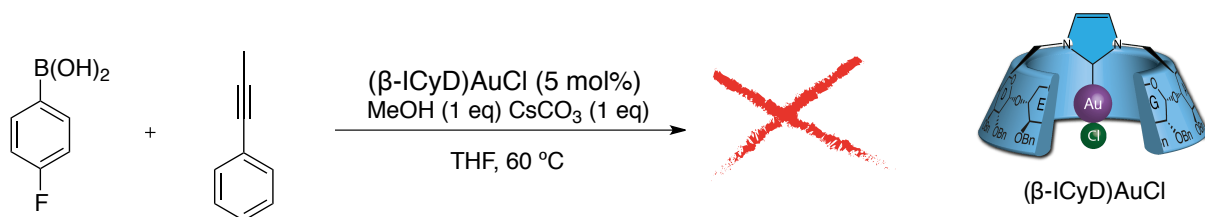


Figure IV-8: Monitoring of the reaction of (β-ICyD)AuAr with **226**

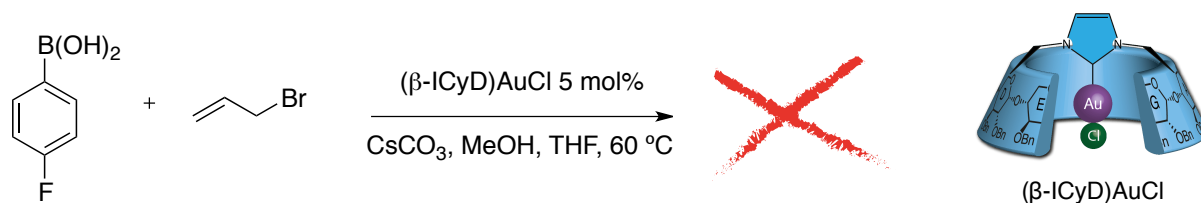
iv. Catalytic tests

To check the reactivity of the last system, (β-ICyD)AuAr **224**, a catalytic test was performed. The first one to test a reactivity of a possible reactivity of the last reaction, the corresponding boronic acid was reacted with PhCCMe in the presence of (β-ICyD)AuCl **127**. 1 equivalent of MeOH and CsCO₃ were added to form (β-ICyD)AuAr **224** in catalytic amounts. In these conditions only protodeborylation of the starting material and the formation of (β-ICyD)AuAr **224** were observed in the crude NMR.



Scheme IV-21: Attempt of catalytic reactivity catalyzed by (β-ICyD)AuCl

The second catalytic trial, was based on the cross-coupling reaction developed by Toste.²²⁶ In the original report, the formation of byproducts produced by intermolecular gold-gold transmetalations was reported. In this case, we expect that the steric hindrance of the cyclodextrin could block the Au-Au intermolecular interactions and reduce the formation of byproducts. Unfortunately, any reactivity was observed using (β -ICyD)AuCl (Scheme).



Scheme IV-22: Attempt of cross-coupling catalyzed by (β -ICyD)AuCl

In conclusion, for an organogold reactivity, the steric hindrance brought by the cyclodextrin skeleton produced a negative effect on the reactivity of the gold complex. High temperatures were required to observe a slow reactivity of the complexes. To continue the study of reactivity with changes in the coordination and the oxidation state, complexes where the reactivity starts with the highest coordinated complex will be evaluated. To do so, the best candidates the Pd(II)-based (ICyD) complexes.

3. Reducing the oxidation state: Palladium(II) to palladium(0)

Since the first synthesis of a palladium NHC by Herrmann in 1995²²⁰, the development and study of N-Heterocyclic carbenes as ligands for Pd-catalyzed cross-coupling increased exponentially.²

In comparison to phosphane ligands, the strong σ -donating character of NHCs favors the oxidative addition, reacting easily with C-Cl bonds²²¹. Nevertheless, this electron-donating character of the ligand made the reductive elimination step harder than in the case of less electron-rich ligands²²².

Different approaches were followed to improve the efficiency of this reductive elimination. The two more popular ones are the increase of the steric bulk on the N-substituents of the ligand producing steric repulsion around the metal center,²²³ and the substitution with electro-withdrawing groups on the C4, and C5 position of the NHC²²⁴.

In most of the systems, the activation of the pre-catalyst is a key step for the reactivity of the system²²⁵. The first study of the reactivity of (β -ICyD)Pd(II) complexes will be the synthesis to Pd(0).

i. Activation of the complex: Towards (β -ICyD)Pd(0) species.

Isolation of NHC-Pd⁰ complexes developed interest in the use of easy-activating precatalysts²²⁶ or phosphorescent complexes²²⁷. No universal reduction conditions for NHC-Pd^{II} complexes were developed and the reducing system, dependent on the chemical structure of the precatalyst, could have an influence on the efficiency of the reaction²²⁸. In this part of the study, preliminary activation tests for the (β -ICyD)Pd^{II} complexes were done to see if the steric hindrance and the low reduction potentials obtained in CV are also a symptom of a low reactivity of the complexes.

²²⁰ W. A. Herrmann, M. Elison, J. Fischer, C. Köchter, G. R. J. Arthus, *Angew. Chem. Int. Ed. Engl.* **1995**, *34*, 2371 – 2373

²²¹ J. C. Green, B. J. Herbert, R. Lonsdale, *J. Organomet. Chem.* **2005**, *690*, 6054 – 6067.

²²² G. Mann, Q. Shelby, A. H. Roy, J. F. Hartwig, *Organometallics* **2003**, *22*, 2775 – 2789.

²²³ For a review on the effect of the steric bulk: R. D. J. Froese, C. Lombardi, M. Pompeo, R. P. Rucker, M. G. Organ, *Acc. Chem. Res.* **2017**, *50*, 2244–2253

²²⁴ Y. Zhang, G. Lavigne, N. Lugan, V. César *Chem. Eur. J.* **2017**, *23*, 13792 – 13801

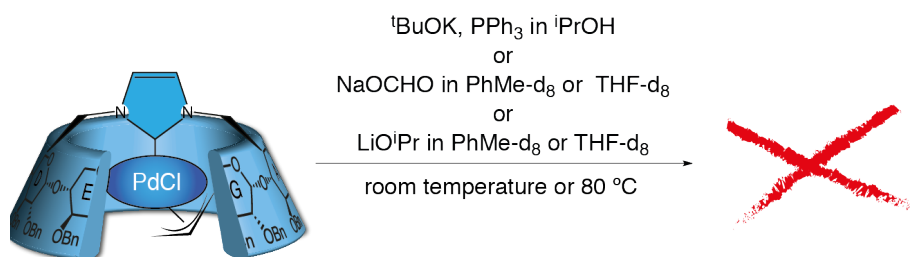
²²⁵ J. Nasielski, N. Hadei, G. Achonduh, E. A. B. Kantchev, C. J. O'Brien, A. Lough, M. G. Organ, *Chem. Eur. J.* **2010**, *16*, 10844 – 10853.

²²⁶ U. Christmann R. Vilar, *Angew. Chem. Int. Ed.* **2005**, *44*, 366 –374.

²²⁷ A. F. Henwood, M. Lesieur, A. K. Bansal, V. Lemaur, D. Beljonne, D. G. Thompson, D. Graham, A. M. Z. Slawin, I. D. W. Samuel, C. S. J. Cazin, E. Zysman-Colman *Chem. Sci.*, **2015**, *6*, 3248–3261.

²²⁸ J. Pytkowicz, S. Roland, P. Mangeney, G. Meyer, A. Jutand, *J. Organomet. Chem.* **2003**, *688*, 166 – 179.

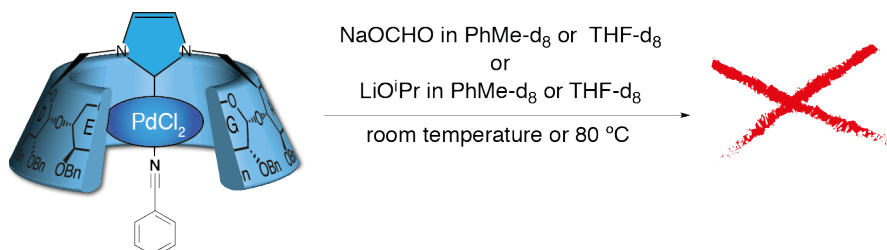
Reducing systems of (NHC)PdCl(Allyl) compounds are mainly based on alkoxides²²⁹, such as ^tBuOK or LiOⁱPr mixed with a phosphine²³⁰. Other methods are based on hydride donors such as LiOⁱPr or Na-formate (HCOONa). Nevertheless, no evolution of the (β-ICyD)PdCl(allyl) complex was observed, in all of the tested conditions.



Scheme IV-23: Test reduction conditions with (β-ICyD)PdCl(allyl).

(NHC)PdCl₂(L) complexes (L = 2e ligand), are frequently reduced by hydride donors such as LiOⁱPr or HCOONa²³¹, β-H eliminating amines such as morpholine²³², NEt₃; or stronger conditions with Grignard reagents.¹⁷²

As for (β-ICyD)PdCl(allyl), reaction of (β-ICyD)PdCl₂(PhCN) with an excess of LiOⁱPr in THF or toluene showed no evolution after 20 hours at 80 °C. The same lack of reactivity was observed when using Na-formate. (Scheme IV)



Scheme IV-24: Tested reduction conditions with hydride donors on (β-ICyD)PdCl₂(PhCN)

Reaction of the same complex with 3 equivalents of morpholine showed a coordination of the amine in the ¹H-NMR at room temperature (Figure IV-9), nevertheless, no evolution was observed when the reaction mixture was heated at 70 °C. Addition of an excess of ^tBuOK, and heating again at 70 °C for an additional 20 hours led to the formation of a mixture of different non-identified species **226**.

²²⁹ M. S. Viciu, O. Navarro, R. F. Germaneau, R. A. Kelly III, W. Sommer, N. Marion, E. D. Stevens, L. Cavallo, and S. P. Nolan *Organometallics* **2004**, *23*, 1629 - 1635, b) R. M. Drost, T. Bouwens, N. P. van Leest, B. de Bruin, C. J. Elsevier, *ACS Catal.* **2014**, *4*, 1349–1357

²³⁰ S. Fantasia, S. P. Nolan, *Chem. Eur. J.*, **2008**, *14*, 6987 - 6993.

²³¹ J. Pytkowicz, S. Roland, P. Mangeney, G. Meyer, A. Jutand, *J. Organomet. Chem.*, **2003**, *678*, 166 - 179

²³² S. Raoufoghaddam, S. Mannathan, A. J. Minnaard, J. G. de Vries, B. de Bruin, J. N. H. Reek, *Chem. Cat. Chem.* **2018**, *10*, 266 – 272

As presented previously, the evolution of the complex was followed by the shifts of the H5A and the CH-NHC. Shifts of those signals was symptomatic of the completion of the reaction and a change of the electronics of the Pd atom.

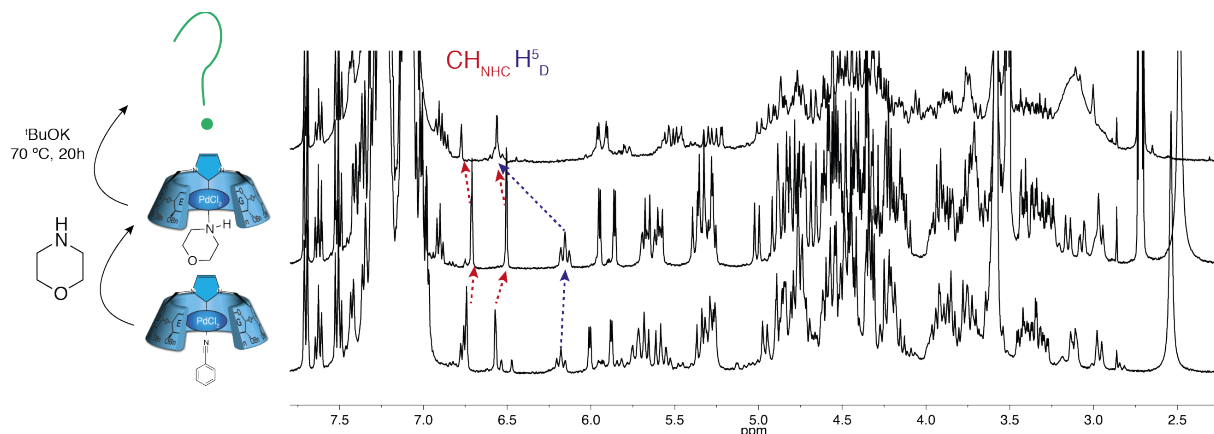


Figure IV-9: Evolution of the $(\beta\text{-ICyD})\text{PdCl}_2(\text{PhCN})$ **171** complex with

This new compound showed two singlets at -3.35 and -3.65 ppm in the proton NMR integrating for one proton each (Figure IV-10). For these two peaks, no cross correlation was found on the HSQC spectrum. Also from the HSQC, an extremely deshielded H5 appeared at 6.55 ppm, confirming the non-decomplexation of an electron-rich palladium atom

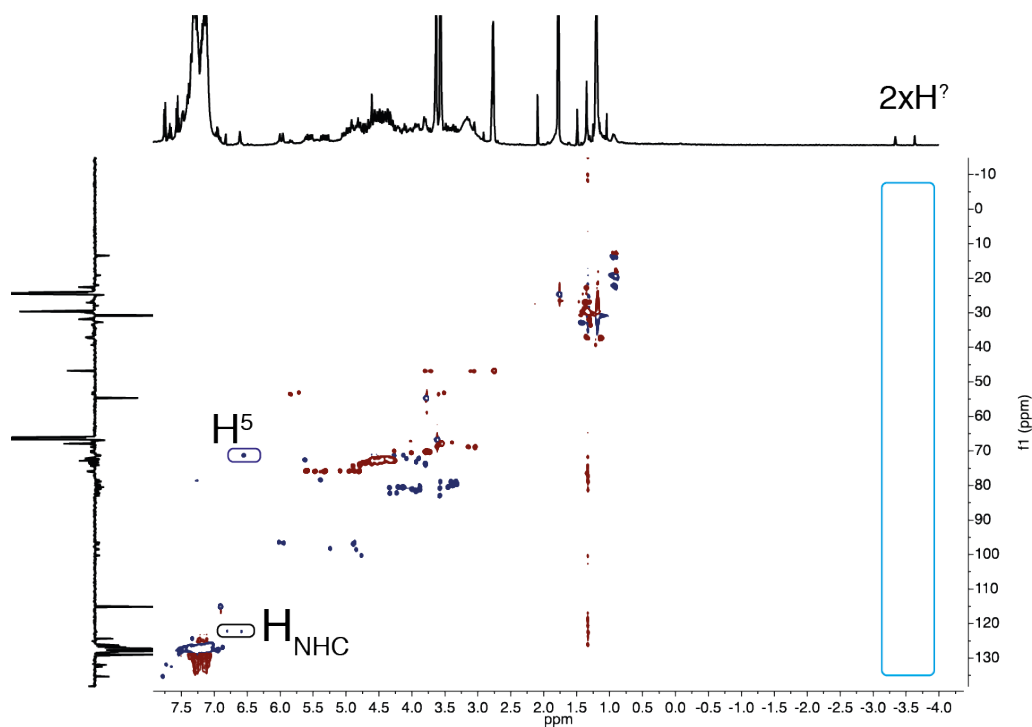


Figure IV-10: HSQC of the non-identified complex formed by reaction of $(\beta\text{-ICyD})\text{PdCl}_2(\text{PhCN})$ with morpholine and $t\text{BuOK}$. THF- d_8 , 600 MHz, 300 K.

The presence of two CH of the NHC and seven anomeric peaks confirms also the presence of a major compound. As for the rest of complexes the resonance frequency of the carbene was found in the HMBC following the cross correlations of the CH of the NHC and the H6 of one of the sugars attached to it (Carbene = 166.2 ppm).

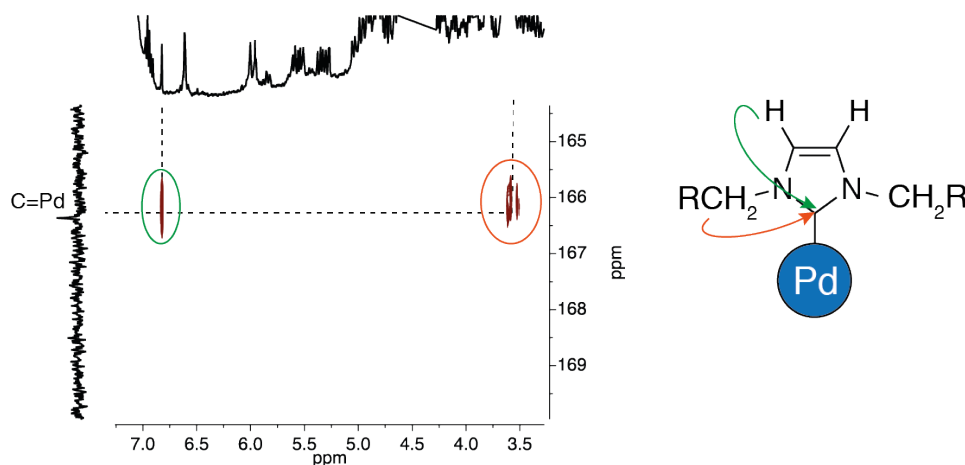


Figure IV-11: Extract of the HMBC of the complex showing the chemical shift of the carbene.

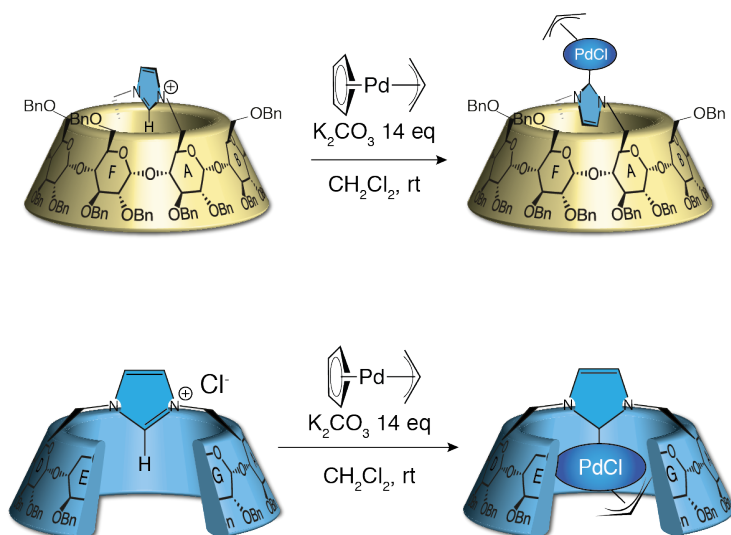
Any reactivity was found after addition of *p*-chloroanisole, excluding the possibility of a Pd(0) complex.

With all these informations the a putative structure for this compound is a (β -ICyD)PdH₂ **226**, with a possible second 2 electron ligand. Nevertheless, no monomeric bis hydride palladium-II complexes were reported in the literature, making impossible any comparison of chemical shifts.²³³

Another user friendly synthesis of low-valent Pd⁰ and Pd^I complexes is based on the direct coordination of the free NHC to (η^3 -Allyl)(η^5 -cyclopentadienyl)palladium(II).²³⁴ The complexation of the precursor produces then a spontaneous reductive elimination forming low valent Pd complexes. Thus, reaction of (α -ICyD)HCl or (β -ICyD)HCl, in the presence of a K₂CO₃ and the Pd-complexes afforded the corresponding (ICyD)PdCl(η^3 -allyl) complexes as single compounds in 48% and 50% yield respectively (Scheme).

²³³ For reports a dimeric (NHC)₂(Pd)₂-H, *Angew. Chem. Int. Ed.* **2010**, 49, 6315 - 6318.

²³⁴ W. Dai, M. J. Chalkley, G. W. Brudvig, N. Hazari, P. R. Melvin, R. Pokhrel, M. K. Takase, *Organometallics*, **2013**, 32 5114–5127



Scheme IV-25: Synthesis of (ICyD)PdCl(η^3 -allyl) with CpPd(η^3 -allyl).

These reduction tests showed that despite the low reduction potentials observed in electrochemistry and the steric hindrance afforded by the cyclodextrin, the (β -ICyD)PdCl₂(PhCN) complex was not inert and chemical transformations could happen inside the cavity. Due to the reaction conditions tested here, the first attempts to use these complexes in Pd cross-coupling reactions were a Buchwald-Hartwig amination reaction.

ii. Towards selectivity with (β -ICyD)Pd(II) complexes

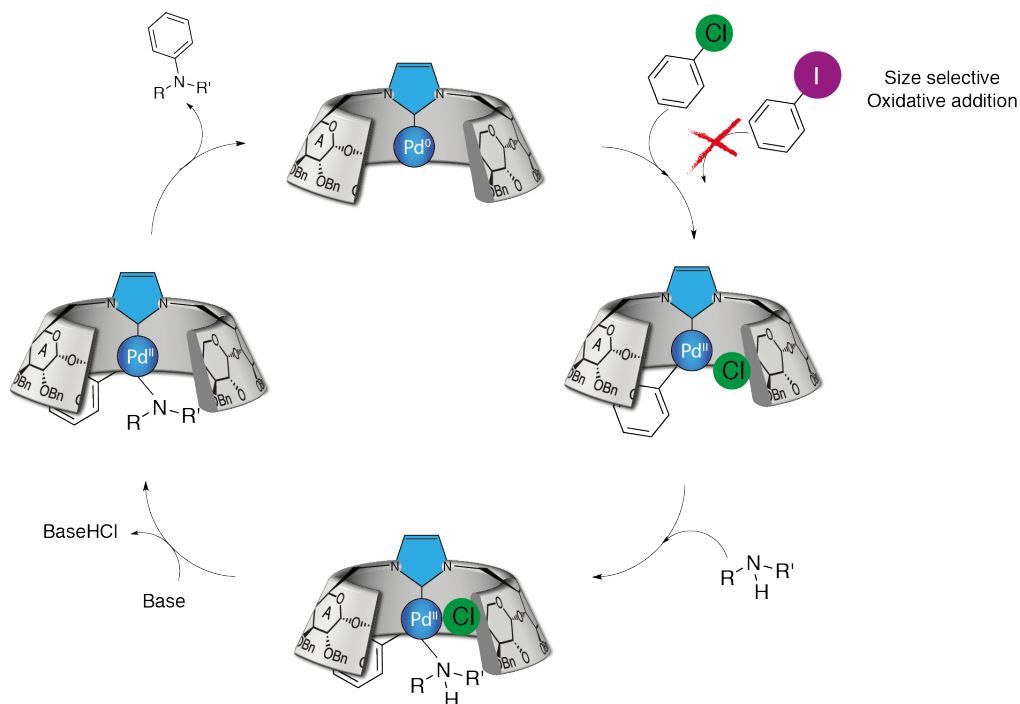
Since the only conditions that showed an evolution of the (β -ICyD)PdCl₂(PhCN) were the use of morpholine and ^tBuOK, the first reaction considered was a Buchwald-Hartwig cross-coupling reaction. It was reported in recent studies that using hindered NHCs in this reaction has many advantages.¹³⁷

In addition, the strong σ -donating character of the NHC facilitates the oxidative addition, making it possible on C-Cl bonds. Besides, from a mechanistic point of view, the same reactivity was found in the case of Ar-Cl and Ar-I substrates. Thus, in contrast to weaker donating phosphane ligands, the oxidative addition is not the limiting step in the case of N-heterocyclic carbenes²³⁵.

From all the studies of the square planar complexes based on (β -ICyD), an important selectivity imposed by the size of the cavity was found on the reactivity towards the oxidation of (β -ICyD)AuCl with Cl₂, Br₂ and I₂. The initial idea of the selectivity with square planar compounds was based on the result that Cl₂ could react inside the cavity while I₂ showed to be non-reactive towards the oxidation of the metal center.

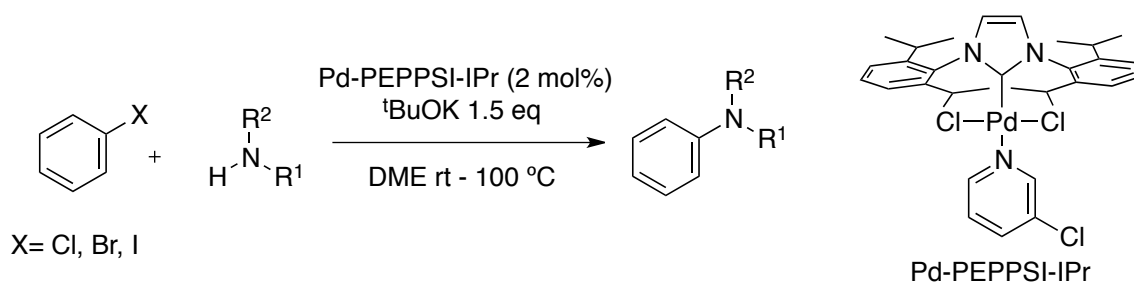
²³⁵ M. G. Organ, M. Abdel-Hadi, S. Avola, I. Dubovyk, N. Hadei, E. A. B. Kantchev, C. J. O'Brien, M. Sayah, C. Valente, *Chem. Eur. J.* **2008**, *14*, 2443 – 2452

The question is: Can we relate the structure and the reactivity obtained with gold(I)/gold(III) oxidations in a Pd(0)/Pd(II) reaction? The aim of this work is to develop a site-selective catalytic reaction where the steric hindrance afforded by the cyclodextrin, made react easier smaller aryl chlorides than bigger aryl iodides?



Scheme IV-26: Design of the attempt of development of a size selective oxidative addition.

Reported reaction conditions for this cross-coupling reaction used an NHC-PEPPSI and a base and in temperatures from room temperature to 100 °C²⁴⁶, depending on the substrate.



Scheme IV-27: Pd-PEPPSI-IPr catalyzed Buchwald Hartwig amination.

The formation of the $(\beta\text{-ICyD})\text{PdCl}_2(3\text{-Chloropyridine})$ **227** complex was monitored by $^1\text{H-NMR}$ starting from the $(\beta\text{-ICyD})\text{PdCl}_2(\text{PhCN})$. Addition of one equivalent of 3-chloropyridine produced a decoordination of HOD and apparition of 2 signals of the corresponding H-ortho of the pyridine confirmed the formation of the expected “PEPPSI-Pd-ICyD” complex **227**. Additionally, apparition of only two signals for the CH of the NHC showed the formation of only one compound.

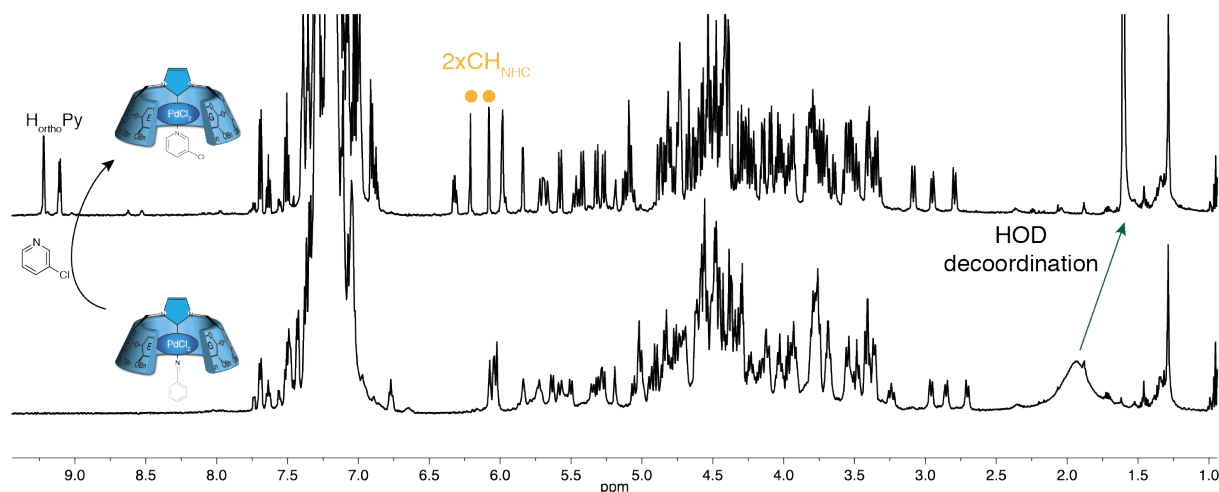
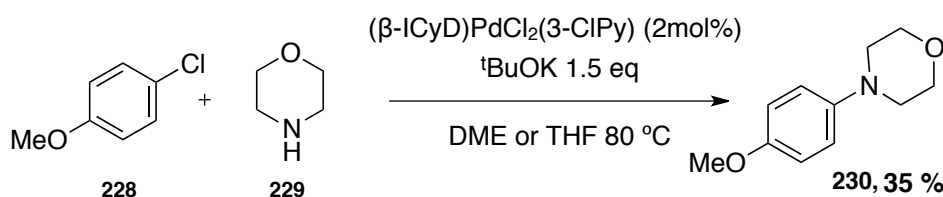


Figure IV-12: Formation of $(\beta\text{-ICyD})\text{PdCl}_2(3\text{-chloropyridine})$ **227** complex

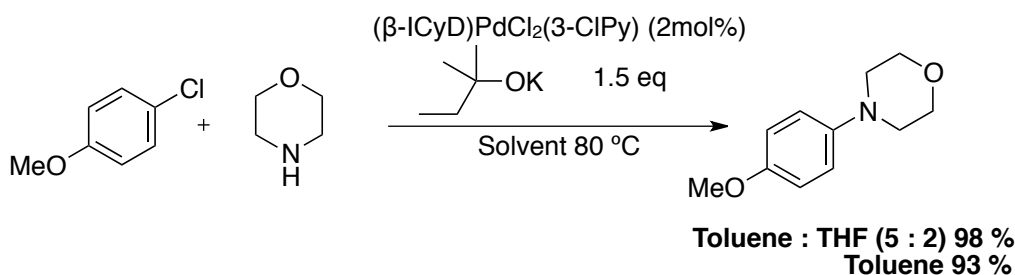
Screening of reaction conditions

The reaction conditions chosen were the same as those proposed by Organ.²⁴⁶ Using morpholine and 4-chloroanisole in DME in presence of $t\text{BuOK}$ and the $(\beta\text{-ICyD})\text{PdCl}_2(3\text{-ClPy})$ complex, the expected cross-coupling product was obtained in 35% isolated yield. The same result was obtained using THF as solvent.



Scheme IV-28: $(\beta\text{-ICyD})\text{PdCl}_2(3\text{-ClPy})$ catalyzed Buchwald-Hartwig amination.

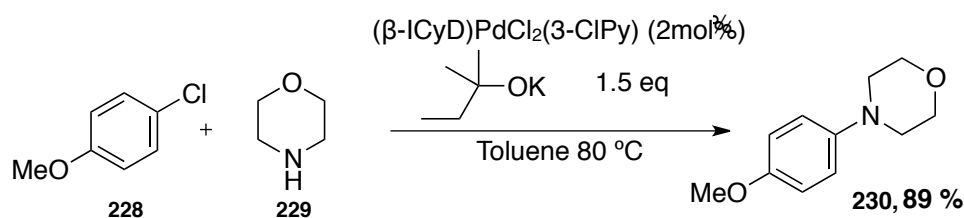
The use of potassium *tert*-amylate as soluble equivalent of $t\text{BuOK}$ led to a significant improvement of the yield. Carrying out the reaction in a toluene : THF 5 : 2 mixture improved the yield to 98%. Using pure toluene as solvent 93% yield was obtained. To avoid mixtures of solvents in future kinetic studies, pure toluene was selected as solvent for the reaction.



Scheme IV-29: Optimization of solvent for the $(\beta\text{-ICyD})\text{PdCl}_2(3\text{-CIPy})$ catalyzed Buchwald-Hartwig amination.

Scope

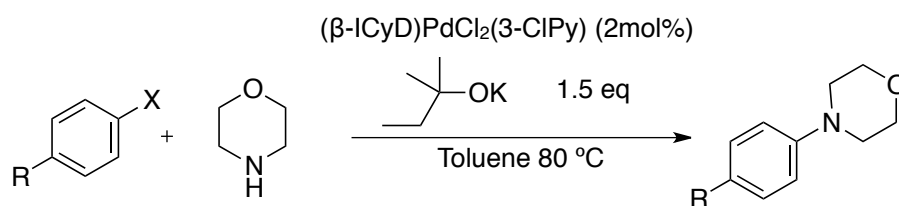
Finally, the loading of the catalyst could be reduced to 0.5 mol% obtaining the cross-coupled amine in 89% yield.



Scheme IV-30: Final conditions for the $(\beta\text{-ICyD})\text{PdCl}_2(3\text{-CIPy})$ reaction

PEPPSI-Pd-ICyD **227** was found to be an efficient catalyst for this reaction. The reactivity of the system was first studied by comparing different aryl substrates with different halogens as partners for the reaction, always using morpholine as model amine. Interestingly, electron-rich chloroanisole gave better yields (entry 1, 89%) than chlorobenzene (entry 4, 67%) or electron-poor *p*-CF₃-substituted aryls (entry 6, 68%).

The opposite trend was observed for the aryl-iodides, that gave lower yields with electron rich MeO- than with electron poor CF₃ substituents (entries 3, 5, 7, 68%, 77%, 89%). In the case of bromo-anisole, an intermediate reactivity between the chloro- and iodo- substrates was obtained (entry 2, 74%). With the aim to develop a site selective reaction, 4-chloriodobenzene was tested as substrate and reacted exclusively at the iodo position.



Entry	R	X	Yield (Product)
1	MeO	Cl	89 % (230)
2	MeO	Br	74 % (230)
3	MeO	I	68 % (230)
4	H	Cl	67 % (231)
5	H	I	77 % (231)
6	CF ₃	Cl	68 % (232)
7	CF ₃	I	89 % (232)
8	Cl	I	63 % (233)

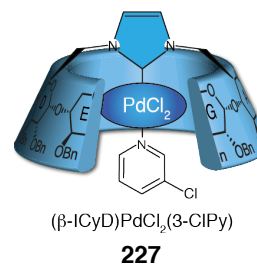


Table IV-6: Yields of the Buchwald-Hartwig amination catalyzed by (β-ICyD)PdCl₂(3-ClPy)

Kinetics:

To verify the initial idea of an easier reaction, the kinetic profiles of the reactions were studied. To do so, the formation of the product was quantified during eight hours by GC using dodecane as internal standard. In the case of the 4-chloroanisole, catalyzed by (β-ICyD)PdCl₂(3-chloropyridine) the reaction reached its maximum of 96% yield in 4 hours of reaction.

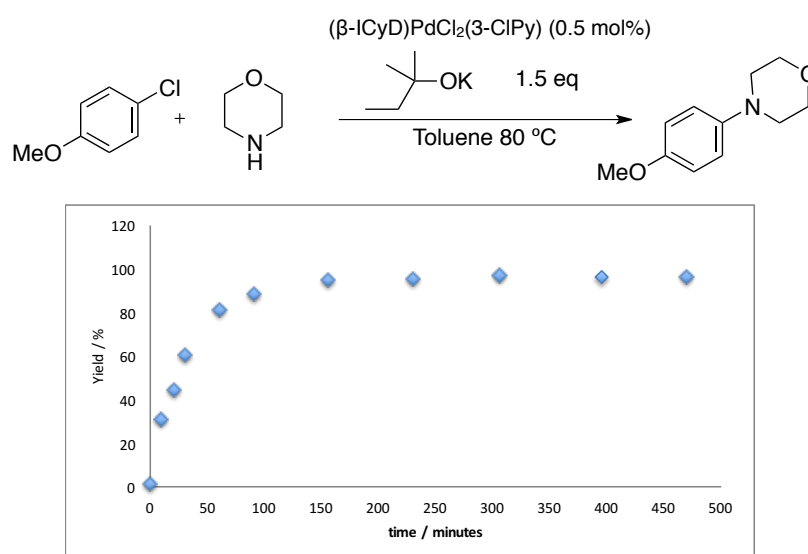


Figure IV-31: Reaction conditions and kinetic profile of the (β-ICyD)PdCl₂(3-ClPy) catalyzed Buchwald-Hartwig amination of 4-chloroanisole.

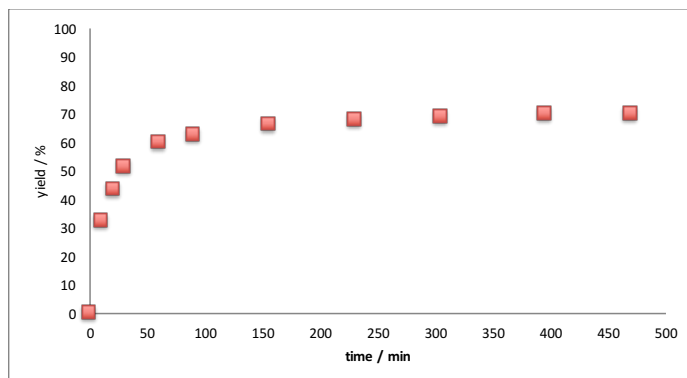
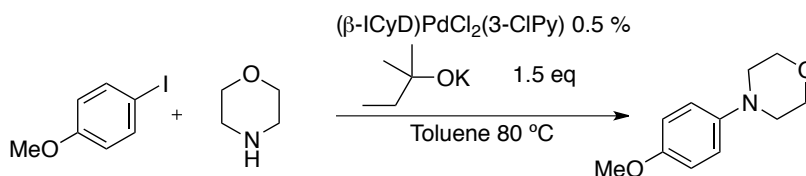


Figure IV-32: Reaction conditions and kinetic profile of the $(\beta\text{-ICyD})\text{PdCl}_2(3\text{CIPy})$ catalyzed Buchwald-Hartwig amination of 4-iodoanisole.

In the case of 4-iodoanisole the plateau of the reaction is also achieved in four hours but only in 68% yield. No appreciable changes were observed in the rates of the reaction, just a reduction of the turnover number from 192 to 138 (Figure IV-32).

Trying to achieve the desired reactivity, the temperature was reduced to 45 °C. In this case, after 4 hours less than a 5% yield was obtained in the case of the 4-Chloroanisole and a 30% in the case of the 4-iodoanisole.

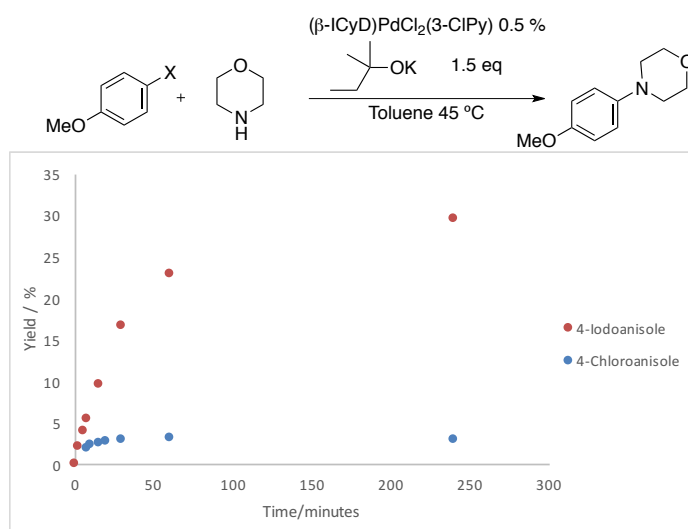


Figure IV-33: Reaction conditions and kinetic profile of the $(\beta\text{-ICyD})\text{PdCl}_2(3\text{CIPy})$ catalyzed Buchwald-Hartwig amination at 45 °C.

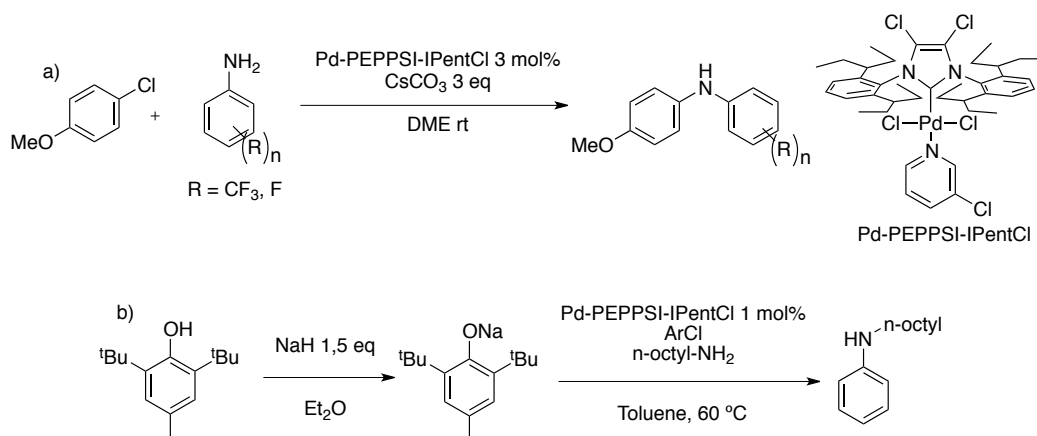
Unfortunately, the attempts to develop a site selective reaction failed (again). Nevertheless, good reaction conditions, with good performances were obtained with different substrates. Those results encouraged us to investigate in more details the possibility of using $(\beta\text{-ICyD})\text{PdCl}_2(3\text{-ClPy})$ in a broader scope for this reaction.

Buchwald-Hartwig amination: Mono-arylation of amines.

Since the first report by Buchwald²³⁶ and almost simultaneously Hartwig²³⁷ of the palladium-catalyzed cross-coupling between arylbromides and amines, researchers focused to improve the original catalytic system to a more methodological reaction. First reports using NHC as ligands for this reaction were started by Nolan²³⁸, and years later Organ's work contributed in the understanding of the role of the sterics and the electronics of the NHC.²²³

Recent researches on this field developed selective cross-coupling reaction to synthesize secondary amines from a Ar-X (X= halogen or pseudo halogen) and a primary amine. First reports showed that using a hindered and electron-poor Pd-PEPPSI-IPentCl could couple electron-poor aryl-amines and electron rich aryl-halides affording the secondary amines in mild conditions²³⁹ without traces of tertiary amines (Scheme IV-a).

Later results showed that the same catalyst could also couple primary amines with a broad scope of aryl chlorides affording the mono-arylated compound as the major product, using the hindered NaBHT as base²⁴⁰ (Scheme IV-31-b). Additionally, to avoid the over-arylation of the secondary amine, the use of an excess of the aryl-halide partner²⁴¹ or the use of a hindered amine are required.²⁴²



Scheme IV-31: Reported examples of selective mono-arylation of primary amines with NHCs.

²³⁶ A. S. Guram, R. A. Rennels, S. L. Buchwald *Angew. Chem. Int. Ed. Engl.* **1995**, *34*, 1348 - 1350

²³⁷ J. Louie, J. F. Hartwig, *Tetrahedron Lett.* **1995**, *36*, 3609 - 3612.

²³⁸ N. Marion, O. Navarro, J. Mei, E. D. Stevens, N. M. Scott, S. P. Nolan, *J. Am. Chem. Soc.* **2006**, *128*, 4101 - 4111

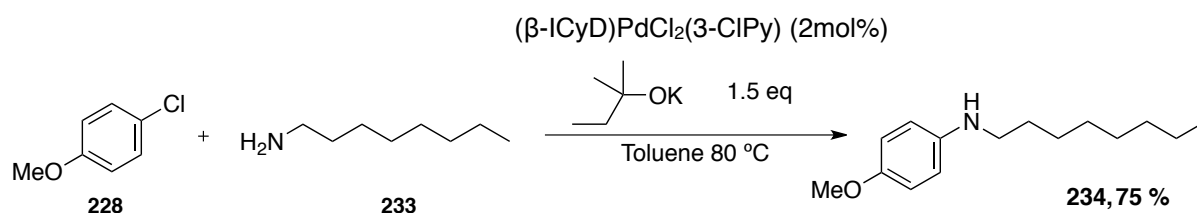
²³⁹ M. Pompeo, J. L. Farmer, R. D. J. Froese, M. G. Organ, *Angew. Chem. Int. Ed.* **2014**, *53*, 3223 - 3226

²⁴⁰ S. Sharif, R. P. Rucker, N. Chandrasoma, D. Mitchell, M. J. Rodriguez, R. D. J. Froese, and M. G. Organ, *Angew. Chem. Int. Ed.* **2015**, *54*, 9507 - 9511

²⁴¹ S. Sharif, D. Mitchell, M. J. Rodriguez, J. L. Farmer, M. G. Organ *Chem. Eur. J.* **2016**, *22*, 14860 - 14863

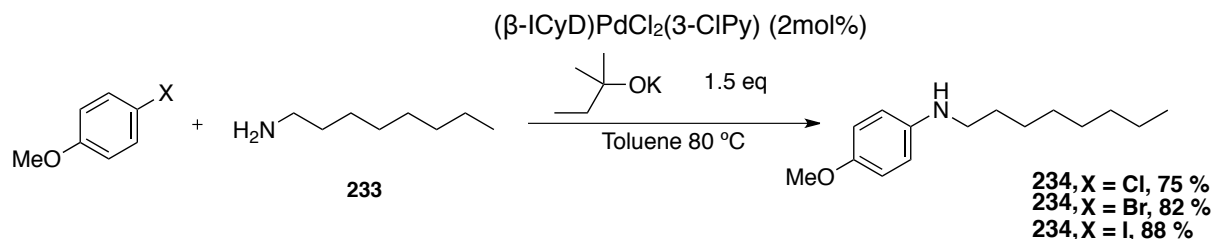
²⁴² a) A. Khadra, S. Mayer, D. Mitchell, M. J. Rodriguez, M. G. Organ, *Organometallics* **2017**, *36*, 3573-3577, b) P. Ruiz-Castillo, D. G. Blackmond, S. L. Buchwald, *J. Am. Chem. Soc.* **2015**, *137*, 3085-3092

Based on these reports, we hoped that a selective method could be developed using our hindered (β -ICyD)PdCl₂(pyridine) complex but with a commercial base, with non-hindered amines and avoiding excesses of reactants. Using the conditions previously developed for the cross-coupling. The reaction was carried out with a 1 : 1 mixture of 4-chloroanisole and *n*-octylamine. The cross-coupled secondary amine was obtained in 75% yield (Scheme). Additionally, no traces of bis-arylated product were detected in the ¹H-NMR of the crude mixture.



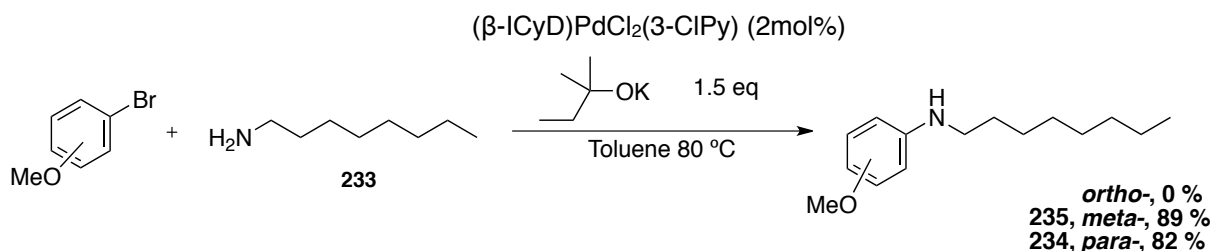
Scheme IV-32: (β -ICyD)PdCl₂(3-CIPy) catalyzed cross-coupling of octylamine with 4-Cl-anisole.

This encouraging result encouraged us to investigate in details the reaction. The first parameter studied was the effect of the halide, showed to be related to the TON of the reaction. This time, 4-iodo-anisole gave better yields than 4-Br-anisole and 4-Cl-anisole (88%, 82% and 74%, respectively).



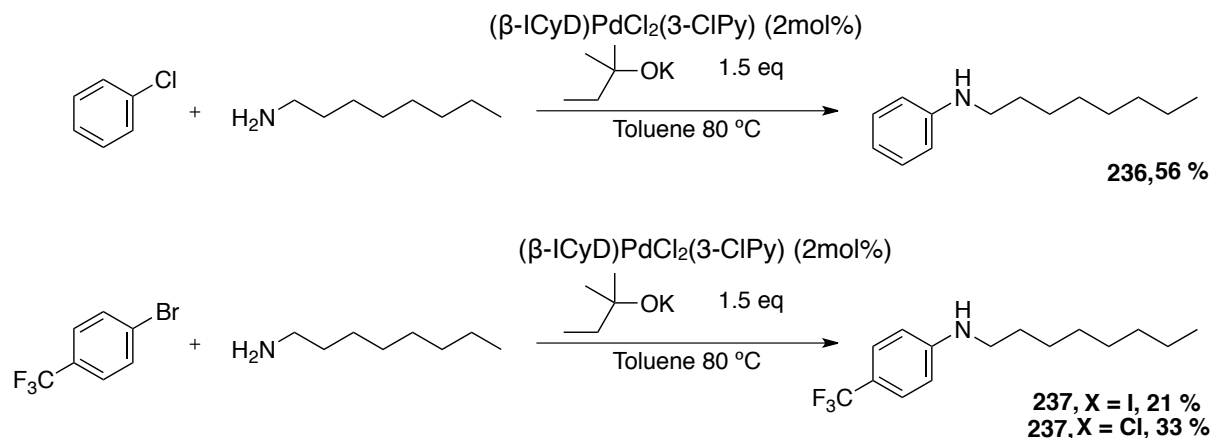
Scheme IV-33: Study of the effect of the halide.

Then, the substitution of the aryl was studied. Reaction of 3-bromoanisole in the same conditions formed the corresponding product in 89% yield, as observed previously, no trace of bis-arylated compound was observed in ¹H-NMR of the crude. In contrast, the ortho substituted 2-bromoanisole gave no trace of product in the same conditions.



Scheme IV-34: Study of the substitution of the aryl.

Less electron rich chlorobenzene afforded the expected N-phenyl-N-octylamine as a single compound in more modest 56% yield. Finally, under the same conditions electro-deficient trifluoromethylbenzene derivatives afforded a 2:1 mixture of mono : bis arylated compound in 21% for the iodo-derivative and in 33% for the chloro-derivative (Scheme IV-35).



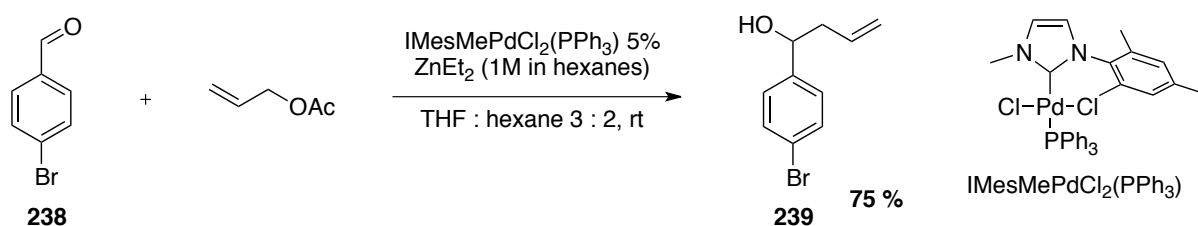
Scheme IV-35: Scope of less electron-rich substrates

In conclusion, $(\beta\text{-ICyD})\text{PdCl}_2(3\text{-chloropyridine})$ appeared as a useful catalyst in a laboratory-scale Buchwald-Hartwig cross-coupling reaction. The system works with electron-rich aryl cross-coupling partners in excellent yields and chlorinated aryl partners and non-hindered primary amines. The reaction can be performed with a commercial base, affording the secondary amines from moderate to excellent yields.

iii. Towards enantioselectivity with $(\beta\text{-ICyD})\text{Pd(II)}$ complexes: Allylation of aldehydes

Another property of $(\beta\text{-ICyD})\text{Pd}^{\text{II}}$ complexes is the intrinsically chiral cyclodextrin skeleton that wraps completely the metal center. Different enantioselective reactions were developed in palladium chemistry, from α -arylation of ketones²⁴³, to assymetric Suzuki-Miyaura cross-coupling reactions.²⁴⁴

In this part of the work, we were interested in a mixed $(\text{NHC})\text{PdCl}_2(\text{PPh}_3)$ catalyzed nucleophilic allylation of aromatic aldehydes. Presented by Roland *et al*, it was developed in the racemic version, never explored in the asymmetric manner with chiral NHCs (Scheme).²⁴⁵



Scheme IV-36: $\text{IMesMePdCl}_2(\text{PPh}_3)$ catalyzed allylation of 4-bromo-benzaldehyde

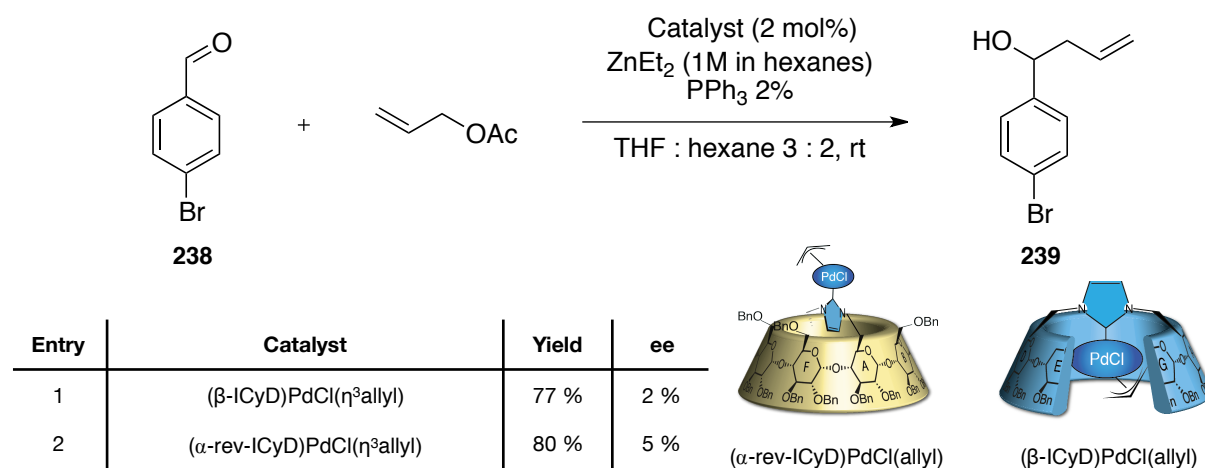
²⁴³ S. Würtz, C. Lohre, R. Fröhlich, K. Bergander, F. Glorius, *J. Am. Chem. Soc.* **2009**, *131*, 8344 - 8345

²⁴⁴ L. Benhamou, C. Besnard, E. P. Kündig, *Organometallics* **2014** *33*, 260-266

²⁴⁵ A. Flahaut, K. Toutah, P. Mangeney, S. Roland, *Eur. J. Inorg. Chem.* **2009**, 5422-5432

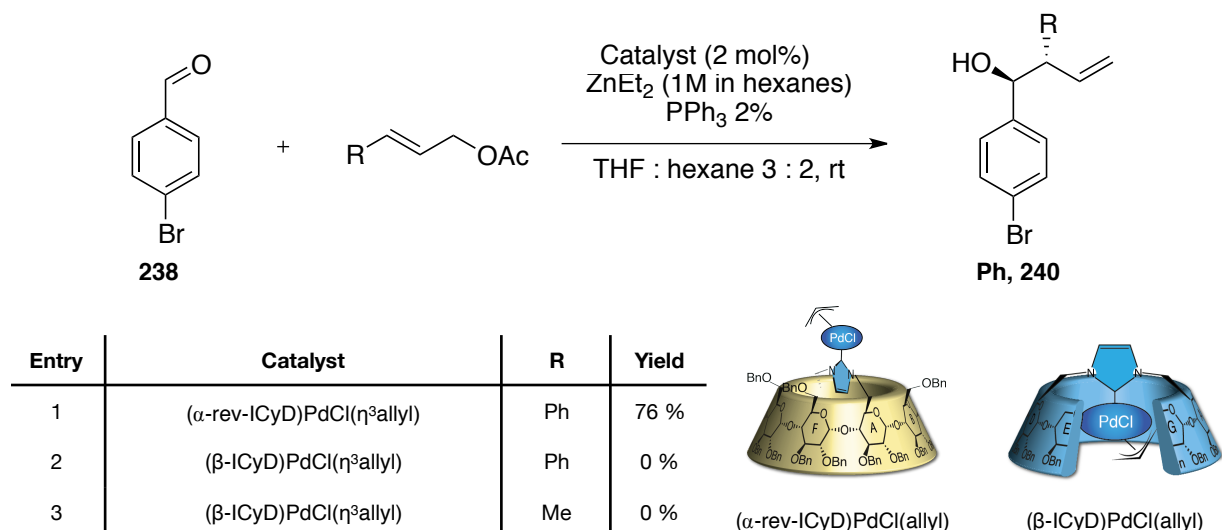
Since the position of the allyl seemed to be blocked in the cavity of the (β -ICyD), the first attempt to perform the reaction was the use (β -ICyD)PdCl(η^3 -allyl) to catalyze the reaction between the 4-bromobenzaldehyde and the allyl acetate afforded the expected product in 77% yield. Unfortunately, only 2% ee was obtained. In contrast, the catalytic efficiency was preserved with lower catalyst loadings of 2%.

Similar catalytic performances were obtained when (α -rev-ICyD)PdCl(η^3 -allyl) was used as catalyst, giving the expected product in 80% yield. Again, only 5% ee was obtained.



Scheme IV-37: (ICyD) catalyzed allylation of **238**

To obtain more insights about the reaction, the reaction was performed on substituted allylic acetates trying to obtain a regioselective reaction. The reaction of cinnamyl acetate catalyzed by (α -rev-ICyD)PdCl(η^3 -allyl) afforded compound **240** in 76% yield. In contrast, the more demanding (β -ICyD)PdCl(η^3 -allyl) gave no conversion to this substrate. Same result was obtained when the crotyl acetate was used showing the size discrimination afforded by the steric hindrance of the cyclodextrin.



Scheme IV-38: (ICyD)PdCl(allyl) catalyzed allylation of 4-bromobenzene.

Studying the behavior of $(\alpha\text{-rev-ICyD})\text{PdCl}(\text{allyl})$ in a reaction mixture 1:1 of cynamyl acetate and allylic acetate (0.6 equivalents each). The complex showed a slight preference for the allyl acetate but both products were obtained in a 42:58 mixture. This result showed that, as expected, the outer coordination of the complex towards the primary rim of the cyclodextrin has almost no effect on the properties of the metal.

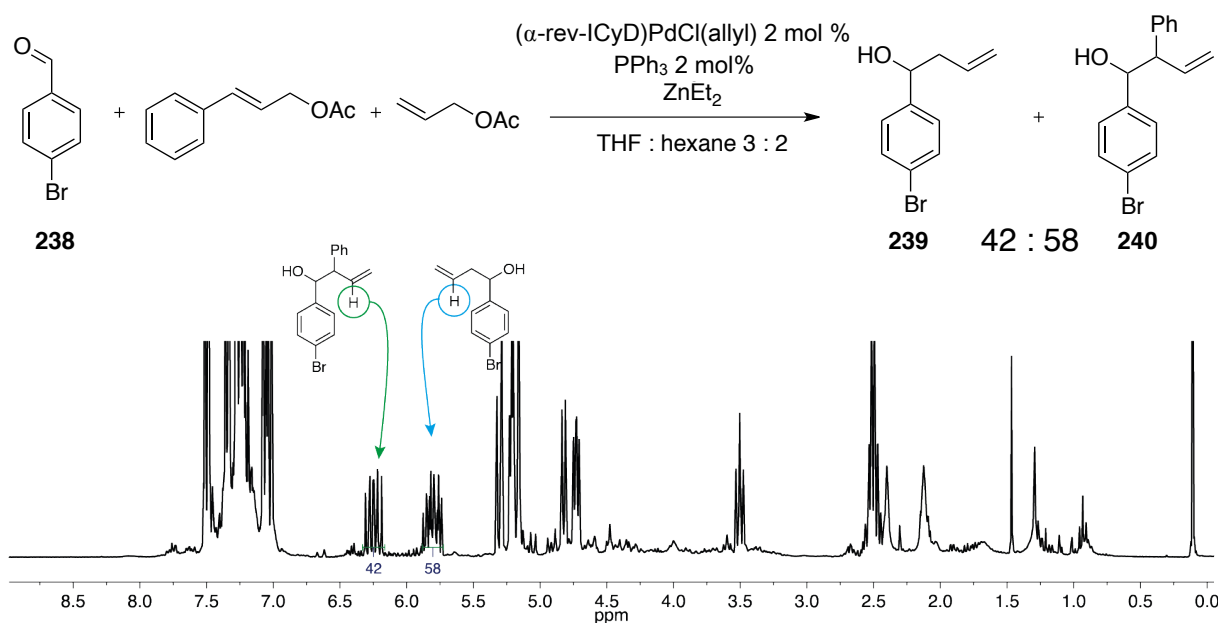


Figure IV-39: Reaction conditions for the “substrate selection” with $(\alpha\text{-rev-ICyD})\text{PdCl}(\text{allyl})$

In contrast, the reaction of 4-bromo anisaldehyde **238** with 0.6 equivalents of allylacetate and 0.6 equivalents of cinammyl acetate, catalyzed by $(\beta\text{-ICyD})\text{PdCl}_2(\text{PhCN})$ afforded a 88 : 12 mixture of **239** and **240** (Figure IV-40). This result showed how the wrapping of the metal center by the cyclodextrin affords an steric hindrance that could be used to develop a substrate selective reaction. In this case, the catalyst favored the reaction with the smallest substrate.

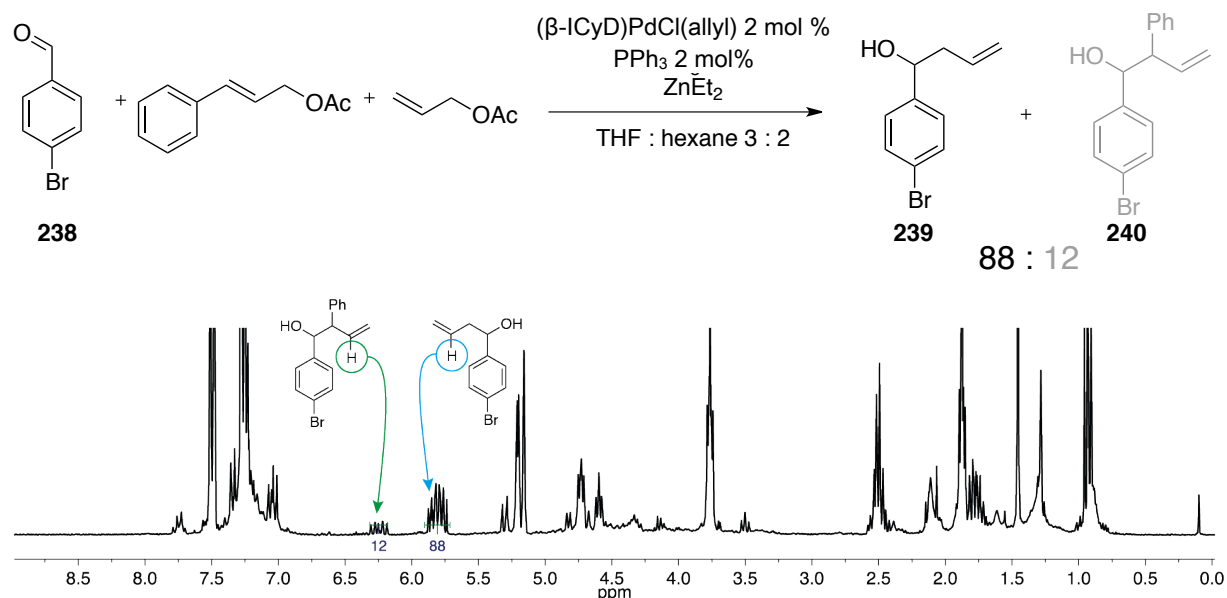


Figure IV-40: Reaction conditions for the substrate selection with $(\beta\text{-ICyD})\text{PdCl}(\eta^3\text{-allyl})$

Size discriminating reactions are an interest topic of interest in bio-inspired reactivity⁶⁷. Enzymes are able to select one single substrate from a extremely complex biological mixture. Using again the active sites of enzymes as inspiration for the development of a highly selective chemical transformation, substrate selective reaction are a topic of interest. In this case, the use of $(\beta\text{-ICyD})\text{PdCl}(\eta^3\text{-allyl})$ where substituted allyls seemed to be unreactive could be used to develop selective reactions. This selectivity was proved to be possible only by the steric of the substrate.

C. Conclusion to chapter IV

In conclusion, during this chapter, a study of the structure-reactivity of the complexes was done. In some cases, the confinement of the metal inside the cavity had negative effects for a catalytic reaction, as showed for the CuAAC and the Pt.

(ICyD)AuCl complexes were found to be efficient catalysts in enyne -cycloisomerization. The addition of the new (γ -AE-ICyD)AuCl and (γ -AD-ICyD)AuCl to the library helped to understand the effect and behavior of the cavity in the selectivity, either in terms of enantioselectivity or product distribution. From a global point of view of this reaction, a laboratory scalable reaction was developed, that in the case of the enyne **144**, the enantiomeric excess was found to be 80%, one of the bests achieved in a cycloisomerization reaction.²⁴⁶

It was also found that the (β -ICyD)Pd^{II} complexes were extremely stable, in agreement with the redox potential obtained in last chapter. However, some reactivity could be achieved. (β -ICyD)PdCl₂PEPPI was found to be an efficient catalyst for a arylation of morpholine, forming the expected cross-coupled products with low catalyst loadings in good yields. This arylation of amines could be developed in a selective manner, to synthesize secondary amines by cross-coupling. This reaction was developed with commercial reactants in 1 : 1 mixtures of both cross-coupling partners. In this conditions, perfect selectivities were obtained, except for electron-poor substrates.

Finally, (β -ICyD)PdCl(allyl) was tested in a Pd-catalyzed allylation of aldehydes. The complex was found to be useful in a substrate selection directed by the size of the cavity. This selection was found to be directed by the size of the substrate, and discriminating substrates with small size differences.

²⁴⁶ S.Y.Kim, Y.C. Chung, *J. Org. Chem.*, **2010**, 75, 1281–1284

General conclusion and perspectives

General conclusion and perspectives

During the course of this PhD work, the synthesis of different families of NHC-capped metal complexes was developed. To begin with, an obtention of the largest analogues (γ -ICyD)AuCl was performed in order to understand the behavior of ICyD complexes in a gold-catalyzed enyne cycloisomerization reaction. This complex was characterized to understand the structure-reactivity relationship of the cyclodextrin skeleton in the selectivity of the reaction.

In the enantioselective version of the enyne cycloisomerization, ICyDs were revealed as efficient catalysts, achieving ee's up to 80%. Nevertheless, due to the largest size of the γ -cyclodextrin cavity, the influence on the reactivity of the metal was less important, and the ee's were lower. Furthermore, with the non-symmetrical isomer, (γ -AD-ICyD)AuCl, the surprising opposite enantiomer was obtained.

During the synthesis of these gold complexes, the formation of (γ -ICyD)AuCl₃ was observed, being this the first time that a squared planar complex was observed inside the cavity of a cyclodextrin. This observation led to the synthesis of palladium and platinum complexes inside the narrower analogues β - and α -ICyDs. This synthesis showed two different coordination modes depending, at the same time, on the size of the metal, the size of the cavity and the synthesis performed.

When the synthesis was made by transmetalation of the inner silver NHC, the complex was obtained inside the cavity, meanwhile, when the free-NHC route was performed, the reactions gave different results. In the case of the α -CD, using an in situ protonation-metallation reaction, the metal complexes were complexed outside of the cavity. In the case of the β analogues, the complexes were obtained mainly inside of the cavity.

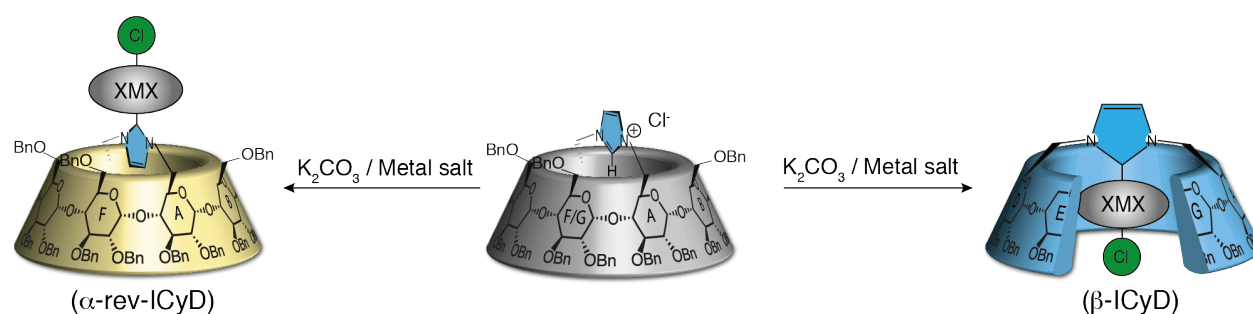


Figure V-1: α - and β -CD based complexes depending on the synthesis.

To elucidate the effect of the cavity on these metal complexes, cyclic voltammetry and catalytic reactions were studied. As expected, when the CV was carried out on the (α -rev-ICyD) complexes, the same behavior as in the model complexes was observed. Surprisingly, in the case of β - and γ -ICyD complexes different behaviors were observed. This result depicts, as far as we are aware of, the first complexes, based on cyclodextrins that are non-silent in electrochemistry. In the case of (ICyD)Au complexes, the same redox potential was obtained for the α -, β - and γ -complexes. In contrast, when the CV was done on the square planar palladium(II) complexes, the redox potentials of the Pd(II)/Pd(0) reduction were lower with the size of the cavity. This different behavior was explained by a reactivity on the entrance of the cavity or a confined reactivity inside the cyclodextrin skeleton by a ligand exchange.

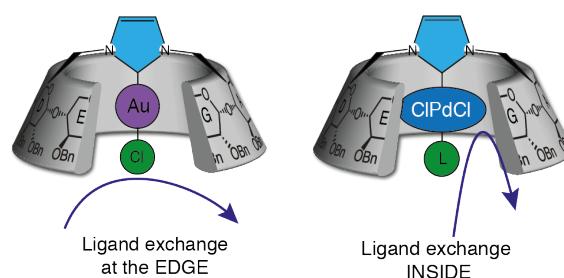


Figure V-2: Schematic reactivity of (ICyD)Au and (ICyD)Pd complexes in electrochemistry

The catalytic applications were broadly studied. In the case of Pd complexes, due to the steric hindrance afforded by the cavity of the (β -ICyD) a selective arylation of primary amines could be developed. In this reaction, the unhindered N-Octylamine was arylated in good to excellent yields. Additionally, enhanced by the steric hindrance of the cyclodextrin, a substrate selective reaction was developed. This reaction was particularly selective with unhindered substrates, while larger ones reacted less efficiently.

All these synthesis of compound, made in a context of the confined space catalysis are the beginning of the development of new reactions that could be useful for synthetic applications.

In this PhD work, in addition to the ones reported previously, CuAAC, amination reactions and hydrosilylation, reactions were the beginning of a broad scope of confined space catalysis. Following this project, different reactivities could be developed. In the case of palladium complexes, since the reductive elimination was revealed as a limiting step, modification of the electronics of the NHC could be developed. In the case of platinum complexes, enantioselective hydrosilylation reactions could be developed in an enantioselective manner.

Experimental Part

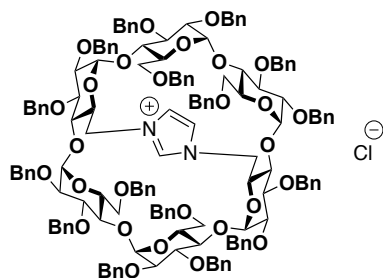
(α -ICyD)HCl (122)	4
(β -ICyD)HCl (124)	5
(α -ICyD)AgCl (123)	7
(β -ICyD)AgCl (125)	8
(α -ICyD)AuCl (126)	10
(β -ICyD)AuCl (127)	11
(α -ICyD)CuCl (128)	13
(β -ICyD)CuCl (129)	14
2A-G, 3A-G, 6B, 6C, 6E, 6F, 6G - Nonadeca-O-benzyl- β -cyclodextrin + 2A-G, 3A-G, 6B, 6C, 6D, 6F, 6G - Nonadeca-O-benzyl- β -cyclodextrin (150)	16
6A,6E-di-O-methylsulfonyl-2A-G,3A-G,6B,6C,6D,6F,6G,6H-Docosa-O-benzyl- γ -cyclodextrin (151)	18
6A,6D-di-O-methylsulfonyl-2A-G,3A-G,6B,6C,6E,6F,6G,6H-Docosa-O-benzyl- γ -cyclodextrin (152)	20
(γ -A,E-ICyD)HCl (153)	22
(γ -A,D-ICyD)HCl (154)	24
(γ -A,E-ICyD)AgCl (155)	26
(γ -A,D-ICyD)AgCl (156)	28
(γ -A,D-ICyD)AuCl (158)	30
(γ -A,E-ICyD)AuCl (157)	32
Free (α -ICyD) (159)	34
(α -rev-ICyD)AuCl + (α -ICyD)AuCl (160 + 127)	37
(γ -ICyD)AuCl ₃ (161)	40
(γ -ICyD)AuBr ₂ Cl (162)	44
(γ -ICyD)AuI ₂ Cl (163)	47
(β -ICyD)AuBr ₂ Cl (165)	54
(γ -AE-ICyD)PdCl(η 3-allyl) (168)	56
(γ -AE-ICyD)PdCl ₂ (PhCN)	59
(β -ICyD)PdCl(η 3-allyl) (170)	62
(β -ICyD)PdCl ₂ (PhCN) (171)	66
(γ -AE-ICyD)PdCl ₂ (pyridine) (173)	69
(β -ICyD)PdCl ₂ (pyridine) (172)	72
(α -rev-ICyD)PdCl ₂ (pyridine) (174)	76
(α -rev-ICyD)PdCl(η 3-allyl) (175)	79
(α -rev-ICyD)PtCl ₂ (pyridine) (180)	83
(β -ICyD)PtCl ₂ (pyridine) + (β -rev-ICyD)PtCl ₂ (pyridine) (181 + 182)	86
(β -rev-ICyD)Pt(dvtms) (183)	89
(β -ICyD)Pt(dvtms) (184)	92
(α -ICyD)CuOH (201)	95
(α -ICyD)CuCCPh (203)	97
(β -ICyD)AuMe (222)	99
(β -ICyD)AuOAc (223)	103
(β -ICyD)Au(4-Fluorobenzene) (224)	105
(β -ICyD)AuCCPh (225)	108
226	110
(β -ICyD)PdCl ₂ (3-Chloropyridine) (227)	111
Gold(I)-catalyzed cycloisomerization	114
(α -ICyD)CuCl catalyzed CuAAC.	117
(β -ICyD)PdCl ₂ (PhCN) catalyzed hydrothiolation	119
NHC-CD-Pt(dvtms) catalyzed hydrosilylation of phenylacetylene	123
(ICyD)Pd-catalyzed Allylation of aldehydes	132
(β -ICyD)PdCl(Allyl) catalyzed allylation of 238	132

General Informations

THF was freshly distilled from sodium/benzophenone. DMF and MeCN were dried over molecular sieves. Reactants were purchased from commercial sources (Sigma Aldrich, Alfa Aesar, Fluorochem, TCI or Strem), and used without further purification. HRMS were recorded on a Bruker micrOTOF spectrometer, using Agilent ESI-L Low Concentration Tuning-Mix as reference. Optical rotations were measured on a Perkin–Elmer 341 digital polarimeter or a Jasco P-2000 polarimeter with a path length of 1 dm. NMR spectra were recorded on a Bruker Avance II 600 MHz or Bruker AM-400 MHz using residual solvent signal as internal reference.¹ Assignments were aided by COSY, HSQC, NOESY, TOCSY and HMBC experiments.

All electrochemical experiments were performed using a Metrohm Autolab PGSTAT101 potentiostat under argon flow in a three-electrode cell. The counter-electrode was a platinum wire; the reference was a saturated calomel electrode separated from the solution by a bridge filled with a 0.3 M solution of $n\text{Bu}_4\text{NBF}_4$ in solvent (2 mL). $n\text{Bu}_4\text{NBF}_4$ (0.3 M) was used as supporting electrolyte. All the cyclic voltammograms (CV) were recorded using a steady GC disk ($d = 3$ mm) as working electrode.

(α -ICyD)HCl (122)



Chemical Formula:

C₁₅₁H₁₅₇ClN₂O₂₈

Molecular Weight:

2483.31

In a round-bottom flask under nitrogen, α -CD(OMs)₂ (1.13 g, 440 μ mol) and imidazole (600 mg, 8.8 mmol) were dissolved in DMF (20 ml). The mixture was heated at 120 °C overnight and the reaction followed by TLC. After cooling down to r.t., the solvent was evaporated under high vacuum and the residue dissolved in a 1:1 mixture of dichloromethane and aqueous HCl (1M). The aqueous layer was extracted with dichloromethane (3 x 20 ml) and the combined organic layers were washed with H₂O (3 times) dried over MgSO₄ and concentrated to dryness. The residue was purified on silica gel chromatography (DCM/MeOH 100:1 then 100:5 then 100:10) to afford **122** (931 mg, 85 %) as a white foam.

The structure of the product was confirmed by comparison with the NMR spectra of the literature.²

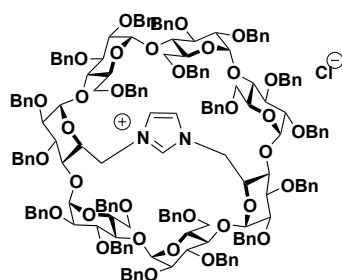
¹H NMR (CD₃CN, 600 MHz, 300 K): δ 9.09 (s, 1H, N-CH=N), 7.43-7.06 (m, 70H, 70 x H-Ar), 6.97-6.95 (m, 4H, 4 x H-Ar), 6.89-6.84 (m, 8H, 6 x H-Ar, 2 x N-CH=CH-N), 5.66 (d, ³J_{1,2} = 3.8 Hz, 2H, 2 x H-1C,F), 5.39 (d, ²J_{Ph-CHH} = 10.7 Hz, 2H, 2 x CHPh), 5.08 (d, ²J_{Ph-CHH} = 10.4 Hz, 2H, 2 x CHPh), 4.85 (d, ²J_{Ph-CHH} = 11.5 Hz, 2H, 2 x CHPh), 4.82 (d, ³J_{1,2} = 3.4 Hz, 2H, 2 x H-1B,E), 4.79 (d, ³J_{1,2} = 3.1 Hz, 2H, 2 x H-1A,D), 4.77 (d, ²J_{Ph-CHH} = 10.7 Hz, 2H, 2 x CHPh), 4.70 (d, ²J_{Ph-CHH} = 11.2 Hz, 2H, 2 x CHPh), 4.65-4.61 (m, 4H, 4 x CHPh), 4.56 (d, ²J_{Ph-CHH} = 12.3 Hz, 2H, 2 x CHPh), 4.54-4.45 (m, 10H, 8 x CHPh, 2 x H-6aA,D), 4.42 (d, ²J_{Ph-CHH} = 12.2 Hz, 2H, 2 x CHPh), 4.40-4.36 (m, 4H, 2 x CHPh, 2 x H-5A,D), 4.29 (d, ²J_{Ph-CHH} = 12.2 Hz, 2H, 2 x CHPh), 4.15 (dd, ³J_{2,3} = 10.1 Hz, ³J_{3,4} = 7.9 Hz, 2H, 2 x H-3C,F), 4.11 (d, ²J_{Ph-CHH} = 12.2 Hz, 2H, 2 x CHPh), 4.03-3.94 (m, 8H, 2 x H-3A,D, 2 x H-4C,F, 2 x H-6bA,D, 2 x H-6aC,F), 3.90 (bd, ²J_{6a,6b} = 10.4 Hz, 2H, 2 x H-6bC,F), 3.88 (dd, ³J_{2,3} = 9.7 Hz, ³J_{3,4} = 8.7 Hz, 2H, 2 x H-3B,E), 3.73 (dd, ³J_{4,5} = 9.8 Hz, ³J_{3,4} = 7.8 Hz, 2H, 2 x H-4A,D), 3.73-3.70 (m, 2H, 2 x H-5C,F), 3.69 (dd, ³J_{4,5} = 9.7 Hz, ³J_{3,4} = 8.6 Hz, 2H, 2 x H-4B,E), 3.57 (dd, ³J_{2,3} = 10.1 Hz, ³J_{1,2} = 3.7 Hz, 2H, 2 x H-2C,F), 3.53 (bdd, ³J_{4,5} = 9.9 Hz, ³J_{5,6} = 4.8 Hz, 2H, 2 x H-5B,E), 3.46 (dd, ³J_{2,3} = 9.8 Hz, ³J_{1,2} = 3.0 Hz, 2H, 2 x H-2A,D), 3.38 (dd, ³J_{2,3} = 9.9 Hz, ³J_{1,2} = 3.3 Hz, 2H, 2 x H-2B,E), 3.25 (dd, ²J_{6a,6b} = 10.8 Hz, ³J_{5,6a} = 1.5 Hz, 2H, 2 x H-6aB,E), 3.11 (dd, ²J_{6a,6b} = 10.8 Hz, ³J_{5,6b} = 5.3 Hz, 2H, 2 x H-6bB,E) ppm.

¹³C NMR (CD₃CN, 151 MHz, 300 K): δ 140.17 (2C), 139.98 (2C), 139.85 (2C), 139.64 (2C), 139.50 (2C), 139.15 (2C), 139.03 (2C), 138.89 (2C) (16 x C-Ar-quat.), 133.52 (N=CH-N), 129.50-127.72 (80 x C-Ar-tert.), 125.29 (2 x N-CH=CH-N), 98.99 (2 x C-1C,F), 98.63 (2 x C-1A,D), 98.10 (2 x C-1B,E), 82.34 (2 x C-4B,E, 2 x C-4C,F), 81.82 (2 x C-3A,D), 81.36 (2 x C-3B,E, 2 x C-3C,F), 80.47 (2 x C-2A,D), 80.19 (2 x C-2B,E), 78.27 (2 x C-2C,F), 77.27 (2 x Ph-CH₂), 77.11 (2 x C-4A,D), 76.52 (2C), 74.85 (2C), 74.61 (2C) (6 x Ph-CH₂), 74.43 (2 x C-5C,F), 74.11 (2C), 73.98 (2C), 73.79 (2C), 73.19 (2C) (8 x Ph-CH₂), 73.03 (2 x C-5B,E), 71.27 (2 x C-5A,D), 71.24 (2 x C-6C,F), 69.23 (2 x C-6B,E), 53.91 (2 x C-6A,D) ppm.

R_f = 0.35 (CH₂Cl₂/MeOH 90:10)

HRMS (ESI) : calculated for C₁₅₁H₁₅₇N₂O₂₈⁺ [M]⁺ 2446.0917, found 2446.0831.

(β -ICyD)HCl (124)



Chemical Formula:

$C_{178}H_{185}ClN_2O_{33}$

Molecular Weight:

2915.82

In a round-bottom flask under nitrogen, β -CD(OMs)₂ (23 g, 7.6 mmol) and imidazole (11 g, 153 mmol) were dissolved in DMF (230 ml). The mixture was heated at 120 °C overnight and the reaction was followed by TLC. After cooling down to r.t., the solvent was evaporated under high vacuum and the residue dissolved in a 1:1 mixture of dichloromethane and aqueous HCl (1M). The aqueous layer was extracted with dichloromethane (3 x 100 ml) and the combined organic layers were washed with H₂O (3 times) dried over MgSO₄ and concentrated to dryness. The residue was purified on silica gel chromatography (DCM / MeOH 100 / 1 then 100 / 5 then 100 / 10) to afford (β -ICyD)HCl after two purifications (14.9 g, 68 %) as a white foam.

The structure of the product was confirmed by comparison with the NMR spectra of the literature.¹

¹H NMR (CD₃CN, 600 MHz): δ 7.36-6.84 (m, 97H, 95 x H-Ar, 2 x N-CH=C), 5.79 (bd, ²J = 3.92 Hz, 2H, 2 x H-1), 5.38 (d, ²J_{Ph-CHH} = 11.33 Hz, 1H, CHPh), 5.27 (d, ²J_{Ph-CHH} = 11.17 Hz, 1H, CHPh), 5.19 (d, ²J_{Ph-CHH} = 10.50 Hz, 1H, CHPh), 5.06 (d, ²J_{Ph-CHH} = 10.63 Hz, 1H, CHPh), 4.98 (d, ³J_{1,2} = 3.25 Hz, 1H, H-1), 4.89 (d, ³J_{1,2} = 3.88 Hz, 1H, H-1), 4.82-4.80 (m, 3H, CHPh, 2 x H-1), 4.76-4.70 (m, 5H, 4 x CHPh, H-1), 4.66(d, ²J_{Ph-CHH} = 10.92 Hz, 1H, CHPh), 4.61-4.30 (m, 31H, H-5, H-3, 2 x H-6, 27 x CHPh), 4.12-4.06 (m, 4H, 2x H-6, H-3, CHPh), 4.00-3.48(m, 28H, 6 x H-6, 4 x H-2, 5 x H-3, 7 x H-4, 6 x H-5), 3.43-3.38 (m, 2H, H-6, H-2), 3.31 (t, ³J_{1,2} = ³J_{2,3} = 2.36 Hz, 1H, H-2), 3.29 (t, ³J_{1,2} = ³J_{2,3} = 2.83, 1H, H-2), 3.20 (d, ²J_{6a,6b} = 11.25 Hz, 1H, H-6), 3.10 (d, ²J_{6a,6b} = 10.65 Hz, 1H, H-6), 2.84 (dd, ²J_{6a,6b} = 10.65 Hz, ³J_{5,6b} = 4.81 Hz, 1H, H-6) ppm.

¹³C NMR (CD₃CN, 151MHz): δ 140.69, 140.58, 140.56, 140.30, 140.08, 139.81, 139.73, 139.68, 139.65, 139.63 (2C), 139.56, 139.48, 139.26, 139.21, 138.98 (3C), 138.82 (19 x C-Ar-quat.), 129.53-128.05 (m, 95 x C-Ar-tert.), 124.98, 124.56 (2 x N-CH=C-N), 100.56, 100.13, 99.28, 98.35, 97.28, 97.16, 96.68(7 x C-1), 83.00 (C-4), 82.56, 82.52(2 x C-3), 82.03, 81.91(2 x C-4), 81.57, 81.54, 81.43(3 x C-3), 81.14, 81.12, 81.11, 81.05(C-4, 2 x C-2, C-3), 80.50, 80.42, 80.28 (2C) (C-4, 2 x C-2, C-3), 79.94 (C-2), 78.72 (C-2), 78.31 (C-2), 77.22, 77.18, 76.80, 76.48, 76.10, 76.09, 75.16, 75.14, 75.02 (9 x Ph-CH₂), 74.19 (C-4), 74.15, 74.09, 73.99 (3 x Ph-CH₂), 74.05 (C-5), 73.94, 73.91 (2 x Ph-CH₂), 73.88 (C-4), 73.85, 73.83, 73.72, 73.49 (4 x Ph-CH₂), 73.35 (C-5), 73.19 (Ph-CH₂), 72.77, 72.73 (2C) (3 x C-5), 72.06 (C-5), 70.54, 70.46, 70.26 (3 x C-6), 70.23 (C-5), 69.12 (C-6), 68.85 (C-6), 53.28 (C-6), 52.86 (C-6) ppm.

[α]_D²⁰ = +49.5 (CHCl₃, c = 0.1)

R_f = 0.31 (DCM/MeOH 95:5)

HRMS (ESI) : calculated for C₁₇₈H₁₈₅N₂NaO₃₃²⁺ [M+Na]²⁺ 1450.6373, found 1450.6434 err. 4.2 ppm

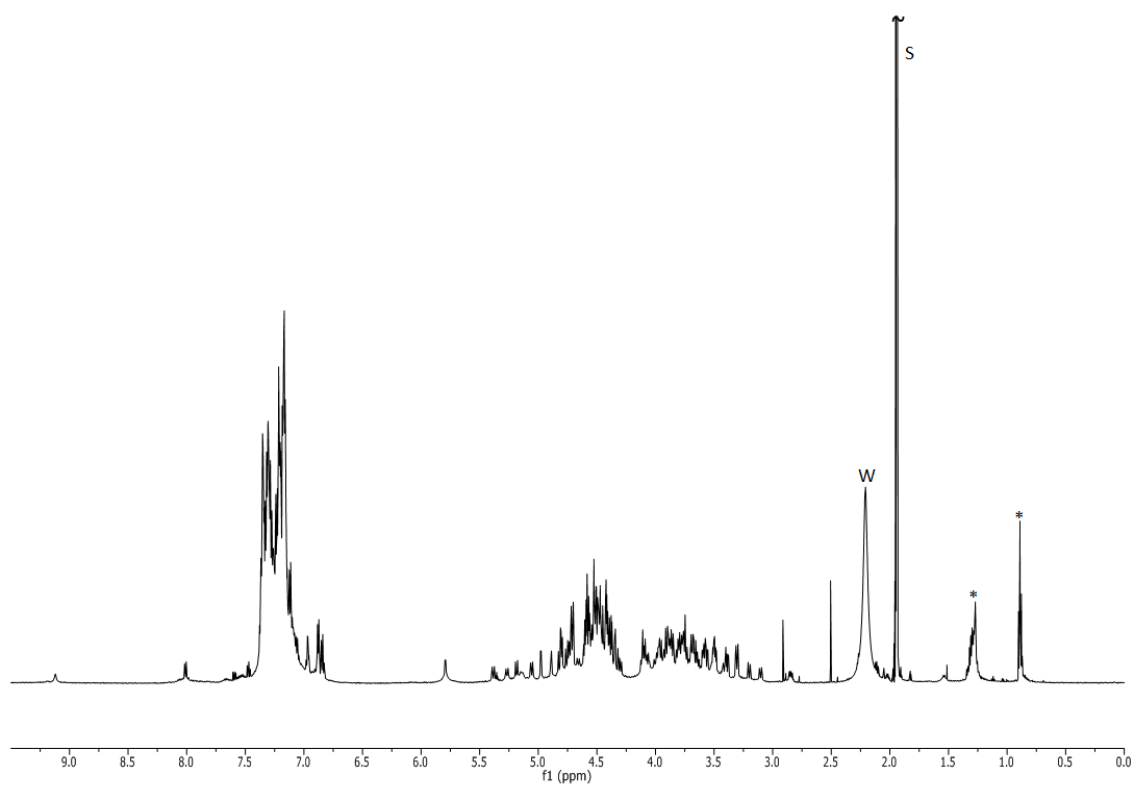


Figure S-1: ^1H NMR of **124** (CD_3CN , 600 MHz, 300 K)

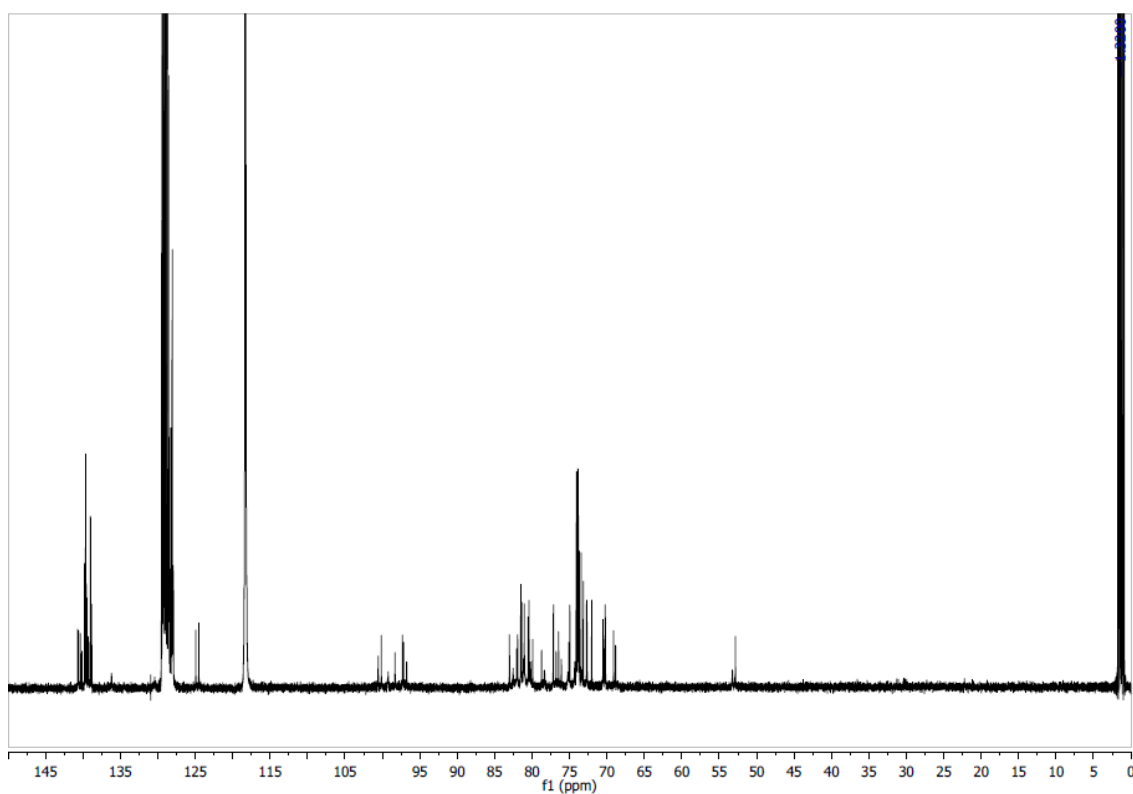
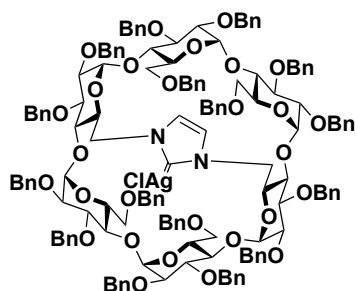


Figure S-2: ^{13}C NMR of $(\beta\text{-ICyD})\text{HCl}$ (CD_3CN , 151 MHz, 300 K)

(α -ICyD)AgCl (123)



Chemical Formula:

$C_{151}H_{156}AgClN_2O_{28}$

Molecular Weight:

2590.17

In a round-bottom flask under nitrogen, imidazolium **122** (570 mg, 230 μ mol) and silver oxide (231 mg, 690 μ mol) were dissolved in dry acetonitrile (5 mL). The black suspension was vigorously stirred at R.T. overnight, then filtrated on celite, rinsed with acetonitrile and concentrated *in vacuo*. The residue was purified on silica gel chromatography (Cyclohexane/AcOEt 4:1 then 3:1) to afford complex **123** (536 mg, 90 %) as a white foam. The structure of the product was confirmed by comparison with the NMR spectra of the literature.¹

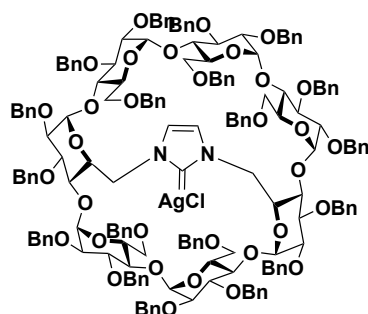
1H NMR : (Chloroform-*d*, 600 MHz, 300 K): δ 7.38-6.97 (m, 74H, 74 x H-Ar), 6.84 (t, $^3J_{o,m} = ^3J_{m,p} = 7.7$ Hz, 4H, 4 x H-*m*-Ar), 6.74 (t, $^3J_{m,p} = 7.4$ Hz, 2H, 2 x H-*p*-Ar), 6.14 (bs, 2H, 2 x N-CH=CH-N), 5.71 (d, $^3J_{1,2} = 3.7$ Hz, 2H, 2 x H-1C,F), 5.65-5.60 (m, 4H, 2 x CHPh, 2 x H-5A,D), 5.37 (d, $^2J_{Ph-CHH} = 10.8$ Hz, 2H, 2 x CHPh), 5.15-5.11 (m, 4H, 4 x CHPh), 4.98 (dd, $^3J_{2,3} = 10.2$ Hz, $^3J_{3,4} = 7.7$ Hz, 2H, 2 x H-3C,F), 4.87 (d, $^2J_{Ph-CHH} = 11.3$ Hz, 2H, 2 x CHPh), 4.65 (d, $^2J_{Ph-CHH} = 11.5$ Hz, 2H, 2 x CHPh), 4.63 (d, $^3J_{1,2} = 3.5$ Hz, 2H, 2 x H-1B,E), 4.60-4.42 (m, 16H, 12 x CHPh, 2 x H-1A,D, 2 x H-6aA,D), 4.29-4.25 (m, 6H, 4 x CHPh, 2 x H-3B,E), 4.22 (d, $^2J_{Ph-CHH} = 12.7$ Hz, 2H, 2 x CHPh), 4.16 (dd, $^3J_{2,3} = 9.7$ Hz, $^3J_{3,4} = 7.7$ Hz, 2H, 2 x H-3A,D), 3.98 (d, $^2J_{Ph-CHH} = 12.2$ Hz, 2H, 2 x CHPh), 3.95 (d, $^2J_{6a,6b} = 10.3$ Hz, 2H, 2 x H-6aC,F), 3.88-3.80 (m, 6H, 2 x H-4C,F, 2 x H-5B,E, 2 x H-5C,F), 3.76 (dd, $^2J_{6a,6b} = 10.5$ Hz, $^3J_{5,6b} = 5.2$ Hz, 2H, 2 x H-6bC,F), 3.71 (t, $^3J_{3,4} = ^3J_{4,5} = 9.2$ Hz, 2H, 2 x H-4B,E), 3.60 (dd, $^3J_{2,3} = 10.2$ Hz, $^3J_{1,2} = 3.8$ Hz, 2H, 2 x H-2C,F), 3.55 (dd, $^3J_{4,5} = 10.1$ Hz, $^3J_{3,4} = 7.7$ Hz, 2H, 2 x H-4A,D), 3.42-3.37 (m, 4H, 2 x H-2B,E, 2 x H-6bA,D), 3.27 (dd, $^3J_{2,3} = 9.8$ Hz, $^3J_{1,2} = 3.0$ Hz, 2H, 2 x H-2A,D), 3.04 (dd, $^2J_{6a,6b} = 10.9$, $^3J_{5,6a} = 3.3$ Hz, 2H, 2 x H-6aB,E), 2.76 (dd, $^3J_{6a,6b} = 11.0$ Hz, $^3J_{5,6b} = 1.7$ Hz, 2H, 2 x H-6bB,E) ppm.

^{13}C NMR (Chloroform-*d*, 151 MHz, 300 K): δ 176.56 (C-Ag), 140.27 (2C), 139.92 (2C), 139.60 (2C), 139.10 (2C), 139.03 (2C), 138.81 (2C), 138.33 (2C), 138.01 (2C) (16 x C-Ar^{quat}), 128.72-126.71 (80 x C-Ar^{tert}), 122.11 (d, $^3J_{C,Ag} = 6.7$ Hz, 2 x N-CH=CH=N), 98.66 (2 x C-1C,F), 98.09 (2C), 98.06 (2C) (2 x C-1A,D, 2 x C-1B,E), 82.60 (2 x C-4C,F), 81.51 (2 x C-3A,D), 81.36 (2 x C-4B,E), 80.26 (2 x C-3B,E), 80.12 (2 x C-2A,D), 79.64 (2 x C-3C,F), 79.11 (2 x C-2B,E), 79.98 (2 x C-2C,F), 76.76 (2 x C-4A,D), 76.64 (2C), 76.39 (2C), 74.16 (2C) (6 x Ph-CH₂), 73.78 (2 x C-5C,F), 73.47 (2C), 73.31 (2C), 73.23 (2C), 72.80 (2C), 72.35 (2C) (10 x Ph-CH₂), 71.92 (2 x C-5B,E), 71.14 (2 x C-6C,F), 70.80 (2 x C-5A,D), 67.82 (2 x C-6B,E), 54.36 (2 x C-6A,D).

$R_f = 0.21$ (Cyclohexane/Ethyl Acetate 4:1)

HRMS (ESI): calculated for $C_{151}H_{156}AgClN_2Na_2O_{28}^{2+}$ [$M+2Na$]²⁺ 1316.4684, found 1316.4674.

(β -ICyD)AgCl (125)



Chemical Formula:
 $C_{185}H_{189}AgClN_3O_{33}$
Molecular Weight:
3125.80

A mixture of perbenzylated imidazolium (β -ICyD)HCl (2.25 g, 0.77 mmol) and silver oxide (534 mg, 2.31 mmol) was dissolved in anhydrous CH_2Cl_2 (50 ml) under a N_2 atmosphere. The reaction mixture was stirred at r.t. overnight. Then the silver oxide was filtered on a celite pad and the residue was washed with CH_2Cl_2 , and the solvents were evaporated. Silica gel chromatography of the residue (CyH/ EtOAc: 4:1) gave the silver complex (β -ICyD)AgCl as a white foam (2.0 g, 85 %).

1H NMR (Chloroform- d , 600 MHz): δ 7.48-6.88 (m, 95H, 95 \times H-Ar), 6.21 (s, 1H, N-CH=C), 5.93 (s, 1H, N-CH=C), 5.88 (d, $^3J_{1,2} = 3.61$ Hz, 1H, H-1G), 5.86 (d, $^3J_{1,2} = 3.61$ Hz, 1H, H-1C), 5.78 (d, $^2J_{Ph-CHH} = 11.78$ Hz, 1H, CHPh), 5.54 (m, 1H, H-5A), 5.45 (d, $^2J_{Ph-CHH} = 10.82$ Hz, 1H, CHPh), 5.42 (d, $^2J_{Ph-CHH} = 11.18$ Hz, 1H, CHPh), 5.35-5.33 (m, 2H, 2 \times CHPh), 5.25 (d, $^2J_{Ph-CHH} = 12.38$ Hz, 1H, CHPh), 5.02 (d, $^2J_{Ph-CHH} = 11.31$ Hz, 1H, CHPh), 5.00 (d, $^2J_{Ph-CHH} = 5.66$ Hz, 1H, CHPh), 4.98-4.94 (m, 3H, 3 \times CHPh), 4.83 (d, $^2J_{6a,6b} = 5.42$ Hz, 1H, H-6aD), 4.82 (d, $^3J_{1,2} = 3.57$ Hz, 1H, H-1D), 4.69 (m, 2H, 2 \times H-1E,F), 4.60 (m, 2H, H-1A, H-3C), 4.58 (d, $^3J_{1,2} = 3.04$ Hz, 1H, H-1B), 4.56 (d, $^2J_{Ph-CHH} = 11.79$ Hz, 1H, CHPh), 4.51-4.38 (m, 23H, H-3B, H-6bA, H-5D, 20 \times CHPh), 4.36 (d, $^2J_{Ph-CHH} = 10.48$ Hz, 1H, CHPh), 4.31 (d, $^2J_{Ph-CHH} = 3.87$ Hz, 1H, CHPh), 4.29 (d, $^2J_{Ph-CHH} = 2.80$ Hz, 1H, CHPh), 4.27 (d, $^2J_{Ph-CHH} = 2.56$ Hz, 1H, CHPh), 4.25-4.20 (m, 3H, 2 \times H-3E,G, CHPh), 4.14-3.94 (m, 7H, H-6aG, H-5B, H-4C, 3 \times H-3A,D,F, CHPh), 3.87-3.63 (m, 11H, H-6aF, H-6bF, H-6aC, H-6bC, H-6bG, 4 \times H-4G,E,B,A, 2 \times H-5C,G), 3.57-3.51 (m, 5H, 2 \times H-2C,G, 2 \times H-4F,D, H-5F), 3.43-3.37 (m, 3H, H-6aA, H-6bD, H-6aE), 3.35-3.30 (m, 5H, 5 \times H-2E,F,D,B,A), 3.25 (m, 1H, H-5E), 2.96 (d, $^2J_{6a,6b} = 10.78$ Hz, 1H, H-6bE), 2.78 (d, $^2J_{6a,6b} = 10.72$ Hz, 1H, H-6aB), 2.71 (dd, $^2J_{6a,6b} = 10.95$ Hz, $^3J_{5,6b} = 3.10$ Hz, 1H, H-6bB);

^{13}C NMR (Chloroform- d , 151 MHz): δ 140.58, 140.21, 140.10, 140.05, 139.57, 139.18, 139.04, 138.98, 138.91, 138.79, 138.72(2C), 138.60, 138.58, 138.52, 138.26, 138.19, 138.08, 137.68, (19 \times C-Ar.quat.), 128.57-126.56 (m, 95 \times C-Ar.tert.), 122.71, 121.26 (2 \times N-CH=C-N), 100.91, 99.69, 98.61, 98.23, 97.52, 97.27, 96.96(7 \times C-1A,B,C,D,E,F,G), 83.32 (C-4F), 82.26 (C-3A), 82.07, 81.94 (2 \times C-4C,G), 81.29 (C-3D), 80.73, 80.46 (2 \times C-4B,E), 80.44 (C-2B), 80.25 (C-3F), 80.17 (C-2A), 80.14, 79.97, 79.89, 79.54 (4 \times C-3B,C,E,G), 78.89, 78.66, 77.99, 77.89, 77.39 (5 \times C-2C,D,E,F,G), 76.94 (Ph-CH $_2$), 76.85 (Ph-CH $_2$), 76.39 (2 \times Ph-CH $_2$), 76.20 (Ph-CH $_2$), 74.37 (C-4A), 74.36 (Ph-CH $_2$), 74.28 (Ph-CH $_2$), 73.86 (C-5C), 73.81, 73.73, 73.57, 73.49, 73.44(5 \times Ph-CH $_2$), 73.43 (C-4D), 73.28 (Ph-CH $_2$), 73.19 (C-5G), 73.18, 73.07, 72.98, 72.76, 72.70 (5 \times Ph-CH $_2$), 72.36 (C-5F), 72.33 (Ph-CH $_2$), 71.89, 71.86, 71.55 (3 \times C-5B,D,E), 70.56 (C-6C), 70.50 (C-5A), 70.34, 69.94, 68.21, 67.63, 55.63, 53.29 (6 \times C-6A,B,D,E,F,G)

$[\alpha]_D^{20} = +46.8$ ($CHCl_3$, $c = 0.1$)

$R_f = 0.21$ (CyH/AcOEt 4:1)

HMRS (ESI) calculated for $C_{178}H_{184}AgN_2O_{33}^+$ $[M-Cl]^+$ 2984.1827, found 2984.1777 err. 1.7 ppm

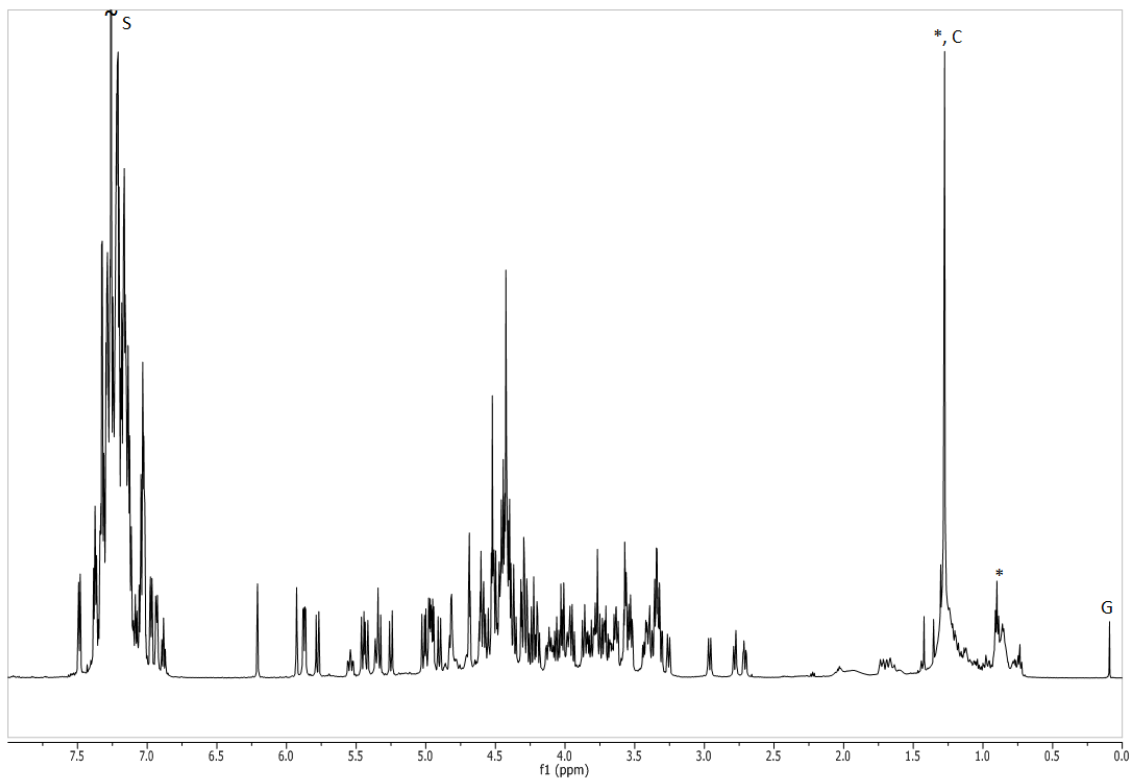


Figure S-3: ^1H NMR of $(\beta\text{-ICyD})\text{AgCl}$ (125) (Chloroform-d, 600 MHz, 300 K)

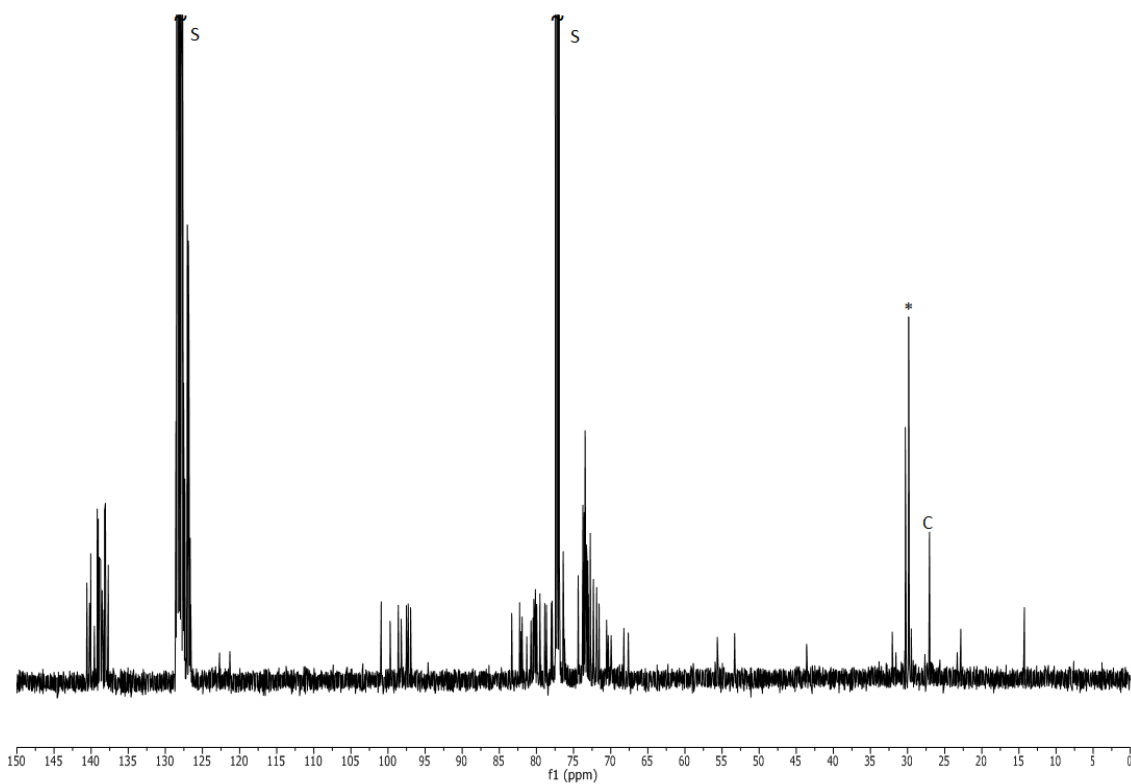
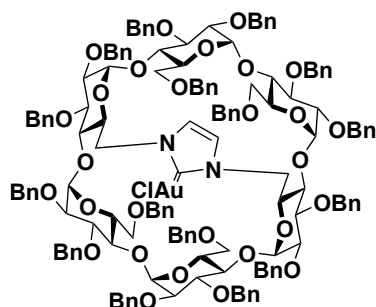


Figure S-4: ^{13}C NMR of $(\beta\text{-ICyD})\text{AgCl}$ 125 (CDCl_3 , 151 MHz, 300 K)

(α -ICyD)AuCl (126)



Chemical Formula:

$C_{151}H_{156}AuClN_2O_{28}$

Molecular Weight:

2679.27

In a round bottom flask under argon, silver complex (α -ICyD)AgCl 123 (1 g, 0.385 mmol) and gold(I) chloride (897 mg, 3.85 mmol) were dissolved in dry acetonitrile (10 mL). The reaction was protected from light and stirred overnight at r.t. The reaction was followed by Mass spectrometry. When finished the solvent was evaporated in vacuo and the residue was purified on silica gel chromatography (Cyclohexane/Ethyl Acetate 4:1) to afford the gold complex (α -ICyD)AuCl 126 (567 mg, 55 %).

The structure of the product was confirmed by comparison with the NMR spectra of the literature.¹

¹H NMR (CDCl₃, 600 MHz, 300 K) : δ 7.41-6.97 (m, 74H, 74 x H-Ar), 6.83 (t, $^3J_{o,m} = ^3J_{m,p} = 7.7$ Hz, 4H, 4 x H-*o*-Ar), 6.73 (t, $^3J = 7.4$ Hz, 2H, 2 x H-*p*-Ar), 6.38 (t, $^3J_{4,5} = ^3J_{5,6} = 10.1$ Hz, 2H, 2 x H-5A,D), 6.09 (s, 2H, 2 x N-CH=CH-N), 5.71 (d, $^3J_{1,2} = 3.8$ Hz, 2H, 2 x H-1C,F), 5.63 (d, $^2J_{Ph-CHH} = 10.6$ Hz, 2H, 2 x CHPh), 5.27 (d, $^2J_{Ph-CHH} = 10.7$ Hz, 2H, 2 x CHPh), 5.17-5.11 (m, 4H, 4 x CHPh), 5.02 (dd, $^3J_{2,3} = 10.2$ Hz, $^3J_{3,4} = 7.9$ Hz, 2H, 2 x H-3C,F), 4.86 (d, $^2J_{Ph-CHH} = 11.2$ Hz, 2H, 2 x CHPh), 4.68-4.40 (m, 20H, 14 x CHPh, 2 x H-1A,D, 2 x H-1B,E, 2 x H-6aA,D), 4.32-4.23 (m, 6H, 6 x CHPh), 4.24 (t, $^3J_{2,3} = ^3J_{3,4} = 9.4$ Hz, 2H, 2 x H-3B,E), 4.18 (dd, $^3J_{2,3} = 9.7$ Hz, $^3J_{3,4} = 7.6$ Hz, 2H, 2 x H-3A,D), 4.14 (bd, $^3J_{4,5} = 9.7$ Hz, 2H, 2 x H-5B,E), 4.01 (d, $^2J_{Ph-CHH} = 12.2$ Hz, 2H, 2 x CHPh), 3.98-3.93 (m, 4H, 2 x H-5C,F, 2 x H-6aC,F), 3.85 (dd, $^3J_{4,5} = 9.4$ Hz, $^3J_{3,4} = 8.0$ Hz, 2H, 2 x H-4C,F), 3.79 (dd, $^2J_{6a,6b} = 10.6$ Hz, $^3J_{5,6b} = 5.4$ Hz, 2H, 2 x H-6bC,F), 3.72 (t, $^3J_{3,4} = ^3J_{4,5} = 9.3$ Hz, 2H, 2 x H-4B,E), 3.61 (dd, $^3J_{2,3} = 10.2$ Hz, $^3J_{1,2} = 3.8$ Hz, 2H, 2 x H-2C,F), 3.57 (dd, $^3J_{4,5} = 10.1$ Hz, $^3J_{3,4} = 7.6$ Hz, 2H, 2 x H-4A,D), 3.43 (dd, $^3J_{2,3} = 9.9$ Hz, $^3J_{1,2} = 3.5$ Hz, 2H, 2 x H-2B,E), 3.33-3.26 (m, 4H, 2 x H-2A,D, 2 x H-6bA,D), 3.10 (dd, $^2J_{6a,6b} = 10.8$ Hz, $^3J_{5,6a} = 3.3$ Hz, 2H, 2 x H-6aB,E), 2.76 (bd, $^2J_{6a,6b} = 10.8$ Hz, 2H, 2 x H-6bB,E) ppm.

¹³C NMR (CDCl₃, 151 MHz, 300 K) : δ 169.73 (C-Au), 140.17 (2C), 139.83 (2C), 139.59 (2C), 139.15 (2C), 139.10 (2C), 138.84 (2C), 138.36 (2C), 138.07 (2C) (16 x C-Ar-quat.), 128.73-126.67 (80 x C-Ar-tert.), 121.52 (2 x N-CH=CH-N), 98.53 (2 x C-1C,F), 98.03 (2C), 97.99 (2C) (2 x C-1A,D, 2 x C-1B,E), 82.59 (2 x C-4C,F), 81.82 (2 x C-3A,D), 81.43 (2 x C-4B,E), 80.36 (2C), 80.25 (2C) (2 x C-2A,D, 2 x C-3B,E), 79.53 (2 x C-3C,F), 79.14 (2 x C-2B,E), 77.12 (2 x C-2C,F), 76.96 (2 x C-4A,D), 76.65 (2C), 76.40 (2C), 74.22 (2C) (6 x Ph-CH₂), 73.73 (2 x C-5C,F), 73.47 (2C), 73.29 (2C), 73.21 (2C), 72.65 (2C), 72.33 (2C) (10 x Ph-CH₂), 71.53 (2 x C-5B,E), 71.12 (2 x C-6C,F), 69.90 (2 x C-5A,D), 67.92 (2 x C-6B,E), 54.32 (2 x C-6A,D) ppm.

$R_f = 0.21$ (Cyclohexane/Ethyl Acetate 4:1)

HRMS (ESI) : calculated for $C_{151}H_{156}AuClN_2NaO_{28}^+$ [M+Na]⁺ 2700.0091, found 2700.0089 err. 0.07 ppm

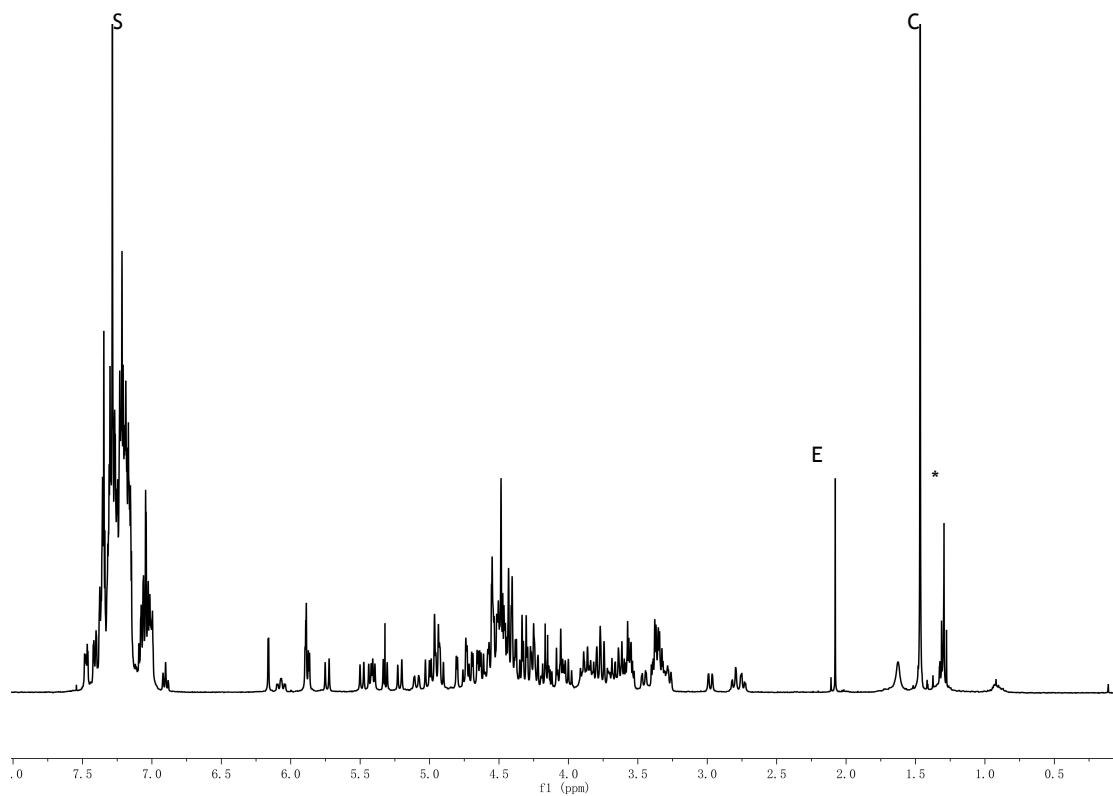


Figure S5: $^1\text{H-NMR}$ of $(\beta\text{-ICyD})\text{AuCl}$ 127. CDCl_3 600 MHz, 300 K

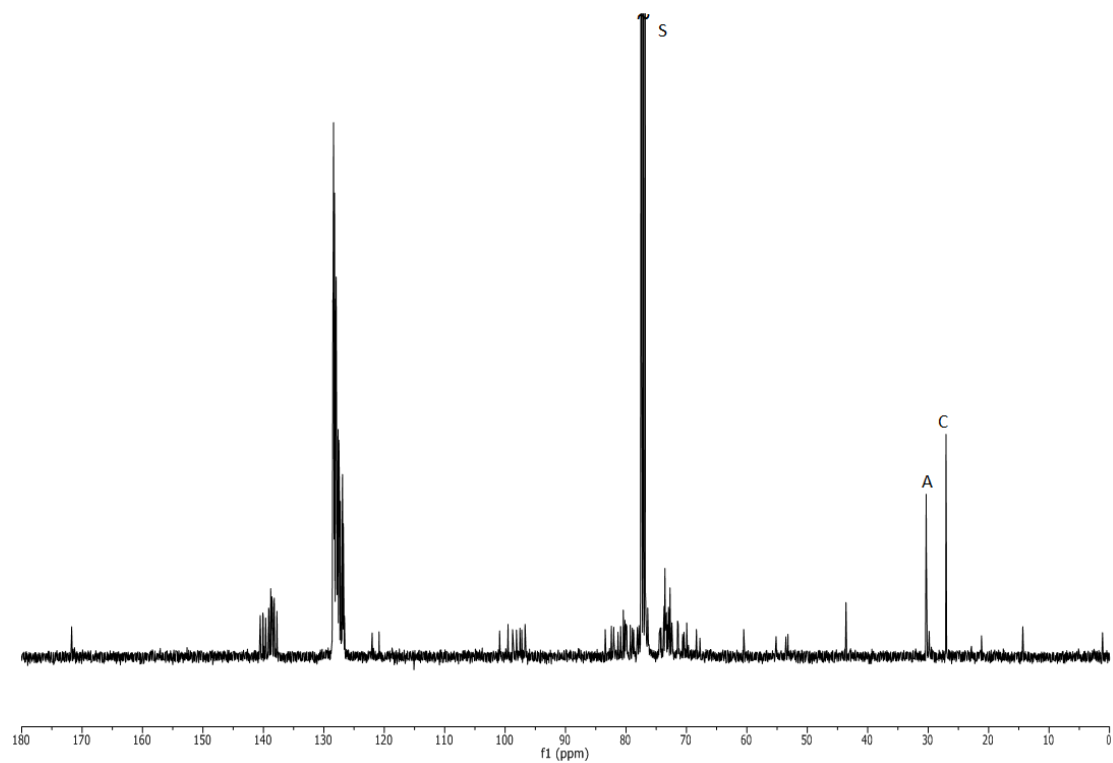
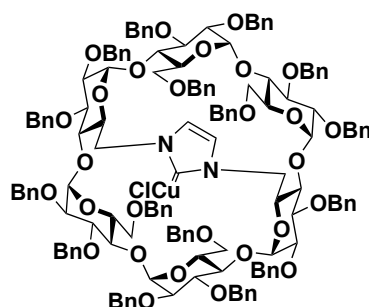


Figure S6: $^1\text{H-NMR}$ of $(\beta\text{-ICyD})\text{AuCl}$ 127. CDCl_3 600 MHz, 300 K

(α -ICyD)CuCl (128)



Chemical Formula:

C₁₅₁H₁₅₆ClCuN₂O₂₈

Molecular Weight:

2545.85

Under argon, (α -ICyD)HCl **122** (5.8 g, 2.3 mmol) and copper(I) oxide (1.2g, 8.3 mmol) were dissolved in 50 ml of 1,4-dioxane previously degassed by bubbling argon for 15 minutes. The mixture was heated at 120 °C overnight, cooled down to R. T., filtered on Celite and washed with CH₂Cl₂ and the solvent evaporated *in vacuo*. The residue was purified on silica gel chromatography (Cyclohexane/Ethyl Acetate 7:3) to afford copper complex (α -ICyD)CuCl **128** (4.7 g, 80 %) as a white foam.

The structure of the product was confirmed by comparison with the NMR spectra of the literature.¹

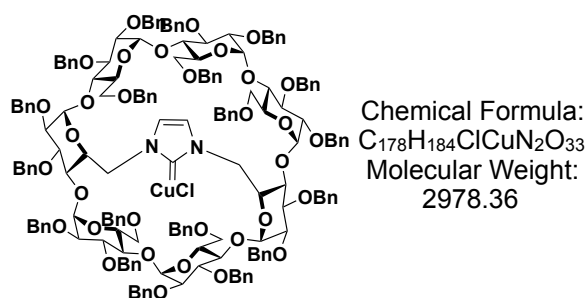
¹H NMR (CDCl₃, 600 MHz, 300 K) : δ 7.39-6.97 (m, 74H, 74 x H-Ar), 6.82 (t, ³J_{o,m} = ³J_{m,p} = 7.7 Hz, 4H, 4 x H-*o*-Ar), 6.69 (t, ³J_{m,p} = 7.4 Hz, 2H, 2 x H-*p*-Ar), 6.16 (s, 2H, 2 x N-CH=CH-N), 5.79-5.74 (m, 4H, 2 x H-1C,F, 2 x H-5A,D), 5.63 (d, ²J_{Ph-CHH} = 10.4 Hz, 2H, 2 x CHPh), 5.23 (d, ²J_{Ph-CHH} = 10.5 Hz, 2H, 2 x CHPh), 5.16-5.11 (m, 4H, 4 x CHPh), 5.07 (dd, ³J_{2,3} = 10.3 Hz, ³J_{3,4} = 7.9 Hz, 2H, 2 x H-3C,F), 4.85 (d, ²J_{Ph-CHH} = 11.3 Hz, 2H, 2 x CHPh), 4.69 (d, ³J_{1,2} = 3.5 Hz, 2H, 2 x H-1B,E), 4.68-4.57 (m, 8H, 8 x CHPh), 4.56 (d, ³J_{2,3} = 3.0 Hz, 2H, 2 x H-1A,D), 4.55-4.45(m, 8H, 6 x CHPh, 2 x H-6aA,D), 4.30-4.24 (m, 6H, 4 x CHPh, 2 x H-3B,E), 4.23 (d, ³J_{1,2} = 12.7 Hz, 2H, 2 x CHPh), 4.20 (dd, ³J_{2,3} = 9.8 Hz, ³J_{3,4} = 7.7 Hz, 2H, 2 x H-3A,D), 4.02-3.87 (m, 10H, 2 x CHPh, 2 x H-4C,F, 2 x H-5B,E, 2 x H-5C,F, 2 x H-6aC,F), 3.83 (dd, ²J_{6a,6b} = 10.5 Hz, ³J_{5,6b} = 4.9 Hz, 2H, 2 x H-6bC,F), 3.73 (t, ³J_{3,4} = ³J_{4,5} = 9.2 Hz, 2H, 2 x H-4B,E), 3.61 (dd, ³J_{2,3} = 10.3 Hz, ³J_{1,2} = 3.7 Hz, 2H, 2 x H-2C,F), 3.56 (dd, ³J_{4,5} = 10.0 Hz, ³J_{3,4} = 7.7 Hz, 2H, 2 x H-4A,D), 3.45 (dd, ³J_{2,3} = 9.9 Hz, ³J_{1,2} = 3.4 Hz, 2H, 2 x H-2B,E), 3.39 (dd, ²J_{6a,6b} = 14.0 Hz, ³J_{5,6b} = 10.1 Hz, 2H, 2 x H-6bA,D), 3.28 (dd, ³J_{2,3} = 9.8 Hz, ³J_{1,2} = 3.0 Hz, 2H, 2 x H-2A,D), 3.05 (dd, ²J_{6a,6b} = 10.9 Hz, ³J_{5,6a} = 3.3 Hz, 2H, 2 x H-6aB,E), 2.76 (dd, ²J_{6a,6b} = 11.0 Hz, ³J_{5,6b} = 1.7 Hz, 2H, 2 x H-6bB,E) ppm.

¹³C NMR (CDCl₃, 151 MHz, 300 K) : δ 173.52 (C-Cu), 140.01 (2C), 139.91 (2C), 139.59 (2C), 139.18 (2C), 139.08 (2C), 138.82 (2C), 138.36 (2C), 138.06 (2C) (16 x C-Ar-quat.), 128.91-126.62 (80 x C-Ar-tert.), 121.56 (2 x N-CH=CH-N), 98.42 (2 x C-1C,F), 98.09 (2 x C-1A,D), 97.71 (2 x C-1B,E), 82.23 (2 x C-4C,F), 81.54 (2 x C-3A,D), 81.43 (2 x C-4B,E), 80.24 (2C), 80.13 (2C) (2 x C-2A,D, 2 x C-3B,E), 79.66 (2 x C-3C,F), 79.25 (2 x C-2B,E), 77.01 (2 x C-2C,F), 76.65 (2 x C-4A,D), 76.54 (2C), 76.45 (2C), 74.13 (2C) (6 x Ph-CH₂), 73.67 (2 x C-5C,F), 73.45 (2C), 73.28 (2C), 73.24 (2C), 72.59 (2C), 72.31 (2C) (10 x Ph-CH₂), 71.85 (2 x C-5B,E), 71.50 (2 x C-5A,D), 71.05 (2 x C-6C,F), 67.91 (2 x C-6B,E), 54.15 (2 x C-6A,D) ppm.

R_f = 0.21 (Cyclohexane/Ethyl Acetate 4:1)

HRMS (ESI) : calculated for C₁₅₁H₁₅₆CuN₂O₂₈⁺ [M-Cl]⁺ 2508.0135, found 2508.0152.

(β -ICyD)CuCl (129)



Under argon, (β -ICyD)HCl **124** (2.8 g, 0.96 mmol) and copper(I) oxide (414 mg, 2.88 mmol) were dissolved in 20 ml of 1,4-dioxane previously degassed by bubbling argon for 15 minutes. The mixture was heated in a Schlenk at 120 °C overnight, cooled down to r. t., filtered on celite, the cake washed with CH_2Cl_2 and the solvent evaporated *in vacuo*. The residue was purified on silica gel chromatography (Cyclohexane/Ethyl Acetate 4:1) to afford copper complex (β -ICyD)CuCl (**2.3 g, 80 %**) as a white foam.

1H NMR (Chloroform-*d*, 600MHz): δ 7.47-6.88 (m, 95H, 95 \times H-Ar), 6.15 (s, 1H, N-CH=C), 5.91-5.90 (m, 2H, N-CH=C, H-1G), 5.87 (d, $^3J_{1,2} = 3.07$ Hz, 1H, H-1C), 5.76-5.74 (m, 2H, CHPh, H-5A), 5.45 (d, $^2J_{Ph-CHH} = 10.02$ Hz, 1H, CHPh), 5.40-5.38 (m, 2H, 2 \times CHPh), 5.26--5.24 (m, 2H, 2 \times CHPh), 4.99 (d, $^2J_{Ph-CHH} = 11.02$ Hz, 1H, CHPh), 4.94-4.89 (m, 6H, 5 \times CHPh, H-6aD), 4.80 (d, $^3J_{1,2} = 3.53$ Hz, 1H, H-1D), 4.72-4.68 (m, 3H, 2 \times H-1E,F, H-3C), 4.64 (d, $^3J_{1,2} = 4.00$ Hz, 1H, H-1B), 4.60-4.59(m, 2H, H-1A, H-3B), 4.57-4.03 (m, 35H, 2 \times H-5D,B, 4 \times H-3E,G,F,A, H-4C, H-6aA, H-6aG, 26 \times CHPh), 3.94 (dd, $^2J_{3,4} = 8.85$ Hz, $^3J_{2,3} = 8.85$ Hz, 1H, H-3D), 3.90-3.52(m, 16H, 2 \times H-2C,G, 6 \times H-4E,G,B,A,D,F, 3 \times H-5C,G,F, H-6bC, H-6bF, H-6bG, H-6aC, H-6aF), 3.43 (br d, 1H, H-6bE), 3.37-3.30(m, 7H, 5 \times H-2B,F,E,D,A, H-6bD, H-6bA), 3.25(br d, 1H, H-5E), 2.99(br d, 1H, H-6aE), 2.79-2.73(m, 2H, H-6aB, H-6bB);

^{13}C NMR (Chloroform-*d*, 151MHz): δ 176.23(Cu-C), 140.48, 140.22, 140.12, 140.02, 139.55, 139.16, 139.05, 138.99, 138.87, 138.85, 138.79, 138.77, 138.61, 138.59, 138.51, 138.27, 138.24, 138.09, 137.74 (19 \times C-Ar.quat.), 128.57-126.50 (m, 95 \times C-Ar-tert.), 122.12, 120.87 (2 \times N-CH=CH-N), 101.03, 99.51, 98.58, 97.94, 97.42, 97.31, 96.83(7 \times C-1A,B,C,D,E,F,G), 83.47(C-4F), 82.22(C-4C), 82.06(C-4G), 81.66(C-3A), 81.41(C-3D), 80.68(C-4E), 80.57(C-4B), 80.38(C-2A), 80.27(C-3F), 80.19, 80.02(2 \times C-3E,G), 79.93(C-3B), 79.89(C-3C), 79.38, 78.99, 78.82, 78.04(4 \times C-2D,E,F,B), 77.96(C-2C), 77.47(C-2G), 76.96, 76.79, 76.41, 76.39, 76.19, 74.41(6 \times Ph-CH₂), 74.33 (C-4A), 74.25(Ph-CH₂), 73.74, 73.73(2 \times Ph-CH₂), 73.70(C-5C), 73.54, 73.49, 73.44, 73.29(4 \times Ph-CH₂), 73.27(C-4D), 73.11(C-5G), 73.07, 72.97, 72.75, 72.72, 72.69(5 \times Ph-CH₂), 72.35(C-5F), 72.34 (Ph-CH₂), 72.05, 71.84, 71.51(3 \times C-5D,E,B), 70.89(C-5A), 70.52, 70.43, 69.81(3 \times C-6C,F,G), 68.27(C-6E), 67.71(C-6B), 55.14(C-6D), 53.01(C-6A).

$[\alpha]_D^{20} = 48.0$ ($CHCl_3$, $c = 1$)

$R_f = 0.21$ (CyH / AcOEt 4:1)

HRMS (ESI) calculated for. $[C_{178}H_{184}N_2O_{33}CuClNa]^+$ $[M+Na]^+$: 2998.1658, found 2998.1513 err. 4.8 ppm

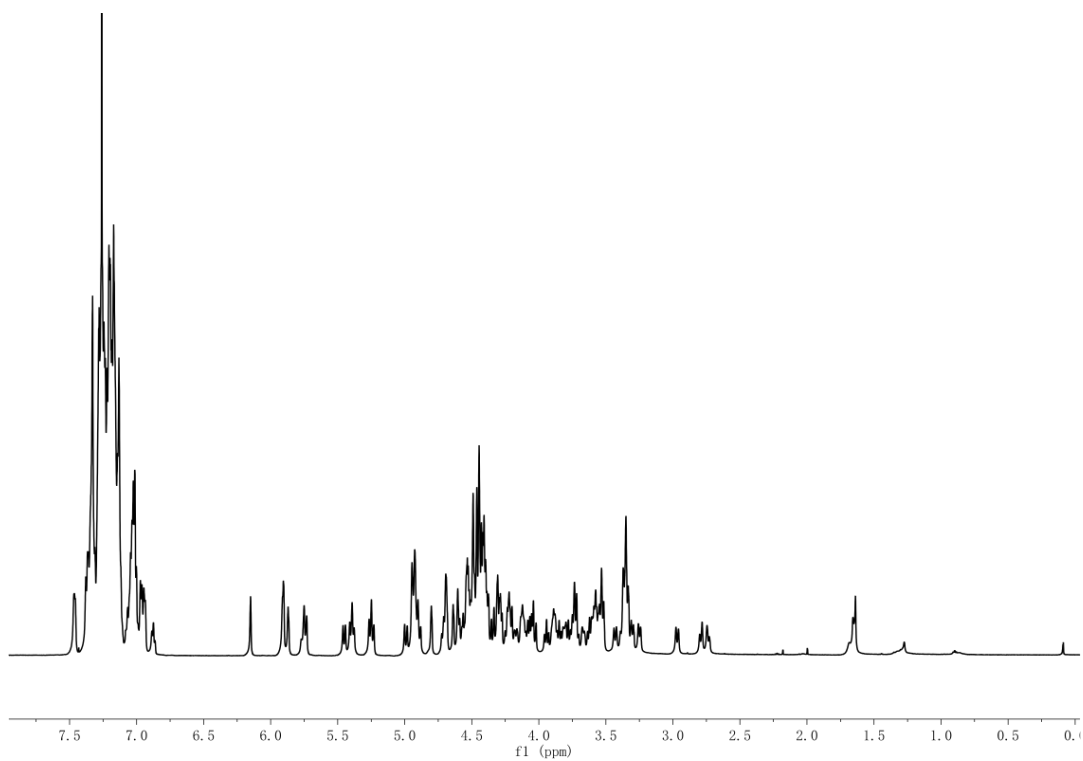


Figure S7: ^1H NMR of $(\beta\text{-ICyD})\text{CuCl}$ 129 (CDCl_3 , 600 MHz, 300 K)

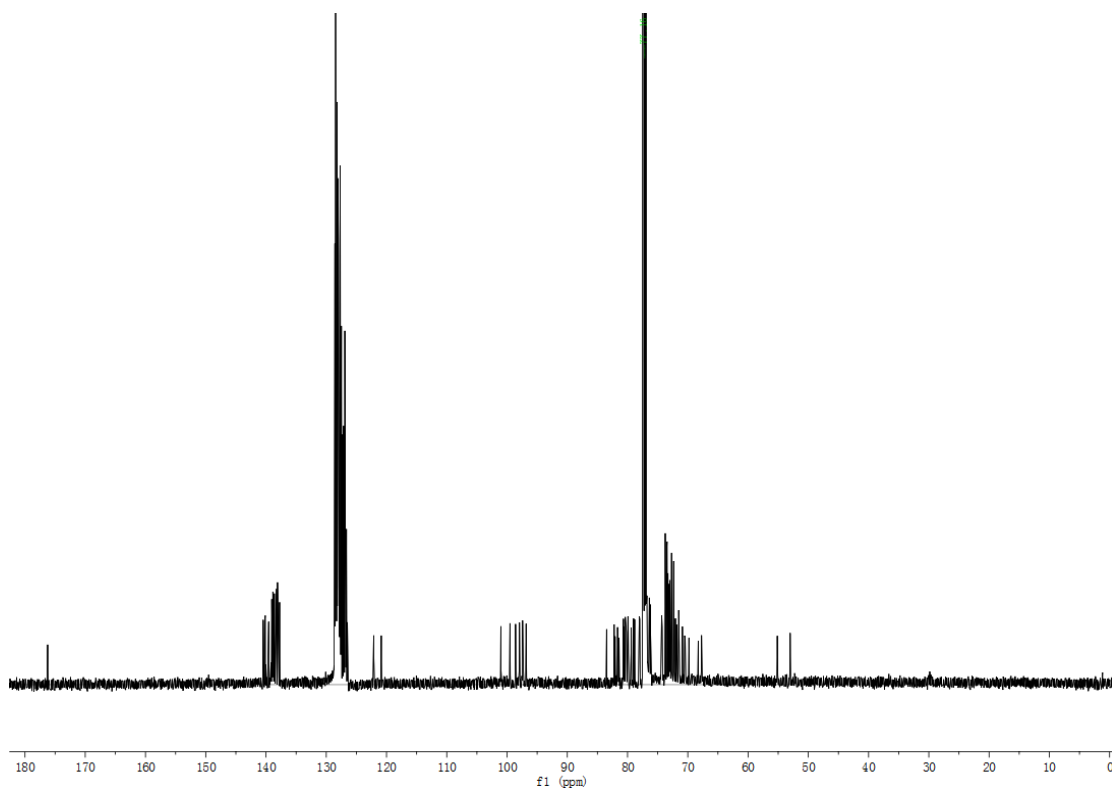
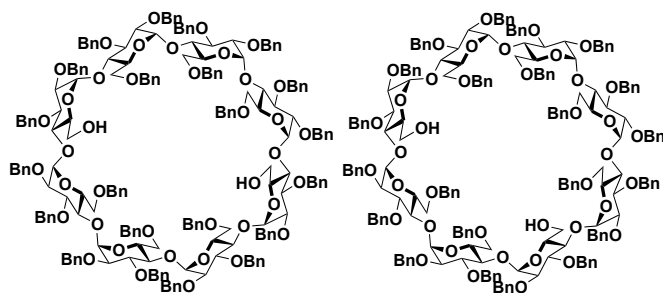


Figure S7: ^{13}C NMR of $(\beta\text{-ICyD})\text{CuCl}$ (CDCl_3 , 151 MHz, 300 K)

2^{A-G}, 3^{A-G}, 6^B, 6^C, 6^E, 6^F, 6^G - Nonadeca-*O*-benzyl-β-cyclodextrin + 2^{A-G}, 3^{A-G}, 6^B, 6^C, 6^D, 6^F, 6^G - Nonadeca-*O*-benzyl-β-cyclodextrin (150)



Chemical Formula:
 $C_{202}H_{212}O_{40}$
Molecular Weight:
3279.82

Perbenzylated γ -CD **167** (15.2 g, 4.4 mmol) under nitrogen was dissolved in freshly distilled toluene (30.7 ml) and the solution stirred. DIBAL-H 1.5M in toluene (61.4 mL, 88 mmol) was added to give a final concentration of 1 M in DIBAL-H. The mixture was heated at 55 °C with a nitrogen flow and the reaction followed by TLC (cyclohexane/AcOEt 3:1). The solution was carefully and slowly poured on 300ml of ice/water while stirring. AcOEt (400 ml) and aqueous HCl 1 M (150 ml) were added and the mixture was stirred at R.T until 2 layers are clearly differentiated (~1h). The layers were then separated and the aqueous one was extracted with AcOEt (3 x 400 ml). The combined organic layers were dried over MgSO₄ and the solvent evaporated. The residue was purified on silica gel chromatography (cyclohexane:AcOEt 3:1) to afford a mixture of AE and AD diols as a white foam (6.6 g, 45%)

R_f=0.4 (CyH:AcOEt 3:1)

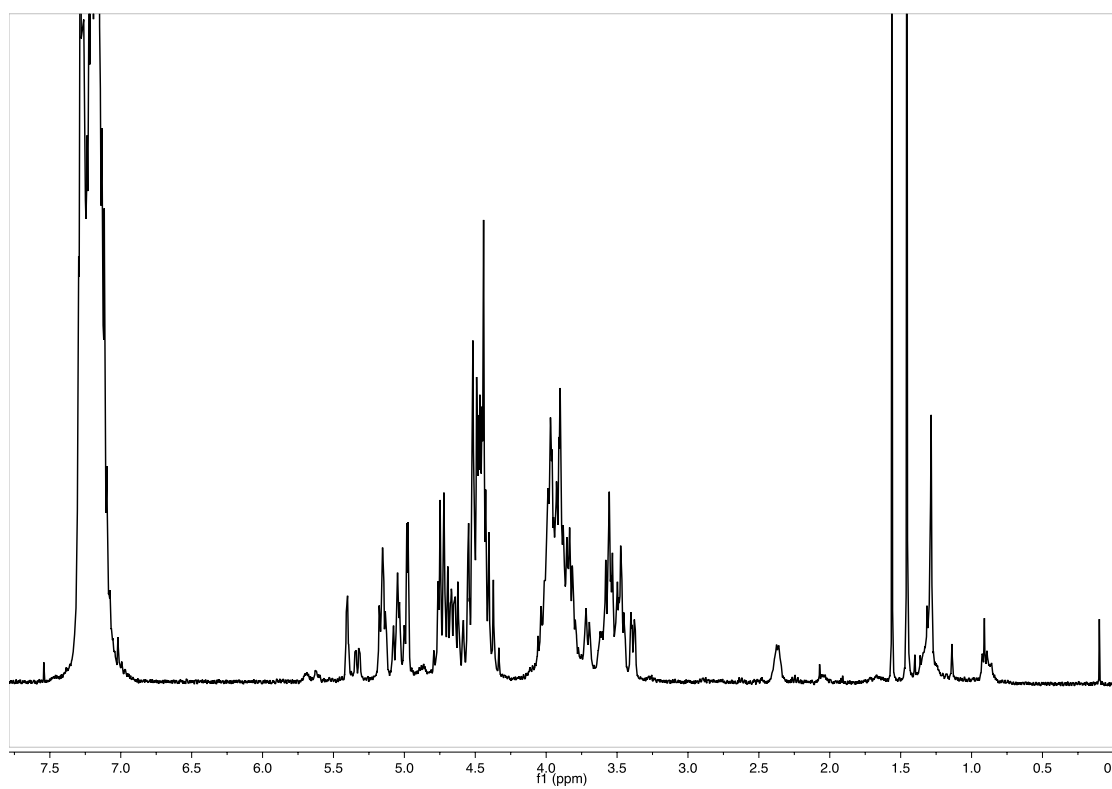
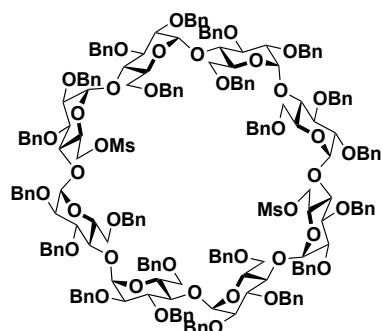


Figure S9: $^1\text{H-NMR}$ of the mixture of $\gamma\text{-AD-CD(OH)}_2$ and $\gamma\text{-AE-CD(OH)}_2$ **150**

6^A,6^E-di-O-methylsulfonyl-2^{A-G},3^{A-G},6^B,6^C,6^D,6^F,6^G,6^H-Docosa-O-benzyl- γ -cyclodextrin (151) and 6^A,6^D-di-O-methylsulfonyl-2^{A-G},3^{A-G},6^B,6^C,6^E,6^F,6^G,6^H-Docosa-O-benzyl- γ -cyclodextrin (152)

To a solution of the mixture of **150** (2 g, 0.611mmol) in anhydrous CH₂Cl₂ (20 mL), triethylamine (200 μ L, 2.444 mmol) was added at 0 °C. The reaction mixture was stirred for 30 minutes at r.t. Then methanesulfonyl chloride (340 μ L, 2.444 mmol) was added at 0 °C. The reaction mixture was stirred at R.T. for 2h under nitrogen, and then water was added slowly, the layers were separated and the aqueous layer was extracted with DCM 3 times. The combined organic layers were dried over MgSO₄, filtered and concentrated. Silica gel chromatography of the residue (Cy/Et₂O 3.5:1) afforded **151** (1,07 g, 51% yield) in a first fraction followed by the second fraction containing **152** (0.589 mg, 30% yield) as a white foam.

6^A,6^E-di-O-methylsulfonyl-2^{A-G},3^{A-G},6^B,6^C,6^D,6^F,6^G,6^H-Docosa-O-benzyl- γ -cyclodextrin (151)



Chemical Formula:
C₂₀₄H₂₁₆O₄₄S₂
Molecular Weight:
3436.00

¹H NMR (600 MHz, CDCl₃): 7.43-6.98 (m, 110H, 110 x H-Ar), 5.59 (d, ³J_{1,2} = 3.9 Hz, 2H, 2 x H-1), 5.50 (d, ²J_{Ph-CHH} = 10.7 Hz, 2H, 2 x CHPh), 5.47 (d, ²J_{Ph-CHH} = 10.4 Hz, 2H, 2 x CHPh), 5.27 (d, ²J_{Ph-CHH} = 10.7 Hz, 2H, 2 x CHPh), 5.07 (d, ³J_{1,2} = 3.3 Hz, 2H, 2 x H-1), 5.03 (d, ³J_{1,2} = 3.1 Hz, 2H, 2 x H-1), 4.92 (d, ³J_{1,2} = 3.4 Hz, 2H, 2 x H-1), 4.88-4.86 (m, 6H, 6 x CHPh), 4.80 (d, ²J_{Ph-CHH} = 10.5 Hz, 2H, 2 x CHPh), 4.69 (d, ²J_{Ph-CHH} = 12.2 Hz, 2H, 2 x CHPh), 4.64-4.56 (m, 4H, 4 x CHPh), 4.55-4.33 (m, 28H, 4 x H-6, 2 x H-5, 22 x CHPh), 4.26 (d, ²J_{Ph-CHH} = 12.9 Hz, 2H, 2 x CHPh), 4.19-3.80 (m, 28H, 8 x H-3, 8 x H-4, 4 x H-5, 8 x H-6), 3.72-3.71 (m, 2H, 2 x H-5), 3.64-3.56 (m, 6H, 2 x H-2, 4 x H-6), 3.50 (dd, 2H, ³J_{1,2} = 9.4Hz, ³J_{2,3} = 3.5 Hz, 2 x H-2), 3.45-3.43 (m, 4H, 4 x H-2), 2.56 (s, 6H, 2 x CH₃);

¹³C NMR (151 MHz, CDCl₃): 139.89(2C), 139.72(2C), 139.59(2C), 138.97(2C), 138.71(4C), 138.56(2C), 138.50(2C), 138.46(2C), 138.00(4C) (22x C-Ar-quat.), 128.44-126.88 (110x C-Ar-tert.), 100.49(2C), 98.78(2C), 98.04(2C), 95.71(2C) (8 x C-1), 81.81(2C), 81.66(2C), 81.25(2C), 81.07(2C), 80.88(4C), 80.13(4C) (8 x C-3, 8 x C-4), 79.07(2C), 78.85(2C), 78.04(2C), 77.38 (2C) (8 x C-2), 76.91(2C), 76.54(2C), 76.40(2C), 74.21(2C), 73.98(2C), 73.43(2C), 73.37(4C), 72.73(2C), 72.70(2C), 72.50(2C) (22 x Ph-CH₂), 71.80(2C), 71.33(4C) (6 x C-5), 69.67(2C), 69.36(2C), 69.30(2C) (6 x C-6), 68.61(2C)(2 x C-5), 67.65(2C) (2 x C-6), 36.60(2 x C-CH₃);

[α]_D²⁵ = +39.1 (CHCl₃, c = 1.0)

R_f = 0.4 (Cy/Et₂O 1:1)

HRMS (ESI) : calculated for C₂₀₄H₂₁₆O₄₄ S₂Na [M+Na]⁺ 3456.3998, found 3456.3979, err. 0.6 ppm

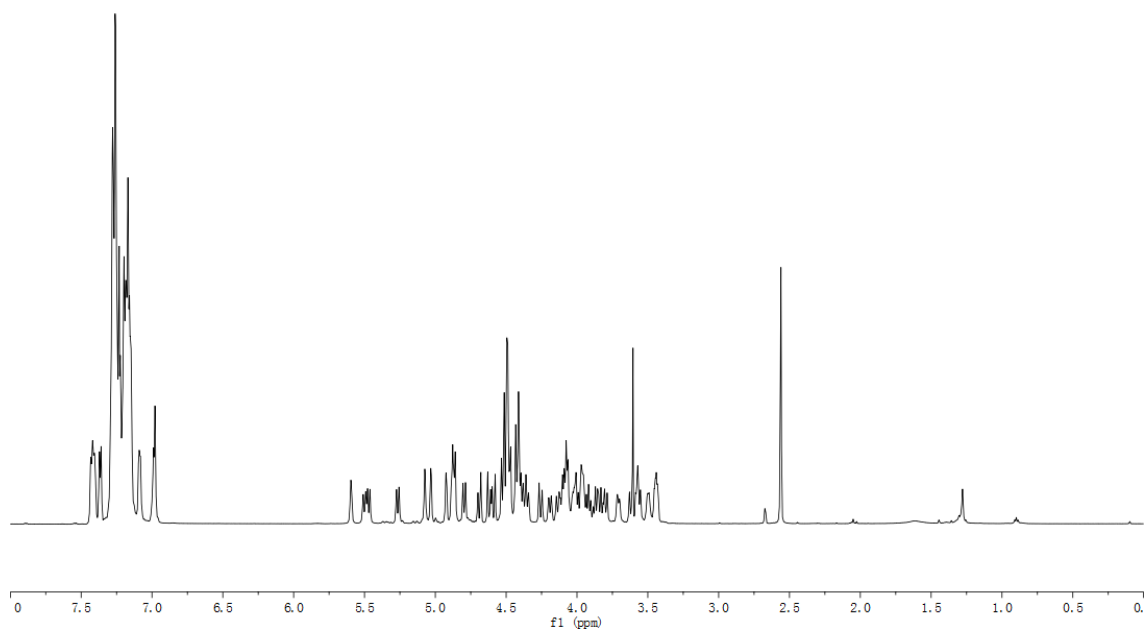


Figure S10: ^1H NMR of **151** (CDCl_3 , 600 MHz, 300 K)

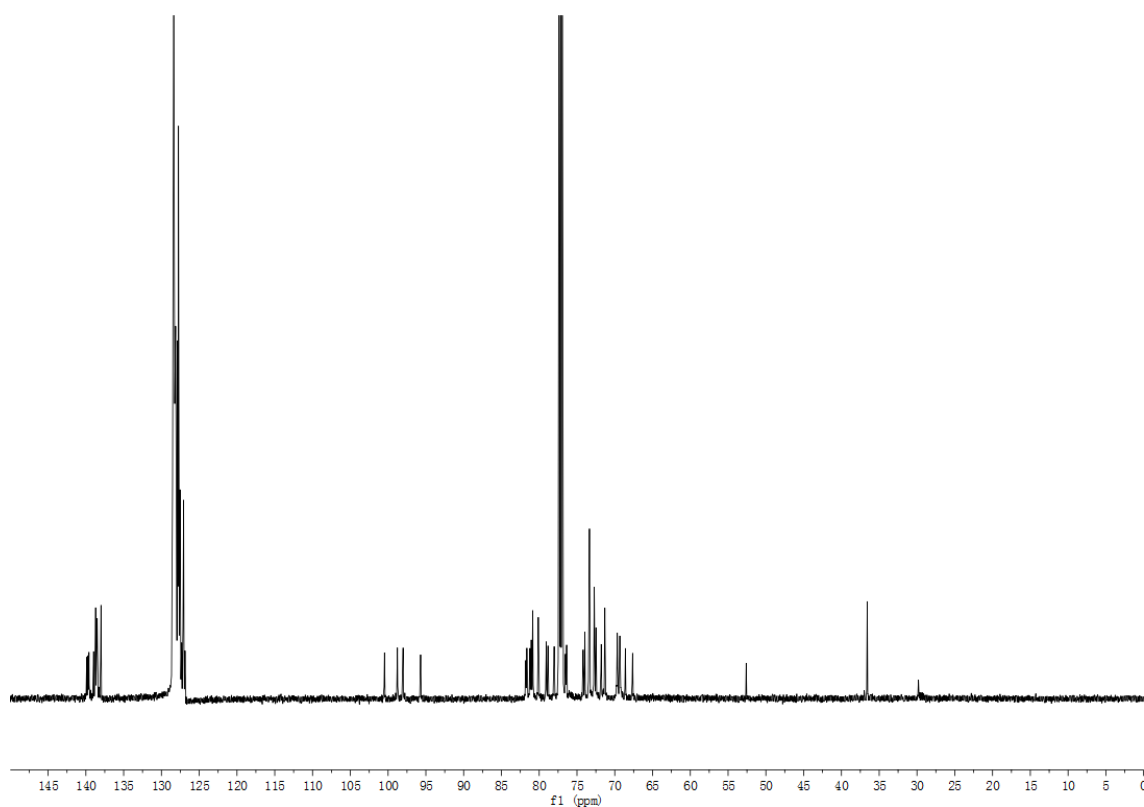
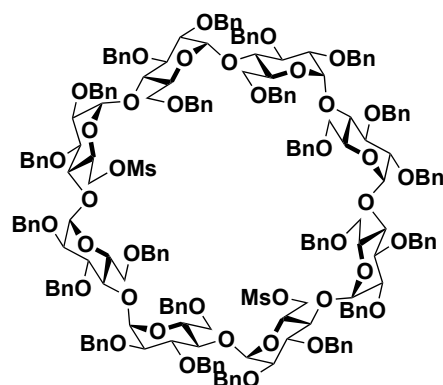


Figure S11: ^{13}C NMR of **151** (CDCl_3 , 151 MHz, 300 K)

6^A,6^D-di-*O*-methylsulfonyl-2^{A-G},3^{A-G},6^B,6^C,6^E,6^F,6^G,6^H-Docosa-*O*-benzyl- γ -cyclodextrin (152)



Chemical Formula:
C₂₀₄H₂₁₆O₄₄S₂
Molecular Weight:
3436.00

¹H NMR (600 MHz, CDCl₃): 7.35-7.08 (m, 110H, 110 x H-Ar), 5.39 (d, ³J_{1,2} = 3.9 Hz, 1H, H-1), 5.36-5.32 (m, 2H, H-1, CHPh), 5.28-5.25 (m, 3H, 3 x CHPh), 5.17 (d, ³J_{1,2} = 3.5 Hz, 1H, H-1), 5.14 (d, ³J_{1,2} = 3.6 Hz, 1H, H-1), 5.11-5.01 (m, 7H, 4 x H-1, 3 x CHPh) 4.85-4.73 (m, 9H, 9 x CHPh), 4.63 (d, ²J_{Ph-CHH} = 12.1 Hz, 1H, CHPh), 4.57-4.38 (m, 30H, 27 x CHPh, 3 x H-6), 4.26 (dd, ²J_{6a,6b} = 10.8 Hz, ³J_{5,6b} = 5.1 Hz, 1H, H-6), 4.10-3.68 (m, 30H, 6 x H-6, 8 x H-3, 8 x H-4, 8 x H-5), 3.58-3.47 (m, 12H, 6x H-2, 6 x H-6), 3.42 (dd, ³J_{1,2} = 9.7Hz, ³J_{2,3} = 3.4 Hz, 1H, H-2), 3.39 (dd, ³J_{1,2} = 9.6Hz, ³J_{2,3} = 3.4 Hz, 1H, H-2), 2.69 (s, 3H, CH₃), 2.68 (s, 3H, CH₃);

¹³C NMR (151 MHz, CDCl₃): 139.55, 139.52, 139.50, 139.35, 139.33, 139.18, 138.95, 138.84, 138.60, 138.57, 138.40, 138.39, 138.38, 138.32, 138.28, 138.28, 138.26, 138.24, 138.20, 138.19, 138.17, 137.95 (22x C-Ar-quat.), 128.52-126.95 (110x C-Ar-tert.), 99.35, 99.01, 98.96, 98.63, 98.31, 98.14, 97.80, 97.77(8 x C-1), 81.25, 81.18, 81.08(2C), 81.03(2C), 80.86, 80.77, 80.33, 80.19, 79.78, 79.45, 79.21, 79.17(2C), 79.10(2C), 79.03(2C), 78.90(2C), 78.54, 78.13, 77.36 (8 x C-3, 8 x C-4, 8 x C-2), 76.37, 76.07, 76.04, 76.00, 75.81, 75.64, 75.16, 75.00, 73.52, 73.42, 73.40(2C), 73.37, 73.32, 73.27(2C), 73.16, 73.01, 72.87(2C), 72.80, 72.77(22 x Ph-CH₂), 72.12, 71.77, 71.57, 71.52, 71.47(2C) (6 x C-5), 69.84 (C-6), 69.51(C-5), 69.41(C-6), 69.35(C-5), 69.30, 69.20, 69.11, 69.06, 68.94(2C) (6 x C-6), 37.00(CH₃), 36.92(CH₃);

[α]_D²⁰ = +41.0 (CHCl₃, c = 1.0);

R_f = 0.33 (CyH/Et₂O 1:1)

HRMS (ESI) : calculated for C₂₀₄H₂₁₆O₄₄ S₂Na [M+Na]⁺ 3456.3998, found 3456.4178, err. -5.2 ppm

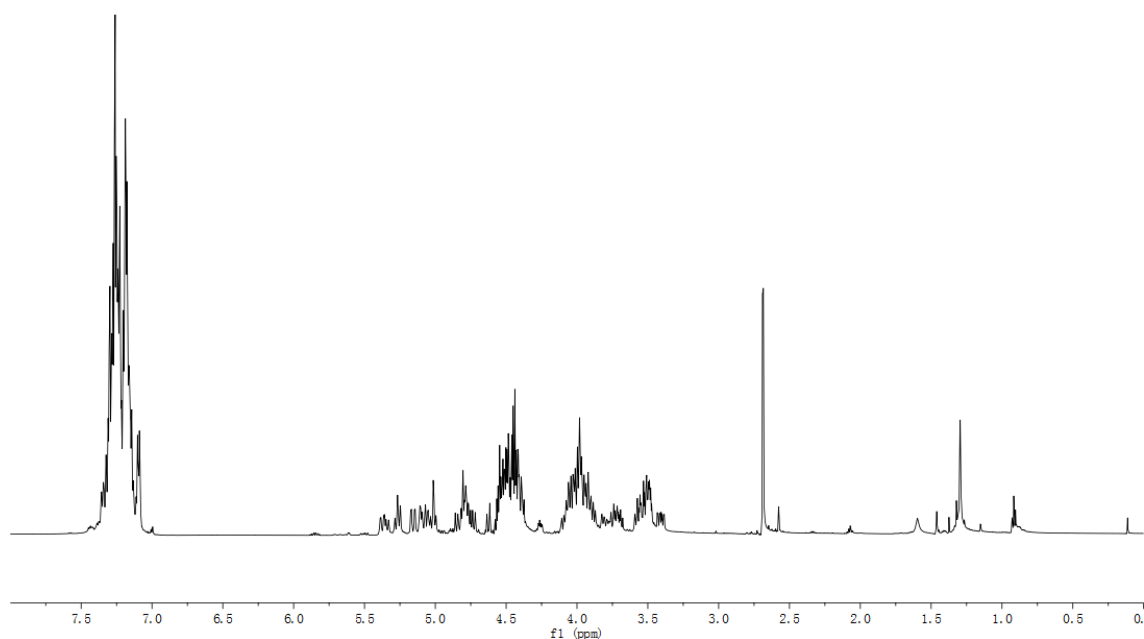


Figure S12: ^1H -NMR of **152** (CDCl_3 , 600 MHz, 300 K)

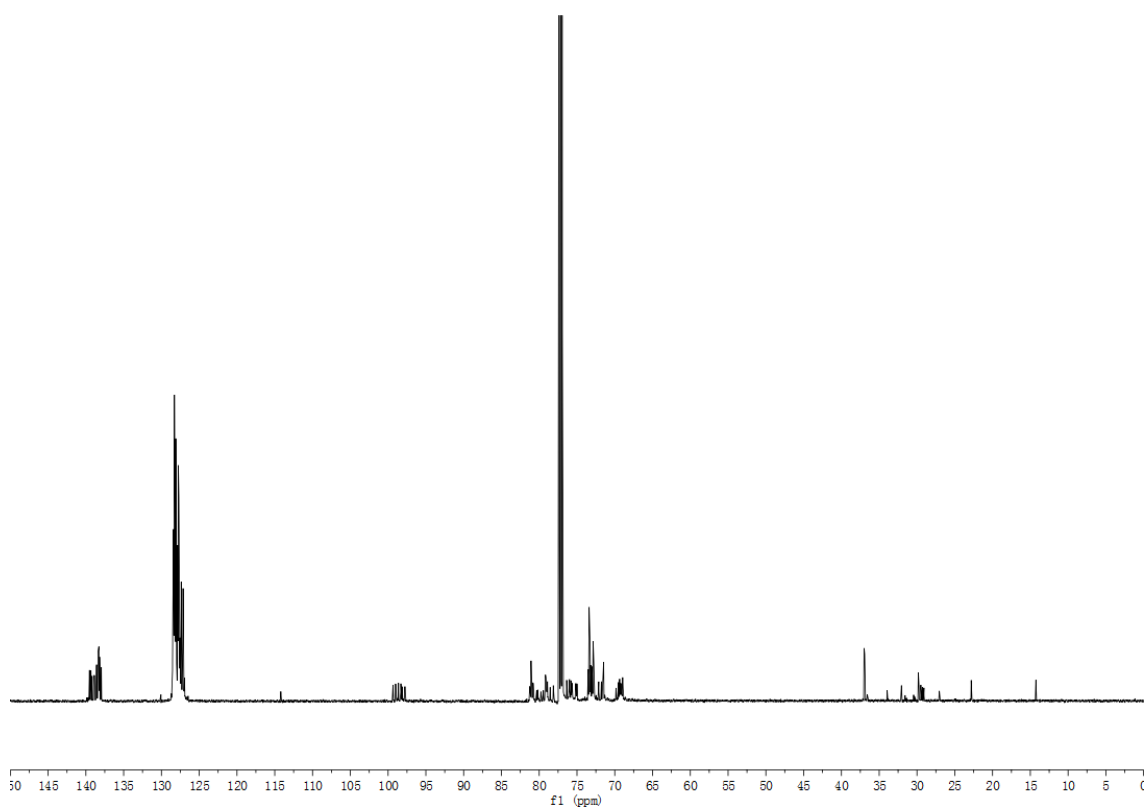
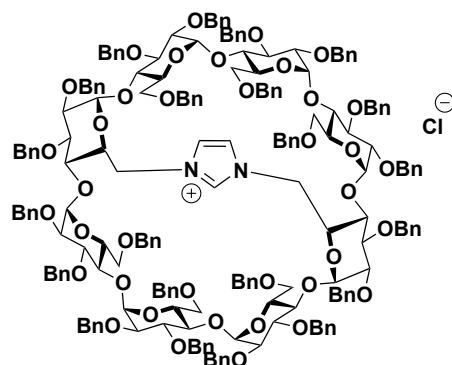


Figure S13: ^{13}C NMR of **152** (CDCl_3 , 151 MHz, 300 K)

(γ -A,E-ICyD)HCl (153)



Chemical Formula:
C₂₀₅H₂₁₃ClN₂O₃₈
Molecular Weight:
3348.33

A mixture of compound **151** (700 mg, 0.203 mmol) and imidazole (277 mg, 4.07 mmol) was dissolved in anhydrous DMF under a N₂ atmosphere. The reaction mixture was stirred at 120°C overnight. When finished, the solvent was evaporated in high vacuo. The crude is dissolved in a 1:1 mixture of CH₂Cl₂ and HCl solution (1 M) (20 mL) was added and the aqueous layer was extracted with DCM 3 times. The combined organic layers were dried over MgSO₄ filtered, and concentrated in *vacuo*. Silica gel chromatography of the residue (DCM/MeOH 95:5) afforded (γ -A,E-ICyD)HCl **153** as a white foam (360 mg, 53 %).

¹H NMR (600 MHz, CD₃CN): 7.41-7.12 (m, 104H, 104 x H-Ar), 6.96 (t, $J = 7.6$ Hz, 4H, 4 x H-Ar), 6.81 (t, $J = 7.4$ Hz, 2H, 2 x H-Ar), 6.69 (s, 2H, 2 x H-imidazolium), 5.61 (d, $^3J_{1,2} = 3.5$ Hz, 2H, 2 x H-1D,H), 5.23 (d, $^2J_{\text{Ph-CHH}} = 10.7$ Hz, 2H, 2 x CHPh), 5.19 (d, $^2J_{\text{Ph-CHH}} = 10.0$ Hz, 2H, 2 x CHPh), 4.93 (d, $^3J_{1,2} = 3.0$ Hz, 2H, 2 x H-1A,E), 4.92 (d, $^3J_{1,2} = 3.5$ Hz, 2H, 2 x H-1C,G), 4.90 (d, $^3J_{1,2} = 3.3$ Hz, 2H, 2 x H-1B,F), 4.85 (d, $^2J_{\text{Ph-CHH}} = 10.9$ Hz, 2H, 2 x CHPh), 4.75 (d, $^2J_{\text{Ph-CHH}} = 10.7$ Hz, 2H, 2 x CHPh), 4.71 (d, $^2J_{\text{Ph-CHH}} = 11.1$ Hz, 2H, 2 x CHPh), 4.66 (d, $^2J_{\text{Ph-CHH}} = 11.3$ Hz, 2H, 2 x CHPh), 4.59-4.37 (m, 32H, 32 x CHPh), 4.31 (dd, $^2J_{6a,6b} = 13.8$ Hz, $^3J_{5,6b} = 2.4$ Hz, 2H, 2 x H-6bA,E), 4.10 (dd, $^2J_{6a,6b} = 11.3$ Hz, $^3J_{5,6b} = 4.7$ Hz, 2H, 2 x H-6aH,D), 3.97-3.72 (m, 26H, H-6aC, H-6aG, H-6bD, H-6bH, H-6bC, H-6bG, H-6aA, H-6aE, 4 x H-5A,E,D,H, 8 x H-3A,B,C,D,E,F,G,H, 6 x H-4B,C,D,F,G,H), 3.64-3.58 (m, 6H, 2 x H-4A,E, 2 x H-5C,G, 2 x H-2D,H), 3.48-3.47 (m, 4H, 2 x H-2A,E, 2 x H-5B,F), 3.39 (ddd, 4H, 4 x H-2B,C,F,G), 3.11 (dd, $^2J_{6a,6b} = 11.2$ Hz, $^3J_{5,6b} = 1.6$ Hz, 2H, 2 x H-6aB,F), 3.11 (dd, $^2J_{6a,6b} = 11.0$ Hz, $^3J_{5,6b} = 3.0$ Hz, 2H, 2 x H-6bB,F).

¹³C NMR (151 MHz, CD₃CN): 140.34(2C), 140.31(2C), 140.18(2C), 139.59(2C), 139.57(4C), 139.56(2C), 139.44(2C), 139.42(2C), 139.01(2C), 138.87(2C), (22x C-Ar-quat.), 129.50-128.05 (110x C-Ar-tert.), 125.08 (2 x N-C=C-N), 99.64(2C), 99.42(2C), 99.05(2C), 94.60(2C) (8 x C-1A,B,C,D,E,F,G,H), 82.38(2 x C-4C,G), 81.79(2 x C-3C,G), 81.28(2 x C-3A,E), 81.22(2 x C-3B,F), 81.02(2C), 80.77(4C) (6 x C-4A,B,D,E,F,H), 80.56(4C) (2 x C-3D,H, 2 x C-2A,E), 80.33(2C), 80.19(2C) (4 x C-2B,C,F,G), 78.27(2 x C-2D,H), 77.46(2C), 77.12(2C), 76.16(2C), 74.76(2C), 73.99(2C), 73.97(2C), 73.93(2C), 73.81 (2C), 73.51(2C), 73.41(2C), 73.22(2C) (22 x Ph-CH₂), 72.74(2 x C-5D,H), 72.36(2C), 72.31(2C) (4 x C-5A,B,E,F), 71.20(2 x C-5C,G), 70.66(2 x C-6C,G), 70.26(2 x C-6D,H), 69.01(2 x C-6B,F), 52.10(2 x C-6A,E);

$[\alpha]_D^{20} = + 35.1$ (CHCl₃, $c = 1.0$)

$R_f = 0.29$ (DCM/MeOH 95:5)

HRMS (ESI) : calculated for C₂₀₅H₂₁₃O₃₈ N₂ [M]⁺ 3310.4791, found 3310.4963, err. -5.2 ppm

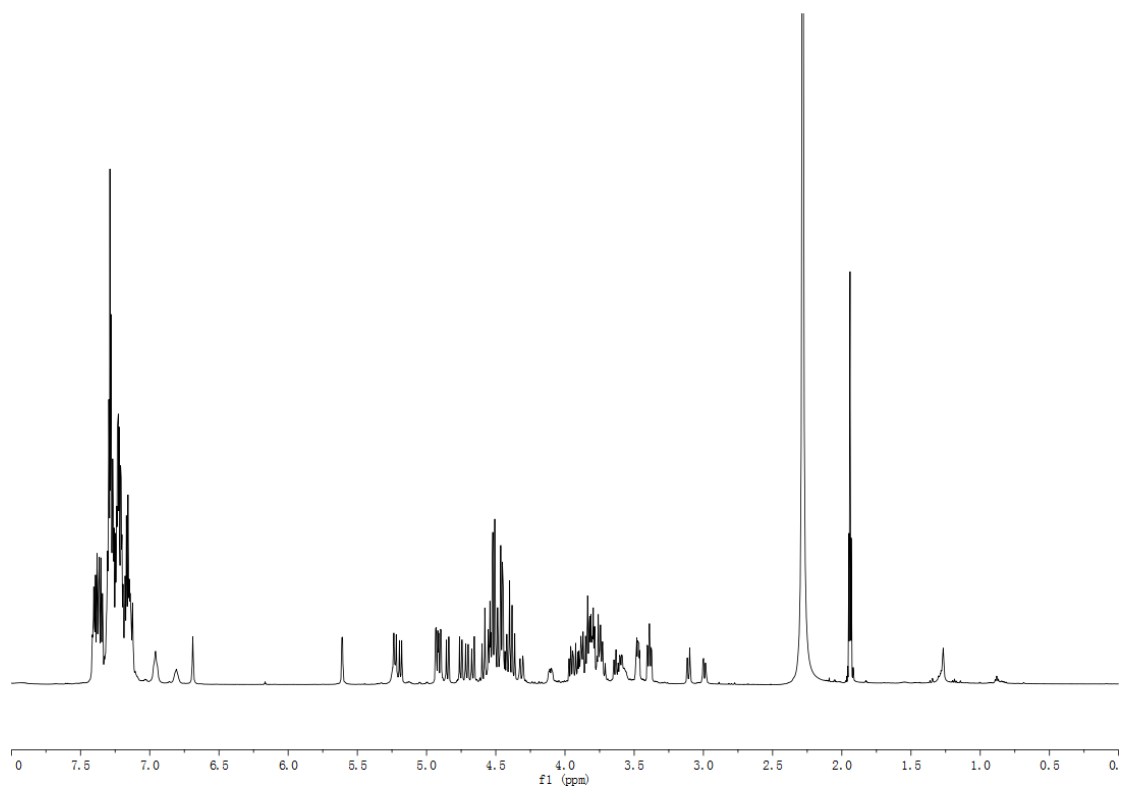


Figure S13: ^1H NMR of (γ -A,E-ICyD)HCl 153 (CD_3CN , 600 MHz, 300K)

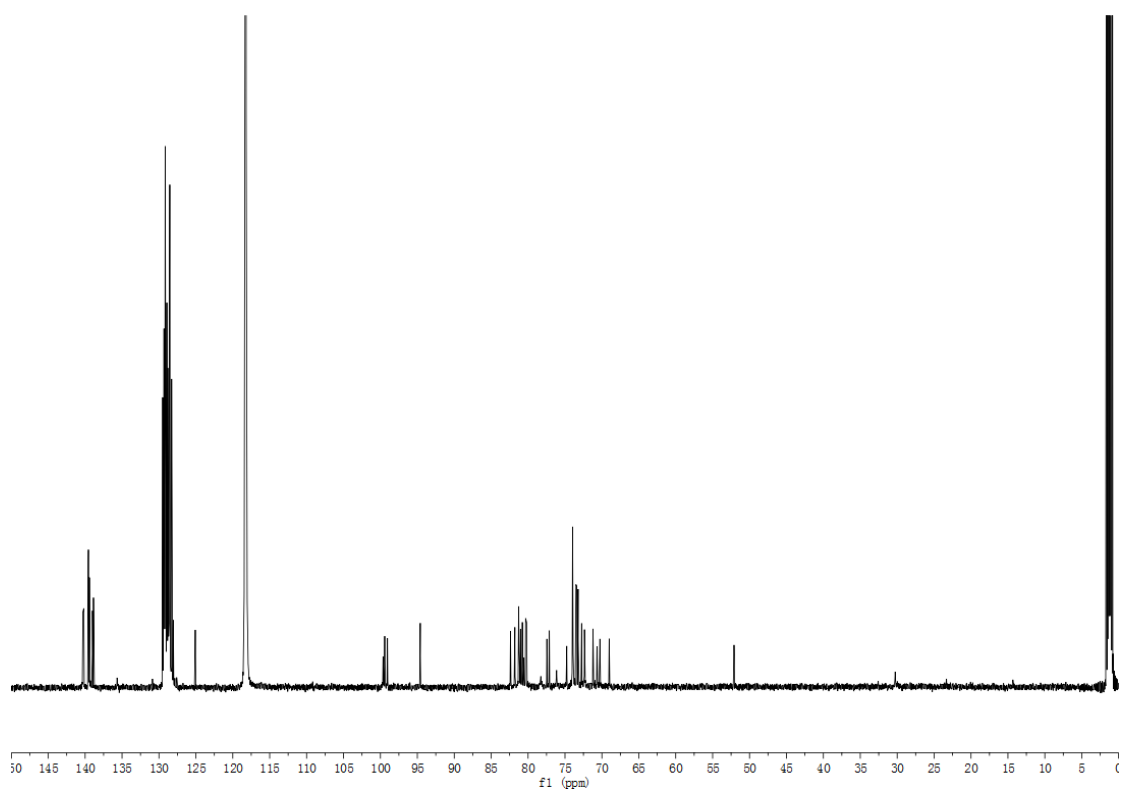
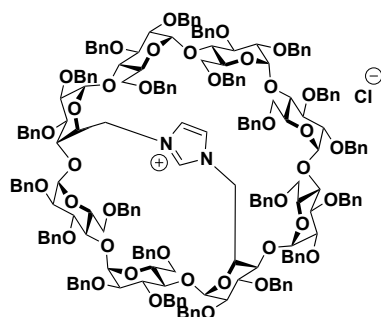


Figure S14: ^{13}C NMR of (γ -A,E-ICyD)HCl 153 (CD_3CN , 151 MHz, 300 K)

(γ -A,D-ICyD)HCl (154)



Chemical Formula:

$C_{205}H_{213}ClN_2O_{38}$

Molecular Weight:

3348.33

A mixture of compound **2 γ -A,D** (500 mg, 0.145 mmol) and imidazole (197 mg, 2.91 mmol) was dissolved in anhydrous DMF under a N_2 atmosphere. The reaction mixture was stirred at $120^\circ C$ overnight. When finished, the solvent was evaporated in high vacuo. The crude is dissolved in a 1:1 mixture of CH_2Cl_2 and HCl solution (1 M) (20 mL) was added and the aqueous layer was extracted with DCM 3 times. The combined organic layers were dried over $MgSO_4$ filtered, and concentrated in *vacuo*. Silica gel chromatography of the residue (DCM/MeOH 95:5) afforded the (**γ -A,D-ICyD**)HCl (360 mg, 53 %).

1H NMR (600 MHz, CD_3CN): 8.73 (s, 1H, N-CH=N), 7.41-7.09 (m, 110H, 110 x H-Ar), 6.95 (s, 1H, H-Im), 6.84 (s, 1H, H-Im), 5.60 (d, $^3J_{1,2} = 3.9$ Hz, 1H, H-1C), 5.32 (d, $^3J_{1,2} = 3.8$ Hz, 1H, H-1H), 5.25-5.18 (m, 2H, 2 x CHPh), 5.14-5.12 (m, 3H, 2 x H-1D,G, CHPh), 5.04 (d, $^3J_{1,2} = 3.5$ Hz, 1H, H-1E), 4.99 (d, $^3J_{1,2} = 3.5$ Hz, 1H, H-1F), 4.94-4.83 (m, 3H, H-1B, 2 x CHPh), 4.77 (d, $^3J_{1,2} = 3.4$ Hz, 1H, H-1A), 4.76-4.37 (m, 38H, H-6aA, H-6aD, H-5A, 35 x CHPh), 4.30-4.27 (m, 2H, 2 x CHPh), 4.23 (d, $^2J_{Ph-CHH} = 11.2$ Hz, 1H, CHPh), 4.17 (d, $^2J_{Ph-CHH} = 11.6$ Hz, 1H, CHPh), 4.13-3.48 (m, 37H, 8 x H-3A,B,C,D,E,F,G,H, 8 x H-4 A,B,C,D,E,F,G,H, 7 x H-5 B,C,D,E,F,G,H, 2 x H-2A,H, H-6bA, H-6aC, H-6bC, H-6bD, H-6aE, H-6bE, H-6aF, H-6bF, H-6aG, H-6bG, H-6aH, H-6bH), 3.45-3.42 (m, 3H, 3 x H-2C,D,G), 3.40-3.38 (m, 2H, 2 x H-2B,E), 3.34 (dd, $^3J_{1,2} = 9.4$ Hz, $^3J_{2,3} = 3.6$ Hz, 1H, H-2F), 3.28 (br d, 1H, H-6aB), 3.03 (dd, $^2J_{6a,6b} = 10.5$ Hz, $^3J_{5,6b} = 6.3$ Hz, 1H, H-6bB);

^{13}C NMR (151 MHz, CD_3CN): 140.44, 140.42, 140.38, 140.35, 139.62, 139.59, 139.57, 139.52, 139.47, 139.42, 139.36, 139.35, 139.29, 139.28, 139.21, 139.18, 139.09, 139.07, 139.04, 138.90, 138.89, 138.88(22x C-Ar-quat.), 129.52-127.61 (110x C-Ar-tert.), 125.05, 124.48(C-Im), 99.82, 99.39, 98.62, 98.35(2C), 98.08, 97.45, 95.49(8 x C-1), 81.90, 81.83, 81.46, 81.23(2C), 81.05, 80.87, 80.78, 80.70(2C), 80.68(2C), 80.40, 80.39, 80.24, 80.22, 80.13, 80.00, 79.91, 79.84, 79.62(7 x C-3A,B,C,D,E,F,G, 8 x C-4A,B,C,D,E,F,G,H, 6 x C-2A,B,C,E,F,G,) 78.95(C-3H), 78.10(C-2D), 77.48, 77.15, 77.05(3 x Ph-CH₂), 76.61 (C-2H), 76.40, 76.10, 76.02, 75.94, 75.71, 74.78, 74.20(2C), (8 x Ph-CH₂), 74.06 (C-5), 73.96, 73.91(2C), 73.84(3C) (6 x Ph-CH₂), 73.72 (C-5), 73.70, 73.51, 73.44(3 x Ph-CH₂), 73.27(C-5), 73.23, 73.01(2 x Ph-CH₂), 72.69, 72.66, 72.61(3 x C-5), 71.16(C-5D), 70.95(C-6), 70.49(C-5A), 70.26, 70.11, 69.98, 69.47, 69.43(5 x C-6), 53.40(C-6D), 52.63(C-6A);

$[\alpha]_D^{20} = + 38.5$ ($CHCl_3$, $c = 1.0$)

$R_f = 0.29$ (DCM/MeOH 95:5)

HRMS (ESI): calculated for $C_{205}H_{213}O_{38} N_2 [M]^+$ 3310.4791, found 3310.4647, err. 4.3 ppm

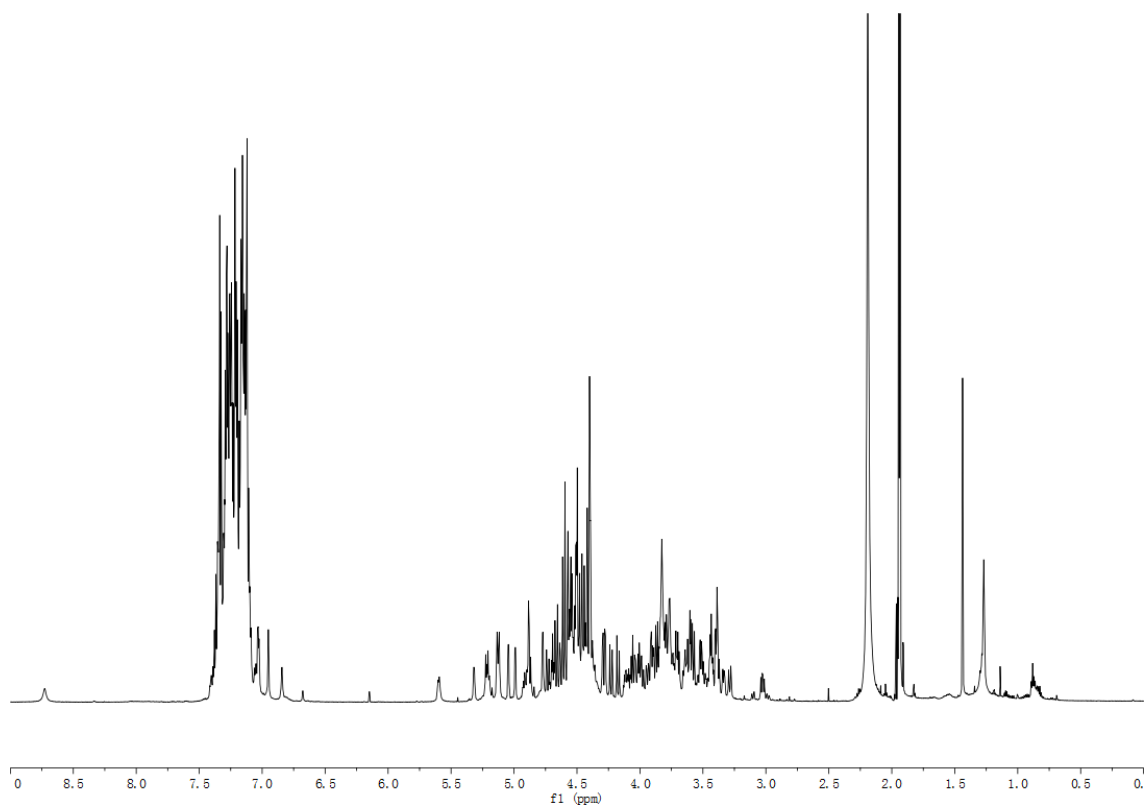


Figure S15: ^1H NMR of (γ -A,D-ICyD)HCl 154 (CD_3CN , 600 MHz, 300 K)

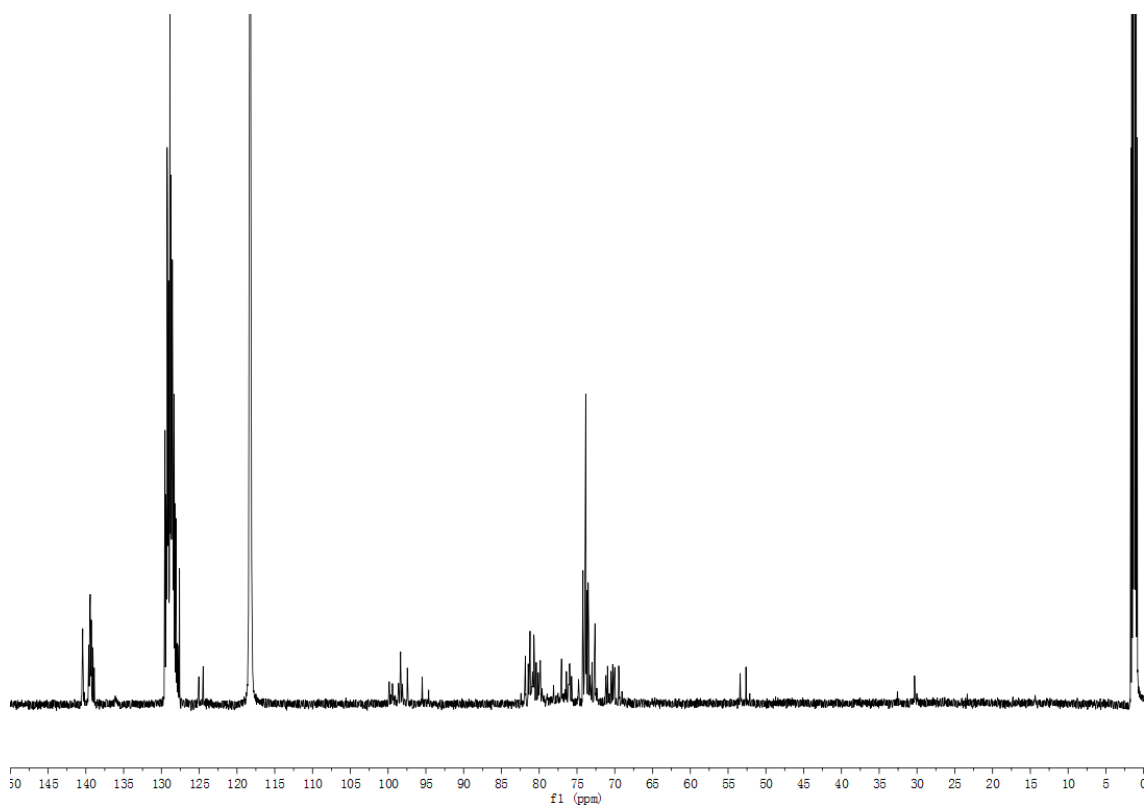
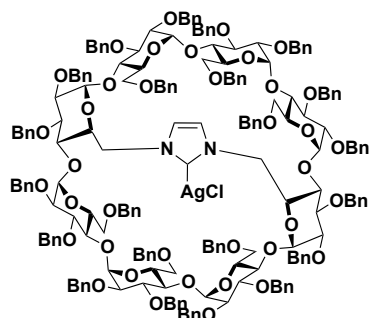


Figure S16: ^{13}C NMR of (γ -A,D-ICyD)HCl 154 (CD_3CN , 151 MHz, 300 K)

(γ -A,E-ICyD)AgCl (155)



Chemical Formula:

$C_{205}H_{213}AgClN_2O_{38}$

Molecular Weight:

3456.20

A mixture of perbenzylated imidazolium (**γ -A,E-ICyD**)HCl **153** (142 mg, 0.042 mmol) and silver(I) oxide (100 mg, 0.42 mmol) was dissolved in anhydrous acetonitrile under a N_2 atmosphere. The reaction mixture was stirred at r.t. overnight. Then the silver oxide was filtered on a celite pad and the residue was washed with acetonitrile, and the solvents were evaporated. Silica gel chromatography of the residue (CyH/ EtOAc: 4:1) gave the silver complex (**γ -A,E-ICyD**)AgCl as white foam (92 mg, 63 %).

1H NMR (600 MHz, CD_3CN): 7.43-7.08 (m, 104H, 104 x H-Ar), 7.03 (t, 4H, 4 x H-Ar), 6.90(t, 2H, 2 x H-Ar), 6.26(s, 2H, 2 x H-Im), 5.63 (d, $^3J_{1,2} = 3.6$ Hz, 2H, 2 x H-1D,H), 5.25-5.24 (m, 4H, 4 x CHPh), 4.95(d, $^3J_{1,2} = 3.2$ Hz, 2H, 2 x H-1A,E), 4.88 (d, $^3J_{1,2} = 3.3$ Hz, 2H, 2 x H-1B,F), 4.86 (d, $^3J_{1,2} = 3.5$ Hz, 2H, 2 x H-1C,G), 3.47 (d, $^2J_{Ph-CHH} = 10.8$ Hz, 2H, 2 x CHPh), 4.73-4.71 (m, 4H, 4 x CHPh), 4.59-4.34 (m, 36H, 34 x CHPh, H-6aA, H-6aE), 4.18-4.16 (m, 4H, 2 x H-3C, G, 2 x H-5A,E), 4.09-4.07 (m, 4H, 2 x H-3D,H, H-6bD, H-6bH), 3.99-3.95 (m, 4H, 4 x H-3A,B,E,F), 3.87-3.53 (m, 24H, 6 x H-5B,C,D,F,G,H, 8 x H-4A,B,C,D,E,F,G,H, 2 x H-2D,H, H-6bA, H-6bE, H-6aC, H-6aG, H-6bC, H-6bG, H-6aD, H-6aH), 3.44 (dd, $^3J_{1,2} = 9.7$ Hz, $^3J_{2,3} = 3.0$ Hz, 2H, 2 x H-2A,E), 3.35 (dd, $^3J_{1,2} = 9.9$ Hz, $^3J_{2,3} = 3.3$ Hz, 2H, 2 x H-2B,F), 3.29 (dd, $^3J_{1,2} = 10.0$ Hz, $^3J_{2,3} = 3.4$ Hz, 2H, 2 x H-2C,G), 3.18 (br d, $^2J = 11.1$ Hz, 2H, H-6aB, H-6aF), 3.01 (d, $^2J = 11.2$ Hz, 2H, H-6bB, H-6bF);

^{13}C NMR (151 MHz, CD_3CN): 141.23(2C), 141.08(2C), 140.64(2C), 139.93(2C), 139.84(2C), 139.74(2C), 139.71(2C), 139.70(2C), 139.68(2C), 139.35(2C), 139.22(2C) (22x C-Ar-quat.), 129.46-127.71 (110x C-Ar-tert.), 99.95(2C), 99.31(2C), 98.82(2C), 94.93(2C) (8 x C-1), 82.69 (2C), 82.05 (2C) (4 x C-4A,C,E,G), 81.95(2C) (2 x C-4D,H), 81.88(2C) (2 x C-3A,E), 81.34(4C) (2 x C-3C,G, 2 x C-2A,E), 81.19(2C), 81.00(2C) (2 x C-3B,F, 2 x C-4B,F), 80.65(4C) (2 x C-3D,H, 2 x C-2B,F), 80.19(2C) (2 x C-2C,G), 78.04 (2C) (2 x C-2D,H), 77.32(2C), 76.99(2C), 74.82(2C), 73.92(2C), 73.90(2C), 73.84(2C), 73.78(2C), 73.68(2C) (16 x Ph- $\underline{C}H_2$), 73.58 (2C) (2 x C-5A,E), 73.43(2C), 73.30(2C), 73.20(2C) (6 x Ph- $\underline{C}H_2$), 72.93(2C) (2 x C-5C,G), 72.39(2C) (2 x C-5B,F), 71.41(2C) (2 x C-5D,H), 70.96(2C), 70.79(2C) (4 x C-6C,D,G,H), 69.33(2C) (2 x C-6B,F), 54.27(2C) (2 x C-6A,E);

$[\alpha]_D^{20} = +31.3$ ($CHCl_3$, $c = 1.0$)

$R_f = 0.43$ (CyH/EtOAc 3:1)

HRMS (ESI): calculated for $C_{205}H_{212}O_{38}N_2Ag$ [M] + 3416.3764, found 3416.3886, err. -3.6 ppm.

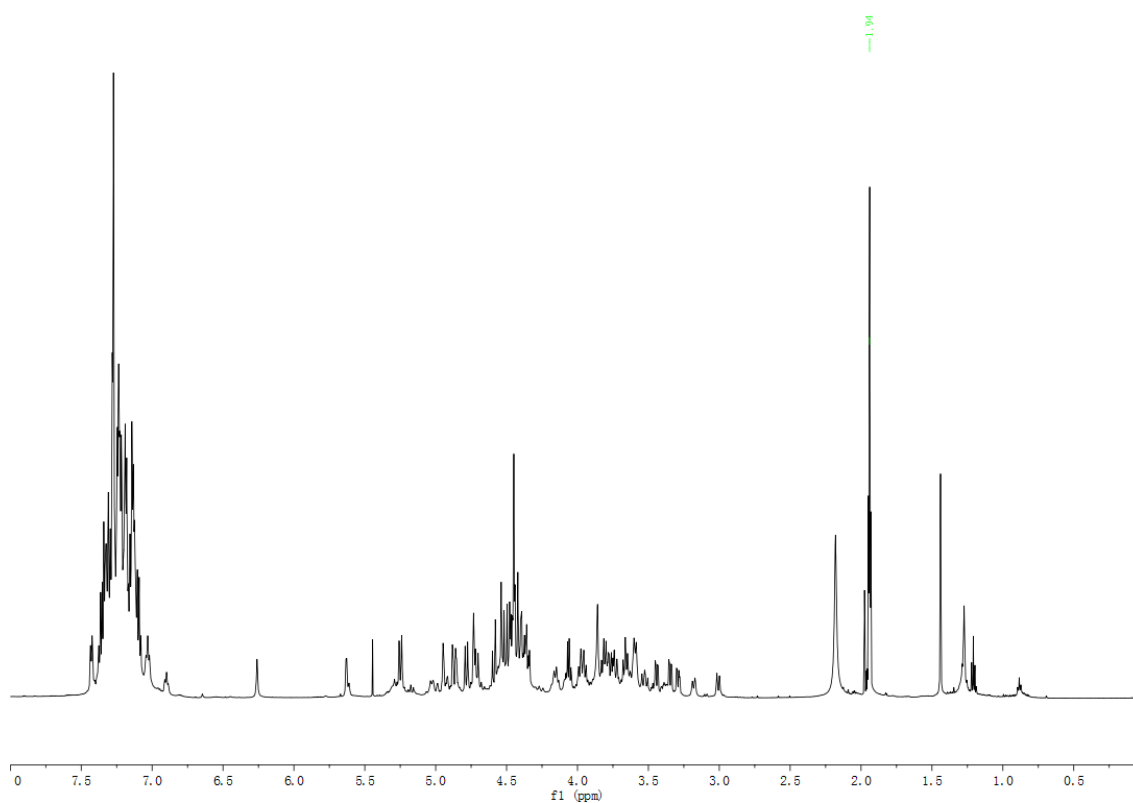


Figure S17: ^1H NMR of $(\gamma\text{-A,E-ICyD})\text{AgCl}$ 155 (CD_3CN , 600 MHz, 300 K)

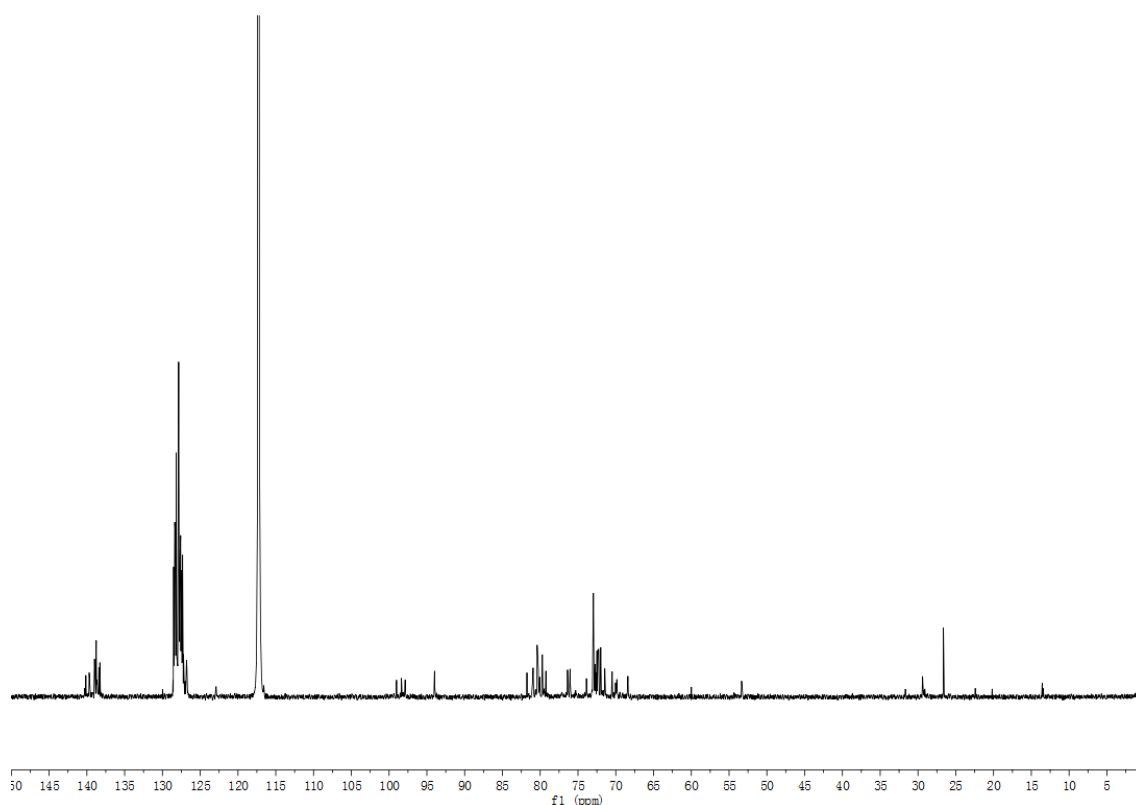
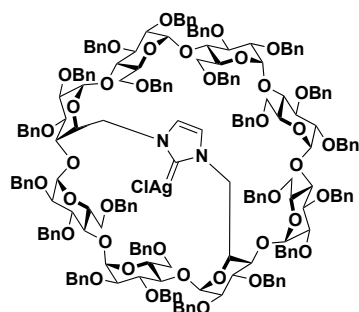


Figure S18: ^{13}C NMR of $(\gamma\text{-A,E-ICyD})\text{AgCl}$ 155 (CD_3CN , 151 MHz, 300 K)

(γ -A,D-ICyD)AgCl (156)



Chemical Formula:

$C_{205}H_{212}AgClN_2O_{38}$

Molecular Weight:

3455.19

A mixture of perbenzylated imidazolium (γ -A,D-ICyD)HCl **154** (250 mg, 0.070 mmol) and silver(I) oxide (250 mg, 0.140 mmol) was dissolved in anhydrous acetonitrile under a N_2 atmosphere. The reaction mixture was stirred at r.t. overnight. Then the silver oxide was filtered on a celite pad and the residue was washed with acetonitrile, and the solvents were evaporated. Silica gel chromatography of the residue (CyH/EtOAc: 4:1) gave the silver complex (γ -A,D-ICyD)AgCl **156** as white foam (118 mg, 45 %).

1H NMR (600 MHz, CD_3CN): 7.46-6.94 (m, 112H, 110 x H-Ar, 2 x H-Im), 5.77 (d, $^3J_{1,2} = 3.38$ Hz, 1H, H-1C), 5.38-5.36 (m, 2H, H-1H, CHPh), 5.18-5.14 (m, 2H, CHPh, H-1D), 5.06 (d, $^3J_{1,2} = 3.5$ Hz, 1H, H-1G), 5.02 (d, $^3J_{1,2} = 3.7$ Hz, 1H, H-1E), 4.98 (d, $^3J_{1,2} = 3.6$ Hz, 1H, H-1F), 4.96 (d, $^2J_{Ph-CHH} = 11.7$ Hz, 1H, CHPh), 4.84-4.82 (m, 3H, CHPh, 2 x H-1A,B), 4.69-4.20 (m, 47H, H-6aA, H-6aD, 3 x H-5 A,D,H, 2 x H-3 B,C, 40 x CHPh), 4.01-3.58 (m, 29H, H-2H, 8 x H-4 A,B,C,D,E,F,G,H, 6 x H-3 A,D,E,F,G,H, 5 x H-5 B,C,E,F,G, H-6bA, H-6bD, H-6aC, H-6bC, H-6aF, H-6aG, H-6bG, H-aH, H-6bH), 3.52-3.43(m, 5H, H-6bF, H-6bE, 3 x H-2A,D,G), 3.36-3.35 (m, 2H, 2 x H-2C,E), 3.32-3.26 (m, 3H, 2 x H-2B,F, H-6aE), 3.05(br d, 1H, H-6aB), 2.90(br d, 1H, H-6bB);

^{13}C NMR (151 MHz, CD_3CN): 140.90, 140.77, 140.71(2C), 140.21, 139.82, 139.78, 139.71, 139.70, 139.67, 139.64, 139.63, 139.61, 139.54, 139.49, 139.45, 139.44, 139.38, 139.31, 139.23, 139.17, 138.14 (22x C-Ar-quat.), 129.42-127.62 (110x C-Ar-tert.), 124.86, 118.72(C-Im), 100.59, 99.12, 99.11, 97.79, 97.75(2C), 97.47, 96.16 (8 x C-1), 83.03(C-3H), 81.96(2C), 81.36(4C), 81.00(4C), 80.73(2C), 80.47(3C)(5 x C-3A,B,C,E,G, 4 x C-4B, D,E,F, 6 x C-2A,B,C,D,E,F,G), 79.64(2C, C-4C, C-2F), 79.09(C-3D), 78.65(C-2C), 78.29(C-3F), 77.35(Ph- $\underline{C}H_2$), 76.52(2C, 2 x C-4G,H), 76.46(Ph- $\underline{C}H_2$), 75.87 (Ph- $\underline{C}H_2$), 75.65(Ph- $\underline{C}H_2$), 75.52(C-4A), 74.93, 74.25, 74.23, 74.15, 74.08, 74.02, 73.81(2C), 73.78(2C), 73.77(3C), 73.74, 73.69(2C), 73.64, 73.55(18 x Ph- $\underline{C}H_2$), 73.50(2C, 2 x C-5), 73.46, 73.36, 73.26, 72.92, 72.69, 72.39, 72.31, 72.18(5 x C-5), 71.19, 70.75, 70.39, 69.90, 69.40, 68.90(6 x C-6B,C,E,F,G,H), 56.74(C-6D), 53.48(C-6A);

$[\alpha]_D^{20} = +38.5$ ($CHCl_3$, $c = 1.0$)

$R_f = 0.43$ (CyH/EtOAc 3:1)

HRMS (ESI): calculated for $C_{205}H_{212}O_{38} N_2AgCl$ $[M+Na]^+$ + 3474.3350, found 3474.3150, err. 5.7 ppm

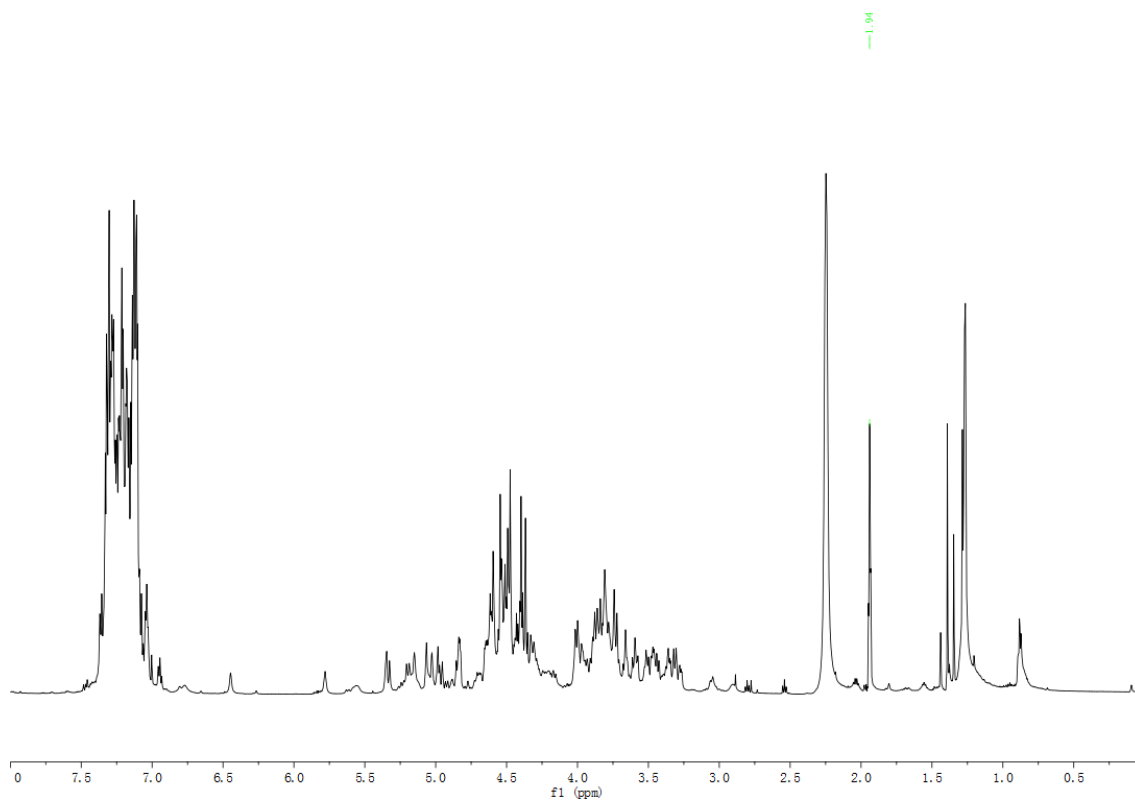


Figure S19: ^1H NMR of $(\gamma\text{-A,D-ICyD})\text{AgCl}$ 156 (CD_3CN , 600 MHz, 300 K)

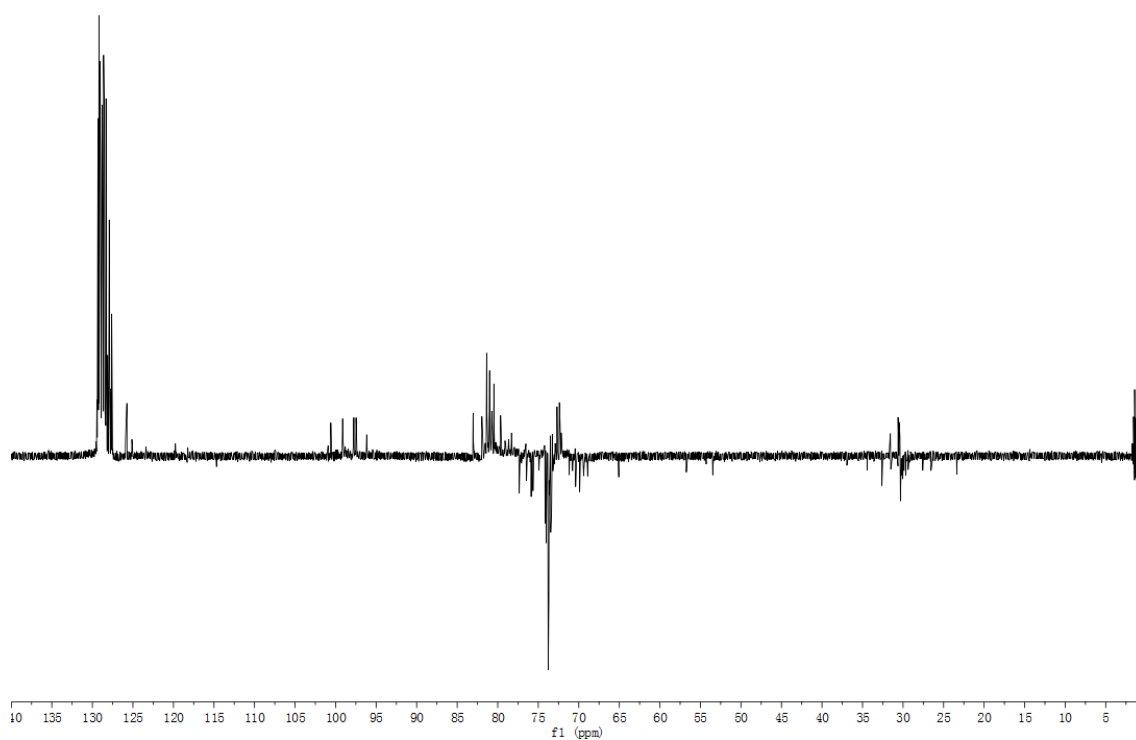
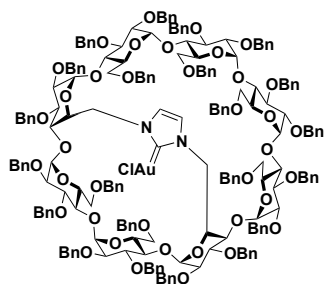


Figure S20: ^{13}C -dept NMR of $(\gamma\text{-A,D-ICyD})\text{AgCl}$ 156 (CD_3CN , 151 MHz, 300 K)

(γ -A,D-ICyD)AuCl 158



Chemical Formula:
 $C_{205}H_{213}AuClN_2O_{38}$
Molecular Weight:
3545.29

A mixture of perbenzylated imidazolium (γ -A,D-ICyD)AgCl 156 (118 mg, 34 μ mol) and Au(Me₂S)Cl (13 mg, 34 μ mol) were dissolved in anhydrous CH₂Cl₂, under nitrogen atmosphere. The reaction was stirred overnight at room temperature for 20 hours. Then, the reaction was filtered on a celite pad and the residue was washed several times with CH₂Cl₂. Then, the reaction mixture was purified in silica gel chromatography (Cyclohexane: Ethyl acetate 2:1) giving the gold complex (γ -A,D-ICyD)AuCl as a white foam (114 mg, 94% yield).

¹H NMR: (CD₃CN, 600MHz): d 7.40-6.85 (m, 112H, 110 x H-Ar, 2 x H-Im), 5.77 (d, *J* = 2.80 Hz, 1H, H-1), 5.33-5.18 (m, 3H, 1 x H-1, 2 x CHPh), 5.15-5.06 (m, 3H, 2 x H-1, 1 x CHPh), 5.04-5.00 (m, 2H, 1 x H-1, 1 x CHPh), 4.93 (d, *J* = 3.43 Hz, 1H, 1 x H-1), 4.85 (d, *J* = 3.45 Hz, 2H, 2 x H-1), 4.75 (d, *J* = 11.2 Hz, 1H, 1 x CHPh), 4.72-4.28 (m, 42H, 1 x H-3, 1 x H-5, 2 x H-6, 38 x CHPh), 4.23-4.16 (m, 4H, 2 x H-5, 1 x H-3, 1 x CHPh), 4.07-3.65 (25H, 6 x H-3, 6 x H-4, 5 x H-5, 8 x H-6), 3.63-3.40 (m, 8H, 4 x H-2, 2 x H-4, 2 x H-6) 3.38-3.22 (m, 6H, 4 x H-2, 2 x H-6), 3.06 (d, *J* = 11.0 Hz, 1H, 1 x H-6), 2.92 (d, *J* = 10.8 Hz, 1H, 1 x H-6);

¹³C NMR: (CD₃CN, 151MHz): d 171.1 (C-Au), 141.5, 141.0, 140.9, 140.8, 140.7, 140.0, 139.8, 139.7, 139.6, 139.5, 139.4, 139.3, 139.3 (22 x C-Ar-quat.), 129.5, 129.4, 129.3, 129.2, 129.1, 129.0, 128.9, 128.8, 128.7, 128.6, 128.5, 128.3, 128.2, 128.2, 128.1, 128.0, 127.8, 128.6 (110 x C-Ar, 2 x C-Im), 100.7 (C-1), 99.0 (3 x C-1), 97.7 (3 x C-1), 96.2 (C-1), 83.1 (C-3), 82.0 (C-2), 81.6, 81.5 (3 x C-3, 2 x C-4), 81.2, 81.1 (1 x C-2, 2 x C-3, 1 x C-4), 80.7 (1 x C-2, 1 x C-3, 1 x C-4), 80.5 (2 x C-2), 79.9 (C-2, C-4), 79.1 (C-3), 78.7 (C-2), 77.7 (C-4), 77.4 (C-4), 76.7, 76.1, 76.0, 75.9, 75.1, 74.1, 73.8, 73.7, 73.6 (21 x Ph-CH₂), 75.6 (C-2), 73.5 (C-4), 73.3 (Ph-CH₂), 73.3 (C-5), 72.8 (C-5), 72.7 (C-5), 72.6 (2 x C-5), 72.4 (C-5), 71.7 (C-5), 71.6 (C-5), 71.2 (C-6), 70.9 (C-6), 70.5 (C-6), 70.0 (C-6), 69.6 (C-6), 69.1 (C-6), 56.0 (C-6), 53.5 (C-6).

HRMS (ESI): calculated for [C₂₀₅H₂₁₂N₂O₃₈AuCl [M+2Na]²⁺: 1794.6956, found 1794.6957 err. 0.05 ppm

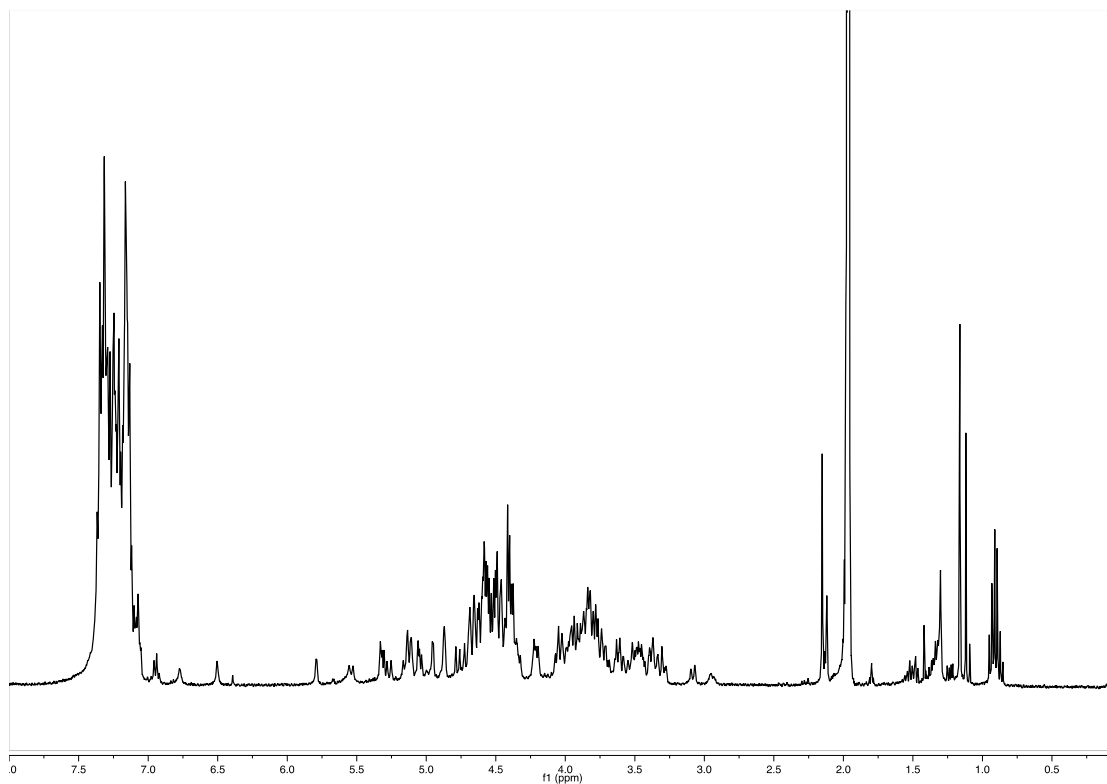


Figure S21: ^1H NMR of $(\gamma\text{-A,D-ICyD})\text{AuCl 158}$ (CD_3CN , 600 MHz, 300 K)

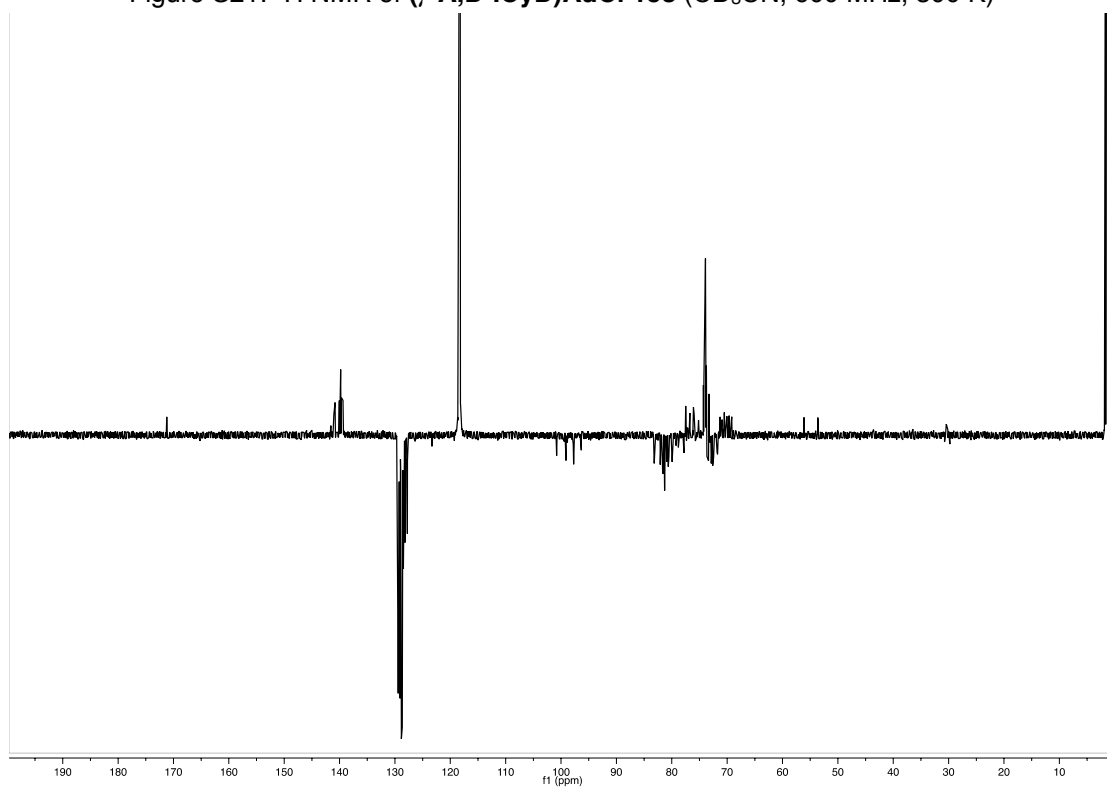
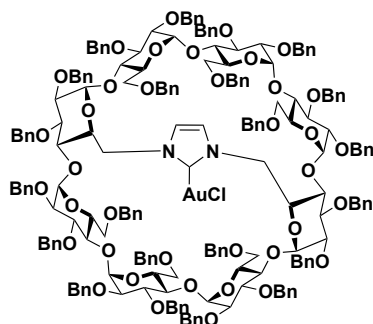


Figure S22: ^{13}C JMod NMR of $(\gamma\text{-A,D-ICyD})\text{AuCl 158}$ (CD_3CN , 151 MHz, 300 K)

(γ -A,E-ICyD)AuCl (157)



Chemical Formula:

$C_{205}H_{213}AuClN_2O_{38}$

Molecular Weight:

3545.29

A mixture of perbenzylated imidazolium (γ -A,E-ICyD)AgCl 155 (150 mg, 61 mmol) and Au(Me₂S)Cl (13 mg, 61 mmol) were dissolved in anhydrous CH₂Cl₂, under nitrogen atmosphere. The reaction was stirred overnight at room temperature for 20 hours. Then, the reaction was filtered on a celite pad and the residue was washed several times with CH₂Cl₂. Then, the reaction mixture was purified in silica gel chromatography (Cyclohexane: Ethyl acetate 2:1) giving the gold complex (γ -A,E-ICyD)AgCl 157 as a white foam (143mg, 93% yield).

¹H NMR (CD₃CN, 400MHz): d 7.43-7.06 (m, 104H, 104 x H-Ar), 6.93 (t, 4H, ³J_{o,m} = ³J_{m,p} = 7.6 Hz, 4 x H-*m*-Ar), 6.79 (t, 2H, ³J_{m,p} = 7.41 Hz, 2 x H-*p*-Ar), 6.36 (s, 2H, 2 x N-CH=CHN), 5.64 (d, ³J_{1,2} = 3.6 Hz, 2H, 2 x H-1D,H), 5.39 (d, ²J = 11.3Hz, 2H, 2 x CHPh), 5.27 (d, ²J=11.7Hz, 2H, 2 x CHPh), 5.21 (d, ²J = 11.1Hz, 2H, 2 x CHPh), 6.06 (d, ²J = 11.3 Hz, 2H, 2 x CHPh), 4.92 (d, ³J_{1,2} = 3.6Hz, 2H, 2 x H-1A,E), 4.87 (d, ³J_{1,2} = 3.6Hz, 2H, 2 x H-1B,F), 4.83 (d, ³J_{1,2} = 3.6Hz, 2H, 2 x H-1C,G), 4.80-4.27 (m, 40H, 2 x H-5A,E, 2 x H-6A,E, 36x CHPh), 4.22-4.05 (m, 6H, 2 x H-6D,H, 2 x H-3C,G, 2 x H-3D,H), 3.98-3.76 (m, 14H, 2 x H-3A,E, 2 x H-3B,F, 2 x H-4B,F, 2 x H-5C,G, 4 x H-6C,G, 2 x H-4D,H), 3.74-3.59 (m, 6H, 2 x H-5B,F, 2 x H-4C,G, 2 x H-6D,H), 3.57-3.48 (m, 4H, 2 x H-5D,H, 2 x H-4A,E), 3.47-3.40 (m, 6H, 2 x H-6A,E, 2 x H-2A,E, 2 x H-2D,H), 3.34 (dd, 2H, ³J_{2,3} = 9.6 Hz, ³J_{2,1} = 3,3 Hz, 2 x H-2B,F), 3.31-3.20 (m, 4H, 2 x H-2C,G, 2 x H-6B,F), 3.05 (d, 1H, ²J=11.2 Hz, 2 x H-6B,F);

¹³C NMR (CD₃CN, 100MHz): d 172.2 (C-Au), 141.4 (2C), 141.0 (2C), 140.8 (2C), 140.9 (2C), 140.7 (2C), 139.9 (2C), 139.8 (2C), 139.77 (2C), 139.7 (2C), 139.3 (2C), 139.2(2C) (22 x C-Ar-quat.), 129.5, 129.4, 129.3, 129.2, 129.1, 129.0, 129.0, 128.9, 128.8, 128.7, 128.6, 128.6, 128.5, 128.4, 128.2, 128.1, 127.9, 127.8, 127.6 (110 x C-Ar-tert), 99.7 (2 x C-1C,G), 99.2 (2 x C-1B,F), 98.7 (2 x C-1A,E), 94.9 (2 x C-1D,H), 82.7 (2 x C-4C,G), 82.4 (2 x C-4D,H), 82.1(2 x C-3A,E), 81.8 (2 x C-3D,H), 81.5 (2 x C-3B,F), 81.2 (4C, 2 x C-4B,F, 2 x C-3C,G), 80.9 (2 x C-2A,E), 80.6 (2 x C-2B,F), 80.31 (2 x C-2C,G), 79.3 (2 x Ph-CH₂), 79.0 (2 x Ph-CH₂), 78.9 (2 x C-2D,H), 78.9 (2 x Ph-CH₂), 78.7 (2 x Ph-CH₂), 78.6 (2 x Ph-CH₂), 78.3 (2 x Ph-CH₂), 77.6 (2 x Ph-CH₂), 77.0 (2 x Ph-CH₂), 76.9 (2 x Ph-CH₂), 74.8 (2 x Ph-CH₂), 74.0 (6 x Ph-CH₂), 73.9 (6 x Ph-CH₂), 73.7 (2 x Ph-CH₂), 73.5 (2 x Ph-CH₂), 73.4 (2 x Ph-CH₂), 73.3 (2 x Ph-CH₂), 73.3 (2 x C-4A,E), 73.2(2 x Ph-CH₂), 73.0 (2 x C-5C,G), 72.4 (2 x C-5B,F), 72.3 (2 x C-5A,E), 71.9 (2 x C-5D,H), 71.1 (2 x C-6C,G), 70.9 (2 x C-6D,H), 69.4 (2 x C-6B,F), 54.2 (2 x C-6A,E)

Rf=0.36 (CyH:AcOEt 3:1)

HRMS (ESI): calculated for C₂₀₅H₂₁₂N₂O₃₈AuClNa₂ [M+2Na]²⁺ : 1794.6956, found: 1794.6959 err. 0.16ppm

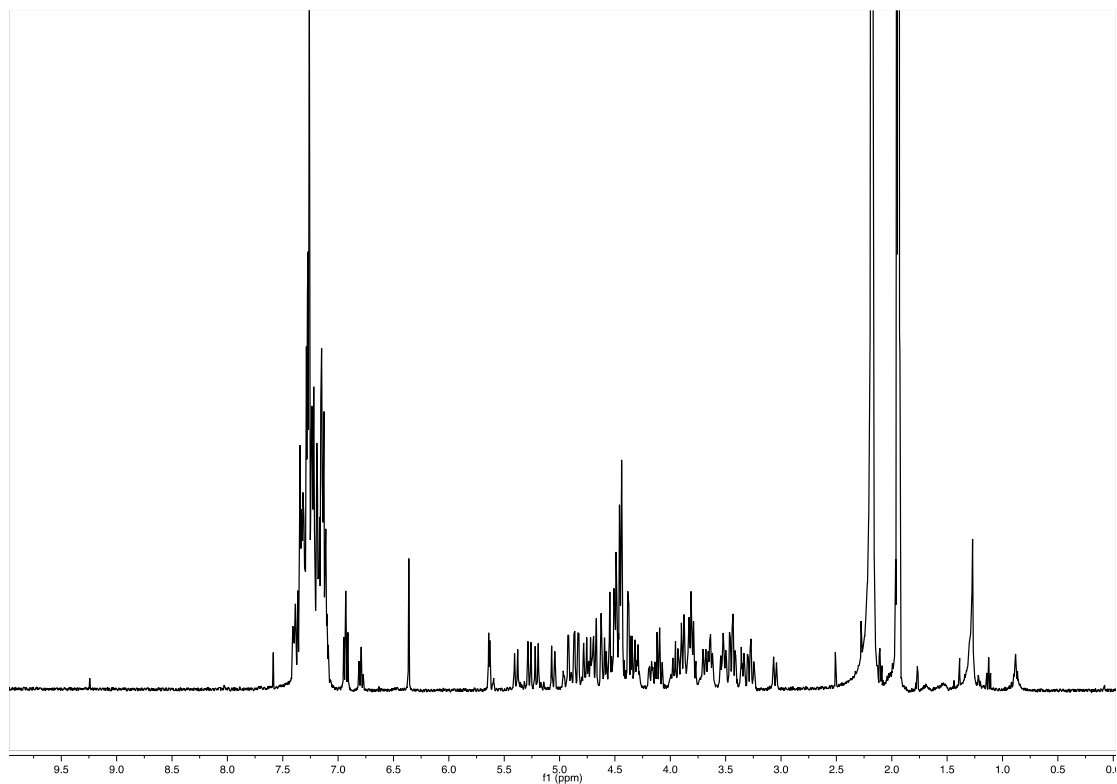


Figure S23: ^1H NMR of (γ -A,E-ICyD)AuCl 157 (CD_3CN , 400 MHz, 300 K)

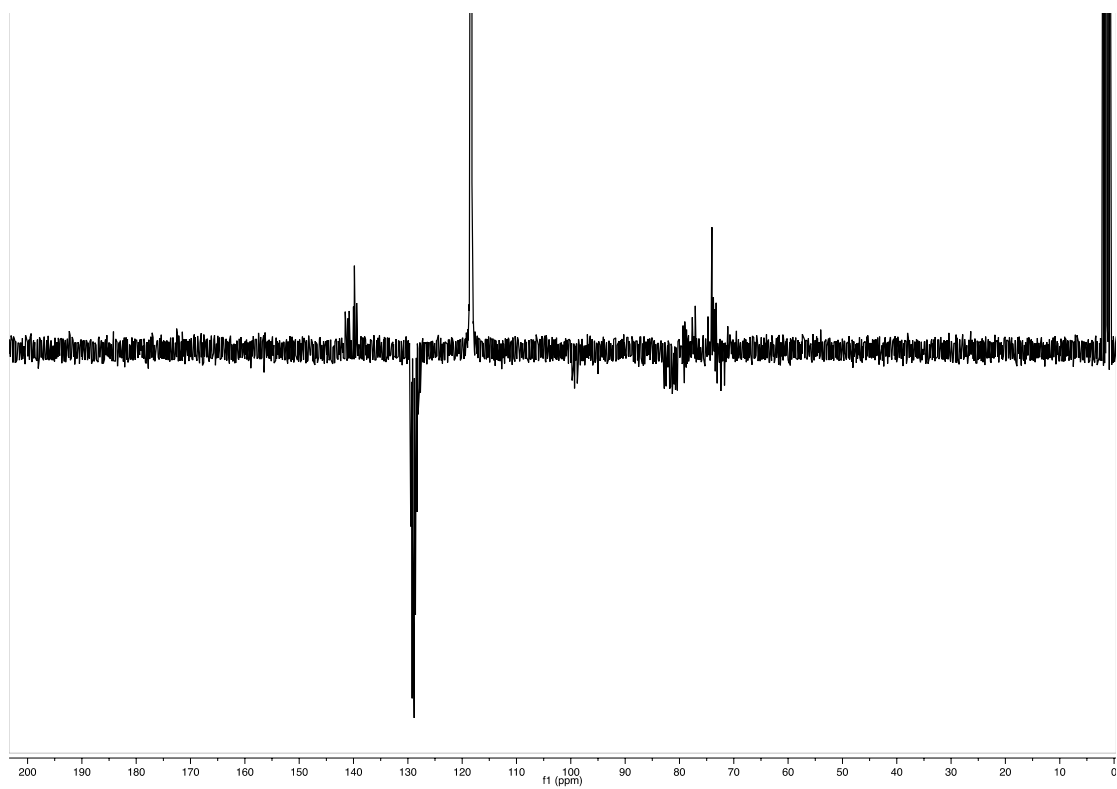
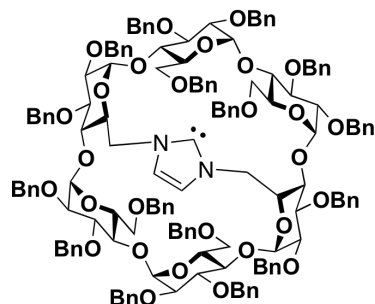


Figure S24: ^{13}C JMod NMR of (γ -A,E-ICyD).AuCl (CD_3CN , 100 MHz, 300 K)

Free (α -ICyD) (159)



Chemical Formula:

$C_{151}H_{156}N_2O_{28}$

Molecular Weight:

2446.91

Under an argon atmosphere, (α -ICyD)HCl **122** (100mg, 40,3 μ mol) was dissolved in THF (2 mL). Then, KH (30% in oil, 27,5 mg, 201 μ mol, 5eq) was added stepwise and the reaction mixture was stirred overnight at room temperature. The crude mixture was directly filtrated over celite and washed with freshly distilled THF. The solvent was evaporated under reduced pressure at 40°C affording the free carbene **159** as a yellow-orange foam without any further purification.

1H NMR (400 MHz, C_6D_6) δ = 7.66 – 7.59 (m, 4H, H-*o*-Ar), 7.43 – 7.33 (m, 9H, H-Ar), 7.30 – 6.87 (m, H_{Ar}), 6.43 (s, 2H, 2xN-CH=C-N), 5.98 (d, $^3J_{1,2}$ = 3.6 Hz, 2H, 2 x H-1C,F), 5.84 (d, $^2J_{Ph-CHH}$ = 10.7 Hz, 2H, 2 x PhCHH), 5.76 (t, $^3J_{5,4}$ = $^3J_{5,6}$ = 9.8 Hz, 2H, 2 x H-5A,D), 5.27 – 5.19 (m, 4H, 2 x PhCHH, 2 x H-1A,D), 5.19 – 5.06 (m, 4H, 4 x PhCHH), 5.04 (d, $^2J_{Ph-CHH}$ = 11.1 Hz, 2H, 2 x PhCHH), 4.90 (d, $^2J_{Ph-CHH}$ = 11.7 Hz, 2H, 2 x PhCHH), 4.82 (d, $^2J_{Ph-CHH}$ = 13.4 Hz, 2H, 2 x PhCHH), 4.76 (d, $^2J_{6a,6b}$ = 13.50 Hz, 2H, 2 x H-6A,D) 4.66 (d, $^3J_{1,2}$ = 3.5 Hz, 2H, 2 x H-1B,E), 4.58 (dd, 3J = 9.7, 3J = 7.8 Hz, 2H, 2 x H-3A,E), 4.50 – 4.14 (m, 20H, 12 x PhCHH, 2 x H-3B,E, 2 x H-4C,F, 2 x H-5C,F, 2 x H-5B,E), 4.07 (d, $^2J_{6a,6b}$ = 10.2 Hz, 2H, 2 x H-6C,F), 3.98 (dd, $^2J_{H6a-H6b}$ = 10.3 Hz, $^3J_{5,6}$ = 5.1 Hz, 2H, 2 x H-6C,F), 3.94 – 3.76 (m, 10H, 2xPhCHH, 2 x H-4A,D, 2 x H-4B,E, 2xH-6B,E, 2 x H-3C,F), 3.66 (dd, $^2J_{6a,6b}$ = 13.6 Hz, $^3J_{6,5}$ = 9.4 Hz, 2H, H-6A,D), 3.62 – 3.48 (m, 6H, 4xPhCHH, 2 x H-2A,D, 2 x H-2B,E), 3.43 (dd, $^3J_{2,3}$ = 9.8 Hz, $^3J_{2,1}$ = 3.6 Hz, 2H, H-2C,F), 3.32 (d, $^2J_{Ph-CHH}$ = 11.0 Hz, 2H, 2 x H-2B,E).

^{13}C NMR (101 MHz, C_6D_6) δ = 212.42 ($C_{carbene}$), 140.7, 140.6, 140.5, 139.5, 139.4x2, 139.3, 138.5 (16 C_{ipso}), 128.6-126.34(CH Ar), 120.3 (2xN-CH=CH-N), 99.0 (2xC-1A,D), 98.4 (2xC-1B,E), 98.1 (2xC-1C,F), 82.9 (2xC-4B,E), 82.6 (2xC-3A,D), 82.03(2xC-4C,F), 81.7 (2xC-3B,E), 81.1 (2xC-2A,D), 80.7 (2xC-3C,F), 80.2 (2xC-2B,E), 78.6 (2xC-2C,F), 77.43 (2xC-4A,D), 75.60, 74.32 (4xCH₂Ph), 74.18 (2xC-5C,F), 73.79 (2xCH₂Ph), 73.61 (2xC-5B,E), 73.55, 73.44, 72.17, 71.78 (8xCH₂Ph), 71.65 (2xC-5A,D), 69.40 (2xC-6C,F), 67.83 (2xC-6B,E), 54.78 (2xC-6A,D).

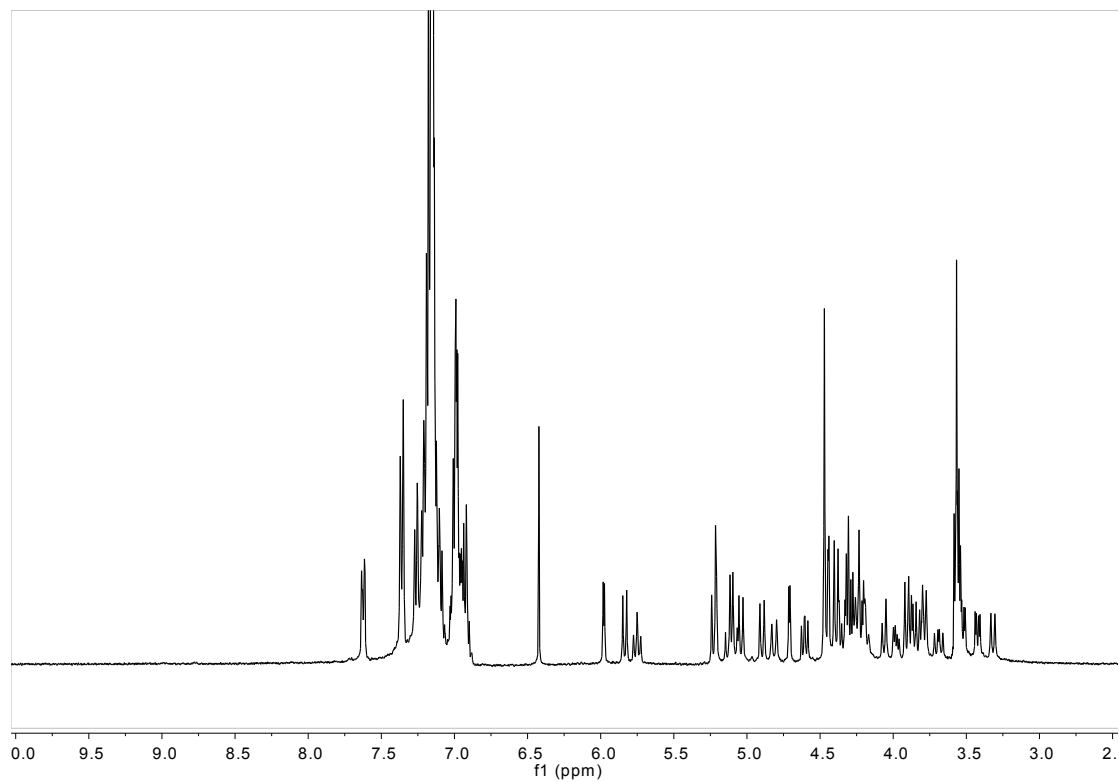


Figure S25: ^1H -NMR of α -ICyD 159. (C_6D_6 , 400 MHz, 300 K)

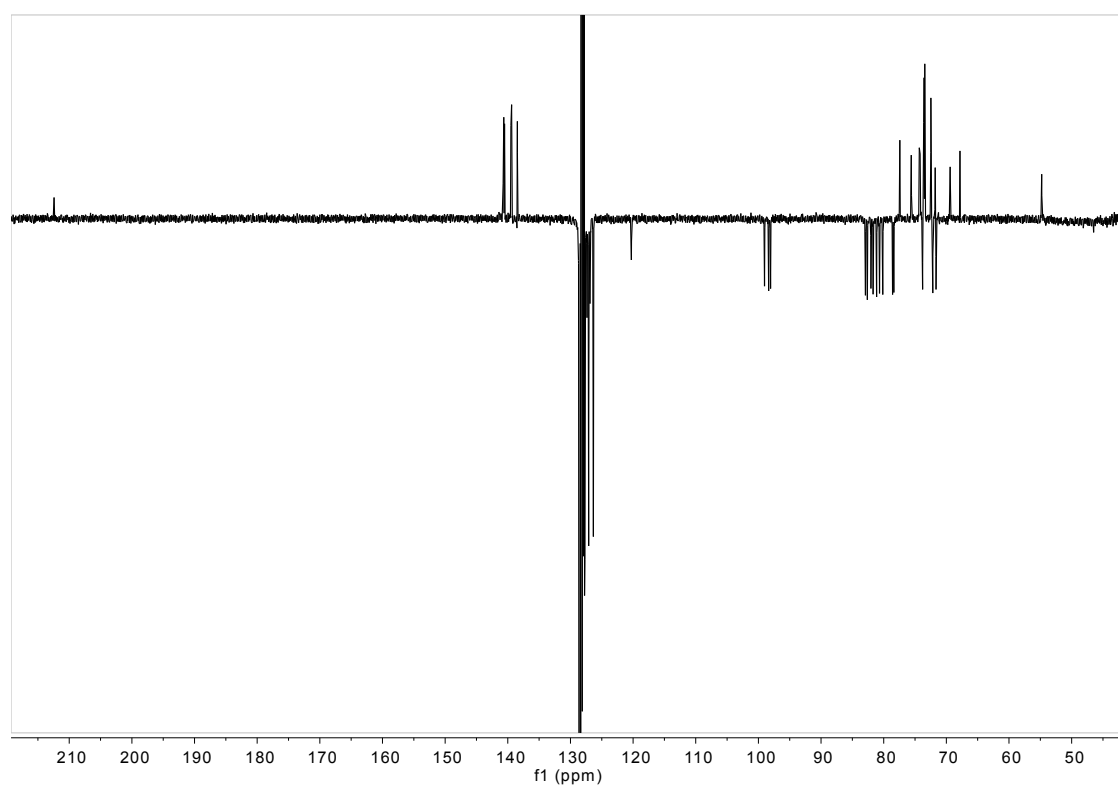


Figure S26: ^{13}C -NMR of α -ICyD 159. (C_6D_6 , 101 MHz, 300 K)

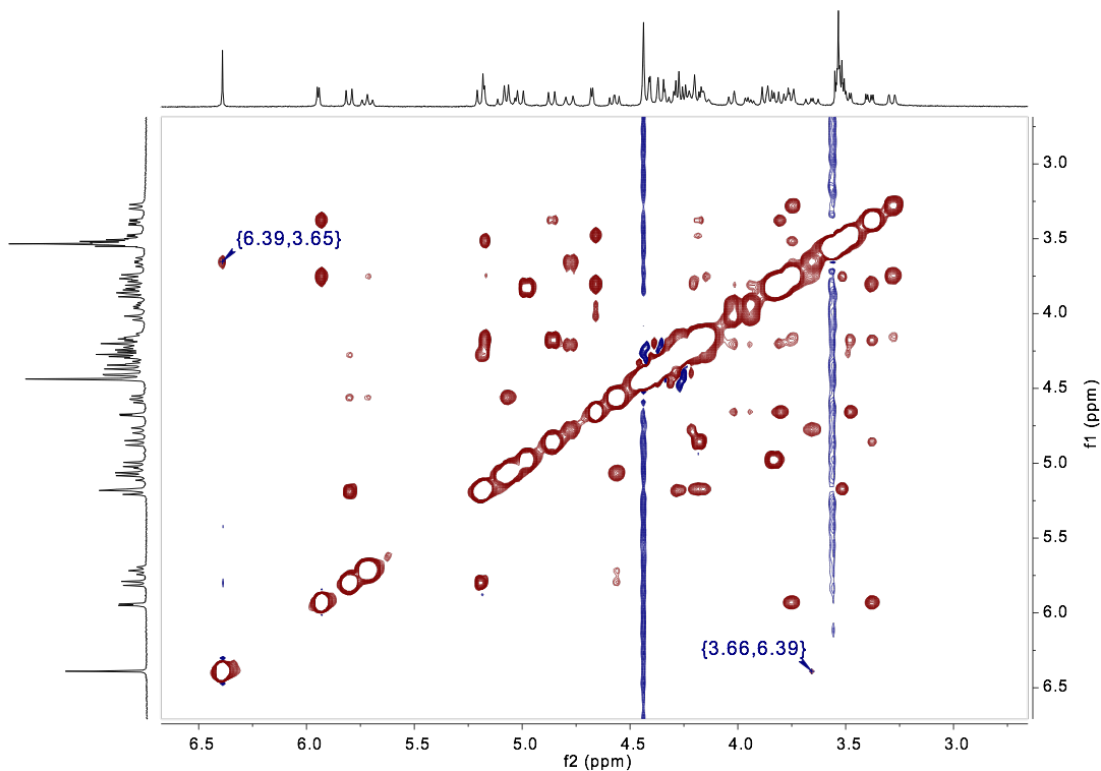
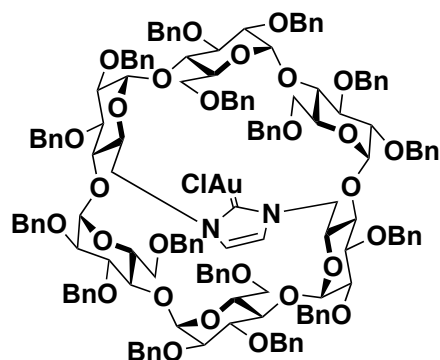


Figure S27: Extract of NOESY Spectrum of α -ICyD 159 showing the cross correlations between H_{NHC} and H-6A,D.

Cycle A	H	C	Cycle B	H	C	Cycle C	H	C
1	5.17	99.01	1	4.66	98.43	1	5.93	98.10
2	3.53	81.1	2	3.48	80.2	2	3.38	78.6
3	4.58	82.6	3	4.29	81.7	3	3.82	80.7
4	3.76	77.43	4	3.82	82.9	4	4.21	82.03
5	5.73	71.65	5	4.15	71.65	5	4.21	73.6
6	3.64		6	3.30		6	3.94	
6'	4.78	54.84	6'	3.77	69.36	6'	4.02	71.9

TableS1: Attribution of the protons of the sugar units of α -ICyD 159

(α -rev-ICyD)AuCl + (α -ICyD)AuCl (160 + 127)



Chemical Formula:

$C_{151}H_{156}AuClN_2O_{28}$

Molecular Weight:

2679.27

In a sealed tube, (α -ICyD) (100 mg, 40 μ mol), Au(Me₂S)Cl (12mg, 40 μ mol) and K₂CO₃ (87mg, 560 μ mol) were dissolved in CH₂Cl₂ (1mL). The reaction mixture was stirred at room temperature for 18h. The solvent was evaporated and the product is filtered by a small silica gel pad CyH : AcOEt 3:1 affording a 77:23 mixture of (α -rev-ICyD)AuCl and (α -ICyD)AuCl as a white foam (87 mg, 81 % yield).

¹H-NMR / ¹³C-NMR

R_f=0.47 (CyH:AcOEt 3:1)

Cycle A	H	C	Cycle B	H	C	Cycle C	H	C
1	4.52	96.73	1	4.57	99.9	1	5.62	99.25
2	3.40	80.69	2	3.30	78.3	2	3.67	77.86
3	4.08	82.37	3	3.78	Overlapped	3	3.80	82.368
4	3.77	80.84	4	Overlap ped	Overlapped	4	3.84	
5	4.54	69.13	5	Overlap ped	Overlapped	5	2.91	71.6
6	4.07		6	3.79		6	3.89	
6'	4.54	53.76	6'	3.68	68.76	6'	3.23	69.1

Table S2: Attribution of the protons of the sugar units of **160**

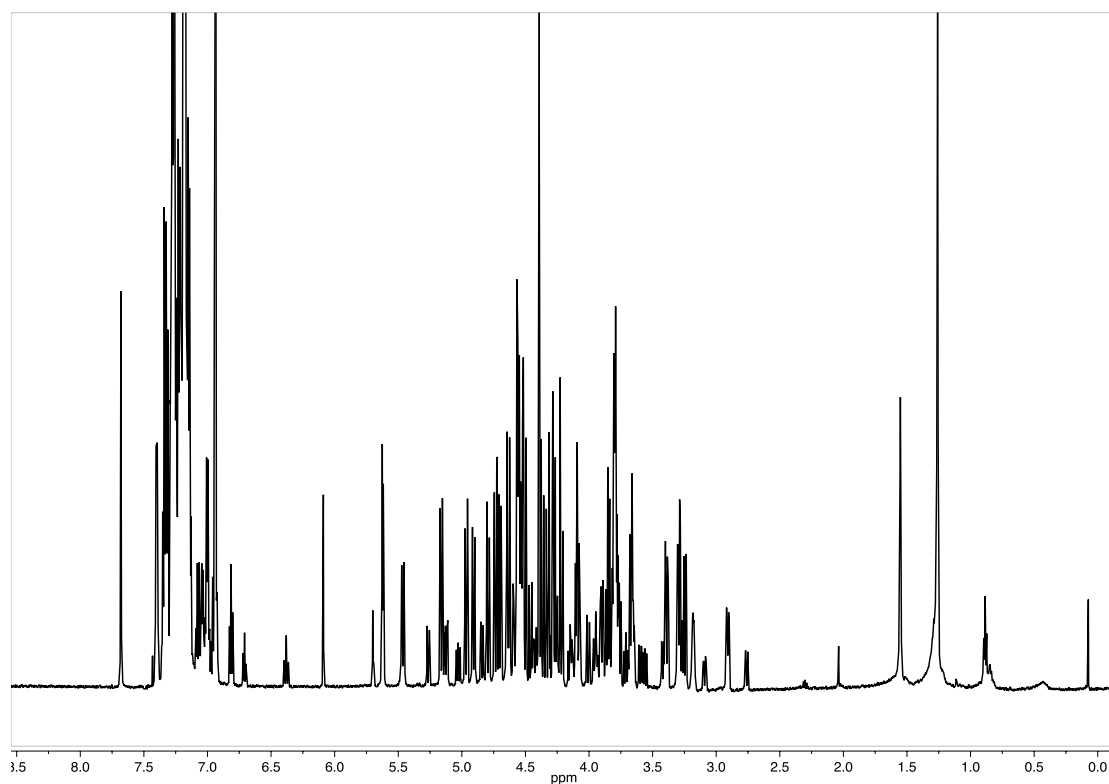


Figure S28: ¹H-NMR of the 77:23 mixture of **160:127** (CDCl₃, 600 MHz, 300 K)

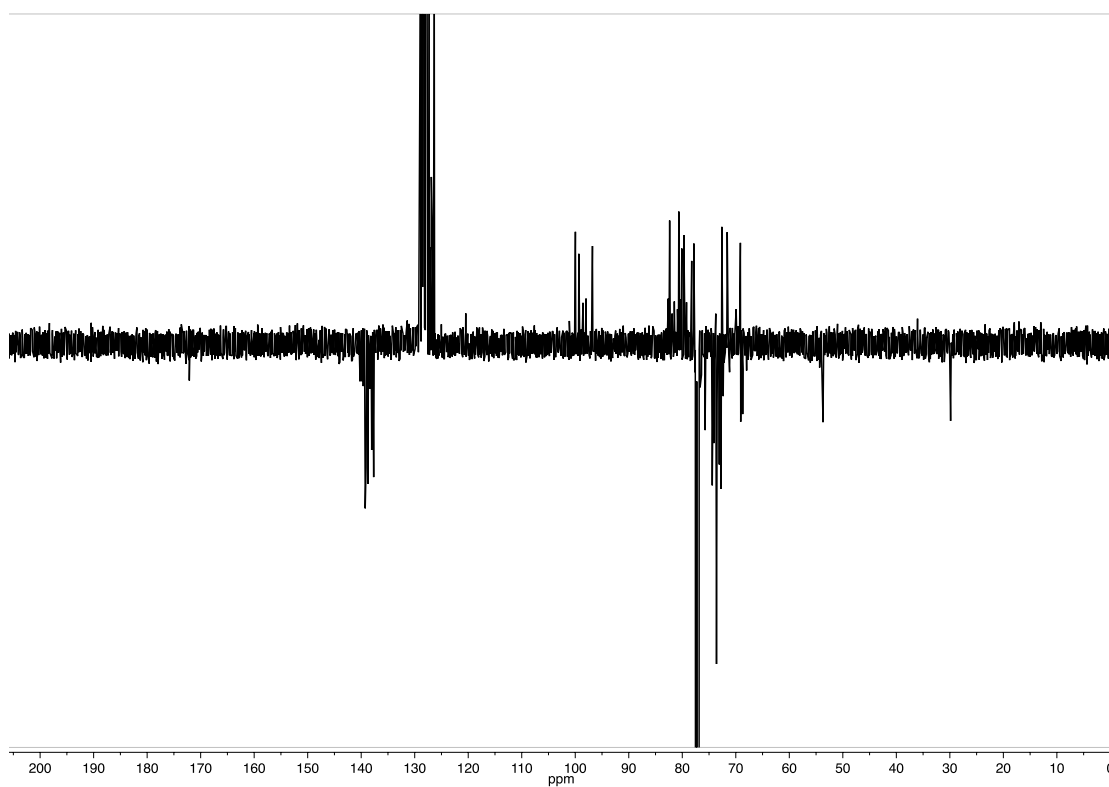


Figure S29: ¹³C-Jmod of the 77:23 mixture of **160:127** (CDCl₃, 600 MHz, 300 K)

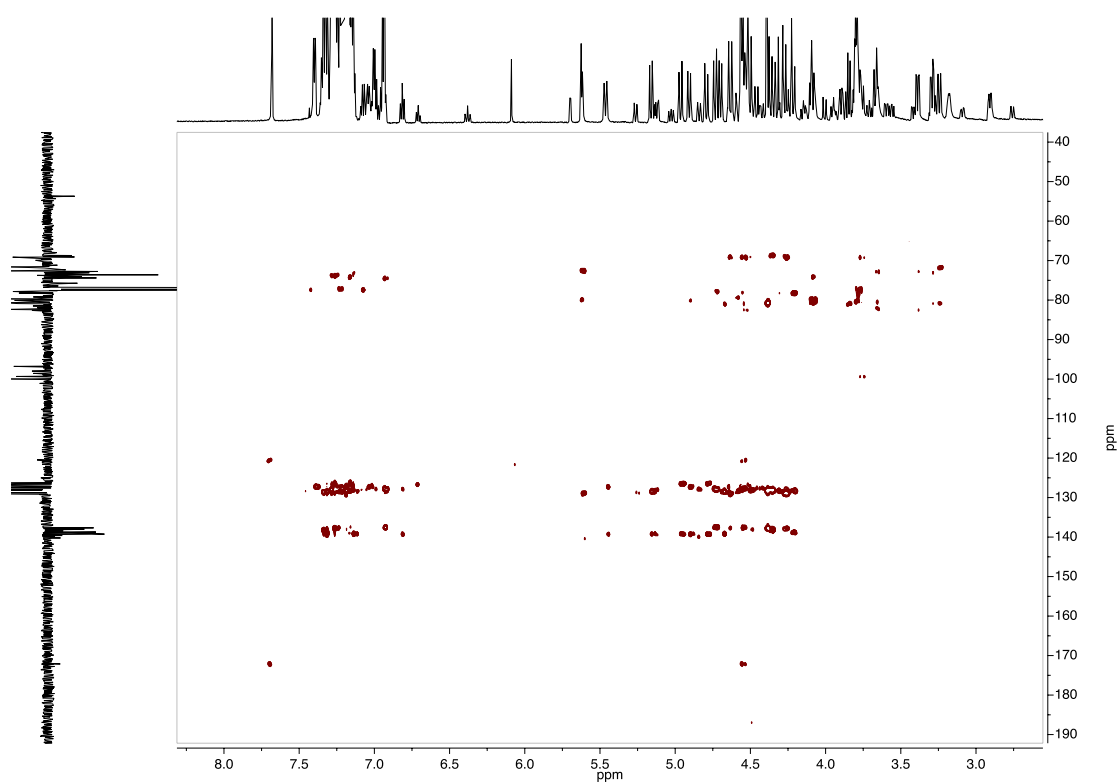
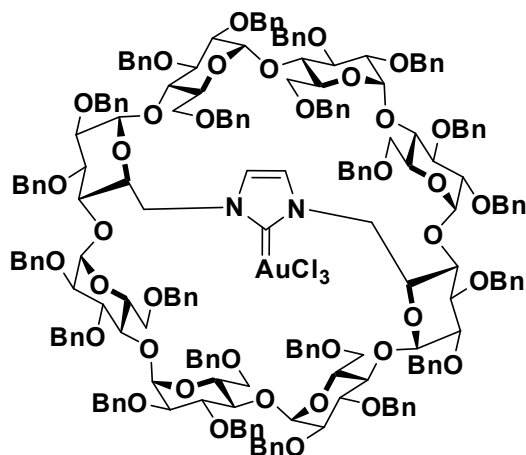


Figure S30: HMBC of the 77:23 mixture of **160:127** (CDCl_3 , 300 K)

Cycle A	H	C	Cycle B	H	C	Cycle C		
							H	C
1	4.52	96.73	1	4.57	99.9	1	5.62	99.25
2	3.40	80.69	2	3.30	78.3	2	3.67	77.86
3	4.08	82.37	3	3.78	Overlapped	3	3.80	82.368
4	3.77	80.84	4	Overlapped	Overlapped	4	3.84	
5	4.54	69.13	5	Overlapped	Overlapped	5	2.91	71.6
6	4.07	53.76	6	3.79	68.76	6	3.89	69.1
6'	4.54		6'	3.68		6'	3.23	

Table S2: Attribution of the protons of the sugar units of **160**

(γ -ICyD)AuCl₃ (161)



Chemical Formula:

C₂₀₅H₂₁₂AuCl₃N₂O₃₈

Molecular Weight:

3615.24

(γ -ICyD)AgCl 155 (55 mg, 18 μ mol) and gold(I) chloride (35.5 mg, 90 μ mol, 8eq) were weighed in a sealed tube and purged with Ar. Then, dry MeCN (2mL) was added. The reaction mixture was stirred at room temperature for 18h. The reaction mixture is evaporated under reduced pressure and charged directly in the column, CyH:EtOAc 5:1 to 4:1 recovering the (γ -ICyD)AuCl₃ **161** complex (22mg, 38%) as a white foam

¹H-NMR(chloroform-d, 600MHz): 7.45 - 7.00 (m, C-H_{Arom}), 6.81 (t, 2H, 2x C-H_{para}), 6.03 (s, 2H, 2 x N-CH=CH-N), 5.69, (d, ²J_{1,2} = 4.1 Hz, 2H, 2 x H-1D,H), 5.43 (d, ²J_{CHHPH} = 11.4 Hz, 2H, 2 x PhCHH), 5.29 (d, ²J_{CHHPH}, 4H, 4 x PhCHH), 5.16 (dd, ²J_{6A,6B} = 14.2 Hz, ³J_{6a,5} = 2.4 Hz, 2H, 2 x H-6A,E), 5.12 (d, ²J_{CHHPH} = 11.7 Hz, 2H, 2 x PhCHH), 4.84 - 4.78 (m, 8H, 6 x PhCHH, 2 x H-1C,F), 4.75 - 4.69 (m, 6H, 2 x PhCHH, 2 x H-1A,E, 2 x H-1B,F), 4.61 (d, ²J_{CHHPH} = 11.5 Hz, 2H, 2 x PhCHH), 4.67 - 4.22 (m, 32H, 2 x H-5A,E, 2 x H-3D,H, 28 x PhCHH), 4.16 (dd, 2H, ²J_{6a,6b} = 11.3Hz, ³J_{6a,5}=4.5Hz, 2 x H-6C,G, 2 x H-6D,H), 4.04 (m, 2H, 2 x H-3C,G) 3.97 - 3.82 (m, 12H, 2 x H-3A,E, 2 x H-6C,G, 2 x H-3B,F, 2 x H-5C,G, 2 x H-6D,H, 2 x H-4D,H), 3.77 - 3.75 (m, 4H, 2 x H-4B,F, 2 x H-5B,F), 3.69 (dd, ²J_{6a-6b} = 10.55 Hz, ³J_{6a,5} = 5.4 Hz, 2H, 2 x H-6C,G), 3.59 (d, 2H, ³J_{4,5} = ³J_{4,3} = 9.2Hz, 2 x H-4C,G), 3.56 - 3.48 (m, 6H, 2 x H-2D,H, 2 x H-4A,E, 2 x H-5D,H), 3.39 - 3.34 (m, 4H, 2 x H-2C,G, 2 x H-2B,F), 3.32 - 3.30 (m, 4H, 2 x H-2A,E, 2 x H-6A,/E) 3.05 (dd, 2H, ²J_{6a-6b} = 10.8 Hz, 2 x H-6B,F), 2.89 (dd, 2H, ²J_{6a-6b} = 11.0 Hz, 2 x H-6B,F).

¹³C-NMR: (151 MHz, Chloroform-d) δ = 145.4 (C=Au^{III}), 140.6 - 138.2 (C_{ipso}), 128.7 - 124.9 (CH_{Arom}), 124.5 (C_{imid}), 99.4 (C-1B/F), 98.9 (C-1C/G), 98.3 (C-1A/E), 94.7 (C-1D/H), 82.5 (C-4C/G), 82.0 (C-4D/H), 80.8 (C-3A/E, C-3C/G), 80.3 (C-2A/E, C-4B/F), 80.0 (C-3B/F), 79.6 (C-3D/H), 79.0 (C-2B/F or C-2C/G), 78.7 (C-2B/F or C-2C/G), 77.5 (C-2D/H), 77.0 (CH₂Ph), 76.9 (CH₂Ph), 76.7 (CH₂Ph), 76.0 (2 x CH₂Ph), 74.0 (CH₂Ph), 73.7 (CH₂Ph), 73.4 (CH₂Ph), 73.0 (CH₂Ph), 73.0 (H-5D/H), 72.6 (CH₂Ph), 72.3 (CH₂Ph), 72.2 (CH₂Ph), 72.1 (C-5C/G), 71.2 (C-4A/E), 71.0 (C-5B/F), 70.9 (C-5A/E), 70.7 (C-6C/G), 70.0 (C-6D/H), 68.7 (C-6B/F), 53.1 (C-6A/E).

Rf: 0.37 (CyH : AcOEt 3 : 1)

HRMS (ESI): calculated for C₂₀₅H₂₁₂AuCl₃N₂O₃₈NaK [M+Na+K]²⁺ 1836.6486 found 1836.6430 err 3.1 ppm

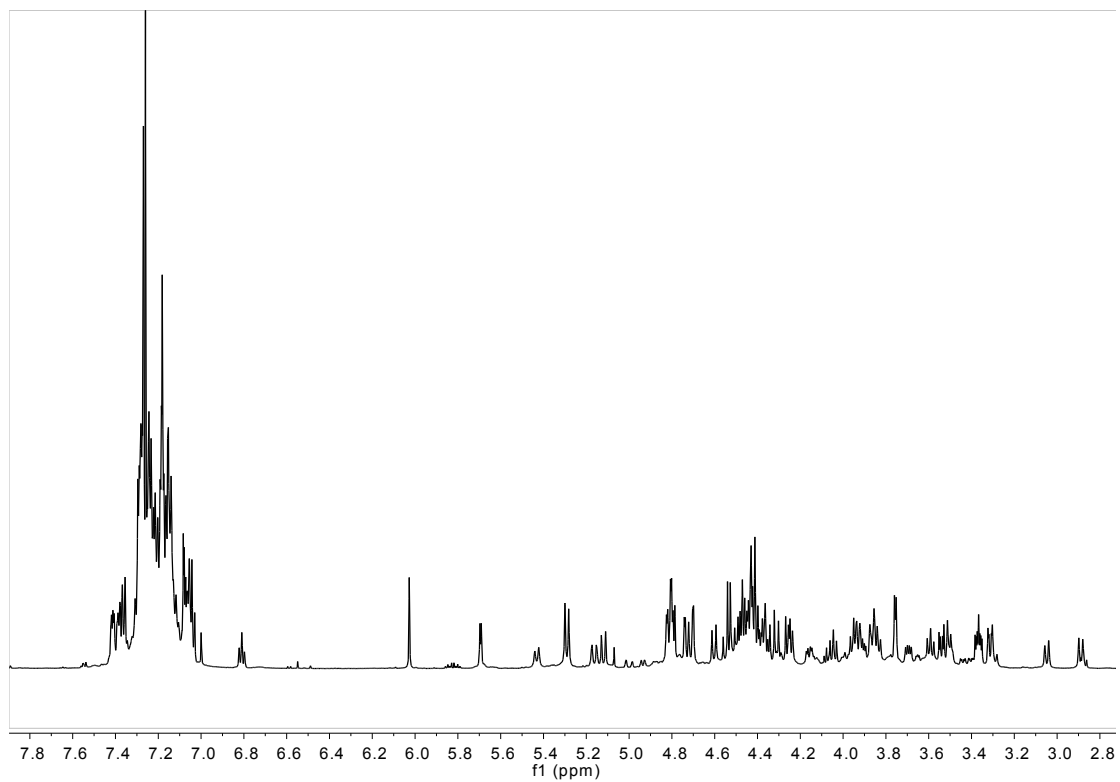


Figure S31: $^1\text{H-NMR}$ of $(\gamma\text{-ICyD})\text{AuCl}_3$ **161** (CDCl_3 , 600 MHz, 300 K)

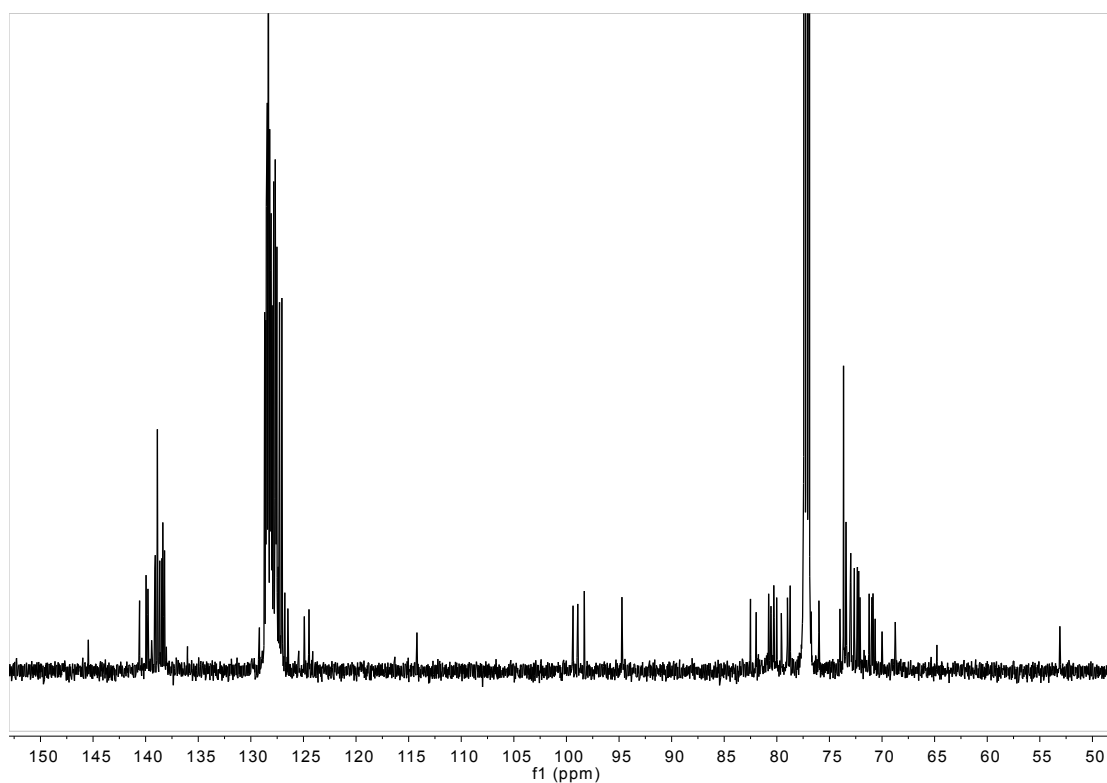


Figure S32: $^{13}\text{C-NMR}$ of $(\gamma\text{-ICyD})\text{AuCl}_3$ **161** (CDCl_3 , 151 MHz, 300 K)

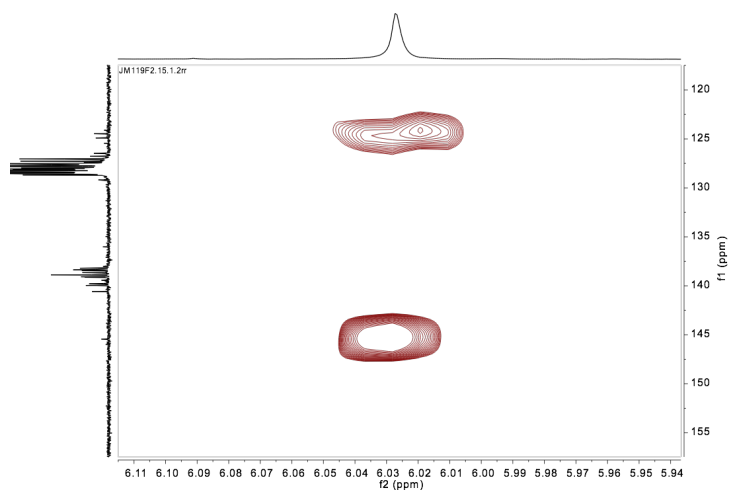


Figure S34: Extract of HMBC of **161** showing the cross correlation between the CH_{NHC} and the C=Au (CDCl₃, 300 K)

Cycle A/E	H/ ppm	C/ ppm	Cycle B/F	H/ ppm	C/ ppm	Cycle C/G	H/ ppm	C/ ppm	Cycle D/H	H/ ppm	C/ ppm
1	4,74	98,3	1	4,70	99,4	1	4,80	98,9	1	5,69	94,7
2	3,31	80,3	2	3,36	78,8	2	3,37	78,8	2	3,54	77,5
3	3,94	80,7	3	3,90	80,1	3	4,04	80,8	3	4,36	79,5
4	3,51	71,2	4	3,76	80,1	4	3,59	82,5	4	3,84	82,0
5	4,43	70,9	5	3,76	72,0	5	3,86	72,1	5	3,50	73,1
6	5,16		6	2,89		6	3,69		6	4,15	
6'	3,30	53,1	6'	3,05	68,8	1	4,80	70,7	1	4,16	70,0

Table S2 :Attribution of the protons of the sugar units of **161**

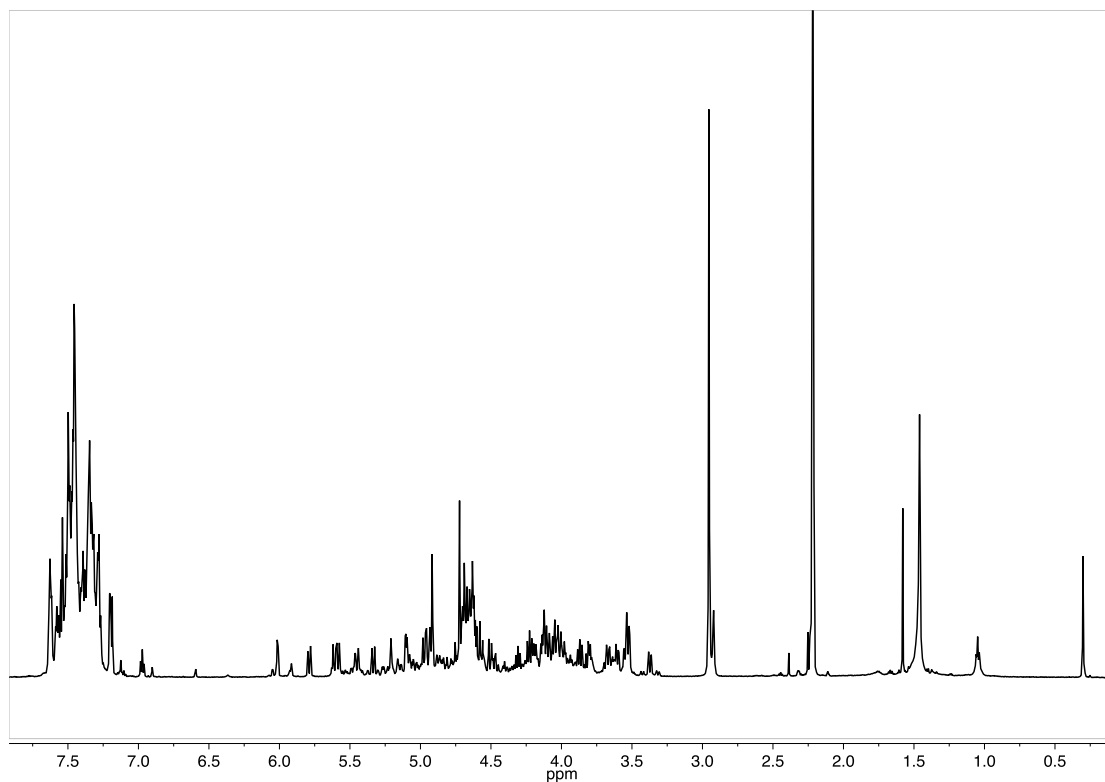
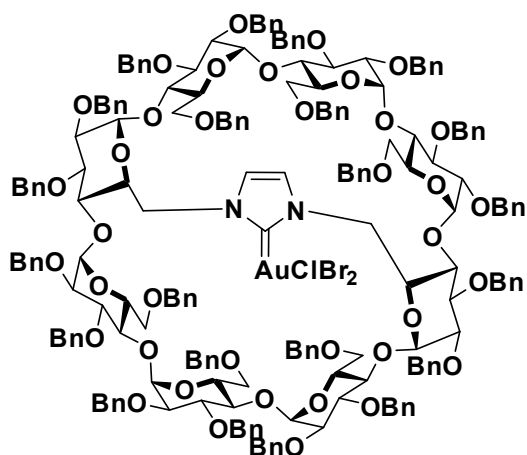


Figure S35: $^1\text{H-NMR}$ of **161** (Acetone- d_6 , 600 MHz, 300K)

Cycle A/E	H/ ppm	C/ ppm	Cycle B/F	H/ ppm	C/ ppm	Cycle C/G	H/ ppm	C/ ppm	Cycle D/H	H/ ppm	C/ ppm
1	5.04	98.66	1	4.94	99.4	1	4.92	99.56	1	5.84	94.96
2	3.43	81.13	2	3.36	80.2	2	3.38	80.2	2	3.50	79.11
3	4.05	81.13	3	4.15	81.96	3	3.96	82.72	3	4.50	80.11
4	3.64	71.77	4	3.71	83.04	4	3.89	81.1	4	3.96	81.13
5	4.54	71.87	5	4.04	73.06	5	3.93	72.77	5	3.62	81.09
6	3.86	53.55	6	3.88	70.6	6	3.36	69.6	6	3.82	70.62
6'	5.28		6'	3.88		6'	4.80		6'	4.31	

Table S3 :Attribution of the protons of the sugar units of **161**

(γ -ICyD)AuBr₂Cl (162)



Chemical Formula:
 $C_{205}H_{212}AuBr_2ClN_2O_{38}$
Molecular Weight:
3704.15

A solution of Br₂ (0.25 μ L in 2 mL of CH₂Cl₂, 4.77 μ mol) was added into another solution of (γ -ICyD)AuCl 157 complex (15mg, 4.34 μ mol, 1 eq) in 1 mL of CH₂Cl₂ previously cooled at -30°C. The reaction is stirred for 30 minutes and followed by TLC and Mass spectrometry. The reaction media was concentrated in vacuum at room temperature and the NMR analysis of 162 was done without any further purification.

¹H-NMR: (400MHz, acetone-d₆): 7.55- 7.10 (m, 100H, H-Ar), 7.05-7.00 (m, 6H, 2 x HAR, 2 x H-Imid), 6.75 (t, ³J = 7.4 Hz, 2H, 2 x HAR), 5.86 (d, ³J_{1,2} = 3.7 Hz, 2H, 2 x H-1D,H), 5.70 (d, ²J_{PhCHH} = 11.5Hz, 2H, PhCHH), 5.44 (d, ²J_{CHHPH} = 10.60 Hz, 2H, PhCHH), 5.25 (dd, 2H, ²J_{6a,6b} = 13.9, ³J_{6,5} = 2.1 Hz, 2 x H-6A,E), 5.13 (d, 2H, ²J_{CHHPH} = 11.6 Hz, PhCHH), 5.07 (d, ³J_{1,2} = 3.0 Hz, 2H, 2 x H-1A,E), 4.93 (2 x d, 2 x ³J_{1,2} = 3.4 Hz, 2H, 2 x H-1B,D, 2 x H-1C,D), 4.83 (d, ²J_{CHHPH} = 10.3 Hz, 2H, 2 x PhCHH), 4.87 - 4.66 (m, 8H, 8 x PhCHH), 4.65 - 4.35 (m, 24H, 2 x H-5A,E, 2 x H-3C,F, 20 x PhCHH), 4.33 - 4.22 (m, 4H, 2 x H-6D,H, 2 x PhCHH), 4.20 - 3.81 (m, 20H, H-6A,E, 2 x H-6C,G, 2 x H-4D,H, 2 x H-3C,G, 2 x H-3B,F, 2 x H-4B,F, 2 x H-6D,H, 2 x H-5B,F, 2 x H-5C,F), 3.76 - 3.60 (m, 6H, 2 x H-5D,H, 2 x H-4C,G, 2 x H-4A,E), 3.52 (dd, ³J_{2,3} = 9.9 Hz, ³J_{2,3} = 3.7 Hz, 2H, 2 x H-2D,H), 3.49 - 3.41 (m, 4H, 2 x H-6B,F, 2 x H-2D,H), 3.40 - 3.30 (2 x dd, ³J_{2,3} = 9.5, ³J_{2,1} = 3.3 Hz, ³J_{2,3} = 9.9, ³J_{2,1} = 3.3 Hz, 4H, 2 x H-2B/F, 2 x H-2C/G), 3.25 (2H, bd, 2 x H-6B,F).

¹³C-NMR (100MHz, acetone-d₆): 142.3 (C=Au), 140.4-139.3 (C_{ipso}), 129.7-127.4 (C_{Ar}), 127.1 (N-CH=CH-N), 100.1 (C-1B,F), 99.8(C-1C,G), 98.5 (C-1A,E), 95.1 (C-1D,H), 83.2 (C-4C,G), 82.9 (C-3B,F), 82.3 (C-3C,G), 81.7 (C-3A,E), 81.5 (C-2A,E), 81.2 (C-4D,H), 80.9 (C-4B,F), 80.3 (C-2B,F, C-2C,G), 80.2 (C-3D,H), 79.4 (C-2D,H), 78.0, 77.6, 76.9, 74.4, 74.18, 74.1 (6 x CH₂Ph), 73.8 (C-5D,H), 74.5 (CH₂Ph), 73.4 (C-5C,G), 73.3, 72.9 (2 x CH₂Ph), 72.4 (C-5B,F), 72.2 (CH₂Ph), 71.9 (C-4A,E), 71.3 (C-5A,E), 71.2 (C-6C,G), 70.8 (C-6D,H), 69.9 (C-6B,F), 50.1 (C-6A,E).

HRMS (ESI): calculated for: C₂₀₅H₂₁₂AuBr₂ClN₂O₃₈Na [M+Na]⁺, 3723.2365 found 3723.2703 err 9.07 ppm

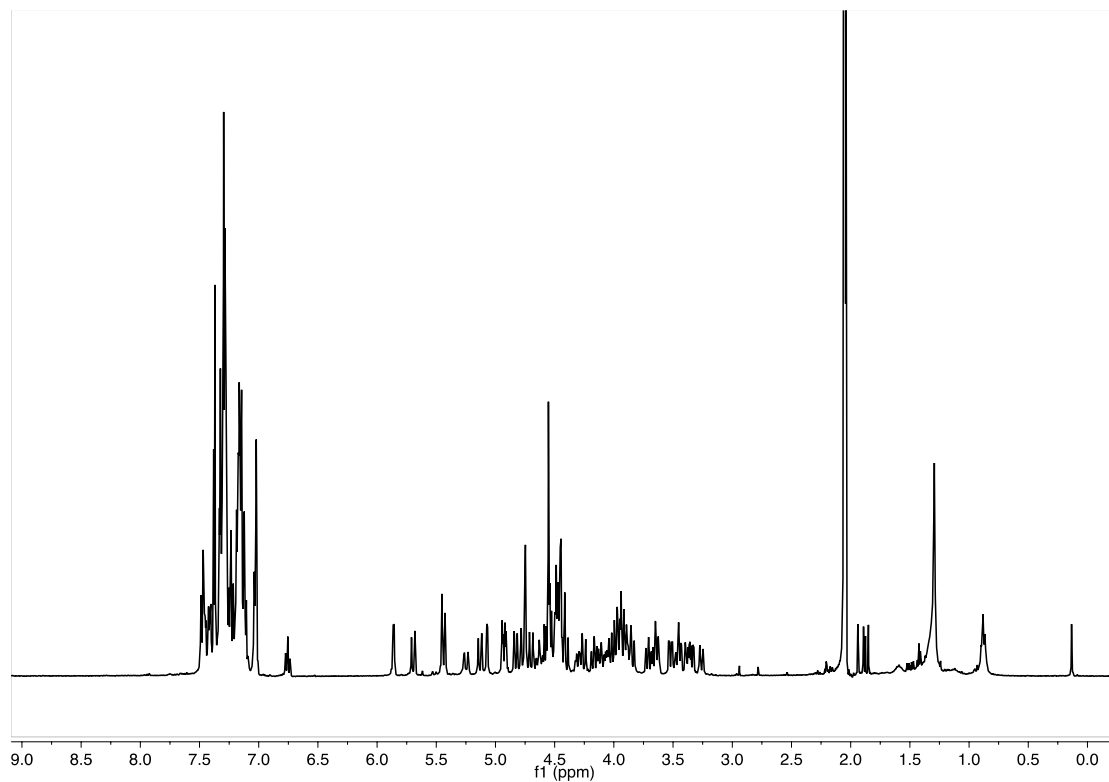


Figure S36: $^1\text{H-NMR}$ of $(\gamma\text{-ICyD})\text{AuBr}_2\text{Cl}$ **162** (Acetone- d_6 , 600 MHz, 300 K)

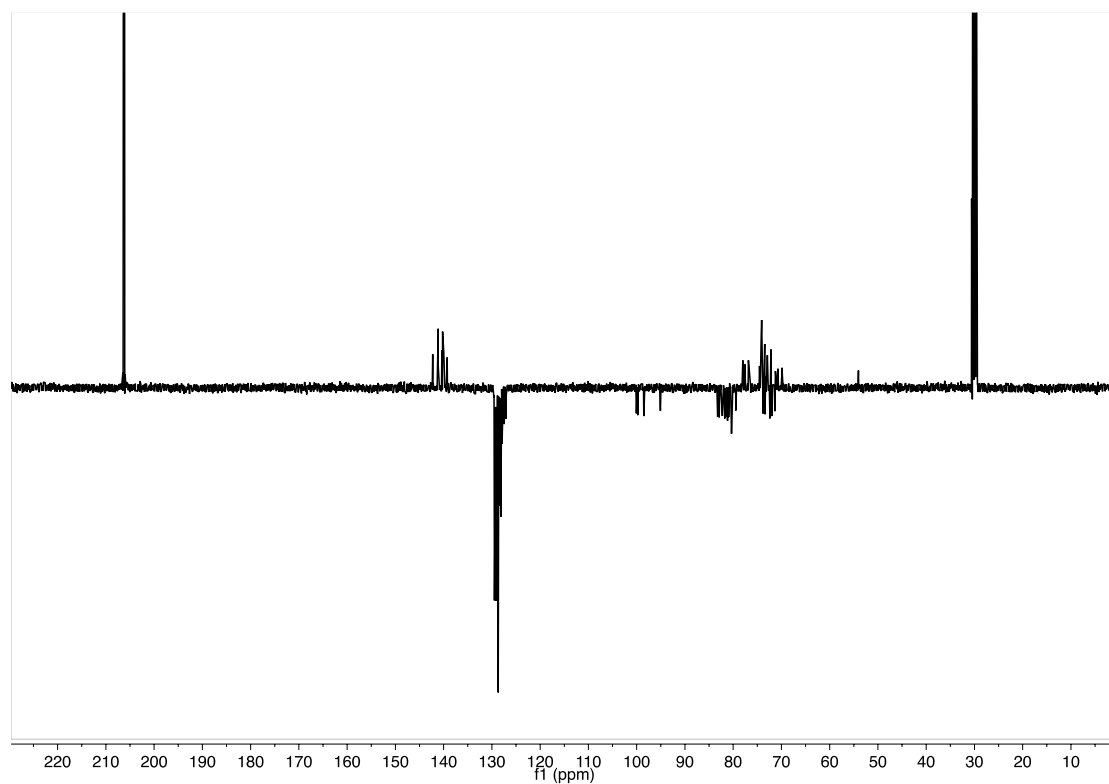


Figure S37: $^{13}\text{C-NMR}$ of $(\gamma\text{-ICyD})\text{AuCl}_3$ **162**. (Acetone- d_6 , 151 MHz, 300 K)

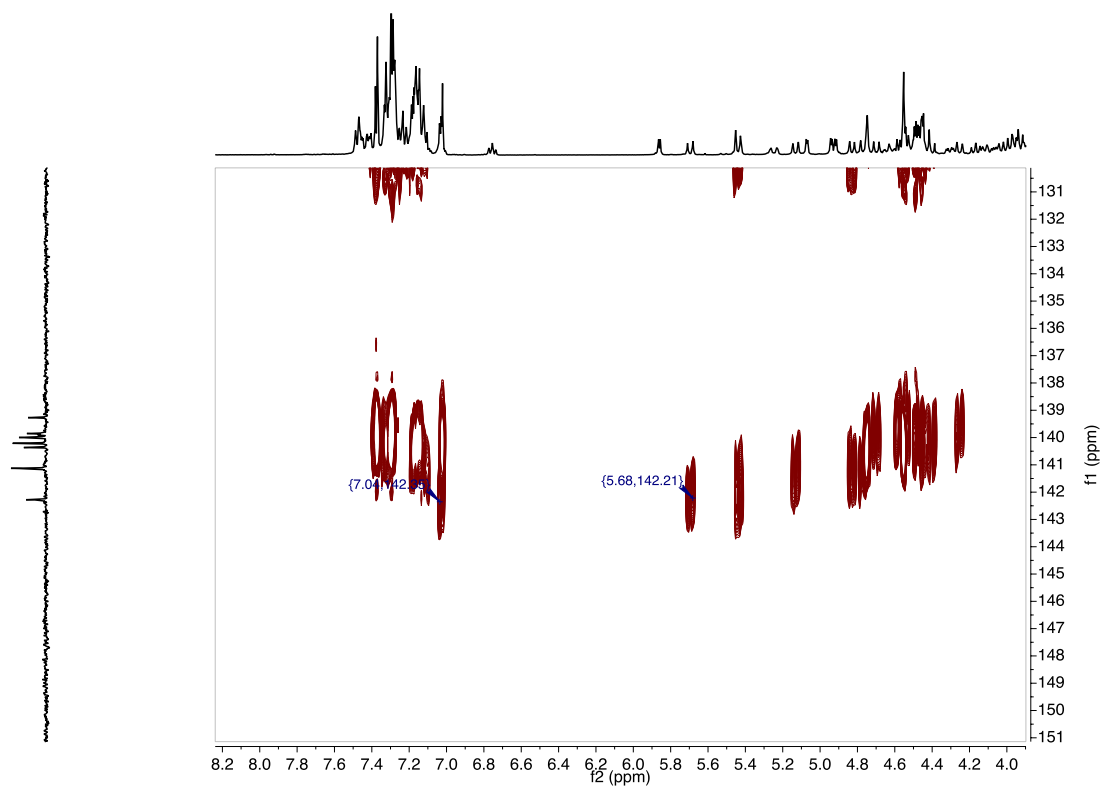
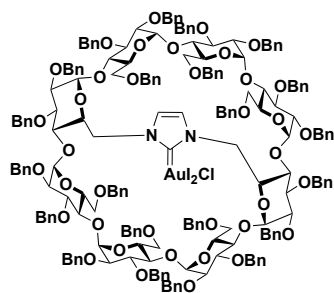


Figure S38: HMBC of (γ -ICyD)AuCl₃ **162**. (Acetone-d₆, 300 K)

(γ -ICyD)Au₂Cl (163)



Chemical Formula:
 $C_{205}H_{212}AuCl_2N_2O_{38}$
Molecular Weight:
3798.10

A solution of I₂ (1.07 mg in 2 mL of CH₂Cl₂, 4.77 μ mol) was added into another solution of (γ -ICyD)AuCl 157 complex (15mg, 4.34 μ mol, 1 eq) in 1 mL of CH₂Cl₂ previously cooled at -30°C. The reaction is stirred for 30 minutes and followed by TLC and Mass spectrometry. The reaction media was concentrated in vacuum at room temperature and the NMR analysis of 163 was done without any further purification.

¹H NMR (600 MHz, Acetone-d₆) δ = 7.50 – 7.01 (m, 108H, H_{Ar}), 7.00 (s, 2H, N-CH=CH-N) 6.80 (t, ³J_{p,m} = 7.4 Hz, 2H, H_{paraBn}), 5.85 (d, ³J_{H1-H2} = 3.8 Hz, 2H, H-1D,H), 5.62 (d, ³J_{PhCHH} = 11.3 Hz, 2H), 5.43 (2 x d, ³J_{PhCHH} = 15.8 Hz, 10.9 Hz, 4H, PhCHH), 5.17 – 5.07 (m, 6H, 2 x PhCHH, 2 x H-1A,E, 2 x H-6A,E), 4.93 (2 x d, ³J_{H1-H2} = 3.4 Hz, 4H, 2 x H-1B,F, 2 x H-1C,G), 4.82 – 4.73 (m, 8H, 2 x H-5A,E, 6 x PhCHH), 4.58 – 4.39 (m, 37H, 2 x H-5B,F, 2 x H-3D,H, PhCHH), 4.30 (dd, ²J_{H6a-H6b} = 11.3 Hz ³J_{H6-H5} = 3.11 Hz, H-6D,H), 4.21 – 4.11 (m, 6H, 2 x H-3C,G, 2 x H-5B,F, 2 x PhCHH), 4.18 – 4.10 (m, 4H, 2 x PhCHH, 2 x H-5C,G), 4.09 – 3.59 (m, 16H, 6 x H-3A,B,C,E,F,G, 8 x H-4A,B,C,D,E,F,G,H, 2 x H-5 D,H, 10 x H-6A,B,C,D,E,F,G,H), 3.54 (dd, ²J_{H2-H3} = 10.0 Hz, ³J_{H1-H2} = 3.6 Hz, 2H, H-6D,H), 3.46 (d, ³J_{H2-H3} = 9.5 Hz, ³J_{H1-H2} = 2.1Hz, 2H, H-2A,E), 3.37 (2 x dd, ³J_{H2-H3} = 9.7, ³J_{H1-H2} = 3.2Hz, 4H, 2 x H-2B,F, 2 x H-2C,G).

¹³C NMR (151 MHz, Acetone) δ 142.0 – 138.9 (C_{ipso}), 131.3 (C=Au^{III}) 129.4 – 126.9 (CH_{Ar}), 119.1 (N-CH=CH-N), 100.5 (C-1B,F), 99.8 (C-1C,G), 98.1 (C-1A;E), 94.9(C-1D,H), 83.3 (C-4C,G), 82.8 (C-4D,H), 82.2 (C-3C,G), 81.8 (C-3A,E), 81.5 (C-2A,E), 80.9, 80.4 (C-3B,F, C-4B,F), 80.1 (C-3D,H), 80.0 (C-2B,F, C-2C,G), 79.5 – 73.9 (CHHPh), 73.5 (C-4A,E), 73.4(CHHPh), 73.2 (C-5C,G), 73.1 (CHHPh), 72.6(CHHPh), 72.4(C-5B,F), 71.7 (CHHPh), 71.6 (C-5D,H), 70.9 (C6-C,G), 70.5 (C-&D,H), 70.3 (C-5A;E), 69.6 (C-6B,F), 54.7 (C-6A,E).

HRMS (ESI): calculated for C₂₀₅H₂₁₂AuCl₂N₂O₃₈Na [M+Na]⁺ 3818.2054 found 3817.8503

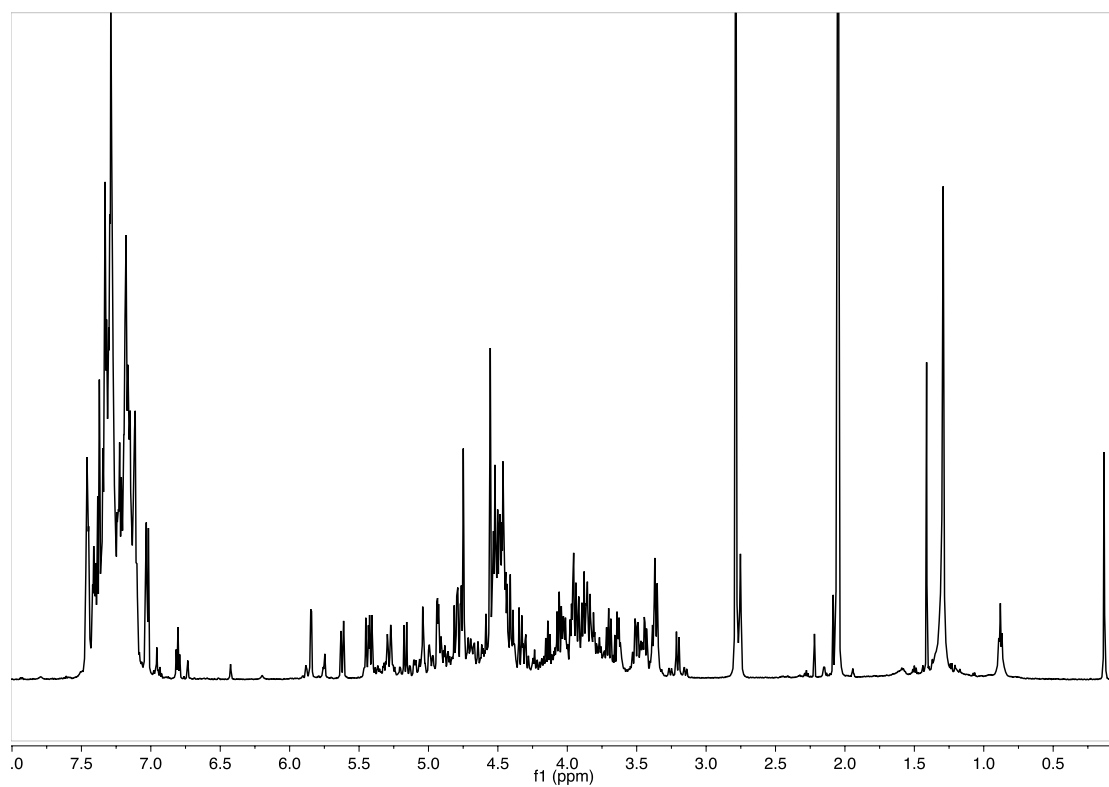


Figure S39: $^1\text{H-NMR}$ of $(\gamma\text{-ICyD})\text{Au}_2\text{Cl}$ **163** (Acetone- d_6 , 600 MHz, 300 K)

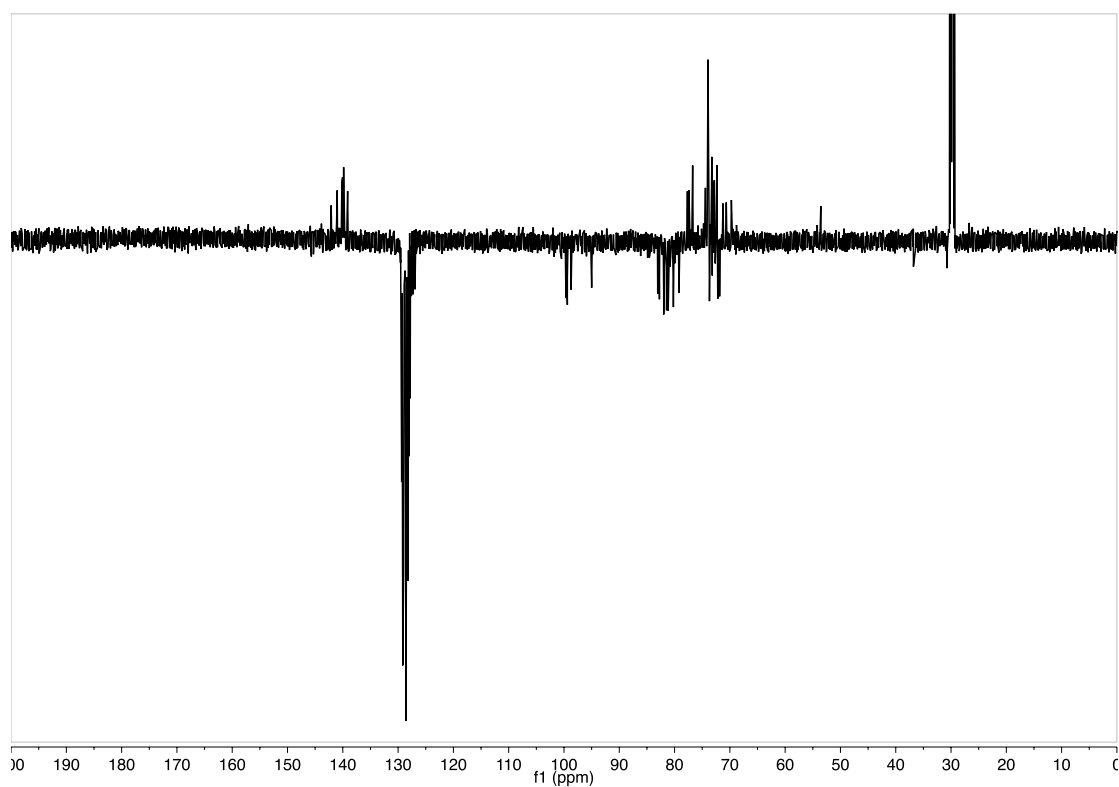


Figure S40: $^{13}\text{C-Jmod}$ of $(\gamma\text{-ICyD})\text{Au}_2\text{Cl}$ **163** (Acetone- d_6 , 151 MHz, 300 K)

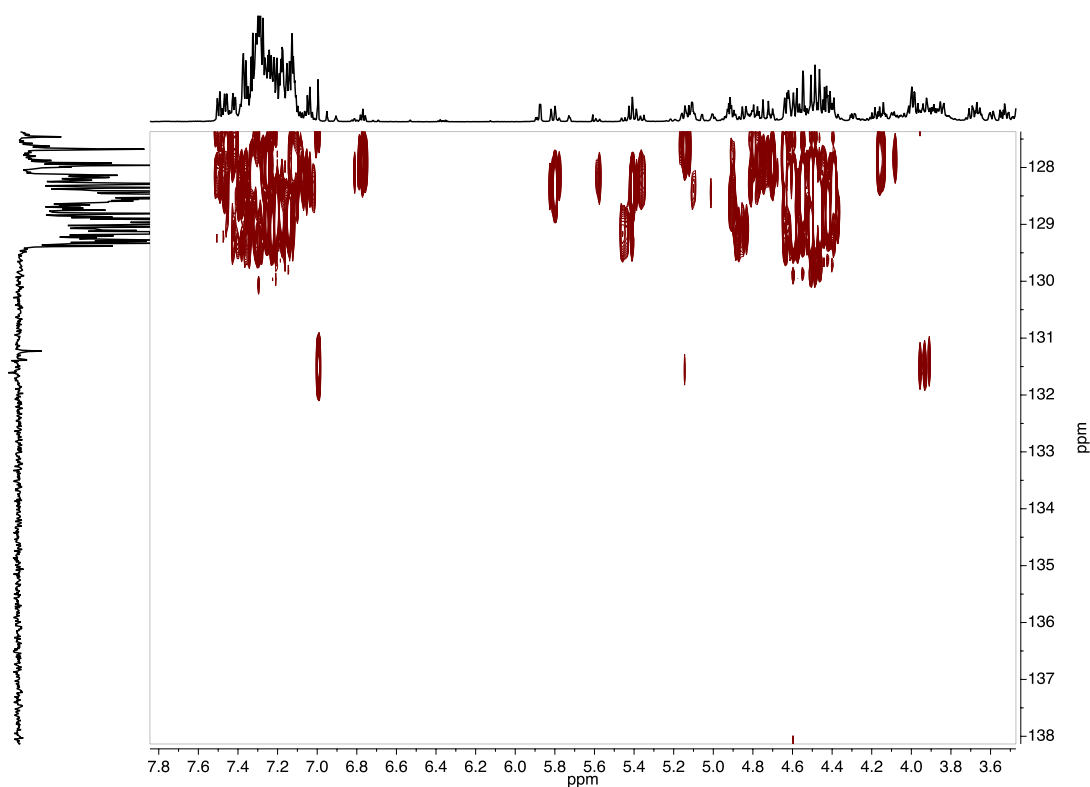
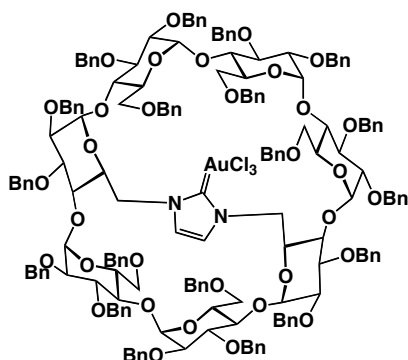


Figure S41: HMBC of (γ -ICyD)Au₂Cl **163** showing the cross correlations with the C=Au.
(Acetone-d₆, 300 K)

Cycl e A/E	H/ ppm	C/ ppm	Cycl e B/F	H/ ppm	C/ ppm	Cycl e C/ G	H/ ppm	C/ ppm	Cycl e D/ H	H/ ppm	C/ ppm
1	5.11	98.0	1	4.92	100.5	1	4.91	99,8	1	5,86	94.9
2	3.47	81.5	2	3.35	79.99	2	3.33	80.0	2	3.54	79,5
3	3.98	81.8	3	4.00	?	3	4.18	82.2	3	4.56	80.1
4	3.66	73.5	4	4.00	?	4	3.69	83.3	4	4.00	82.7
5	4.80	70.3	5	4.39	72.3	5	4.13	73.3	5	3.66	71.6
6	3.93	54.3	6	3.33	69.6	6	3,89	70.85	6	4.29	70.6
6'	5.15		6'	3.59		6'	3.89		6'	3.85	

Table S4 :Attribution of the protons of the sugar units of **163**

(β -ICyD)AuCl₃ (164)



Chemical Formula:
 $C_{178}H_{184}AuCl_3N_2O_{33}$
Molecular Weight:
3182.73

Into a solution of **β -ICyD-AuCl 127** (20mg, 6,4 of μ mol) in CH_2Cl_2 (2,5 mL)at $-78^\circ C$, Cl_2 is slowly bubbled until the reaction mixture becomes slightly yellow.The reaction is monitored by TLC (CyH:EtOAc 3:1) and Cl_2 is slowly bubbled until completion. When finished, solid K_2CO_3 is added, Ar bubbled and slowly warmed up at $-30^\circ C$, Ar is bubbled until loss of yellow coloration. K_2CO_3 was filtered over cotton and CH_2Cl_2 is evaporated in vacuo until dryness without heating and the compound is characterized without any further purification.

1H -NMR: (600 MHz, Acetone- d_6) δ 7.55 - 6.93 (m, 96H, 94xH-Ar, 2xN-CH=C), 6.81 (t, $J = 7.5$ Hz, 2H, H-Ar), 5.91 (d, $^3J_{1,2} = 3.8$ Hz, 1H, H-1G), 5.82 (d, $^3J_{1,2} = 3.5$ Hz, 1H, H1-C), 5.70 (d, $J = 11.4$ Hz, 1H, PhCHH), 5.64 (d, $^2J_{Ph-CHH} = 10.8$ Hz, 1H, PhCHH), 5.54 (dd, $J = 13.4, 2.6$ Hz, 1H, H-6D), 5.37 - 5.29 (m, $^2J_{6a,6b} = 13.2$ Hz, $^3J_{6,5} = 2.6$ Hz, 2H, H-6A,CHPh), 5.28 - 5.22 (m, 2H, 2 x PhCHH), 5.20 - 5.15 (m, 2H, PhCHH, H-1D), 5.05 (d, $^2J_{Ph-CHH} = 11.1$ Hz, 1H, PhCHH), 5.02 - 4.66 (m, 16H, H-5A, H-5D, H-3C, H-3E, H-1A, H-1B, H-1E, H-1F, 8 x PhCHH), 4.65 - 4.07 (m, 33H, H-5B, H-5E, H-5F, H-3B, H-3D, H-3F, H-3G, H-4C, H-6G, H-6D, 23xCH₂Ph) 4.05 - 3.54 (m, 19H, H-3A, H-4A, H-4B, H-4D, H-4E, H-4F, H-4G, H-5C, H-5G, H-6A, 2 x H-6C, H-6D, 2xH-6F, H-6G, H-2D, H-2G, PhCHH), 3,51 (d, $^3J_{2,3} = 10.8$ Hz, $^3J_{2,1} = 3.7$ Hz, 1H, H-2C), 3,44 (d, $^3J_{2,1} = 9.8$ Hz, $^3J_{2,1} = 2.9$ Hz, 1H, H-2A), 3,37 - 3.30 (m, 2H, H2-B, H2-F), 3.30 - 3.12 (m, $^3J_{2,1} = 9.7$, $^3J_{2,1} = 2.7$ Hz, 4H, H-2E, 2 x H-6B, H-6E)

^{13}C -NMR(151 MHz, Acetone- d_6) δ 143.0 (C=Au), 141.8, 141.5, 141.2, 140.9, 140.8, 140.2, 140.1, 140.0, 140.0, 139.9, 139.9, 139.8, 139.7, 139.6, 139.1, (C_{ipso}), 129.3-, 127.4 (CH Ar, 2xN-CH-CH-N), 101.3 (C-1E), 99.8 (C-1F), 99.1 (C-1D), 98.6 (C-1B), 98.5 (C-1A), 98.4 (C-1C), 97.8 (C-1G), 84.0 (C-4F), 83.0 (C-4G), 2x82.7 (C-4C, C-4E), 82.6 (C-3A), 82.5 (C-3D), 2x81.70 (C-2D,C-4B), 81.40 (C-2A), 81.2 (C-3F), 80.9 (C-2F), 80.5 (C-2B), 80.3 (C-3E), 80.0 (C-3G), 79.8 (C-2E), 78.96(C-3C), 78.3 (C-2C), 78.3(C-2G), 77.0-75.2 (CH₂Ph), 74.8 (C-5GorC-5C), 74.5 (C-4D), 74.1 (C-5G or C-5C), 74.3-72.6 (CH₂Ph), 73.7 (C-4A), 73.2 (C-5F), 72.9 (C-5A), 72.85 (C-5B), 72.1 (C-5E), 71.1 (C-6C), 70,9 (C-6F), 70.8 (C-5D) 70,5 (C-6G), 69.8 (C-6E), 69.7 (C-6B) 54.8 (C-6D), 53.8 (C-6A).

Rf=0.43 (CyH:AcOEt 3:1)

HRMS (ESI, injection in MeCN): calculated for $C_{178}H_{184}AuCl_3N_2O_{33}Na$ [M+Na]⁺ found 3205.1386 calculated 3205.1416 err=-0.935ppm

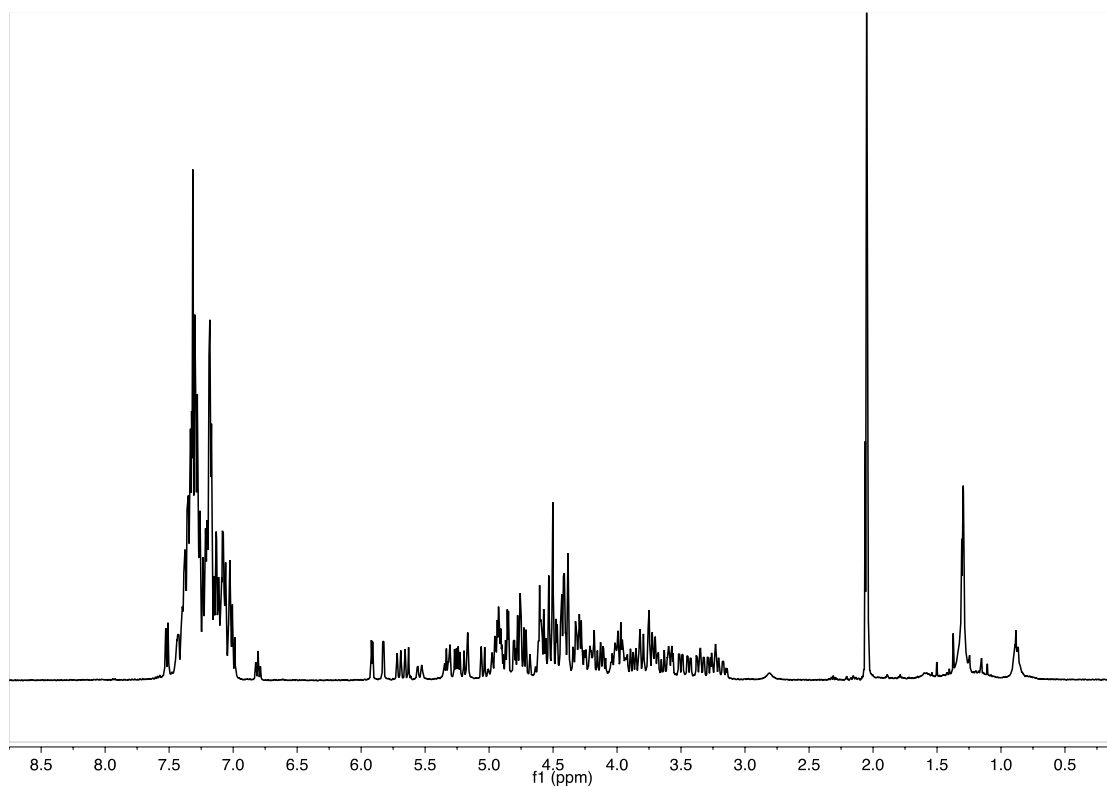


Figure S42: ^1H -NMR of $(\beta\text{-ICyD})\text{AuCl}_3$ **164** (Acetone- d_6 , 600 MHz, 300 K)

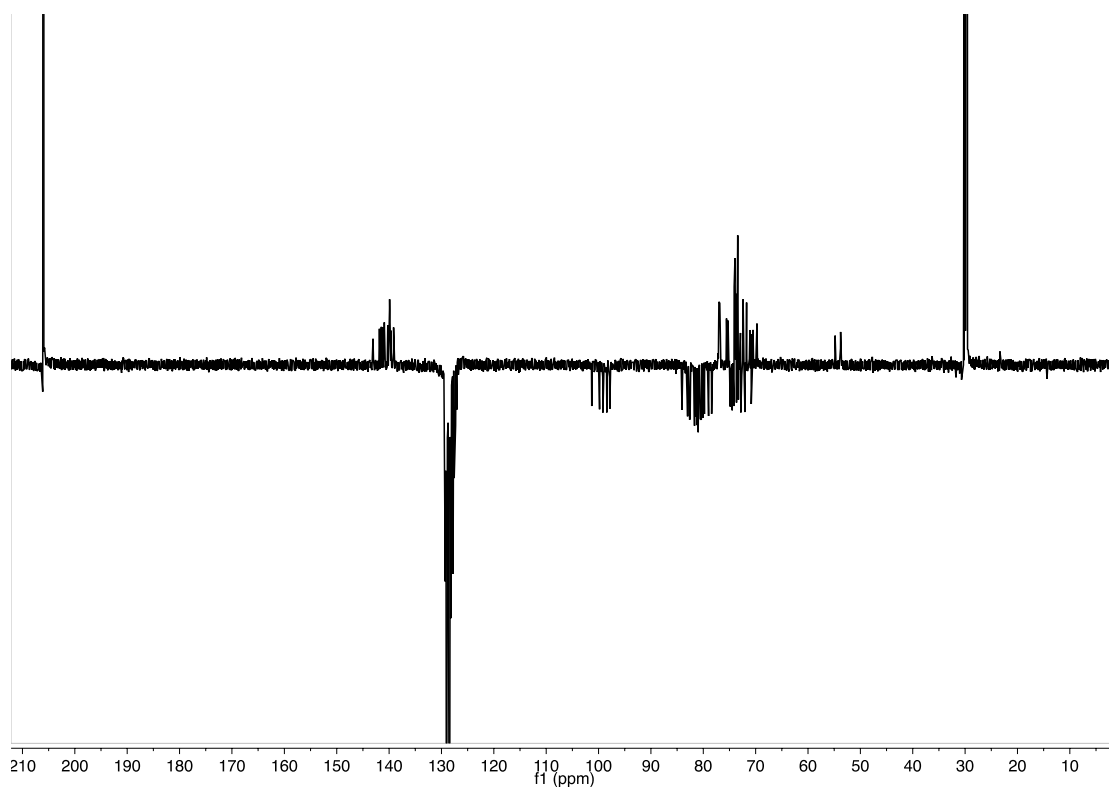


Figure S43: ^{13}C -Jmod of $(\beta\text{-ICyD})\text{AuCl}_3$ **164** (Acetone- d_6 , 151 MHz, 300 K)

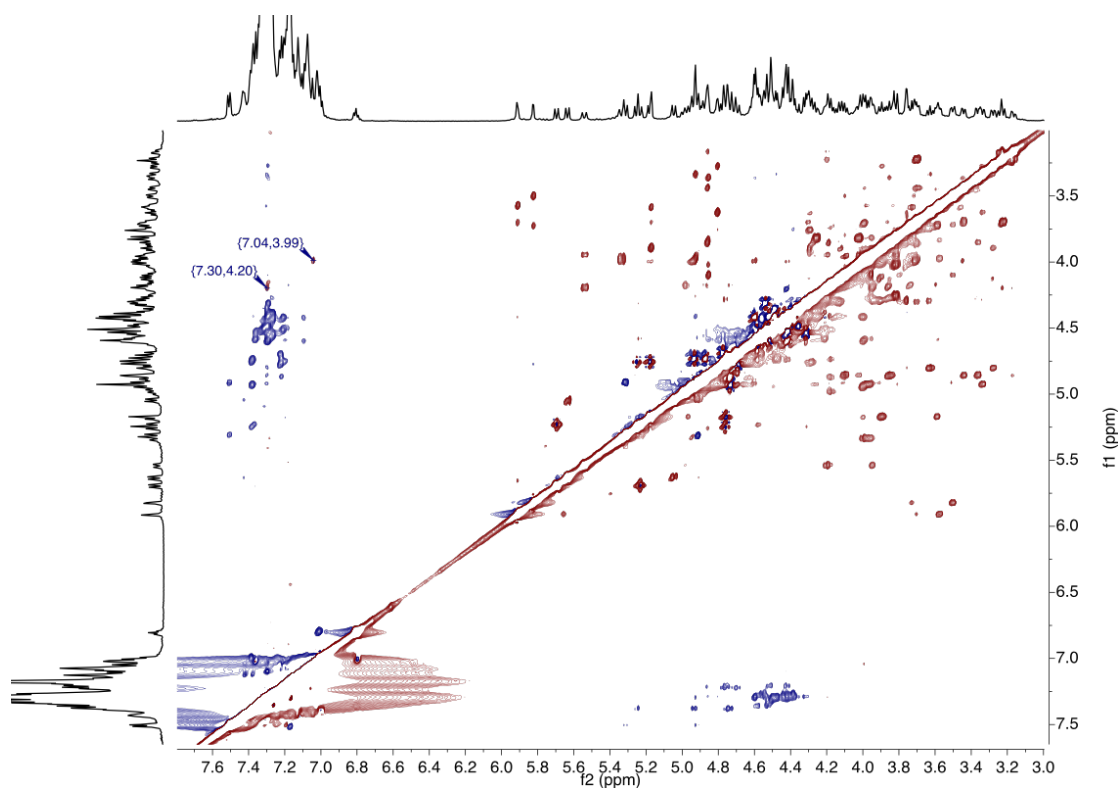


Figure S44: 2D-NOESY spectrum of $(\beta\text{-ICyD})\text{AuCl}_3$ **164** showing the cross correlations between the H_{NHC} and the H6 (Acetone- d_6 , 600 MHz, 300 K)

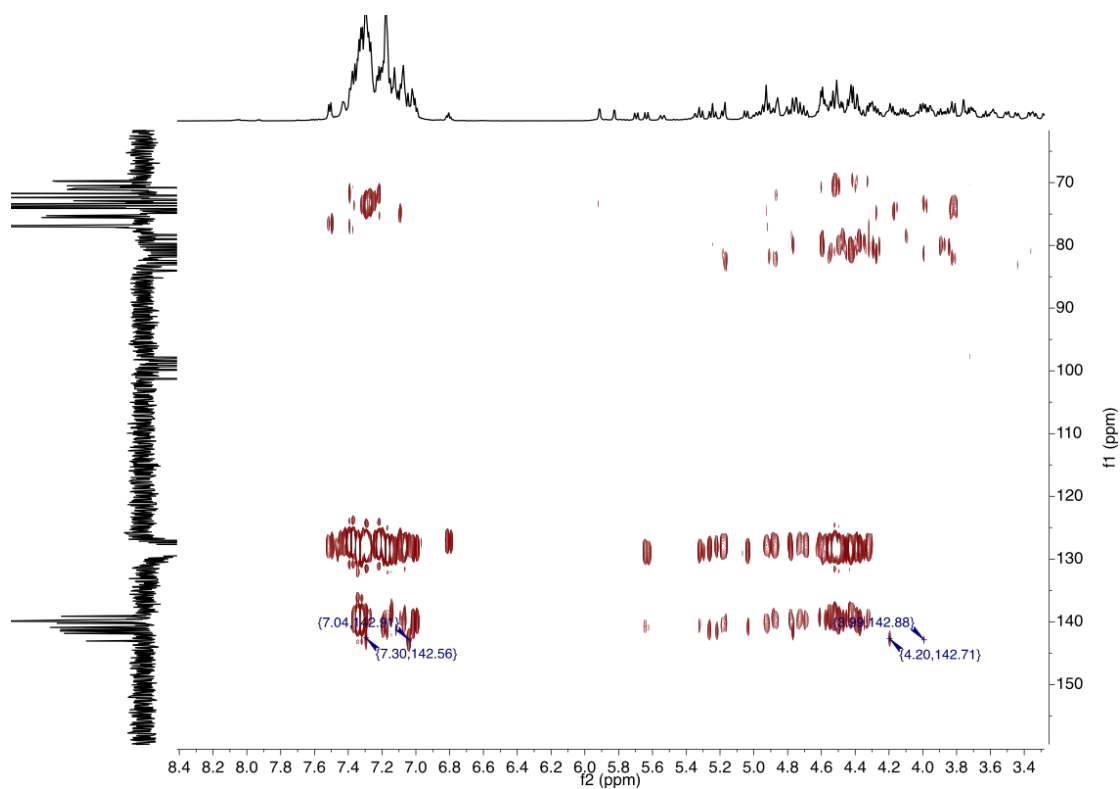
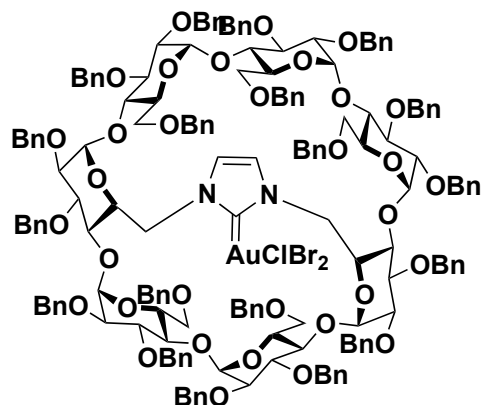


Figure S45: 2D-HMBC spectrum of $(\beta\text{-ICyD})\text{AuCl}_3$ **164** showing the cross correlations between the H_{NHC} , the H6 and the $\text{C}=\text{Au}$ (Acetone- d_6 , 300 K)

Cycle A	H	C	Cycle B	H	C
1	4,87	98,59	1	4,86	98,95
2	3,44	81,44	2	3,37	80,53
3	4,00	82,6	3	4,28	80,85
4	3,70	73,74	4	3,86	81,69
5	4,95	72,95	5	4,20	72,84
6	4,00	53,81	6	3,18	69,74
6'	5,33		6'	3,24	
Cycle C	H	C	Cycle D	H	C
1	5,82	98,54	1	5,17	99,17
2	3,51	78,32	2	3,58	81,70
3	4,91	79,02	3	4,17	82,49
4	4,10	82,72	4	3,73	74,51
5	3,95	74,14/74,85	5	4,99	70,85
6	3,81	71,13	6	4,19	54,82
6'	4,02		6'	5,53	
Cycle E	H	C	Cycle F	H	C
1	4,80	101,33	1	4,93	99,83
2	3,27	78,3	2	3,34	80,90
3	4,13	80,11	3	4,32	81,21
4	3,90	82,58	4	3,63	84,02
5	4,31	74.14/74.85	5	4,29	73,27
6	3,70	69,79	6	3,76	70,86
6'	3,23		6'	3,76	
Cycle G	H	C			
1	5,91	97,86	ImidA	7,05	
2	3,58	80,39	ImidD	7,29	
3	4,58	80,11	C=Au	143.1	
4	3,98	82,58			
5	3,95	72,09			
6	3,82	70,50			
6'	4,25				

Table S5: Attribution of the protons of the sugar units of **164**

(β -ICyD)AuBr₂Cl (165)



Chemical Formula:
 $C_{178}H_{184}AuBr_2ClN_2O_{33}$
Molecular Weight:
3271.59

In a round bottom flask, (**β -ICyD**)AuCl 127 (30 mg, 9.6 μ mol, 1 eq) was dissolved under argon in CH₂Cl₂, the solution was cooled down to -78 °C during 5 minutes. Then, a solution of Br₂ (0.5 μ L in 10 μ L of CH₂Cl₂) was added. The reaction mixture was stirred at -78 °C during 30 minutes and monitored by ESI-TOF. When finished, the solution is let to warm up slowly and the solvent is evaporated until dryness. The NMR and the Mass Spectra were done without any further purification.

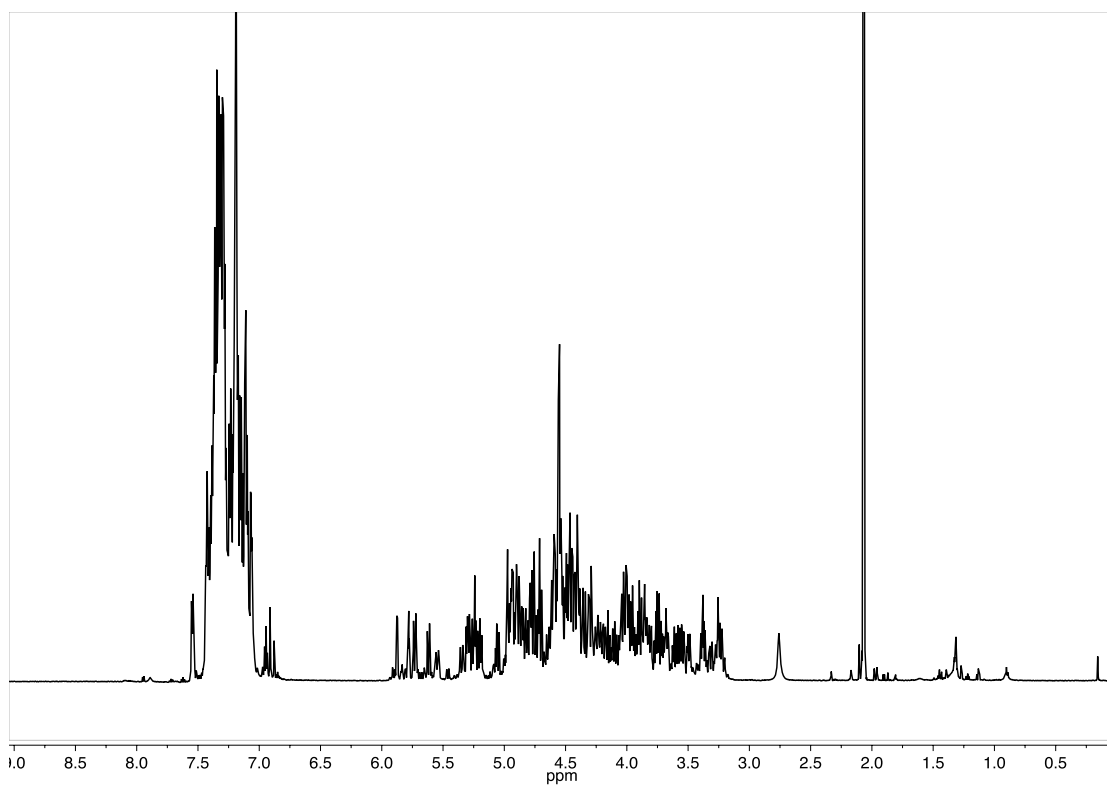


Figure S46: $^1\text{H-NMR}$ of $(\beta\text{-ICyD})\text{AuBr}_2\text{Cl}$ **165** (Acetone- d_6 , 600 MHz, 300K)

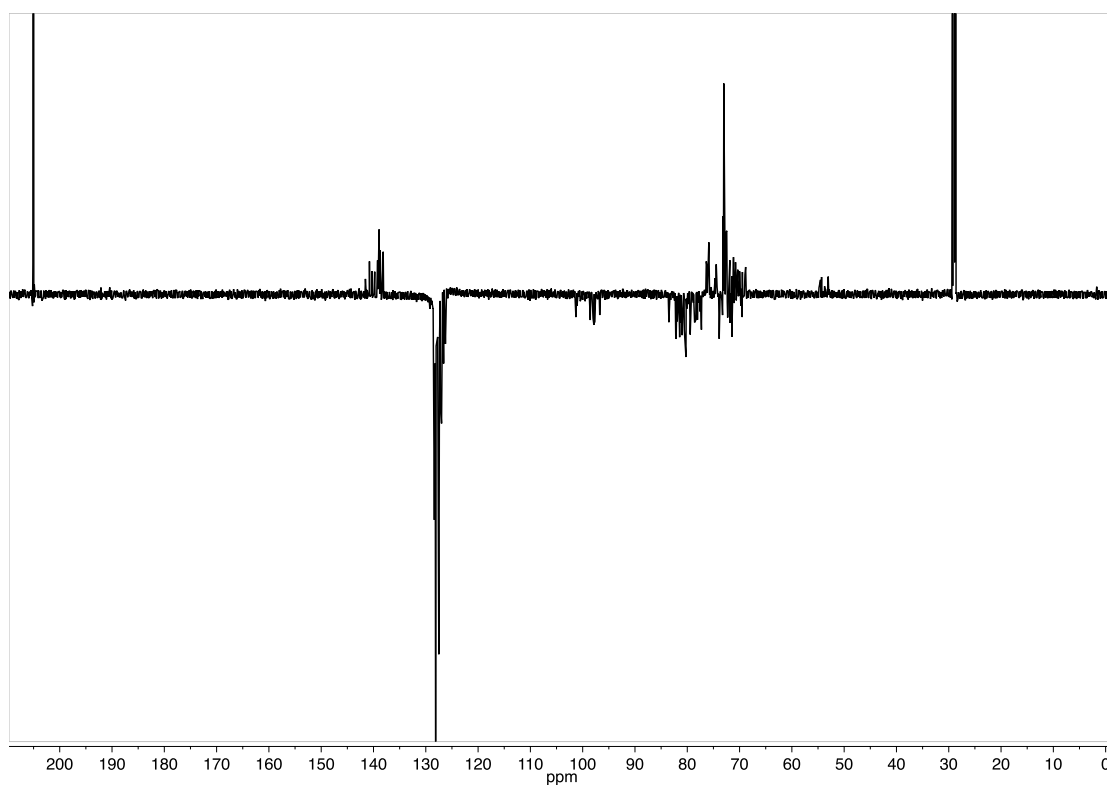
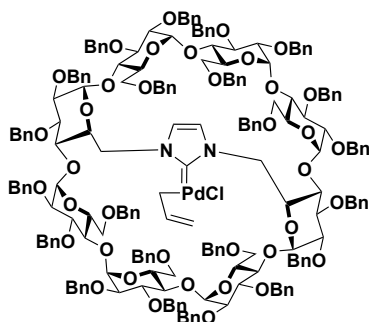


Figure S47: $^{13}\text{CJmod}$ of $(\beta\text{-ICyD})\text{AuBr}_2\text{Cl}$ **165** (Acetone- d_6 , 151 MHz, 300K)

(γ -AE-ICyD)PdCl(η^3 -allyl) (168)



Chemical Formula:

$C_{208}H_{217}ClN_2O_{38}Pd$

Molecular Weight:

3494.81

(γ -ICyD)AgCl **155** (10mg, 2.8 μ mol) and allylpalladium(II) chloride dimer (0.5 mg, 1.4 μ mol) were weighed in a sealed tube and purged with Ar, then, dry DCM (1.5 mL) was added. The reaction mixture was stirred at room temperature for 30 minutes. The reaction is checked by Mass Spectrometry and TLC, when finished, silver salts are removed by filtration with a 0.2 μ m PET filter, washed with DCM recovering the (γ -AE-ICyD)PdCl(η^3 allyl) **168** complex (9 mg, 88%) characterized without any further purification.

1H NMR (600 MHz, Acetone- d_6) δ 7.52 – 7.44 (m, 10H), 7.47 – 7.20 (m, 110H), 7.20 (s, 6H), 7.17 (ddd, J = 6.8, 4.9, 1.9 Hz, 20H), 7.17 – 7.07 (m, 10H), 7.10 – 6.97 (m, 10H), 6.81 (dt, J = 17.9, 7.5 Hz, 6H), 6.67 – 6.55 (m, 6H), 5.97 (d, J = 4.0 Hz, 1H), 5.91 – 5.82 (m, 6H), 5.78 – 5.69 (m, 3H), 5.56 (dd, J = 27.9, 10.8 Hz, 4H), 5.47 – 5.38 (m, 5H), 5.32 – 5.12 (m, 11H), 5.10 (dd, J = 7.2, 3.1 Hz, 4H), 5.08 – 4.79 (m, 25H), 4.79 – 4.68 (m, 9H), 4.70 – 4.21 (m, 85H), 4.20 – 3.28 (m, 68H), 3.29 – 3.06 (m, 10H), 3.02 (d, J = 12.0 Hz, 4H), 2.60 (d, J = 11.8 Hz, 2H, HAllylcis-anti(isomer a)), 2.34 (d, J = 11.7 Hz, 1H, HAllylcis-anti (isomer b)).

Rf=0.34 (CyH:AcOEt 3:1)

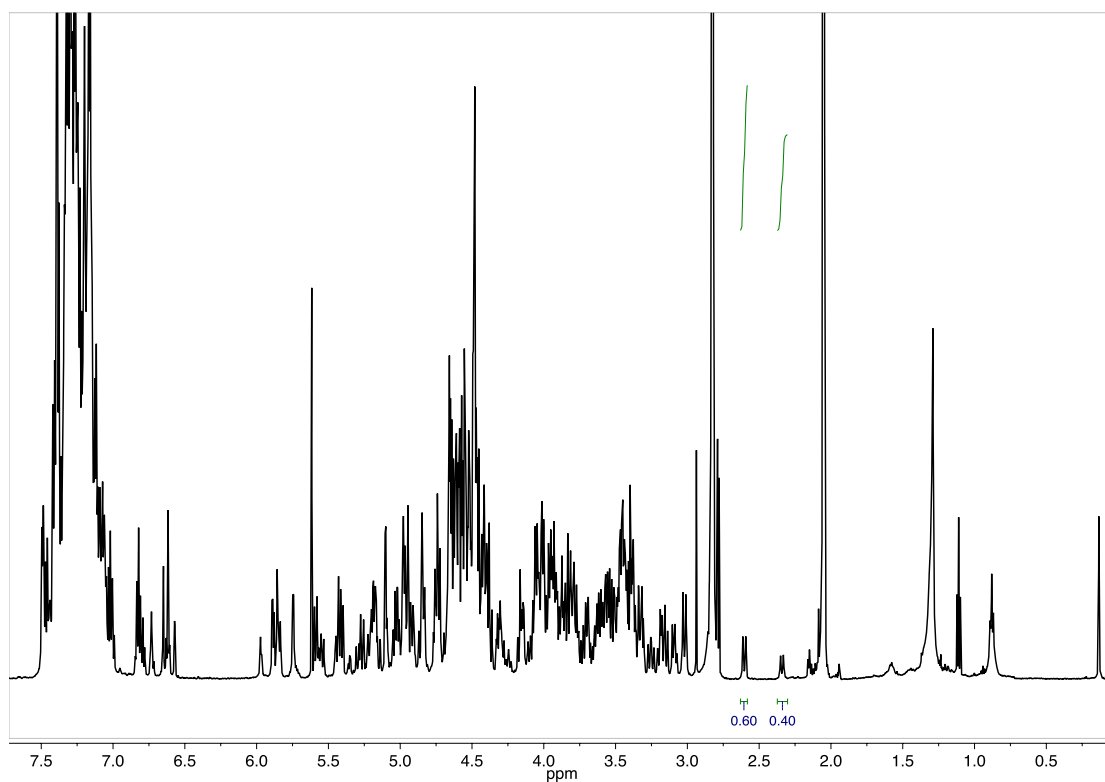


Figure S46: $^1\text{H-NMR}$ of $(\gamma\text{-AE-ICyD})\text{PdCl}(\eta^3 \text{ allyl})$ **168** (Acetone- d_6 , 600 MHz, 300K)

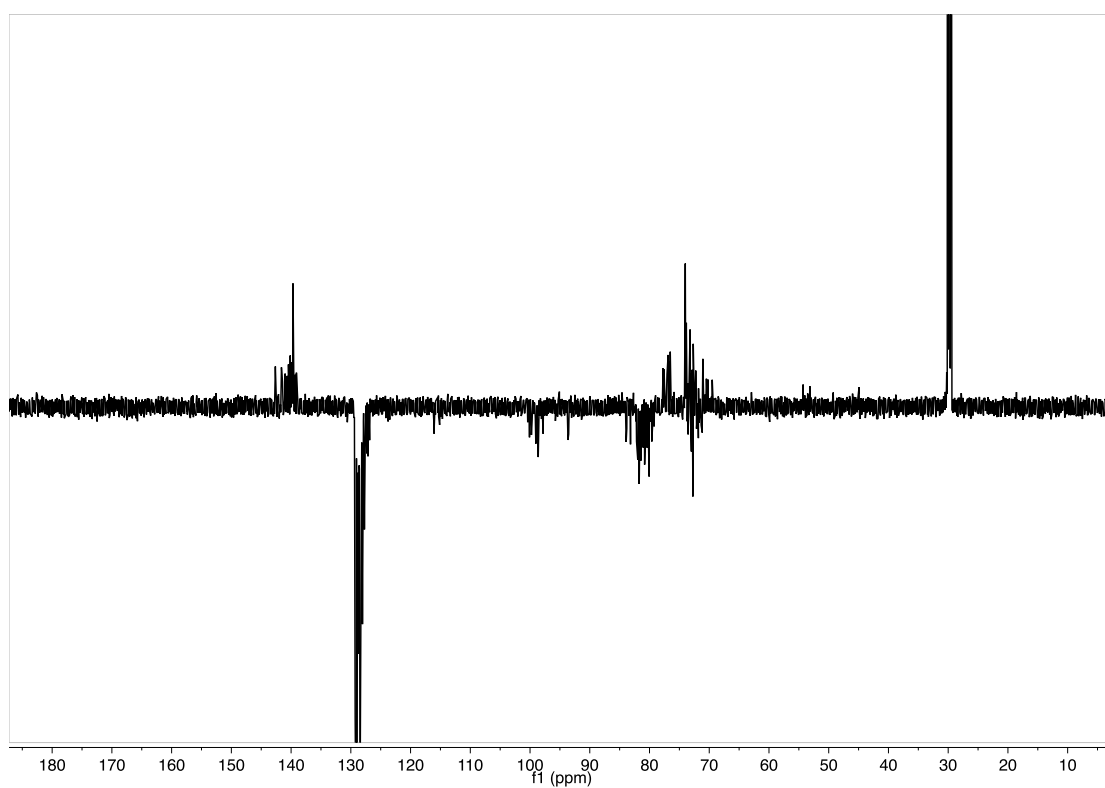


Figure S47: $^{13}\text{C-Jmod}$ of $(\gamma\text{-AE-ICyD})\text{PdCl}(\eta^3 \text{ allyl})$ **168** (Acetone- d_6 , 151 MHz, 300 K)

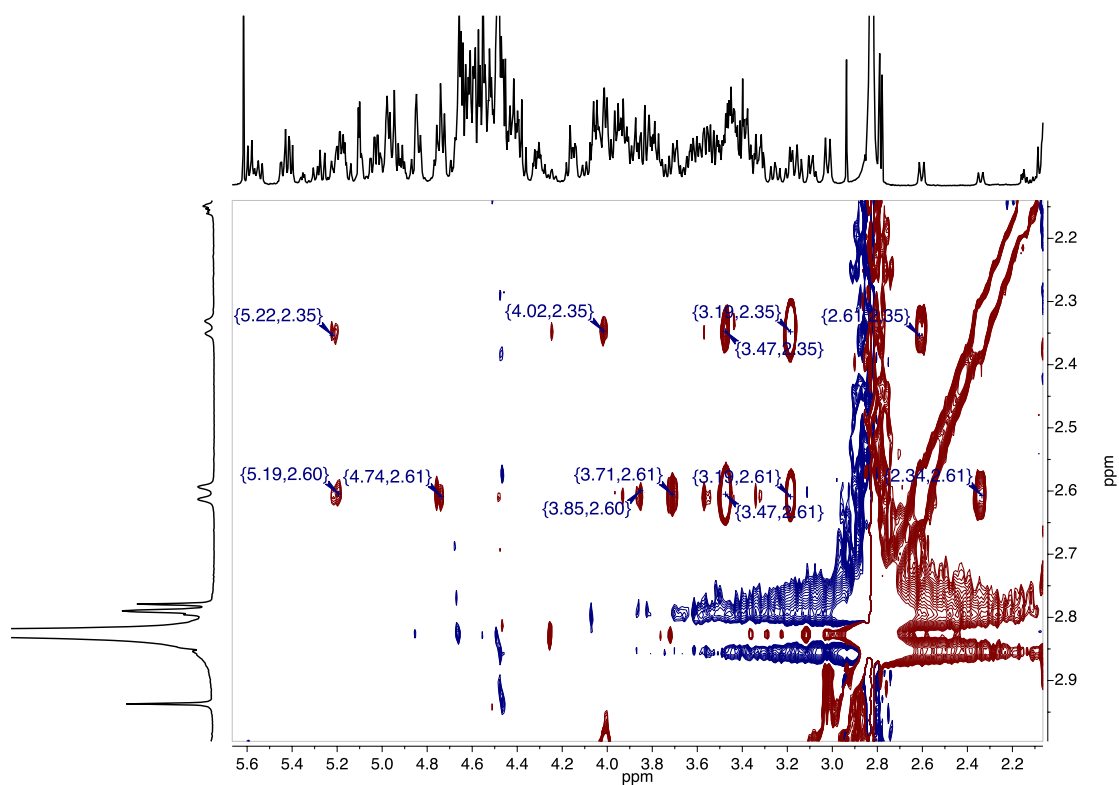
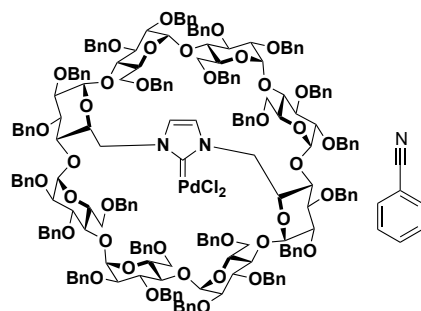


Figure S48: 2D-NOESY showing the cross correlations of the Hcis-anti of the allyl Acetone-d₆, 600 MHz, 300 K

(γ -AE-ICyD)PdCl₂(PhCN)



Chemical Formula:
C₂₁₂H₂₁₇Cl₂N₃O₃₈Pd
Molecular Weight:
3592.31

(γ -AE-ICyD)AgCl 155 (10 mg, 2.8 μ mol) and bis(benzonitrile) palladium(II) chloride (1.1 mg, 2.8 μ mol) were weighed in a sealed tube and purged with Ar, then, dry DCM (1 mL) was added. The reaction mixture was heated at 40°C for 30 minutes. The reaction was monitored by Mass Spectrometry and TLC. When finished, silver salts were removed by filtration with a 0.2 μ m PET filter, washed with CH₂Cl₂ recovering the (**γ -AE-ICyD)PdCl₂(PhCN) 169** complex (9mg, 88%) characterized without any further purification.

¹H NMR (600 MHz, Acetone-d₆) δ 7.78 (dd, $J = 8.2, 1.4$ Hz, 2H, H_{PhCN}), 7.65 (m, 1H, H_{PhCN}), 7.60 (m, 1H, H_{PhCN}), 7.46 – 6.97 (m, 106H, H_{Ar}), 6.88 (t, $J = 8.2$, 2H, H_{Ar}), 6.73 (s, 2H, N-CH=CH-N), 6.03 – 5.91 (m, 4H, 2 x H-1D,H, 2 x H-6A,E), 5.58 (d, $^2J_{\text{PhCHH}} = 12.1$ Hz, 2H, PhCHH), 5.49 (d, $^2J_{\text{PhCHH}} = 10.6$ Hz, 2H, 2 x PhCHH), 5.34 (d, $^3J_{\text{PhCHH}} = 11.3$ Hz, 2H, PhCHH), 5.17 – 5.05 (m, 4H, 2 x H-1A,E, 2 x H-5A,E), 4.93 (2 x d, $^3J = 3.3$ Hz, 4H, H-1B,F, H-1C,G), 4.87 (2 x d, $^3J_{\text{PhCHH}} = 11.4$ Hz, 4H, 2 x PhCHH), 4.80 - 4.71 (m, 6H, 6 x PhCHH), 4.68 – 4.36 (m, 28H, 2 x H-3D,H, 16 PhCHH), 4.32 – 4.27 (m, 4H, 2 x H-3C,G, 2 x H-6D,H), 4.25 – 4.13 (m, 10H, 2 x H-3A,E, 2 x H-5B,F, 2 x H-5C,G, 4 x PhCHH), 4.05 (t, $J = 9.4$ Hz, 2H, H-3B,F), 3.93 (m, 4H, H-6C,G), 3.90 – 3.82 (m, 6H, 2 x H-4B,F, 2 x H-4D,H, 2 x H-6D,H), 3.80 – 3.73 (m, 4H, 2 x H-5D,H, 2 x H-4A,E), 3.70 (t, $^3J_{4,5} = ^3J_{4,3} 9.2$ Hz, 2H, 2 x H-4C,G), 3.61 (bt, 2H, 2 x H-6A,E), 3.55 (dd, $^3J_{2,3} = 10.2$ Hz, $^3J_{2,1} = 3.7$ Hz, 2H, 2 x H-2D,H), 3.53 – 3.50 (m, 1H, 2 x H-2A,E), 3.42 – 3.30 (m, 6H, 2 x H-2C,G, 2 x H-2B,F, 2 x H-6B,F), 3.09 (bd, $^3J_{6a,6b} = 11.7$ Hz, 2H, 2 x H-6B,F).

¹³C NMR (151 MHz, Acetone) δ , 144.6 (C=Pd), 144.6 - 139.2 (C_{ipso}), 133.9 - 127.0 (C_{HAr}, C_{HArPhCN}), 125.2 (N-CH=CH-N), 99.1 (C-1C,G), 98.6 (C-1A,E, C-1B,F), 94.8 (C-1D,G), 83.1 (C-4D,H, C-2D,H), 82.9 (C-4C,G), 82.2 (C-3A,E), 81.7(C-3C,G), 81.5 (C-2B,F, C-3B,F), 81.5 (C-2A,E), 80.6 (C-2B,F), 80.4 (C-2C,G), 80.0 (C-2D,H, C-3D,H), 77.5 (C_{HHPH}), 76.9 (C_{HHPH}), 76.6 (C_{HHPH}), 74.2 (C_{HHPH}), 73.8 (C_{HHPH}), 73.8 (C_{HHPH}), 73.5 (C-4A,E, C-5D,H), 73.1 (C_{HHPH}), 73.0 (C_{HHPH}), 72.9 (C-5C,G), 72.8 (C_{HHPH}), 72.7(C_{HHPH}), 72.4, 72.1 (C-5A,E), 71.9 (C-6B,F), 71.2 (C-2C,G), 70.8 (C-2D,H), 69.9 (C_{HHPH}), 68.8 (C_{HHPH}), 68.3 (C_{HHPH}), 66.8 (C_{HHPH}), 66.4 (C-2B,F), 54.1(C-6A,E)

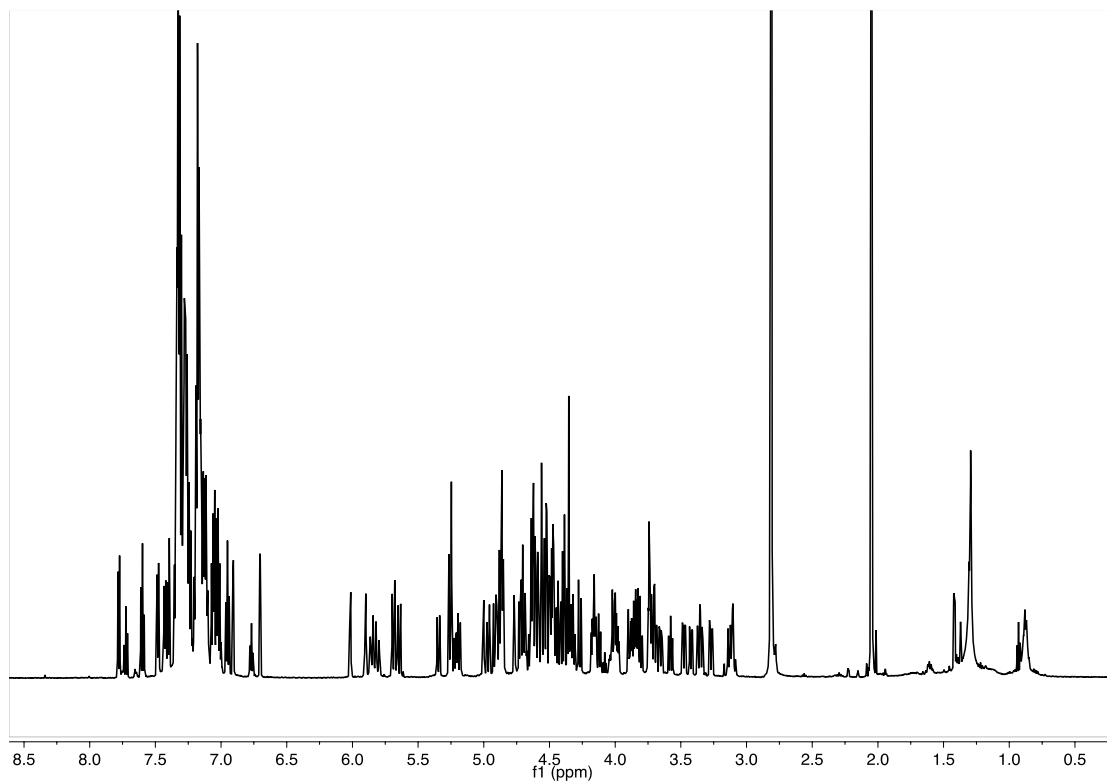


Figure S49: $^1\text{H-NMR}$ of $(\gamma\text{-AE-ICyD})\text{PdCl}_2(\text{PhCN})$ **169** (Acetone- d_6 , 600 MHz, 300K)

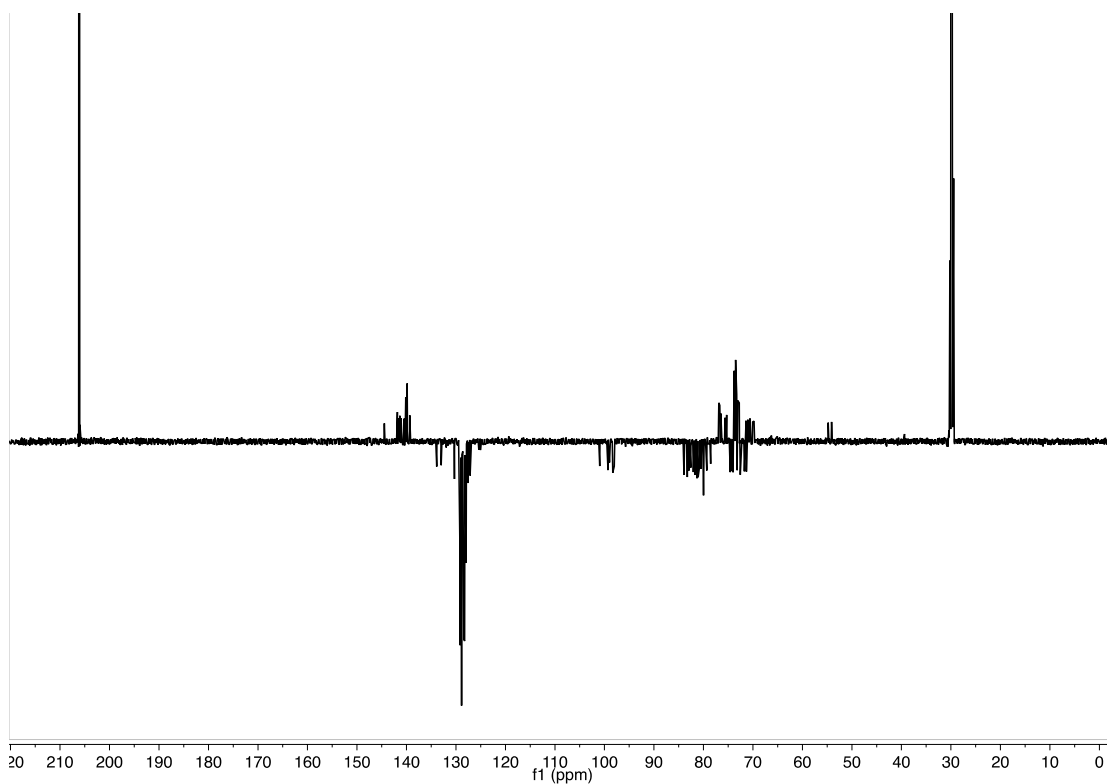
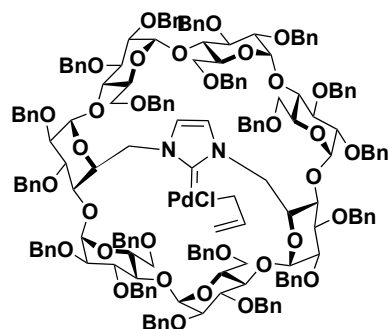


Figure S50: $^{13}\text{C-NMR}$ of $(\gamma\text{-AE-ICyD})\text{PdCl}_2(\text{PhCN})$ **169** (Acetone- d_6 , 151 MHz, 300K)

Cycl e A/E	H	C	Cycl e B/F	H	C	Cycl e C/ G	H	C	Cycl e D/ H	H	C
1	5,14	98,6	1	4,92	98,6	1	4,94	99,1	1	5,99	94,9
2	3,52	81,5	2	3,40	80,6	2	3.34	80.43	2	3,55	80,0
3	4,21	82,16	3	4,06	81,47	3	4.29	81.75	3	4,65	80,0
4	3,76	73,46	4	3,88	81,45	4	3.70	82.86	4	3,88	83.1
5	5,08	72,1	5	4,20	71,95	5	4.16	72.86	5	3,78	73,5
6	3,61	54,1	6	3.30	66,55	6	3.93	71.2	6	4,31	70,8
6'	5,95		6'	3.09		6'	3.93		6'	3,84	

Table S6:Attribution of the protons of the sugar units of **169**

(β -ICyD)PdCl(η^3 -allyl) (170)



Chemical Formula:

$C_{181}H_{189}ClN_2O_{33}Pd$

Molecular Weight:

3062.30

(β -ICyD)AgCl 125 (150mg, 49.7 μ mol, 1eq) and allylpalladium(II) chloride dimer (9 mg, 49.7 μ mol, 1eq) were weighed in a sealed tube and purged with Ar, then, dry DCM (1,5 mL) was added, and the reaction mixture is then stirred at room temperature for 30 minutes. The reaction is checked by Mass Spectrometry and TLC when finished, silver salts are removed by filtration with a 0.2 μ m PET filter, and the solvent is evaporated *in vacuo*. After silica gel filtration (CyH:AcOEt 3:1) **(β -ICyD)PdCl(η^3 allyl) 170** was obtained as a yellow palish foam (141 mg, 93%)

1H -NMR: (600 MHz, acetone- d_6) 7.49 - 6.94 (m, 94H, H Ar), 6.91 (d, $^2J_{NCH=CHN} = 1.7$ Hz, 1H, HImD), 6.80 (d, $^2J_{NCH=CHN} = 1.7$ Hz, 1H, HImA), 6.77 (m, 1H, HARp), 5.97 (d, $^2J_{1,2} = 3.8$ Hz, 1H, H-1G), 5.94 (d, $^2J_{1,2} = 3.3$ Hz, 1H, H-1C), 5.83 (d, $^2J_{CHHPH} = 11.7$ Hz, 1H, CHPh), 5.69 (1H, heptuplet? Hallylmeso), 5.65 - 5.58 (m, 2H, H-6A, CHPh), 5.43 (d, $^2J_{1,2} = 11.2$ Hz, 1H, CHPh), 5.33 - 5.28 (m, 2H, 2xCH₂Ph), 5.13 (dt, $^2J_{CHHPH} = 10.7$ Hz, $^3J_{6,5} = 1.8$ Hz, 1H, H-5A), 5.08 (d, $^2J_{CHHPH} = 11.5$ Hz, 1H, CHPh), 5.03 (d, $^3J_{1,2} = 3.6$ Hz, 1H, H-1D), 5.01 - 4.96 (m, 3H, H-1F, 2xCHPh), 4.96 (d, $^3J_{1,2} = 3.6$ Hz, 1H, H-1B), 4.94 - 4.71 (m, 11H, H-1A, H-1E, H-5D, H-5E, H-5F, H-3G, 5xCHPh), 4.69 - 4.30 (m, 25H, H-6D, H-3F, H-6G, Hallylcis-syn, 21xCHPh) 4.30 - 4.18 (m, 7H, H-3B, H-3C, H-4C, Hallyltrans, 3xCH₂Ph) 4.12 - 4.03 (m, 3H, H-3D, H-3E, H-5G) 4.02 - 3.42 (m, 22H, H-2A, H-2B, H-2C, H-2G, H-3A, H-4A, H-4B, H-4D, H-4E, H-4F, H-4G, H-5B, H-6B, H-5C, H-6A, 2xH-6C, H-6D, H-6G, 2xH-6F, Hallylcis), 3.39 (dd, $^3J_{2,3} = 10.0$ Hz, $^3J_{1,2} = 3.2$ Hz, 1H, H-2F), 3.30 (dd, $^3J_{2,3} = 9.7$ Hz, $^3J_{1,2} = 3.3$ Hz, 1H, H2-E), 3.05 (m, 3H, H6-B, 2xH6-E), 2.78 (m, 1H, Hallylcis-anti).

^{13}C -NMR: 183.5 (C=Pd), 142.1-139.8 (Cipso), 129.2-127.1 (CAr), 124.2 (N-CH=CH-N, A), 123.7 (N-CH=CH-N,D), 114.4 (CAllylmeso), 101.17 (C-1D), 101.12 (C-1E), 98.48x2 (C-1A, C-1F), 98.2 5 (C-1B) 97.3 (C-1C), 96.4 (C-1G), 84.0 (C-4F), 83.9 (C-3A), 83.5 (C-4E), 82.3 (C-4G), 82.1 (C-4C), 81.5x2(C-4B, C3/F), 81.3 (C-3G), 81.2-81.1 (2xC-2A/B/D, C-2G, C-3G, C-3B, C-3E/D), 81.0 (C-3E/D), 80.9 (C-3C), 80.6 (C-2E), 80.5 (C-2A/B/D), 79.8 (C-2F), 78.7 (C-2C), 74.8 (CAllylcis), 74.4 (C-4D), 73.7(C-5C), 73.6 (C-5B), 73.4 (C-5G), 73.3 (C-4A), 73.1 (C-5A), 72.5 (C-5F), 71.7 (C-5D), 71.5 (C-5E), 71.3 (C-6F), 70.8 (C-6C)70.7 (C-6G), 69.9 (C-6E), 69.3 (C-6A), 56.0 (C-6D), 53.1 (C-6A), 51.2 (CAllyltrans).

HRSM (ESI) : calculated for $[C_{181}H_{189}ClN_2O_{33}PdNa]^+$ 3082.1828, found 3081.1738 err 1.3 ppm

Rf=0.35 (CyH:AcOEt 3:1)

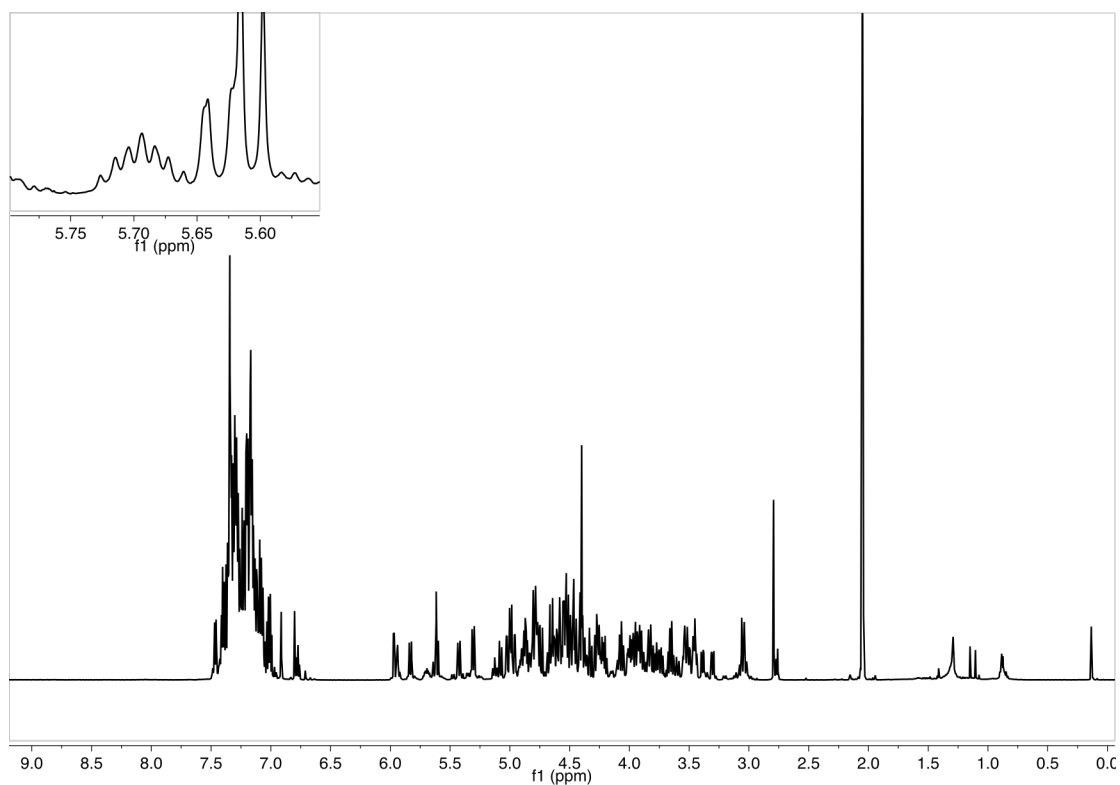


Figure S51: $^1\text{H-NMR}$ of $(\beta\text{-ICyD})\text{PdCl}(\eta^3 \text{ allyl})$ **170** (Acetone- d_6 , 600 MHz, 300K)

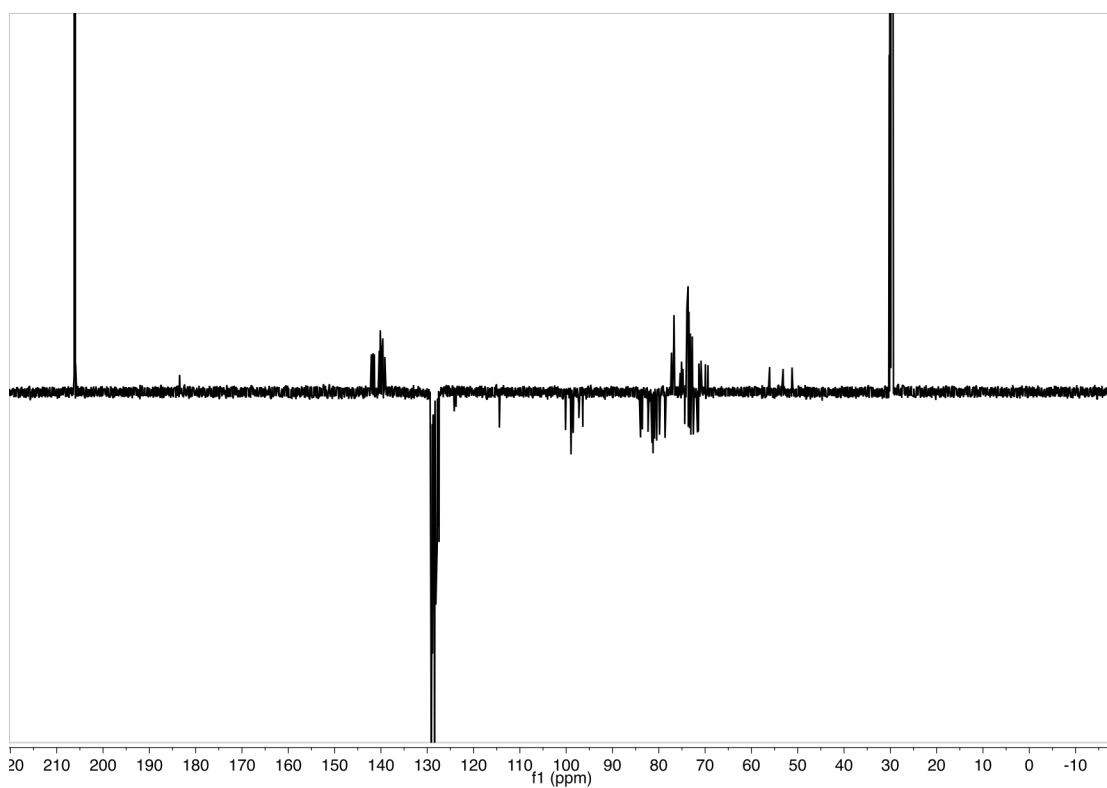


Figure S52: $^{13}\text{C-JmodNMR}$ of $(\beta\text{-ICyD})\text{PdCl}(\eta^3 \text{ allyl})$ **170** (Acetone- d_6 , 151 MHz, 300K)

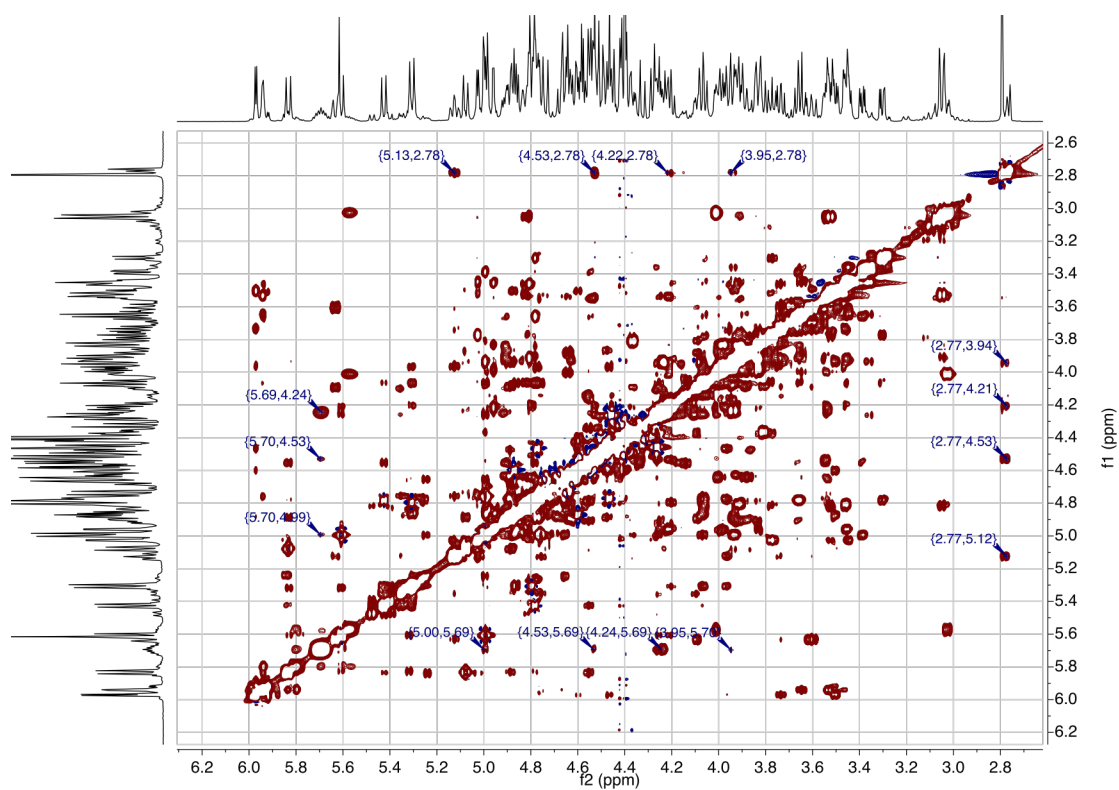
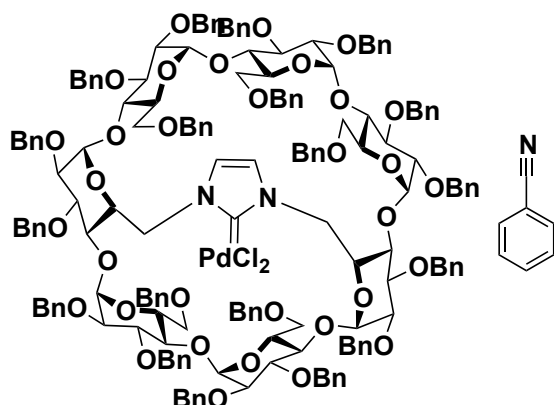


Figure S53: 2D-NOESY of $(\beta\text{-ICyD})\text{PdCl}(\eta^3 \text{ allyl})$ **170** showing the cross correlations of the *H*_{cis-anti}(Acetone-*d*₆, 600 MHz, 300K)

Cycle A	H	C	Cycle B	H	C
1	4,81	98,91	1	4,96	98,47
2	3,46	80,50/81,23	2	3,46	81,22/80,50
3	3,96	83,94	3	4,20	81,23
4	3,74	73,23	4	3,92	81,48
5	5,13	73,10	5	3,54	73,64
6	3,60		6	3,54	
6'	5,63	53,15	6'	3,05	69,93
Cycle C	H	C	Cycle D	H	C
1	5,94	97,25	1	5,03	100,15
2	3,53	78,70	2	3,45	81,23/80,50
3	4,25	80,9	3	4,07	81,08/82,40
4	4,23	82,13	4	3,64	74,40
5	4,01	73,66	5	4,79	71,67
6	3,98		6	3,87	
6'	3,84	70,80	6'	4,67	56,04
Cycle E	H	C	Cycle F	H	C
1	4,78	100,15	1	4,99	98,92
2	3,30	80,55	2	3,39	81,28
3	4,06	81,07	3	4,55	81,49
4	3,78	83,55	4	3,66	84,04
5	4,82	71,49	5	4,91	72,52
6	3,05		6	3,91	
6'	3,05	70,80	6'	3,83?	71,34
Cycle G	H	C	allyl	H	C
1	5,97	96,4	Hcis-anti	2,78	
2	3,50	79,22	Hcis-syn	4,53	51,21
3	4,89	81,24	Hmeso	5,69	114,43
4	3,93	82,3	Htrans-anti	4,24	
5	4,09	73,40	Htrans-syn	3,94	74,81
6	4,36		HImA	6,80	124,15
6'	3,80	70,70	HImD	6,91	123,66

Table S7: Attribution of the protons of the sugar units of **170**

(β -ICyD)PdCl₂(PhCN) (171)



Chemical Formula:
C₁₈₅H₁₈₉Cl₂N₃O₃₃Pd
Molecular Weight:
3159,81

(β -ICyD)AgCl 125 (227mg, 73 μ mol, 1eq) and bis(benzonitrile)palladium(II) chloride (28,8mg, 73umol, 1eq) were weighed in a sealed tube and purged with Ar, then, CH₂Cl₂ (2 mL) was added, and the reaction mixture was heated at 40°C for 30 minutes. The reaction was checked by Mass Spectrometry and TLC. When finished, silver salts are removed by filtration with a 0.2 μ m PET filter, and evaporated to dryness. After silica gel filtration (CyH : EtOAc, 3 : 1) **(β -ICyD)PdCl₂(PhCN) 171** was obtained as a palish yellow foam (218mg, 94%)

¹H-NMR: (600 MHz, acetone-d₆): 7.80 - 7.76 (m, 2H, Hortho Benzonitrile), 7.75 - 7.70 (m, 1H, Hpara Benzonitrile), 7.62 - 7.57 (m, 2H, Hmeta Benzonitrile), 7.50 - 6.98 (m, 94H, HAr) 6.95 (t, J = 7.7 Hz, 2H, HArmeta), 6.91 (d, J = 1.9 Hz, 1H, NH-CH=CH-NH), 6.77 (t, J = 6.7 Hz, 1H, HArpara) 6.70 (d, J = 1.9Hz, 1H, HImD), 6.02 (d, J = 3.8 Hz, 1H, H1-G), 5.90 (d, J = 3.8 Hz, 1H, H1-C), 5.89 - 5.77 (m, 3H, H5-D, H6-A, H6-D), 5.73 - 5.63 (m, 3H, 2 x CHPh, H5-A), 5.35 (d, J = 11.4 Hz, 1H, CHPh), 5.29 - 5.16 (m, 5H, 3xCHPh, H1-D, H3-C), 5.00 (d, J = 3.2 Hz, 1H, H1-F), 4.98 - 4.82 (m, 10H, H3-G, H1-F, 8xCHPh), 4.77 (d, J = 3.3 Hz, 1H, H1-E), 4.75 - 4.25 (m, 38H, H1-A, H1-B, H3-B, H3-F, H5-B, H5-E, H5-F, H6-C, H6-G, 30xCHPh), 4.21 - 4.10 (m, 4H, H5-G, H3-A, H3-D, H3-E) 4.05 - 3.95 (m, 5H, H4-G, H4-C, H5-G, H5-C, CHPh), 3.92 - 3.78 (m, 6H, H4-B, H4-D, H4-E, H6-G, H6-D, H6-C) 3.77 - 3.67 (m, 5H, H2-G, H4-A, H6-A H6-B, H6-B, H6-E, 2XH6-F), 3.65 (dd, J = 9.5, 3.8 Hz, 1H, H2-D), 3.58 (dd, J = 10.0, 8.1 Hz, 1H, H4-F), 3.48 (dd, J = 10.4, 3.8 Hz, 1H, H2-C), 3.42 (dd, J = 9.8, 3.3 Hz, 1H, H2-A), 3.38 - 3.32 (2 x dd, J = 10.0, 3.6 Hz, 2H H2-F, H2-B) 3.27 (dd, J = 10.0, 3.3 Hz, 1H, H2-E), 3.18 - 3.06 (m, 2H, H6-B, H6-E)

¹³C-NMR(151MHz) 144.5 (C=Pd), 141.8-139.2 (Cipso), 133,9 (CBenzonitrile meta) 132,9 (CBenzonitrileOrtho), 130,3 (CBenzonitrile Para), 129,3-127,2 (CAr), 101,0 (C1-E), 99.3 (C1-D) 99.0 (C1-F), 98.3 (C1-B), 98.2 (C1-A), 98.1 (C1-G), 98.0 (C1-C), 83.9 (C4-F), 83.4 (C3-D), 83.3 (C3-A), 83.0 (C4-E), 82.6 (C4-G), 82.2 (C4-C), 82.0 (C2-D), 81.76 (C4-B), 81.71 (C2-A), 81.32 (C2-F), 81.30 (C4-E), 81.1 (C2-B), 80.85 (C3-B), 80.5 (C3-E), 80.0X2(C2-E, C3-G), 79.5(C3-C), 79.32 (C2-C), 78.54 (C2-G), 76.9x2, 76.7x2, 76.7, 76.5, 75.6, 75.3 (7x CH2Ph), 74.6(C4-D), 74.4(C5-C), 74.0(C4-A), 73.9 (CH2Ph), 73.8(C5-G), 73.8x3, 73.6, 73.5, 73.3, 73.2 (7xCH2Ph), 73.2 (C5-A), 73.0, 72.8 (2xCH2Ph), 72.5X2 (C5-B, C5-F), 71.7(C5-E), 71.4 (C6-C), 71.3(C5-D), 71.0 (C6-B), 70.6 (C6-F), 69.8 (C6-E), 69.7 (C6-B), 54.7 (C6-D), 54.1 (C6-A).

HRMS (ESI): calculated for [C₁₈₅H₁₈₉Cl₂N₃O₃₃PdNa₂]²⁺ [M+2Na]²⁺+1549.5507 found 1549.5483 err = 1.6 ppm

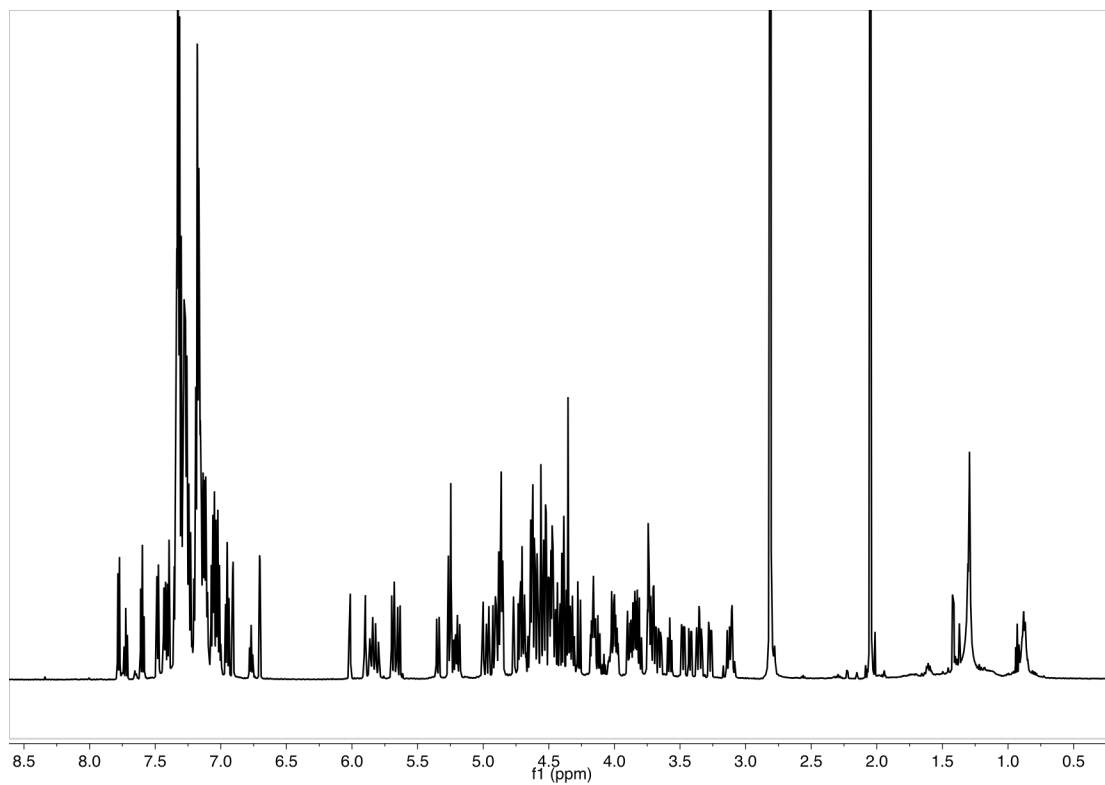


Figure S55: $^1\text{H-NMR}$ of $(\beta\text{-ICyD})\text{PdCl}(\text{PhCN})$ 171 (Acetone- d_6 , 600 MHz, 300K)

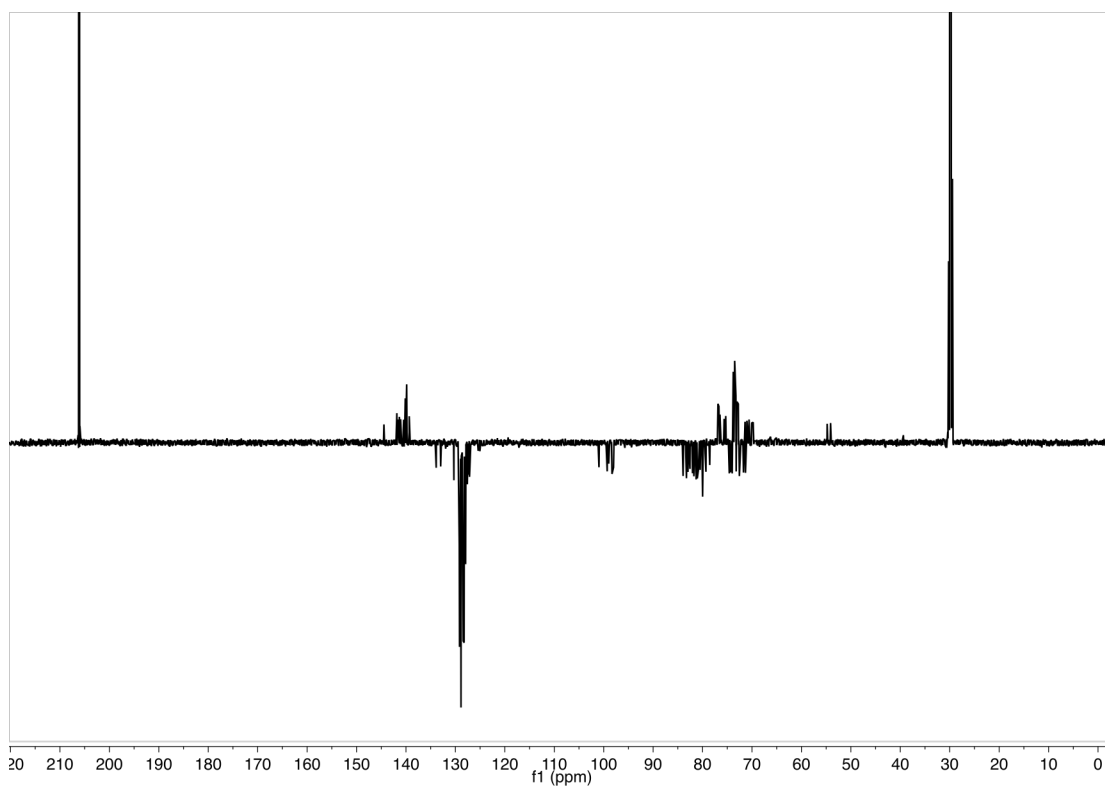
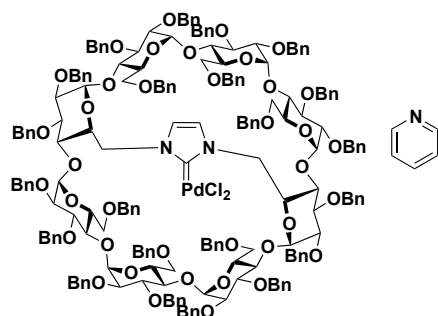


Figure S56: $^{13}\text{C-Jmod}$ of $(\beta\text{-ICyD})\text{PdCl}(\text{PhCN})$ 171 (Acetone- d_6 , 151 MHz, 300K)

Cycle A	H	C	Cycle B	H	C
1	4.86	98.2	1	4.86	98.26
2	3.42	81.67	2	3.34	81.08
3	4.12	83.26	3	4.55	80.85
4	3.73	74.06	4	3.84	81.78
5	5.67	73.20	5	4.47	72.5
6	5.84	54.1	6	3.70	69.7
6'	3.72		6'	3.13	
Cycle C	H	C	Cycle D	H	C
1	5.90	98.02	1	5.25	99.30
2	3.48	79.3	2	3.65	82.04
3	5.21	79.51	3	4.15	83.26
4	4.00	82.22	4	3.81	74.61
5	4.03	74.36	5	5.83	71.32
6	4.33	71.4	6	3.87	54.7
6'	3.83		6'	5.81	
Cycle E	H	C	Cycle F	H	C
1	4.76	100.97	1	5.00	99.00
2	3.27	80.00	2	3.36	81.32
3	4.16	80.53	3	4.31	81.33
4	3.86	82.98	4	3.58	83.96
5	4.63	71.73	5	4.68	72.5
6	3.13	69.8	6	3.74	71.03
6'	3.71		6'	3.74	
Cycle G	H	C			
1	6.02	98.1	ImidA	6.70	125.04
2	3.70	78.55	ImidD	6.91	125.37
3	4.90	80.00	C=Pd		144.5
4	4.01	82.6	Hortho	7.80-7.76	132.9
5	4.15	73.83	Hmeta	7.48	133.9
6	4.33	70.6	Hpara	7.60	130.3
6'	3.83				

Table S8: Attribution of the protons of the sugar units **171** (Acetone-d₆, 600 MHz, 300K)

(γ -AE-ICyD)PdCl₂(pyridine) (173)



Chemical Formula:
C₂₁₀H₂₁₇Cl₂N₃O₃₈Pd
Molecular Weight:
3568.29

(γ -AE-ICyD)HCl 153 (50mg, 0.14 μ mol), K₂CO₃ (30 mg, 1.96 μ mol) and PdCl₂(PhCN)₂ (5.9 mg, 0.14 μ mol) were dissolved in Pyridine (1 mL) under Ar atmosphere. The reaction mixture was stirred for 18 hours at 80°C. After cooling down the mixture to room temperature, the solvent was evaporated and the product was filtrated on a silica gel chromatography (CyH:AcOEt 5:1) affording **(γ -AE-ICyD)PdCl₂(pyridine) (173)** as a pale yellow foam (47 mg, 88 %).

¹H NMR: (600 MHz, Chloroform-d) δ = 8.57 (d, 2H, J=5.5, 2 x H_{orthoPy}), 7.47 (d, 4H, J = 7.7, 4 x H_{Bn}), 7.43 (d, 4H, J = 7.5 Hz, 4 x H_{orthoBn}), 7.31 – 7.02 (m, 92H, 94 x H_{Ar}), 7.04 – 6.92 (m, 6H, H_{Ar}), 6.84 (m, 4H, 4 x H_{Ar}), 6.72 (t, 2 H, J = 7.5 Hz, H_{Ar}), 6.10 (s, 1H, N-CH=CH-N), 5.97 (m, 3H, 2 x H-1D,H, H_{paraPy}), 5.78 (d, 2H, ²J_{H6a-H6b} = 13.3 Hz, H-6A,E), 5.53 (t, 1H J = 6.7 Hz, CH_{metaPy}), 5.49 (d, 2H, J = 10.0 Hz, 2 x PhCHH), 5.33 (d, 2H, J = 11.1Hz, 2 x CHHPh), 5.08 (t, 2H, ³J_{H5-H6} = ³J_{H5-H4} = 10.4 HZ, 2 x H-5A,D), 4.96 – 4.89 (m, 4H, H-1A,D, 4 x PhCHH), 4.84 – 4.75 (m, 6H, 4 x PhCHH, 2 x H-1B,F), 4.78 (d, 2H, ²J_{H1-H2} = 3.3 Hz, 2 x H-1C,G), 4.64 – 4.50 (m, 10H, 10 x PhCHH), 4.52 – 4.40 (m, 10H, 10 x PhCHH), 4.35 – 4.09 (m, 22H, 2xH-3A,D, 2 x H-3B,F, 2 x H-5B,F, 2 x H-3C,G, 2 x H-3D,H, 2 x H-6D,H, 10 x PhCHH), 4.00 (dd, 2H ³J_{H5-H4} = 10.0 Hz, ³J_{H5-H6} = 4.6, 2 x H-5C,G), 3.84 (m, 8H, 4 x H-6C,G, 2 x H-6D,H, 2 x H-4B,F), 3.75 (t, 2H ³J_{H4-H5} = ³J_{H4-H3} = 9.2 Hz, 2 xH-4D,H), 3.69 – 3.62 (m, 4H, 2 x H-4C,F, H-4A,E), 3.58 (dd, ³J_{H5-H4} = 9.9 Hz, ³J_{H5-H6} = 3.9 Hz, 2 x H-5D,H), 3.49 – 3.42 (m,6H, 2xH-2B,F, 2 x H-2A,E, 2 x H2-D,H), 3.35 – 3.21 (m, 6H, 2 x H-2C,G, 2 x H-6A,D, 2 x H-6B,F), 2.95 (d, 2H, ²J_{PhCHH} = 11.7 Hz, PhCHH), 2.89 (d, 2H, ²J_{H6a-H6a}=11.0, 2 x H6-B,F).

¹³C NMR: (151 MHz, Chloroform-d) δ = 155.9 (C=Pd), 151.7 (C_{orthoPy}), 140.7, 140.1, 140.0, 139.1, 139.00, 138.98, 138.9, 138.8, 138.7, 138.6, 138.30 (11 x C_{ipso}), 136.6 (C_{paraPy}), 128.8 – 125.9 (CH_{Ar}), 123.4 (CH_{meta}), 122.9 (N-CH=CH-N), 98.9 (C-1C,G), 98.6 (C-1B,F), 98.2 (C-1A,E), 93.1(C-1D,H), 82.0 (C-4C,G), 81.9 (C-4D,H), 81.4 (C-3A,E), 80.9 (C-3C,G), 80.8 (C-3B,F), 80.7 (C-2A,E), 80.7 (C-4B,F), 79.3 (C-2D,H), 79.2 (C-2B,F), 78.9 (C-3D,H), 78.9 (C-2C,G), 77.4, 77.0, 76.2, 74.9, 73.8, 73.5, 73.4, 73.2, 72.7 (9 X PhCHH), 72.4 (C-5D,H), 72.2, 72.1 (2 x PhCHH), 71.8 (C-5C,G), 71.5, 71.4 (C-4A,E, C-5A,E), 70.7 (C-5B,F), 70.4(C-6C,G), 69.7 (C-6D,H), 69.3 (C-6B,F), 53.2 (C-2A,E).

HRMS (ESI): Calculated for C₂₁₀H₂₁₇Cl₂N₃O₃₈PdNa₂ [M+2Na]²⁺ 1805.1689, found 1805.1566 err 6.8 ppm

Rf=0.35 (CyH:AcOEt 3:1)

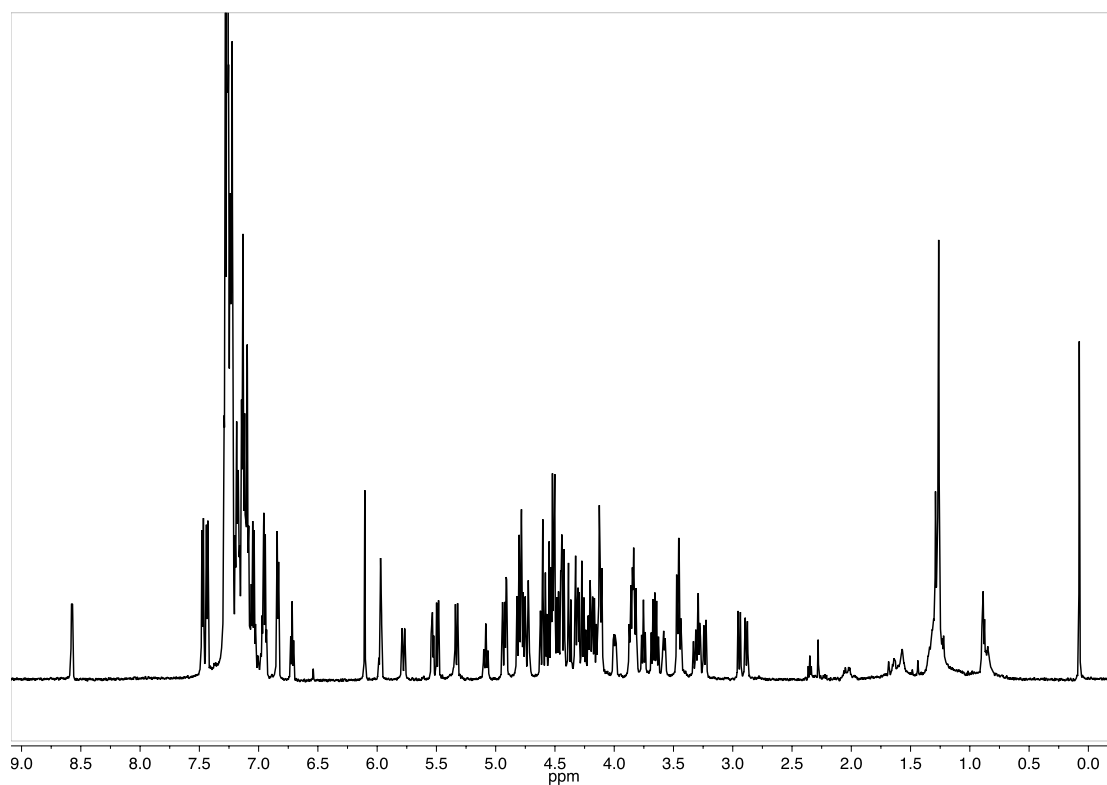


Figure S57: $^1\text{H-NMR}$ of $(\gamma\text{-AE-ICyD})\text{PdCl}_2(\text{pyridine})$ **173** (CDCl_3 , 600 MHz, 300K)

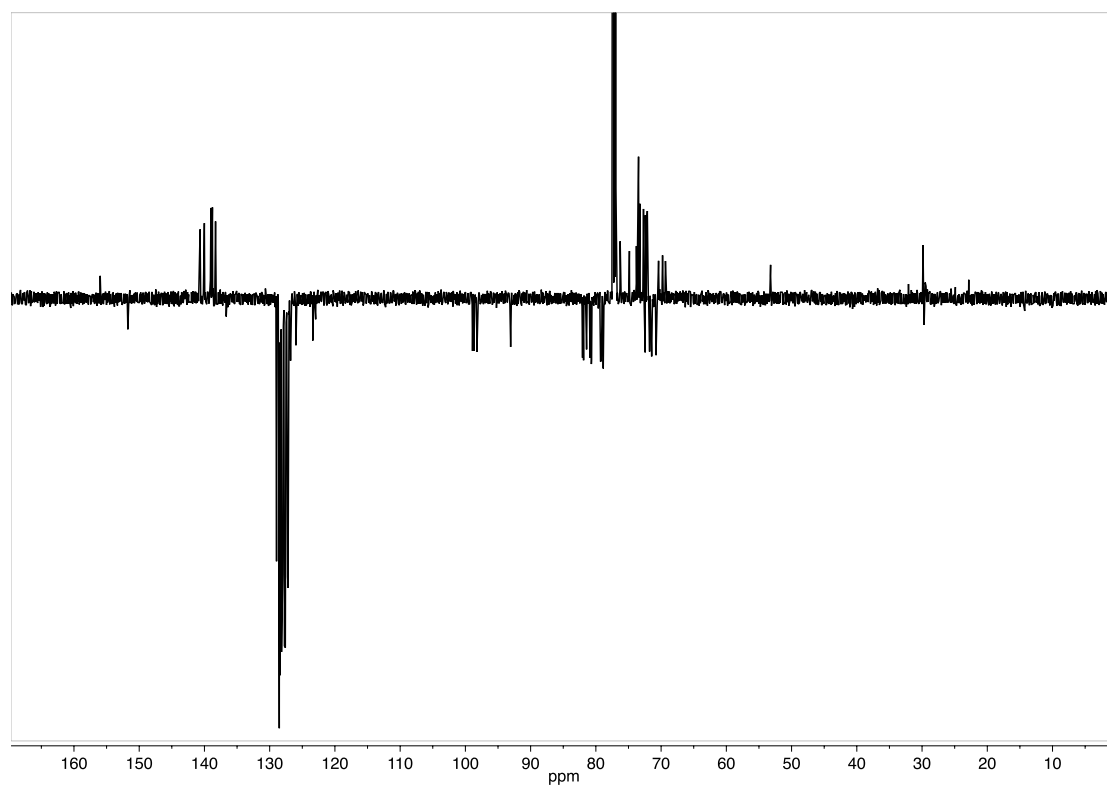
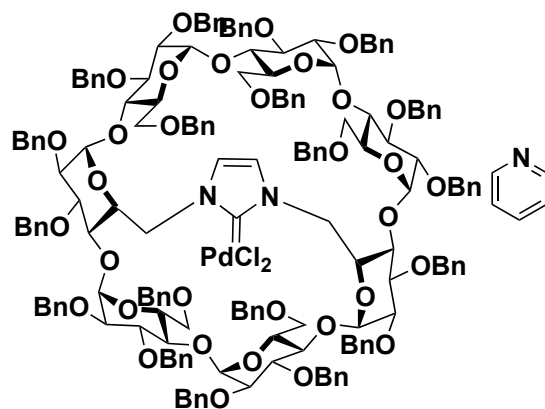


Figure S58: $^{13}\text{C-Jmod}$ of $(\gamma\text{-AE-ICyD})\text{PdCl}_2(\text{pyridine})$ **173** (CDCl_3 , 151 MHz, 300K)

Cycle AE	H	C	Cycle BF	H	C	Cycle CG	H	C	Cycle DH	H	C
1	4.91	98.22	1	4.78	98.72	1	4.72	98.88	1	5.97	93.04
2	3.44	80.66	2	3.47	79.25	2	3.29	78.87	2	3.46	79.25
3	4.25	81.41	3	4.11	80.75	3	4.16	80.89	3	4.12	78.93
4	3.67	71.39	4	3.85	80.67	4	3.64	82.00	4	3.75	81.83
5	5.08	71.39	5	4.21	70.78	5	3.99	71.75	5	3.58	72.43
6	3.31	53.25	6	3.24	69.32	6	3.85	70.42	6	4.19	69.7
6'	5.78		6'	2.89		6'	3.85		6'	3.83	

Table S9 :Attribution of the protons of the sugar units of **173**

(β -ICyD)PdCl₂(pyridine) (**172**)



Chemical Formula:
C₁₈₃H₁₈₉Cl₂N₃O₃₃Pd
Molecular Weight:
3135.79

(β -ICyD)HCl (100 mg, 0.34 μ mol), K₂CO₃ (64 mg, 2.76 μ mol) and PdCl₂(PhCN)₂ (12.7 mg, 0.34 μ mol) were dissolved in Pyridine (1 mL) under Ar atmosphere. The reaction mixture was stirred for 18 hours at 80°C. After cooling down the mixture to room temperature, the solvent was evaporated and the product was filtrated on a silica gel chromatography (CyH : AcOEt 5 : 1) affording **172** as a pale yellow foam (73, 68%).

¹H NMR (600 MHz, Chloroform-d) δ 9.17 – 9.14 (m, 2H, H_{ortho}Py), 7.42 – 6.92 (m, 95H, H_{Arom}, H_{para}Py), 6.81 (t, J = 7.4 Hz, 1H, H_{para}), 6.64 (t, J = 7.0 Hz, 2H, H_{meta}Py), 6.19 (d, J = 1.8 Hz, 1H, H_{imid}D), 6.12 (t, J = 10.4 Hz, 1H, H5-D), 6.04 (d, J = 1.7 Hz, 1H, H_{imid}A), 5.97 (d, J = 4.2 Hz, 1H, H1-G), 5.89 (d, J = 3.9 Hz, 1H, H1-C), 5.74 – 5.67 (m, 2H, H6b-A, H6b-D), 5.52 (d, J = 11.0 Hz, 1H, CH₂Ph), 5.43 (td, J = 10.4, 2.5 Hz, 1H, H5-A), 5.26 – 5.20 (m, 3H, 2xCH₂Ph, H3-C), 5.14 (2xd, J = 11.0 Hz, 2H, 2xCH₂Ph), 5.05 (d, J = 3.8 Hz, 1H, H1-D), 4.84 – 4.09 (m, 46H, H1-A, H1-B, H1-E, H1-F, H5-E, H5-F, H5-G, H5-B, H3-A, H3-B, H3-D, H3-F, H3-G, 23xCH₂Ph), 4.06 (dd, J = 10.7, 3.9 Hz, 1H, H6a-G), 3.92 (m, 3H, H3-E, H5-C, H6b-C), 3.86 – 3.72 (m, 8H, H4-B, H4-C, H4-D, H4-E, H4-G, H6a-C, H6a-F, H6b-G), 3.69 (t, J = 9.4 Hz, 1H, H4-A), 3.64 (t, J = 9.1 Hz, 1H, H4-F), 3.62 – 3.55 (m, 3H, H2-G, H6b-F, H6a-E), 3.54-3.48 (m, 2H, H2-C, H2-D), 3.46 (dd, J = 13.2, 11.1 Hz, 1H, H6a-D), 3.41 – 3.27 (m, 5H, H2-A, H2-B, H2-E, H2-F, H6a-A), 3.06 (d, J = 11.1 Hz, 1H, H6b-E), 2.92 (dd, J = 11.3, 2.5 Hz, 1H, H6b-B), 2.77 (d, J = 10.7 Hz, 1H, H6a-B).

¹³C NMR (151 MHz, Chloroform-d) δ = 153.1 (C=Pd), 151.96 (C_{ortho}Py), 140.4, 140.3, 140.2, 140.1, 134.0, 139.23, 139.22, 139.1, 139.05, 139.00, 138.95, 138.93, 138.89, 138.8, 138.7, 138.5, 138.35, 138.30, 138.15 (19xC_{ipso}), 137.5 (C_{para}Py), 128.50, 127.26-126.5 (C_HArom), 124.14 (C_{meta}Py), 123.3 (C_{imid}A), 122.95 (C_{imid}D), 100.4 (C1-E), 99.9 (C1-F), 98.3 (C1-D), 98.2 (C1-B), 97.8 (C1-C), 97.6 (C1-A), 97.1 (C1-G), 82.8 (C4-F), 82.2 (C4-C, C4-D), 82.1 (C3-D), 81.95 ?, 81.6 (C4-E), 81.10 (C2-D), 80.90 (C4-B), 80.8 (C2-A), 80.77 (C3-A, C3-G), 80.7 (C3-F), 80.2 (C3-E, C3-B), 79.7 (C2-F), 79.55 (C2-B), 78.80 (C2-E), 78.6 (C2-G), 78.3 (C3-C), 78.2 (C2-C), 76.45, 76.34, 76.17, 76.08, 75.54, 74.66 (6xCH₂Ph), 74.62 (C4-D), 74.41 (5C4-A), 74.20(CH₂Ph), 73.80 (C5-C), 73.60, 73.43, 73.38, 73.33, 73.09, 73.01, 72.81, 72.64, 72.47 (11xCH₂Ph), 72.26 (C5-G), 72.23 (CH₂Ph), 71.7 (C5-A), 71.5 (C5-F), 71.16 (C5-B), 71.12 (C6-C), 70.7 (C5-D), 70.6 (C5-E), 70.0 C6-F, 69.68 (C6-G), 68.96 (C6-E), 68.93 (C6-B), 54.77 (C6-D), 53.79 (C6-A).

HRMS (ESI): Calculated for [C₁₈₃H₁₈₉Cl₂N₃O₃₃PdNaK]²⁺ 1557.5377, found 1557.5403 err -1.7 ppm

R_f=0.42 (CyH:AcOEt 3:1)

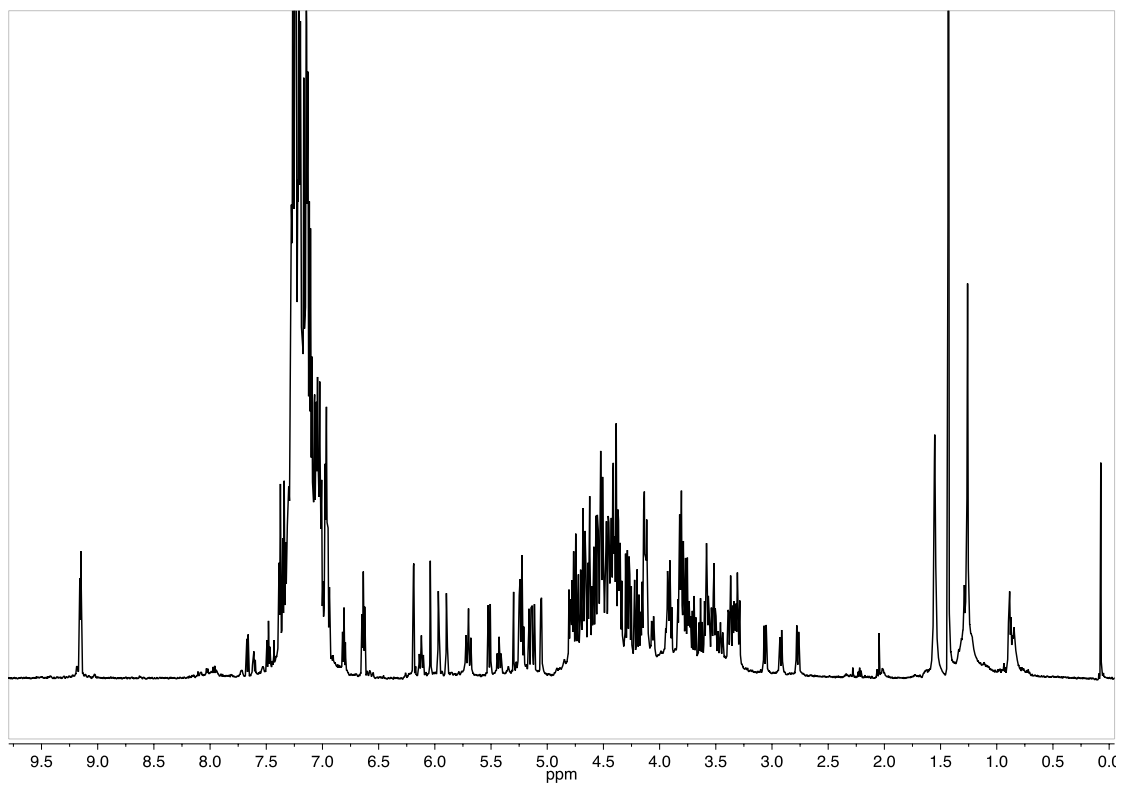


Figure S59: $^1\text{H-NMR}$ of $(\beta\text{-ICyD})\text{PdCl}_2(\text{pyridine})$ **172** (CDCl_3 , 600 MHz, 300 K)

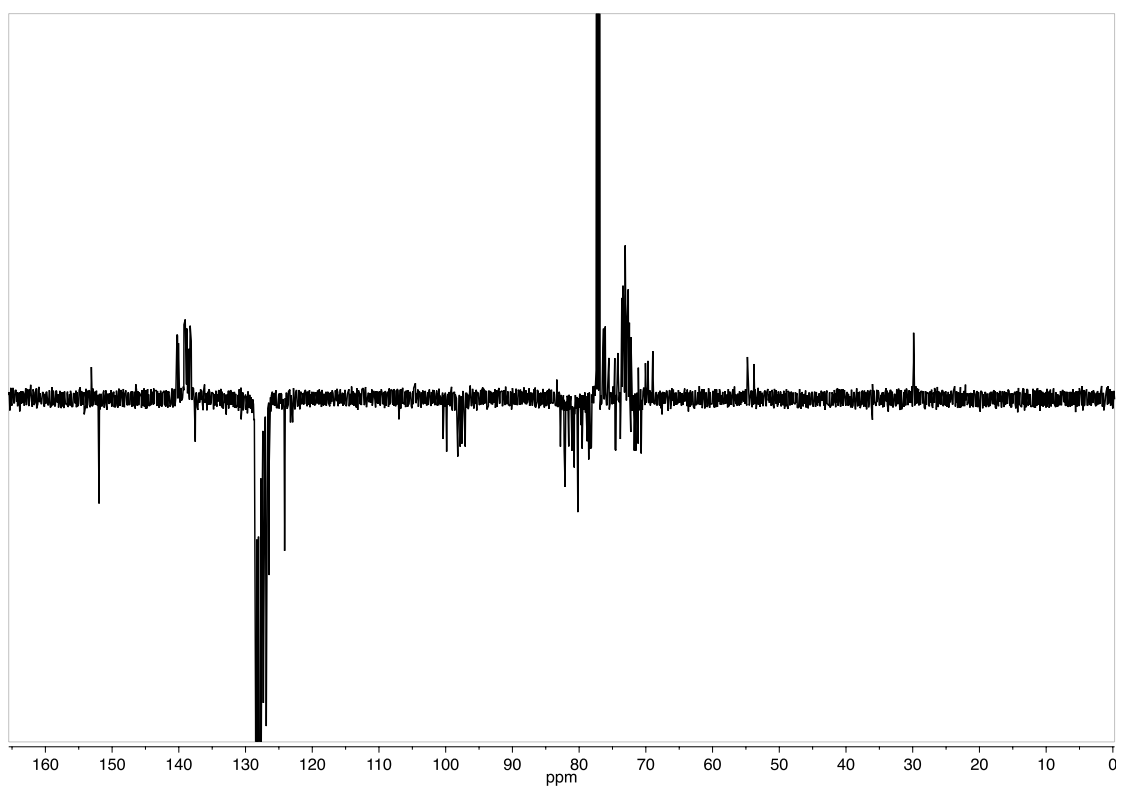


Figure S60: $^{13}\text{C-Jmod}$ of $(\beta\text{-ICyD})\text{PdCl}_2(\text{pyridine})$ **172** (CDCl_3 , 151 MHz, 300 K)

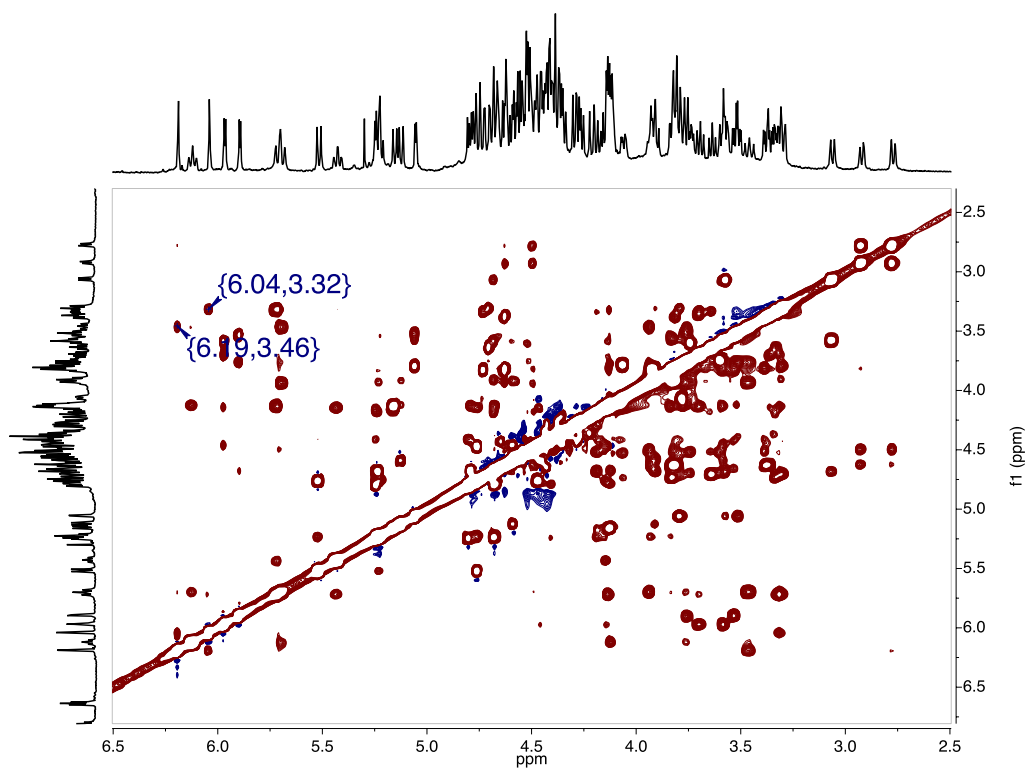
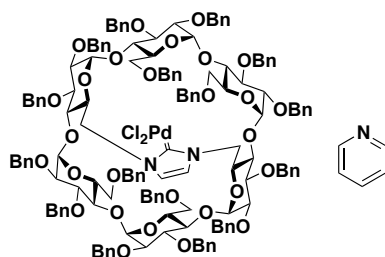


Figure S61: 2D-NOESY of **172** showing the cross correlations of the H_{NHC} with the H_{6A} and D (CDCl₃, 600 MHz, 300 K)

Cycle A	H	C	Cycle B	H	C
1	4.62	97.52	1	4.62	98.14
2	3.36	80.82	2	3.38	79.50
3	4.14	80.77	3	4.40	80.20
4	3.69	74.41	4	3.80	80.93
5	5.42	71.72	5	4.49	71.17
6	3.31	53.8	6	2.29	68.88
6'	5.71		6'	2.79	
Cycle C	H	C	Cycle D	H	C
1	5.89	97.73	1	5.05	98.19
2	3.53	78.14	2	3.52	81.10
3	5.22	78.28	3	4.12	82.09
4	3.82	82.11	4	3.75	74.62
5	3.93	73.80	5	6.12	70.67
6	3.80	71.14	6	3.46	54.7
6'	3.91		6'	5.69	
Cycle E	H	C	Cycle F	H	C
1	4.70	100.34	1	4.72	99.89
2	3.29	78.76	2	3.33	79.7
3	3.91	80.20	3	4.19	80.76
4	3.79	81.61	4	3.63	82.78
5	4.68	70.60	5	4.52	71.5
6	3.57	68.96	6	3.74	69.99
6'	3.07		6'	3.91	
Cycle G	H	C			
1	5.97	97.05	ImidA	6.04	123.2
2	3.58	78.58	ImidD	6.19	122.9
3	4.14	80.76	C=Pd		153.1
4	3.82	82.10	Pyridine	H	C
5	4.12	72.27	Ortho	9.15	151.95
6	4.05	69.6	Meta	6.63	124.15
6'	3.77		Para	7.11	137.58

Table S10: Attribution of the protons of the sugar units **171** (CDCl₃, 600 MHz, 300K)

(α -rev-ICyD)PdCl₂(pyridine) (174)



Chemical Formula:
C₁₅₆H₁₆₁Cl₂N₃O₂₈Pd
Molecular Weight:
2703,28

(α -ICyD)HCl (100 mg, 40 μ mol), K₂CO₃ (87mg, 560 μ mol), and PdCl₂(PhCN)₂ (mg, 40 μ mol) were dissolved in pyridine (1 mL) under Ar atmosphere. The reaction mixture was stirred for 18 hours at 80°C. After cooling down the mixture to room temperature, the solvent was evaporated and the product was filtrated on a silica gel chromatography (CyH : AcOEt 4 : 1) affording (α -rev-ICyD)PdCl₂(pyridine) **174** as a pale yellow foam (69 mg, 62 % yield).

¹H-NMR: (600 MHz, Chloroform-d): 9.01 (dd, ²J_{ortho}= 2H, H_{orthoPy}), 7.83 (1H, H_{paraPy}) 7.77 (s, 2H, H_{imid}), 7.43 (m, 2H, H_{metaPy}), 7.40-7.05 (m, H_{arom}), 6.92-6.88 (m, 6H, H_{meta/paraBn}, 2 x C-2C,F), 5.71 (d, ²J_{H1,H2} = 4.1 Hz, 2H, 2x H-1C/F), 5.52 (d, ²J_{PhCHH} = 11.3 Hz, 2H, PhCHH), 5.24 (dd, ²J_{H6a-H6b} = 15.2 Hz, ³J_{H6a-H5} = 1.7 Hz, 2H, H-6A,D), 5.19 (d, ²J_{PhCHH}=10.3, 2H, PhCHH) 4.91 (2xd, ²J_{PhCHH}=11.3Hz, 4H, 2xPHCHH), 4.78 (d, ²J_{PhCHH} = 11.4 HZ, 2H, PhCHH) 4.75 – 4.69 (m, 10H, 4 x PhCHH, 2 x H-1A,D, 2 x H-1B,D, H-5A,D), 4.60 (d, 2H, ²J_{PhCHH} = 11.9 Hz, PhCHH), 4.53 – 4.35 (m, 12H, 12 x PHCHH), 4.33 (d, ²J_{PhCHH} = 11.9 Hz, 2H, 2 x PhCHH), 4.28 (dd, ²J_{H6a,H6b} = 12.4 Hz, ³J_{H6,H5} = 2.75 Hz, 2H, 2 x H-6B,E), 4.25 - 4.10 (m, 2 x PhCHH, 10H, 2 x H-3A,D, 2 x H-6A,D, 2 x H-4B,E, 2 x H-5C,F), 4.03 (t, ³J_{H4,H5} = ³J_{H4,H3} = 9.3 Hz, 2H, H-4C,F), 3.93 – 3.86 (m, 4H, 2xH3-B/D, 2xH3-C/F), 3.84 – 3.78 (m, 4H, 2 x H-4A,D, 2 x H-6B,D), 3.73 (dd, ²J_{H6b-H6a} = 12.0 Hz ³J_{H6b,H5} = 2.4 Hz, 2H, 2 x H-6C,F), 3.67 (d,, ³J_{H2,H3} = 10.1 Hz, ³J_{2,1} = 4.1 Hz, 2H, 2 x H-2C,F), 3.44 (d, ³J_{H2,H3} = 9.2 Hz, ³J_{2,1} = 3.4 Hz, 2H, 2 x H-2A,D), 3.32 (d, 2H, ³J_{H2-H3} = 10.1 Hz, ³J_{H2-H1} = 3.4 Hz, 2 x H-2B,E), 3.21 (bdd, 2H, 2 x H-5C,F), 3.13 (d, 2H, 2xH-5B,E)

¹³C-NMR: (151MHz, Chloroform-d) 152.0 (C=Pd), 151.36 (2xC_{orthoPy}), 139.4, 139.3, 139.2, 139.9, 138.6 (12xC_{ipso}), 138.3 (C_{paraPy}), 137.8, 137.7 (4xC_{ipso}), 129.3-127.2 (C_{arom}), 126.4 (C_{ortho-Bn3-A/D}), 124.7 (2 x C_{metaPy}), 121.2 (2 x N-CH=CH-N), 100.2 (C-1C,F), 99.4 (C-1B,E), 96.2 (C-1A,D), 82.6 (C-3A,D), 81.8 (C-4C,F), 81.03 (C-3B,D), 80.99 (C-2A,D), 80.5 (C-3C,F), 79.86 (C-4B,E), 79.8 (C-4A,D), 78.6 (C-2B,D), 78.2 (C-2C,F), 77.0, 75.8, 74.3, 74.0,73.5, 73.4, 72.8, 72.55 (18xCHHPh), 72.4, (C-5C,F), 71.6 (C-5B,D), 70.3 (C-6B,E), 69.8 (C-6C,F), 68.9 (C-5A,D), 54.2 (C-6A,D)

Rf=0.35 (CyH:AcOEt 3:1)

HRMS (ESI): [C₁₅₆H₁₆₁Cl₂N₃O₂₈PdNa₂]²⁺ msrd 1304.4702 calce 1304.4751 err 3.8 ppm

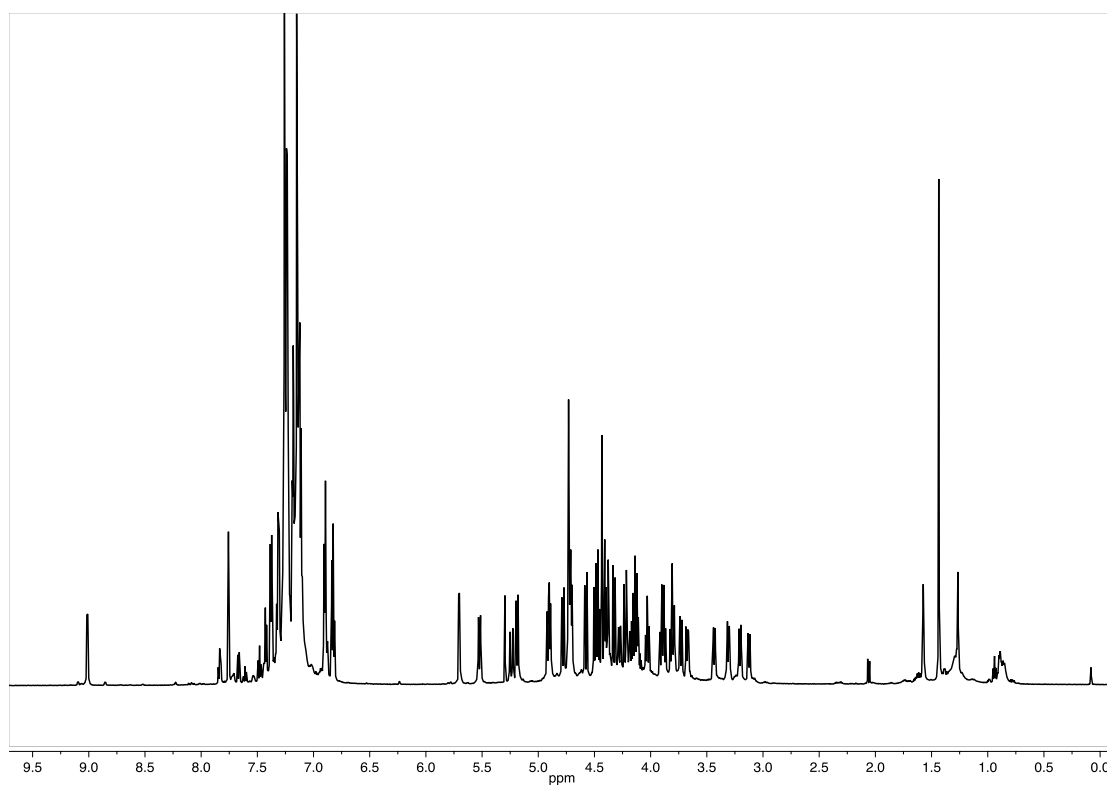


Figure S62: $^1\text{H-NMR}$ of $(\alpha\text{-rev-ICyD})\text{PdCl}_2(\text{pyridine})$ **174** (CDCl_3 , 600 MHz, 300 K)

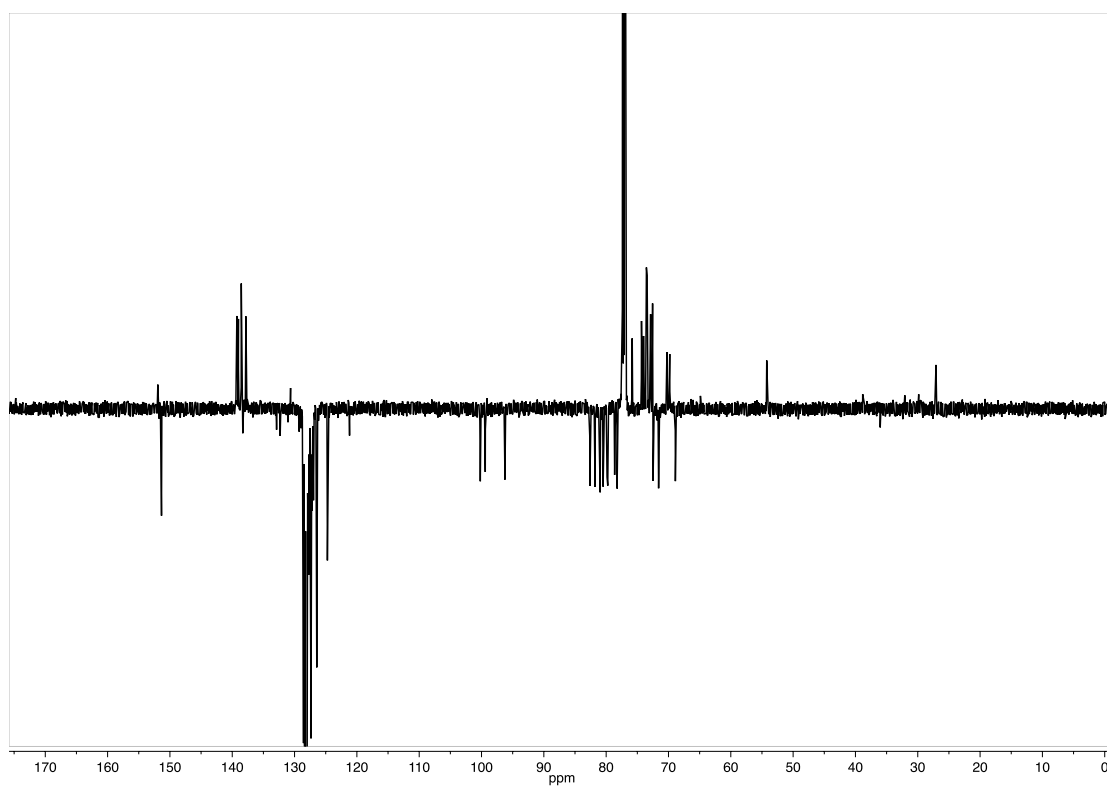


Figure S63: $^{13}\text{C-Jmod}$ of $(\alpha\text{-rev-ICyD})\text{PdCl}_2(\text{pyridine})$ **174** (CDCl_3 , 151 MHz, 300 K)

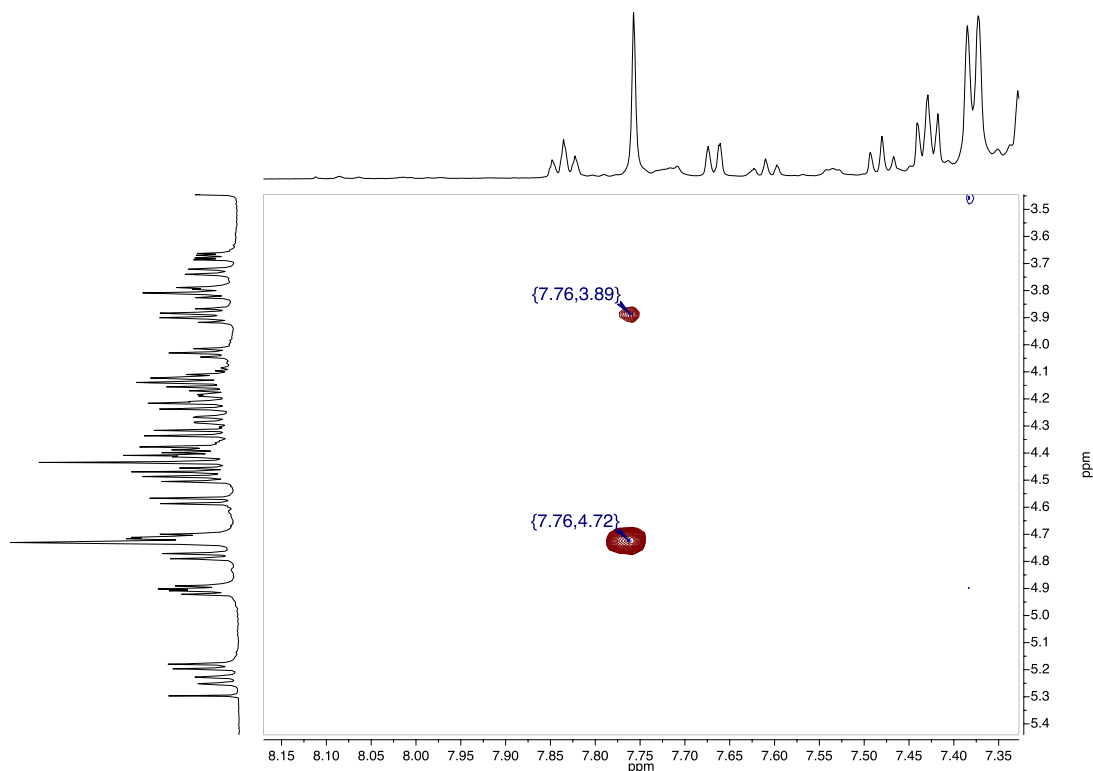


Figure S64: 2D-NOESY of **174** showing the cross correlations of the H_{NHC} with the H₅ and H₃ (CDCl₃, 600 MHz, 300 K)

Cycle A	H	C	Cycle B	H	C	Cycle C	H	C
1	4.73	96.24	1	4.74	100.23	1	5.70	99.40
2	3.44	80.99	2	3.32	78.64	2	3.68	78.26
3	4.11	82.62	3	3.89	81.06	3	3.87	80.50
4	3.81	79.76	4	4.14	79.88	4	4.02	81.80
5	4.71	68.89	5	3.13	71.57	5	3.20	72.48
6	4.20		6	4.27		6	4.12	
6'	5.23	54.23	6'	3.80	70.22	6'	3.72	69.70

Table S11: Attribution of the protons of the sugar units of **174**

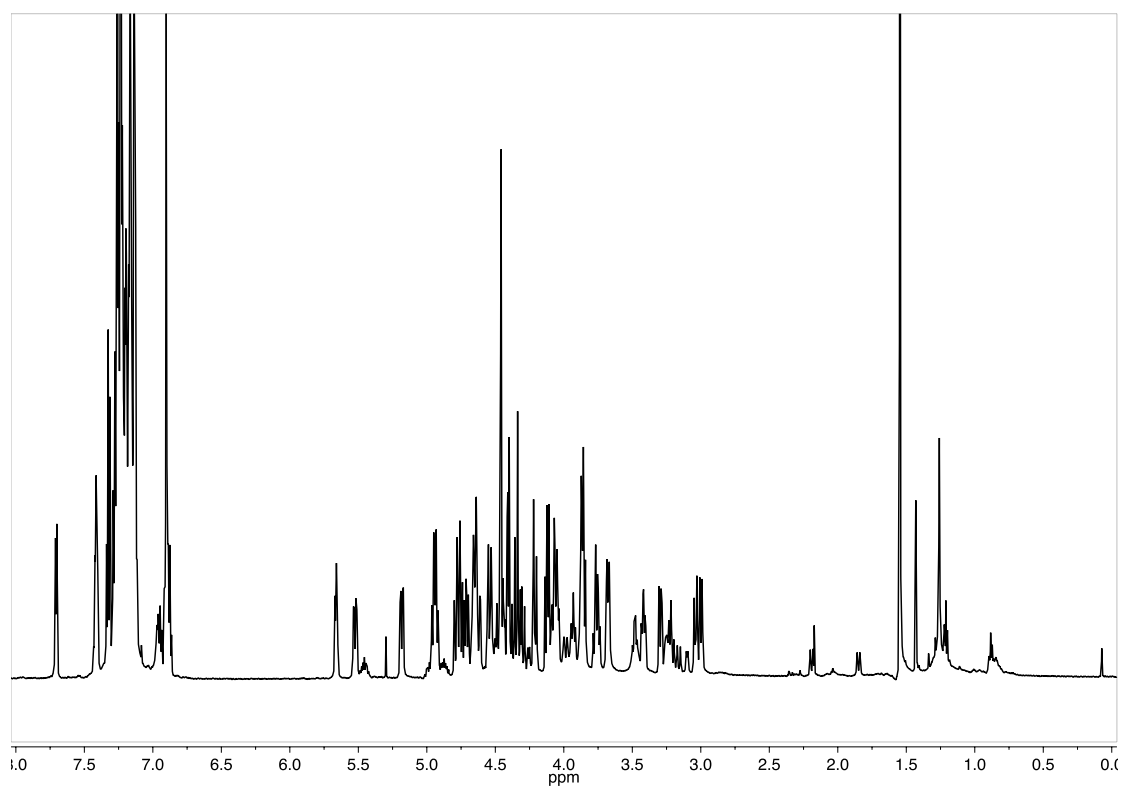


Figure S65: $^1\text{H-NMR}$ of $(\alpha\text{-rev-ICyD})\text{PdCl}(\eta^3\text{-allyl})$ **175** (CDCl_3 , 600 MHz, 300 K)

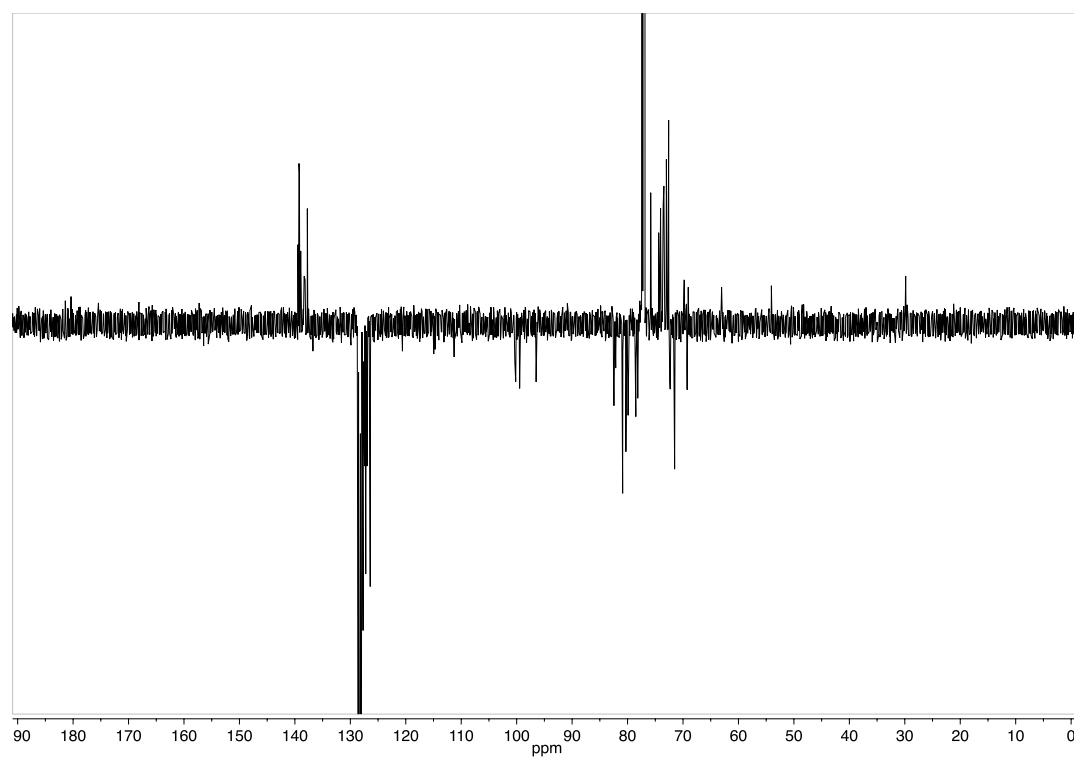


Figure S65: $^{13}\text{C-Jmod}$ of $(\alpha\text{-rev-ICyD})\text{PdCl}(\eta^3\text{-allyl})$ **175** (CDCl_3 , 151 MHz, 300 K)

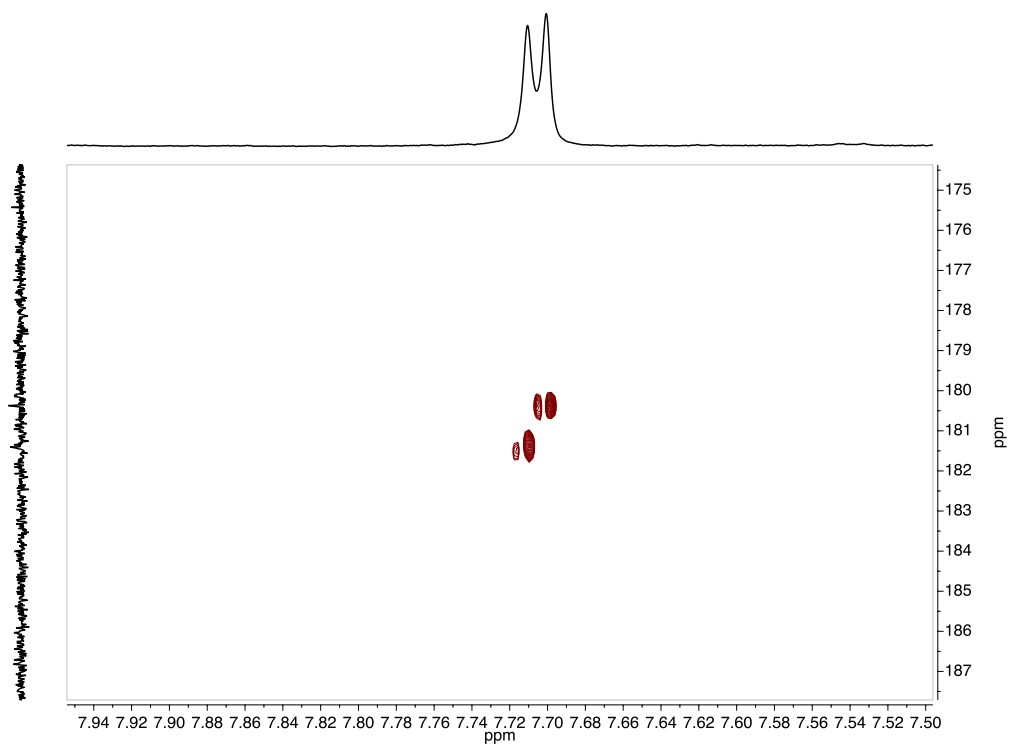


Figure S66: HMBC of **175** showing the presence of two C=Pd (CDCl₃, 300 K)

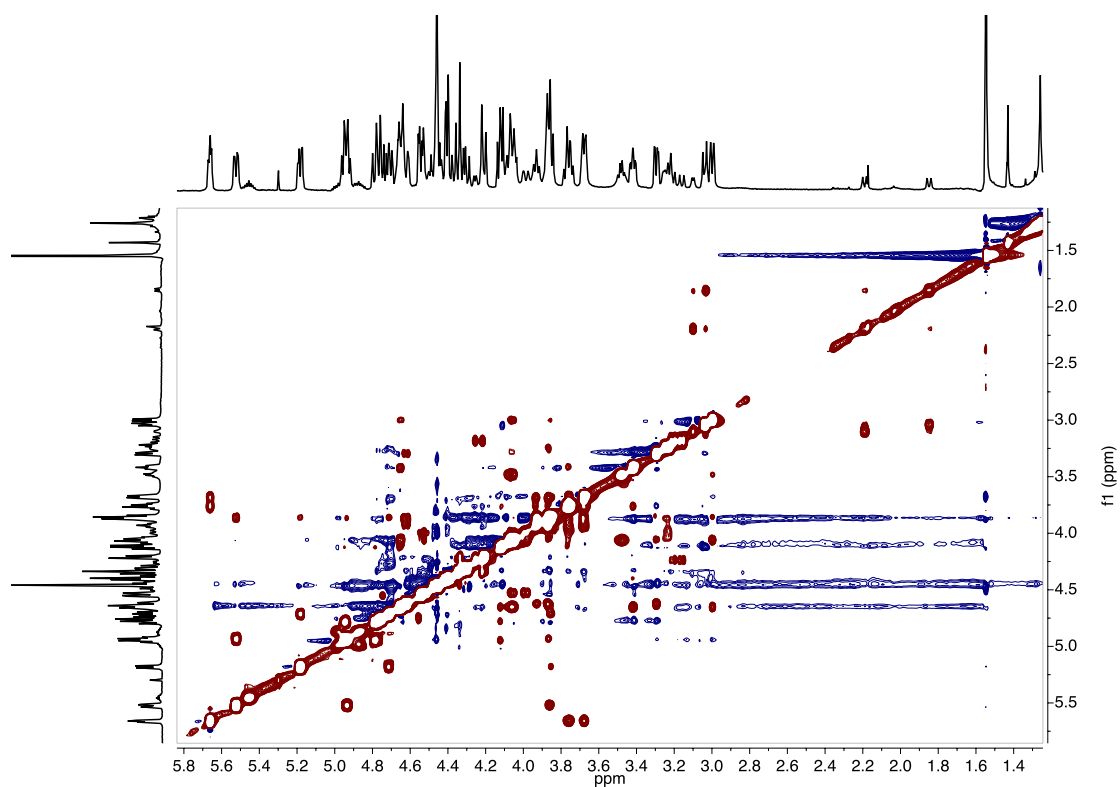


Figure S67: 2D-NOESY of (α -rev-ICyD)PdCl(η^3 -allyl) **175** (CDCl₃, 151 MHz, 300 K)

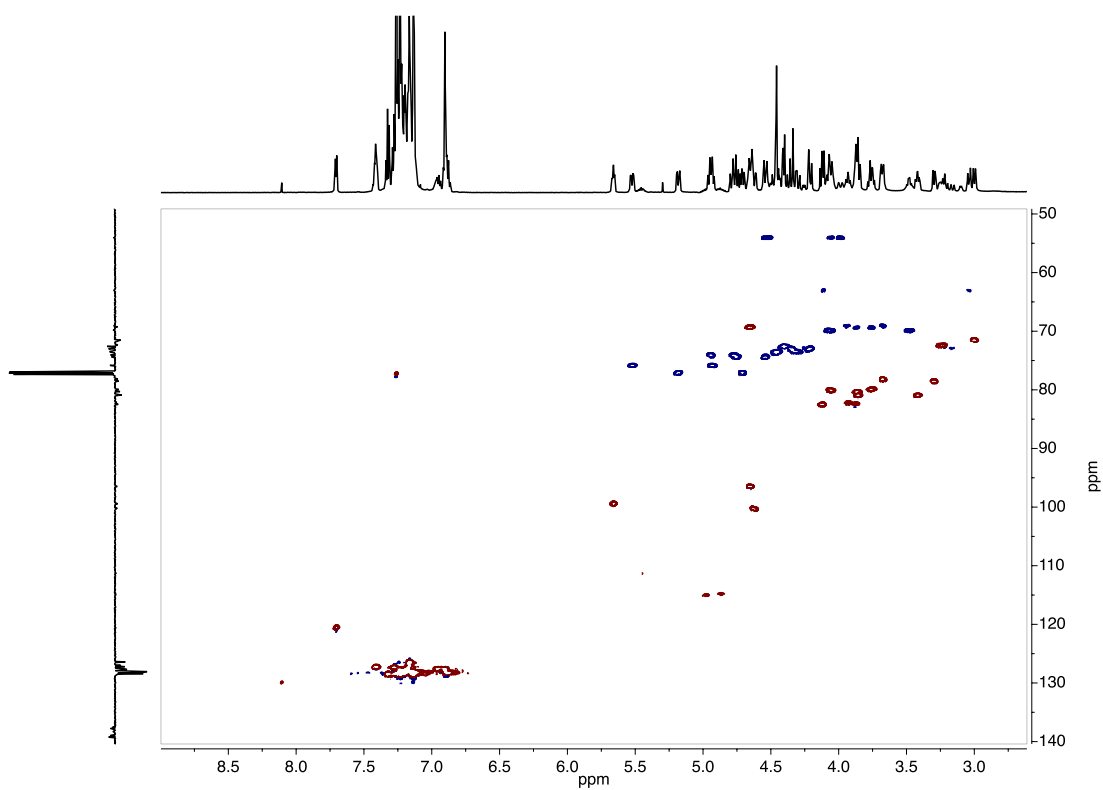
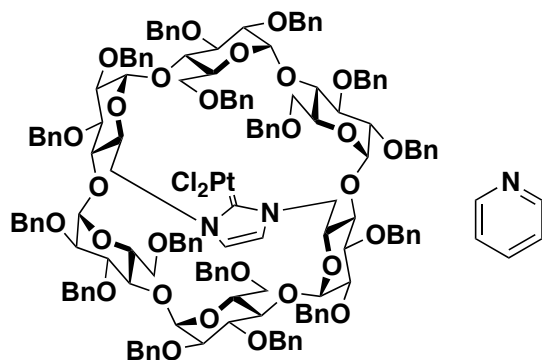


Figure S68: HSQC of (α -rev-ICyD)PdCl(η^3 -allyl) 175 (CDCl_3 , 600 MHz, 300 K)

(α -rev-ICyD)PtCl₂(pyridine) (180)



Chemical Formula:

C₁₅₆H₁₆₁Cl₂N₃O₂₈Pt

Molecular Weight:

2791.94

(α -ICyD)HCl **122** (100 mg, 40 μ mol), K₂CO₃ (120 mg, 560 μ mol) and PtCl₂ (10.7 mg, 40 μ mol) were dissolved in Pyridine (1 mL) under Ar atmosphere. The reaction mixture was stirred for 18 hours at 80°C. After cooling down the mixture to room temperature, the solvent was evaporated and the product was filtrated on a silica gel chromatography (CyH : AcOEt 4 : 1) affording (α -rev-ICyD)PtCl₂(pyridine) **180** as a pale yellow foam (67 mg, 60 % yield).

¹H NMR (600 MHz, Chloroform-*d*) δ 9.02 (d, ³J_{o-m} = 5.6 Hz, 2H, H_{orthoPy}), 7.86 (t, *J* = 7.7 Hz, 1H, H_{metaPy}), 7.70 (s, 2H, N-CH=CH-N), 7.49 – 6.84 (m, 121H, H_{Ar}), 5.70 (d, ³J_{1,2} = 4.2 Hz, 2H, H-1A,D), 5.55 (d, ²J_{PhCHH} = 11.1 Hz, 2H, 2 x PhCHH), 5.35 (d, *J* ²J_{PhCHH} = 15.0 Hz, 2H, 2 x PhCHH), 5.20 (d, ²J_{PhCHH} = 10.3 Hz, 4H, 4 x PhCHH), 4.96 – 4.88 (m, 4H, 4 x PhCHH), 4.78 - 4.75 (m, 4H, 4 x PhCHH), 4.74 - 4.65 (m, 12H, 2 x H-6A,D, 2 x H-5A,D, 2 x H-1B,E, 2 x H-1C,F, 2 x PhCHH), 4.56 (d, ²J_{PhCHH} = 12.0 Hz, 2H, 2 x PhCHH), 4.52 (d, ²J_{PhCHH} = 11.2 Hz, 2H, 2 x PhCHH), 4.48 – 4.27 (m, 17H, 15 x PhCHH, 2 x H-6B,E), 4.21 (d, ²J_{PhCHH} = 12.8 Hz, 2H, PhCHH), 4.16 – 4.08 (m, 8H, 2 x H-6B,E, 2 x H-3A,D, 2 x H-4B,E, 2 x H-6C,F), 4.04 (t, ³J_{4,5} = ³J_{4,3} = 9.3 Hz, 2H, H-4C,F), 3.89 (m, 4H, 2 x H-3B,E, 2 x H-3C,F), 3.82 – 3.66 (m, 12H, 2 x H-6B,E, 2 x H-6C,F, 2 x H-4A,D, 2 x H-3B,F, 2 x H-3C,F, 2 x H-2C,F), 3.42 (dd, ³J_{2,3} = 9.3, ³J_{2,1} = 3.4 Hz, 2H, 2 x H-2A,D), 3.32 – 3.25 (m, 4H, 2 x H-2B,E, 2 x H-5C,F), 3.09 (d, ³J_{5,4} = 9.3 Hz, 2H, 2 x H-2B,E).

¹³C NMR (151 MHz, Chloroform-*d*) δ 151.4 (CH_{orthoPy}), 139.5 – 137.70 (C_{ipso}, C_{paraPy}), 128.72 – 125.14 (CH_{Ar}), 120.2 (NH-CH=CH-NH) 100.1 (C-1B,E), 99.5 (C-1C,F), 96.38 (C-1A,D), 82.6 (C-3A,D), 81.8 (C-4C,F), 81.4 (C-3B,E), 81.1 (C-3C,F), 80.9 (C-2A,D), 80.4 (PhCHH), 80.0 (C-4B,E), 79.8 (C-4A,D), 78.6 (C-2B,E), 78.3 (C-2C,F), 77.1 (PhCHH), 75.8 (PhCHH), 74.4 (PhCHH), 74.00 (PhCHH), 73.5 (PhCHH), 73.4 (PhCHH), 72.9 (PhCHH), 72.5 (PhCHH), 72.4 (C-5B,F), 71.5 (C-5B,E), 69.9 (C-6C,F), 69.7 (C-6C,F), 69.1 (C-5A,D), 53.0 (C-6C,F).

R_f=0.33 (CyH:AcOEt 3:1)

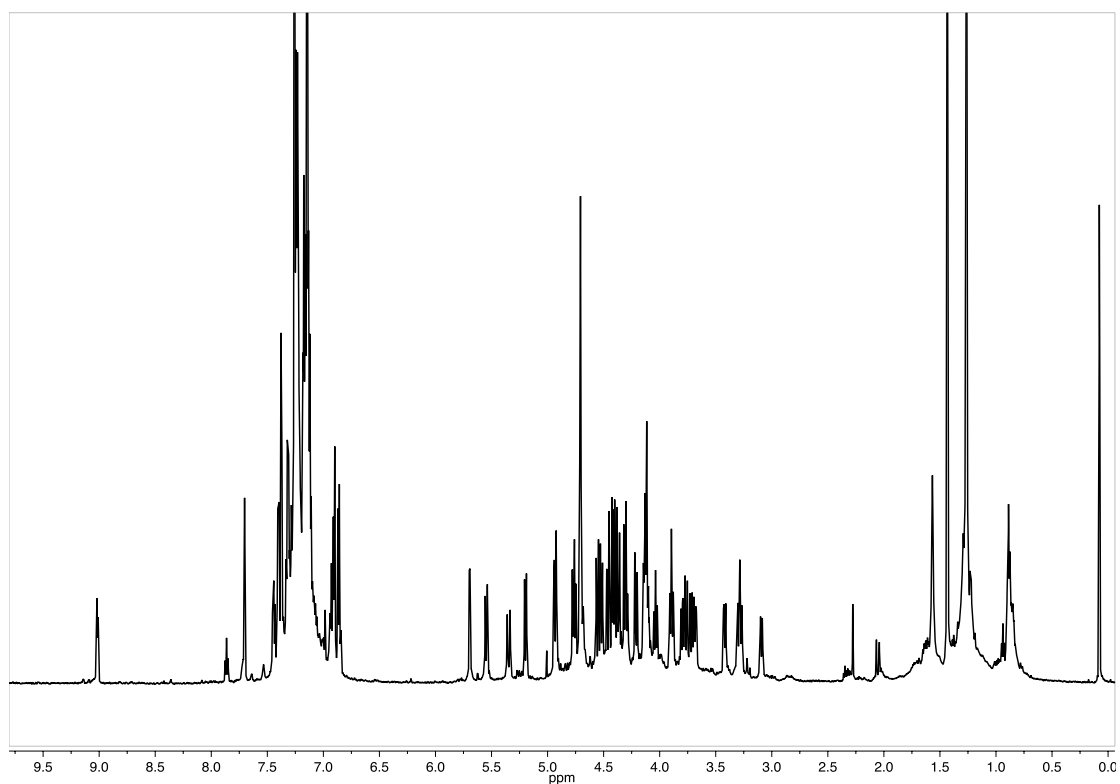


Figure S69: $^1\text{H-NMR}$ of $(\alpha\text{-rev-ICyD})\text{PtCl}_2(\text{pyridine})$ **180** (CDCl_3 , 600 MHz, 300 K)

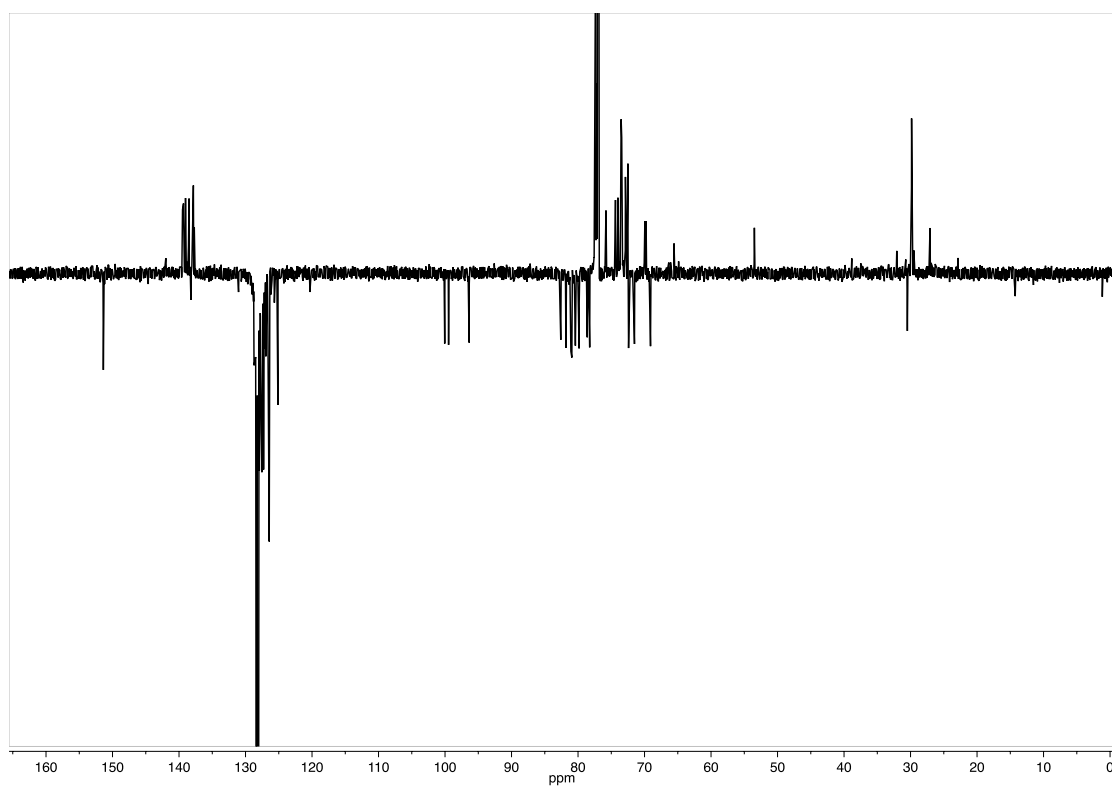


Figure S70: $^{13}\text{C-Jmod}$ of $(\alpha\text{-rev-ICyD})\text{PtCl}_2(\text{pyridine})$ **180** (CDCl_3 , 151 MHz, 300 K)

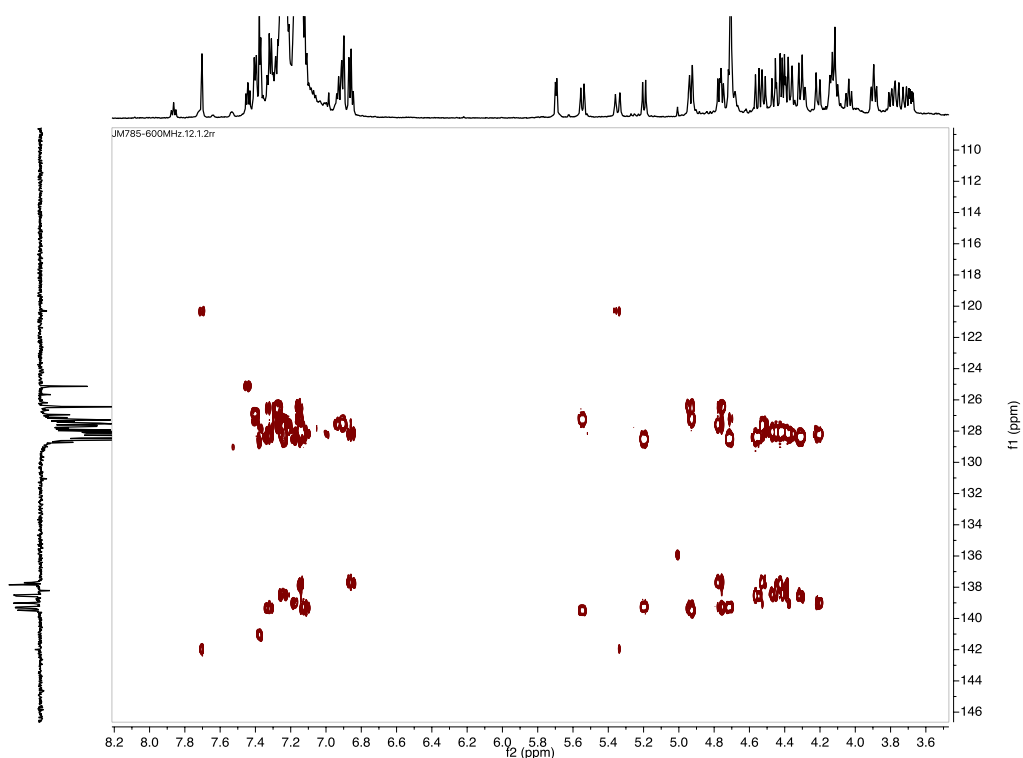


Figure S71: HMBC of (α -rev-ICyD)PtCl₂(pyridine) **180** (CDCl₃, 300 K)

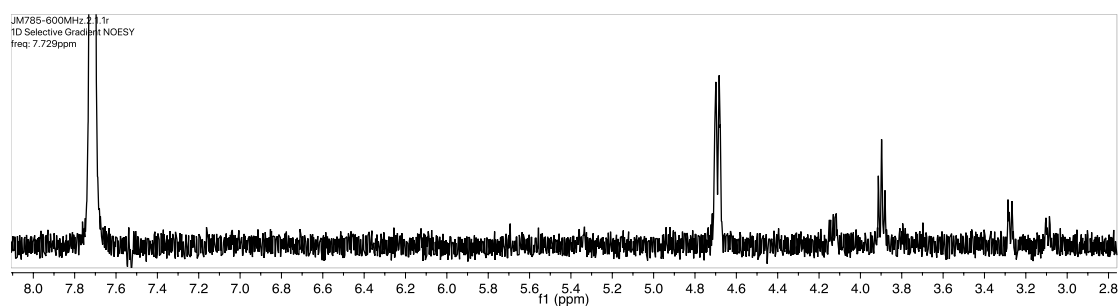
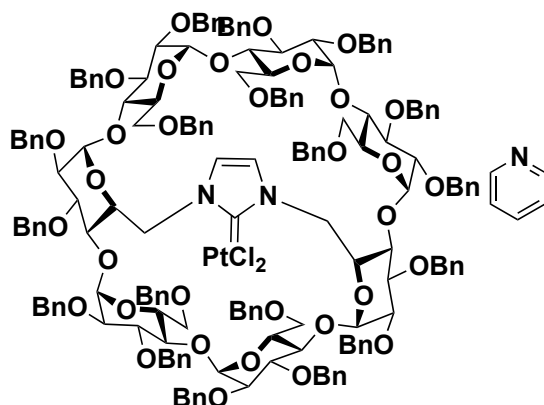


Figure S71: 1D-NOESY of (α -rev-ICyD)PtCl₂(pyridine) **180** (CDCl₃, 600 MHz, 300 K, Irradiation at 7.73 ppm H_{NHC})

Cycle A	H	C	Cycle B	H	C	Cycle C	H	C
1	4.71	96.37	1	4.71	100.05	1	5.69	99.40
2	3.43	80.93	2	3.29	78.63	2	3.68	78.29
3	4.13	82.60	3	3.89	81.41?	3	3.90	81.07?
4	3.80	79.85	4	4.11	79.97	4	4.04	81.82
5	4.69	69.09	5	3.09	71.49	5	3.28	72.39
6	5.36		6	3.68		6	4.12	
6'	4.12	53.03	6'	4.30	69.93	6'	3.71	69.73

Table S12: Attribution of the protons of the sugar units of **180**

(β -ICyD)PtCl₂(pyridine) + (β -rev-ICyD)PtCl₂(pyridine) (**181** + **182**)



Chemical Formula:
C₁₈₃H₁₈₉Cl₂N₃O₃₃Pt
Molecular Weight:
3224.45

(β -ICyD)HCl **124** (100 mg, 32 μ mol), K₂CO₃ (120 mg, 448 μ mol) and PtCl₂ (8.5 mg, 32 μ mol) were dissolved in Pyridine (1 mL) under Ar atmosphere. The reaction mixture was stirred for 18 hours at 80°C. After cooling down the mixture to room temperature, the solvent was evaporated and the product was filtrated on a silica gel chromatography (CyH : AcOEt 4 : 1) affording a 55:45 mixture of **181**:**182** as a white foam (58 mg, 55 % yield).

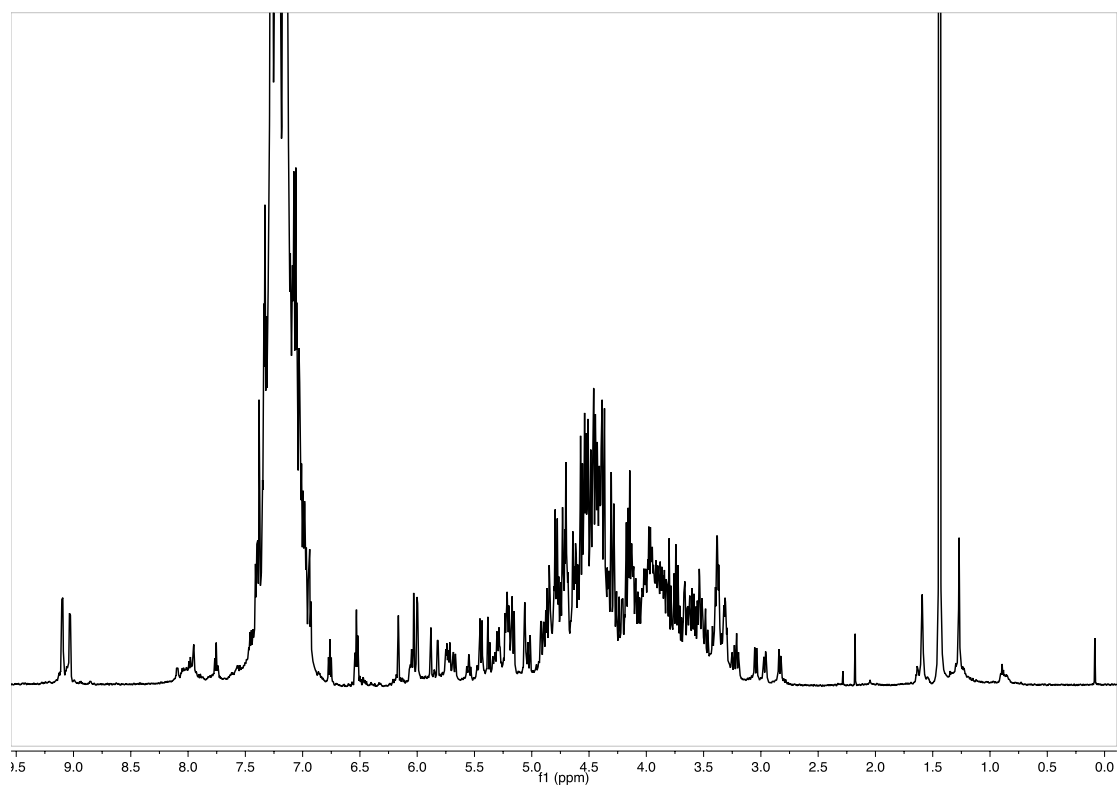


Figure S72: $^1\text{H-NMR}$ of **181+182** (CDCl_3 , 600 MHz, 300 K)

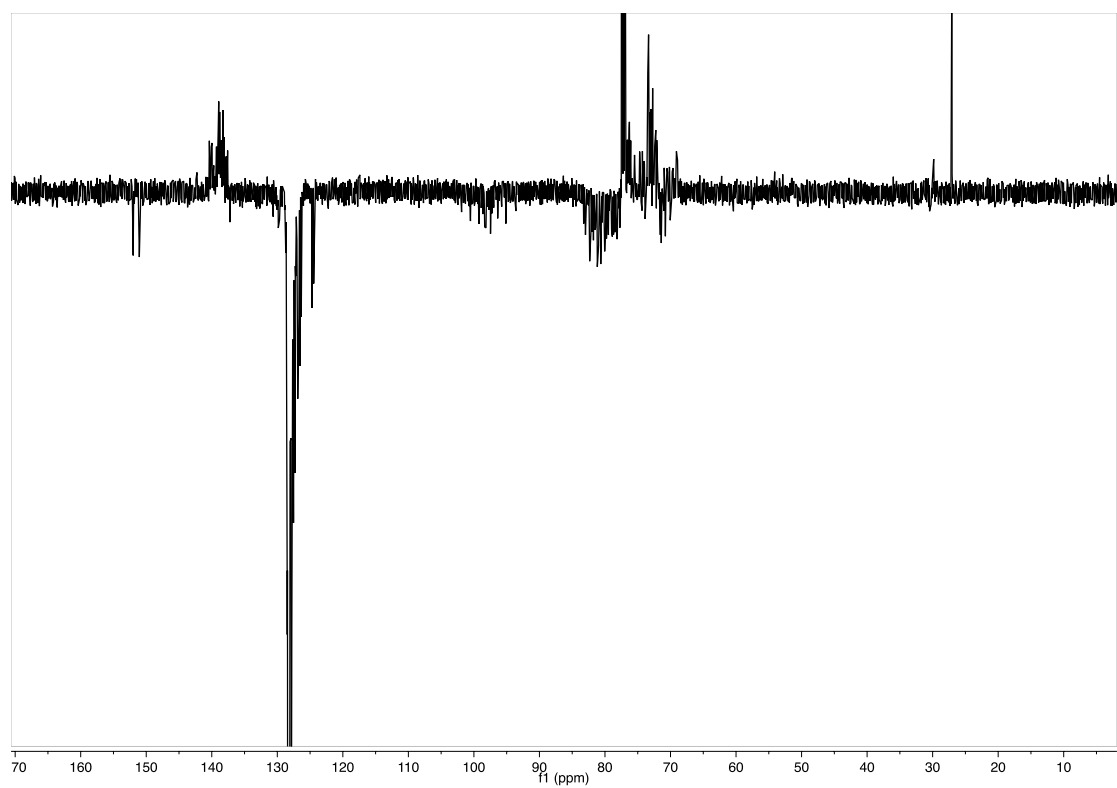


Figure S73: $^{13}\text{C-Jmod}$ of **181+182** (CDCl_3 , 151 MHz, 300 K)

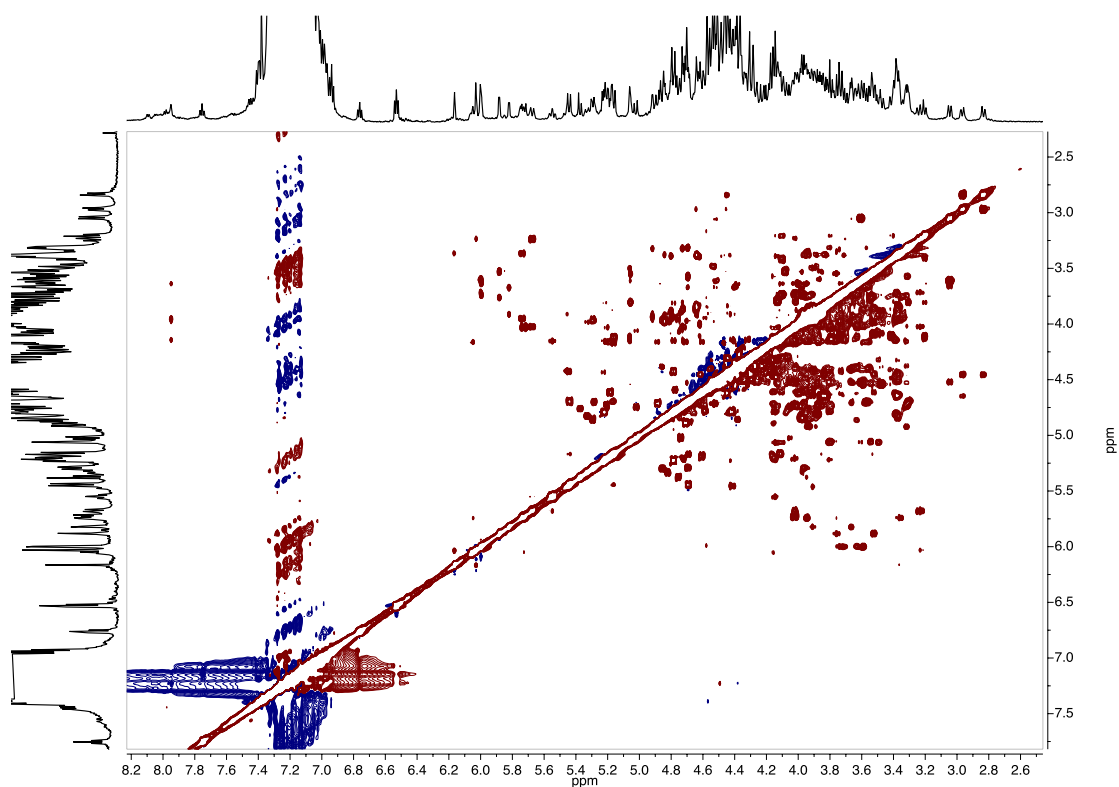


Figure S74: 2D-NOESY of **181+182** (CDCl₃, 600 MHz, 300 K)

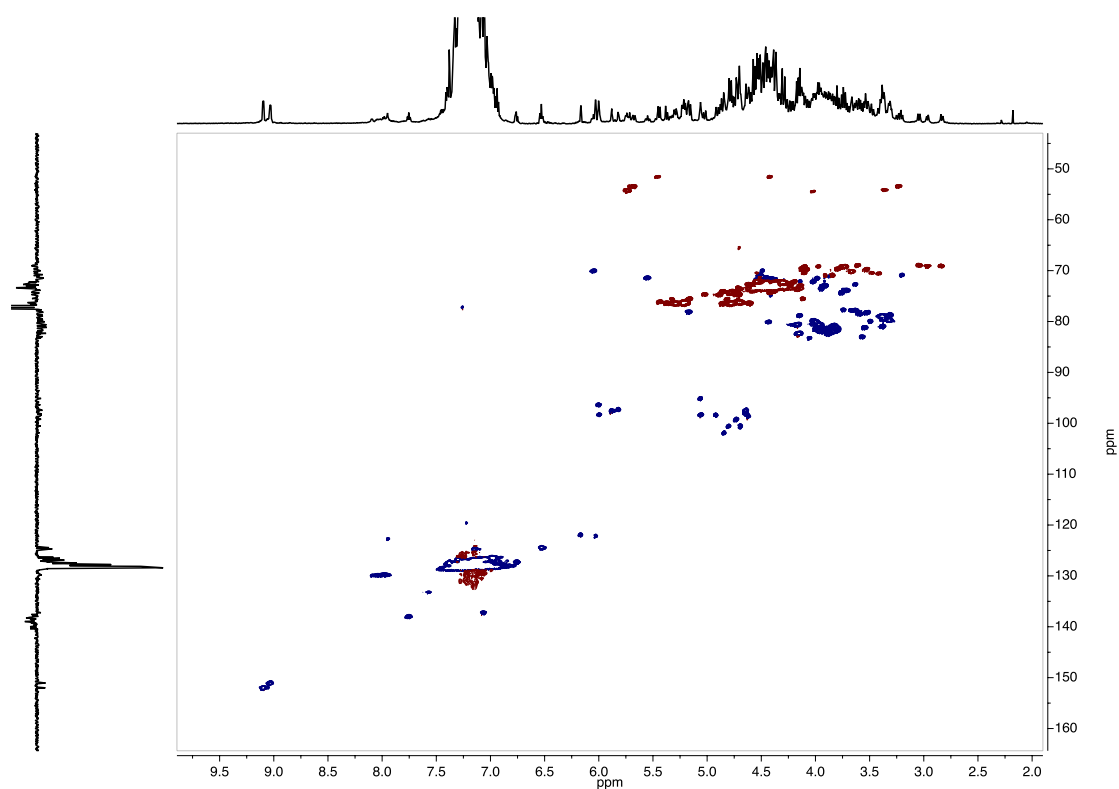
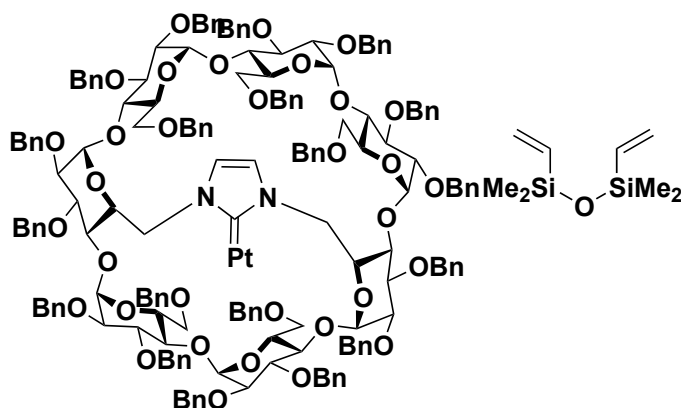


Figure S75: HSQC of **181+182** (CDCl₃, 151 MHz, 300 K)

(β -rev-ICyD)Pt(dvtms) (183)



Chemical Formula:
C₁₈₆H₂₀₂N₂O₃₄PtSi₂
Molecular Weight:
3260.84

In a sealed tube (β -ICyD)HCl 124 (100 mg, 32 μ mol) was dissolved in toluene (1mL) under a Ar atmosphere. KHMDS (340 μ L, 0.5M in toluene 0.171 μ mol) was slowly added. The solution was stirred for 30 minutes and Pt₂(dvtms)₃ (400 μ L, 2% in xylene, ~32 μ mol) was added. The reaction mixture was stirred for 18h. The solvent was evaporated and the product was purified by a silica gel flash chromatography. (15g 40-63 μ m + 15g 15 μ m) affording (β -rev-ICyD)Pt(dvtms) 184 as a white foam (31 mg, 30%)

In a sealed tube (β -ICyD)HCl 124 (500 mg, 160 μ mol) and ^tBuOK (89 mg, 800 μ mol) were dissolved in toluene (5mL) under a Ar atmosphere at r.t. Pt₂(dvtms)₃ was added and the reaction mixture was stirred for 18h. The solvent was evaporated and the product was purified by a silica gel flash chromatography. (15g 40-63 μ m + 15g 15 μ m) affording (β -rev-ICyD)Pt(dvtms) as a white foam (166 mg, 30%)

¹H NMR (600 MHz, Chloroform-d) δ 7.98 (s, 1H, N-CH=CH-N), 7.42 – 6.89 (m), 5.95 (d, J = 4.3 Hz, 1H, H1), 5.88 (d, J = 3.7 Hz, 1H, H1), 5.39 (m, 2H, H6, PhCHH), 5.35 – 5.26 (m, 2H, 2 x PhCHH), 5.22 (d, J = 10.4 Hz, 1H), 5.08 (d, ³J_{PhCHH} = 3.8 Hz, 1H, PhCHH), 5.00 (d, J = 11.6 Hz, 1H, H1), 4.89 – 4.67 (m, 13H, 2 x H1, 11 x PhCHH), 4.67 – 4.20 (m, 28H, H-5, H-6A, H-6D, 25 x PhCHH), 4.17 (t, J = 9.0 Hz, 1H, H-3), 4.14 – 3.90 (m, 13H, H-6A, H5, 7 x H3/H4, 4xH6), 3.89 – 3.83 (m, 2H, 2 x H3/H4), 3.75 (m, 4H, 2 x H6, 2 x H6-D), 3.63 (m, 6H), 3.54 (m, 3H), 3.39 (m, 4H), 3.23 (dt, J = 9.8, 3.3 Hz, 2H), 3.17 (d, J = 11.3 Hz, 1H), 2.32 – 2.28 (m, 1H, =CH₂), 1.94 (d, J = 13.4 Hz, 1H, =CH₂), 1.87 – 1.80 (m, 2H, =CH), 0.39 (s, 3H, SiCH₃), 0.22 (s, 3H, SiCH₃), -0.27 (s, 3H, SiCH₃), -0.46 (s, 2H, SiCH₃).

¹³C NMR (151 MHz, Chloroform-d) δ = 182.1 (C=Pt), 139.9 – 137.5 (C_{ipso}), 128.5 – 126.4 (CH_{Ar}), 122.8 (N-CH=CH-N), 119.5 (N-CH=CH-N), 101.1, 101.0, 99.1, 98.2, 98.1, 96.9, 95.2 (7 x C1), 83.4, 82.1, 82.0, 81.7, 80.8, 80.8, 80.6, 80.4, 80.2, 80.2, 79.6, 79.3, 78.9, 78.4, 78.0, 77.8, 77.7 (7 x C2, 7 x C3, 5x C4) 76.6, 76.5, 76.4, 76.1, 75.8, 74.5, 74.2, 74.1, 73.8, 73.7, 73.6, 73.4, 73.3, 73.3, 73.2, 73.1, 72.6 (C4), 72.6(C4), 72.4, 72.4, 72.2, 71.9, 71.9 (2 x C5), 71.7(C5), 71.3(C5), 70.4(2 x C5), 70.3(C5), 70.3(C5), 69.3, 68.5, 68.2, 66.0, 53.8 (C6), 50.9 (C6), 40.7 (=CH₂), 33.5 (=CH), 15.4, 1.8 (SiCH₃), 1.7(SiCH₃), -1.0(SiCH₃), -1.1(SiCH₃).

R_f=0.35 (CyH:AcOEt 3:1)

HRMS (ESI) [C₁₈₆H₂₀₂N₂O₃₄PtSi₂Na₂]²⁺ 1652.1599 msrd 1652.1561 calcd err -2.3 ppm

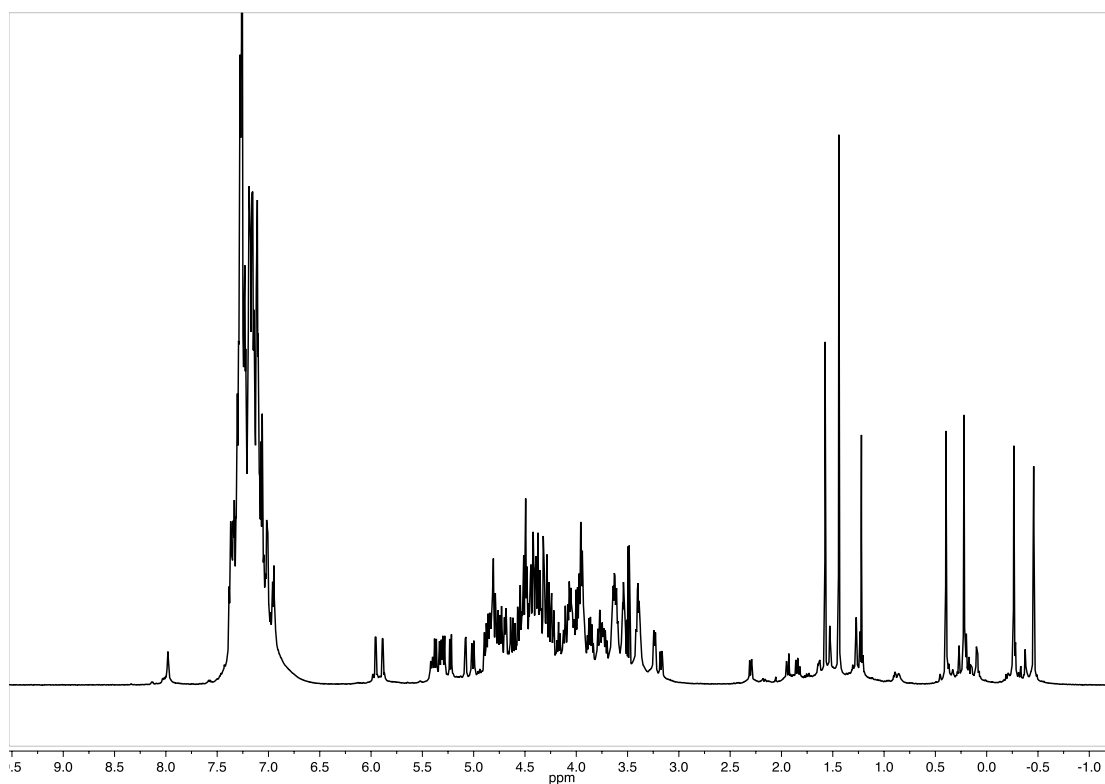


Figure S76: $^1\text{H-NMR}$ of $(\beta\text{-rev-ICyD})\text{Pt}(\text{dvtms})$ **183** (CDCl_3 , 600 MHz, 300 K)

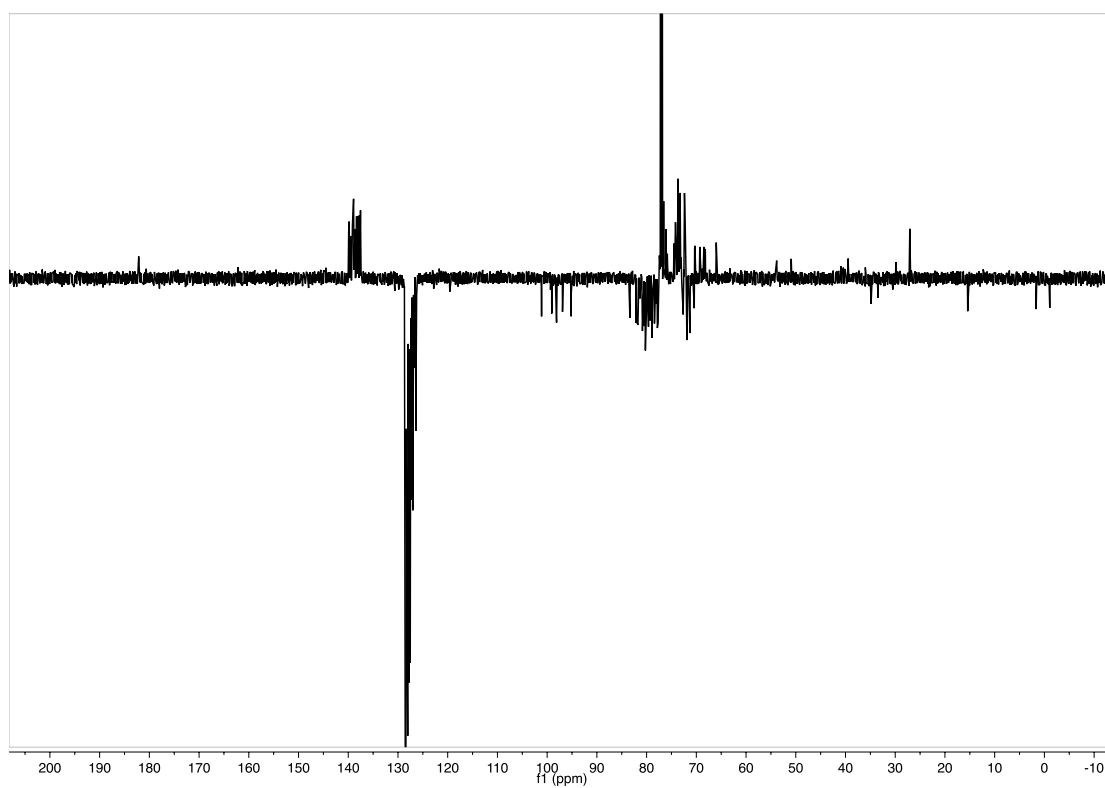


Figure S77: $^{13}\text{C-Jmod}$ of $(\beta\text{-rev-ICyD})\text{Pt}(\text{dvtms})$ **183** (CDCl_3 , 151 MHz, 300 K)

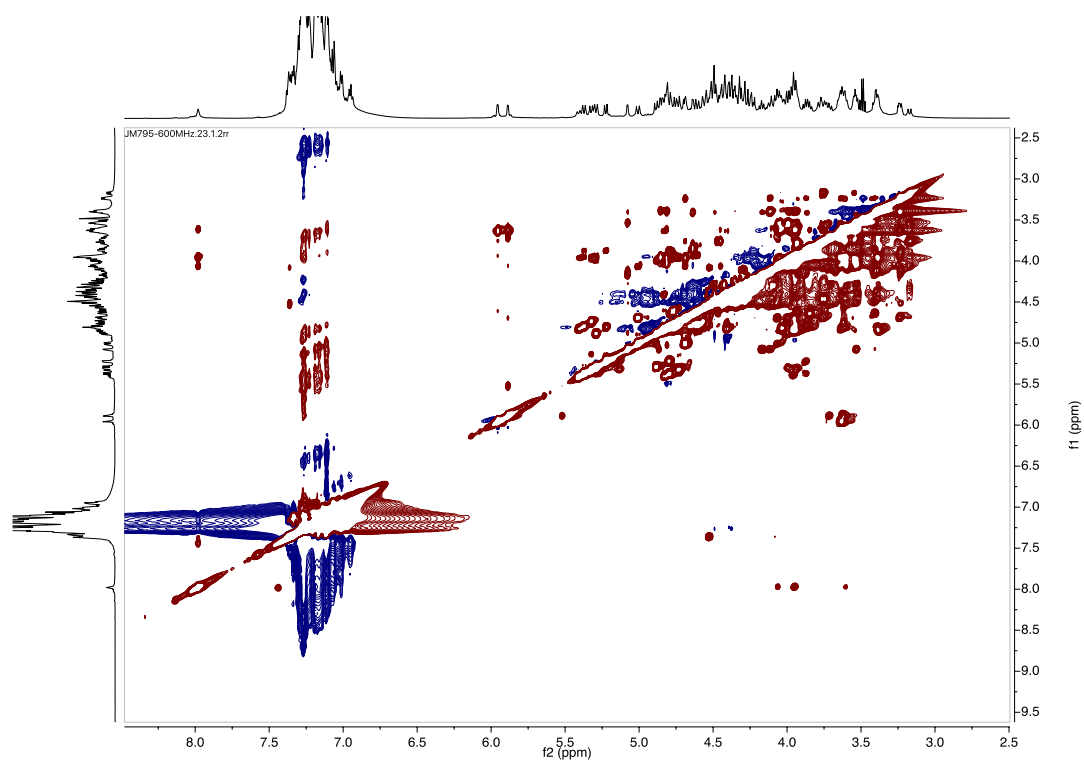


Figure S78: NOESY of (β -rev-ICyD)Pt(dvtms) 183 (CDCl₃, 600 MHz, 300 K)

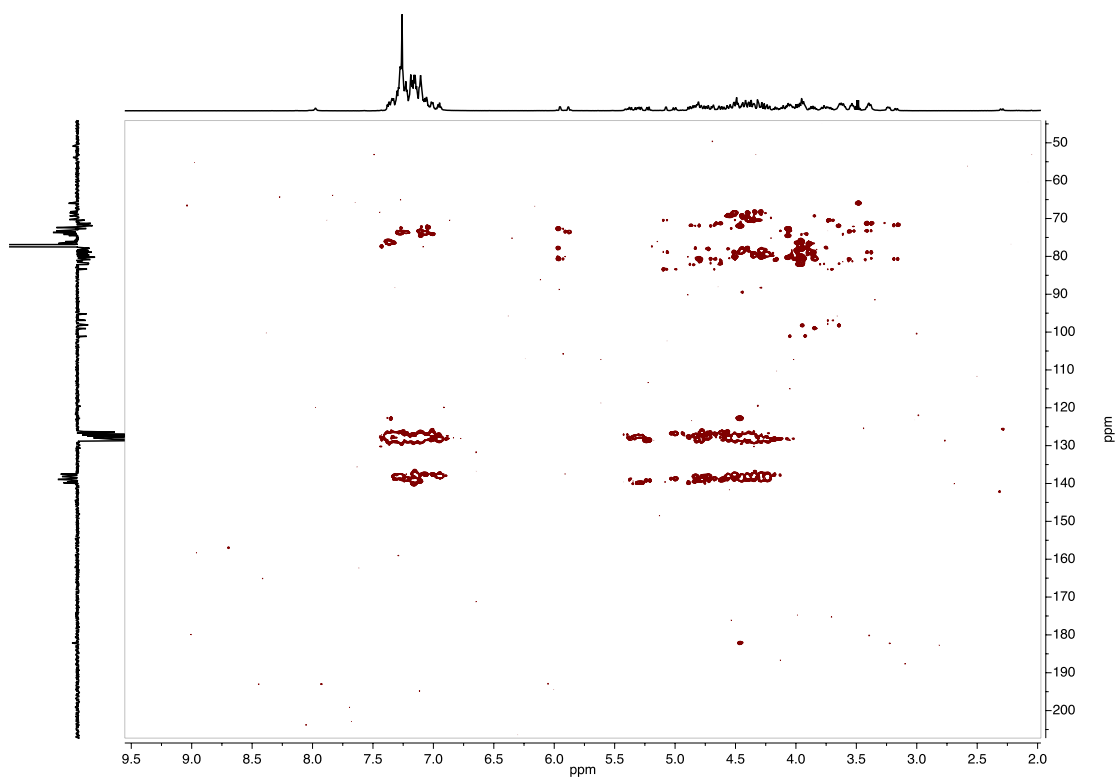
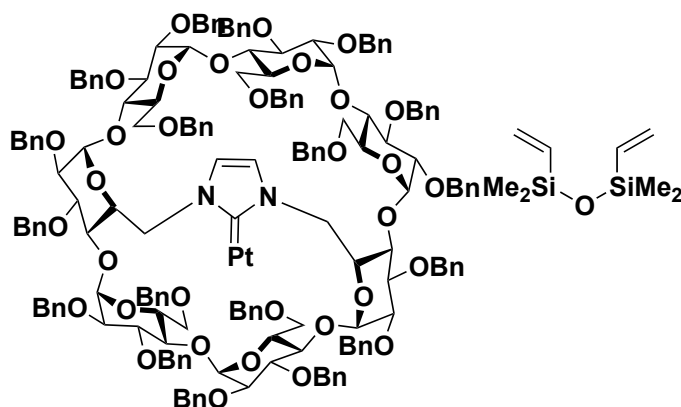


Figure S79: HMBC of (β -rev-ICyD)Pt(dvtms) 183 (CDCl₃, 300 K)

(β -ICyD)Pt(dvtms) (184)



Chemical Formula:
 $C_{186}H_{202}N_2O_{34}PtSi_2$
Molecular Weight:
3260.84

In a sealed tube (β -ICyD)HCl (200 mg,) K_2CO_3 (100 mg, XX) were dissolved in CH_2Cl_2 (2mL). The solution is cooled at $-30\text{ }^\circ\text{C}$ and $Pt_2(dvtms)_3$ was added (0.8 mL, 2% Pt in xylene). The reaction mixture is stirred for 18 hours. The reaction mixture is warmed up slowly to room temperature and stirred for 24 hours. The solvent was evaporated and the product was purified by a silica gel flash chromatography. (15g 40-63 μm + 15g 15 μm) affording (β -ICyD)Pt(dvtms) as a white foam (60 mg, 26%)

R_f=0.29 (CyH:AcOEt 3:1)

HRMS (ESI-TOF): [$C_{186}H_{202}N_2O_{34}PtSi_2Na_2$] 3280.3115 msrd calcd 3281.3229 err 1.7 ppm

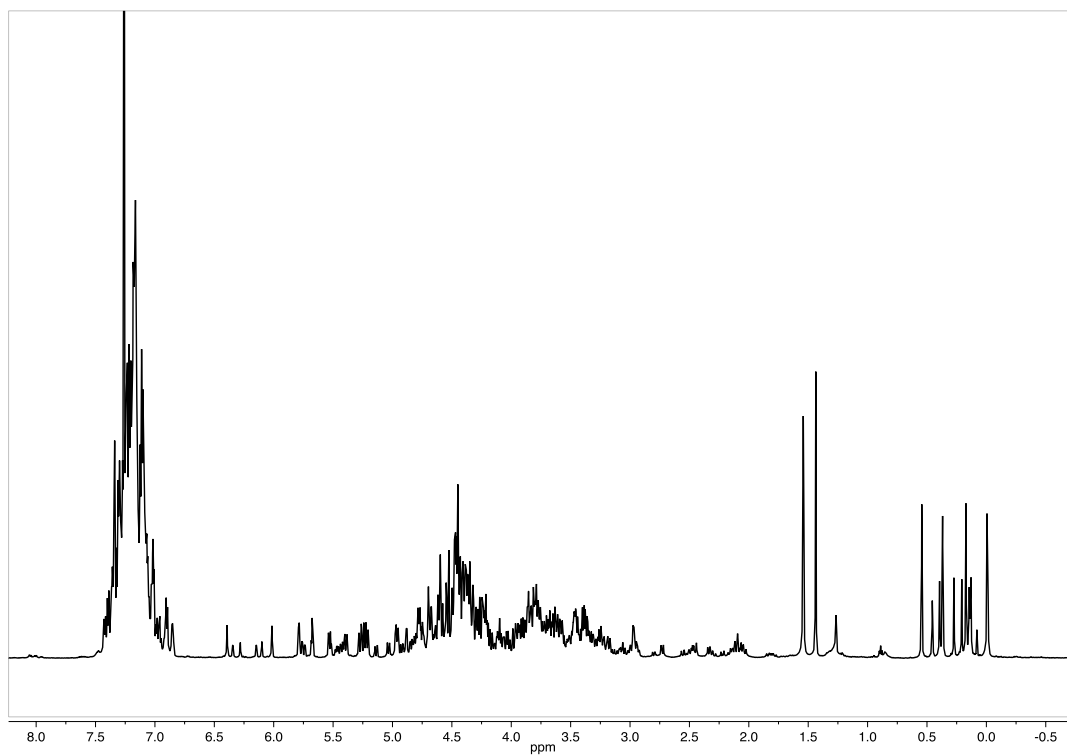


Figure S80: $^1\text{H-NMR}$ of $(\beta\text{-ICyD})\text{Pt}(\text{dvtms})$ **184** (CDCl_3 , 600 MHz, 300 K)

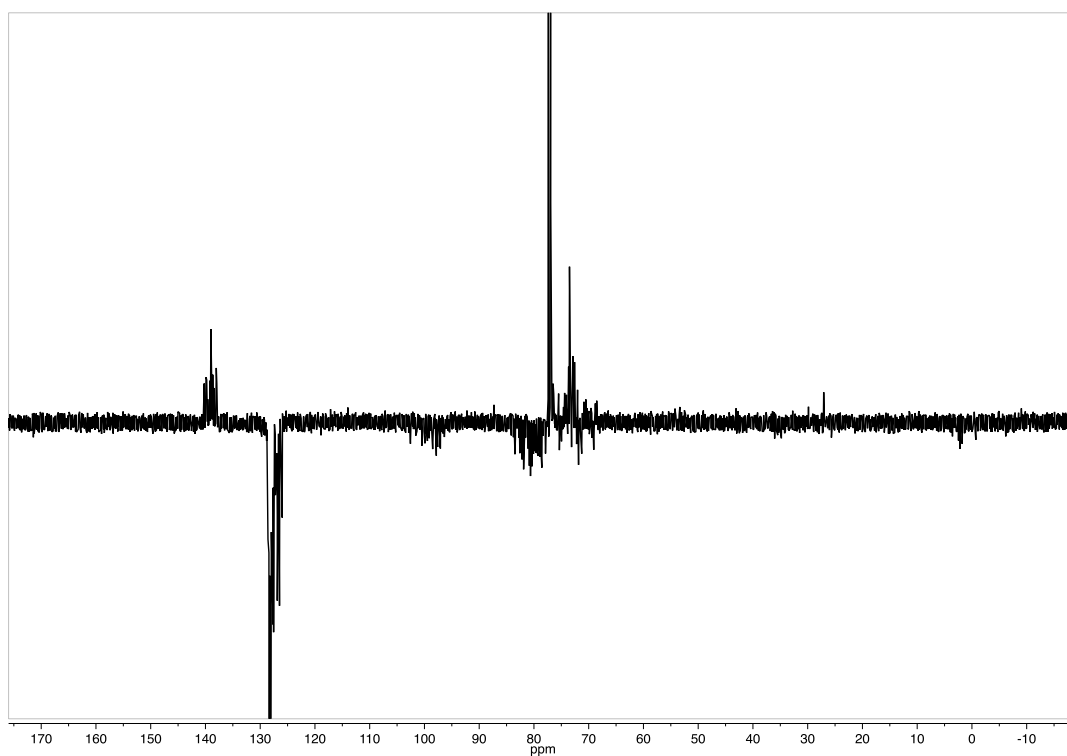


Figure S81: $^{13}\text{C-Jmod}$ of $(\beta\text{-ICyD})\text{Pt}(\text{dvtms})$ **184** (CDCl_3 , 151 MHz, 300 K)

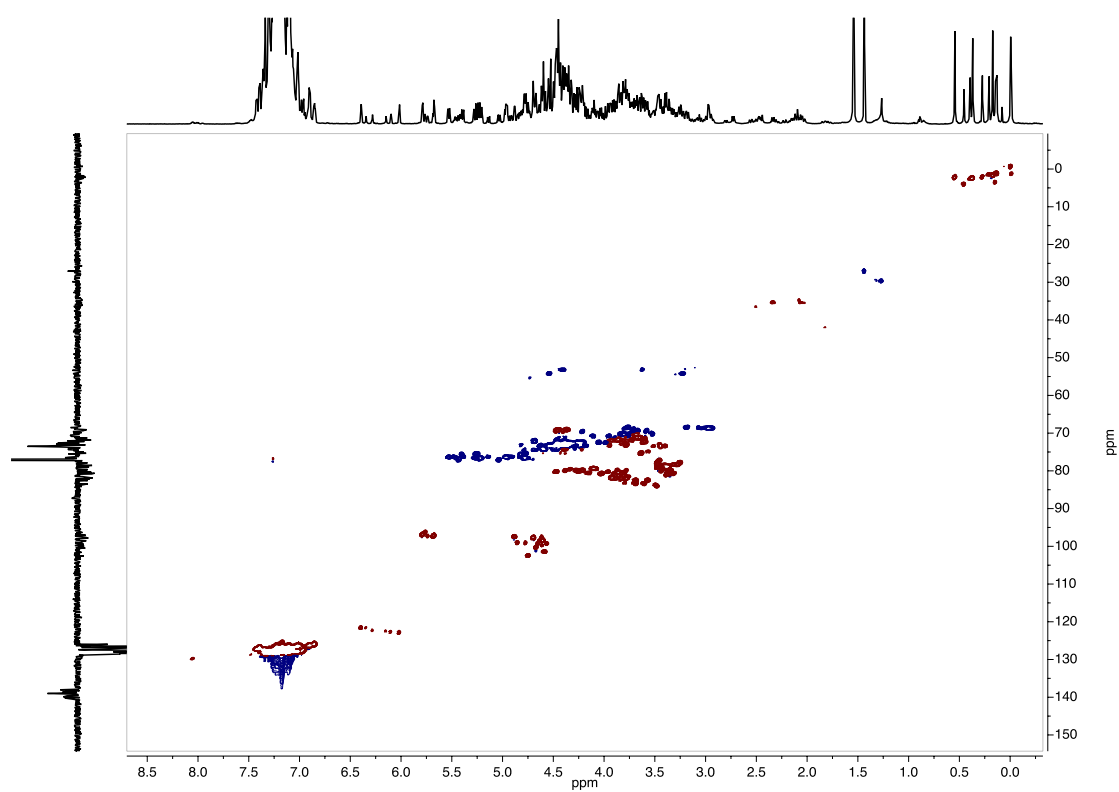


Figure S82: ^{13}C -Jmod of $(\beta\text{-ICyD})\text{Pt}(\text{dvtms})$ 184 (CDCl_3 , 151 MHz, 300 K)

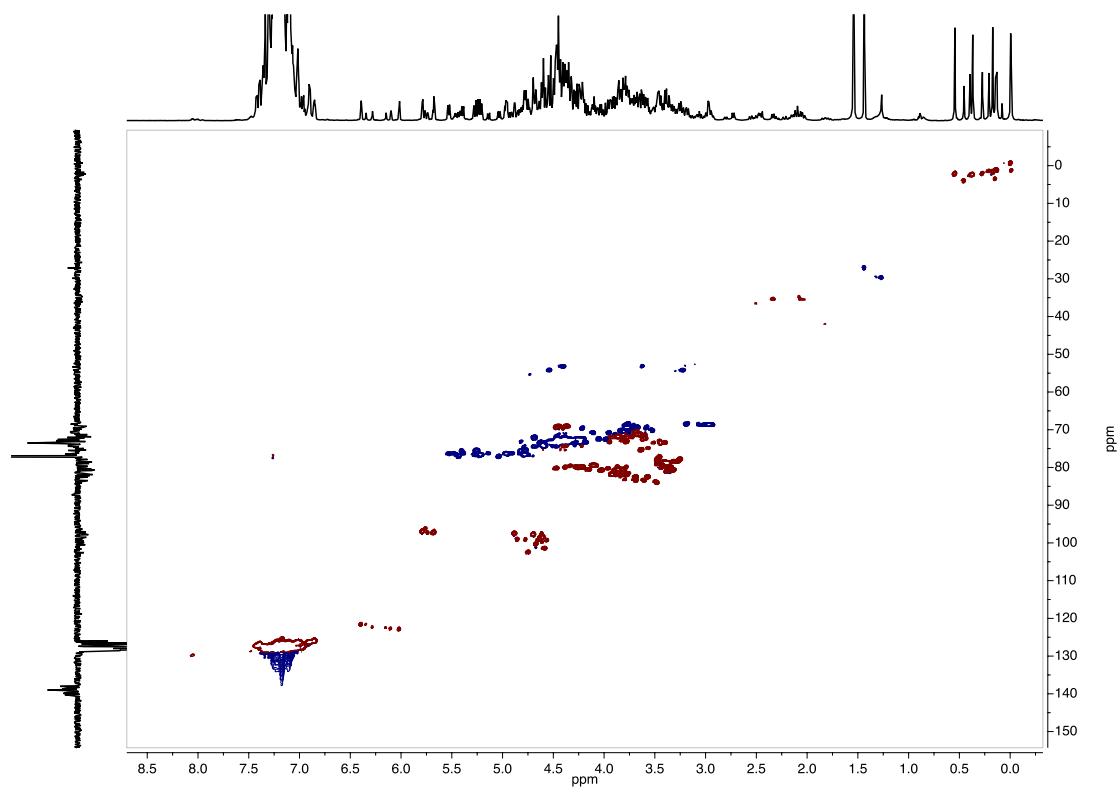
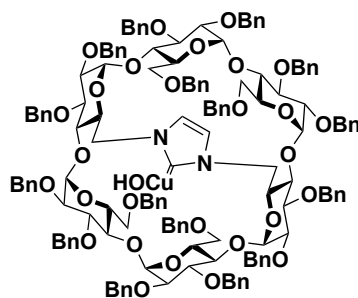


Figure S83: HSQC of $(\beta\text{-ICyD})\text{Pt}(\text{dvtms})$ 184 (CDCl_3 , 600 MHz, 300 K)

(α -lCyD)CuOH (201)



Chemical Formula:

C₁₅₁H₁₅₇CuN₂O₂₉

Molecular Weight:

2527.40

A mixture of (α -lCyD)CuCl (478 mg, 1 equiv.) and KOH (105 mg, 10 equiv.) was dissolved in anhydrous THF (8ml) under a N₂ atmosphere. The reaction mixture was stirred at r.t. for 24h. Then the excess KOH was filtered on a micropore and the residue was washed with THF. The residue was evaporated and **279** was obtained as a foam (403 mg, 85%).

¹H NMR (THF-d₈, 600MHz): δ 7.56 (d, $2J = 6.6$ Hz, 4H, 4 \times H-*o*-Ar), 7.32-6.94 (m, 72H, 72 \times H- Ar), 6.70 (s, 2H, 2 \times H-Im), 6.68-6.61 (m, 4H, 4 \times H-*m*-Ar), 5.97 (t, $3J_{4,5} = 3J_{5,6} = 9.9$ Hz, 2H, 2 \times H-5A, D), 5.77 (d, $2J_{Ph-CHH} = 11.4$ Hz, 2H, 2 \times CHPh), 5.71 (d, 2H, $3J_{1,2} = 3.6$ Hz, 2 \times H-1C, F), 5.39 (d, $2J_{Ph-CHH} = 11.5$ Hz, 2H, 2 \times CHPh), 5.21 (d, $2J_{Ph-CHH} = 11.4$ Hz, 2H, 2 \times CHPh), 5.11-5.00 (m, 4H, 2 \times CHPh, 2 \times H-3C,F), 4.90-4.81 (m, 4H, 2 \times CHPh, 2 \times H-1B, E), 4.78 (d, 2H, $3J_{1,2} = 2.8$ Hz, 2 \times H-1A, D), 4.61-4.57 (m, 8H, 8 \times CHPh), 4.52-4.46 (6H, 2 \times H-6aA,D, 4 \times CHPh), 4.38 (t, $3J_{2,3} = 3J_{3,4} = 9.3$ Hz, 2H, 2 \times H-3B,E), 4.35-4.31 (m, 6H, 2 \times H-3A,D, 4 \times CHPh), 4.28 (d, $2J_{Ph-CHH} = 12.4$ Hz, 2H, 2 \times CHPh), 4.23-4.16 (m, 4H, 2 \times H-5B,E, 2 \times CHPh), 4.10-4.00 (m, 6H, 2 \times H-5C, F, 2 \times H-6aC,F, 2 \times CHPh), 3.96 (t, $3J_{3,4} = 3J_{4,5} = 8.7$ Hz, 2H, 2 \times H-4C,F), 3.82 (d, $2J = 10.5$ Hz, 2H, 2 \times H- 6bC,F), 3.76-3.67 (m, 4H, 2 \times H-4B,E, 2 \times H-6bA,D), 3.62-3.59 (m, 2H, 2 \times H-4A,D), 3.48 (dd, $3J_{1,2} = 3.6$ Hz, $3J_{2,3} = 10.3$ Hz, 2H, 2 \times H-2C,F), 3.36 (dd, $3J_{1,2} = 3.4$ Hz, $3J_{2,3} = 9.9$ Hz, 2H, 2 \times H- 2B,E), 3.30 (dd, $3J_{1,2} = 2.7$ Hz, $3J_{2,3} = 9.7$ Hz, 2H, 2 \times H-2A,D), 3.25 (dd, $2J_{6a,6b} = 10.9$ Hz, $3J_{5,6b} = 4.1$ Hz, 2H, 2 \times H-6aB,E), 2.99 (wd, $2J_{6a,6b} = 10.2$ Hz, 2H, 2 \times H-6bB,E) ppm;

¹³C NMR (THF-d₈, 151MHz): δ 175.95 (C-Cu), 142.10(2C), 141.56(2C), 140.93(2C), 140.32(2C), 140.11(2C), 139.90(2C), 139.55(2C), 139.36(2C)(16 \times C-Ar-quat.), 129.36-126.82 (80 \times C-Ar-tert.), 122.70(2 \times N-C=C-N), 98.77(2 \times C-1C,F), 98.44(2 \times C-1B,E), 97.90(2 \times C- 1A,D), 82.52, 82.42, 82.30(2 \times C-3A,D, 2 \times C-4C,F, 2 \times C-4B,E), 81.39(2C)(2 \times C-3B,E, 2 \times C- 2A,D), 81.18(2 \times C-3C,F), 80.80(2 \times C-2B,E),79.12(2 \times C-2C,F), 77.31(2 \times Ph-CH₂), 77.26(2 \times C- 4A,D), 77.19(2 \times Ph-CH₂), 75.39(2 \times Ph-CH₂), 74.67(2 \times Ph-CH₂), 74.63(2 \times C-5C,F), 73.86(2 \times Ph-CH₂), 73.80(2 \times Ph-CH₂), 73.66(2 \times Ph-CH₂), 72.85(2 \times C-5B,E), 72.70(2 \times Ph-CH₂), 72.66(2 \times C-5A,D), 71.71(2 \times C-6C,F), 69.65(2 \times C-6B,E), 54.85(2 \times C-6A,D)ppm.

$[\alpha]_D^{20} = 42.5^\circ$ (CHCl₃, c=1.0)

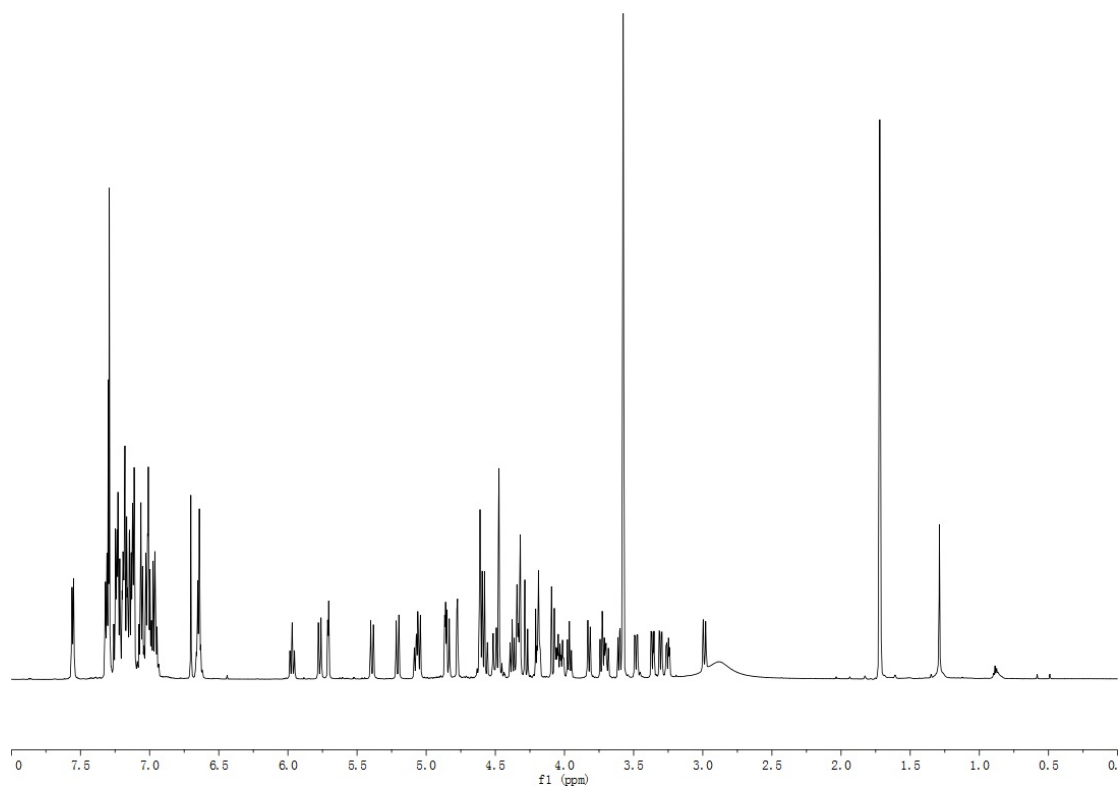


Figure S84: $^1\text{H-NMR}$ of $(\alpha\text{-ICyD})\text{CuOH 202}$ (THF-d_8 , 600 MHz, 300 K)

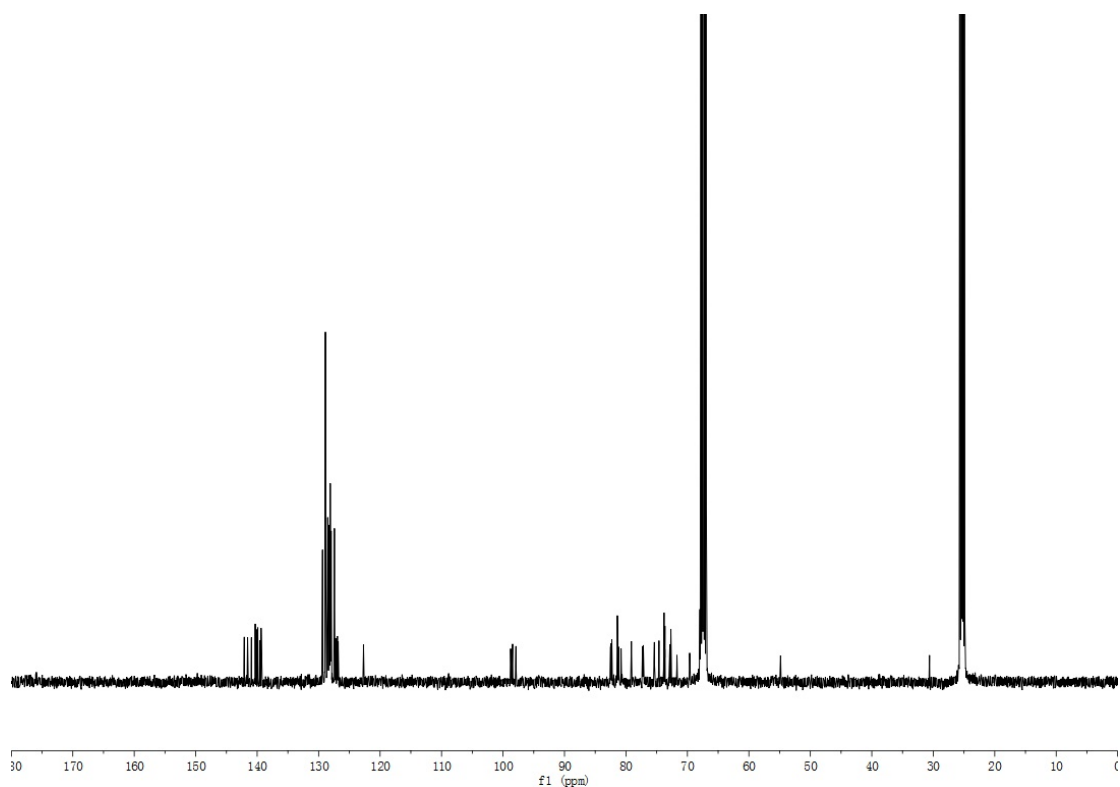
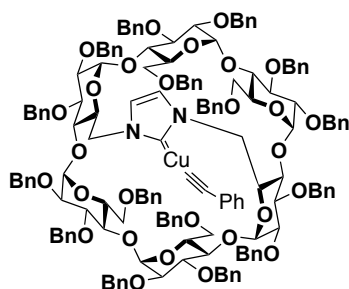


Figure S85: $^{13}\text{C-NMR}$ of $(\alpha\text{-ICyD})\text{CuOH 202}$ (THF-d_8 , 151 MHz, 300 K)

(α -ICyD)CuCCPh (203)



Chemical Formula:

$C_{159}H_{161}CuN_2O_{28}$

Molecular Weight:

2611.52

(α -ICyD)CuCl (15 mg, 1 equiv.) was dissolved in anhydrous THF- d_8 (400 μ L) under Ar atmosphere in a NMR tube. Then 2 μ L (2 equiv.) of phenylacetylene was added into the solution. The mixture was left at r.t. for 4d and the reaction was followed by 1H NMR.

1H NMR (THF- d_8 , 600MHz): δ 7.57 (dd, $3J=6.6$, $3J=3.0$, 2H, 2 \times H- σ -Acetylide), 7.34-6.79 (m, 80H, 80 \times H-Ar), 6.68(s, 2H, 2 \times H-Im), 6.66-6.63 (m, 3H, 2 \times H- m -Acetylide, H- p -Acetylide), 36.03 (t, $3J_{4,5} = 3J_{5,6} = 9.8$ Hz, 2H, 2 \times H-5A,D), 5.59(d, $J_{1,2}=3.5$ Hz, 2H, 2 \times H-1C,F), 5.47-5.45 (m, 4H, 4 \times CHPh), 4.96 (d, $3J_{1,2} = 3.1$ Hz, 2H, 2 \times H-1A,D), 4.92 (d, $2J_{Ph-CHH} = 11.0$ Hz, 2H, 2 \times CHPh), 4.90-4.85 (m, 6H, 4 \times CHPh, 2 \times H-3C,F), 4.79 (d, $2J_{Ph-CHH} = 11.8$ Hz, 2H, 2 \times CHPh), 4.70-4.63 (m, 6H, 2 \times CHPh, 2 \times H-1B, E, 2 \times H-6aA,D), 4.45-4.33 (m, 18H, 4 \times H- 3A,B,D,E, 14 \times CHPh), 4.21 (d, $2J_{Ph-CHH} = 12.1$ Hz, 2H, 2 \times CHPh), 4.14-4.05 (m, 6H, 4 \times H- 5B,C,E,F, 2 \times CHPh), 3.95 (d, 2H, $2J_{6a,6b} = 10.4$ Hz, 2H, 2 \times H-6aC,F), 3.81-3.71 (m, 8H, 4 \times H- 4B,C,E,F, 2 \times H-6bA,D, 2 \times H-6bC,F), 3.62 (td, $3J_{3,4} = 3J_{4,5} = 7.7$ Hz, 2H, 2 \times H-4A,D), 3.44-3.39 (m, 4H, 4 \times H-2A,C,F,D), 3.32-3.24 (m, 4H, 2 \times H-2B,E, 2 \times H-6aB,E), 3.00 (wd, 2H, $2J_{6a,6b} = 11.2$ Hz, 2 \times H-6bB,E) ppm;

^{13}C NMR (THF- d_8 , 151MHz): δ 176.74 (C-Cu), 141.35(2C), 141.23(2C), 141.03(2C), 140.17(2C), 140.02 (2C), 139.65(2C), 139.63(2C), 139.09(2C) (16 \times C-Ar-quat.), 133.16 (2C, m - C-Acetylide), 132.62 (2C, σ -C-Acetylide), 129.18 (Cu-CC-Ph), 128.93-126.24 (80 \times C-Ar-tert.), 124.70 (C-Acetylide quat), 123.44(p -C-Acetylide) 122.75(2 \times N-C=C-N), 106.83 (Cu-CC-Ph), 99.73(2 \times C-1C,F), 98.90(2 \times C-1B,E), 98.15(2 \times C-1A,D), 83.81(2 \times C-4C,F), 82.44(2 \times C-3A,D), 82.33(2 \times C-4B,E), 81.93(2 \times C-3B,E), 81.60 (2 \times C-2A,D), 80.26(2 \times C-3C,F), 79.98 (2 \times C-2B,E), 78.68(4C)(2 \times C-4A,D, 2 \times C-2C,F), 77.51(2 \times Ph-CH₂), 76.19(2 \times Ph-CH₂), 75.09 (2 \times C-5C,F), 74.42(2 \times Ph-CH₂), 73.96(2 \times Ph-CH₂), 73.64(4C) (4 \times Ph-CH₂), 73.24 (2 \times Ph-CH₂), 72.98(2 \times C- 5B,E), 72.53(2 \times Ph-CH₂), 72.47(2 \times C-5A,D), 72.33(2 \times C-6C,F), 69.31(2 \times C-6B,E), 54.85(2 \times C- 6A,D)ppm.

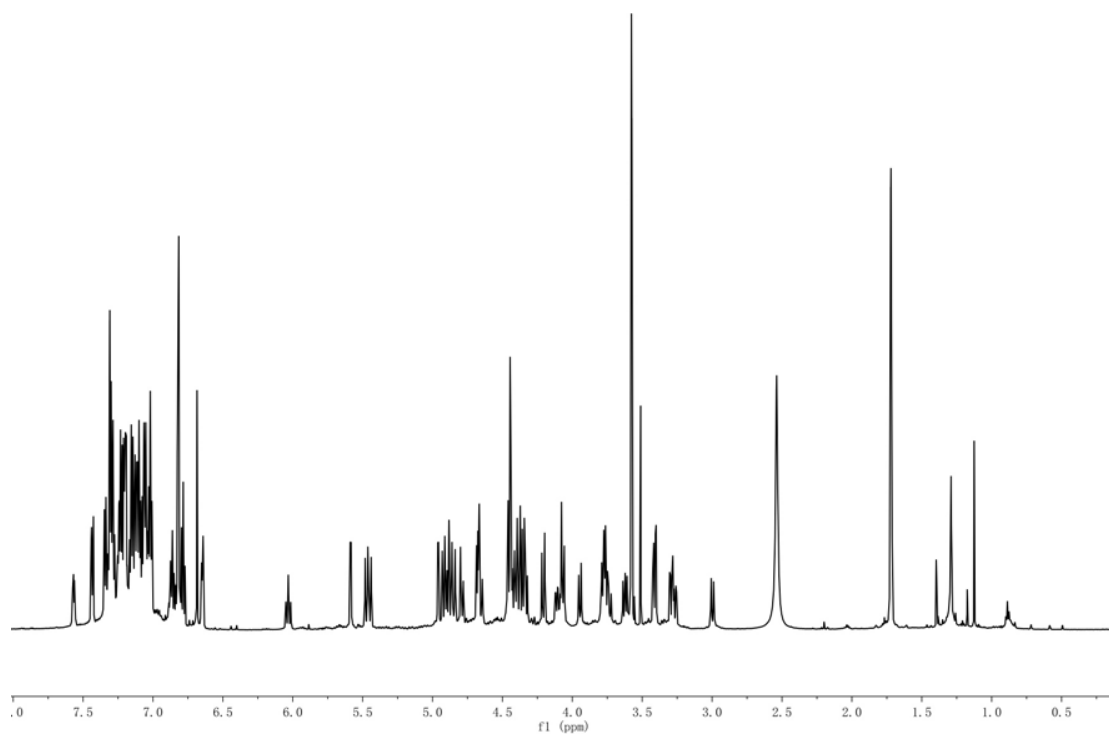


Figure S86: $^1\text{H-NMR}$ of $(\alpha\text{-ICyD})\text{CuCCPh 203}$ (THF- d_8 , 600 MHz, 300 K)

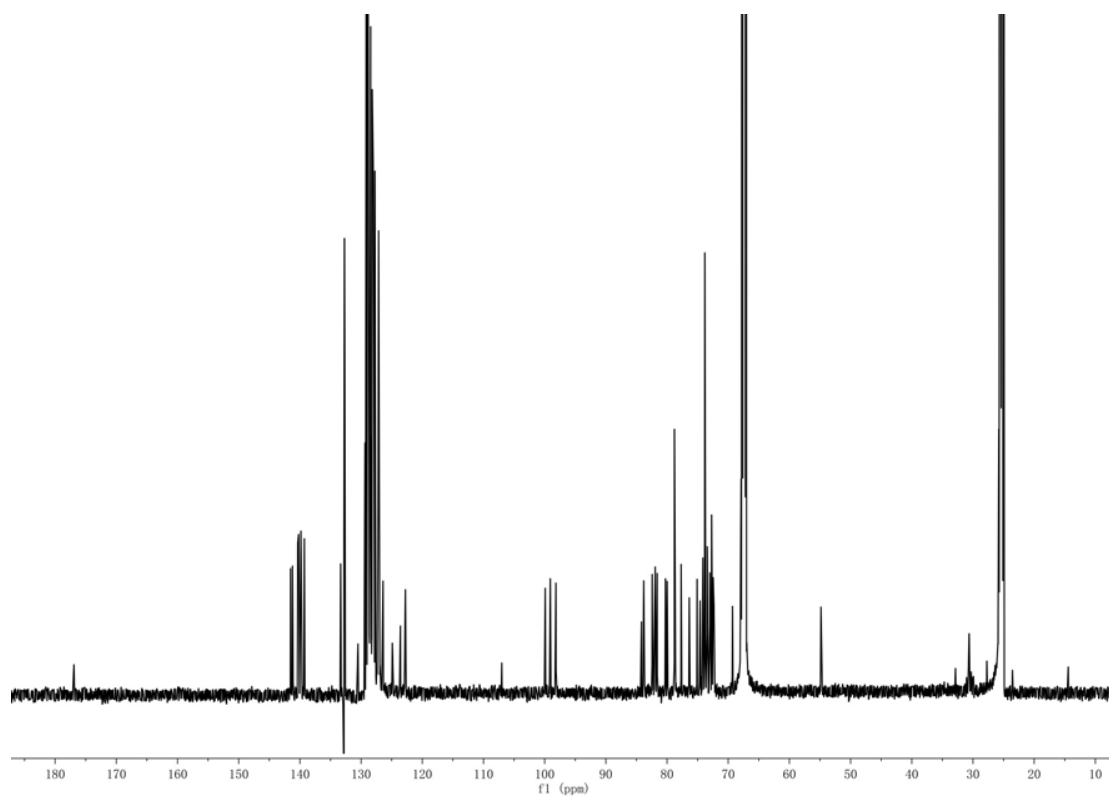
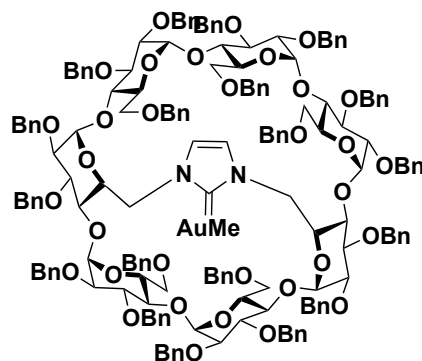


Figure S86: $^{13}\text{C-NMR}$ of $(\alpha\text{-ICyD})\text{CuCCPh 203}$ (THF- d_8 , 151 MHz, 300 K)

(β -ICyD)AuMe (222)



Chemical Formula:

$C_{179}H_{187}AuN_2O_{33}$

Molecular Weight:

3091.36

Under an Ar atmosphere, (**β -ICyD**)AuCl (90mg, 30 μ mol) was dissolved in anhydrous toluene. Then MeMgBr (10 μ L, 3.0 M in Et₂O, 30 μ mol) was added. The reaction mixture was stirred at room temperature and followed by TLC. When finished, the product is directly filtrated on silica (CyH:AcOEt 3:1) affording (**β -ICyD**)AuMe **222** as a white solid (63 mg, 70%)

¹H NMR (600 MHz, Chloroform-d) δ 7.44 – 6.94 (m, H_{Ar}), 6.87 (t, J = 7.4 Hz, 1H), 6.32 – 6.19 (m, 1H), 6.14 (d, J = 1.7 Hz, 1H), 5.96 (d, J = 1.7 Hz, 1H), 5.90 (d, J = 3.7 Hz, 1H), 5.86 (d, J = 3.6 Hz, 1H), 5.55 (d, J = 10.7 Hz, 1H), 5.42 (dd, J = 17.9, 10.7 Hz, 2H), 5.34 (d, J = 11.2 Hz, 1H), 5.22 (dd, J = 19.1, 11.5 Hz, 2H), 5.02 (d, J = 10.7 Hz, 1H), 4.97 – 4.82 (m, 6H), 4.83 – 4.73 (m, 2H), 4.72 – 4.14 (m, 44H), 4.13 – 3.97 (m, 5H), 3.91 – 3.66 (m, 10H), 3.61 – 3.52 (m, 4H), 3.37 – 3.31 (m, 2H), 3.34 – 3.25 (m, 2H), 2.96 (dd, J = 11.3, 1.8 Hz, 1H), 2.73 (t, J = 1.9 Hz, 2H), 0.83 (s, 3H, Au-CH₃).

¹³C NMR (151 MHz, CDCl₃) δ 199.1, 140.2, 140.1, 140.0, 139.8, 139.7, 139.1, 139.0, 138.9, 138.9, 138.8, 138.8, 138.8, 138.6, 138.6, 138.3, 138.2, 138.2, 137.9, 128.6, 128.5, 128.5, 128.5, 128.4, 128.4, 128.4, 128.3, 128.3, 128.3, 128.2, 128.2, 128.2, 128.1, 128.1, 128.1, 128.0, 128.0, 128.0, 128.0, 127.9, 127.9, 127.9, 127.9, 127.8, 127.8, 127.8, 127.7, 127.7, 127.6, 127.5, 127.5, 127.3, 127.2, 127.1, 127.0, 126.9, 126.8, 126.8, 126.6, 121.3, 120.4, 100.8, 99.4, 98.8, 97.9, 97.3, 97.2, 96.4, 83.3, 82.7, 82.0, 81.6, 81.5, 81.0, 80.7, 80.6, 80.4, 80.3, 80.1, 79.9, 79.8, 79.0, 78.8, 78.4, 78.1, 77.9, 76.9, 76.7, 76.5, 76.4, 74.6, 74.3, 74.0, 73.6, 73.5, 73.3, 73.3, 73.1, 73.0, 72.8, 72.7, 72.6, 72.5, 72.2, 71.6, 71.4, 71.4, 70.5, 70.4, 70.4, 69.7, 68.6, 68.0, 54.5, 52.9, 29.9, 1.5.

HRMS (ESI) calculated for C₁₇₉H₁₈₇AuN₂O₃₃ [M-Na]⁺ 3112.2574 found 3112.2580 err -0.2 ppm

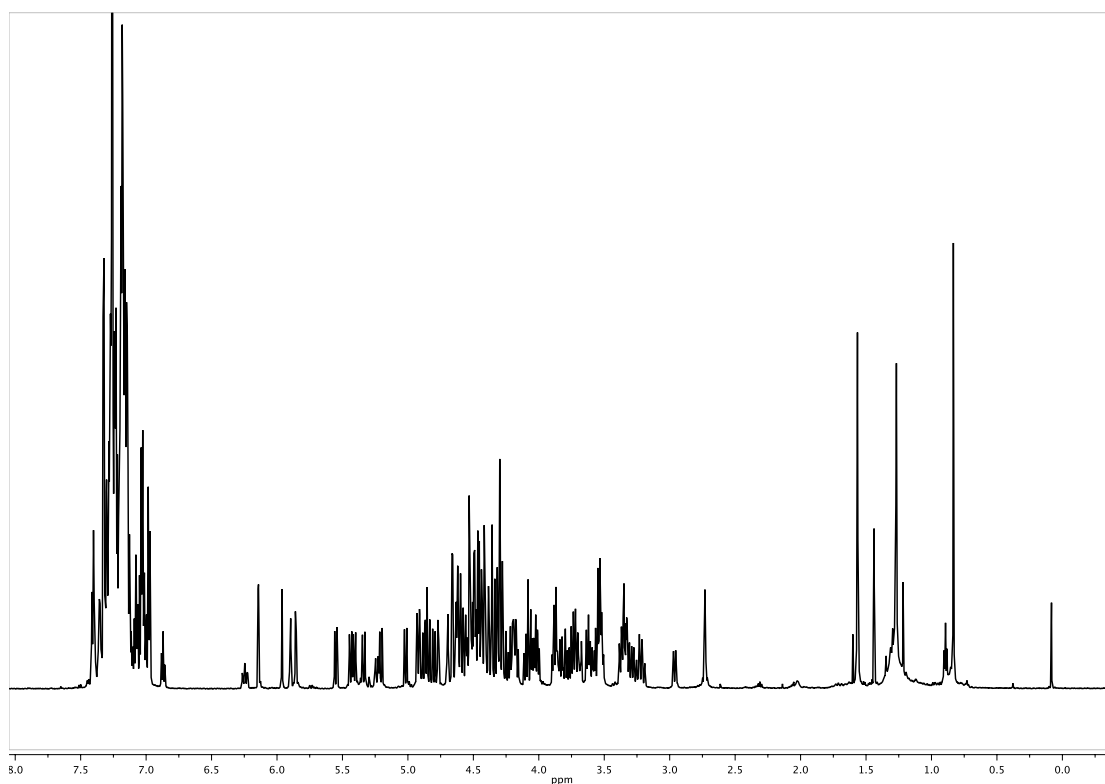


Figure S87: ^{13}C -NMR of $(\beta\text{-ICyD})\text{AuMe 222}$ (THF-d_8 , 600 MHz, 300 K)

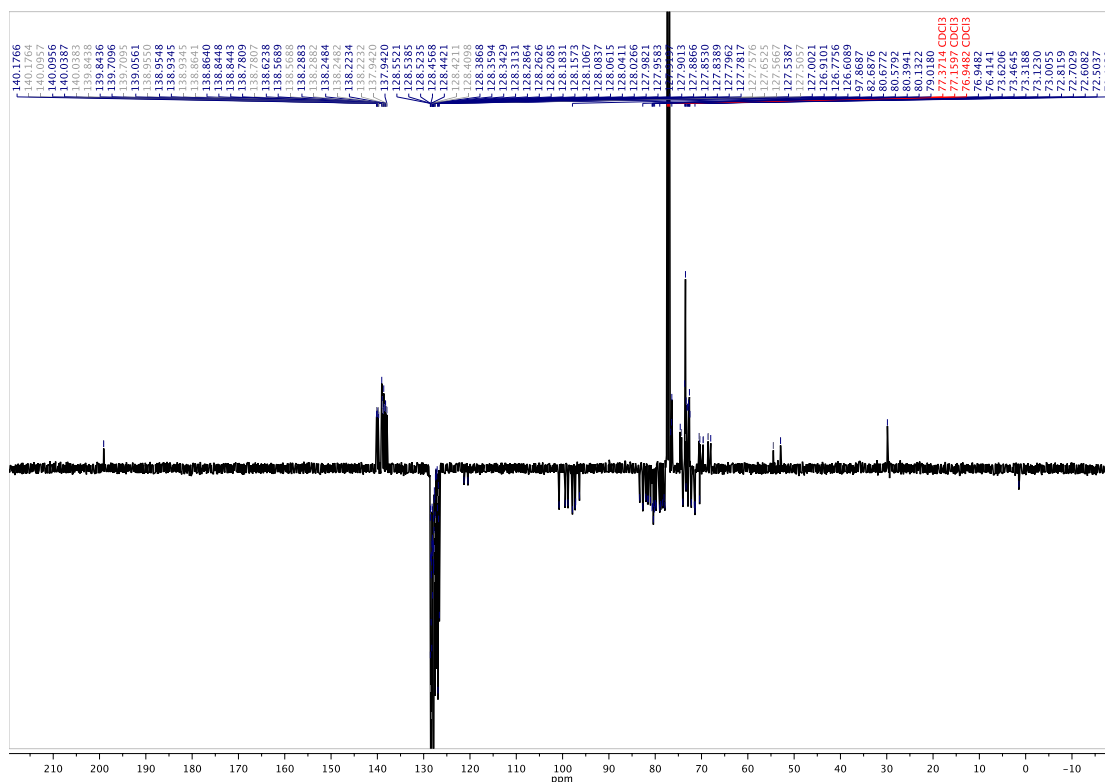


Figure S88Figure S86: ^{13}C -NMR of $(\beta\text{-ICyD})\text{AuMe 222}$ (THF-d_8 , 151 MHz, 300 K): ^{13}C -NMR of $(\beta\text{-ICyD})\text{AuMe 222}$ (THF-d_8 , 151 MHz, 300 K)

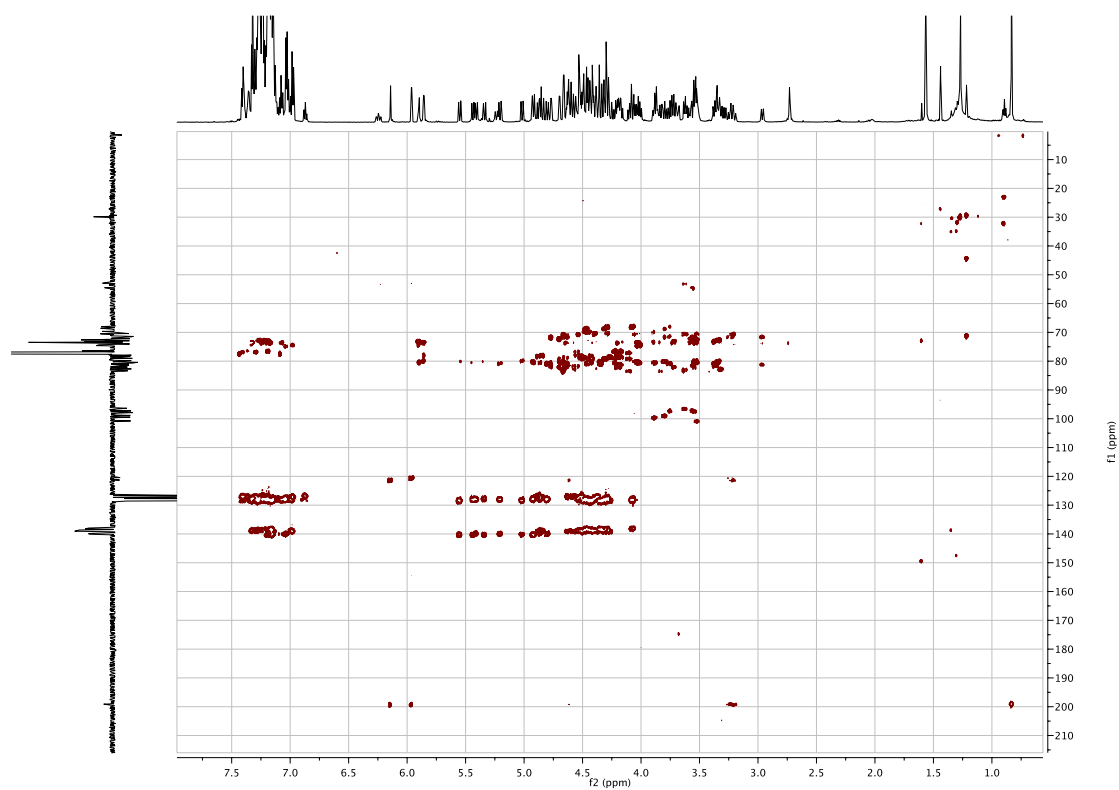


Figure S89: HMBC of (β -ICyD)AuMe 222 (THF- d_8 , 300 K)

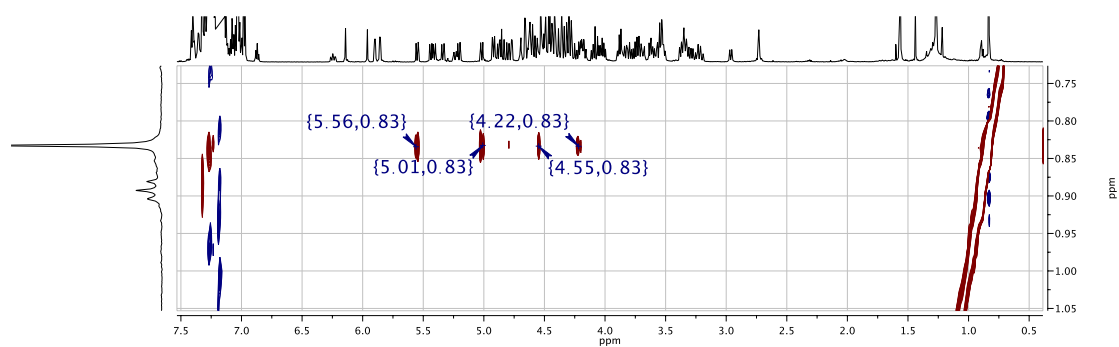
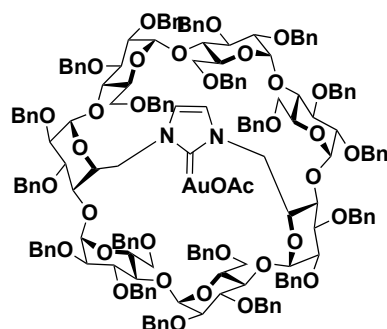


Figure S91: NOESY of (β -ICyD)AuMe 222 showing the cross correlations with the Me (THF- d_8 , 600 MHz, 300 K)

Cycle A	H	C	Cycle B	H	C
1	4,66		1	4,63	97,78
2	3,31		2	3,37	
3	4,01		3	4,21	
4	3,61	73,9	4	3,75	
5	6,24	70,28	5	4,30	71,22
6	3,20		6	2,73	
6'	4,60	52,79	6'	2,73	
Cycle C	H	C	Cycle D	H	C
1	5,85	97,07	1	4,77	98,74
2	3,54		2	3,36	
3	4,54		3	4,01	
4	4,04		4	3,54	73,33
5	3,86	73,27	5	4,61	71,41
6	3,73		6	3,23	
6'	4,19	69,51	6'	5,23	54,27
Cycle E	H	C	Cycle F	H	C
1	4,66		1	4,70	99,26
2	3,34		2	3,34	
3	4,17		3	4,09	
4	3,80		4	3,51	
5	3,28	71,37	5	3,62	72,05
6	3,52		6	3,58	
6'	2,96	68,43	6'	3,83	70,32
Cycle G	H	C			
1	5,90	96,26	ImidA	5,96	121,14
2	3,54		ImidD	6,14	120,29
3	4,18		C=Au		199,1
4	3,88	82,01	CH3	0,84	1,46
5	3,69	72,82			
6	3,70				
6'	4,19	69,52			

Table S13: Attribution of the protons of the sugar units of **222**

(β -ICyD)AuOAc (223)



Chemical Formula:

$C_{180}H_{187}AuN_2O_{35}$

Molecular Weight:

3135.37

In a sealed tube (**β -ICyD**)**AuCl** (100 mg, 32.1 μ mol) and AgOAc (5.3 mg, 32.1 μ mol) were dissolved in dry toluene (1 mL). The reaction was stirred overnight. The solution was filtrated in a 0.2 μ m PET filter and washed with toluene. The solvent is evaporated and (**β -ICyD**)**AuOAc 223** was obtained as a white foam (100 mg, 99%).

1H NMR (600 MHz, Chloroform-d) δ 7.41 – 6.83 (m, 83H), 6.16 – 6.08 (m, 2H), 5.92 (d, J = 1.8 Hz, 1H), 5.83 (dd, J = 7.8, 3.5 Hz, 2H), 5.54 (d, J = 10.5 Hz, 1H), 5.40 (m, 4H), 5.05 (dd, J = 12.2, 7.2 Hz, 2H), 4.98 (d, J = 11.0 Hz, 2H), 4.94 – 4.81 (m, 5H), 4.78 (d, J = 3.6 Hz, 1H), 4.73 – 4.33 (m, 33H), 4.33 – 4.25 (m, 7H), 4.27 – 4.03 (m, 8H), 3.93 – 3.56 (m, 14H), 3.55 – 3.21 (m, 14H), 2.96 (d, J = 10.5 Hz, 1H), 2.75 (d, J = 2.6 Hz, 2H), 1.69 (s, 3H).

^{13}C NMR (151 MHz, Chloroform-d) δ 175.5, 164.9, 139.2, 138.9, 128.5, 128.4, 128.3, 128.3, 128.3, 128.2, 128.2, 128.1, 128.1, 128.1, 128.1, 128.0, 128.0, 128.0, 127.9, 127.9, 127.8, 127.8, 127.7, 127.7, 127.7, 127.6, 127.6, 127.6, 127.5, 127.5, 127.4, 127.3, 127.1, 127.1, 127.0, 126.9, 126.8, 122.2, 120.8, 100.9, 99.8, 98.7, 97.8, 97.4, 97.2, 96.8, 83.4, 82.5, 82.1, 81.5, 81.4, 80.9, 80.8, 80.6, 80.2, 80.1, 79.9, 79.8, 79.7, 79.0, 79.0, 78.2, 78.1, 77.9, 76.9, 76.6, 76.5, 76.4, 76.3, 74.6, 74.5, 73.8, 73.7, 73.5, 73.5, 73.3, 73.2, 73.2, 73.0, 72.7, 72.6, 72.5, 72.3, 71.5, 71.4, 70.4, 69.9, 69.7, 68.4, 68.0, 55.0, 53.7, 24.2.

HRMS (ESI): calculated for $C_{180}H_{187}AuN_2O_{35}Na$ $[M+Na]^+$ 3112.2574 found 3112.2580, err -0.2 ppm

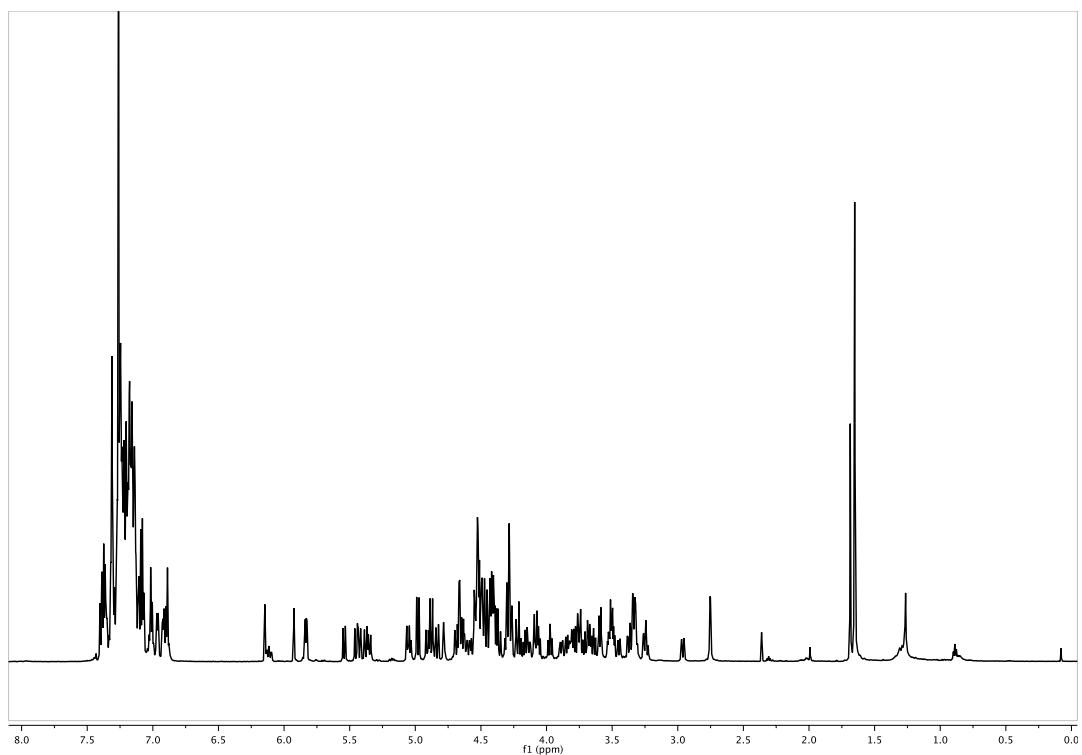


Figure S92: $^1\text{H-NMR}$ of $(\beta\text{-ICyD})\text{AuOAc}$ 223 (CDCl_3 , 600 MHz, 300 K)

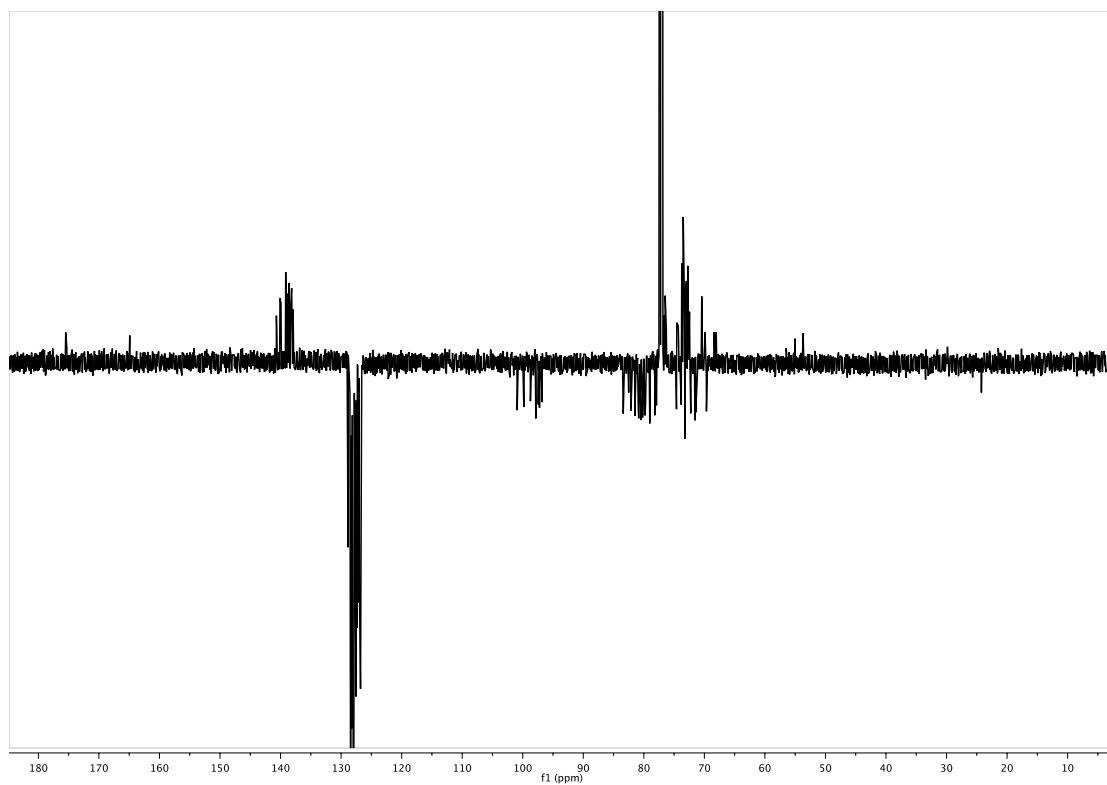


Figure S93: $^{13}\text{C-NMR}$ of $(\beta\text{-ICyD})\text{AuOAc}$ 223 (CDCl_3 , 151 MHz, 300 K)

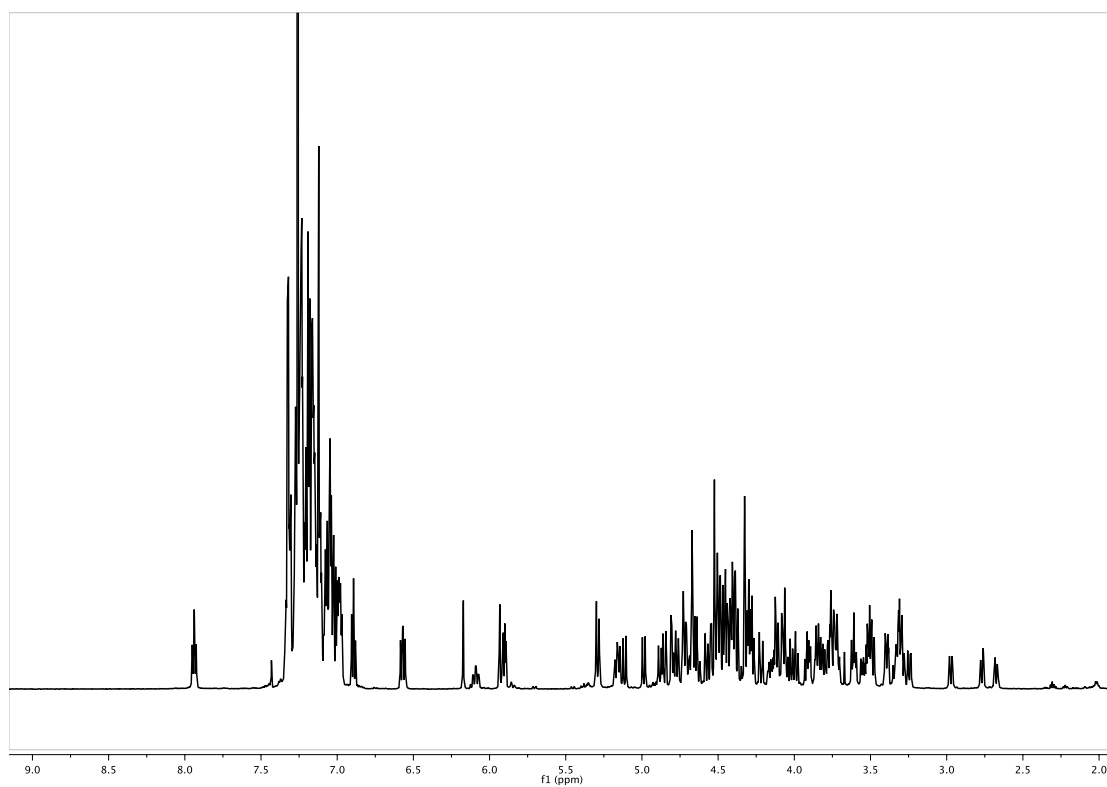


Figure S94: $^1\text{H-NMR}$ of **224** (CDCl_3 , 600 MHz, 300 K)

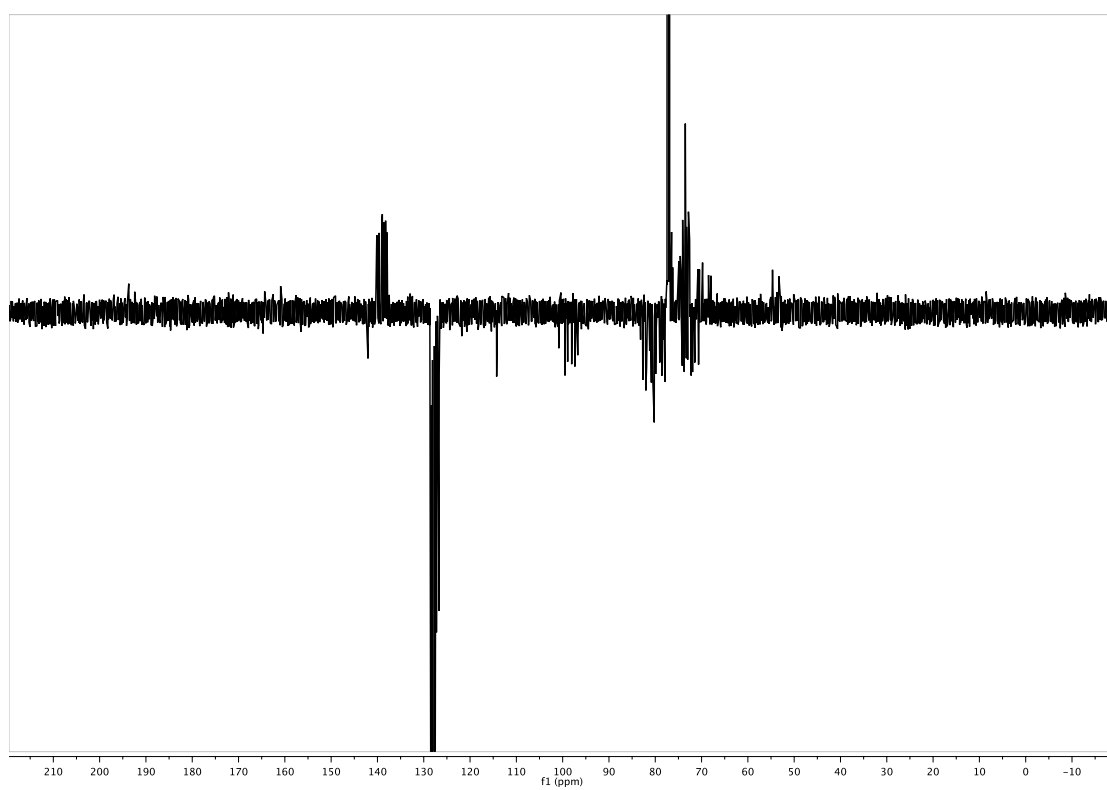
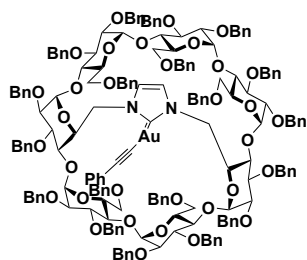


Figure S95: $^{13}\text{C-NMR}$ of **224** (CDCl_3 , 151 MHz, 300 K)

Cycle A	H	C	Cycle B	H	C
1	4,72	97,26	1	4,54	98,03
2	3,40	80,84	2	3,25	78,6
3	4,12	79,82?	3	3,91	80,42
4	3,74	74,14	4	3,71	80,55
5	6,09	71,95	5	4,06	71,60
6	3,32	53,32	6	2,76	67,99
6'	4,67		6'	2,67	
Cycle C	H	C	Cycle D	H	C
1	5,89	97,35	1	4,81	98,87
2	3,51	77,93	2	3,39	80,17
3	4,42	79,93	3	3,99	81,88
4	3,91	82,01	4	3,61	72,26
5	3,86	73,30	5	4,78	71,95
6	3,80	74,15	6	3,33	54,67
6'	3,75		6'	5,16	
Cycle E	H	C	Cycle F	H	C
1	4,66	100,89	1	4,67	99,47
2	3,31	78,32	2	3,30	80,17
3	4,12	82,7?	3	4,02	81,88
4	3,76	81,22?	4	3,49	83,17
5	3,28	71,45	5	3,60	73,75
6	2,97	68,50	6	3,56	70,47
6'	3,47		6'	3,84	
Cycle G	H	C			
1	5,91	96,72	ImidA	6,17	120,61
2	3,52	78,33?	ImidD	5,93	121,7
3	4,08	80,23	C=Au		193,7
4	3,83	81,98	Cipso		193,7(3Hz)
5	3,73	74,95	Hortho	7,94	142,06(5Hz)
6	4,16	69,78	Hmeta	6,57	114,18(18Hz)
6'	3,77		CF		164,4(241,4Hz)

Table S14: Attribution of the protons of the sugar units of **222**

(β -ICyD)AuCCPh (**225**)



Chemical Formula:
 $C_{186}H_{189}AuN_2O_{33}$
Molecular Weight:
3177.45

In a NMR tube, **224** (3.5 μ mol) were dissolved in $CDCl_3$, then phenyl acetylene **132** (0.39 μ L, 3.5 μ mol) was added. The mixture was left at r.t. overnight and the reaction is followed by NMR. In 18h **225** was quantitatively formed.

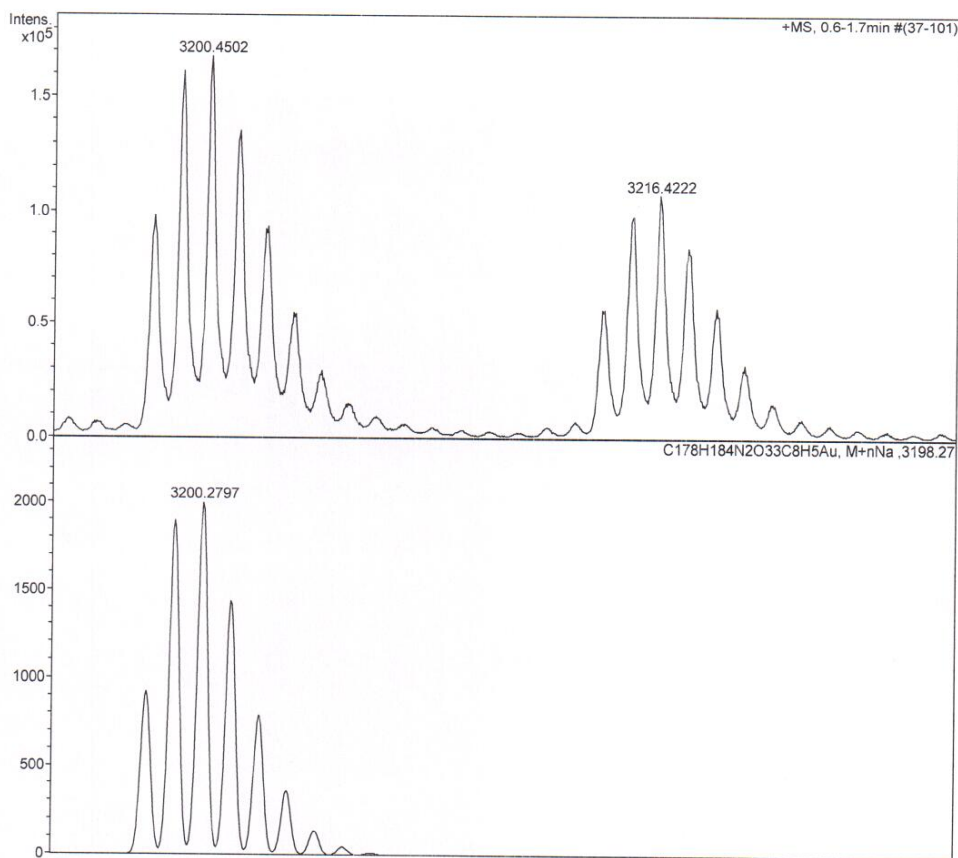


Figure S96: Mass Spectra **225** (CDCl₃, 400 MHz, 300 K)

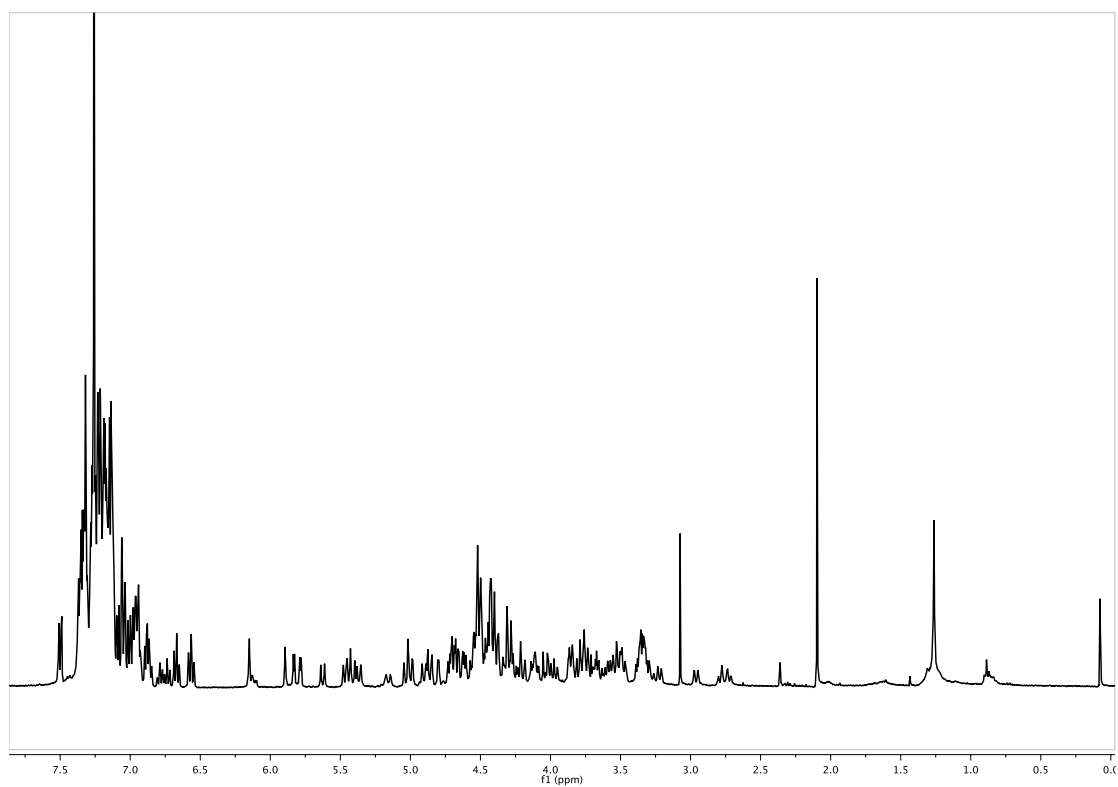


Figure S97: $^1\text{H-NMR}$ of **225** Figure S94: $^1\text{H-NMR}$ of **224** (CDCl_3 , 600 MHz, 300 K) (CDCl_3 , 600 MHz, 300 K)

226

In a NMR tube (β -ICyD) $\text{PdCl}_2(\text{PhCN})$ (10 mg, 0.3 μmol), $t\text{BuOK}$ (5 mg) and morpholine (0.25 μL , 0.3 μmol) were dissolved in THF- d_8 . The reaction mixture was heated at 80 $^\circ\text{C}$ for 18 hours and the reaction was monitored by $^1\text{H-NMR}$ leading to a formation of one major compound.

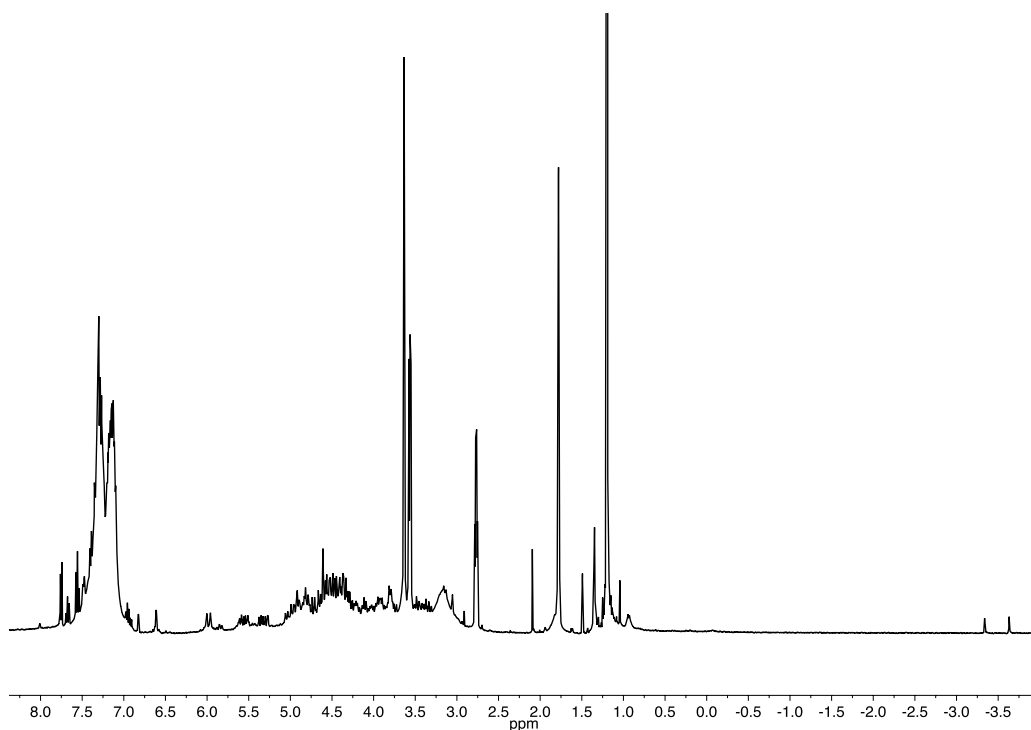


Figure S98: $^1\text{H-NMR}$ of **226** (THF- d_8 , 600 MHz, 300 K)

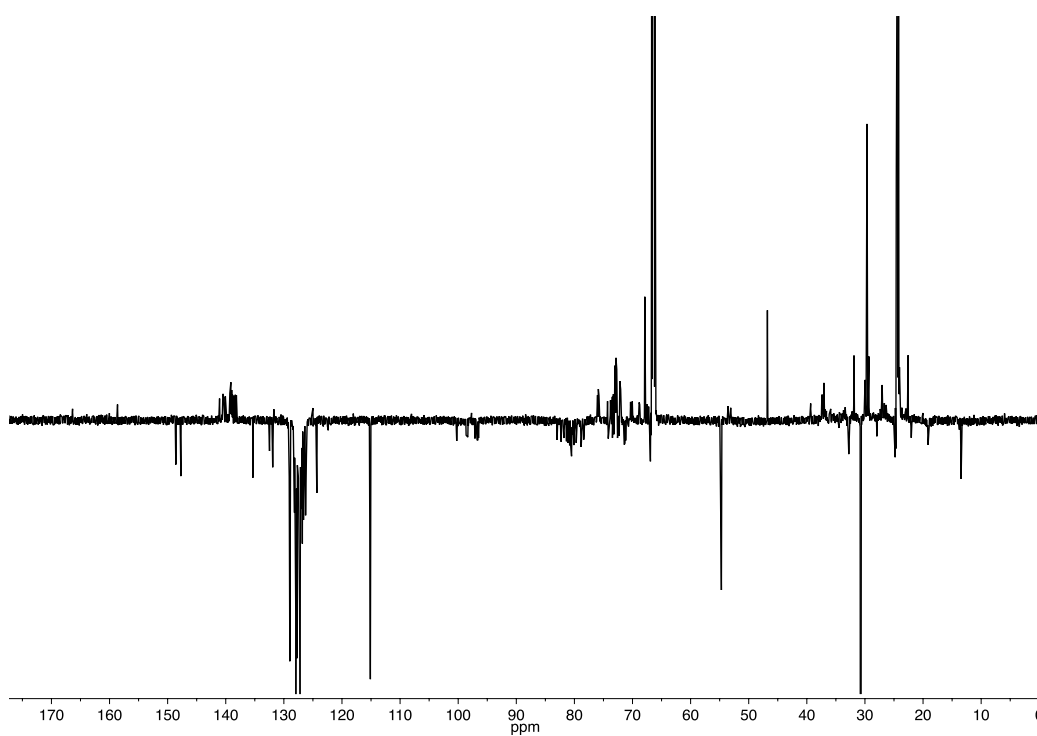
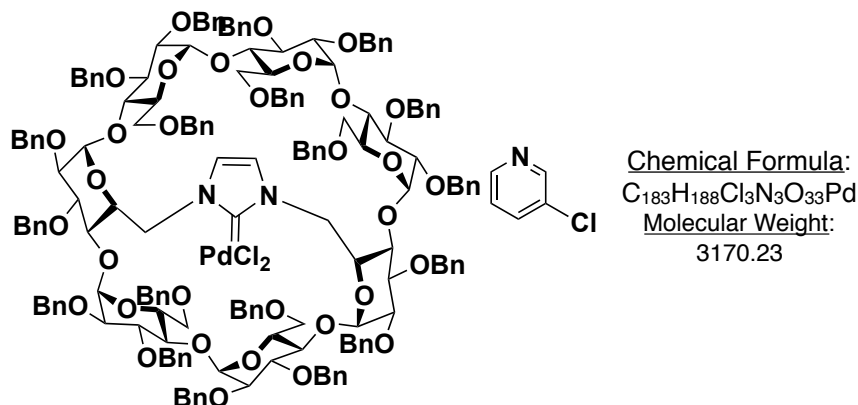


Figure S99: $^{13}\text{C-Jmod}$ of **226** (THF- d_8 , 151 MHz, 300 K)

(β -ICyD)PdCl₂(3-Chloropyridine) (227)



In an NMR tube. (β -ICyD)PdCl₂.PhCN (15 mg, 47 μ mol, 1 eq) has been dissolved in chloroform-d (300 μ L). Then, 3-Chloropyridine was added in a Chloroform-d solution (100 μ L). The complexed formed (**227**) has been characterized without any further purification.

¹H NMR (600 MHz, Chloroform-d) δ 9.20 (d, J = 2.4 Hz, 1H, H_{orthoPy}), 9.11 – 9.04 (m, 1H, H_{5Py}), 7.40 – 6.94 (m, H_{Arom} + H_{3Py}), 6.90 – 6.82 (m, 3H, H_{Arom}), 6.30 (dd, J = 8.2, 5.5 Hz, 1H, H_{4Py}), 6.19 (d, J = 1.8 Hz, 1H, H_{imidD}), 6.05 (d, J = 1.8 Hz, 1H, H_{imidA}), 5.99 – 5.92 (m, 2H; H-1-G, H-5D), 5.82 (d, J = 3.8 Hz, 1H, H_{1-C}), 5.67 (2xdd, J = 13.5, 2.7 Hz, 2H, H_{6b-A}, H_{6b-D}), 5.55 (d, J = 11.0 Hz, 1H, CH₂Ph), 5.44 (td, J = 10.6, 2.5 Hz, 1H, H_{5-A}), 5.40 (d, J = 10.7 Hz, 1H, CH₂Ph), 5.31 – 5.27 (d, J = 11.5 Hz 1H, CH₂Ph), 5.24 (d, J = 11.2 Hz, 1H, CH₂Ph), 5.13 – 5.01 (m, 4H, H_{3-CH1-D}), 4.89 – 4.67 (m, 11H), 4.67 – 4.33 (m, 33H), 4.32 – 4.15 (m, 7H), 4.15 – 4.09 (m, 2H), 4.09 – 3.87 (m, 9H), 3.85 – 3.64 (m, 12H), 3.62 (d, J = 10.4 Hz, 1H), 3.58 – 3.41 (m, 6H), 3.40 – 3.27 (m, 5H), 3.06 (d, J = 11.1 Hz, 1H), 2.93 (dd, J = 11.3, 2.5 Hz, 1H), 2.77 (dd, J = 11.2, 1.9 Hz, 1H).

¹³C-NMR: (151 MHz, Chloroform-d) δ = 151.2 (C=Pd), 150.5 (CH_{orthoPy})150.1 (CH_{orthoPy}), 140.39, 140.32, 140.08, 140.08, 139.80, 139.18, 139.17, 139.12, 139.01, 138.96, 138.92, 138.91, 138.78, 138.77, 138.61, 138.49, 138.46, 138.25, 138.23, 138.08 (19 x C_{ipso} + .H_{PhCN}) 137.7 (CH_{py}), 132.89 (CH_{Py}), 132.31, 131.95, 131.01, 130.65 (C_{Py}), 129.2 - 126.4 (CH_{Ar}), 124.7 (C_{metaPy}), 100.5 (C-1E), 99.8 (C-1G), 98.4 (C-1D), 98.32 (C-1B), 97.9 (C-1C), 97.5 (C-1A), 96.9 (C-1F), 83.3 (PhCHH), 82.8 (PhCHH), 82.4 (PhCHH), 82.2 (C-3A), 81.92, 81.9 (C-2F), 81.7 (C-4E), 81.0 (C-3D), 80.88 (C-2D), 80.80, 80.7 (C-4-G), 80.7 (C-3E), 80.65, 80.2 (C-3B), 79.6 (C-2G), 79.4 (C-2A), 78.69 (PhCHH), 78.54 (C-2E), 78.0 (C-3C), 77.7 (C-2C), 76.61 (PhCHH), 76.4 (PhCHH), 76.1 (PhCHH), 75.41 (PhCHH), 74.73 (PhCHH), 74.6 (C-4D), 74.2 (C-4A), 74.2 (PhCHH), 73.9 (C-5C), 73.6 (PhCHH), 73.4 (PhCHH), 73.3 (PhCHH), 73.3 (PhCHH), 73.1 (PhCHH), 73.2 (PhCHH), 72.8 (PhCHH), 72.7 (PhCHH), 72.5 (PhCHH), 72.4 (PhCHH), 72.3 (PhCHH), 72.2 (C-5F), 71.8(C-5A), 71.5 (C-5D), 71.1 (C-5B), 71.2 (C-6C), 70.5 (C-5D), 70.5 (C-5E), 70.1 (C-6G), 69.64 (C-6F), 68.9 (C-6D), 68.8 (C-6E), 68.32 (C6-B), 54.80 (C-6A), 53.7 (C-6D).

HRMS(ESI) 3189.1153 msrd 3189.1375 err -7 ppm

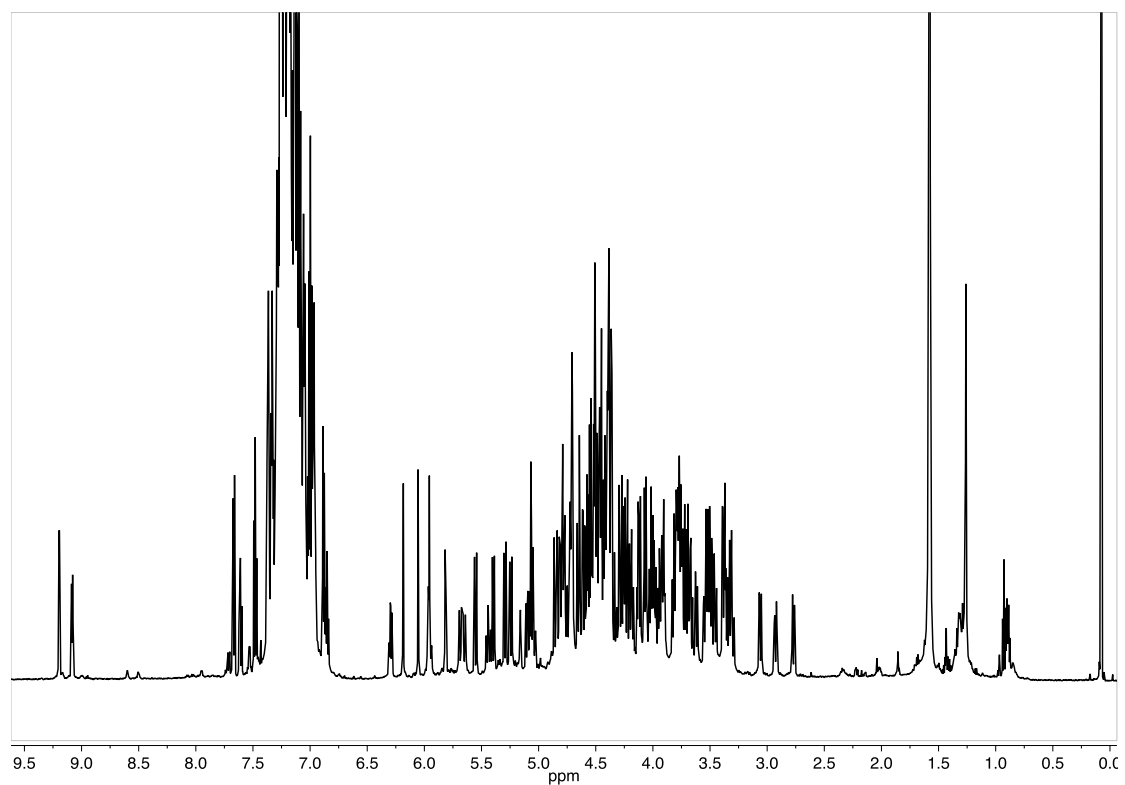


Figure S100: ^1H -NMR of **227** (CDCl_3 , 600 MHz, 300 K)

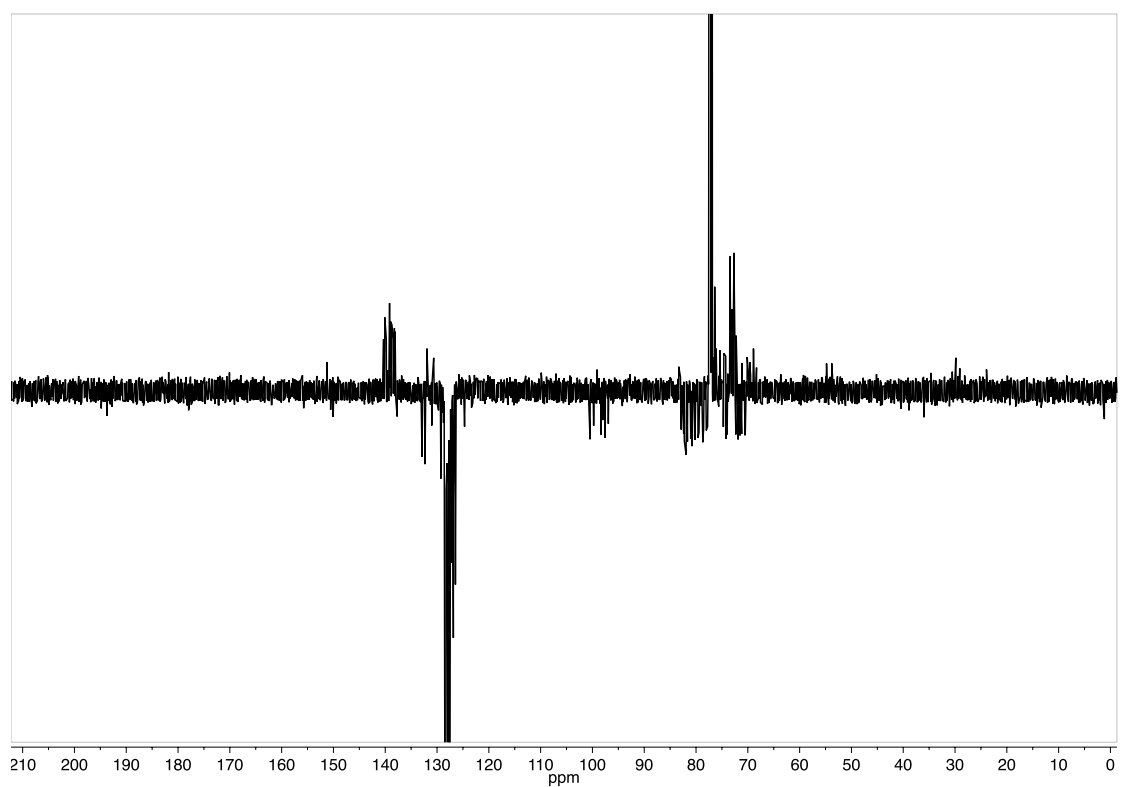


Figure S101: ^{13}C -Jmod of **227** (CDCl_3 , 151 MHz, 300 K)

Cycle A	H	C	Cycle B	H	C
1	4.65	97.44	1	4.62	98.22
2	3.38	79.43	2	3.38	80.7/79.4
3	4.19	82.19	3	4.44	80.16
4	3.71	74.19	4	3.80	82.28
5	5.44	71.65	5	4.41	71.14
6	3.30	53.77	6	2.75	68.78
6'	5.68		6'	2.94	
Cycle C	H	C	Cycle D	H	C
1	5.82	97.9	1	5.07	98.38
2	3.50	77.70	2	3.51	80.97
3	5.10	77.96	3	4.11	81.83
4	3.78	81	4	3.72	74.68
5	3.90	73.9	5	5.95	70.41
6	3.92	71.17	6	3.46	54.70
6'	3.79		6'	5.65	
Cycle E	H	C	Cycle F	H	C
1	4.70	100.36	1	5.96	96.79
2	3.32	78.62	2	3.53	¿
3	4.01	80.83	3	3.99	¿
4	3.80	81.7	4	3.77	81.8
5	4.71	70.48	5	4.06	72.16
6	3.55	68.81	6	3.76	69.60
6'	3.06		6'	4.08	
Cycle G	H	C			
1	4.72	99.65	ImidA	6.05	123.03
2	3.36	79.6	ImidD	6.19	124.59
3	4.20	¿	C=Pd		151.2
4	3.67	82.77			
5	4.50	71.48			
6	3.75	70.0			
6'	3.61				

Table S15: Attribution of the protons of the sugar units of **227**

Catalytic Reactions

Gold(I)-catalyzed cycloisomerization

*(α -ICyD)AuCl-catalyzed cycloisomerization of **141**:*

(α -ICyD)AuCl (19.3 mg, mmol, 2 mol%) and AgSbF_6 (2.6 mg, 17.4 mmol, 2 mol%) were introduced in a round bottom flask under an argon atmosphere and anhydrous CH_2Cl_2 (5 mL) was added. The solution was stirred at room temperature for 5 minutes, then enyne **141** was introduced (103 mg, mmol, 0.025 M). The reaction mixture was stirred at 40°C for 18 h and monitored by TLC. After completion, the solution was filtered through a pad of silica and the pad was washed with AcOEt. The solvent was vaporized under reduced pressure and the crude mixture was purified by silica gel flash chromatography (pentane:Et₂O, 85:15) to afford (R,R) **143** (84 mg, 0.289 mmol, 83%, 43 % ee) as a white powder.

$[\alpha]^{20}_{\text{D}} + 40.5$ (c 0.62, CHCl_3). $\{[\alpha]^{20}_{\text{D}}$ (*ent*-**143**) – 93 (c 1.07, CHCl_3) for 88% ee (1*S*,6*S*) $\}^3$

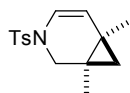
Chromatogram was recorded on a CO₂ supercritical fluid chromatography (SFC) using AD-H column, pressure: 100 Bars, with a debit of 5 mL/min and 4 % MeOH as eluent at $\lambda = 254$ nm. (+)-1,6-dimethyl-3-tolylsulfonyl-3-azabicyclo[4.1.0]hept-4-ene **7** was obtained as the major enantiomer.

*(β -ICyD)AuCl-catalyzed cycloisomerization of **141**:*

(β -ICyD)AuCl (23 mg, 0.0073 mmol, 2 mol%) and AgSbF_6 (2.6 mg, 0.0073 mmol, 2 mol%) were dissolved in CH_2Cl_2 (14.6 mL) in a round bottom flask under an argon atmosphere was added. The solution was stirred at room temperature for 5 minutes, then enyne **5** was introduced (101 mg, 0.365 mmol, 0.025 M). The reaction mixture was stirred at r.t. for 15 h monitored by TLC. After completion, the solution was filtered through a pad of silica and the pad was washed with diethyl ether. The solvent was removed under reduced pressure and the crude mixture was purified by flash chromatography on silica gel (Pentane/Et₂O : 85/15) to afford **143** (78 mg, 0.282 mmol, 77%). The enantiomer (+)-(R,R)-**143** (60% ee) was obtained as the major isomer.

$[\alpha]^{20}_{\text{D}} = + 59.3$ (c 0.62, CHCl_3).

¹H NMR of 141:



¹H NMR (400 MHz, Chloroform-d) δ 7.69 – 7.58 (m, 2H), 7.34 – 7.27 (m, 2H), 6.24 (dd, $J = 8.0, 1.2$ Hz, 1H), 5.16 (d, $J = 8.0$ Hz, 1H), 3.76 (d, $J = 11.4$ Hz, 1H), 2.66 (dd, $J = 11.4, 0.9$ Hz, 1H), 2.40 (s, 3H), 1.10 (s, 3H), 1.09 (s, 3H), 0.71 (d, $J = 4.3$ Hz, 1H), 0.31 (dd, $J = 4.3, 1.2$ Hz, 1H); The spectral data for 1,6-dimethyl-3-tolylsulfonyl-3-azabicyclo[4.1.0]hept-4-ene correspond to those previously reported.⁴

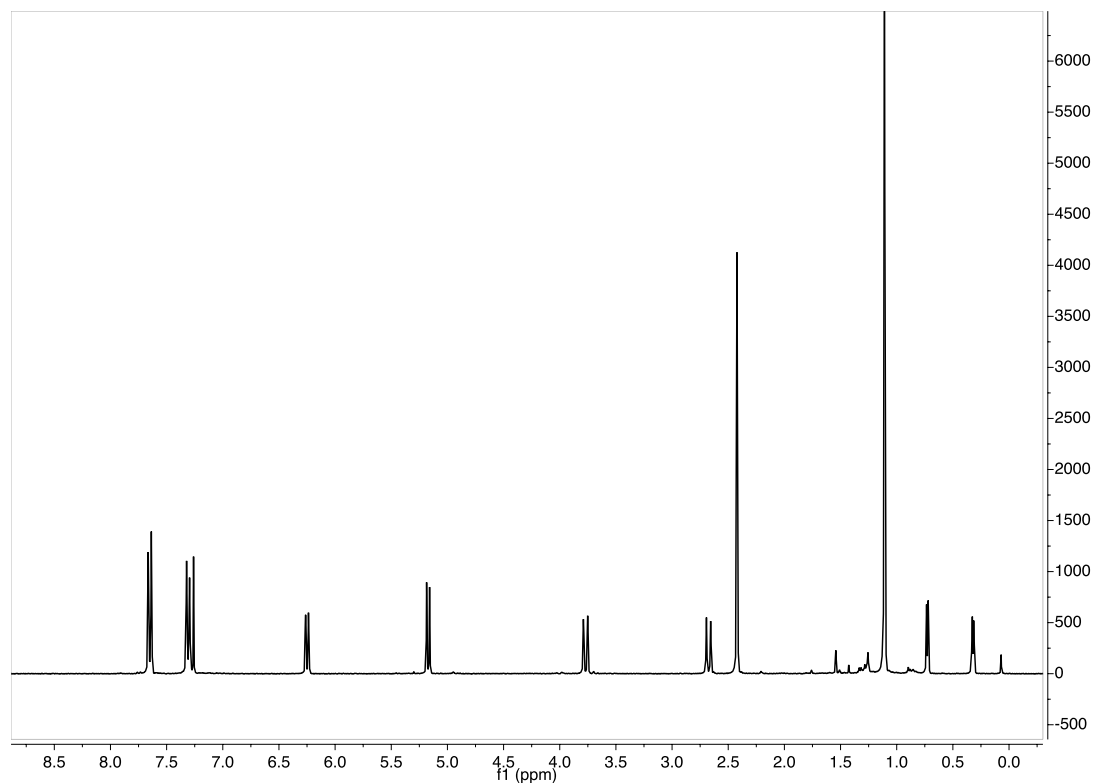


Figure S102: ¹H-NMR of **141** (CDCl₃, 400 MHz, 300 K)

(β -ICyD)AuCl-catalyzed cycloisomerization of **142:**

Using (β -ICyD)AuCl (18 mg, 0.006 mmol, 2 mol%) and AgSbF₆ (2.1 mg, 0.006 mmol, 2 mol%) and **142** (100 mg, 0.30 mmol). The reaction mixture was stirred at rt for 15 h. After completion, the solution was filtered through a pad of silica and the pad was washed with diethyl ether. The solvent was removed under reduced pressure and the crude mixture was purified by flash chromatography on silica gel (Pentane/Et₂O : 85/15) to afford **8** (99 mg, 0.29 mmol, 99 %) as a pale yellow solid. (+)-(R,R)-6-methyl-1-phenyl-3-tolyl-3-azabicyclo[4.1.0]hept-4-ene (**144**) was obtained (80% ee) as the major enantiomer.

¹H NMR of 6-methyl-1-phenyl-3-tolyl-3-azabicyclo[4.1.0]hept-4-ene **144:**

¹H NMR (300 MHz, Chloroform-d) δ 7.89 (d, J = 7.6 Hz, 1H), 7.46 (t, J = 7.4 Hz, 1H), 7.33-7.21 (m, 7 H), 6.47 (d, J = 7.9 Hz, 1H), 5.40 (d, J = 7.9 Hz, 1H), 3.81 (d, J = 12.0 Hz, 1H), 3.19 (d, J = 12.0 Hz, 1H), 2.61 (s, 3 H), 1.19 (d, J = 4.6 Hz, 1H), 1.02 (d, J = 4.5 Hz, 1H), 0.89 (s, 3H). The spectral data for 6-methyl-1-phenyl-3-(*p*-tolylsulfonyl)-3-azabicyclo[4.1.0]hept-4-ene correspond to those previously reported.⁵

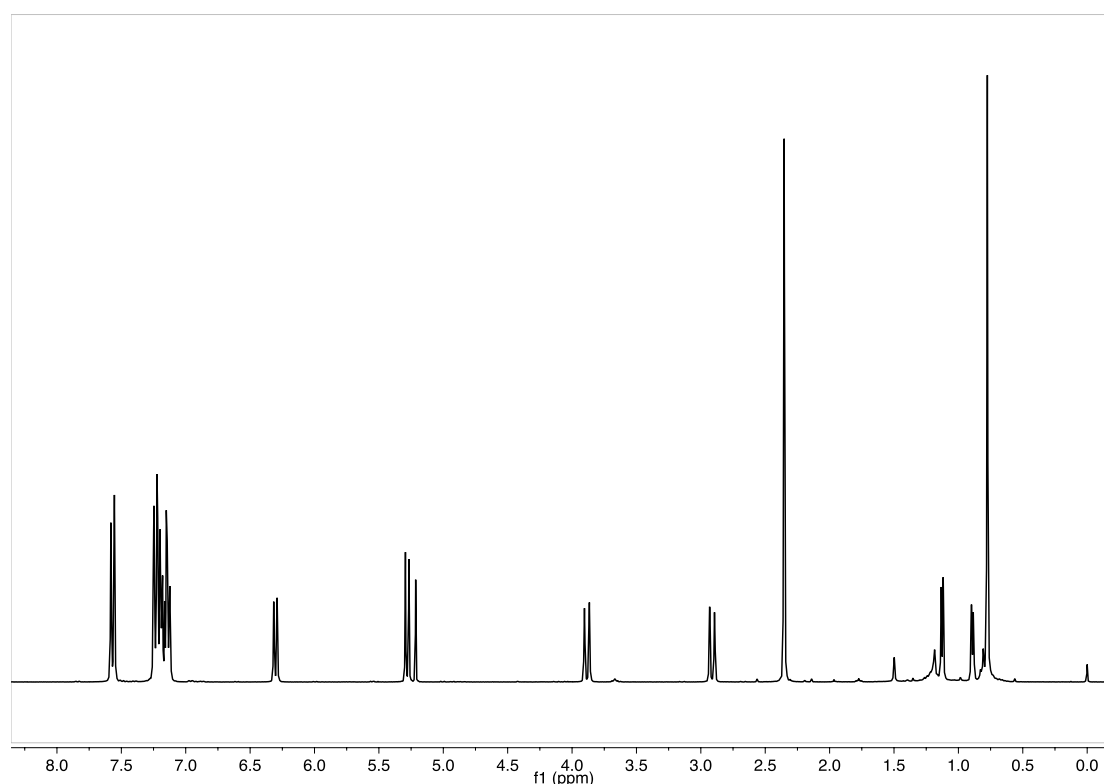


Figure S103: ¹H-NMR of **142** (CDCl₃, 400 MHz, 300 K)

(α -ICyD)CuCl catalyzed CuAAC.

In a round bottom flask, benzyl azide (44 mg, 0.354 μ mol), phenylacetylene (0.236 μ mol) and (α -ICyD)CuCl (60 mg, 0.06 μ mol) were weight. THF (1.5 mL) and an aqueous solution of KOH (1M 1.5mL) were added. The reaction was stirred at room temperature for 18 hours and monitored by TLC. When finished, the solvent was evaporated and the crude reaction was purified by silica gel flash chromatography (CyH : EtOAc 6 : 1) To obtain **200** (35 mg, 63%) and **199** (18 mg, 35%) as white solids. The reported NMR data were in agreement with the one reported on the literature.⁶

199

¹H NMR (300 MHz, Chloroform-d) δ 7.56 – 7.41 (m, 2H, CH_{Ar}), 7.32 – 7.04 (m, 6H, CH_{Ar}), 6.89 – 6.80 (m, 2H, CH_{Ar}), 4.80 – 4.57 (m, 2H, PhCHH).

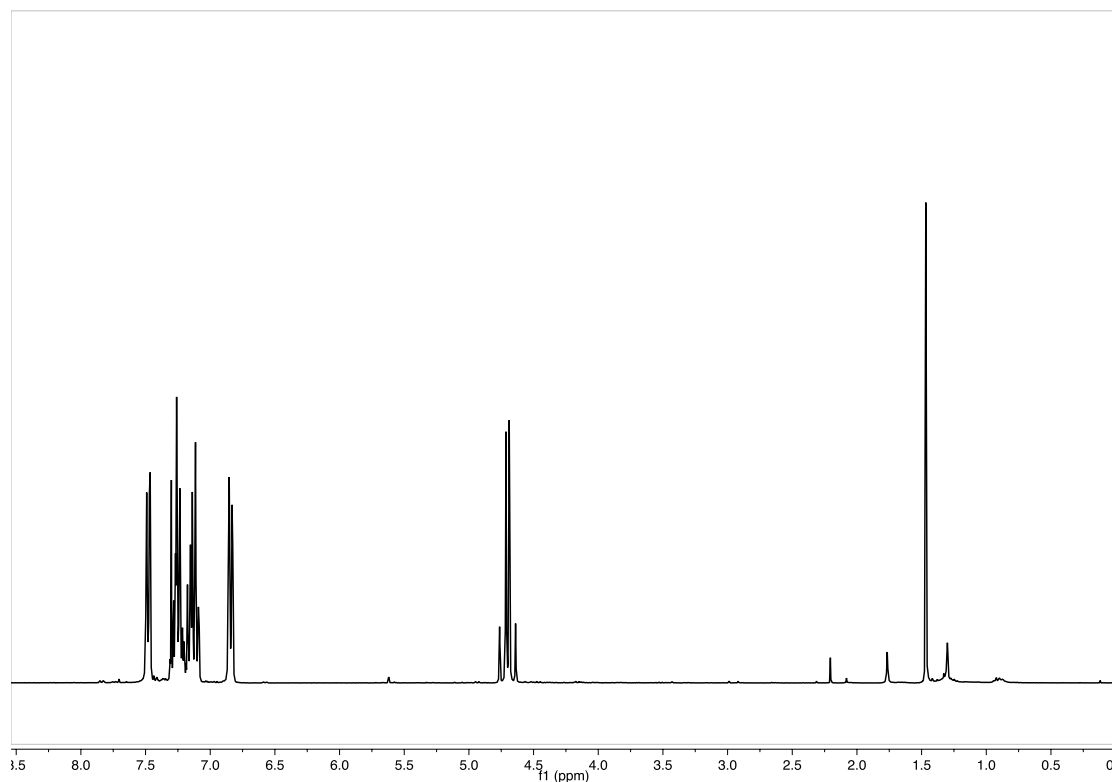


Figure S104: ¹H-NMR of **199** (CDCl₃, 600 MHz, 300 K)

200

¹H NMR (300 MHz, Chloroform-d) δ 7.90 – 7.73 (m, 2H, CH_{Ar}), 7.66 (s, 1H, CH_{triazole}), 7.49 – 7.27 (m, 8H, CH_{Ar}), 5.58 (s, 2H, PhCH₂H).

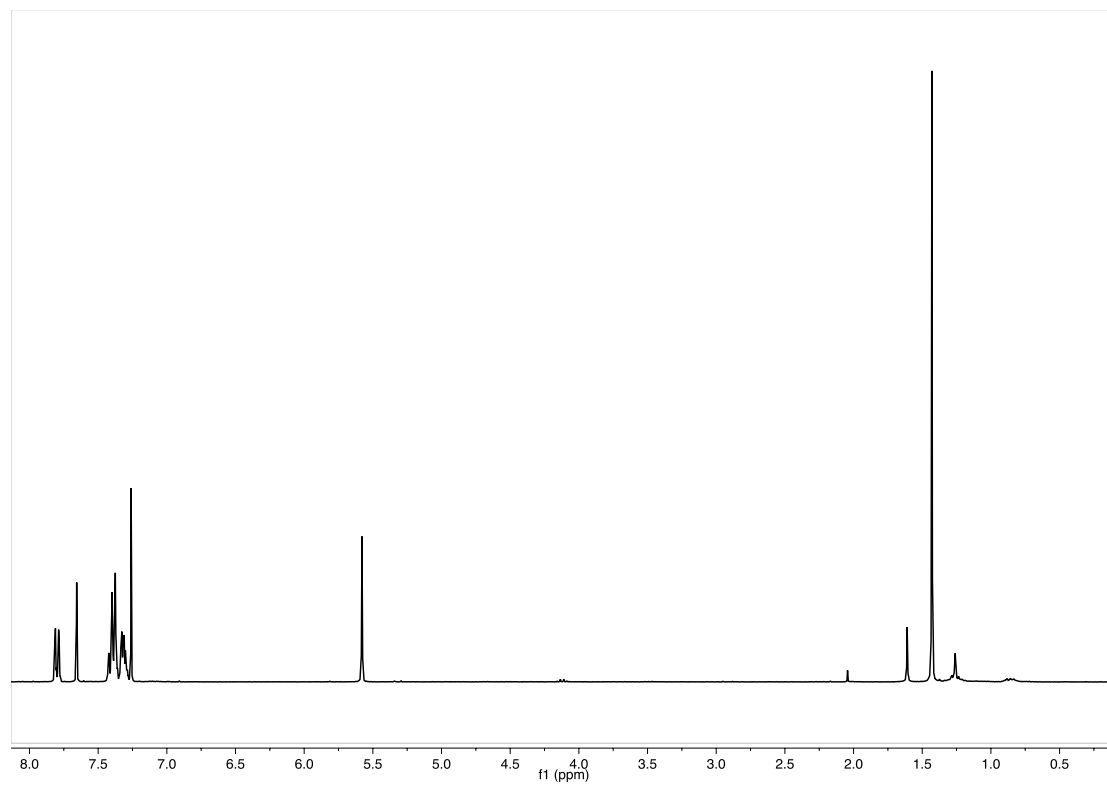


Figure S105: ¹H-NMR of **200** (CDCl₃, 400 MHz, 300 K)

(β -ICyD)PdCl₂(PhCN) catalyzed hydrothiolation

209

In a sealed tube *p*-thiocresol (19.7 mg, 170 μ mol), was introduced under Ar. Then a solution of (β -ICyD)PdCl₂(PhCN) (10mg, 3 μ mol), NEt₃ (0.9 μ L, 6.9 μ mol), γ -terpinene (50 μ mL, 340 μ mol) and phenylacetylene (17.4 μ L, 170 μ mol) in THF (300 μ L) was added. The reaction mixture was stirred during 18 hours and monitored by TLC, when finished, the solvent was removed under reduced pressure and 1,4-dinitrobenzene (0.3 eq) was added. The crude NMR was done without any further purification.

The NMR data was in agreement with those reported in the literature.⁷

Selected examples:

(β -ICyD)PdCl₂(PhCN): 7.6 mg 1,4-dinitrobenzene = 89 %

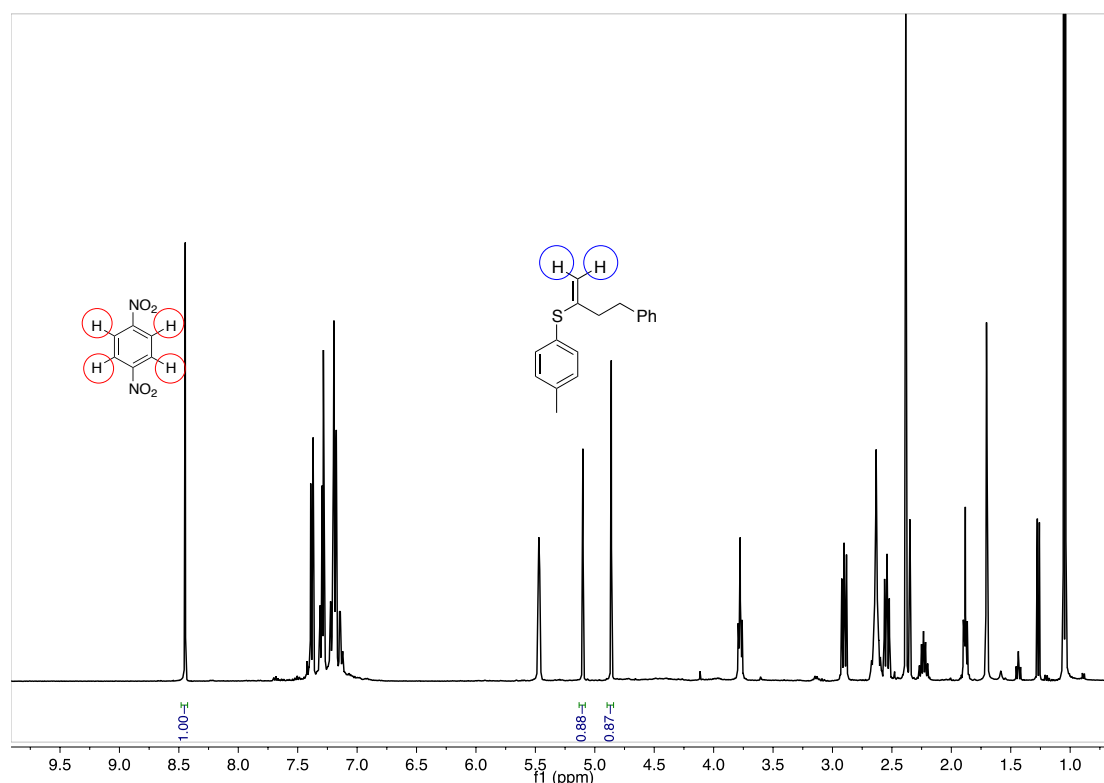


Figure S106: Crude ¹H-NMR of **209** (CDCl₃, 400 MHz, 300 K)

[(IPr)PdCl₂]: 7.8mg 1,4-dinitrobenzene

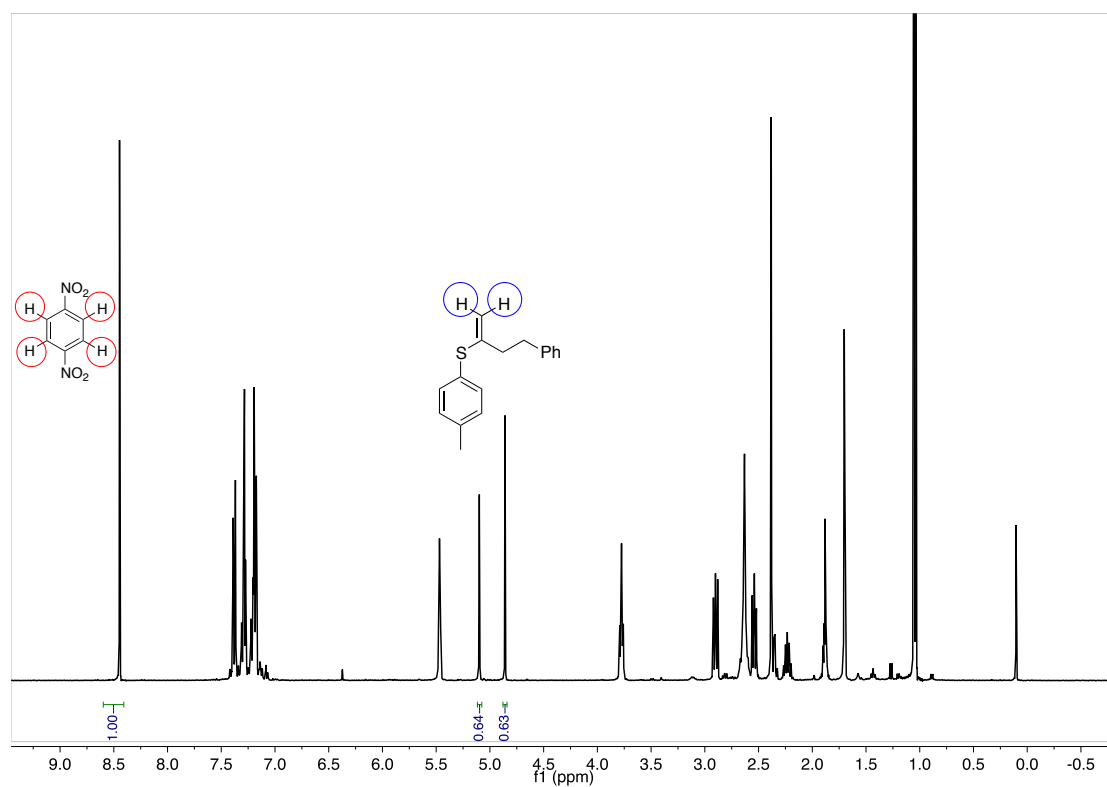


Figure S107: Crude ¹H-NMR of **209** (CDCl₃, 400 MHz, 300 K)

Kinetics of the reaction

In an NMR tube. A ^1H -NMR of a solution in THF ($500\ \mu\text{L}$) of Phenylbutyne (100 mM), *p*-thiocresol (100 mM), NEt_3 (4 mM) and γ -terpinene (200 mM) was recorded. The catalyst was added (1 mM in Pd) and a proton NMR was run each 5 minutes.

$[(\text{IPr})\text{PdCl}_2]_2$

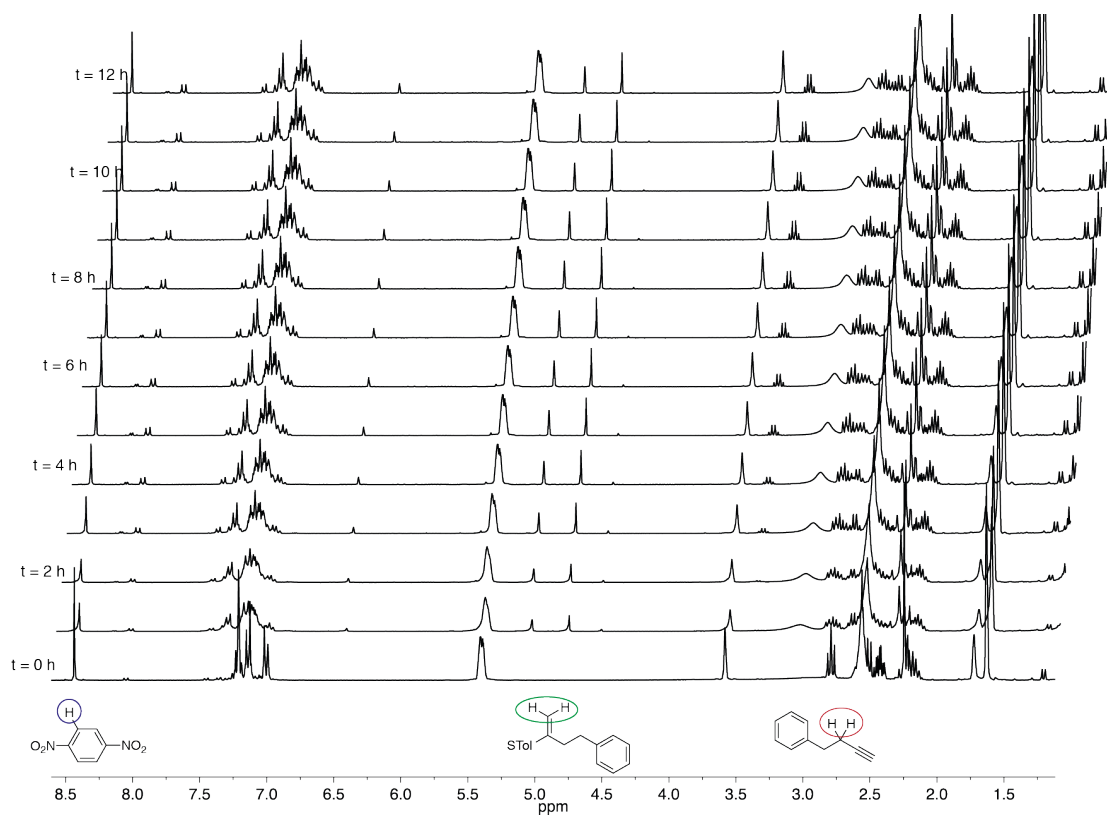


Figure S108: ^1H -NMR kinetics of the formation of **209** (THF- d_8 , 300 MHz, 300 K)

(β -ICyD)PdCl₂(PhCN)

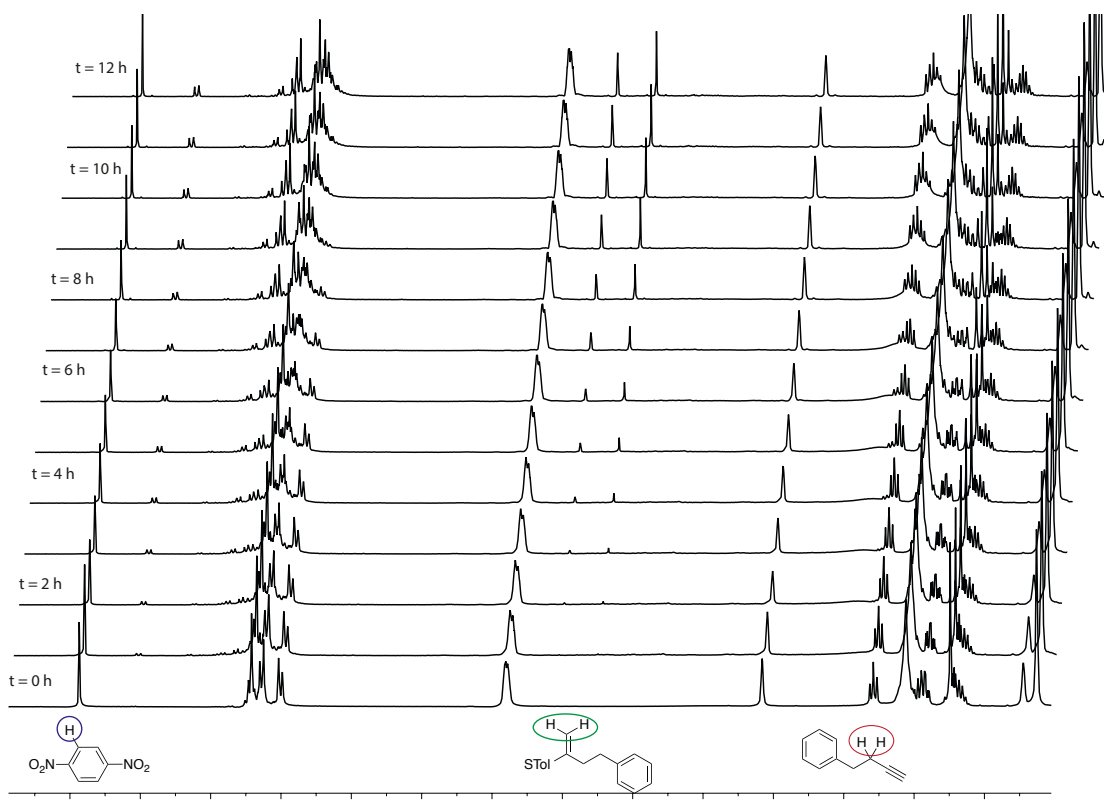


Figure S109: ¹H-NMR kinetics of the formation of **209** (THF-d₈, 300 MHz, 300 K)

NHC-CD-Pt(dvtms) catalyzed hydroacylation of phenylacetylene

In a sealed tube the catalyst (5mg, 1.54 μmol), phenylacetylene (17 μL , 15.4 μmol) and triethylsilylamine (24.7 μL , 15.4 μmol) were dissolved in toluene (300 μL). The reaction was stirred for 18 hours and the crude NMR of an aliquot was done.

Crude NMR of (β -ICyD)Pt(dvtms)

210:212 obtained in a 8:2

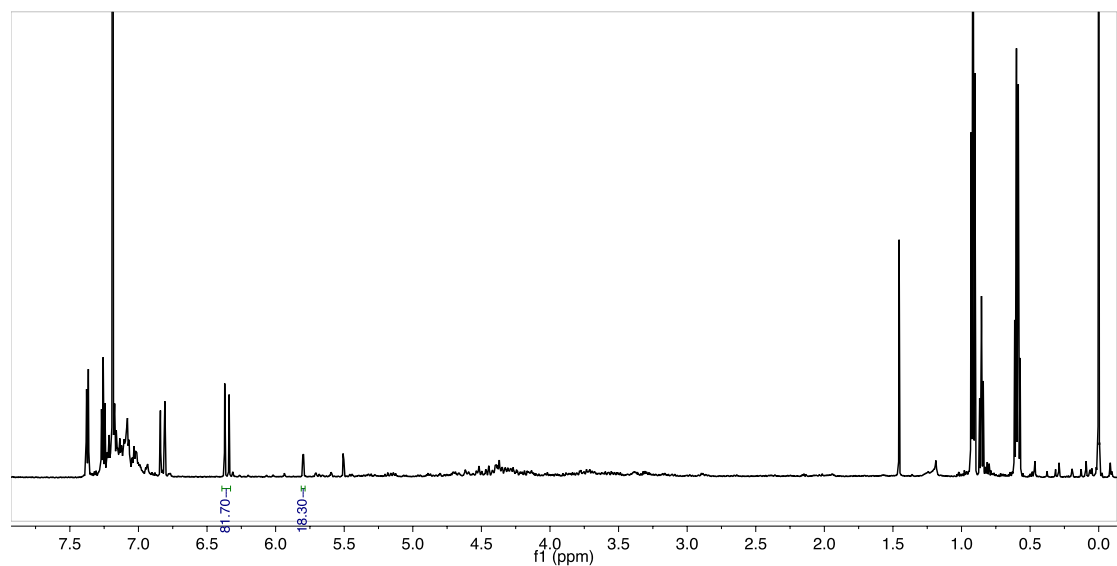


Figure S110: Crude $^1\text{H-NMR}$ of the reaction with (β -ICyD)Pt(dvtms)(CDCl_3 , 600MHz, 300K)

Crude NMR of (β -rev-ICyD)Pt(dvtms)

210:212 obtained in a 9:1

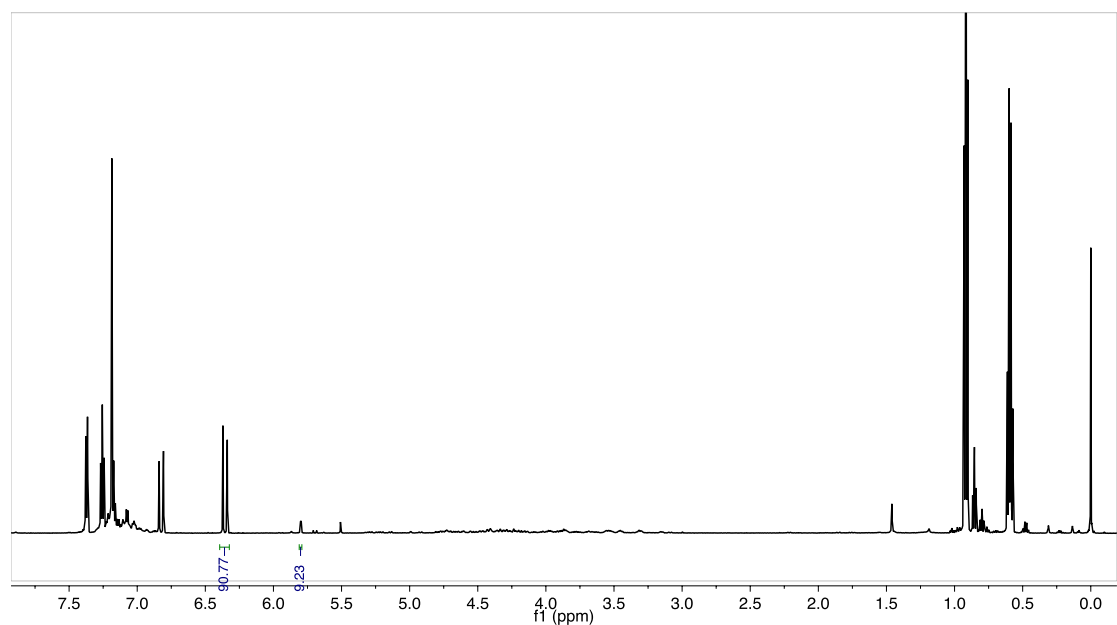
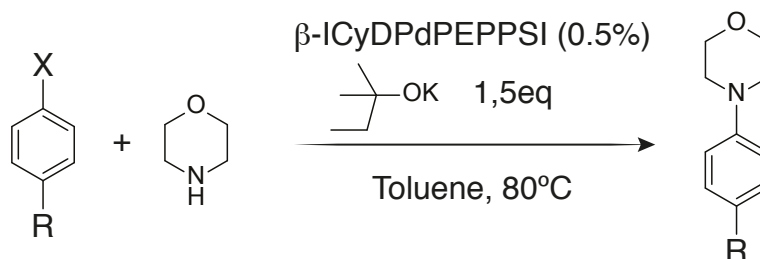


Figure S111: Crude $^1\text{H-NMR}$ of the reaction with (β -rev-ICyD)Pt(dvtms) (CDCl_3 , 600MHz, 300K)

Representative procedure for the arylation of morpholine.



Under an Ar atmosphere (β -ICyD)PdCl₂(PhCN) (4,75mg, 1,41 μ mol), and 3-chloropyridine (0,1 μ L, 1,41 μ mol) were dissolved in 500 μ L of anhydrous toluene. Then morpholine (40 μ L, 485 μ mol), a solution of potassium tert-amylate 1.7M in toluene (240 μ L, 364 μ mol) and the aromatic substrate (243 μ mol) were added to the mixture. The reaction mixture was stirred at 80°C. When finished the reaction crude is directly purified by flash chromatography.

Representative purification.

Sample: JM660A

RediSep Column: Silica 12g
Flow Rate: 30 ml/min
Equilibration Volume: 5.4 CV
Initial Waste: 0.0 CV
Air Purge: 0.0 min
Solvent A: Cyclohexane
Solvent B: ethyl acetate

Rf+

Peak Tube Volume: Max.
Non-Peak Tube Volume: Max.
Loading Type: Liquid
Wavelength 1 (red): 254nm
Peak Width: 1 min
Threshold: 0.20 AU
Wavelength 2 (purple): 280nm

Monday 09 October 2017 10:00AM

Run Notes:

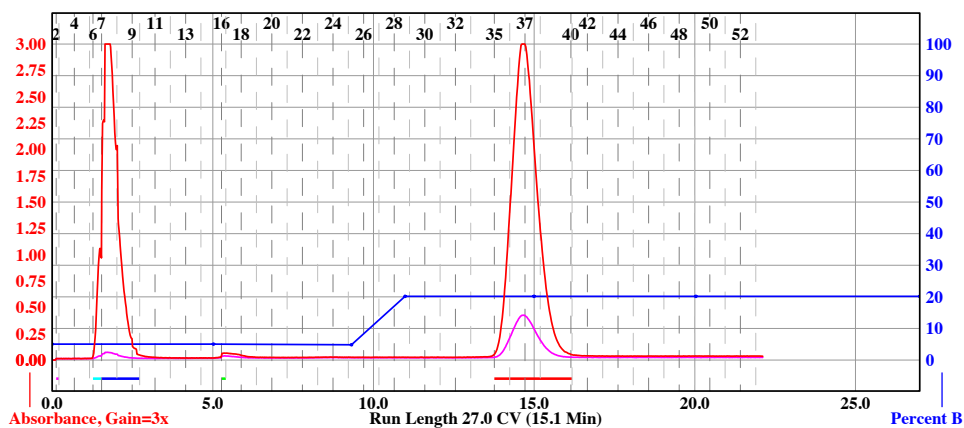


Figure S112: Flash purification of 230

	X=Cl	X=Br	X=I
R=MeO	89% (45mg)	74% (34mg)	68% (30mg)
R=H	68 % (27mg)		78 % (30mg)
R=CF ₃	80% (50mg)		89 % (55 mg)
R=Cl	63% (30mg)		

Table S16: Yield of the acylation reaction for the morpholine with (β -ICyD)PdCl₂(3-ClPy)

N-Phenylmorpholine.

Following general procedure 27mg (68% X=Cl) 30mg (78%, X=I) of the title compound were obtained as a yellow oil.

The spectral data were in accordance with those reported in the literature.⁸

N-(4-Methoxyphenyl)morpholine

Following general procedure 45mg (89% X=Cl) 34mg (74%, X=Br), (68%, X=I) of the title compound were obtained as a yellow oil.

The spectral data were in accordance with those reported in the literature.⁹

¹H NMR (400 MHz, Chloroform-d) δ = 7.03 – 6.68 (m, 4H), 3.95 – 3.82 (m, 4H), 3.77 (s, 3H), 3.17 – 2.95 (m, 4H).

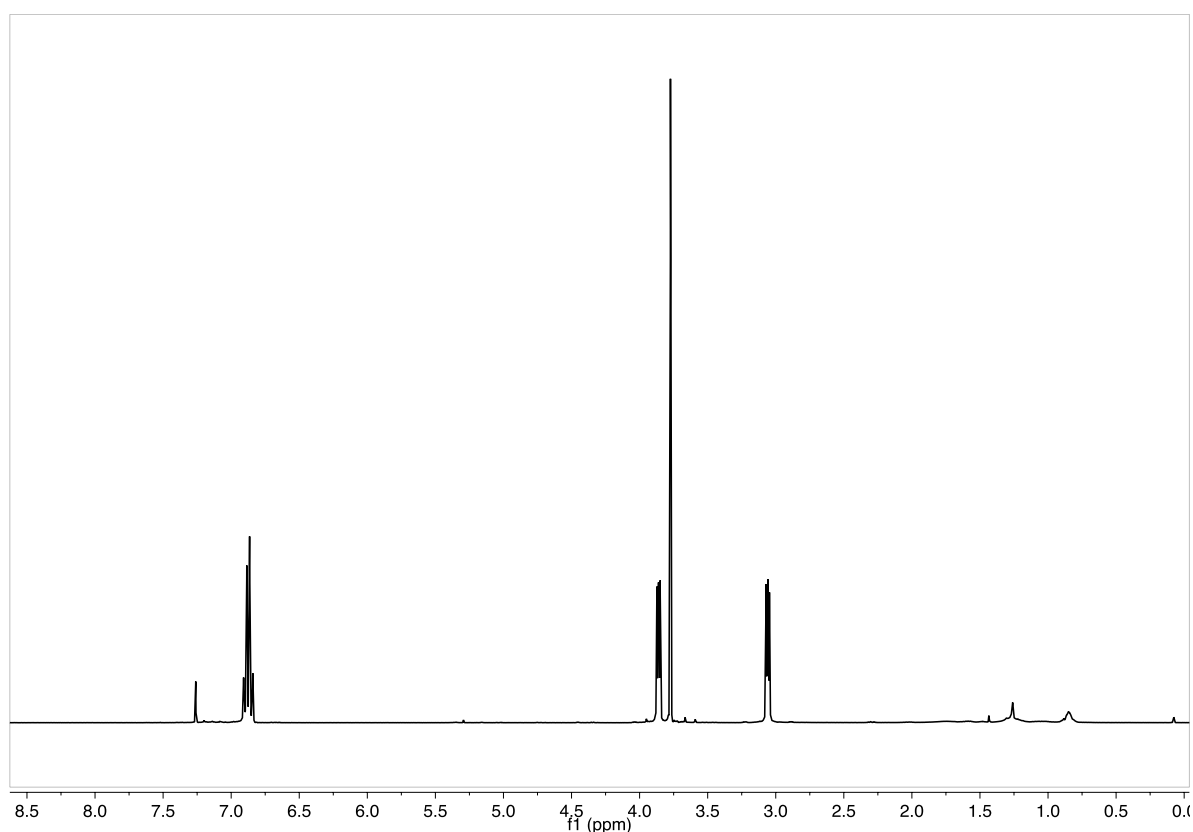


Figure S113: ¹H-NMR of **230** (CDCl₃, 400 MHz, 300 K)

N-(4-Trifluoromethylphenyl)morpholine (**232**)

Following general procedure 50mg (80% X=Cl) 55mg (89%, X=I) of the title compound was obtained as a yellow oil.

The spectral data were in accordance with those reported in the literature.¹⁰

¹H NMR (400 MHz, Chloroform-d) δ = 7.72 – 7.34 (m, 1H), 7.07 – 6.70 (m, 1H), 4.00 – 3.61 (m, 2H), 3.37 – 3.06 (m, 2H).

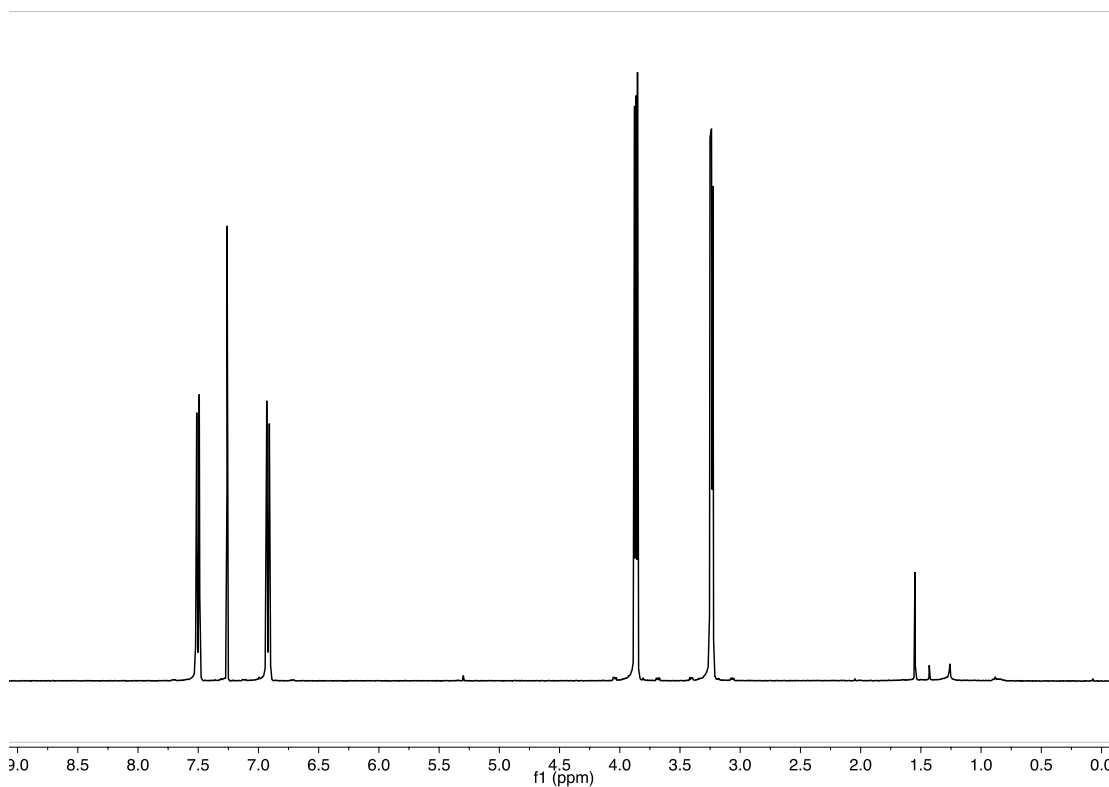
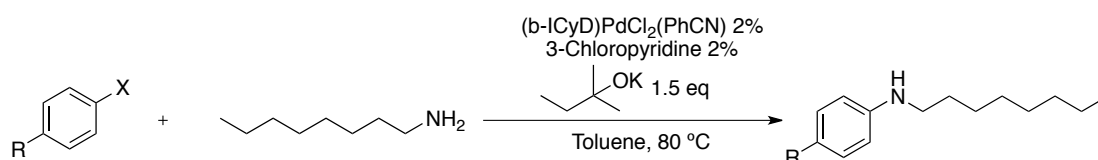


Figure S114: ¹H-NMR of **232** (CDCl₃, 400 MHz, 300 K)

Representative procedure for the arylation of N-octylamine.



Under an Ar atmosphere (β-ICyD)PdCl₂(PhCN) (15 mg, 4,5 μmol), and 3-chloropyridine (0,4 μL, 4,5 μmol) were dissolved in 500 μL of anhydrous toluene. Then *n*-octylamine (40 μL, 243 μmol), a solution of potassium tert-amylate 1.7 M in toluene (240 μL, 364 μmol) and the aromatic substrate (243 μmol) were added to the mixture. The reaction mixture is stirred at 80°C until finished and the reaction crude was directly purified by flash chromatography.

N-octyl-4-(trifluoromethyl)aniline **237**

Following general procedure 14 mg (21% X=Cl) 22 mg (31%, X=I) of a 2:1 mixture of **N-octyl-4-(trifluoromethyl)aniline** and **N-octyl-bis(4-(trifluoromethyl)aniline)** were obtained as a yellow oil.

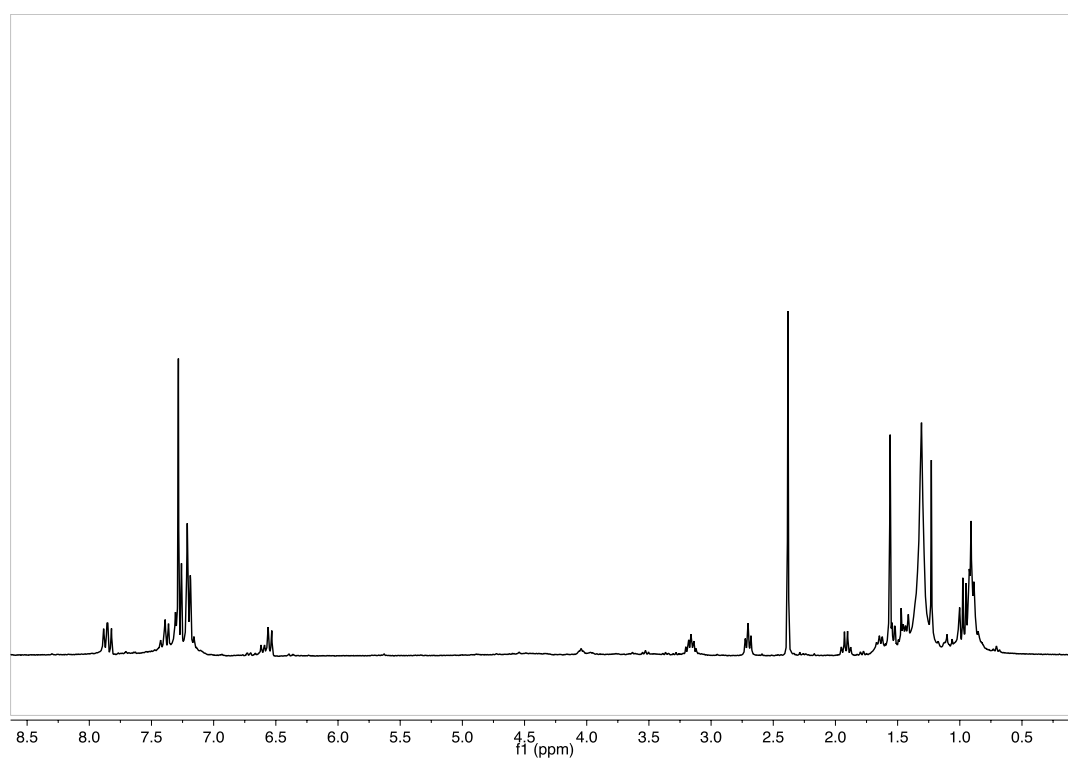


Figure S115: ¹H-NMR of **237** (CDCl₃, 400 MHz, 300 K)

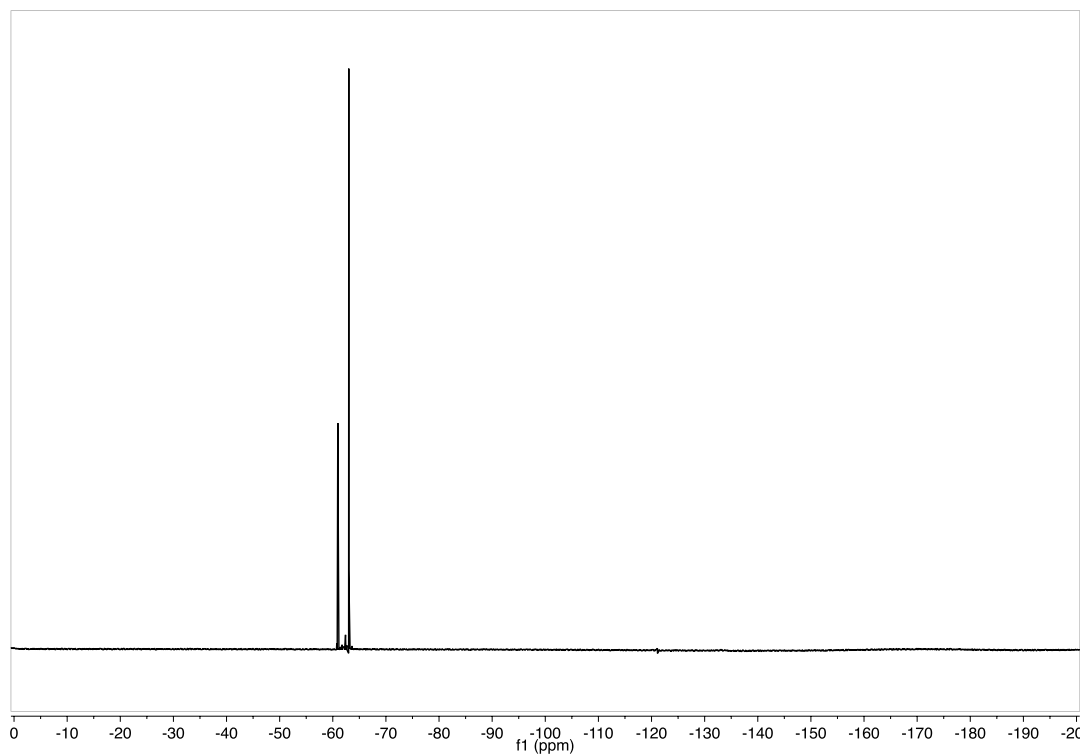


Figure S116: ^{19}F -NMR of **234** (CDCl_3 , 376 MHz, 300 K)

N-octylaniline **236**

Following general procedure 37mg (56% X=Cl), of the title compound was obtained as a yellow oil.

¹H NMR (400 MHz, Chloroform-d) δ 7.23 – 7.12 (m, 5H), 6.73 – 6.56 (m, 2H), 3.10 (t, $J = 7.1$ Hz, 2H), 2.36 (d, $J = 0.7$ Hz, 3H), 1.68 – 1.46 (m, 3H), 1.44 – 1.17 (m, 2H), 1.20 (s, 3H), 0.97 – 0.82 (m, 5H).

The spectral data were in accordance with those reported in the literature.

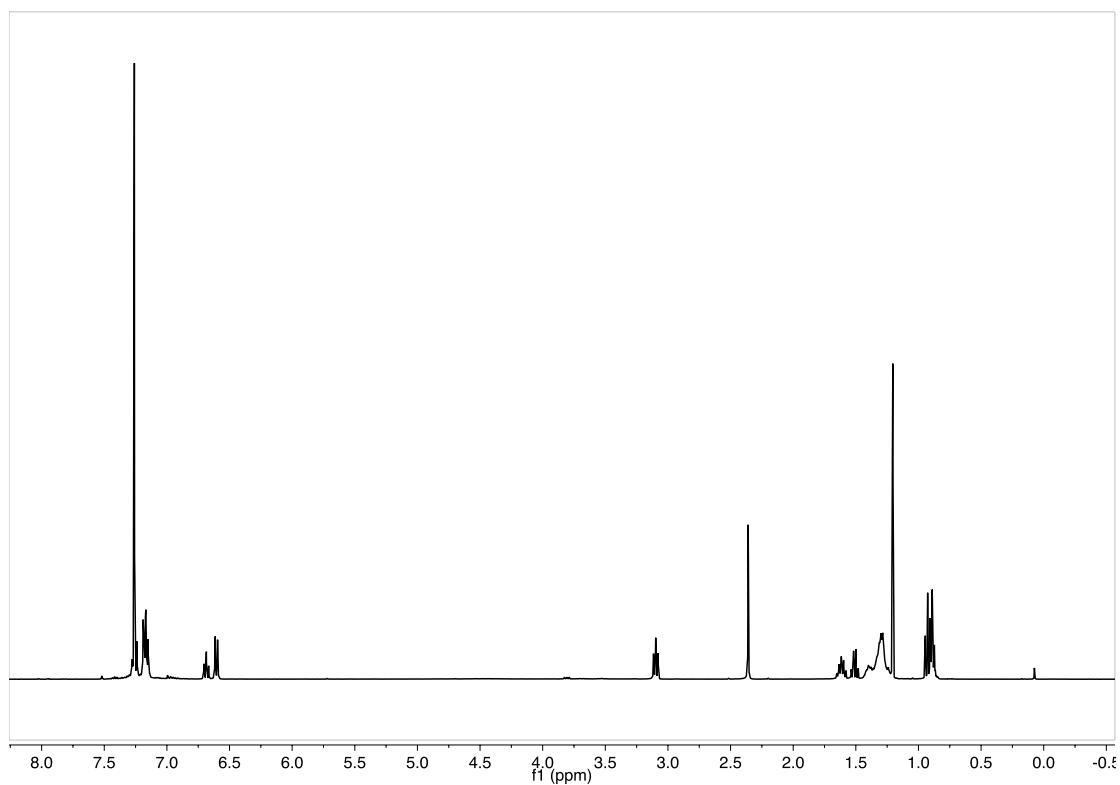


Figure S117: ¹H-NMR of **236** (CDCl₃, 400 MHz, 300 K)

N-octyl-4-methoxyaniline **235**

Following general procedure 42 mg (74% X=Cl) 47 mg (88%, X=I) of the title compound were obtained as a yellow oil.

The spectral data were in accordance with those reported in the literature.¹¹

¹H NMR (300 MHz, Chloroform-d) δ 6.83 – 6.73 (m, 2H), 6.64 – 6.53 (m, 2H), 3.75 (s, 3H), 3.05 (t, J = 7.1 Hz, 2H), 1.66 – 1.44 (m, 3H), 1.20 (s, 3H), 0.98 – 0.83 (m, 4H).

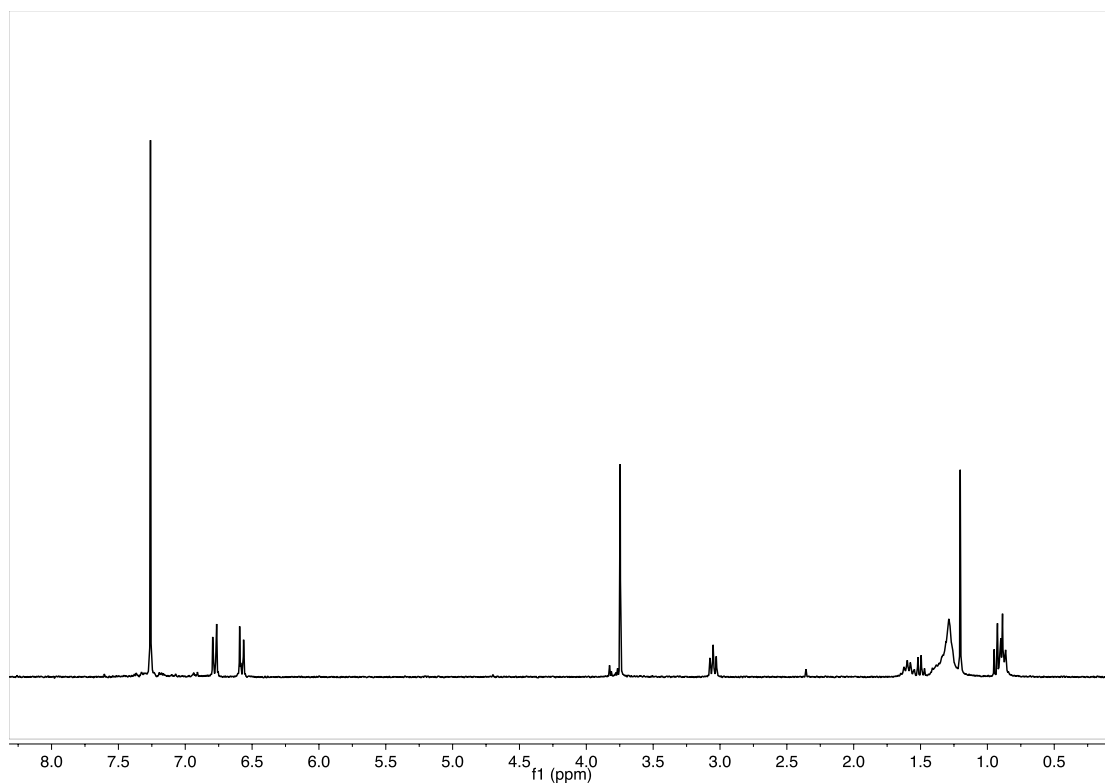


Figure S118: ¹H-NMR of **235** (CDCl₃, 400 MHz, 300 K)

N-octyl-3-methoxyaniline

Following general procedure 48mg (89% X=Br) of the title compound were obtained as a yellow oil.

¹H NMR (300 MHz, Chloroform-d) δ 7.07 (t, J = 8.1 Hz, 1H), 6.24 (m, 2H), 6.16 (t, J = 2.3 Hz, 1H), 3.77 (s, 3H), 3.08 (t, J = 7.1 Hz, 2H), 1.67 – 1.53 (m, 2H), 1.50 – 1.24 (m, 13H), 1.00 – 0.81 (m, 5H).

The spectral data were in accordance with those reported in the literature.¹²

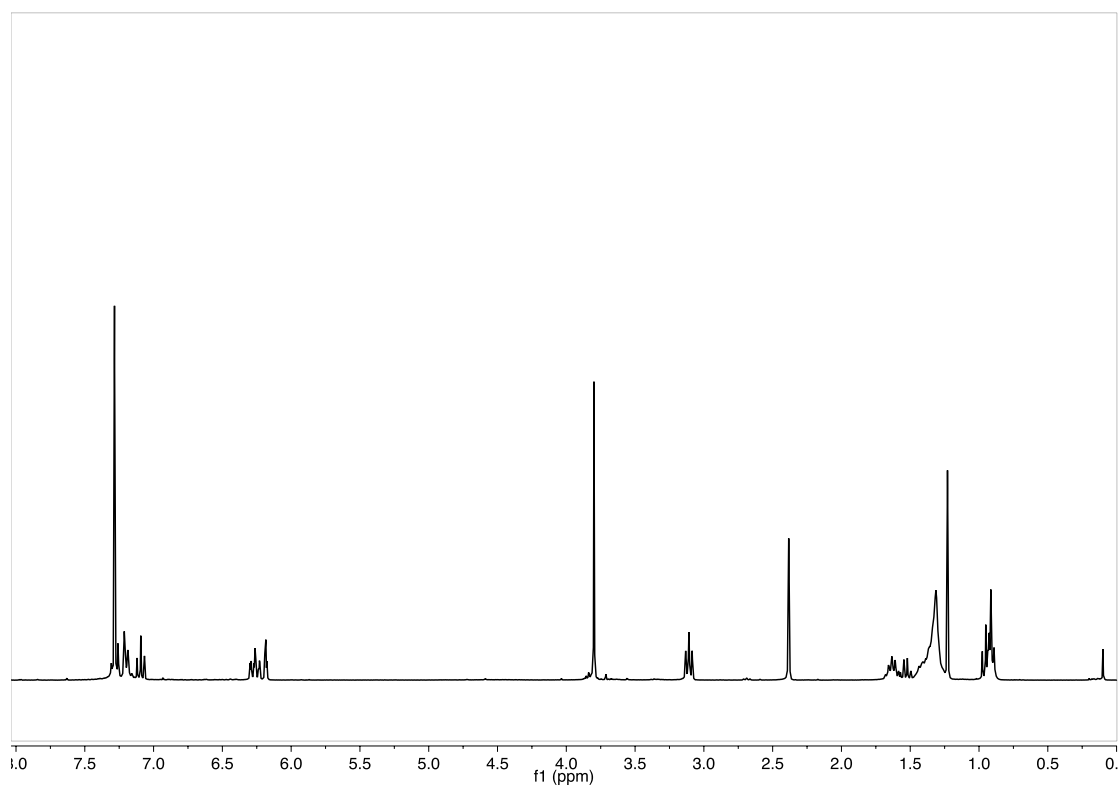


Figure S119: ¹H-NMR of **235** (CDCl₃, 400 MHz, 300 K)

(ICyD)Pd-catalyzed Allylation of aldehydes

(α -rev-ICyD)PdCl(Allyl) catalyzed allylation of **238**

In a sealed tube (α -rev-ICyD)PdCl(allyl) (10.5 mg, 4.0 μ mol), PPh₃ (1.05 mg 4.0 μ mol) were dissolved in THF (1.5 mL) under Ar. Then, 4-Bromobenzaldehyde (37 mg, 0.200 μ mol) and allyl acetate (24 mg, 240 μ mol) were added. Then, a solution of ZnEt₂ in hexanes (700 μ L, 700 μ mol) was added dropwise. The reaction mixture was monitored by TLC. When finished, a saturated aqueous solution of NH₄Cl (4mL) was added dropwise and vigorously stirred for 30 minutes. The product is extracted with Et₂O (2 x 10 mL), dried with Na₂SO₄ and evaporated in vacuo. The crude is purified by silica gel flash chromatography (CyH:AcOEt 95:5) affording **239** (36 mg, 80%) as a pale yellow oil.

The spectral data were in accordance with those reported in the literature.¹³

¹H NMR (300 MHz, Chloroform-d) δ 7.52 – 7.42 (m, 2H), 7.24 (m, 2H), 5.89 – 5.68 (m, 1H), 5.23 – 5.10 (m, 2H), 4.71 (dd, J = 7.7, 5.1 Hz, 1H), 2.59 – 2.36 (m, 2H).

$[\alpha]_D^{20} + 1.05$ (c 1, benzene) 5% ee.

(β -ICyD)PdCl(Allyl) catalyzed allylation of **238**

In a sealed tube (β -ICyD)PdCl(allyl) (10.5 mg, 4.0 μ mol), PPh₃ (1.05 mg 4.0 μ mol) were dissolved in THF (1.5 mL) under Ar. Then, 4-Bromobenzaldehyde (37 mg, 0.200 μ mol) and allyl acetate (24 mg, 240 μ mol) were added. Then, a solution of ZnEt₂ in hexanes (700 μ L, 700 μ mol) was added dropwise. The reaction mixture was monitored by TLC. When finished, a saturated aqueous solution of NH₄Cl (4mL) was added dropwise and vigorously stirred for 30 minutes. The product is extracted with Et₂O (2 x 10 mL), dried with Na₂SO₄ and evaporated in vacuo. The crude is purified by silica gel flash chromatography (CyH:AcOEt 95:5) affording **239** (36 mg, 80%) as a pale yellow oil.

The spectral data were in accordance with those reported in the literature.

¹H NMR (300 MHz, Chloroform-d) δ 7.52 – 7.42 (m, 2H), 7.24 (m, 2H), 5.89 – 5.68 (m, 1H), 5.23 – 5.10 (m, 2H), 4.71 (dd, J = 7.7, 5.1 Hz, 1H), 2.59 – 2.36 (m, 2H).

$[\alpha]_D^{20} + 0.42$ (c 1, benzene) 2% ee.

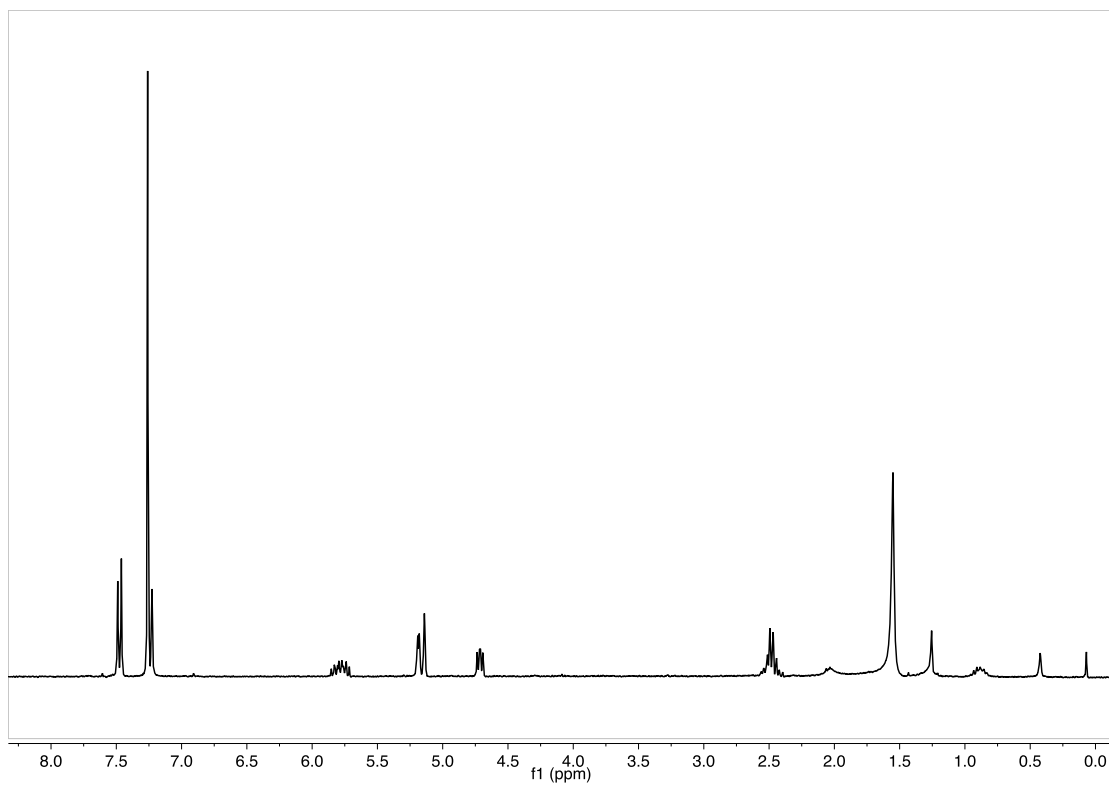


Figure S120: $^1\text{H-NMR}$ of **239** (CDCl_3 , 400 MHz, 300 K)

(α -rev-ICyD)PdCl(Allyl) catalyzed allylation of **238**

In a sealed tube (α -rev-ICyD)PdCl(allyl) (10.5 mg, 4.0 μ mol), PPh₃ (1.05 mg, 4.0 μ mol) were dissolved in THF (1.5 mL) under Ar. Then, 4-Bromobenzaldehyde (37 mg, 0.200 μ mol) and cinnamyl acetate (39.9 μ L, 240 μ mol) were added. Then, a solution of ZnEt₂ in hexanes (700 μ L, 700 μ mol) was added dropwise. The reaction mixture was monitored by TLC. When finished, a saturated aqueous solution of NH₄Cl (4 mL) was added dropwise and vigorously stirred for 30 minutes. The product is extracted with Et₂O (2 x 10 mL), dried with Na₂SO₄ and evaporated in vacuo. The crude is purified by silica gel flash chromatography (CyH:AcOEt 95:5) affording **240** (45 mg, 75%) as a pale yellow oil.

The spectral data were in accordance with those reported in the literature.

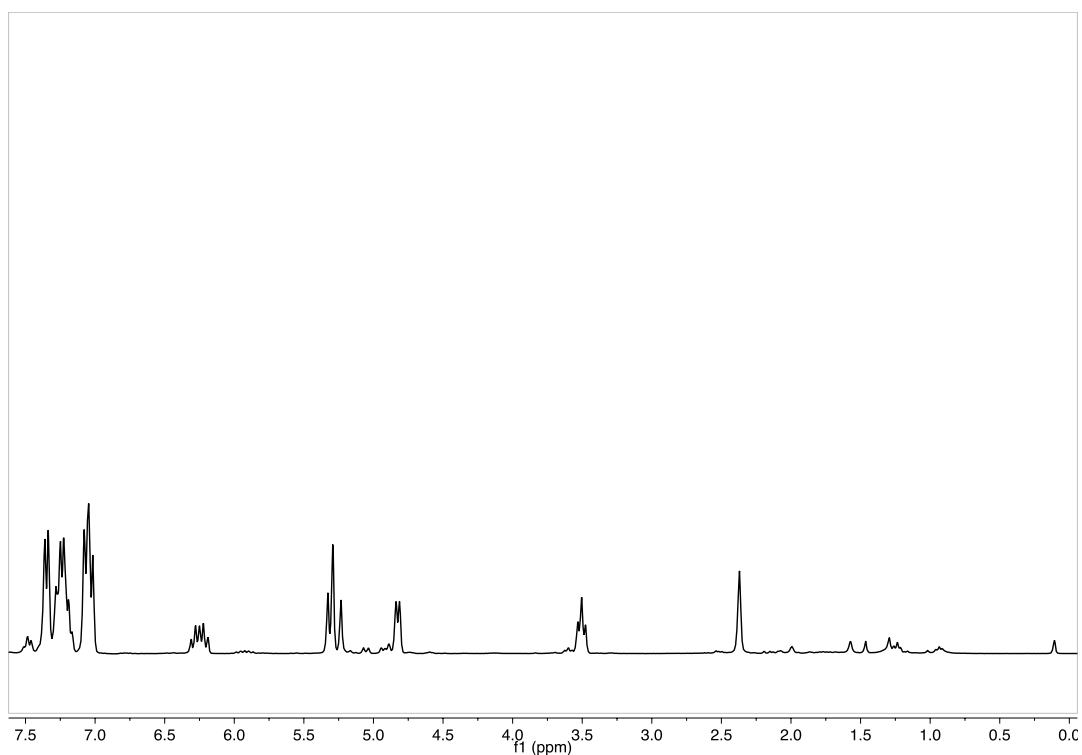


Figure S121: ¹H-NMR of **239** (CDCl₃, 300 MHz, 300 K)

(α -rev-ICyD)PdCl(Allyl) substrate selection

In a sealed tube (α -rev-ICyD)PdCl(allyl) (10.5 mg, 4.0 μ mol), PPh₃ (1.05 mg 4.0 μ mol) were dissolved in THF (1.5 mL) under Ar. Then, 4-Bromobenzaldehyde (37 mg, 0.200 μ mol), allyl acetate (12 mg, 120 μ mol) and cinnamyl acetate (20 μ L, 120 μ mol) were added. Then, a solution of ZnEt₂ in hexanes (700 μ L, 700 μ mol) was added dropwise. The reaction mixture was monitored by TLC. When finished, a saturated aqueous solution of NH₄Cl (4mL) was added dropwise and vigorously stirred for 30 minutes. The product is extracted with Et₂O (2 x 10 mL), dried with Na₂SO₄ and evaporated in vacuo.

The crude is analyzed by NMR. By integration of the internal vinyl proton a ratio 58:42 of **238:239** was obtained.

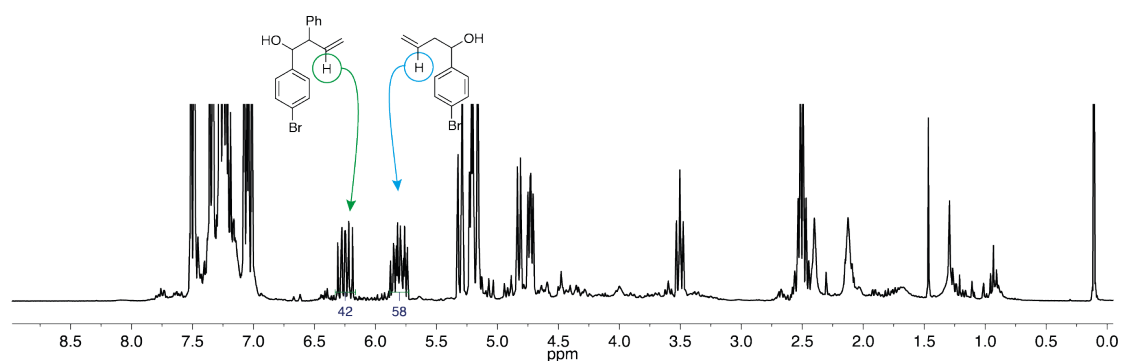


Figure S122: Crude ¹H-NMR of **238+239** (CDCl₃, 400 MHz, 300 K)

(β -ICyD)PdCl(Allyl) substrate selection

In a sealed tube (β -ICyD)PdCl(allyl) (10.5 mg, 4.0 μ mol), PPh₃ (1.05 mg 4.0 μ mol) were dissolved in THF (1.5 mL) under Ar. Then, 4-Bromobenzaldehyde (37 mg, 0.200 μ mol), allyl acetate (12 mg, 120 μ mol) and cinnamyl acetate (20 μ L, 120 μ mol) were added. Then, a solution of ZnEt₂ in hexanes (700 μ L, 700 μ mol) was added dropwise. The reaction mixture was monitored by TLC. When finished, a saturated aqueous solution of NH₄Cl (4mL) was added dropwise and vigorously stirred for 30 minutes. The product is extracted with Et₂O (2 x 10 mL), dried with Na₂SO₄ and evaporated in vacuo. The crude is purified by silica gel flash chromatography (CyH:AcOEt 95:5) affording a 30 mg of a mixture of **238** and **239**

By integration of the internal vinyl proton a ratio 88:12 of **238:239** was obtained.

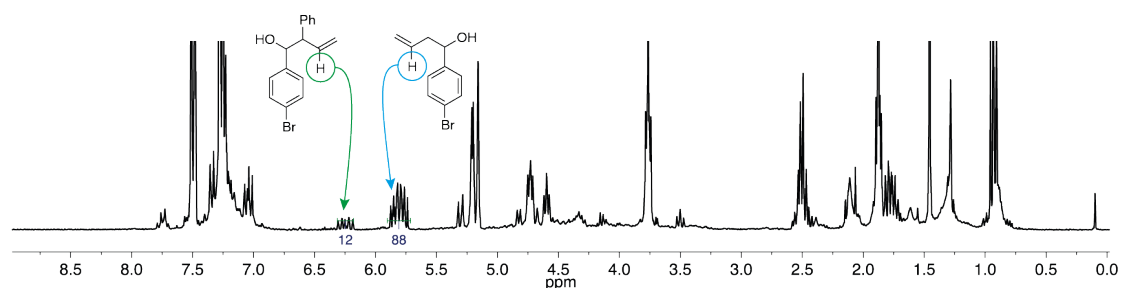


Figure S123: ¹H-NMR of **238+239** (CDCl₃, 400 MHz, 300 K)

Supplemental References

- ¹ G. R. Fulmer, A. J. M. Miller, N. H. Sherden, H. E. Gottlieb, A. Nudelman, B. M. Stoltz, J. E. Bercaw, K. I. Goldberg, *Organometallics* **2010**, *29*, 2176–2179
- ² M. Guitet, P. Zhang, F. Marcelo, C. Tugny, J. Jiménez-Barbero, O. Buriez, C. Amatore, V. Mouriès-Mansuy, J.P. Goddard, L. Fensterbank, Y. Zhang, S. Roland, M. Ménand, M. Sollogoub, *Angew. Chem. Int. Ed.* **2013**, *52*, 7213–7218
- ³ T. Nishimura, Y. Maeda, T. Hayashi, *Org. Lett.* **2011**, *13*, 3674-3677
- ⁴ A. Fürstner, H. Szillat, F. Stelzer, *J. Am. Chem. Soc.* **2000**, *122*, 6785-6786
- ⁵ T. Shibata, Y. Kobayashi, S. Maekawa, N. Toshida, K. Takagi *Tetrahedron* **2005**, *61*, 9018-9024
- ⁶ J. González, V. M. Pérez, D. O. Jiménez, G. Lopez-Valdez, D. Corona, E. Cuevas-Yañez, *Tet. Lett.* **2011**, *52*, 3514-3517
- ⁷ E. S. Degtyareva, J. V. Burykina, A. N. Fakhrutdinov, E. G. Gordeev, V. N. Khrustalev, V. P. Ananikov *ACS Catal.* **2015**, *5*, 7208–7213
- ⁸ D. Guo,; H. Huang, J. Xu, H. Jiang, H. Liu, *Org. Lett.* **2008**, *10*, 4513-4516
- ⁹ L. Ackermann, R. Born, *Angew. Chem. Int. Ed.* **2005**, *44*, 2444-2447
- ¹⁰ D. Guo, H. Huang, J. Xu, H. Jiang, H. Liu, *Org. Lett.*, **2008**, *10*, 451-4516
- ¹¹ Q. Shen, T. Ogata, J. F. Hartwig, *J. Am. Chem. Soc.*, **2008**, *130*, 6586-6596
- ¹² S. Ge, R. A. Green, J. F. Hartwig, *J. Am. Chem. Soc.* **2014**, *136*, 1617-1627
- ¹³ A. Flahaut, K. Toutah, P. Mangeney, S. Roland, *Eur. J. Inorg. Chem.* **2009**, 5422–5432